MOLECULAR SPECTROSCOPIC ANALYSIS AND DOCKING STUDIES OF SOME THIAZOLEPYRAZOLE DERIVATIVES



Thesis submitted to

Bharathidasan University, Tiruchirappalli

in partial fulfillment of the requirements for the award of the degree of

DOCTOR OF PHILOSOPHY IN PHYSICS

By

N. SHANMUGAPRIYA M.Sc., M.Phil., B.Ed.

(Ref.No.05677/Ph.D.K2/Physics/Part-Time/April-2017 /01.04.2017)

Under the Guidance of

Dr. V. BALACHANDRAN M.Sc., M.Phil., M.Ed., PGDCA., Ph.D.



CENTRE FOR RESEARCH – DEPARTMENT OF PHYSICS ARIGNAR ANNA GOVERNMENT ARTS COLLEGE

(Affiliated to Bharathidasan University, Tiruchirappalli - 620 024)

MUSIRI, TIRUCHIRAPPALLI - 621 211, TAMILNADU, INDIA

AUGUST - 2022

Dr. V. BALACHANDRAN M.Sc., M.Phil., M.Ed., PGDCA., Ph.D., Assistant Professor and Research Supervisor, Centre for Research – Department of Physics, Arignar Anna Government Arts College, Musiri, Tiruchirappalli – 621211, Tamilnadu, India.



Date:

CERTIFICATE

This is to certify that the work incorporated in this thesis titled "MOLECULAR SPECTROSCOPIC ANALYSIS AND DOCKING STUDIES OF SOME THIAZOLE-PYRAZOLE DERIVATIVES" submitted to the Bharathidasan University in partial fulfilment of the requirements for the degree of "DOCTOR OF PHILOSOPHY IN PHYSICS" is a bonafide record of work done by N. SHANMUGAPRIYA (Ref No:05677/Ph.D.K2/Physics/Part-Time/April-2017) who carried out the research under my supervision. Certified further that to the best of my knowledge, the contents of this thesis have not been formed the basis for the award of any degree, associateship, diploma, fellowship or any other similar title of any university or institution.

Research Supervisor

N. SHANMUGA PRIYA M.Sc., M.Phil., B.Ed.,

Guest Lecturer of Physics,

Arignar Anna Government Arts College,

Musiri, Tiruchirappalli – 621211, Tamilnadu, India.



DECLARATION

The research work presented in this thesis titled, "MOLECULAR SPECTROSCOPIC ANALYSIS AND DOCKING STUDIES OF SOME THIAZOLE-PYRAZOLE DERIVATIVES" was carried out by me independently under the supervision of Dr. V. BALACHANDRAN, Assistant Professor and Research Supervisor, Centre for Research – Department of Physics, Arignar Anna Government Arts college, Musiri. This work is original and has not been submitted in part or full for any other degree or diploma of this or any other university.

Place: Signature of the Candidate

Date:



CENTRE FOR RESEARCH – DEPARTMENT OF PHYSICS, ARIGNAR ANNA GOVERNMENT ARTS COLLEGE, MUSIRI, TIRUCHIRAPPALLI – 621211, TAMILNADU, INDIA.

CERTIFICATE OF PLAGIARISM CHECK

1.	Name of the research scholar	N. SHANMUGAPRIYA
2.	Course of study	Ph.D., PHYSICS
3.	Title of the thesis / dissertation	Molecular spectroscopic analysis and docking studies of some thiazole-pyrazole derivatives
4.	Name of the research supervisor	Dr. V. BALACHANDRAN
5.	Department / Institution / Research Center	Centre for Research Department of Physics, Arignar Anna Government Arts College, Musiri, Tiruchirappalli – 621211.
6.	Acceptable maximum limit	10%
7.	Percentage of similarity of content identified	4%
8.	Software used	OURIGINAL
9.	Date of verification	24/08/0022

Report on plagiarism check item with 4% of similarity attached.

Signature of the Research Supervisor

Signature of the Candidate



Document Information

Analyzed document N.Shanmugapriya Thesis PhD PHYSICS.pdf (D143213773)

Submitted 8/24/2022 11:15:00 AM
Submitted by Srinivasa ragavan S
Submitter email bdulib@gmail.com

Similarity 4%

Analysis address bdulib.bdu@analysis.urkund.com

Sources included in the report

W

 ${\tt URL:\ http://przyrbwn.icm.edu.pl/APP/PDF/136/app136z3p02.pdf}$

Fetched: 1/3/2022 7:44:07 AM

W

URL: https://annalsofrscb.ro/index.php/journal/article/download/4608/3696/8484

Fetched: 12/11/2021 6:16:53 AM

W

URL: https://www.researchsquare.com/article/rs-1752702/latest.pdf

Fetched: 7/29/2022 6:32:45 AM

W

URL: http://www.joics.org/gallery/ics-2830.pdf

Fetched: 4/25/2022 1:30:19 PM

w

URL: https://www.researchgate.net/publication/346736779_Analysis_of_spectroscopic_quantum_chemical_calculations_molecular_docking_RDG_ELF_anticancer_and_antimicrobial_activity.

 $\hbox{$3-4-Chlorophenyl-5-4$-propane-$2$-yl_phenyl-$45$-dihy}$

Fetched: 4/17/2022 3:32:38 AM

W

URL: https://ijisrt.com/assets/upload/files/IJISRT20NOV356.pdf

Fetched: 7/9/2021 9:45:18 AM

w

 ${\tt URL: http://oam-rc.inoe.ro/articles/spectra-and-normal-coordinate-analysis-of-poly-vinyl-acetate/full texture.} \\$

Fetched: 6/26/2021 2:48:08 PM

W

URL: http://ijrar.com/upload_issue/ijrar_issue_1844.pdf

Fetched: 11/3/2021 6:14:30 AM

Entire Document

1 CHAPTER – 1 MOLECULAR SPECTROSCOPY-AN INTRODUCTION 1.1 Introduction The study of spectroscopy deals with emission as well as absorption spectra. An emission spectrum is produced by atom. Atoms can be excited thermally (by heating the substance rapidly) or electrically (by passing an electric discharge through the vapours of the substance at a very low pressure). Energy is absorbed to meta-stable states when an electric discharge passes through the vapours of the substance. When electrons from the meta stable state jump to the lower energy state, then some energy of definite radiation is analysed with the help of a spectrometer [1]. 1.2 Electromagnetic radiation Electromagnetic (EM) radiation is a periodically changing or oscillating electric field propagating in a certain direct frequency but perpendicular to the electric field [2]. The electric and magnetic field are mutually perpendicular to each other and are coplanar. These are characterized by their wavelengths or frequency representation of EM radiation is shown in Fig. 1.1. Fig.1.1 A schematic representation of EM radiation

2 EM radiation may be considered as a traveling wave or as a stream of mass less elementary particles, often called photons. As a wave, it can be characterized by its wavelength λ (the length of one w unit time) and its wave number k (the number of waves per unit length) [3]. The velocity for EM - waves proves to be a constant for the medium in which the waves are propagating, that is 3*10 8 m/s wavelength is being inversely proportional to the frequency. Using the quantum character of EM radiation, there is the relation E=hv (1.2) where E is the photon energy and h is Planck's constant [4]. Ea energy proportional to its frequency v [5]. By this means, a photon with a higher frequency contains more energy. 1.3 Electromagnetic spectrum and absorption of radiations Electromagnetic spectrum radiant energy from cosmic rays to X-rays to visible light to microwaves, each of which can be considered as a wave or radiation or particle traveling at the speed of light. When radiation will be absorbed molecular vibration if the frequency of the radiation matches the frequency of the molecule. These radiation differ from each other in the wavelength and frequency, as illustrated in Fig. 1.2.

3 Fig. 1.2 Electromagnetic spectrum The EM spectrum can be divided into several regions differing in frequency only. It extends from gamma (v≥10 20 Hz) and X-rays (3·10 16 ≤v>10 20 Hz) to radio (7.5·10 14 ≤v>3·10 16 Hz), visible (4·10 14 ≤v>7.5·10 14 Hz) and infrared (IR) regions (0.003≤v>4·10 14 Hz). 1.4 Spectroscopy Spectroscopy is a branch of physics which deals with the interaction result of this interaction, electromagnetic radiation characteristic of the interacting system may be absorbedor emitted. In such a case, the experimental data consists of the nature (frequencyor wavel characteristic radiation absorbedor emitted. In spectroscopy, we correlate these data with the molecular and electronic structure of the substance and with intramolecular and intermolecular interact spectroscopic technique could be considered under the following heads: i. Radiation that interacts with the matter. ii. Energy levels that affect transitions among different energy levels.

4 iii. Absorption (or emission) bands obtained as a result of these transitions. The position, band width, number and intensity of the absorption (or emission) may be correlated with the molecular and expess of spectroscopy. When light is allowed to pass through the substance that absorber, the radiation causes an excitation of molecules from a lower to a higher energy level. At the atomic or molecular spectroscopy. The characters like molecular absorption, emission and vibration are studied in molecular spectroscopy. The characters like molecular absorption, emission and vibration are studied, etc. This method of spectroscopy is widely used due to many applications. The methods are quick, easy and accurate in determining. Further, they are easily integrated into other analytical tespectroscopy. Here energy change takes place at atomic levels. The measurement is done to study the atoms and their quantity. Atomic spectroscopy classified in two types as (a) Atomic absorption spectroscopy As the term suggests, light is absorbed by the sample. The wavelength of the absorbed light and the extent of absorption are considered. The nature of the compound absorbed, while the intensity of absorbed light determines the concentration. The following are a few examples of spectroscopic.

5 methods that belong to this category:calorimetry, UV-spectroscopy, infrared spectroscopy and Nuclear magnetic resonance (NMR). (b) Atomic emission spectroscopy In contrast to the previous method light hitting the sample is absorbed. This absorption of light results in transition of electrons from ground state to an excited state. These excited electrons return back to ground state with the aid (light) of a particular wavelength. The concentration is determined by the intensity, whereas the nature of the substance is deduced by the wavelength. Fluorimetry and flame photometry are example system that is based on the electrical or magnetic properties of the compound. Light is an electromagnetic radiation, as we all know. It possesses electrical and magnetic properties, in other words. Elewithout the use of a magnetic field. The substance under test is exposed to light without being influenced by a magnetic field in this method. (iv) Magnetic spectroscopy In this spectroscopy, the substance of an external magnetic field. Examples Nuclear magnetic resonance spectroscopy (NMR) and Electron spins resonance spectroscopy (ESR).

ACKNOWLEDGEMENT

Immeasurable gratitude for the help and support is extended to the following people who, in one way or another, have contributed to making this study possible.

First of all, I would like to express my thanks, admiration, and gratitude to my guide and research supervisor, **Dr. V. BALACHANDRAN**, Assistant Professor, Centre for Research – Department of Physics, Arignar Anna Government Arts College, Musiri, for his valuable guidance that made the study possible. In spite of his extremely busy academic pursuits, he spared so much time for me. In fact, he has motivated me with his unstained kindness, affectionate guidance, and noble generosity during the course of my study period.

I wish to thank **Dr. M.K. Rajkumar, Principal,** Arignar Anna Government Arts College, Musiri, for supporting and allowing me to do this research work in this esteemed institution.

I wish to place on record my sincere thanks and humble gratitude to **Dr. B. Revathi, Head and Associate Professor**, Center for Research, Department of Physics, Arignar Anna Government Arts College, Musiri, for encouraging, and motivating me to carry out my research work in this Department of Physics.

I would like to thank my doctoral committee members Dr. K. Renuga Devi, Associate Professor and Head, Department of Physics, Government Arts College for Women (Autonomous), Pudukkotottai and Dr. M.K. Murali, Head, Department of Physics, J.J.College of Arts and Science, Pudukkotottai for their helpful comments and suggestions.

I express my sincere thanks to **Dr. B. Narayana**, Professor, Department of Studies in Chemistry, Mangalor University, Mangalagangotri, India, for providing all samples to my research work.

I take immense pleasure to offering my special thanks to **Dr. K. Vanasundari,** Assistant Professor of Physics, Arignar Anna Government Arts College, Musiri, for her good vibration, immense knowledge, and plentiful experience have encouraged me in all the time of my academic research and daily life.

I am incredibly grateful to all of the faculty members, Department of Physics, Arignar Anna Government Arts College, Musiri. Thank you for the encouraging words of wisdom.

I have no words to thank my brother, **Dr. C. Sivakumar**, Guest Lecturer, Department of Physics, Government Arts and Science College, Musiri. Thank you for the strength you gave me.

My warm and heartfelt thanks go to my research family Dr. A. Viji, Assistant Professor, Kongunadu College of Engineering and Technology (Autonomous), Thottiam, **Dr. Vijaykumar**, Assistant Professor of Srimad Andavan Arts Science Physics, and College, Tiruchirappalli, Miss. S. Babiyana, Holy Cross College (Autonomous), Tiruchirappalli, Mr. N. Thirughana Sambantham and Mrs. Malarvizhi Full-Time Research Scholar Department of Physics, Arignar Anna Government Arts College, Musiri, for their tremendous support and hope they had given to me. Without that hope, this thesis would not have been possible.

I would like to thank all of my friends, students and colleagues who supported me and incented me to strive towards my goal.

A special thanks to **Dr. K. Rajam,** Assistant Professor of Commerce, Srimad Andavan Arts and Science College, Tiruchirappalli, wife of my research guide for her help and encouragement during my research work. I express my sincere thanks to **B.R. Snega M.A** and **B.R. Sangeetha B.Sc** who has shown hospitability during the period of my research.

I would like to thank my beloved teacher Late **B. Rajeshwari** who is looking at me from heaven. I thank **Thiyagarajan** and **Shanmugam** family members for supporting me to complete this work.

Last, but not least, **My father Shri. T.N.T. Natesanar** for their love, caring, patience, understanding and their support in financial aspects to pursue this manuscript. I would also like to thank my mother **Mrs. N. Isaivani**, and my young sister **Miss. N. Devi Jayakkalyani M. Phil.,** whom without this would have not been possible. I cannot express my gratitude in mere words to their prayers, affectionate and support throughout.

Finally, I thank all the people who have supported me to complete the research work directly or indirectly.

N. Shanmugapriya

PREFACE

Molecular spectroscopy is an invaluable tool to identify and characterize the molecule with the help of its molecular vibrational modes. Depending on its geometry, conformation, and electronic structure, each molecule has typical molecular spectra that are measured with the help of FT-IR and FT-Raman spectroscopy. These studies of organic molecules are of great interest in biochemical, pharmaceutical, and many other industries because of their applications. Molecular docking is an efficient tool to get an insight into ligand-receptor interactions and screen molecules for the binding affinities against a particular receptor. This work may be helpful to the researchers who are pursuing research on the functions of drug design.

In the present investigation, quantum chemical calculations were carried out using the GAUSSIAN 09W program package with Beeke-3-Lee-Yang-Parr (B3LYP), the standard 6-31G, 6-311G, cc-pVDZ basis sets. Optimized geometrical parameters, vibrational assignments, HOMO-LUMO, molecular interactions, and NBO parameters were discussed. Topological parameters are studied by a multi-wave function (Multiwfn) and visualize molecular dynamics (VMD) programs. Molecular docking studies were also carried out by Auto Dock-Tool 4.0 software and ligand-protein interactions were visualized by Discovery studio 4.1 software. This computational work has been implemented in eight chapters. They are as follows:

Chapter 1: introduces the fundamentals of molecular spectroscopy as well as the necessary theory for the simplification of problems in molecular spectroscopy. It appears to contain infrared and Raman spectroscopy principles and normal modes of vibration,

Chapter 2: quantum chemical calculations are dealtwith in this chapter. The different quantum mechanical methods like *ab-initio* methods, semi-empirical methods, and density functional theory have been discussed. The effect of scaling on vibrational wavenumbers, and basis set combinations in the computations of molecular geometry optimization, energy, and vibrational wavenumbers are discussed in this chapter. The general procedure of normal coordinate analysis in the calculation of potential energy distribution (PED) is also discussed. The highest occupied molecular orbital (HOMO) and lowest unoccupied molecular orbital (LUMO), Molecular electrostatic potential (MEP), and Natural bond orbital (NBO) analysis were used to predict the essential chemical reactivity andstability of the molecule. The topological parameters, reduced density gradient (RDG), and molecular docking studies are also discussed.

Chapter 3: discusses the FT-IR and FT-Raman instrumental analysis sample handling techniques.

Chapter 4: Based on the systematic process the structure of thiazol-pyrazol compound 4-[{2-[3-(4-chlorophenyl)-5- (4-chlorophenyl)-5- (4-propan-2-yl) phenyl)-4, 5-dihydro- 1*H*- pyrazol-1-yl]-4-oxo-1, 3-thiazol-5(4H)-ylidene} methyl] benzonitrile (CPTBN) was investigated. In the first level, the spectral statistics on experimental FT-IR and FT-Raman were reported. At the next level, geometrical parameters were theoretically acquired from density functional theory (DFT) using B3LYP/6-31G and 6-311G basis sets. The computed wavenumber was collected and compared with the experimental wavenumber. The vibrational modes were interpreted in terms of potential energy distribution (PED) results. The FMO, MEP, and NBO analysis further validated the charge transfer, reactivity sites, and stability of the molecule. The antimicrobial activity against four bacteria and two fungal strains using disc diffusion and broth

microdilution susceptibility assays. Two grams- positive bacterial strains *staphylococcus* aureus, Bacillus subtilis, and two gram-negative bacterial strains Esherichia coli, and Pseudomonas aeruginosawere performed for antibacterial activity. Two fungal strains Candida albicans and Aspergillus Niger were carried out against a ligand using antifungal activity. The molecular docking analysis explores the antimicrobial and selective potential inhibitory nature of the binding molecule. Besides, RDG and ELF analyses were also performed to show the nature of interactions between the molecules.

Chapter 5: A comprehensive investigation of the molecular structure, electronic properties and vibrational spectra of 5-(4-Propoxybenzylidene)-2-[3-(4-chlorophenyl)-5-[4-(propan-2-yl) phenyl]-4, 5-dihydro-1*H*-pyrazol-1-yl]-1, 3-thiazol-4(5*H*)-one have been studied. Thiazol is one of the leading heterocyclic five-member ring compounds that contain one nitrogen and one sulphur atom. Many natural and synthetic compounds contain, thiazol which are attractive compounds found in the building of numerous natural products and certain pharmaceutical agents. To understand the molecular-orbital interaction and structural investigation of the title compound, the density functional theory (DFT) calculation has been carried out using B3LYP/6-31G and 6-311G basis sets combination. The experimental FT-IR and FT-Raman spectral data along with theoretical quantum chemical calculation were investigated. For potential energy distributions (PED) analysis, the VEDA 4 program is utilized to do comparative wavenumber assignments. With the optimized structures, the highest occupied molecular orbital (HOMO), the lowest unoccupied molecular orbital (LUMO) energies, and Natural Bond Orbital (NBO) was applied to describe the chemical reactivity of the molecule. The electron density interactions distributed in space, which exist within these compounds are analyzed by different topological parameters namely, atoms in the molecule (AIM), localized orbital locator (LOL), electron localization function (ELF), and the reduced gradient of the density (RDG). Finally, the molecular docking studies of the title compound for potent Pim-1 kinase cancerPDB ID: 3a99, 1gj8, 1xqz were investigated using the Auto Dock program.

Chapter 6: The experimental FT-IR (4000-0 cm⁻¹) and FT-Raman (3500-0 cm⁻¹) absorption data of the 5-(4-Hydrobenzylidene)-2-[3-(4-chlorophenyl)-5- [4-(propan-2-yl) phenyl]-4, 5- dihydro-1*H*-pyrazol-1-yl]-1, 3-thiazol-4(5*H*)-one (HCPPT) were combined with a theoretical quantum chemical calculation. For the theoretical computations, the optimized geometrical parameters and the vibrational assignment of the HCPPT were determined by density functional theory using the B3LYP method cc-PVDZ and 6-311G basis sets. The charge transfer (donor and acceptor) within the molecule is easily identified by density plots across the highest occupied molecular orbital (HOMO) and lowest unoccupied molecular orbital (LUMO) energy surfaces. It also provides information about the chemical activity of the title compound. A molecular electrostatic potential surface was plotted to assess the molecule's electrophilic and nucleophilic reactivity sites. The charge delocalization and stability of the title molecule were investigated using natural bond orbital (NBO) analysis. Non-covalent interactions, topology, and two- and three-dimension finger-print plots were also studied using reduced density gradient analysis. In addition, the anti-microbial activity of the title compound is evaluated against bacterial: gram-positive organisms (staphylococcus aureus, Bacillus subtilis), gram-negative organisms (Escherichia coli, Pseudomonas aeruginosa), and fungal organisms (candida albicans and Aspergillus Niger) to investigate its biological action. Furthermore, molecular docking studies of the title compound revealed that it may exhibit Antineoplastic (solid tumors), anti-cancerous and anti-inflammatory activity.

Chapter 7: In this work, a structural and electronic properties of 5-(4-Methoxybenzylidene)-2-[3-(4-chlorophenyl)-5-[4-(propan-2-yl) phenyl]-4, 5-dihydro-1*H*-pyrazol-1-yl]-1, 3-thiazol-4(5H)-one have been presented. The optimized geometrical parameters bond length, bond angles, dihedral angles, and vibrational wavenumber are obtained with the help density functional theory (DFT) along with B3LYP/6-31G and 6-311G hybrid functional is employed. For the experimental calculation vibrational spectrum was obtained in the region of 4000-0 cm⁻¹ and 3500-0 cm⁻¹ for FT-IR and FT-Raman spectrum, respectively. Moreover, frontier molecular orbital (HOMO-LUMO), MEP, and NBO analyses were performed for the optimized structure. Various intermolecular interactions in the MCPPT have been thoroughly investigated using topological as atoms in molecules (AIM) analysis and the non-covalent interactions (NCI) approach. Finally, the molecular docking between the molecule and protein-Antinneurogenic pain (5pbe), Anti-inflammatory (4x7s), Myeloid cell leukemia-1 (6dm8), Myeloblastin (1fuj), Naproxen (4ot2) was investigated. These ligand-enzyme interactions were attempting to exhibit the drug's nature of the compound.

Chapter 8: The FTIR and FT-Raman spectra of 5-Chloro-1-(4-chlorobenzyl)-3-[2-(3-(4-chlorophenyl)-5-[4-(propan-2-yl)phenyl]-4,5-dihydro-1*H*-pyrazol-1-yl)-4-oxo-4,5-dihydro-1,3-thiazol-5(4H)-ylidene]-2,3-dihydro-1*H*-indole-2-one was measured in the range of 4000-400 cm⁻¹ and 3500-100 cm⁻¹, respectively. Using the B3LYP/6-31G and 6-311G basis sets, density functional theory was used to optimize the geometrical parameters, frequency, and vibrational bands of these molecules. Optimized geometrical parameters such as bond length and bond angles were computed. The scaled values were compared to the experimental FT-IR and FT-Raman spectrums. Based on the potential energy distribution, a thorough interpretation of FT-IR and FT-Raman spectra were also

reported. The HOMO-LUMO and MEP surface investigations, along with their essential chemical parameters, reveal the reactivity of electrophilic, nucleophilic, and electronic properties of the compound. The natural bond orbital method was used to study the molecular stability and bond strength. Topology studies were conducted to identify critical points in the molecule. Molecular docking analysis was used to assess its activity against COVID-19, HIV, insulin, and anti-inflammatory proteins. Among these, the highest binding affinity was observed against the HIV target protein 2m8n with a docking score of -10.83 kcal/mol.

LIST OF PUBLICATIONS

- 1. Quantum chemical calculation, performance of selective antimicrobial activity using molecular docking analysis, RDG and experimental (FT-IR, FT-Raman) investigation of 4-[{2-[3-(4-chlorophenyl)-5-(4-propan-2-yl) phenyl)-4, 5-dihydro- 1*H* pyrazol-1-yl]-4-oxo-1, 3- thiazol-5(4*H*)-ylidene}methyl] benzonitrile, **Heliyon,** 7(2021) e07634.
- 2. Spectroscopic Identification, Structural Features and Molecular Docking Studies on 5-(4-Propoxybenzylidene)-2-[3-(4-chlorophenyl)-5-[4(propan-2-yl) phenyl-4,5-dihydro-1*H*-pyrazol-1-yl]-1,3-thiazol-4(5*H*)-one using Pim-1 Kinase Cancer Protein, **Asian Journal of Chemistry**, Vol.34,No.4 (2022) 857-870.

PARTCIPATION AND PAPER PRESENTATION IN SEMINARS / CONFERENCES

- 7th International Conference on Perspectives in Vibrational Spectroscopy
 [ICOPVS-2018] 25-29 November 2018, Bhabha Atomic Research Center, at
 DAE-Convention Center, Anushaktinagar, Mumbai-400094, India.
- 2. International Conference on Recent Advances in Materials Science [ICRAMS-2019] 04-06 February 2019, National College (Autonomous), Trichy-620 001, Tamil Nadu.
- 3. National Level Virtual Conference on Recent Trends in Materials Science and Technology [NCMST-2021] 28 May 2021, Kongunadu College of Engineering and Technology (Autonomous), Thottiam, Trichy-621210, Tamil Nadu.
- International Conference on Growth of Crystals and their Technological Applications [GCTA-2022] 10-12 January 2022, SSN Research Centre, SSN Institutions, Chennai-603110, Tamil Nadu.

CONTENT

CERTIFICATE		ii	
ACK	NOWLE	EDGEMENT	V
PRE	FACE		vii
LIST	OF PUI	BLICATIONS	xiv
PAP	ER PRES	SENTED IN	XV
SEM	INARS/	CONFERENCE/WORKSHOPS	
		CHAPTER – 1	
		MOLECULAR SPECTROSCOPY-AN INTROD	UCTION
1.1	Introduc	ction	1
1.2	Electron	nagnetic radiation	1
1.3	Electron	nagnetic spectrum and absorption of radiations	2
1.4	Spectros	scopy	3
	1.4.1	Elements of spectroscopy	3
	1.4.2	The different types of spectroscopy	4
	1.4.3	Importance of spectroscopy	6
1.5	Vibratio	onal spectroscopy	7
1.6	Theory	of Infrared and Raman spectroscopy	7
1.7	Molecul	lar vibrations	8
1.8	Normal	modes of vibrations	9
		CHAPTER – 2	
		QUANTUM CHEMICAL CALCULATION	NS
2.1	Introdu	ction	11
2.2	Survey	of computational chemistry methods	12
	2.2.1	Molecular mechanics	12
	2.2.2	Electronic structure methods	12
	2.2.3	Ab initio methods	13
	2.2.4	Density functional theory	14
2.3	Basis se	et	16
2.4	Types	of basis set	17
	2.4.1	Minimal basis set	17
		1	

	2.4.2	Extended basis set	18
	2.4.3	Correlation-consistent basis sets	21
2.5	5 Gaussian-09		22
2.6	6.6 Gauss view 5.0		22
2.7	2.7 Geometry optimization		22
2.8	Frequer	ncy calculations	23
2.9	Frontie	molecular orbital theory (HOMO-LUMO)	24
2.10	Molecu	lar electrostatic potential (MEP)	25
2.11	Natural	bond orbital analysis (NBO)	26
2.12	Topolo	gy Analysis	27
	2.12.1	Atoms in molecules (AIM)	27
	2.12.2	Localized orbital locator (LOL) and electron	28
		localization function (ELF)	
	2.12.3	Reduced density gradient (RDG)	28
2.13	Molecu	30	
	2.13.1	Binding site identification and mapping	32
	2.13.2	Types of Docking	33
	2.13.3 Brief introduction of the software and websites used		34
		for docking study AutoDock Vina	
	2.13.4	Pymol	35
	2.13.5	RCSB-PDB	35
		CHAPTER – 3	
		INSTRUMENTATION TECHNIQUES	
3.1	Introdu	ction	37
3.2	Instrum	entation	37
	3.2.1	Basic components of FT-IR	37
	3.2.2	Source	38
	3.2.3	Interferometer	38
	3.2.4	Sample handling techniques	39
	3.2.5	Detector	40
	3.2.6	Amplifiers and recorders	41
	3.2.7	Computers	41
	ı		

	3.2.8	Spectra	41
3.3	Raman	spectroscopy	42
	3.3.1	Source	43
	3.3.2	Monochromator	44
	3.3.3	Detectors	44
	3.3.4	Data acquisition and control	45
	3.3.5	Sample handling techniques in Raman spectroscopy	46
3.4	Advantages of FT-IR and FT-Raman spectrometers		46

QUANTUM CHEMICAL CALCULATION, PERFORMANCE OF SELECTIVE ANTIMICROBIAL ACTIVITY USING MOLECULAR DOCKING ANALYSIS, RDG AND EXPERIMENTAL (FT-IR, FT-RAMAN) INVESTIGATION OF 4-[{2-[3-(4-CHLOROPHENY)-5-(4-PROPAN-2-YL)PHENYL)-4, 5-DIHYDRO- 1H- PYRAZOL-1-YL]-4-OXO-1, 3-THIAZOL-5(4H)-YLIDENE}METHYL] BENZONITRILE

4.2	Experi	mental details	40
			48
4.3	Compu	ntational details	49
4.4	Results and discussion		50
	4.4.1	Molecular geometry	50
	4.4.2	Vibrational assignments	52
	4.4.3	Reactivity cite of CPTBN	59
	4.4.4	HOMO- LUMO energy and global reactivity	61
		descriptors	
	4.4.5	Fock matrix for bonds	62
	4.4.6	Reduced density gradient (RDG)	64
	4.4.7	Localized orbital locator (LOL) and electron localization function (ELF)	65
	4.4.8	Antibiotic and antifungal activity	67
	4.4.9	Molecular docking	67
4.5	Conclu	ision	73

SPECTROSCOPIC IDENTIFICATION, STRUCTURAL FEATURES AND MOLECULAR DOCKING STUDIES ON 5-(4-PROPOXYBENZYLIDENE)-2-[3-(4-CHLOROPHENYL)-5-[4(PROPAN-2-YL) PHENYL-4,5-DIHYDRO-1H-PYRAZOL-1-YL]-1,3-THIAZOL-4(5H)-ONE USING PIM-1 KINASE CANCER PROTEIN

5.1	Introduction		85
5.2	Experimental Profile		86
5.3	Computational details		86
5.4	Results and discussion		87
	5.4.1	Molecular geometry	87
	5.4.2	Vibrational assignments	89
	5.4.3	Global reactivity descriptors	95
	5.4.4	Molecular electrostatic potential (MEP)	97
	5.4.5	NBO analysis	98
	5.4.6	Topology analysis	99
	5.4.7	Molecular docking	103
5.8	Conclusion		106

CHAPTER - 6

EXPLORATION MECHANISM OF SPECTRAL CHARACTERIZATION, DFT STUDIES, BIOLOGICAL ACTIVITY AND MOLECULAR INTERACTION DATA OF 5-(4-HYDROBENZYLIDENE)-2-[3-(4-CHLOROPHENYL)-5- [4-(PROPAN-2-YL) PHENYL]-4, 5- DIHYDRO-1*H*-PYRAZOL-1-YL]-1, 3-THIAZOL-4(5*H*)-ONE

6.1	Introdu	uction	122
6.2	Experi	mental details	123
6.3	Comp	utational details	123
6.4	Result	s and discussion	124
	6.4.1	Molecular geometric properties	124
	6.4.2	Vibrational frequency assignments	126
	6.4.3	Frontier molecular orbital analysis	132
	6.4.4	Global reactivity descriptors	134
	6.4.5	Molecular Electrostatic Potential	134

	6.4.6	NBO analysis	135
	6.4.7	Topology analysis	136
	6.4.8	Antimicrobial activity	140
	6.4.9	Molecular Docking	141
6.5	Conclusion		145

SPECTRAL INVESTIGATIONS, TOPOLOGY, COMBINING DFT COMPUTATIONS WITH MOLECULAR DOCKING STUDIES OF 5-(4METHOXYBENZYLIDENE)-2-[3-(4-CHLOROPHENYL)-5-[4(PROPAN-2-YL) PHENYL]-4,5-DIHYDRO-1H-PYRAZOL-1-YL]-1,3-THIAZOL-4(5H)-ONE

7.1	Introduction		160
7.2	Experimental details		161
7.3	Computational techniques		161
7.4	.4 Results and discussion		162
	7.4.1	Molecular geometrical optimization	162
	7.4.2	Vibrational Analysis	163
	7.4.3	Frontier Molecular Orbital Analysis	169
	7.4.4	Molecular Electrostatic Potential (MEP)	171
	7.4.5	Donor-acceptor interaction	172
	7.4.6	Topology analysis	173
	7.4.7	Molecular Docking	175
7.5	Conclusion		178

CHAPTER – 8

SPECTROSCOPIC INVESTIGATION (FT-IR, FT-RAMAN), VIBRATIONAL ASSIGNMENTS, TOPOLOGY EVALUATION AND MOLECULAR DOCKING STUDY OF 5-CHLORO-1-(4-CHLOROBENZYL)-3-[2-(3-(4-CHLOROPHENYL)-5-[4-(PROPAN-2-YL) PHENYL]-4,5-DIHYDRO-1H-PYRAZOL-1-YL) -4-OXO- 4,5-DIHYDRO-1,3-THIAZOL-5(4H)-YLIDENE]-2,3-DIHYDRO-1H-INDOL-2-ONE

8.1	Introduction	189
8.2	Experimental details	190
8.3	Computational details	190

onal analysis or molecular orbitals ular electrostatic potential (MEP)	191 191 197
r molecular orbitals	
	197
ılar electrostatic potential (MEP)	
	198
rface analysis	199
nd LOL analysis	200
nalysis	201
ılar docking study	203
	204
F CONCLUSION	220
s	
)	OF CONCLUSION

Molecular Spectroscopy - An Introduction

Abstract

Molecular spectroscopy is the collective term used to describe two analytical techniques: infrared (IR) and Raman spectroscopy. They are non-destructive, non-invasive tools that use vibrational energy levels to provide information about the molecular composition, structure elucidation, and characterization interactions within a sample. These methods are used to identify vibrational energy levels along with the spectrum of the chemical bonds. Molecular vibrations which modulate the molecular dipole moment are visible in the infrared spectrum, while those vibrations, which modulate the polarizability appear in the Raman spectrum. These two techniques yield complementary and confirmatory information regarding molecular vibrations. Thus, both these methods should necessarily be used for a complete vibrational analysis of a molecule.

MOLECULAR SPECTROSCOPY-AN INTRODUCTION

1.1 Introduction

The study of spectroscopy deals with emission as well as absorption spectra. An emission spectrum is produced by the emission of radiant energy by an excited atom. Atoms can be excited thermally (by heating the substance rapidly) or electrically (by passing an electric discharge through the vapours of the substance at a very low pressure). Energy is absorbed and electrons in the ground state are promoted to metastable states when an electric discharge passes through the vapours of the substance. When electrons from the met a stable state jump to the lower energy state, then some energy of definite frequency is released as radiation. This emitted radiation is analysed with the help of a spectrometer [1].

1.2 Electromagnetic radiation

Electromagnetic (EM) radiation is a periodically changing or oscillating electric field propagating in a certain direction with a magnetic field oscillating at the same frequency but perpendicular to the electric field [2]. The electric and magnetic field are mutually perpendicular to each other and are coplanar. These are characterized by their wavelengths or frequencies or wavenumbers. The schematic representation of EM radiation is shown in Fig. 1.1.

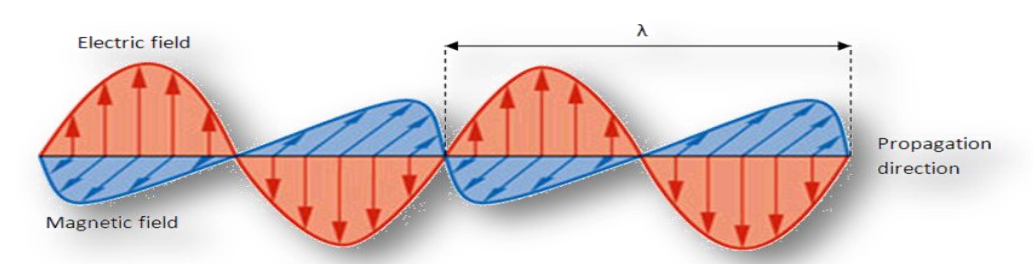


Fig. 1.1 A schematic representation of EM radiation

EM radiation may be considered as a traveling wave or as a stream of mass less elementary particles, often called photons. As a wave, it can be characterized by its wavelength λ (the length of one wave), its frequency v (the number of vibrations per unit time) and its wavenumber k (the number of waves per unit length) [3]. The velocity for EM - waves proves to be a constant for the medium in which the waves are propagating, that is $3*10^8$ m/s in vacuum. It can be easily seen that

$$c=\lambda v$$
 (1.1)

wavelength is being inversely proportional to the frequency. Using the quantum character of EM radiation, there is the relation

$$E=hv$$
 (1.2)

where E is the photon energy and h is Planck's constant [4]. Each quantum of radiant energy or photon has energy proportional to its frequency v [5]. By this means, a photon with a higher frequency contains more energy.

1.3 Electromagnetic spectrum and absorption of radiations

Electromagnetic spectrum refers to the "seemingly" diverse collection of radiant energy from cosmic rays to X-rays to visible light to microwaves, each of which can be considered as a wave or radiation or particle traveling at the speed of light. When radiation will be absorbed and identify the change in the amplitude of molecular vibration if the frequency of the radiation matches the frequency of the molecule. These radiation differ from each other in the wavelength and frequency, as illustrated in Fig. 1.2.

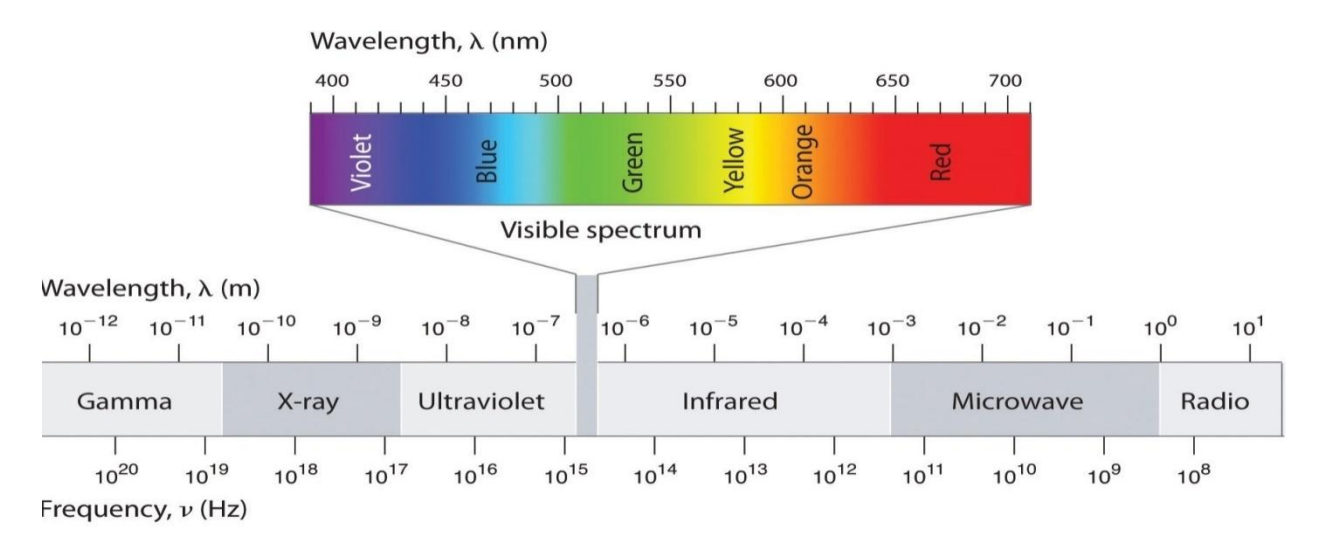


Fig. 1.2 Electromagnetic spectrum

The EM spectrum can be divided into several regions differing in frequency only. It extends from gamma ($v \ge 10^{20} \,\text{Hz}$) and X-rays ($3 \cdot 10^{16} \le v < 10^{20} \,\text{Hz}$) to radio frequencies ($v < 0.003 \,\text{Hz}$) and includes ultraviolet ($7.5 \cdot 10^{14} \le v < 3 \cdot 10^{16} \,\text{Hz}$), visible ($4 \cdot 10^{14} \le v < 7.5 \cdot 10^{14} \,\text{Hz}$) and infrared (IR) regions ($0.003 \le v < 4 \cdot 10^{14} \,\text{Hz}$).

1.4 Spectroscopy

Spectroscopy is a branch of physics which deals with the interaction of electromagnetic radiation with matter [6]. As a result of this interaction, electromagnetic radiation characteristic of the interacting system may be absorbed or emitted. In such a case, the experimental data consists of the nature (frequency or wavelength) and the amount (intensity) of the characteristic radiation absorbed or emitted. In spectroscopy, correlate these data with the molecular and electronic structure of the substance and with intramolecular and intermolecular interactions.

1.4.1 Elements of spectroscopy

Any spectroscopic technique could be considered under the following heads:

- i. Radiation that interacts with the matter.
- ii. Energy levels that affect transitions among different energy levels.

iii. Absorption (or emission) bands obtained as a result of these transitions.

The position, band width, number and intensity of the absorption (or emission) may be correlated with the molecular and electronic structure and bonding.

1.4.2 The different types of spectroscopy

When light is allowed to pass through the substance that absorber, the radiation causes an excitation of molecules from a lower to a higher energy level. At the atomic or molecular level, absorption radiation is classified as follows:

(i) Molecular spectroscopy

Energy changes occurring at the level of molecules are studied in molecular spectroscopy. The characters like molecular absorption, emission and vibration are studied. The examples include UV-spectroscopy, infrared, etc. This method of spectroscopy is widely used due to many applications. The methods are quick, easy and accurate in determining. Further, they are easily integrated into other analytical techniques like chromatography.

(ii) Atomic spectroscopy

Here energy change takes place at atomic levels. The measurement is done to study the atoms and their quantity. Atomic spectroscopy classified in two types as

- (a) Atomic absorption spectroscopy
- (b) Atomic emission spectroscopy

(a) Atomic absorption spectroscopy

As the term suggests, light is absorbed by the sample. The wavelength of the absorbed light and the extent of absorption are considered. The nature of the compound is determined by the wavelength of light absorbed, while the intensity of absorbed light determines the concentration. The following are a few examples of spectroscopic

methods that belong to this category: calorimetry, UV-spectroscopy, infrared spectroscopy and Nuclear magnetic resonance (NMR).

(b) Atomic emission spectroscopy

In contrast to the previous method, the emitted light is measured here. Some of the light hitting the sample is absorbed. This absorption of light results in transition of electrons from ground state to an excited state. These excited electrons return back to ground state with the aid of using the discharge of electromagnetic radiation (light) of a particular wavelength. The concentration is determined by the intensity, whereas the nature of the substance is deduced by the wavelength. Fluorimetry and flame photometry are examples.

(iii) Electronic spectroscopy

A classification system that is based on the electrical or magnetic properties of the compound. Light is an electromagnetic radiation, as we all know. It possesses electrical and magnetic properties, in other words. Electronic spectroscopy is the study of a compound without the use of a magnetic field. The substance under test is exposed to light without being influenced by a magnetic field in this method.

(iv) Magnetic spectroscopy

In this spectroscopy, the substance is exposed to electromagnetic radiation in the presence of an external magnetic field.

Examples

Nuclear magnetic resonance spectroscopy (NMR) and

Electron spins resonance spectroscopy (ESR).

1.4.3 Importance of spectroscopy

The techniques used in spectroscopy are exceedingly sensitive. Among 10²⁰ or more atoms of a different species, single atoms and even various isotopes of the same atom can be recognised. Spectroscopic techniques are frequently the most successful at detecting trace levels of pollutants or contaminants. Infinite frequency changes in narrow spectroscopic lines can be measured using microwave, optical, and gammaray spectroscopy techniques.

Frequency shifts as small as one part in 10¹⁵ of the frequency being measured may be located with ultra high resolution laser techniques. Because of this sensitivity, the most accurate physical measurements had been frequency measurements. Spectroscopic analysis has been crucial in the development of the most fundamental theories in physics, including quantum mechanics, the special and general theories of relativity, and quantum electrodynamics.

Spectroscopy has been a vital instrument in gaining a scientific understanding of not only the electromagnetic force, but also the strong and weak nuclear forces, when applied to high-energy collisions. In almost every technical discipline of science and technology, spectroscopic techniques have been used.

It is already mentioned earlier that the frequency of the radiation absorbed or emitted depends on the energy difference (E) between the two levels involved in the transition and this energy difference is different for rotational, vibrational, electronic, etc. energies. Consequently, the corresponding spectra occur indifferent regions of the electromagnetic spectrum.

1.5 Vibrational spectroscopy

Vibrational spectroscopy is a powerful technique for evaluating the structure of molecules. Its main applications are to study the intramolecular forces, intermolecular forces and in the determination of the strength of the chemical bond and the calculation of thermodynamic properties. Modern methods of spectroscopy, in the different regions of the electromagnetic spectrum have provided indispensable tools for the investigation of molecular structure. Among which, vibrational spectroscopy is undoubtedly the most powerful physical technique for the elucidation of molecular structure.

1.6 Theory of Infrared and Raman spectroscopy

Molecular vibrations can be excited via two physical mechanisms: the absorption of light quanta and the inelastic scattering of photons [7]. Direct absorption of photons is achieved by irradiation of molecules with polychromatic light that includes photons of energy matching the energy difference hv_k between two vibrational energy levels, the initial (e.g., ground state) and the final (e.g., first excited state) vibrational state.

$$hv_k = hv_f - hv_i \tag{1.3}$$

As these energy differences are in the order of 0.5 and 0.005eV, light with wavelengths longer than 2.5 mm, that is infrared (IR) light, is sufficient to induce the vibrational transitions. Thus, vibrational spectroscopy that is based on the direct absorption of light quanta is denoted as IR absorption or IR spectroscopy.

In contrast to IR spectroscopy, the scattering mechanism for exciting molecular vibrations requires monochromatic irradiation. A portion of the incident photons is scattered in elastically such that the energy of the scattered photons (hv_R) differs from that of the incident photons (hv_0) . According to the law of conversation of energy, the

energy difference corresponds to the energy change of the molecule, which refers to the transition between two vibrational states. Thus, the energy differences

$$hv_0 - hv_r = hv_f - hv_i \tag{1.4}$$

lie in the same range as the transitions probed by the direct absorption of mid-IR quanta, although photons of UV, visible, or near-infrared light are used to induce scattering. This inelastic scattering of photons was first discovered by the Indian scientist C.V. Raman in 1928 and is thus denoted as the Raman effect.

In IR and Raman spectroscopy, the same or different vibrational transitions are investigated depending on the molecule, and both methods frequently offer complementing data. In order to make comparisons easier, IR and Raman spectra are typically plotted in a similar manner. The energy of the vibrational transition, expressed in terms of wavenumbers (cm⁻¹), is given on the abscissa, corresponding to the frequency of the absorbed light v_{abs} in IR spectroscopy and to the frequency difference between the exciting and scattered light, $hv_0 - hv_R$, in Raman spectroscopy.

1.7 Molecular vibrations

A molecular vibration occurs when atoms in a molecule are in periodic motion while the molecule as a whole has constant translational and rotational motion. The frequency of the periodic motion is known as a vibration frequency. A molecule can be imagined as a system of balls and springs with varying strengths that correspond to the atoms and chemical bonds within the molecule. A molecule is not a rigid arrangement of atoms. As a result, the positions of atoms in molecules are not fixed; they are subjected to a number of different vibrations. These vibrations fall into the two main categories of stretching and bending. Stretching, in which the distance between two atoms decreases or increases, but the atoms remain in the same bond axis, and bending (or deformation),

in which the position of the atom changes relative to the original bond axis. Each of the vibrational motions of a molecule occurs with a certain frequency, which is characteristic of the molecule and of the particular bond. The stretching comprises of symmetric and asymmetric stretching whereas the bending involves in-plane (such as rocking, scissoring vibrations) and out-of-plane bending (such as twisting, wagging) vibrations. The energy involved in a particular vibration is characterized by the amplitude of the vibration, so that higher the vibrational energy, larger will be the amplitude of the motion [8].

1.8 Normal modes of vibrations

Normal modes are used to describe the different vibrational motions in molecules. Each mode can be characterized by a different type of motion and each mode has a certain symmetry associated with it. Group theory is a useful tool in order to determine what symmetries the normal modes contain and predict if these modes are IR and Raman active. Consequently, IR and Raman spectroscopy is often used for vibrational spectra.

In general, a normal mode is an independent motion of atoms in a molecule that occurs without causing movement in any of the other modes. Normal modes, as implied by their name, are orthogonal to each other. In order to discuss the quantum-mechanical equations that govern molecular vibrations it is convenient to convert Cartesian coordinates into so called normal coordinates. Vibrations in polyatomic molecules are represented by these normal coordinates.

There exists an important fact about normal coordinates. Each of these coordinates belongs to an irreducible representation of the point the molecule under investigation. Vibrational wavefunctions associated with vibrational energy levels share

this property as well. The normal coordinates and the vibration wavefunction can be categorized further, according to the point group they belong to. From these, the frequency can be predicted for which symmetries can exist. The irreducible representation offers insight into the IR and/or Raman activity of the molecule. Each atom within a molecule has three degrees of freedom for its motion in three-dimensional space. If there are N atoms within a molecule there are 3N degrees of freedom. However, the molecule as a whole has to move as a unit and the x, y, z transitional motion of the entire molecule reduces the degrees of freedom by three. The molecule has rotational degrees of freedom. For a non-linear molecule this rotation has three degrees of freedom reducing the number of degrees of freedom to 3N-6. A linear molecule can be rotated around its axis with no change and only two significant rotations. Therefore, a linear molecule has 3N-5 degrees of freedom. The number of peaks actually observed in an infrared spectrum is often less than the maximum because some of the vibrations are energetically identical or degenerate. A real molecule will often have two or more vibrations that may differ only by their orientation in space. These will have exactly the same energy and result in one absorption peak. In addition to the degeneracy of vibrational modes, there is also the requirement that a vibration result in a change in the dipole moment of the molecule needs to be observed [9].

Table 1.1: Degrees of freedom for polyatomic molecules

Type of degrees of freedom	Linear molecule	Non-linear molecule
Translational	3	3
Rotational	2	3
Vibrational	3N-5	3N-6
Total degrees of freedom	3N	3N

Quantum Chemical Calculations

Abstract

The theoretical methods which are suitable for the prediction of vibrational normal modes are discussed. The software packages utilized for the complete study of the title thesis are explained to a greater extent. The functional theories of density functional theory methods and basis set combinations for the molecules are illustrated with necessary theory.

QUANTUM CHEMICAL CALCULATION

2.1 Introduction

The progress of computational approaches to chemical problems has been remarkable. Computers, associated with appropriate software, have gradually become clear as instruments of new experimental methodology, i.e., computer experiment, which means that computers, in combination with appropriate software, form a fundamental extension of our means of obtaining experimental information [10]. Molecular modeling, a subset of computational chemistry, concentrates on predicting the behaviour of individual molecules within a chemical system. The most accurate molecular models use *ab initio* or 'first principles' electronic structure methods, based upon the principles of quantum mechanics, and are generally very computer-intensive. However, due to advances in computer storage capacity and processor performance, molecular modeling has been a rapidly evolving and expanding field, to the point that it is now possible to solve relevant problems in an acceptable amount of time.

The types of predictions possible for molecules and reactions include: (1) Heats of formation (2) Bond and reaction energies (3) Molecular energies and structures (thermochemical stability) (4) Energies and structures of transition states (activation energies) (5) Reaction pathways, kinetics and mechanisms (6) Charge distribution in molecules (reactive sites) (7) Substituent effects (8) Electron affinities and ionization potentials (9) Vibrational frequencies (IR and Raman spectra) (10) Electronic transitions (UV/Visible spectra) (11) Magnetic shielding effects (NMR spectra).

2.2 Survey of computational chemistry methods

All molecular modeling techniques can be classified under three major categories:

- i. Molecular mechanics
- ii. Electronic structure methods and
- iii. Ab initio electronic structure calculations.

2.2.1 Molecular mechanics

Molecular Mechanics (MM) is a standard form which predicts the properties and structures of molecules using classical physics laws. There are different molecular mechanics methods. Each atom (i.e., electrons and nucleus) is represented as one particle with a characteristic mass. A chemical bond is represented as a spring, with a characteristic force constant determined by the potential energy of interaction between the two participating atoms. Potential energy functions can describe intramolecular bond stretching, bending and torsion, or intermolecular phenomenon such as electrostatic interactions or van der Waals interaction which is a potential energy functions on empirically derived parameters obtained from experiments or from other calculations.

2.2.2 Electronic structure methods

Electronic structure methods utilize the laws of quantum mechanics, which is the basis for computational calculations. Quantum mechanics states that the energy and other related properties of the molecule can be obtained by solving the Schrodinger equation,

$$H \psi = E \psi \tag{2.1}$$

However, exact solutions to the Schrödinger equation are not practical. Electronic structure methods are characterized by their various mathematical

approximations and their solutions. There are two major classes of electronic structure methods.

Semi-empirical methods employ simpler Hamiltonian by parameter values that are adjusted to fit the experimental data. That means they solve the approximate parameters available for the type of chemical system of interest. There is no unique method for the choice of parameters.

Ab initio force fields provide solutions to these problems. Ab initio methods utilize the correct Hamiltonian and do not use experimental data other than the values of the fundamental physical constants (i.e., c, h, mass and charges of electrons and nuclei). Moreover, it is a relatively successful approach to perform vibrational spectral calculations.

2.2.3 *Ab initio* methods

Ab initio translated from Latin means "from first principle". This refers to the fact that no experimental data is used and computations are based on quantum mechanics. Ab initio methods first optimize the molecular geometry and then evaluate the second derivative at the equilibrium positions usually using analytical derivatives. Such methods provide reliable values for harmonic vibrational frequencies for fairly large sized molecules. Additionally, such calculations can be used to predict barriers to internal rotation as well as relative stabilities of different conformers. The information obtained from structural parameters, conformational stabilities, force constants, vibrational frequencies as well as infrared and Raman band intensities give significant contributions to the field of vibrational spectroscopy.

Harmonic force constants in Cartesian coordinates can be directly derived from *Ab initio* calculations. These force constants can be transformed to force constants in

internal or symmetry coordinates. *Ab initio* calculations followed by normal coordinate analysis are very helpful in making reliable vibrational assignments. Band intensities from *ab initio* studies are another important output. Such band intensity data can also be very useful in making vibrational assignments. Two principally different quantum mechanical methods addressing the vibration problems are namely Hartree-Fock method and density functional theory (DFT) [11-14].

2.2.4 Density functional theory

Density functional theory calculation has emerged in the past few years as a successful alternative to the traditional Hartree-Fock (HF) method. The DFT methods, particularly hybrid functional methods have evolved as a powerful quantum chemical tool for the determination of the electronic structure of molecules. In the framework of the DFT approach, different exchange and correlation functionalities are routinely used. Among these, the Becke-3-Lee-Yang-Parr (B3LYP) combination is the most used since it proved its ability in reproducing various molecular properties, including vibrational spectra, electronic transitions, nonlinear optical activity (NLO), NMR chemical shifts, molecular electrostatic potential [15-19].

The combined use of B3LYP functional and various standard basis sets, provide an excellent compromise between accuracy and computational efficiency of molecular properties, vibrational spectra, electronic transitions, NMR chemical shifts, NLO properties and natural bond orbital analysis (NBO) for large and medium size molecules. The vibrational frequencies calculated by applying DFT methods are normally overestimated than the experimental values by 2-5% on an average. This overestimation is due to the neglect of electron correlation, anharmonicities and incomplete basis sets.

This overestimation can be narrowed down by applying empirical corrections called scaling, where the empirical scaling factors are ranging from 0.8 to 1.0. The scaling factors depend on both method and basis sets and they partially compensate for the systematic errors in the calculation of frequencies. Global scaling or uniform scaling, multiple or selective scaling is some scaling methods advocated to minimize the overestimation of the frequency differences. *Ab initio* calculation could be performed using Gaussian 09 software package [20].

Although density functional theory has its conceptual roots in the Thomas Fermi model, density functional theory was put on a firm theoretical footing by Hohenberg Kohn theorems [21]. The first theorem demonstrates the existence of a one to one mapping between the ground state electron density and the ground state wave function of a many particle system. The second theorem proves that the ground state density minimizes the total electronic energy of the system. The most common implementation of density functional theory is through the Kohn-Sham method [22]. Within the framework of Kohn-Sham DFT, the intractable many body problems of interacting electrons in a static external potential is reduced to a tractable problem of non interacting electrons moving in an effective potential. The effective potential includes the external potential and the effects of the coulomb interactions between the electrons, such as the exchange and correlation interactions.

Despite recent improvements, there are still difficulties in using density functional theory to suitably describe intermolecular interactions, especially van der Waals forces (dispersion), charge transfer excitations, transition states, global potential energy surfaces and some other strongly correlated systems; and in calculations of the band gap in semiconductors. Its incomplete treatment of dispersion can adversely affect

the accuracy of DFT in the treatment of systems which are dominated by dispersion (e.g. Interacting noble gas atoms) or where dispersion competes significantly with other effects [23, 24].

2.3 Basis set

A basis set is the mathematical description of the orbitals within a system used to perform the theoretical calculation. When molecular calculations are performed, it is common to use basis composed finite number of atomic orbitals, centred at each atomic nucleus within the molecule. Most molecular quantum mechanical methods initiate the calculation with the choice of a set of basis functions. Larger basis sets include more and a greater range of basis functions. Therefore, larger basis sets can better refine the approximation to the "true" molecular wave function, but require correspondingly more computer resources. Alternatively, accurate wave functions may be obtained from different treatments of electrons in atoms. For instance, molecules containing large atoms (Z > 30) are often modeled using basis sets incorporating approximate treatments of inner-shell electrons which account for relativistic phenomena. 'Minimal' basis sets contain the minimum number of atomic orbitals (AO) basis functions needed to describe each atom (e.g., 1s for H and He; 1s, 2s, $2p_x$, $2p_y$, $2p_z$ for Li to Ne). The general expression for a basis function is given as:

Basis Function=
$$N^*e^{(-\alpha^*r)}$$
 (2.2)

Where, N is the normalization constant, α is the orbital exponent, r is the radius in angstroms.

2.4 Types of basis set

2.4.1 Minimal basis set

The most common minimal basis set is the Slater-type orbital (STO-XG), where X is an integer. This X value represents the number of Gaussian primitive function comprising a basis function was developed by Pople and co-workers [25]. Originally formulated for first row elements [26] it was later extended to second row [27] third row [28] and fourth row [29] main group elements. It has also been applied to first-and second row transition metals [30]. The main attraction of this basis other than its small size is its effectiveness in predicting geometries. Thus, STO-3G has only one basis function per hydrogen, five per atom from Li to Ne (1s, 2s, 2px, 2py, and 2pz), and nine for the second row elements Na - Ar (1s, 2s, 2px, 2py, 2pz, 3s, 3px, 3py, 3pz). Note the inclusion of the "core" orbitals, which are omitted in semi-empirical calculations. Only one best fit to a given type of Slater orbital is possible for a given number of Gaussian functions. Hence, all STO-3G basis set for any row of the periodic table are the same, except for the exponents of the Gaussian functions. The exponents are expressed as scale factors, the squares of which are used as multipliers of the adjusted exponents in the original best-fit Gaussian functions. The small computers' increased power and unsatisfactory, but significantly less expensively priced, outcomes that are nonetheless insufficient for publication as research. As a result, the STO-3G basis set is now never used. Commonly used minimal basis sets of this type are:

STO-2G,

STO-3G,

STO-6G, and

STO-3 G* (Polarized version of STO-3G).

2.4.2 Extended basis set

a) Split valence basis set

One problem with minimal basis sets is that they do not allow alteration of the basis orbitals in response to changing molecular environments. Consider a *p*-orbital on oxygen in an ether compared to that same ether when protonated. The inability of a basis set like STO-3G to reflect these changes makes comparison between charged and uncharged species unreliable. Anisotropic environments are another problem for minimal basis sets. The use of split valence basis sets is one way to respond to these problems. In these bases, the Atomic orbitals (AOs) are split into two parts,

An inner compact orbital and

An outer more diffuse one.

The coefficients of these two kinds of orbitals can be varied independently during construction of the Molecular orbitals (MOs). Thus the size of the AO can be varied between the limits set by the inner and outer functions. Split valence basis sets treat only the valence orbitals in this way, basis sets that similarly split the core orbitals are called *double zeta* (DZ). The simplest split valence basis set provided by GAUSSIAN is the 3-21G is shown in Fig. 2.1.

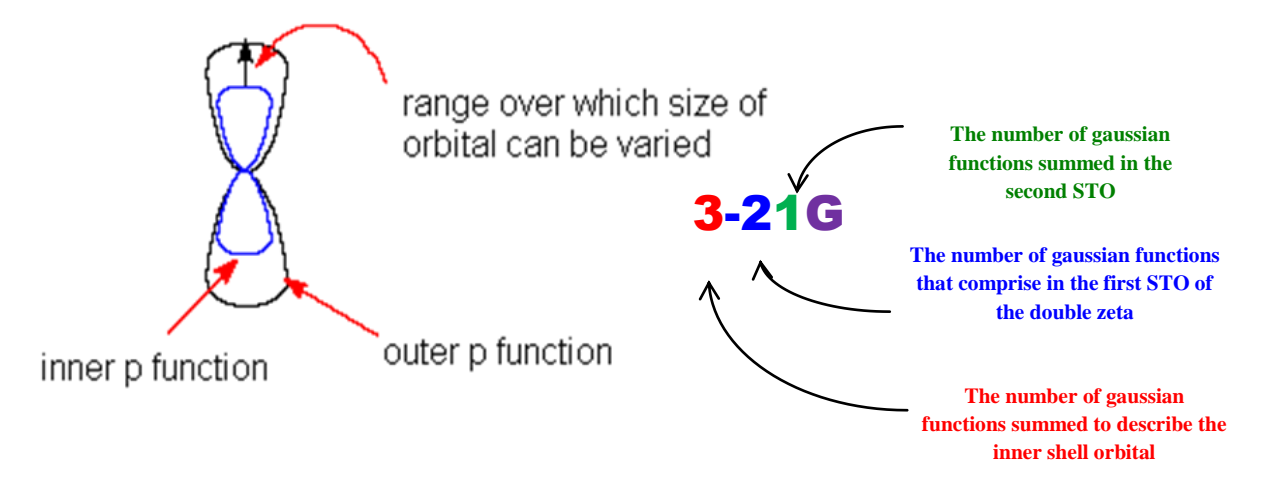
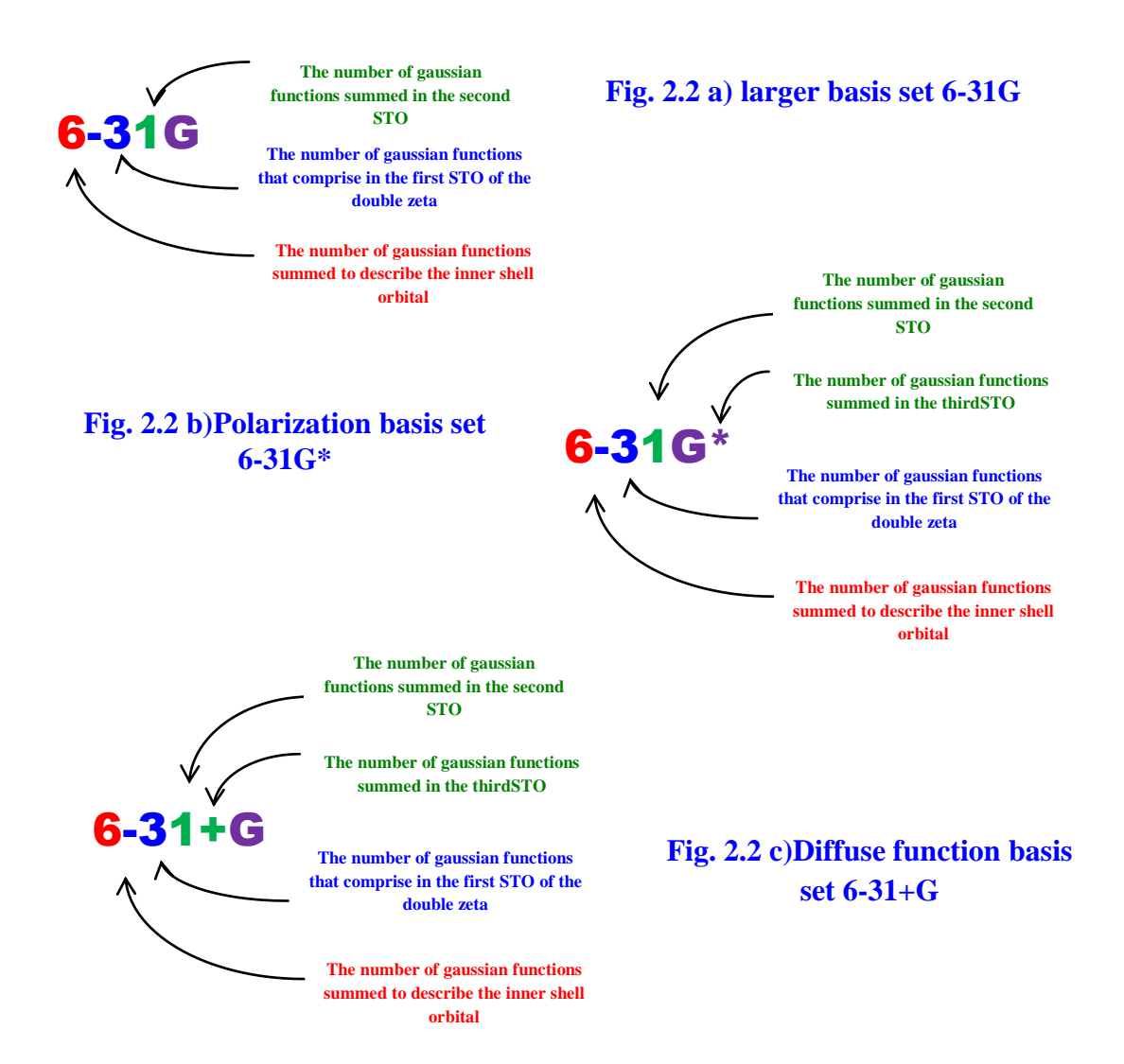


Fig. 2.1 Split valence basis set 3-21G

This description means that the core orbitals are represented by three Gaussians, whereas the inner and outer valence orbitals consist of two and one Gaussians, respectively. If we were to name, bases consistent, of course, this one would be labeled STO-3-21G, but the STO is customarily omitted from all split valence descriptors. GAUSSIAN offers two other split valence bases, the 6-31G and the 6-311G. Both have six Gaussian cores. The 6-311G is a triply split basis, with an inner orbital represented by three Gaussians, and middle and outer orbitals represented as single Gaussians. The triple split improves the description of the outer valence region.

b) Polarization

Further improvement of basis functions is achieved by adding d-orbital to all heavy (non-hydrogen) atoms. For typical organic compounds these are not used in bond formation, as are the *d*-orbitals of transition metals. They are used to allow a shift of the center of an orbital away from the position of the nucleus. The presence of polarization functions is indicated in the Pople notation by appending an asterisk to the set designator. The larger basis set 6-31G with polarization function is shown in Fig.2.2 (a). Typically, six d-functions (x², y², z², xy, xz, and yz), equivalent to five *d*-orbitals and one *s*, are used (for computational convenience). Most programs can also use five "real" *d*-orbitals. An alternative description of this kind of basis is DZP, double zeta, polarization. A second asterisk, as in the 6-31G** basis set implies the addition of a set of p-orbitals to each hydrogen to provide for their polarization. Again, an alternative notation exists: DZ2P, double zeta 2 polarizations. An asterisk in parentheses signals that polarization functions are added only to second-row elements. This is the standard setup for the 3-21G basis set in GAUSSIAN. Another alternative to the asterisk for specifying polarization functions is (d), placed after the G is shown in Fig. 2.2 (b).



(c) Diffuse function

The basis sets are also frequently augmented with the so-called diffuse functions. These Gaussians have very small exponents and decay slowly with distance from the nucleus. Diffuse Gaussians are usually of s and p type. Diffuse functions are necessary for the correct description of anions and weak bonds (e.g. Hydrogen bonds) and are frequently used for calculations, magnetic properties (e.g. Dipole moment, polarizabilities etc.). The presence of diffuse functions is symbolized by the addition of a plus sign, +, to the basis set designator, 6-31+G is shown in Fig. 2.2 (c). Again, a second

+ implies diffuse functions added hydrogens, however, little improvement in results is noted for this addition unless the system under investigation includes hydride ions.

2.4.3 Correlation-consistent basis sets

Correlation consistent basis sets are built up by adding shells of functions to a core set of atomic Hartree-Fock functions. Each function in a shell contributes very similar amounts of correlation energy in an atomic calculation. For first and second row atoms, the basis sets are cc-pVNZ where N=D, T, Q, 5, 6... (D=double, T=triples, etc.) and 'cc-p', stands for 'correlation-consistent polarized', 'V' indicates they are valence-only basis sets. They include successively larger shells of polarization (or correlating) functions (d, f, g, etc.). More recently these 'correlation-consistent polarized' basis sets have widely used for HatreeFock methods.

Examples of these basis sets are

cc-pVDZ - Double-zeta,

cc-pVTZ - Triple-zeta,

cc-pVQZ - Quadruple-zeta,

cc-pV5Z - Quintuple-zeta,

aug-cc-pVDZ, etc.

Here, aug represents augmented versions of the preceding basis sets with added diffuse functions. These basis sets can be augmented with core functions for geometric and nuclear property calculations and with diffuse functions for electronic excited-state calculations, electric field calculations and long-range interactions such as Van der Waals forces. The steps for constructing additional augmented functions exist in the literature as many five augmented functions have been used in second

hyperpolarizability calculations. Because of the precise construction of these basis sets, extrapolation can be done for several molecular properties.

2.5 Gaussian-09

GAUSSIAN-09 [20] is a computational chemistry software program used for performing the quantum chemical calculations. It is well-known; the Gaussian program is widely-used electronic structure programs for advanced quantum chemistry research and other fields.

2.6 Gauss View 5.0

Gauss View [31] is an affordable, full featured graphical user interface for Gaussian-09. With the help of Gauss View, one can submit the inputs to Gaussian and to examine the output graphically which are generated by Gaussian-09 software. Gauss View incorporates an excellent molecule built. One can use it to rapidly sketch the molecules and possibly view three dimensional molecular pictures. It is used to build an atom, ring group, amino acids and nucleic acids. Gauss View can graphically display a variety of Gaussian results such as animation of the normal modes, molecular orbital, atomic charges, electrostatic potential, NMR shielding density and potential energy surface scans.

2.7 Geometry optimization

Optimization of molecular geometry is a first step in quantum chemical calculation. This is mostly done on an isolated molecule in the gas phase. Geometry optimization is performed to locate the lowest energy molecular energy structure in close proximity to the specified starting structure. A geometry optimization will adjust the atomic arrangements in a molecule until an energy minimum is reached. This is the

lowest position on the potential energy surface. Optimized geometry is generally used to compare with experimental data. In the absence of experimental data, construction of models is based on intuitively reasonable values for bond distances, inter-bond angles and dihedral angles.

2.8 Frequency calculations

Vibrational spectra of molecules in their ground and excited states can be computed by employing the Gaussian program. Frequency calculations are valid only at stationary points on the potential energy surface, for this reason it is necessary to run a geometry optimization prior to a frequency calculation. In addition to predicting the frequencies and intensities of spectra, the program can also describe the displacements of the molecule as it undergoes normal modes of vibrations. Molecular frequencies depend on the second derivative of energy with respect to the position of nuclei. Analytic second derivatives are provided by the density functional (B3LYP) theoretical procedures. An optimized energy is used as input for the frequency calculation. The frequency calculations should be performed using the same theoretical model and the basis set as the one that was used to obtain the optimized geometry of the molecule [32-36]. Harmonic force fields derived from quantum mechanics are widely used at present for the calculation of frequencies and the modes of normal vibrations. This opened the way to calculate the frequencies and intensities of spectral bands with a minimum degree of arbitrariness and finding the rational explanations for a number of chemical and physical properties of substances. However, in numerous current quantum calculations of vibrational spectra performed at different levels of approximation, calculated frequencies are higher than their experimental counterparts. These calculations required empirical corrections. To improve agreement with experiment, quantum-mechanical force fields are corrected in one way or another, e.g. using empirical corrections called scale factors which are estimated from the experimental vibrational spectra of small molecules with reliable frequency assignments.

Single point energy gives a prediction of the energy of a molecule with specific geometry. This is usually followed by a Mulliken population analysis which is used to estimate the charge distribution. Electrostatic moments are also calculated, which then allow to calculate the dipole moments. Single point energy calculations can be performed at any level of theory, with small or large basis sets.

2.9 Frontier molecular orbital theory (HOMO-LUMO)

Two major characteristics of an atom or molecule that are very important to computational chemists are the highest occupied molecular orbital (HOMO) and the lowest unoccupied molecular orbital or the virtual orbital (LUMO). Together, they are called the frontier orbitals. The HOMO can be found by locating the outermost orbital containing an electron. The LUMO is the first orbital that does not contain the electron. Koopman's theorem [37] can be used for the computation of approximate ionization energy.

By this theorem, for the closed-shell systems, the first ionization energy is equal to the energy of the HOMO. That is, the energy required to form the caution from the system provided that the ionization process is adequately represented by the removal of an electron from an orbital without change in the wave functions of the other electrons. Similarly, electron affinity can be found as the negative of the energy of the lowest unoccupied, i.e., virtual, orbital (the LUMO).

2.10 Molecular electrostatic potential (MEP)

The molecular electrostatic potential (MEP) is a useful method for studying the interaction of a molecular system with its surroundings and is used for predicting sites and relative reactivity towards electrophilic attack and in studies of biological recognition. The MEP surface which is a method of mapping electrostatic potential on to the isoelectron density surface and it provides a visual method to understand the relative polarity [38]

Computationally, it is usually evaluated within the formalism of either HF or DFT theories. The MEP is particularly useful when visualized on surfaces or in regions of space, since it provides information about local polarity it simultaneously displays molecular size, shapes as well as positive, negative and neutral electrostatic potential regions in terms of the colour grading. The different values of the electrostatic potential are represented by different colours. Potential increases in the order red<orange< yellow< green< blue [39]. The most negative potential is assigned to be red, the most positive potential is assigned to be blue, and the colour spectrum is mapped to all other values by linear interpolation. If this is done on the molecular van der Waals surface, one can immediately distinguish regions of local negative and positive potential, which may be informative for purposes of predicting chemical reactivity.

MEP plot provides a visual representation of the chemically active sites and comparative reactivity of atoms. The negative electrostatic potential corresponds to an attraction of protons by the aggregate electron density in the molecule (shades of red and yellow) and the positive electrostatic potential corresponds to the repulsion of protons by the nuclei (shades of blue).

2.11 Natural bond orbital analysis (NBO)

The NBO analysis provides an efficient method for studying intra and intermolecular bonding and interaction among bonds. The NBO analysis provides a description of the structure of a compound by a set of localized bond, anti-bonds and Rydberg extra valence orbital to identify and confirm the possible intra and intermolecular interaction between the units that would form the proper and improper hydrogen bonding.

From the NBO analysis a large number of stabilizing orbital interactions are observed in molecules. The hyper conjugative interaction energy was deduced from the second-order perturbation approach [40]. The hyper conjugative interactions are formed by the orbital overlap between σ (C-C) bond orbital σ^* (C-C) anti-bonding orbital, which results in intramolecular charge transfer (ICT) causing stabilization of the system. The hyper conjugative interaction energy was deduced from the second order perturbation approach.

$$E(2) = \Delta E_{ij} = q_{i} \frac{(F_{i,j})^{2}}{(E_{i} - E_{i})}$$
(2.3)

where q_j is the donor orbital occupancy, ε_j and ε_i are diagonal elements and F (ij) is the off diagonal NBO Fock matrix element.

From the larger second order interaction energy E(2) value, the more intensive is the interaction between electron donors and electron acceptors, (i-e) the more donating tendency from electron donors to electron acceptors and the greater the extent of conjugation of the whole system. These interactions can be identified by finding the increase in electron density (ED) in anti-bonding orbital that weakens the respective bonds. NBO localization is a multistep process the details of which are sufficiently complicated. In an initial step, orbitals that are associated almost entirely with a single

atom, e.g., core orbitals and lone pairs, are localized as so called natural atomic orbitals (NAO_S). Next, orbitals involving bonding or antibonding between pairs of atoms are localized by using only the basis set AOs of those atoms. Finally, the remaining Rydberg-like orbitals are identified, and all orbitals are made orthogonal to one another. The result is that, except for very small contributions from other AOs to ensure orthogonality, all NAOs and Rydberg orbitals are described through the basis-set AOs of two atoms. Thus, NBO analysis provides an orbital picture that is as close as possible to a classical Lewis structure for a molecule.

Another useful chemical concept is hyperconjugation, which rationalizes certain chemical phenomena in terms of filled-orbital-empty-orbital interactions. NBOs analysis can be used to quantify this phenomenon. Since the NBOs do not diagonalize the Fock operator, when the Fock matrix is formed in the NBO basis, off-diagonal elements will be non-zero. Second-order perturbation theory gives the off-diagonal elements between filled and empty NBOs, and can be recognized with the stabilization energies obtained from hyperconjugation

2.12 Topology Analysis

2.12.1Atoms in molecules (AIM)

The quantum theory of atoms in molecules (AIM) is a useful tool for the characterization of hydrogen bonding; intra-inter molecular interactions within the molecule [41]. The chemical structure of an element is identified using critical point's (CP's). The type of critical point described as:(3, -3) nuclear critical point (NCP); (3, -1) bond critical point (BCP); (3, +1) ring critical point (RCP); and (3,+3) cage critical point (CCP). The number and type of critical points that can coexist in a molecule or crystal follow a strict topological relationship which states equation (2.4) that:

$$n_{NCP} - n_{BCP} + n_{RCP} - n_{CCP} = \begin{cases} {}^{1(Isolated-molecules)} \\ {}^{0(Infinite-crystals)} \end{cases} \tag{2.4}$$

where 'n' denotes the number of the subscripted type of CP. The topology relationship of an isolated system is known as the Poincare – Hopf relationship (PH).

2.12.2 Localized orbital locator (LOL) and electron localization function (ELF)

The topologies of the localized orbital locator (LOL) and electron localization function (ELF) are investigated electron density (gradient) in an attempt to elucidate cores and the valence shell of the atoms. To define Fermi hole curvature Becke and Edgecombe [37] proposed as a local scalar function V(r) and show the excess kinetic energy of the Pauli repulsion regions (absence of LOL) of space. Extensively, Savin and Silvi [42] explain the two main types of basins in a molecule: core and valence. Core basins engulf centre nuclei present in the molecule and valence basins identifies the boundaries shared by the cores and lone pair. The localized orbital locator (LOL) shows the surface topology of interaction bond path. From electron localization function (ELF) analysis, it finds the positions of isosurface, shared and unshared in space where ELF is maximal, and to use the value of ELF in these points. By defining the electron localization (ELF) gradient in terms of η by the mapping its values on to range $0 \le \eta \le 1$: The value of ELF, $\eta(r)$ ranges from 0.0 to 1.00, where relatively high values in the interval 1.00 to 0.5 indicate regions containing bonding and antibonding localized electrons, whereas lower values (>0.5) describe domains where electrons are expected to be delocalized.

2.12.3 Reduced density gradient (RDG)

Non-covalent interactions (NCI) constitute the machinery through which distinct molecules 'recognize' themselves, determining how they will approach and eventually pack together [43-46]. They encompass a wide range of bonding types, such as hydrogen

and halogen bonds, CH... π and π ... π interactions, and several binding or anti-binding forces, like those due to dispersion, electro- statics or to Pauli's principle. Indeed, a considerable effort has been spent in the last decade to disclose the role of each of the above in the self-assembly [47] and crystallization [48] processes, whose underlying general rules are however well far away to be fully rationalized and understood. Decoding the interplay of intermolecular NCI in setting up supramolecular assemblies represents a fundamental step in making progress in structural prediction [49], to say nothing of molecular reactivity and drug-receptor docking processes. Therefore, it is not surprising that the research on this topic spans over a wide range of scientific disciplines, including molecular pharmacology, crystal structure prediction and crystal engineering, as well as over a plethora of quite diverse investigative tools. Among the later, of a particular relevance are those based on the electron density observable, $\rho(r)$, that may be obtained from ab initio calculations or from single crystal X-ray diffraction experiments. Actually, the electron density(ED) scalar field inherently bears a vast amount of information on how molecules in close contact influence each other [50, 51]. Descriptors derived from the ED are clearly potentially suited to study non covalent interactions (NCI) and, moreover, they allow for a comparison of theoretical predictions with experimental results on the same grounds, being based on a quantum observable and a measurable quantity. Johnson et al. [52] and Contreras García et al. [53] introduced a novel NCI descriptor, based on the reduced electron density gradient (RDG) that leads to an easy-to-catch pictorial visualization of various kinds of NCI directly in the real space using Multiwfn and plotted by visual molecular dynamics (VMD) program [54, 55]. Moreover, when combined with the sign of the second principal local curvature of the electron density q(r), it enables one to distinguish the

allegedly attractive or repulsive nature of the interactions and to rank their relative strength on a qualitative, visual basis.

RDG index is able to depict inherently delocalized interactions in terms of extended and flat RDG isosurfaces, in contrast to the bond path analysis that is often bound to a too localized and possibly discontinuous description. The extension to experimental EDs will hopefully represent a key step forward for the possible applications of the RDG-based NCI descriptor and for the study of the vast variety of NCI leading to the complex, fascinating crystalline structures of interest to materials science and biology. RDG leads to an easy-to-catch pictorial visualization of various kinds of non-covalent interactions directly in the real space.

2.13 Molecular docking

Molecular docking is a well established computational technique which predicts the interaction energy between two molecules. Molecular docking studies are used to determine the interaction of two molecules and to find the best orientation of ligands which would form a complex with overall minimum energy. The small molecule, known as ligand usually fits within the protein's cavity which is predicted by the search algorithm. These protein cavities become active when they come in contact with any external compounds and are thus called as active sites. Docking is frequently used to predict the binding orientation of small molecule drug candidates to their protein targets in order to predict the affinity and activity of the small molecule. Hence docking plays an important role in rational drug design. The results are analyzed by a statistical scoring function which converts interacting energy into numerical values called as the docking score; and also the interacting energy is calculated. The 3D pose of the bound ligand can be visualized using different visualization tools like Pymol [56] and

Discovery studio [57], which could help in inference of the best fit of ligand. Predicting the mode of protein- ligand interaction can assume the active site of the protein molecule and further help in protein annotation. Moreover molecular docking has major application in drug designing and discovery [58-60].

The prediction of the protein–ligand complex is usually done by searching the translational and rotational degrees of freedom of the ligand within the receptor binding site, and by searching the conformational degrees of freedom of the ligand itself. Binding conformations generated by docking programs are thus defined by both a position of the ligand on the receptor surface and a particular ligand conformer. The first docking algorithm for small molecules was developed by the Kuntz group at UCSF in 1982 [61] since then, many different docking algorithms have been developed, and structure-based drug design has become a standard tool in drug discovery. A flow chart of Computer-Aided Drug Discovery Process used in molecular docking methodology as shown in Fig. 2.3.

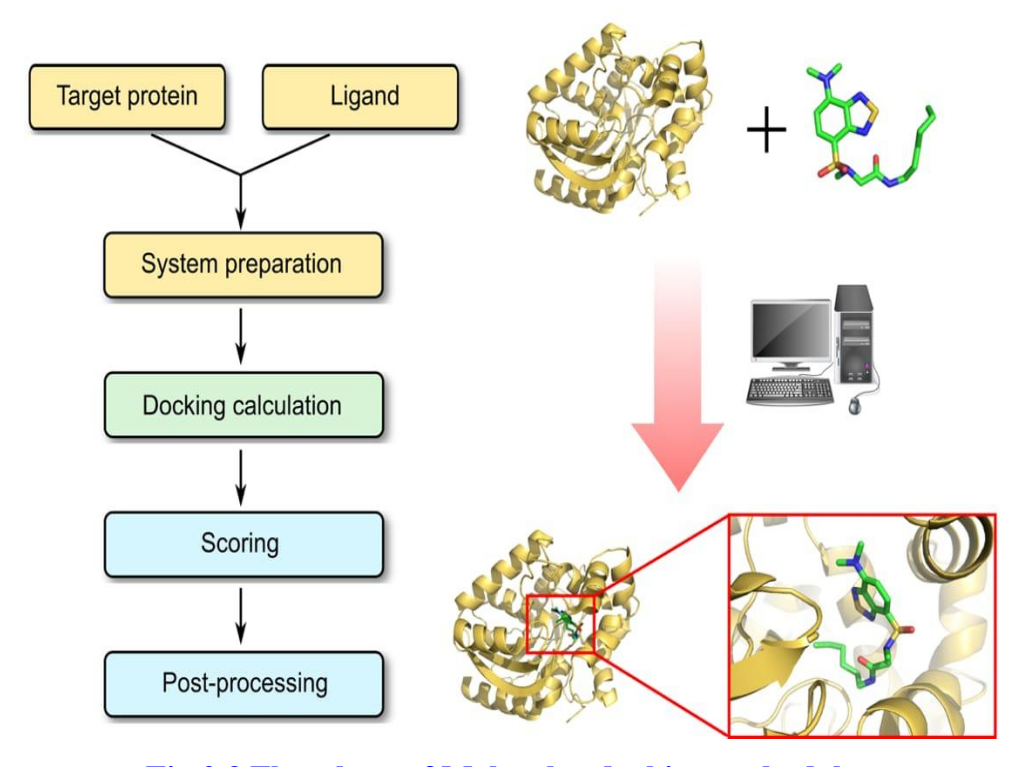


Fig.2.3 Flowchart of Molecular dockingmethodology

2.13.1 Binding site identification and mapping

Docking methods generally rely on a demarcation of the search space on the receptor surface to address the computational intensive nature of the search problem in finding the correct ligand binding conformation. The space searched spans only the active site and requires some knowledge about the position of the binding site on the receptor. Often the active site of a receptor is known from an X-ray crystallography structure, or perhaps NMR, of a protein–ligand complex. However, sometimes the active site, or additional binding sites, has to be predicted. It is often assumed that the largest cleft on a protein surface corresponds to the active site, but this is not always the case.

After drug candidates have been identified with the search algorithms that have been discussed, optimization of these leads begins. For structure-based drug design to have an impact on lead optimization, the binding mode of the lead with the receptor has to be known. Docking tools play a critical role in predicting binding modes, and the ability of a docking program to correctly identify the biologically relevant binding mode from the other possibilities is the most basic test of docking algorithms. The success rate in retrieving binding modes of known protein-ligand complexes is an important validation for docking programs [62]. The measure that is usually used to determine whether a binding mode prediction is a success is the root mean square distance (RMSD). Before ligands can be docked against a receptor, generally the binding site has to be identified first. This is done to limit the search space on the receptor surface and thus minimize the degrees of freedom that have to be searched. The active site is often known from crystal structures of ligand-bound receptors, but it can also be predicted. The large cavity on a protein surface is frequently the active site, but this is not always the case and different active site prediction and analysis methods have been developed.

The basis for the DOCK search algorithm can be found in distance geometry and consists of sets of ligand atoms that are being matched to sets of receptor spheres. The receptor spheres describe the binding site and can be viewed as a "negative image" of the active site and thus match what the ideal ligand shape would look like. The matching of ligand atoms to receptor spheres is used to search the translational and rotational degrees of freedom of a rigid ligand in the active site. The second part of a docking program consists of a scoring function, which will distinguish among the generated binding modes the best solution that closely matches the actual mode of binding. The most-favorable predicted protein—ligand complex is considered to be the biologically relevant one.

2.13.2 Types of docking

The following type of docking is used often.

Lock and key or rigid docking

In rigid docking, both the internal geometry of the receptor and ligand is kept fixed during docking.

Induced fit or flexible docking

In this model, both the ligand and side chain of the protein is kept flexible and the energy for different conformations of the ligand fitting into the protein is calculated. For induced fit docking, the main chain is also moved to incorporate the conformational changes of the protein upon ligand binding, though it is time consuming and computationally expensive, yet this method can evaluate many different possible conformations which make it more exhaustive and possibly simulate real life phenomenon and hence trustworthy.

2.13.3 Brief introduction of the software and websites used for docking study Auto Dock Vina

Auto Dock Vina and Autodock Tools are free of charge techniques that have been extensively cited in the literature as essential tools in structure-based drug design. Moreover, these methods are fast enough to permit virtual screening of ligand libraries containing tens of thousands of compounds. However, using Auto dock requires some knowledge in programming which creates a limitation for biologists and makes them prone for commercial applications.

Auto Dock Vina is a comparatively new open-source program for drug discovery, molecular docking and virtual screening, offering multi-core capability, high performance, enhanced accuracy and ease of use. Auto dock vina has been designed and implemented by Oleg Trott (2010) [63] in the Molecular Graphics Lab at the Scripps Research Institute. Auto Dock Vina automatically calculates the grid maps and clusters the results in a way transparent to the user. Auto Dock Vina significantly improves the average accuracy of the binding mode predictions compared to Autodock4. Additionally, Auto Dock Vina has been tested against a virtual screening benchmark called the Directory of Useful Decoys by the Watowich group, and was found to be "a strong competitor against the other programs and at the top of the pack in many cases". It should be noted that all six of the other docking programs, to which it was compared, are distributed commercially.

For its input and output, Vina uses the PDBQT (Protein Data Bank, Partial Charge (Q), & Atom Type (T)) molecular structure file format used by Autodock. PDBQT files can be generated (interactively or in batch mode) and viewed using MGL

[Molecular graphics Laboratory] Tools. Other files, such as the Autodock and AutoGrid parameter files (GPF, DPF) and grid map files are not needed.

2.13.4 PyMOL

PyMOL [56] is a computer software, which is a molecular visualization system created by Warren Lyford De Lano. It is user-sponsored, open-source software, with more than 600 settings and 20 representations to provide users with precise and powerful control. Spheres provide a CPK-like view, surface and mesh provide more volumetric views, lines and sticks put the emphasis on bond connectivity and ribbon and cartoon are popular representations for identifying secondary structure and topology. PyMOL can produce high-quality 3D images of small molecules and biological macromolecules, such as proteins. Pymol can interpret over 30 different file formats from PDB files to SDF-files to volumetric electron density maps.

2.13.5 RCSB-PDB

Research Collaboratory for Structural Bioinformatics (RCSB)-PDB [64] is an online portal for teachers, students, and the general public to promote exploration in the world of proteins and nucleic acids. Learning about the diverse shapes and functions of these biological macromolecules helps to understand all aspects of biomedicine and agriculture, from protein synthesis to health and disease to biological energy. Researchers around the world are studying these molecules at the atomic level. These 3D structures are freely available at the Protein Data Bank (PDB), the central storehouse of biomolecular structures. This website builds introductory materials to help beginners get started in the subject ("101", as in an entry level course) as well as resources for extended learning. PDB is developed by the RCSB-PDB, a global resource for the advancement of research and education in biology and medicine. Along with our

Worldwide PDB collaborators, RCSBPDB curates, annotates, and makes publicly available the PDB data deposited by scientists around the globe.

The RCSB PDB then provides a window to these data through a rich online resource with powerful searching, reporting, and visualization tools for researchers. This information is then streamlined for students and teachers at PDB. RCSB PDB is funded by the National Science Foundation, the National Institutes of Health, and the Department of Energy. The Protein Data Bank (PDB) archive is the single worldwide repository of information about the 3D structures of large biological molecules, including proteins and nucleic acids. These are the molecules of life that are found in all organisms, including bacteria, yeast, plants, flies, other animals, and humans. Understanding the shape of a molecule deduce a structure's role in human health and disease, and in drug development.

The structures in the archive range from tiny proteins and bits of DNA to complex molecular machines like the ribosome. The PDB archive is available at no cost to users. The PDB archive is updated weekly. PDB was formed to maintain macromolecular structural data that is free and publicly available to the global community. It consists of organizations that act as deposition, data processing and distribution centers for PDB data. In addition, the RCSB PDB supports a website where visitors can perform simple and complex queries on the data, analyze, and visualize the results.

Instrumentation

Abstract

The experimental techniques of infrared and Raman spectroscopy and sample handling techniques are briefly dealt with. The advantages of Fourier Transform-infrared (FT-IR) and FT-Raman technique are also explained

CHAPTER - 3

INSTRUMENTATION

3.1 Introduction

Infrared and Raman spectroscopy is a versatile experimental technique and it is is relatively easy to obtain spectra from samples in solution or in the liquid, solid or gaseous states. In this chapter, how samples can be introduced into the instrument, the equipment required to obtain spectra and the pre-treatment of the samples are examined.

3.2 Instrumentation

3.2.1 Basic components of FT-IR

Infrared (IR) spectroscopy is one of the most common spectroscopic techniques used by organic and inorganic chemists. Simply, it is the absorption measurement of different IR frequencies by a sample positioned in the path of an IR beam. The main goal of IR spectroscopic analysis is to determine the chemical functional groups in the sample. There are five components for FT-IR instruments: a radiation source, a sample, an interferometer, a detector (amplifiers and recorders), computer. Radiation beam from a broadband source is collimated and directed into the interferometer. The beam passes through the sample is focuses on the detector. The recorded detector signal is amplified using analog-to-digital converter and transferred to the computer for Fourier-transformation [65]. The basic components of a Fourier-transform infrared (FT-IR) spectrometer are shown in schematic Fig.3.1.

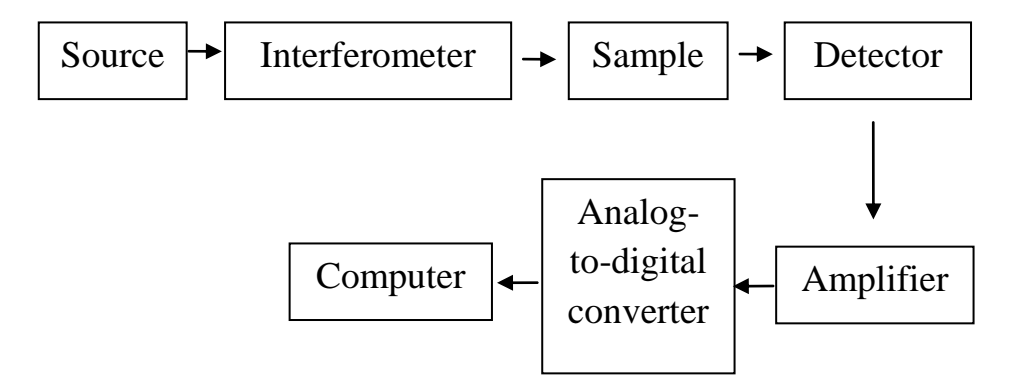


Fig. 3.1 Basic components of FT-IR

3.2.2 Source

Infrared radiation is produced by electrically heating a source (glowing black-body source are shown in Fig.3.2, usually a Nernst filament or a Globar to 1000–1800°C. The Nernst filament is fabricated from a binder and oxides of thorium, cerium, zirconium and yttrium. The Globar is a small rod of silicon carbide usually 5 cm in length and 0.5 cm in diameter. The maximum radiation for the Globar occurs in the 5500–5000 cm⁻¹ region. Nichromewire, carbon arc, rhodium wire and tungsten filament lamp are also used as light source. In a commercial infrared spectrometer either a nichrome wire or aplatinum filament contained in a ceramic tube is commonly used as infrared source for the range 4000–0 cm⁻¹ [66].

3.2.3 Interferometer

The most common interferometer used in FT-IR spectrometry is a Michelson interferometer [67-69], which consists of two perpendicularly plane mirrors, one of which can travel in a direction perpendicular to the plane. The opticalarrangement of FT-IR spectrophotometer is shown in Fig. 3.2. A semi-reflecting film, the beam splitter, bisects the planes of these two mirrors. The beam splitter material has to be chosen according to the region to be examined. (Materials such as germanium or iron oxide are coated onto an 'infrared transparent' substrate such as potassium bromide or cesium

iodide to producebeam splitters for the mid- or near-infrared regions. Thin organic films, such aspoly (ethylene terephthalate), are used in the far-infrared region.)

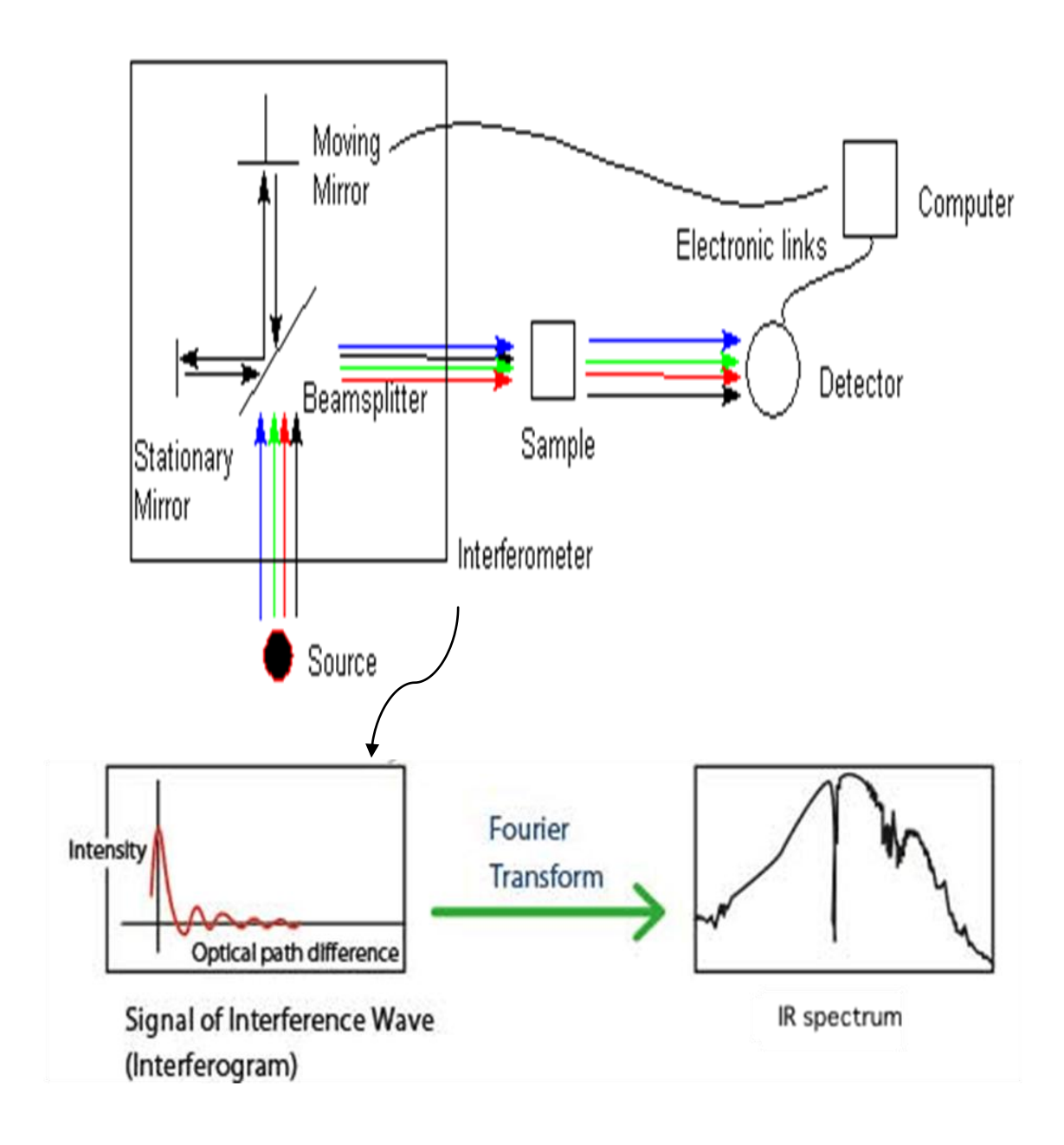


Fig. 3.2 Optical arrangement of a FT-IR spectrometer

3.2.4 Sample handling techniques

Sample handling is considered as an important technique in infrared spectroscopy. The spectra of solid samples can be obtained in awide variety of ways. If the sample is soluble, it may be dissolved and handled as a liquid. Solid samples for

which no solvent is suitable can be prepared for analysis by incorporating them into a pressed pelletof alkali halide, usually potassium bromide. Sample is mixed with a weighed amount of powdered potassium bromide and the mixture is admitted to a pressureof several tones in a die, to produce a highly transparent plate or disc which can beinserted into the spectrophotometer. The use of KBr eliminates the problems of additional bands due to mullingagent. KBr does not absorb infrared light in the region 2.5–15 µm and a complete spectrum of the sample is obtained. Solid samples have also been examined in the form of a thin layer deposited by sublimation or solvent evaporation on the surface of a salt plate. Another method, called mulling has also been developed, in which the powdered sample is mixed to form a paste with little heavy paraffin oil. The mull is sandwiched between salt plates for measurement. Mulls are formed by grinding 2 to 5 mg of finely powered sample in the presence of one or two drops of a heavy hydrocarbon oil called Nujol [70].

3.2.5 Detector

Detectors used in infrared spectrophotometers usually convert the thermal radiant energy into electrical energy, which can subsequently be plotted on a chart recorder.

Two Types of the detectors are commonly used:

- **Thermal Detectors**, in which the infrared radiation produces a heating that alters some physical property of the detector.
- **Photon detectors**, which use the quantum effects of the infrared radiation to change the electrical properties of a semiconductor [71].

3.2.6 Amplifiers and recorders

The radiant energy received by the detector is converted into measurable electrical signal and is amplified by the amplifiers. The amplified signal is registered by a recorder or a plotter. The recorder is driven with a speed which is synchronized with that of a monochromator, so that, the pen moving across the chart, records the transmittance of the sample as a function of the wavenumber.

3.2.7 Computers

The computer forms a crucial component of modern infrared instruments and performs a number of functions. The computer controls the instrument, for example, it sets scan speeds and scanning limits, and starts and stops scanning. It reads spectra into the computer memory from the instrument as the spectrum is scanned; this means that the spectrum is digitized. Spectra may be manipulated using the computer, for example, by adding and subtracting spectra or expanding areas of the spectrum of interest. The computer is also used to scan the spectra continuously and average or add the result in the computer memory.

3.2.8 Spectra

Early infrared instruments recorded percentage transmittance over a linear wavelength range. It is now unusual to use wavelength for routine samples and the wavenumbers scale is commonly used. The output from the instrument is referred to as a spectrum. Most commercial instruments present a spectrum with the wavenumbers decreasing from left to right. Most commercial instruments present a spectrum with the wavenumbers decreasing from left to right. The infrared spectrum can be divided into three main regions: the far-infrared (<400 cm⁻¹), the mid-infrared (4000–400 cm⁻¹) and the near-infrared (13000–4000 cm⁻¹) [72-74].

3.3 Raman spectroscopy

Raman spectroscopy is a popular technique for the analysis of molecular structure and is considered complementary to infrared spectroscopy. The spectrometer which provides maximum Raman collection efficiency and which uses light most efficiency to convert it into a spectrum is the Fourier transform (FT) spectrometer. A major advantage of FT-Raman over conventional dispersive Raman spectroscopy is that the low excitation energy (Nd:YAG laser of 1064 nm) renders spectra that are generally from fluorescence interference [75]. The spectrometer through-put is high. Both the FT-IR and FT-Raman enjoys wavelength precision so that spectra may be co-added, resulting in a rapid improvement in signal-to-noise (S/N) performance. Since the intensity of Raman lines is proportional to the fourth power of the excitation frequency there is a reduction in sensitivity on using Nd:YAG laser. However, multiplex gain of Fourier spectroscopy increases the sensitivity. The simultaneous detection of all frequencies leads to lower recording time of the experimental data. Once the optical path of the FT spectrometer has been properly aligned, the same instrument can be operated either as an infrared spectrometer or as a Raman spectrometer by simply interchanging sources, beam splitters and detectors. The optical arrangement of Raman spectrometer is shown in Fig. 3.3

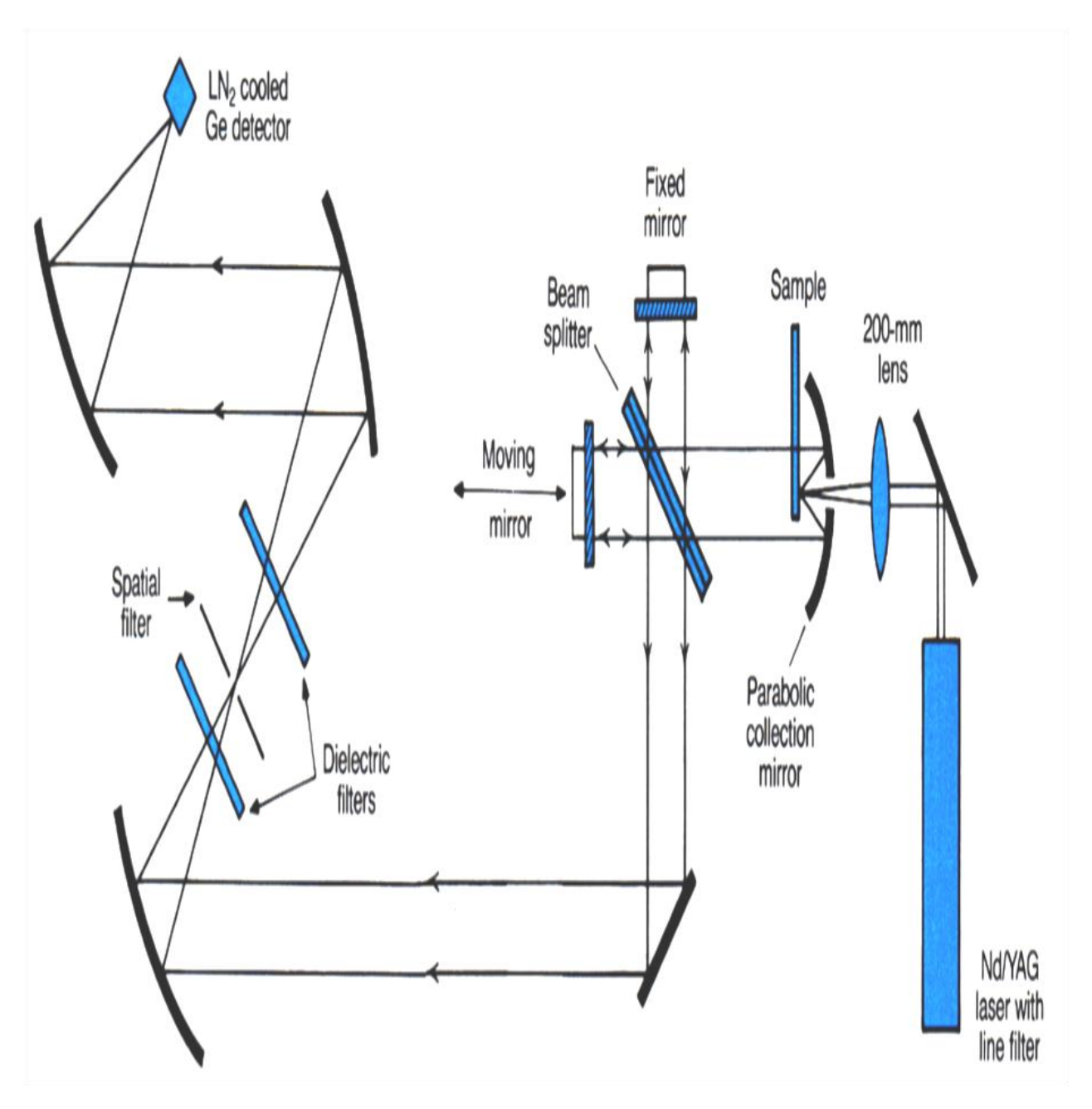


Fig. 3.3 Optical diagram of Fourier Transform Raman Spectrophotometer

3.3.1 Source

The source used in FT-Raman spectrometer is an air cooled, diode pumped Nd:YAG laser with a maximum output power of 200 mW operating at a wavelength of 1064 nm. The laser is attached to the rear side of the FRA 106 which is driven by its own source of power (110 V or 220 V Ac). The laser radiation travels through optics

base plate to the front mounted sample compartment and can be switched on and off by computer software commands when running the application program.

3.3.2 Monochromator

A commercial Raman spectrometer is equipped with a double or a triple monochromator with a view to eliminating even the strong light radiation. In a double monochromator, one monochromator is coupled with another monochromator in sequence and this arrangement causes the escape of both the stray and the Raman radiations through the exit slit of the first monochromator, irrespective of the nominal frequency, set for that monochromator. This radiation, escaping through the exit slit of the first monochromator, is allowed to enter the second monochromator of the double monochromator where the radiation is redispersed, as a result of which, the unwanted radiation is completely eliminated. The procedure involves the setting up of a slit at some narrow width so that operation of the laser causes the shine of the monochromator. Then the transmitted radiation is recorded first at the laser frequency and then at the frequency of the nominal monochromator. [76-79]

The Raman spectrometer (BRUKER RFS 27V) used for recording the spectra in the present investigation is equipped with a triple monochromator and this arrangement eliminates the unwanted radiation completely and more effectively than the one equipped with a double monochromator. When light enters the monochromator, the grating of the spectrometer disperses it and then allows it to pass through one or more narrow slits. Hence the light entering the detector always has a narrow band width and hence it is considered to be monochromatic. However, a spectrograph uses wider slits and hence causes the display of a broad band of light on the detector.

3.3.3 Detectors

Photomultipliers are employed as detectors in BRUKER RFS 27V Raman spectrometer. The light from the monochromator is collected and focussed on the

cathode surface of the photomultiplier tube, where it is converted into an electric signal. The electrical signal is further amplified by the preamplifier. The efficiency of detection of the weak signal is enhanced by two factors, viz. high efficiency and low thermionic dark current. The term quantum efficiency is defined as the ratio of the number of signal pulses appearing at the anode per second to the number of photons reaching the cathode per second. This ratio is the function of wavelength. Various types of photo surfaces are used as a detector depending on the wavelength of the laser used. In the absence of light, few thermally excited electrons should leave the cathode of photomultiplier tube. Photo cathodes which are capable of producing five dark pulses per second at room temperature are available commercially. But as the photo cathodes are cooled at -30°C, no dark pulses are produced. Hence at room temperature, the output of the photomultiplier tube contains this dark current. This must be taken into account when the output of the photomultiplier tube is considered. The output of photomultiplier tube is a measure of number of pulses of electrons.

3.3.4 Data acquisition and control

The Raman spectrometer, BRUKER RFS 27V used in the present investigation is interfaced with computer for data acquisition and control. The spectrometer position is incremented by a pre-set step size between initial and final wavenumber positions. Data acquired for the orthogonal orientation can be chosen for the entire run. After the completion of the run, Raman spectra are displayed on the monitor screen. The library functions in the computer are useful in several aspects, such as smoothening of the peaks, expansion of the selected peaks, calculation and comparison of the peak intensities. A plotter, interfaced with the Raman spectrometer is used to take the printout, displayed on the screen, after the completion of the run.

3.3.5 Sample handling techniques in Raman spectroscopy

Sample handling for Raman spectroscopic measurements is simpler than for IR spectroscopy because, glass can be used for windows, lenses, and other optical components instead of the more fragile and atmospherically less stable crystalline halides. In addition, the laser source is easily focused on a small sample area and the emitted radiation efficiently focused on a slit. As a result, relatively small samples can be studied. For the solid sample KBr or solvent is needed. A few milligrams of the solid samples are required. Solid can be packed into a capillary tube as powder. The crystal can be mounted in a goniometer on a glass or silica fiber. The spectra can be measured for different orientations of the crystal. For single crystals, the Raman spectrum varies depending on the direction of the crystal axis, when polarized light is used as incident radiation. Raman spectra of absorbed species can be recorded. Raman spectra can also be recorded at different temperatures and pressures.

3.4 Advantages of FT-IR and FT-Raman spectrometers

- ❖ As the absorption at all wavelengths is recorded in spectrometer gives a spectrum with a better signal-to-noise (S/N) ratio at the same time. These are much faster and saves a lot of experiment time. This provides for taking multiple scans for low concentration samples and then averaging them.
- **!** It gives better frequency resolution and reproducibility.
- ❖ Due to its simple mechanical design with only one moving part (the moving mirror in interferometer), there is less wearing out of the components and hence better reliability of the spectrometer.

Quantum chemical calculation, performance of selective antimicrobial activity using molecular docking analysis, RDG and experimental (FT-IR, FT-Raman) investigation of 4-[{2-[3-(4-chloropheny)-5-(4-propan-2-yl) phenyl)-4, 5-dihydro- 1H-pyrazol-1-yl]-4-oxo-1, 3-thiazol-5(4H)-ylidene}methyl] benzonitrile

Abstract

The research received a great deal of worldwide attention due to the nature of interpretation before the experimental process. Based on the systematic process the structure of thiazole-pyrazole compound 4-[{2-[3-(4-chlorophenyl)-5- (4-chlorophenyl)-5-(4-propan-2-yl) phenyl)-4, 5-dihydro- 1H- pyrazol-1-yl]-4-oxo-1, 3-thiazol-5(4H)-ylidene} methyl] benzonitrile [CPTBN] were investigated. In the first level, the spectral statistics on experimental FT-IR and FT-Raman was reported. At the next level, geometrical parameters were theoretically acquired from density functional theory (DFT) using B3LPY/6-31G and 6-311G basis sets. The computed wavenumber was collected and compared with the experimental data. The vibrational modes were interpreted in terms of potential energy distribution (PED) results. The FMO, MEP, and NBO analysis further validated the electrophilic and nucleophilic interaction in the molecular systems. Two gram-positive bacteria: staphylococcus aureus, Bacillus subtilis and two gram- negative bacteria: Esherichia coli, pseudomonas aeruginosa were performed for antibacterial activity. Two fungal strains: Candida albicans and Aspergillus Niger were carried out against a ligand using anti-fungal activity. The molecular docking analysis explores the antimicrobial and selective potential inhibitory nature of the binding molecule. Besides, RDG and ELF analysis were also performed to show the nature of interactions between the molecule.

CHAPTER - 4

Quantum chemical calculation, performance of selective antimicrobial activity using molecular docking analysis, RDG and experimental (FT-IR, FT-Raman) investigation of 4-[{2-[3-(4-chloropheny)-5-(4-propan-2-yl) phenyl)-4, 5-dihydro- 1H-pyrazol-1-yl]-4-oxo-1, 3-thiazol-5(4H)-ylidene}methyl] benzonitrile

4.1 Introduction

Recently, the investigation of vibrations of substituent azoles compounds was an incredible arrangement of enthusiasm among the spectroscopists because of their physical and chemical properties. Thiazole is one of the most intensively studied classes of aromatic amalgamation and one of the most intensively studied classes of aromatic amalgamation that was initially outlined by Hantzsch and Weber in 1887 [80]. It belongs to the family of azoles, the heterocyclic five-membered compounds containing sulfur and nitrogen atoms at 1,3 positions in their fragrant ring structure [81]. Thiazole core occupies a very important position among the heterocyclic compounds which are naturally bioactive. Attached to various active elements like pyrazole, phenyl, nitrile-contains compounds were synthesized in a laboratory environment and were eventually introduced to be used to treat various diseases and varieties of industrial purposes such as fungicides, dye, and paint production [82, 83]. Consistently, the active elements nitrile is a common choice as both a chemical and physical barrier to these hazards, especially nitrile gloves were useful to a huge number of human services and industry labourers who are exposed to chemical and organic risk [84]. Benzonitrile often plays a key role in the inhibition of hydrogen absorption [85]. The present work involves the study of comprehensive molecular geometry and vibrational modes of CPTBN using quantum chemical calculations; it has a molecular formula C₂₉H₂₃C1N₄OS. The global reactivity descriptors like highest occupied molecular orbital (HOMO), lowest unoccupied molecular orbital (LUMO), and molecular electrostatic potential (MEP) analysis were interpreted with the theoretical value. The energy gap values (ΔE) have been calculated using B3LYP/6-31G and 6-311G basis sets and reported as a result of the molecular transitions. The investigation of natural bond orbital (NBO) provides information on the chemical features such as intra and intermolecular charge transfer, second-order perturbation characteristic relationships between the Lewis (donor) and non-Lewis (acceptor) [86]. The title molecule's reduced density gradient (RDG) and electron localization function (ELF) were investigated using Multiwfn software. The disc diffusion method was used to successfully evaluate antimicrobial activity of the compound at 25, 50, 75, and 100 µg/ml concentration levels with established bacterial and fungus strains. To explore the potential biological activity of the thiazole (CPTBN) compound, few studies included in the molecular docking analysis and report on the drug- like behaviors of the title compound. The anti-microbial, monoclonal antibodies, Nitric oxide synthase inhibitor, consistent with the results of docking pose provide key insight of selective antimicrobial and medical potential inhibitors. The above findings are opening up new avenues of medicinal chemistry and are important for clinical manifestation.

4.2 Experimental details

The structure of CPTBN along with the synthesis procedure was screened by Salian et al. [87]. In the present work, the following techniques and biological studies were carried out.

- Fourier transform infrared spectrum was recorded between 4000-0 cm⁻¹ using the Perkin Elmer spectrometer, which was calibrated using an MCT Mid-IR range detector with KBr (potassium bromide) pellets technique.
- FT-Raman spectrum was obtained within the interval of 3500-0 cm⁻¹ using a Bruker RFS27 the 1064nm line of a Nd: YAG laser device for excitation controlled at 200

mW power. At room temperature, the spectrum was recorded at a scanning speed of 10 cm^{-1} and a spectral resolution of 1.0 cm^{-1} .

Using the disc diffusion method, the title compound with four concentrations of 25, 50, 75 and 100 μg/ml in distilled DMSO was prepared and tested against antimicrobial strains were maintained on agar medium at 4°C. Antimicrobial cultures such as *Staphylococcus aureus*, *Bacillus subtilis*, *Esherichia coli*, *Pseudomonas aeruginosa*, *Candida albicans and Aspergillus Niger* were tested.

4.3 Computational details

In the present work, the optimized geometrical parameters namely bond lengths, bond angles of the CPTBN were first performed by B3LYP functional with 6-31G and 6-311G basis sets, using the Gaussian 09 program [17]. The correlation function is used to predict the molecular structure (Vibrational spectra) of the CPTBN. The potential energy distribution (PEDs) is done with the help of (VEDA) program [88]. GAUSSVIEW program [31,89] provided a visual presentation of vibrational modes. Screening the calculations exposed that, the density functional theory (DFT) computations with the promising vibrational properties, molecular geometry, and orbital energy of CPTBN. Besides natural bond orbital (NBO) calculations were carried out using the NBO program implemented in Gaussian 09 [90]. Multiwfn software provides a route for a consistent description of interactions between the atoms in terms of the topological properties of the electron density $\rho(r)$. Electron Localization Function (ELF) map and Reduced Density Gradient (RDG) were calculated using the Multiwfn program [20]. Molecular docking studies were performed with the help of an Auto dock [57] software, discovery Studio Visualizer 4.1 [57] and Pymol software [56, 92].

4.4 Results and discussion

4.4.1 Molecular geometry

The density functional theory is one of the most reliable computational approaches for the theoretical investigation of the structure of the molecule. The optimized molecular form of CPTBN computed by B3LYP/6-31G, B3LYP/6-311G, and visualized through the Gauss View program shown in Fig. 4.1. The optimized bond lengths and bond angle of the title compound were tabulated in Tables 4.1 and 4.2, respectively. The optimized structure is found to be with C1 point group symmetry having its ground state energy of -2271.46 a.u with a dipole moment of 8.9529 Debye. Elaboration of the collected data is as follows:

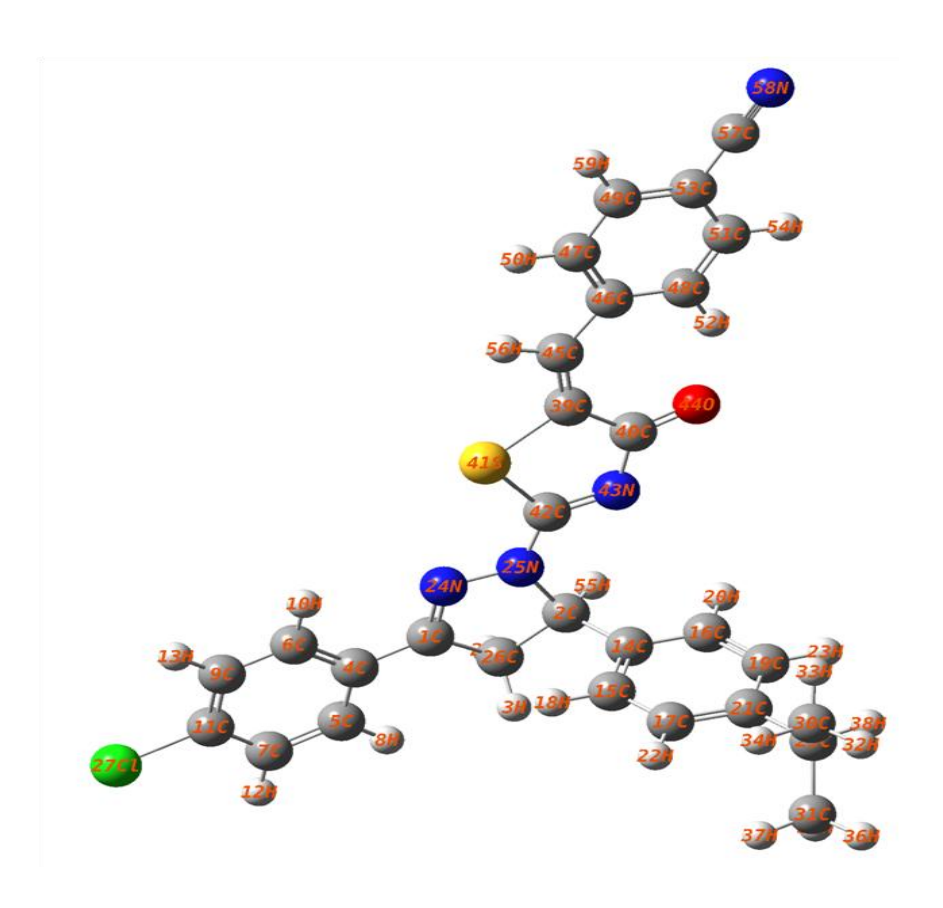


Fig. 4. 1 Optimized structure of CPTBN using B3LYP/6-311G basis set

The optimized geometrical structure of the title molecule benzonitrile substituent in the thiazole ring system, chain with pyrazol bounds by two phenyl rings (one is chlorophenyl - PhI and the other is 4-(Propan-2-yl) phenyl- PhII. Normally, the C-C bond lengths of aromatic rings formed by the phenyl ring are greater than range $1.3900\ \text{Å}$, although the computed value falls in the range C_4 - $C_6 = 1.4102/1.4120$ Å, C_9 - $C_{11} =$ 1.3933/1.3964 Å, $C_5-C_7=1.3959/1.3977$ Å, for PhI and $C_{14}-C_{15}=1.4038/1.405$ Å, $C_{16}-C_{19}=1.4038/1.405$ Å = 1.3964/1.3982 Å, C_{17} - C_{21} = 1.4056/1.4076 Å for PhII. The title compund is somewhat regular and the spread of C-C bond distance is 1.3900 - 1.5500 Å in (phenyl ring I) PhI and 1.3900- 1.4500Å in (phenyl ring II) PhII, which is similar to the report by Parveen et al. [93]. The computed bond lengths of the C=C double bond values are C_4 - C_5 = 1.4067/1.4083 Å, C_6 - $C_9 = 1.3907/1.3931$ Å, C_7 - $C_{11} = 1.3886/1.3922$ Å for PhI and C_{14} - C_{16} = $1.3981/1.4009 \text{ Å, } C_{15}\text{-}C_{17} = 1.394/1.3957 \text{ Å, } C_{19}\text{-} \ C_{21}\text{=} \ 1.4011/1.4036 \text{ Å for PhII. This}$ observation reveals that the C-C atoms in both rings are between the conventional C-C single and C=C double bond lengths, indicating that the electron density is conjugated on all rings. The outer shell carbon-hydrogen bond length values are experimentally falling in the range of 0.90 Å to 1.09 Å, whereas the calculated C-H (ring) and C-H (methyl) values are 1.0800 Å and 1.0900 Å, respectively. The C-H length in both phenyl rings is found almost equal to around 1.08 Å, is very close to the experimental value 1.09 Å, which indicates that C-H bond lengths remain unaffected by the substitution in rings. Generally, the thiazole ring has a difference in bond length is due to the presence of a sulphur and nitrogen atom. The theoretical value of the C_{39} - S_{41} bond length is 1.8653/1.8592 Å and the experimental value is found to be 1.86 Å [82]. The C_{40} = O_{44} carbonyl moiety present in thiazole has a double bond character, as evidenced by the compound's estimated bond length (DFT) of 1.2450/1.2472 Å. The shortening of these C-N bonds reveals the effect of resonance in this part of the molecule. It attempts to draw the electron density of the neighboring atoms which as a result move closer together to share the electrons more easily. The literature value of C-N, C=N, C=N bond length (XRD) is 1.300 Å, 1.31 Å and 1.160 Å [93]. In the current studies C_1 - N_{24} = 1.3046/1.3061 Å, C_2 - N_{25} = 1.5079/1.5097 Å present in pyrazole ring, C_{42} - N_{43} = 1.3051/1.3059Å present in thiazole ring, and C_{57} - N_{58} = 1.1682/1.1748 Å present in benzonitrile ring indicating that π - electron in the molecules are delocalized in the C=C of the molecule which is similar in reported by Mustafa et al [94]. The chlorine is extremely electronegative, it strives to get more electron density, and the computed value is 1.825 Å, that is found near the phenyl ring PhI. The experimental values are taken from a similar C-Cl bond length observed in 1.8200 Å by Vanasundari et al. [95]. The magnitude of the length N-N bond is described in 1.38 Å assigned by Priyanka Singh et al. [96]. In CPTBN it to be 1.3963/1.3946Å for the CPTBN molecule. The angle formed between two adjacent bonds shows the internal bond angles N_{25} - C_{42} - N_{43} , C_1 - N_{24} - N_{25} , C_{39} - C_{40} - O_{44} and N_{43} - C_{40} - O_{44} are found around the range to be 123°, 108°, 124° and 122° in the CPTBN respectively. The shortest bond angle formed between thiazol is C_{39} - S_{41} - C_{42} in 86°.

4.4.2 Vibrational assignments

The main aim of this vibrational assignment is to provide a clear interpretation of both experimental and theoretical results. The experimental and theoretical FT-IR and FT-Raman spectra are shown in Figs 4.2 and 4.3, respectively

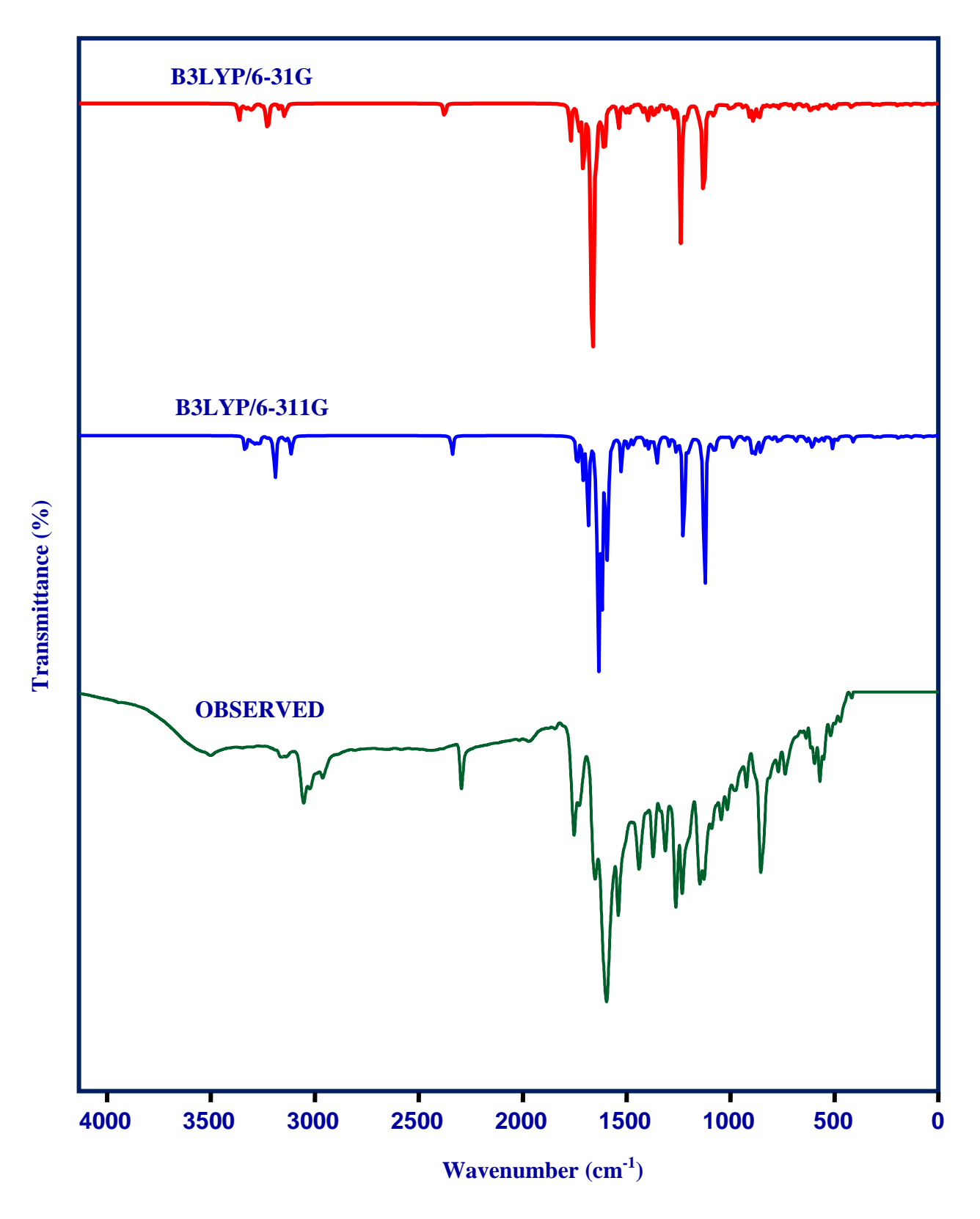


Fig. 4.2 Observed FT-IR and simulated spectra of CPTBN

Fig.4.3 Observed FT-Raman and simulated spectra of CPTBN

The theoretical calculations were performed using the B3LYP method with 6-31G and 6-311G basis sets were reported in Table 4.3. Generally, the vibrational modes of a compound with N atoms have (3N-5) vibrational modes for a linear compound and (3N - 6) modes for a nonlinear compound. The CPTBN is a nonlinear molecule has 59 atoms and 171 fundamental vibrational modes. Based on the optimized structure, the detailed spectral information is interpreted as follows:

C-H vibrations

In the present study, there are three different benzene rings attached to the combination of thiazole with pyrazol. The occurrence of benzene C-H stretching vibration extends often above 3000 cm⁻¹ for aromatic composition and less than 3000 cm⁻¹ for nonaromatic composition. In the FT-IR, FT-Raman spectra, aromatic compounds predominantly have a C-H vibration of 3000-3100 cm⁻¹. The essence and location of the replacement are affected in this region by the band. Because of their high polarization, these C-H stretching mode typically appear with Raman strength. These bands observed at 3074 cm⁻¹ and 3053 cm⁻¹ in FT-Raman by Sathish et al. [97]. In the case of the title compound, it exhibits multiple weak band shoulders on the stronger C-H stretching vibrations at 3067, 3013 cm⁻¹ in FT-IR and 2957, 2868 cm⁻¹ in FT-Raman. Normally, the C-H in-plane vibrational bending mode occurs in the region 1530-1000 cm⁻¹. In the present case, C-H in-plane vibrational bending mode observed at 1424 cm⁻¹ (w), 1396 cm⁻¹ (ms), and 1114 cm⁻¹ (ms) in FT-IR spectrum and 1285 cm⁻¹ (ms), 1251 cm⁻¹ (s), 1173 cm⁻¹ (ms) in FT-Raman spectrum, the computed wavenumbers for this mode were coincident with 1429, 1394, 1290, 1253, 1120 cm⁻¹ for B3LYP/6-31G and 1425, 1395, 1286, 1250, 1116 cm⁻¹ for B3LYP/6-311G. The out-of-plane C-H bending mode of the phenyl ring are observed at 804 cm⁻¹ (IR), 928, 832, 806 cm⁻¹ (FT-Raman) and computed values are in the range 932-810 cm⁻¹ (DFT) by Begume et al. [98]. The correlated vibrations observed at 896 (w), 829(ms), 811 cm⁻¹ (w) in FT-IR and 945 cm⁻¹ (m) in FT-Raman were coincident with 933, 900, 833, 814 cm⁻¹ for B3LYP/6-311G.

Methyl group vibrations

The CH₃ group frequencies are generally associated with nine fundamental modes of vibration. These vibrations are CH₃ symmetrical stretch, CH₃ asymmetrical stretching, CH₃ in-plane bending (δ), CH₃ out-of-plane bending (γ), CH₃ symmetric deformations, CH₃ asymmetrical deformations, CH₃ in-plane rocking (δ rock), CH₃ out-of-plane rocking (γ rock), and twisting bending (Γ CH₃) [99]. From the structure of the title molecule posses two CH₃ (5-(4- Propan-2-yl) phenyl) group substitutions in the pyrazole ring chain.

The CH₃ asymmetric stretching vibration is recorded in the FT-IR at 2929(w) cm⁻¹, and FT-Raman at 2947, 2933 cm⁻¹, are coincides with computed values at 2952, 2936, 2934, 2928, 2903, 2881 cm⁻¹ in B3LYP/6-31G and 2948, 2932, 2924, 2930, 2900, 2879 cm⁻¹ in B3LYP/6-311G. The in-plane (δ_{ipb}) bending modes have been calculated at 1390 and 1385 cm⁻¹ by 6-31G, and 1389, 1382, 998 cm⁻¹ by 6-311G. The out-of-plane bending vibrations of title compound occur in medium peak (γ_{opb}) 1409 cm⁻¹ in FT-Raman is assigned and deformation is predicted at (γ_{opb}) 1420, 1415 cm⁻¹ for B3LYP/6-31G and 1418, 1410 cm⁻¹ for B3LYP/6-311G. The rocking mode of the CH₃ group is computed at 1103, 1025 cm⁻¹ for B3LYP/6-31G and 1100,1021 cm⁻¹ for B3LYP/6-311G well in agreement with a recorded value of 1099 cm⁻¹ in the FT-Raman spectrum. Moreover, the twisting vibration of Γ CH₃ falls below 500 cm⁻¹. In the present study, the twisting vibration for CH₃ is assigned to weak band at 181 (w) in FT- Raman. These observation are in very good agreement with literature values.

CH₂ vibrations

For the assignment of CH_2 group frequencies basically there are six fundamental modes namely, asymmetric stretching mode- v_{ass} (CH_2), symmetric stretching mode- v_{ss}

(CH₂), a rocking mode- rock (CH₂), Wagging mode ω (CH₂), twisting mode - Γ (CH₂) and a scissoring mode - ρ (CH₂). According to the literature, CH₂ symmetric and asymmetric vibration falls in the range around 3000-2800 cm⁻¹ [100]. The CH₂ asymmetric stretching modes are computed at 2955, 2915 cm⁻¹ for B3LYP/6-31G and 2953, 2912 cm⁻¹ for B2LYP/6-311G, but no peaks can be observed in this region on the recorded spectrum. The twisting mode of the CH₂ group is observed at 1195 cm⁻¹ in FT-IR and 1196 cm⁻¹ in FT- Raman. The CH₂ scissoring vibration of the title compound was observed at 1375 cm⁻¹ (w) in FT-Raman.

Nitrile vibrations

Nitrogen compounds with triple bonds, such as nitrile and cyanates, have a specific spectrum, typically with a single, usually intense absorption peak at 2280- 2200 cm⁻¹ [85]. The saturated cyclic nitrile is detected by the presence of a band near 2250 cm⁻¹ while their aromatic counterparts absorb at lower frequencies near 2230 cm⁻¹. Generally, the IR and Raman spectra exhibits C≡N stretching vibrations at 2235 cm⁻¹ and 2290 cm⁻¹ [101,102]. In the present investigation, the band observed at 2223 (m) cm⁻¹ in FT-IR and 2222 (m) cm⁻¹ in FT-Raman are attributed to C≡N stretching vibrations.

C-C vibrations

In general, C-C stretching vibration of heterocyclic aromatic compounds occurs in the region 1650-1200 cm⁻¹ [102-104]. Fatima et al. [101] reported that carbon-carbon stretching vibration occur in the region 1625-1400 cm⁻¹. The C-C stretching vibrations at 1428 cm⁻¹, 1235 cm⁻¹, 1002 cm⁻¹ in the IR spectra and 1579 cm⁻¹, 1531cm⁻¹, 1439 cm⁻¹, 1380 cm⁻¹, 1123 cm⁻¹ in the Raman spectra are assigned by Kuruvilla et al. [105]. In the present study, above similar wavenumbersare observed at 1493(ms), 1600(vs), 1225(vs) cm⁻¹ in FT-IR spectrum and 1441(w), 1596(vs), 1561(vs), 1551(m) 1225(vs) cm⁻¹ in FT- Raman spectrum are assigned as a C-C stretching vibrations. The corresponding

values theoretically computed at 1600, 1564, 1230 cm⁻¹ in B3LYP/6-31G and 1598, 1562, 1226 cm⁻¹ B3LYP/6-311G are assigned to C-C stretching vibrations of the title molecule. The C-C in- plane bending vibration occurs between 1000-600 cm⁻¹ [104].

In the present case, bending and ring vibration of C-C falls below 1000 cm⁻¹ and are shown in Table 4.3. A medium intense FT-Raman band is identified at 823 cm⁻¹, the corresponding calculated value lies at 826 cm⁻¹ in 6-31G and 821 cm⁻¹ in 6-311G. From the FT-Raman spectrum the values predicted at $\delta_{ring} = 945$ (ms), 631 (m), 551 (vw), 353 (ms) cm⁻¹ that confirms the formation of δ_{ring} at 632, 671, 622, 339, 332, 327, 310, 81,76,71, 23 cm⁻¹ (B3LYP/6-311G), and δ_{ring} at 684, 675, 625, 340, 334, 331, 314, 84, 75, 25, 23 cm⁻¹ (B3LYP/6-31G). The C-C in-plane bending vibration mode calculated at δ_{ipb} = 695, 440, 390, 345 cm⁻¹ (B3LYP/6-31G), and δ_{ipb} = 694, 396, 388, 343 cm⁻¹ (B3LYP/6-311G). The out-of-plane C-C bending modes are calculated at 850, 844, 622, 405, 375, 310, 298, 35, 29, 18, 14, 8 cm⁻¹ (B3LYP/6-311G) and 855, 847, 625, 444, 379, 314, 300, 38, 30, 20, 15, 10 cm⁻¹ (B3LYP/6-31G).

C= O vibrations

The C=O stretching vibration of the carbonyl group, is generally expected in the region 1740-1660 cm⁻¹. In the present study, this vibration has been observed at 1698/1697 cm⁻¹ in FT-IR/FT-Raman spectra are assigned as C=O stretching vibration of the title molecule. The strong band in the FT-IR and FT-Raman, near 1750-1655 cm⁻¹ confirms the possibility of a carbonyl group in an aromatic compound [106]. The C=O in-plane bending vibration occurs in the range of 820- 630 cm⁻¹. El- Azab et al. reported that C=O in-plane bending vibration was appearing at 694 cm⁻¹ [107]. In the present molecule it was observed as a weak intense peak at 694 (w) cm⁻¹ in the FT-Raman spectrum, the corresponding calculated in-plane bending modes of C=O occurs at 695 cm⁻¹ in B3LYP/6-31G and 694 cm⁻¹ in B3LYP/6-311G. The prominent absorptions bands of δCC, the medium-strong

peak is observed in FT- IR at 1094 (ms) cm⁻¹, the corresponding theoretical value bound at 1095 cm⁻¹ at both B3LYP/6-31G and B3LYP/6-311G.

C-Cl vibrations

The vibrational assignments of the benzene ring belong to Carbon-Halogen (F, Cl, Br) bonds, which are formed between the ring carbon and the halogen atoms are particularly important. Because of the lowering of molecular symmetry and the presence of heavy atoms, vibrations indeed are mixed [108-111]. In the FT-Raman spectrum, a strong band is observed due to the presence of Cl, Br, and F atoms. The C-Cl band at 720 (vs) cm⁻¹ in FT-Raman is a stretching vibration found by Govindarajan et al. [112]. For a simple benzene ring chlorine containing atom, C-Cl absorptions are in the region between 750-700 cm⁻¹. In the title molecule, C-Cl stretching vibration is observed at 460 (vw) cm⁻¹ (FT-IR), and the corresponding computed value is 465 cm⁻¹ in B3LYP/6-31G and 462 cm⁻¹ in B3LYP/6-31IG.

C-S vibrations

The characteristic frequency for the C-S stretching mode appears as a weak band in the region 800- 600 cm⁻¹. The C-S stretching modes are reported at 783, 632 cm⁻¹ in FT- IR, 633 cm⁻¹ in FT-Raman, and 785,635 cm⁻¹ theoretically assigned by Fatima et al. [113]. In the current study, FT-Raman spectrum with very low intensity is assigned to C-S symmetric stretching vibrations. The weak band observed at 720(w) cm⁻¹ in FT-Raman and the calculated values at 878, 740, 724 cm⁻¹ for B3LYP/6-31G and 875, 738, 720 cm⁻¹ for B3LYP/6-311G are assigned C-S stretching vibrations of the title molecule.

4.4.3 Reactivity cite of CPTBN

The molecular electrostatic potential (MEP) plot is a visual illustration of the foremost reactive sites during a molecule and mapped with the colour scheme [114]. Potential will increase within the order of red< orange < yellow < green < blue. Using the

Gaussian 09 program, we tracked and plotted the alpha density (e⁻⁴), density difference (e⁻³), and MEP (e⁻²) surface mapping. It provides a visual method to understand the relative step-by-step polarity of the molecule.

Based on the three electrostatic potential surface deepest red, blue potential value in this molecule ranges from -4.055e⁻⁴ a.u to 4.055e⁻⁴ a.u, -6.088e⁻³ a.u to 6.088e⁻³ a.u and -7.960e⁻² a.u to 7.960 e⁻² a.u. Alpha density represents the full electrophilic region which is represented by blue colour. Density difference shows the region of energy difference between alpha density and MEP. In the reactive properties of MEP, the nucleophilic reactive site (red colour) shows the molecule's negative regions, and is located on the thiazole ring and partly above the benzonitrile. The other site is the electrophilic reactive site (blue colour) which indicates the positive regions of the molecule and is located on all hydrogen atoms in the molecule. The more dominant area are marked by green colour over the MEP surface indicates that the electrostatic potential is midway between the vicinity of the red and blue regions. Therefore, intermolecular interaction of the compound was confirmed by the reactive site regions, the electrostatic potential surface along with the Alpha density, and complete title compound density are shown in Fig. 4.4.

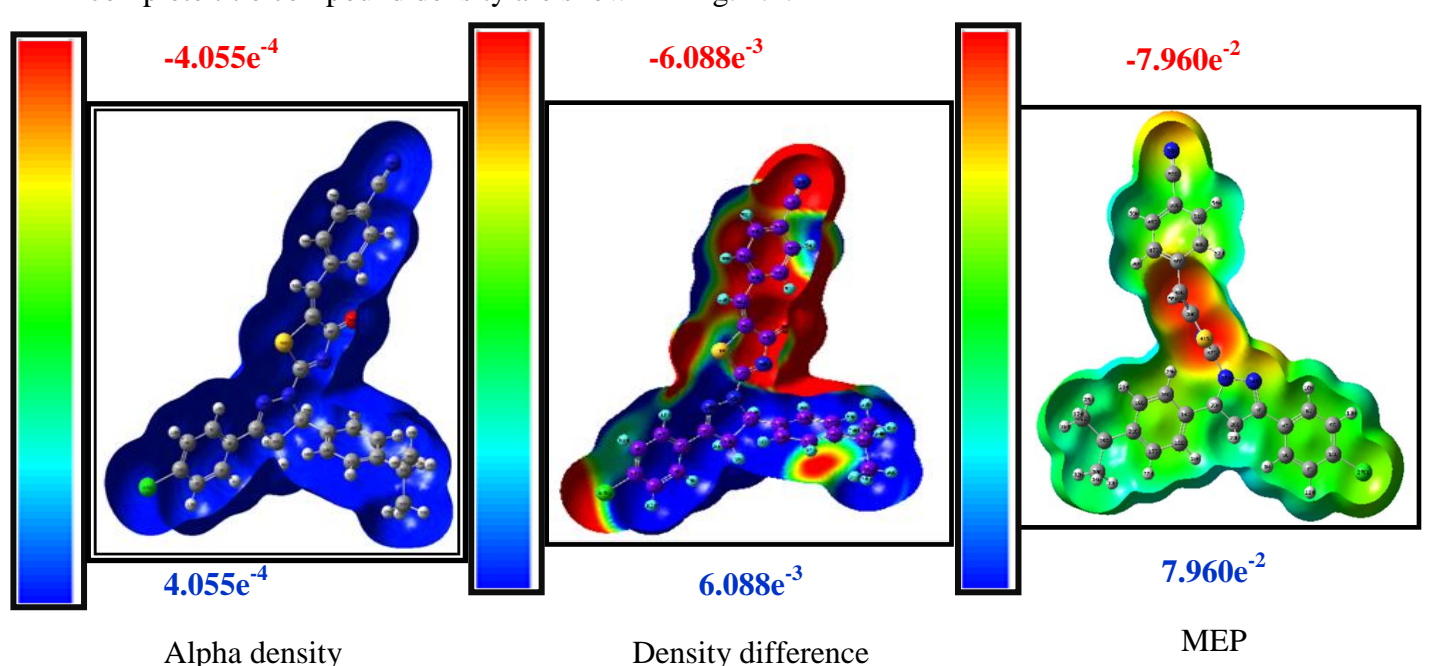


Fig. 4.4 Alpha density (e⁻⁴), density difference (e⁻³), and MEP (e⁻²) of CPTBN

4.4.4 HOMO- LUMO energy and global reactivity descriptors

The energies of the highest occupied molecular orbital (HOMO), the outermost orbital containing electrons, tend to give electrons and act as an electron donor. On the other hand, lowest unoccupied molecular orbital (LUMO), the innermost orbital containing is vacant and can accept electrons. The energy gap between HOMO and LUMO orbital difference is a very useful factor in determining the chemical reactivity of the molecule. In a simple molecule, orbital theory approaches HOMO and LUMO can offer a reasonable qualitative prediction of the excitation properties and the ability of electron transport. The energies of the HOMO and LUMO orbital for the possible excitations were carried as 3.57 eV for B3LYP/6-31G and 3.58 eV for B3LYP/6-311G. Using HOMO and LUMO orbital energies, the ionization energy (I) and electron affinity (A) can be expressed as Eqs. (4.1) and (4.2)

Ionization potential =
$$-E_{HOMO}(E_H)$$
 (4.1)

Electron affinity
$$A = -E_{LUMO}(E_L)$$
 (4.2)

Koopman [37] stated that the negative energies of E_{HOMO} were 6.46 eV, 6.70 eV, 6.99 eV and E_{LUMO} were 2.88 eV, 2.32 eV, 1.21 eV. Moreover, the energy gap is calculated with the occurrence of orbital diagram HOMO- LUMO, HOMO-1-LUMO+1, HOMO-2-LUMO+2, and the most significant higher orbital energy gaps were determined in 6-311G are 3.58 eV, 4.37 eV, 5.78 eV respectively, which are shown in Fig. 4.5. Based on the root density functional descriptors, global reactivity descriptors of the title molecule described the ionization potential (I), electron affinity (A), chemical potential (μ), electro-negativity (χ), global hardness(η), global softness(σ), and global electrophilicity (ω) calculation, according to the equations given below 4.3 to 4.7.

Global hardness
$$\eta = (I - A)$$
 (4.3)

Global softness
$$\sigma = 1/\eta$$
 (4.4)

Chemical potential
$$\mu = -(I + A)/2$$
 (4.5)

Electro negativity
$$\chi = (I + A)/2$$
 (4.6)

Global electrophilicity index
$$\omega = \mu^2/2\eta$$
 (4.7)

The values of the global reactive descriptor [17,116] are computed and listed in Table 4.4, which ensures the molecule's indisputable biological activity.

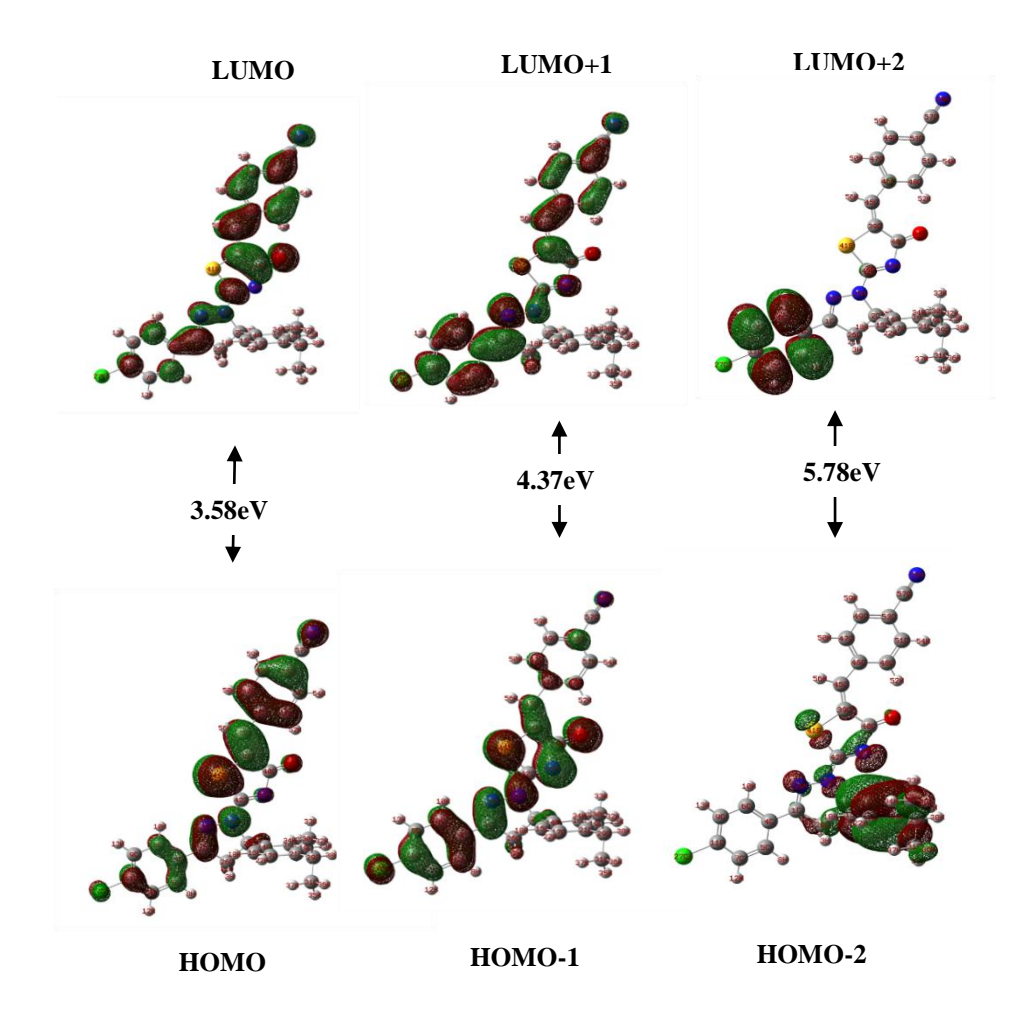


Fig. 4.5 HOMO - LUMO energy distribution plots of CPTBN at DFT/B3LYP/6-311G basis set

4.4.5 Fock matrix for bonds

Calculations of the bond fock matrix [90] were made using the Gaussian 09 [20] program to interpret the many second—order perturbation interactions between the full orbits

of one subsystem and the empty orbits of another subsystem, which is a measure of hyperconjugation intermolecular delocalization. The natural bond orbital (NBO) analysis in the donor–acceptor interactions basis was evaluated using the second-order Fock matrix [117]. This analysis is carried out by examining all possible interactions between 'filled' (donor) Lewis-type NBOs and 'empty' (acceptor) non-Lewis NBOs. For each donor (i) and acceptor (j), the stabilization energy in the Eq. (4.8) E(2) associated with the delocalization $[i \rightarrow j]$ is estimated at

$$E(2) = \Delta E_{ij} = q_{i} \frac{(F_{i,j})^{2}}{(E_{i} - E_{i})}$$
(4.8)

where q_i is the orbital occupancy of the donor, E_i and E_j are diagonal elements and F (i, j) is the off- diagonal NBOFock matrix element. The transmission of this electron to electron from a bonding orbital (donor- σ , π) with depreciation in its occupancy, an antibonding orbital (acceptor- σ^* , π^*) and Lone pair (LP) can be defined as charge transfer. Several other types of valuable data, such as directionality, hybridization and partial loading, have been analyzed from the NBO results.

The strong intra- molecular hyperconjugation interaction of the π^* electrons from C_7 - C_{11} to the π^* anti-bonding orbital's of C_4 - C_5 bond shows leading to the stabilization of 215.88 kcal/mol. The bonding $\pi^*(C_7$ - $C_{11})$ NBO further conjugates with $\pi^*(C_4$ - $C_5)$, $\pi^*(C_6$ - $C_9)$, have an enormous stabilization energy of 215.88, 141.93 kcal/mol, as shown in Table 4.5. The interaction between $\pi^*(C_6$ - $C_9)$, $\pi^*(C_7$ - $C_{11})$ to $\pi^*(S_{41}$ - $C_{42})$ the electrons are heavy intermolecular. In addition to these interactions, there is also a strong lone pair show stabilization capacity, such as LP (1) N_{25} - $\pi^*(C_1$ - $N_{24})$ = 26 kcal/mol, LP (2) N_{43} - $\pi^*(S_{41}$ - $C_{42})$ = 144.68 kcal/mol calculated by the basis set B3LYP/6-311G. These charge transfers are responsible for the structure-activity relationship analysis of the molecule.

4.4.6 Reduced density gradient (RDG)

The RDG method is a powerful way to analyze non-covalent inter-molecular interactions. The RDG function is a fundamental dimensionless quantity used to describe the deviation from a homogeneous electron distribution, which succeeding Eq. (4.9) was developed by E. R. Johnson et al. [57].

RDG(r) =
$$\frac{1}{2(3\pi r^2)^{1/2}} \frac{|\nabla \rho(r)|}{\rho(r)^{4/3}}$$
 (4.9)

where $\rho(r)$ and RDG (r) are the electron density and its first derivative, respectively. The gradient subsurface plots of RDG versus the electron density $\rho(r)$ multiplied by the sign of the second Hessian eigen value sign [k2(r)] were rendered by the VMD 1.9.2 program [118] based on outputs of Multiwfn software 4.1 program [54], shown in Fig 4. 6(a). In RDG surface blue colour indicates the presence of strong hydrogen bond appeared red in benzonitrile and green colour represent van der Waals interaction appeared in the center thiazole ring and red colour represent the strong repulsion that appears in the centre of the ring system.

The density value of the low- gradient spikes (the RDG versus ρ plot) appears to be a good indicator of the strength of the interaction. When 2D is plotting RDG values versus ρ is more meaningful to distinguish the bonding (λ_2 <0) from nonbonding (λ_2 >0) interactions, plotted in Fig 4.6 (b).

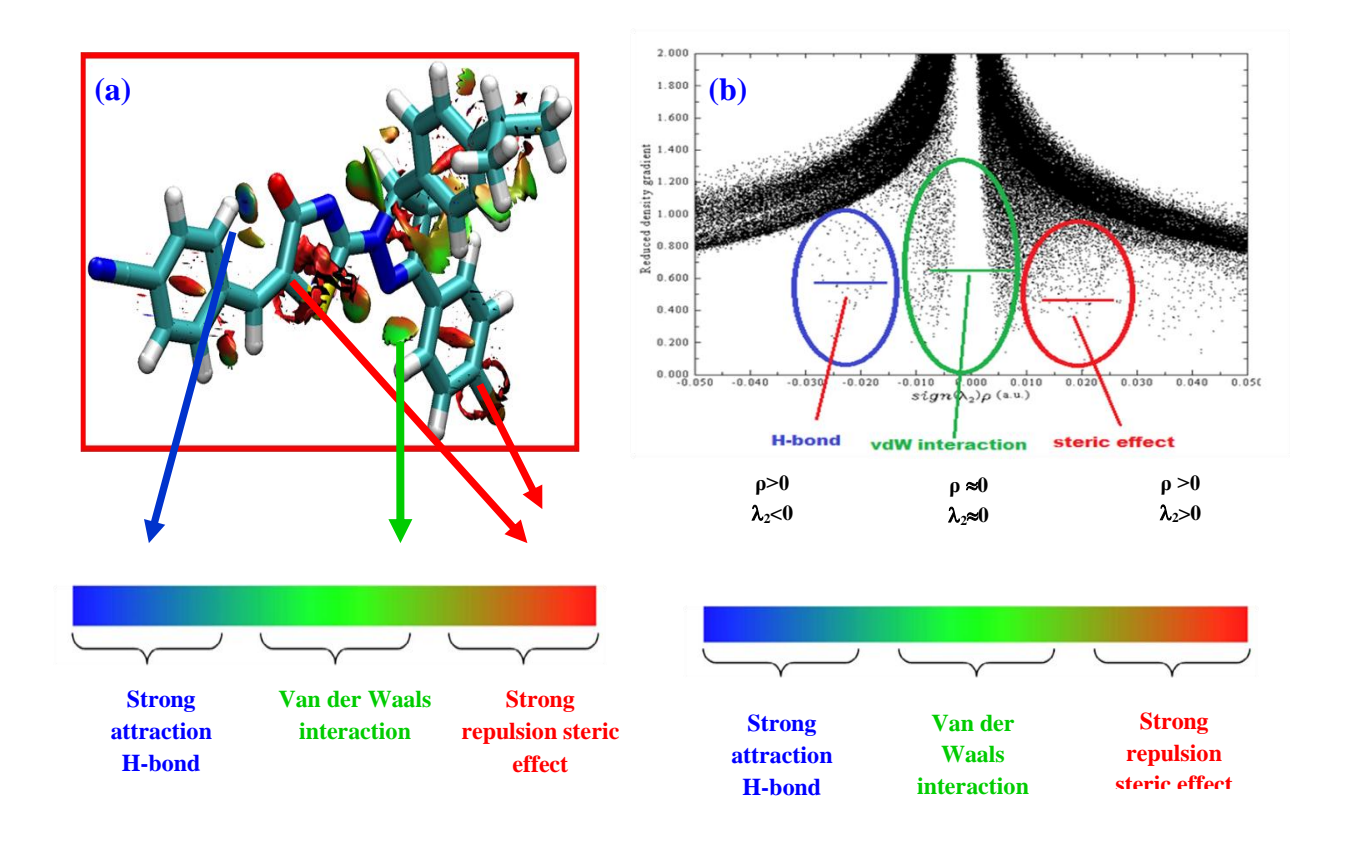


Fig. 4.6 RDG (a) 3D colour scaling of non-covalent interaction and (b) 2D scatter graph of the electron density ρ versus RDG interaction in CPTBN

4.4.7 Localized orbital locator (LOL) and electron localization function (ELF)

The localized orbital locator (LOL) and electron localization function (ELF) is one of the most powerful methods for understanding chemical bonding because it allows the identification of chemically relevant locations in the molecular space where electrons concentrate, such as a bonding, non-bonding and lone pair. This analysis was defined by LOL $[\gamma(r)]$ and ELF $[\eta(r)]$ which is related with Fermi hole curvature [119]. It is defined as a measure of excess kinetic energy density due to the Pauli repulsion. The shaded surface map of electron localization function and localized orbital locator - LOL are drawn using Multi-wfn software [54,120] they are presented in Figs 4.7 and 4.8 respectively.

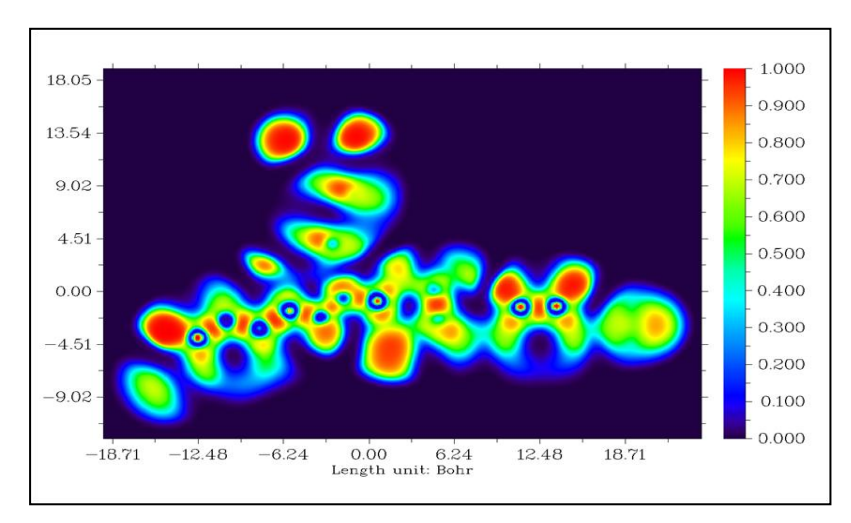


Fig. 4.7 Localized orbital locator (LOL) for CPTBN obtained in xy plane

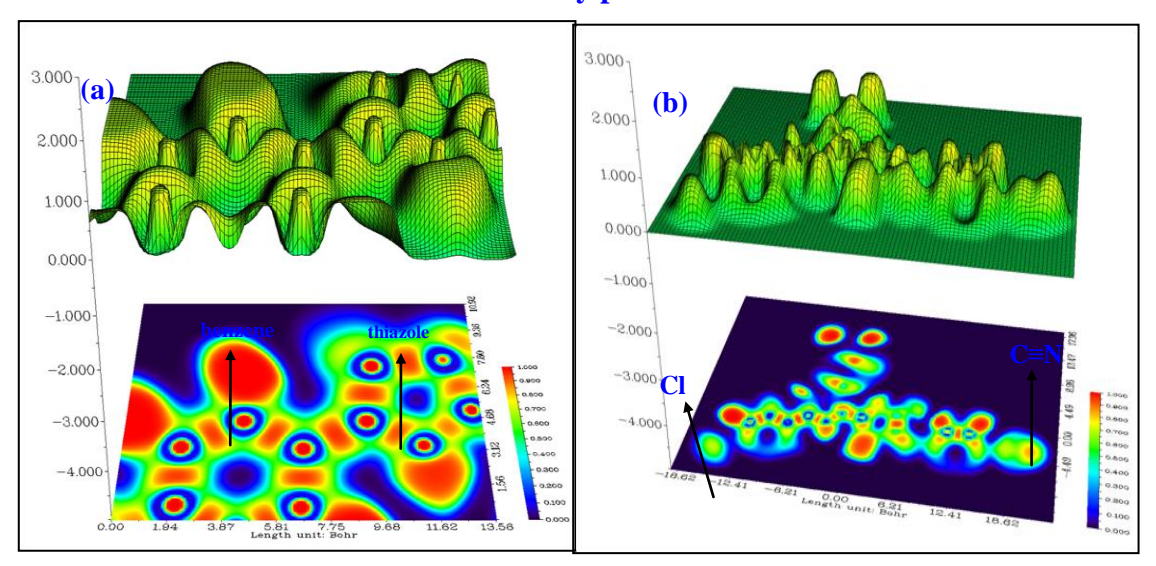


Fig. 4.8 Electron localization function (ELF) or shaded surface map with projection effect of (a) thiazole and benzene ring and (b) full CPTBN

There are basically two types of basins. On the one hand are core basins organized around nuclei (with Z > 2) and on the other are valence basins in the remaining space. The inner atomic shell structure is quite similar to the structure provided by the core is connected [121,122]. In our description, the localization colour code (Fig. 4.7) used for the domain are: red-dot blue ring shows the carbon core, red-dot yellow ring shows the joining bond between core atoms and white shell rounded with rings of red, yellow, green show the valence shell. An electron localization function shows the shaded surface map obtained from localization orbits. Depending upon the density of electron it notifies the boundary region are highly localized with broad peak, the ring bond region is localized with a sharp

peak (like water droplet) and $C \equiv N$ region are low localized with small peak which is shown in Fig. 4.8.

4.4.8 Antibiotic and antifungal activity

Microbial is killed and ruled out from reproduction by antimicrobial drugs. Nevertheless, these microorganisms are caused by improper and unnecessary use of antibiotics to develop resistance to these substances [82, 123]. Thiazole compound was assayed at a concentration range of 25 µg/ml, 50 µg/ml, 75 µg/ml, 100 µg/ml and total control are shown in bar chart Fig. 4.9 against two Gram-positive bacteria: Bacillus subtilis, Staphylococcus aureus and two Gram- negative bacteria: Escherichia coli, Pseudomonas aeruginosa Fig. 4.10. The anti- fungal activity was carried out against a well- known fungal strain Candida albicans and Aspergillus Niger (Fig. 4.11) by the disc diffusion method [124]. Bacterial and fungal pathogens standardized using the DMSO standard were diluted (1:100) and added to an aliquot into respective wells. The plates were incubated in a static incubator at 37°C for 18-24 hr and the determined zone of inhibitory concentration values are listed in Table 4. 6. Results revealed that the compound showed varying zones of inhibitation against the test panel of pathogens were plotted in the form of bar graph (Fig. 4.9). The compound showed the highest inhibition against bacterial strains Staphylococcus aureus, whereas 24 µl respectively at 100 µl/ml. Furthermore, significant inhibition against fungi strains Candida Aabicans whereas 20 µl showed inhibitation at 100 µl/ml against A. Niger is shown in Figs. 4.10 and 4.11.

4.4.9 Molecular docking

Molecular docking is a computational technique that tries to predict the sub-region or binding composites from a multi – dimensional image of the macromolecule (protein) non-covalent bonding and a small molecule (ligands) [125]. Multiple views of the visualization are a useful way of extending 3D, the 2D display shows dimensional

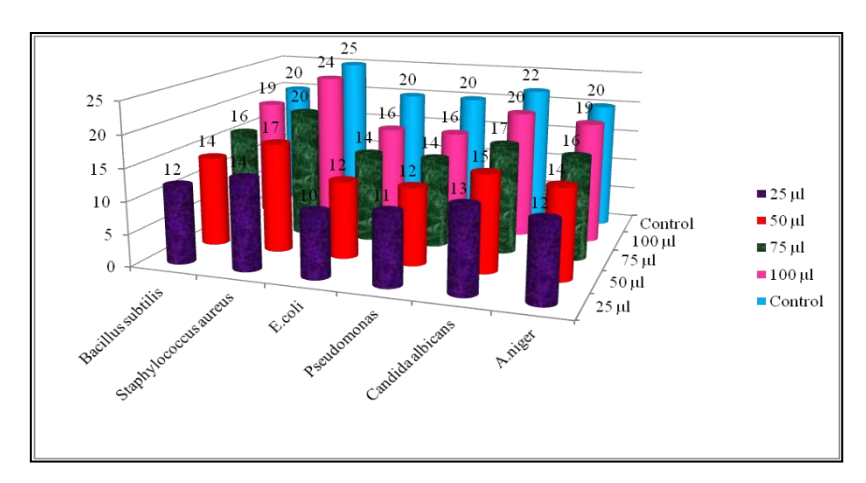


Fig. 4.9 Bar chart for antibacterial and antifungal of CPTBN

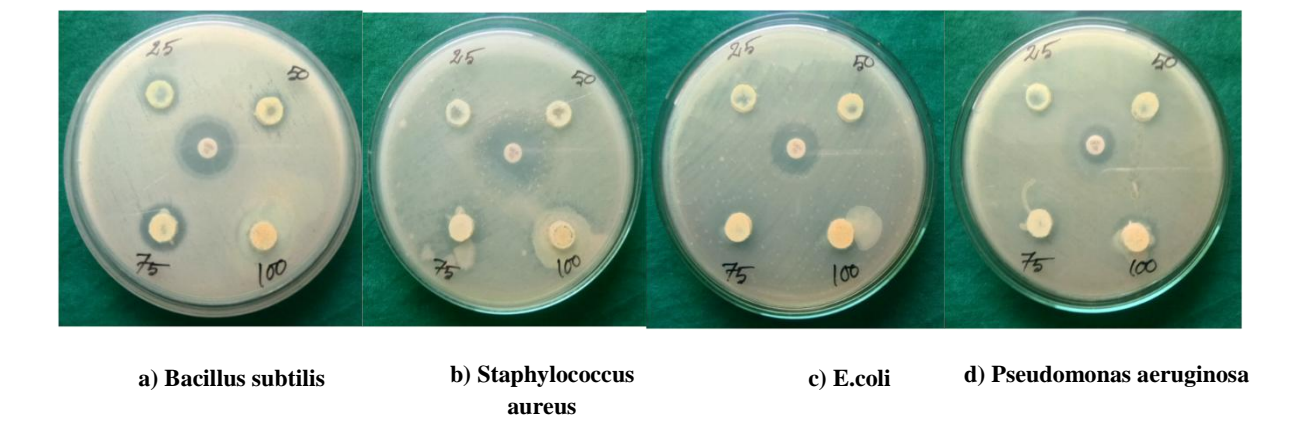


Fig. 4.10 CPTBN microbial tests against bacterial microorganisms a) Bacillus subtilis, b) Staphylococcus aureus, c) Escherichia coli and d) Pseudomonas aeruginosa using disk-diffusion method

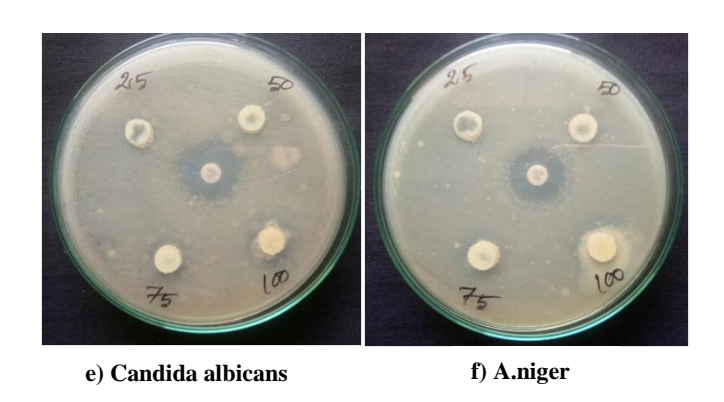
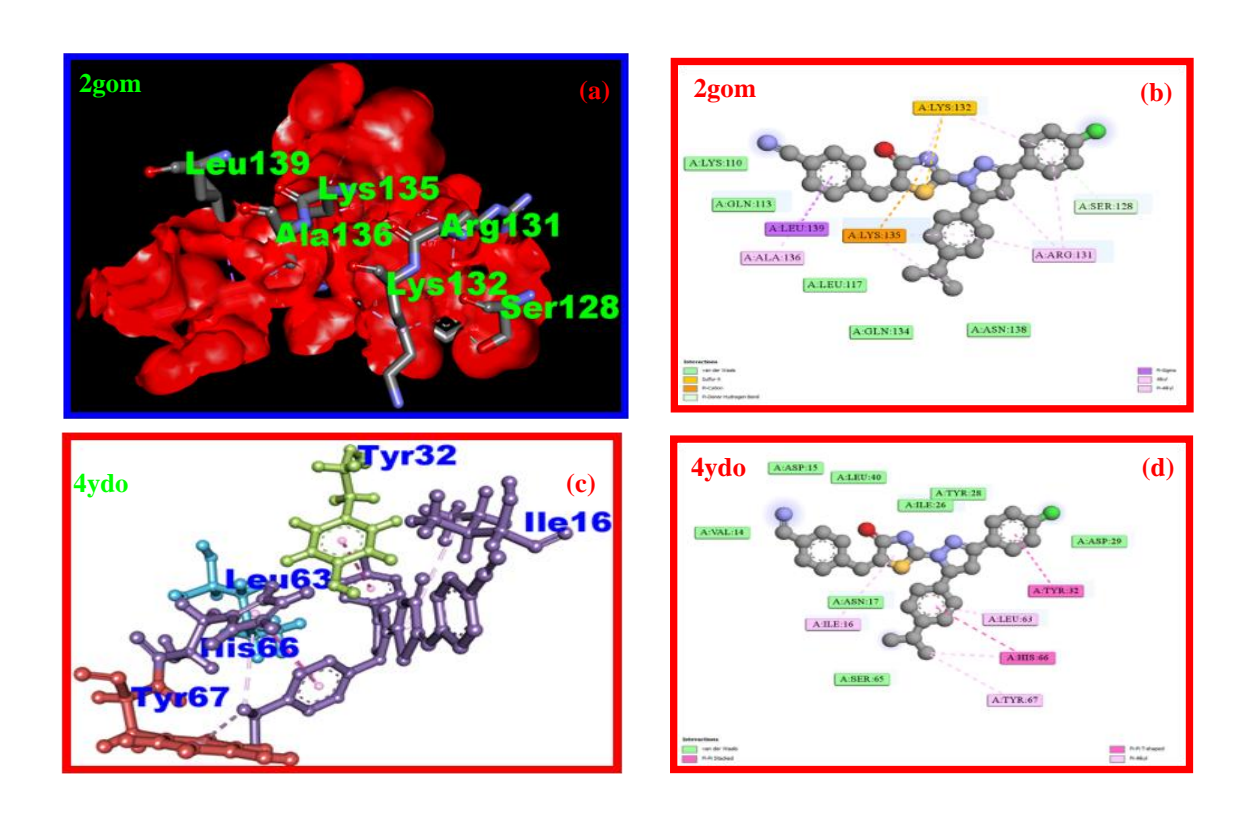


Fig 4.11 CPTBN microbial testing of fungal microorganism e) Candida albicans and f) Aspergillus Niger using Disk-diffusion method

limitations. To collect such views directly from the PDB (protein data bank). Based on the antibiotics, antifungal and biological behaviours of the CPTBN, different type of protein activities such as high- resolution antibacterial, antifungal, Monoclonal antibodies, nitric oxide synthase inhibitor, Staphylococcal protein A. The selected protein structureshave been downloaded from the RCSB [64] PDB ID website of the database 2gom, 4ydo, 5178, 4d7o and 1bdc. Initially, the title molecule was minimized as a pdb file based on the DFT method and bind with downloaded protein. Finding 3D structures with the lowest binding energy of the compound were constructed using auto dock tools and minimum docking energy values were investigated. The dotted lines show the bond formation between the ligand and targeted proteins. The docking process were analyzed for the predicted binding interactions, including binding energy, inhibition constant, and intermolecular energy, between the receptors and ligand in the best scoring pose, which was listed in Table 4.7. Discovery studio [57] generates the binding position of a ligand- protein dock in 3D view (Figs. 4.12a, 4.12c, 4.12e, 4.12g and 4.12i) and 2D represent (Figs. 4.12b, 4.12d, 4.12f, 4.12h and 4.12j) represent a residual interaction energy conformation.



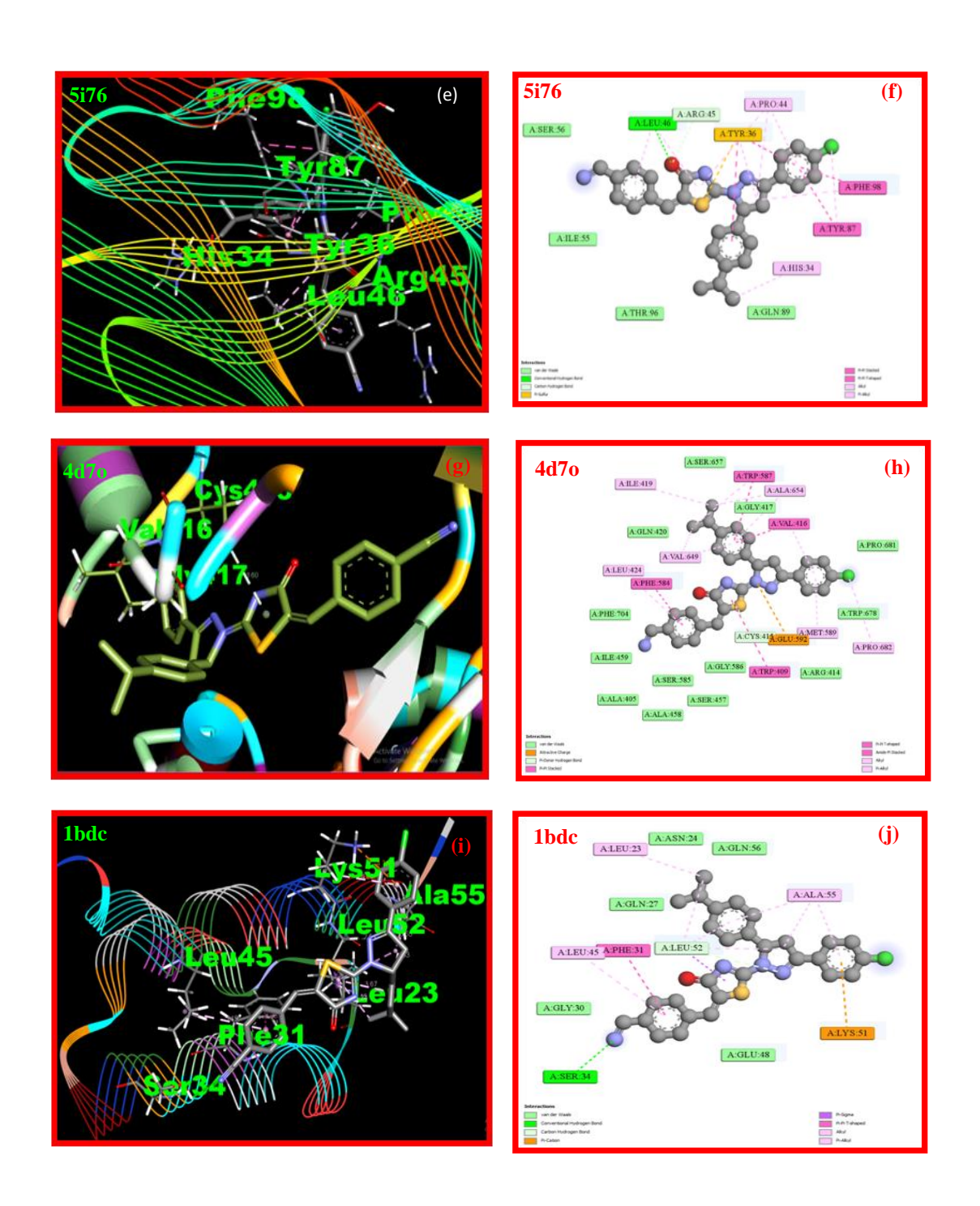


Fig.4.12 a) Antibacterial Docked interaction pose, b) 2D binding modes of CPTBN structure, c) Antifungal Docked interaction pose, d) residual 2D modes of CPTBNstructure, e) Monoclonal antibodies Docked interaction pose, f) targeting 2D modes of CPTBN structure, g) Nitric oxide synthase inhibitor docked interaction pose, h) 2D amino acid bonding modes of CPTBN structure, i) Staphylococcal Protein A docked interaction pose and j) 2D protein interaction modes of CPTBN structure

Antibacterial activity

Antibacterial activity and virtual screening by molecular docking of staphylococcus aureus is a protein tied to its complementary target to provide bacterial suppression of structure. Staphylococcus aureus (PDB ID- 2gom) protein resolution is 1.25 Å having unit cell length a = 59.59 Å, c = 45.63 Å, and angle $\alpha = 90^{\circ}$, $\beta = 90^{\circ}$, $\gamma = 90^{\circ}$ [126]. The docking result of CPTBN ligand interaction has shown (Fig 4.12a and 4.12b) a binding affinity to the target protein 2gom, as indicated by the bonding interaction between the ligand and catalytic site amino acids. Glutamine (GLN) from a van der Waals interaction was found near benzonitrile and Lysine (LYS) forms a Pi- Cation interaction near the thiazole ring. Binding energy and inhibition constant are -7.913 kcal/mol and 1.42 μ M.

Antifungal activity

Antifungal are medicines that kill or stop the growth of fungi that causes infections. One of the antifungal protein target Candida Albicans PDB ID: 4ydo are examined ligand (CPTBN) using molecular docking studies. This work aim to verify amino acid (residue) interaction of protein 4ydo are Crystal Structure (Fig 4.12c and 4.12d) of Candida Albicans a unit cell length a = 96.824 Å, b = 96.824 Å, c= 183.082 Å and angle α = 90°, β = 90°, γ = 90° [127]. The binding interaction between the ligand and catalytic site amino acids Tyrosine (TYR) and Isoleucine (ILE) forms a van der Waals interaction near Thiazole ring, Leucine (LEU) forms a Pi- Alkyl interaction and Tyrosine (TYR) forms a Pi- Pi T-shaped interaction. Binding energy and inhibition constant are - 10.62 kcal/mol and 16.35 Nanomolar.

Monoclonal antibodies

To develop highly efficient therapeutic and diagnostic agents. Monoclonal antibodies (mAbs) structure of the protein PDB ID: 5i76 protein has a resolution 1.922 having unit cell length a = 72.482 Å, b = 68.037 Å, c = 97.689 Å, and angle $\alpha = 90^{\circ}$, $\beta = 68.037$ Å, $\beta = 68.037$ Å, $\beta = 68.037$ Å, and angle $\beta = 90$

 101.85° , $\gamma = 90^{\circ}$. Examination of the binding energy (-7.85) kcal/mol, inhibition constant (1.76µM) and shown in Figs. 12e and 12f. CPTBN ligand binds at the active site of protein by lower amino acid (residue) interaction. Amino acid Leucine (LEU) forms a conventional hydrogen bond with carbonyl present in the thiazole ring. van der Waals interaction Serine (SER):Glutamine (GLN): was found near both benzonitrile and propane-2-ly. Proline (PRO) residual alkyl and Pi-alkyl bind with O atom and interaction with the core of the chlorophenyl ring, thiazole ring, and pyrazole ring.

Nitric oxide synthase inhibitor

PDB ID-4d7o protein (Figs 4.12g and 4.12h) [128] has a resolution 1.78 had a unit cell length a = 51.77 Å, b = 110.58 Å, c = 165.16 Å and angle $\alpha = 90^{\circ}$, $\beta = 90^{\circ}$, $\gamma = 90^{\circ}$. Amino acid Tryptophan (TRP) and Phenylalanine (PHE) forms Amide- Pi stacked and van der Waals interaction with a CH₃ atom in the propan group. Most of the core rings are interactive with alkyl Pi-Pi, T- Shaped, and amide Pi stacked presented in protein. Two van der Waals interactions with Isoleucine (ILE) and Glycine (GLY) bound with benzonitrile ring. Binding energy and inhibition constants were -7.85 kcal/mol and 1.63 μ M.

Staphylococcal Protein A

Staphylococcal Protein A (PDB ID-1bdc) receptor is a persistent human pathogen that causes a variety of diseases, both in clinical appearance and in severity found in normal human flora, located on the skin and mucous membranes. To investigate nanomolar bacterial binding targets for complementary ligand interaction. Staphylococcal Protein A interaction protein [129] shows (Figs 4.12i and 4.12j) the existence of many conventional bonds, which are as follows: π - π T- shaped, conventional hydrogen bond, van der Waals interactions. Leucine (LEU) form carbon – hydrogen bond interaction with the core thiazole ring. Asparagine (ASN) form a van der Waals interaction was found near CH₃. The inhibition constant was 428.64 Nanomolar and the observed binding energy was -8.69 kcal/mol.

4.5 Conclusion

In the integrating work, analysis of 4-[{2-[3-(4-chlorophenyl)-5-(4-propan-2-lye) phenyl)-4, 5-dihydro- 1H- pyrazol-1-yl]-4-oxo-1, 3-thiazol- 5(4H)-ylidene} methyl] benzonitrile [CPTBN] molecule through the first level of the spectral statistics on experimental FT-IR, and FT-Raman are recorded and at the next level, detailed vibrational assignments using DFT/B3LYP/6-31G and B3LYP/6-311G basis level were computed. The geometry of the title molecule was analyzed theoretically. The three different zone mapped surfaces provide a visual plot to understand the atoms in an intermolecular polarity. Positive and negative regions of the MEP map that are localized around the title compound indicate possible sites of nucleophilic and electrophilic reactivity of the molecule. The energy flow from the gap is generally low to high, and Gaussian diagrams have been used to visualize it. The reactive nature of the CPTBN is hypothetically dissected using techniques for the quantum system and addressed by electronic properties, such as hardness, chemical potential, electro-negativity, global hardness, and global softness. The NBO interprets the conjugate relationship of the orbital donor and the unoccupied illustration, hydrogen bond, van der Waals and steric effects depict the interaction of the atoms inside the molecule. The electron localization of the region in the molecular space at which identified chemically significant regions as a bond and lone pair. Antimicrobial inhibitory activity against the compound was explored through the tests. Utilizing the molecular restraining nature of the particle was seen as the most vulnerable restricting ligand to a catalyst and the most grounded hydrogen authoritative. The title molecule is docked with receptors high resolution antibacterial (2gom), antifungal (4ydo), Monoclonal antibodies (5i76), Nitric oxide synthase inhibitor (4d7o), Staphylococcal protein A (1bdc) and gives good binding affinity values. Acceptable and delicate antibacterial effects against all screened pathogens and the definitive medicine support the docking results. The nature of the molecules shows the binding activity of thiazole with biological targets were examined and discussed in terms of interaction energy. The inclusion of antimicrobial resistance rises to the development of new antibiotics through a direct further rational work mode of action.

Table 4.1: Optimized structural parameters (bond length) of CPTBN calculated by DFT/B3LYP method with 6-31G and 6-311G basis sets

Bond	B3LYP/	B3LYP/	Bond	B3LYP/	B3LYP/
Length(Å)	6-31G	6-311G	Length(Å)	6-31G	6-311G
C1-C4	1.46	1.46	C26-H28	1.09	1.10
C1-N24	1.3	1.31	C29-C30	1.55	1.55
C1-C26	1.52	1.52	C29-C3I	1.54	1.55
C2-C14	1.52	1.52	C29-H38	1.09	1.10
C2-N25	1.51	1.51	C30-H32	1.09	1.10
C2-C26	1.56	1.56	C30-H33	1.09	1.10
C2-H55	1.09	1.09	C30-H34	1.09	1.10
H3-C26	1.09	1.09	C31-H35	1.09	1.10
C4-C5	1.41	1.41	C31-H36	1.09	1.10
C4-C6	1.41	1.41	C31-H37	1.09	1.10
C5-C7	1.4	1.4	C39-C40	1.50	1.50
C5-H8	1.08	1.08	C39-S41	1.87	1.86
C6-C9	1.39	1.39	C39-C45	1.35	1.36
C6-H10	1.08	1.08	C40-N43	1.40	1.40
C7-C11	1.39	1.39	C40-O44	1.25	1.25
C7-H12	1.08	1.08	S41-C42	1.84	1.84
C9-C11	1.39	1.4	C42-N43	1.31	1.31
C9-H13	1.08	1.08	C45-C46	1.46	1.46
C11-CL27	1.83	1.82	C45-H56	1.09	1.09
C14-C15	1.4	1.41	C46-C47	1.42	1.42
C14-C16	1.4	1.4	C46-C48	1.41	1.41
C15-C17	1.39	1.4	C47-C49	1.39	1.39
C15-H18	1.08	1.09	C47-H50	1.08	1.09
C16-C19	1.4	1.4	C48-C51	1.39	1.39
C16-H20	1.08	1.09	C48-H52	1.08	1.08
C17-C21	1.41	1.41	C49-C53	1.41	1.41
C17-H22	1.08	1.09	C49-H59	1.08	1.08
C19-C21	1.4	1.4	C51-C53	1.41	1.41
C19-H23	1.08	1.09	C51-H54	1.08	1.08
C21-C29	1.53	1.53	C53-C57	1.43	1.43
N24-N25	1.4	1.39	C57-N58	1.17	1.17
N25-C42	1.34	1.34			

Table 4.2: Optimized structural parameters (bond angle) of CPTBN calculated by DFT/B3LYP method with 6-31Gand6-311G basis sets.

Bond	B3LYP/6	B3LYP/6	Bond	B3LYP/6	B3LYP/6
angle(degree)	-31G	-311G	angle(degree)	-31G	-311G
C4-C1-N24	121.66	121.57	C2-C26-H28	111.73	111.63
C4-C1-C26	125.16	125.26	H3-C26-H28	107.50	107.49
N24-C1-C26	113.17	113.16	C21-C29-C30	111.67	111.74
C14-C2-N25	112.28	112.16	C21-C29-C31	111.97	112.07
C14-C2-C26	115.28	115.36	C21-C29-H38	107.05	106.93
C14-C2-H55	109.32	109.24	C30-C29-C31	110.93	111.07
N25-C2-C26	100.08	100.12	C30-C29-H38	107.46	107.36
N25-C2-H55	107.21	107.31	C31-C29-H38	107.48	107.37
C26-C2-H55	112.16	112.15	C29-C30-H32	110.48	110.46
C1-C4-C5	120.62	120.65	C29-C30-H33	111.13	111.11
C1-C4-C6	120.57	120.67	C29-C30-H34	111.11	111.21
C5-C4-C6	118.81	118.69	H32-C30-H33	108.29	108.22
C4-C5-C7	120.86	120.92	H32-C30-H34	107.81	107.81
С4-С5-Н8	120.29	120.37	H33-C30-H34	107.90	107.91
С7-С5-Н8	118.86	118.71	C29-C31-H35	111.19	111.16
C4-C6-C9	120.73	120.78	C29-C31-H36	110.45	110.43
C4-C6-H10	119.09	119.12	C29-C31-H37	111.19	111.29
C9-C6-H10	120.18	120.10	H35-C31-H36	108.24	108.17
C5-C7-C11	118.80	118.74	H35-C31-H37	107.92	107.94
C5-C7-H12	120.73	120.72	H36-C31-H37	107.72	107.72
C11-C7-H12	120.47	120.53	C40-C39-S41	108.92	108.90
C6-C9-C11	118.96	118.93	C40-C39-C45	132.84	132.96
C6-C9-H13	120.71	120.71	S41-C39-C45	118.24	118.14
C11-C9-H13	120.32	120.36	C39-C40-N43	113.46	113.45
C7-C11-C9	121.84	121.95	C39-C40-O44	124.41	124.31
C7-C11-CL27	119.10	119.07	N43-C40-O44	122.14	122.24
C9-C11-CL27	119.06	118.99	C39-S41-C42	86.38	86.28
C2-C14-C15	121.47	121.46	N25-C42-S41	119.48	119.70
C2-C14-C16	119.90	120.00	N25-C42-N43	123.19	123.01

C15-C14-C16	118.63	118.54	S41-C42-N43	117.33	117.29
C14-C15-C17	120.62	120.67	C40-N43-C42	113.91	114.08
C14-C15-H18	120.23	120.30	C39-C45-C46	134.89	134.95
C17-C15-H18	119.15	119.03	C39-C45-H56	113.98	113.95
C14-C16-C19	120.53	120.59	C46-C45-H56	111.13	111.10
C14-C16-H20	119.55	119.56	C45-C46-C47	115.75	115.85
C19-C16-H20	119.90	119.82	C45-C46-C48	126.30	126.28
C15-C17-C21	121.06	121.10	C47-C46-C48	117.96	117.87
C15-C17-H22	119.11	119.04	C46-C47-C49	121.69	121.70
C21-C17-H22	119.84	119.86	C46-C47-H50	119.20	119.23
C16-C19-C21	121.24	121.28	C49-C47-H50	119.11	119.07
C16-19-H23	119.38	119.35	C46-C48-C51	120.52	120.58
C21-C19-H23	119.37	119.37	C46-C48-H52	119.11	119.14
C17-C21-C19	117.91	117.82	C51-C48-H52	120.37	120.29
C17-C21-C29	121.37	121.41	C47-C49-C53	119.75	119.80
C19-C21-C29	120.71	120.76	C47-C49-H59	120.49	120.42
C1-N24-N25	108.58	108.59	C53-C49-H59	119.77	119.78
C2-N25-N24	113.47	113.35	C48-C51-C53	120.85	120.87
C2-N25-C42	125.02	124.98	C48-C51-H54	119.73	119.66
N24-N25-C42	121.46	121.62	C53-C51-H54	119.43	119.47
C1-C26-C2	103.65	103.71	C49-C53-C51	119.24	119.17
C1-C26-H3	112.34	112.39	C49-C53-C57	120.26	120.29
C1-C26-H28	110.44	110.44	C51-C53-C57	120.50	120.54
C2-C26-H3	111.23	111.25			
					-

Table 4.3: Experimental and calculated wavenumbers along with vibrational assignments CPTBN using B3LYP/6-31G and B3LYP/6-311G

Mode No	Observed wavenumbers (cm ⁻¹)		waven	ulated umbers n ⁻¹)	Vibrational assignments		
NO	ET ID	ET DAMAN	B3LYP/	B3LYP/	(PED %)		
	FT-IR	FT-RAMAN	6-31G	6-311G			
1		3067m	3075	3067	νCH(98)		
2			3060	3061	νCH(98)		
3	3049w		3054	3050	νCH(99)		
4			3036	3027	νCH(98)		
5		3013w	3018	3012	νCH(98)		
6			3010	3008	νCH(98)		
7			3002	3001	νCH(97)		
8			2999	2997	νCH(97)		
9			2995	2994	νCH(97)		
10			2994	2990	νCH(98)		
11			2988	2986	νCH(98)		
12			2982	2979	νCH(99)		
13			2975	2972	νCH(98)		
14	2957w		2966	2960	ν CH(99)		
15			2955	2953	$v_{ass}CH_2(88)$		
16		2947w	2952	2948	$v_{ass}CH_3(89)$		
17			2928	2924	$v_{ss}CH_3(89)$		
18		2933w	2936	2932	$v_{ss}CH_3(89)$		
19	2929w		2934	2930	$v_{ass}CH_3(89)$		
20			2915	2912	$v_{ass}CH_2(96)$		
21			2903	2900	$v_{ass}CH_3(96)$		
22			2881	2879	$v_{ass}CH_3(89)$		
23	2868w	2868w	2870	2868	νCH(97)		
24	2223w	2222ms	2228	2223	νCN(98)		
25	1698ms	1697w	1702	1699	νCO(82),δCC(14)		
26			1655	1653	νCC(75), δCH(15)		
27	1600ms	1596vs	1600	1598	νCC(74), δCH(16)		
28		1561vs	1564	1562	νCC(74), δCH(15)		
29		1551m	1552	1550	νCC(72), δCH(14)		
30	1548vs		1550	1548	νCN(72), νCC(12), δCH(10)		

31			1525	1522	νCC(88), δCH(16)
32	1493ms	1493w	1498	1495	vCC(78), δCH(10),vCO(10)
33			1455	1453	ν CN(72), ν CO(14), δ CH(10),
34		1441w	1442	1440	vCC(70), vCN(15), vCO(12)
35			1440	1436	δCH(69), νCC(18)
36	1424w		1429	1425	δ CH(68), ν CC(18)
37			1420	1418	δ_{opb} CH ₃ (72)
38		1409m	1415	1410	δ_{opb} CH ₃ (72)
39	1396ms	1397ms	1394	1395	δCH(68), νCCl(20)
40			1390	1389	δ_{ipb} CH ₃ (82)
41			1385	1382	δ_{ipb} CH ₃ (82)
42		1375w	1379	1376	ρ_{scis} CH ₂ (80)
43	1370ms		1370	1368	δ CH(69), ν CC(10)
44			1345	1343	δ CH(68), ν CC(12)
45	1331ms	1334ms	1333	1330	δ_{sb} CH ₃ (69)
46			1325	1322	δCH(62)
47			1314	1312	δCH(66)
48	1306w		1304	1305	δ_{sb} CH ₃ (72)
49			1300	1296	δ CH(67), ν CN(10)
50			1293	1290	δCH(69)
51		1285ms	1290	1286	δCH(70)
52			1283	1280	δCH(70)
53	1274ms		1278	1275	δCH(72)
54			1265	1262	γCH(59)
55		1251s	1253	1250	δCH(63)
56			1250	1246	δCH(64)
57			1245	1241	δCH(69)
58			1240	1237	vCC(70)
59	1225s	1225s	1230	1226	vCC(70), δCC(12)
60			1205	1203	δCH(72)
61	1195ms	1196ms	1196	1194	$\Gamma \text{CH}_2(69)$
62			1192	1189	δCH(64)
63			1185	1182	δCH(64)
64		1173ms	1178	1175	δCH(64)
65			1154	1151	δCH(63)
66			1140	1137	δCH(63)
67	1114ms	1115ms	1120	1116	δCH(62)

 1114 1110 νCC(71), δCH(12) 1107 1107 Γ CH₂(68) 1099ms 1103 1100 δ_{ipr}CH₃(62) 1094ms 1095 1095 δCC(66), δCO(22) 	
70 1099ms 1103 1100 $\delta_{ipr}CH_3(62)$	
71 1094ms 1095 1095 δCC(66), δCO(22)	
72 $1058w$ 1061 1056 $\delta CH(69)$	
73 1033w 1035 1033 δCH(63)	
74 1030 1028 δCH(62)	
75 $1025 1021 \delta_{Opr} CH_3(62)$	
76 1014w 1012w 1015 1014 νCCL(78)	
77 998 998 δ _{ipr} CH ₃ (70)	
78 985w 995 993 νCN(68), νNN(12)	
79 980w 980 981 γCH(66)	
80 975 973 δ _{ipr} CH ₃ (69)	
81 966 965 $\delta_{\text{ring}}(58)$	
82 958 957 $\delta_{\text{ring}}(56)$	
83 949w 951 949 $\delta_{\text{ring}}(57)$	
84 948 945 $\delta_{\text{ring}}(60)$	
85 945m 933 932 γCH(58)	
86 928 925 γCH(57)	
87 920 918 γCH(58)	
88 910 906 γCH(58)	
89 896w 900 898 γCH(58)	
90 889w 893 890 νCH(59)	
91 878 875 ν CS(78),	
92 870 866 νCH(59)	
93 850w 853 850 γCC(68)	
94 847 844 γCC(68)	
95 837w 840 838 γCS(78), νCN(12)	
96 829ms 833 829 γCH(68)	
97 823w 826 821 γCC(68)	
98 820 816 γCH(58)	
99 811w 814 810 γCH(56)	
100 793 790 γCH(58)	
101 784 781 γCH(58),	
102 770 767 $\delta_{\text{ring}}(60)$	
103 748w 753 750 νCH(55)	
104 740 738 $\delta_{\text{ring}}(58)$, vCS(12)	

105		720w	724	720	$\delta_{\rm ring}(60), \nu \rm CS(12)$
106	716w		718	715	$\delta_{\rm ring}(59)$
107		694w	695	694	δ CC(62), δ CO(17)
108	685vw		684	682	$\gamma_{\rm ring}(62)$
109		668vw	675	671	$\gamma_{\rm ring}(63)$
110	662vw		663	660	γCO(72)
111			650	647	$\delta_{\rm ring}(68)$
112			641	638	γCH(58)
113		631m	632	630	$\delta_{\rm ring}(59)$
114	619vw		625	622	γ CC(58), $\gamma_{ring}(20)$
115			605	602	$\delta_{\rm ring}(57)$, $\delta {\rm CN}(18)$
116	579w		582	580	δ CN(58), δ _{ring} (17)
117			566	564	δ CN(58), δ _{ring} (20)
118	554ms	551vw	554	552	$\delta_{\rm ring}(60)$
119			530	528	γCH(62)
120			520	517	γCH(60)
121	504w		505	503	γCH(60)
122	494vw		498	495	γCH(61)
123			481	479	$\delta_{\rm ring}(58)$
124	460vw		465	462	$vCCL(53)$, $\delta CC(19)$
125		440w	444	440	δCC(52)
126			430	427	$\delta_{\text{ring}}(58)$, δ CC(12)
127	406vw		408	405	γCC(56)
128			400	396	δCC(60)
129			390	388	δCC(60)
130			379	375	γCC(58)
131			365	363	γCCH ₃ (57)
132		353ms	358	355	$\delta_{\rm ring}(58)$
133			345	343	δCC(58)
134			340	339	$\gamma_{\rm ring}(53)$
135			334	332	$\gamma_{\rm ring}(54)$
136		325w	331	327	$\gamma_{\rm ring}(54)$
137			320	319	δ CCH ₃ (56)
138			314	310	γ CC(52), γ _{ring} (21)
139		297w	300	298	γCC(53)
140			280	275	δCCC(58)
141			255	253	δCCC(60)

142	233w	236	233	γCCC(52)
143		215	212	δCCC(60)
144		207	202	$\Gamma \text{ CH}_3(58)$
145		190	188	γCCC(58)
146	181w	185	180	Γ CH ₃ (58)
147		172	169	γCCC(53)
148		166	162	Γ CCCC(52)
149		153	151	Γ CCCC(52)
150		148	145	γCCH ₃ (62)
151		140	138	$\delta_{\text{ring}}(63)$
152	129w	133	130	δCCC(67)
153		128	122	γCCN(62)
154		125	117	δCCC(63)
155		116	111	γCCC(60)
156		105	103	δCCC(60)
157	92	97	93	γCCC(62)
158		95	89	δCCC(60)
159	79s	84	81	$\gamma_{ring}(56)$
160		80	76	$\gamma_{ring}(55)$
161		75	71	$\gamma_{ring}(55)$
162	64s	68	65	γCCC(54)
163		62	59	γCCC(54)
164		53	51	γCCC(50)
165		45	42	γCCC(52)
166		38	35	γCC(54)
167		30	29	γ CC(54)
168		25	23	$\gamma_{ring}(52)$
169		20	18	γCC(52)
170		15	14	γCC(52)
171		10	8	γCC(51)

s-strong, ms-medium strong, w-weak, vw-very weak, vs-very strong, v-stretching, v_{sym}-sym stretching, v_{ass}-asymstretching , δ -in-plane, δ _{inb}-in-plane bending. δ _{inr}-in-plane rocking, γ -out-of-plane, γ _{opb}-out-of-plane bending, γ _{ring}- out-of-plane ring, scis-scissoring, ρ _{scis}-in plane scissoring, w-wagging, rock-rocking, Γ -twisting, δ ring-ring vibration.

Table 4.4: Calculated E-HOMO, E-LUMO (H-1 \rightarrow L+1, H-2 \rightarrow L+2), energy gap (E_L-E_H), Ionization potential (I), Electron affinity (A), global hardness (η), electronegativity (χ), chemical softness (σ), chemical potential (μ) and global electrophilicity (ω) using the 6-311G levels of theory

Molecular	Energy	Energygap	(I)	(A)	(η)	(X)	(σ)	-(µ)	(ω)
properties	(eV)	(eV)	(eV)	(eV)	(eV)	(eV)	(eV)	(eV)	(eV)
E _{HOMO}	-6.4673								
$\mathbf{E}_{\mathbf{LUMO}}$	-2.8841	3.5832	6.4673	2.8841	1.7916	4.6757	0.558	-4.6757	6.1013
$\mathbf{E}_{\text{HOMO-1}}$	-6.7003								
$\mathbf{E}_{\text{LUMO+1}}$	-2.3211	4.3792	6.7003	2.3211	2.1896	4.5107	0.457	-4.5107	4.6461
$\mathbf{E}_{\text{HOMO-2}}$	-6.9990								
$\mathbf{E}_{\text{LUMO+2}}$	-1.2128	5.7862	6.9990	1.2128	2.8931	4.1059	0.346	-4.1059	2.9136

Table 4.5: Second-order perturbation theory analysis of Fock matrix in NBO basis corresponding to the intramolecular bonds of the title compound

Donor(i)	Type	ED/o	Acceptor	Type	ED/o	E(2) ^a	E(j)-E(i) ^b	F(i,j) ^c
Donor(i)	Type	ED/e	(j)	Type	ED/e	Kcal/mol	a.u	a.u
π	$(C_6 - C_9)$	1.66281	π *	$(C_4 - C_5)$	0.39139	21	0.28	0.069
π	$(C_6 - C_9)$	1.66281	π *	$(C_7 - C_{11})$	0.39379	22	0.26	0.068
σ	$(C_6 - H_{10})$	1.97641	σ*	$(C_4 - C_5)$	0.02245	5	1.06	0.064
π	$(C_7 - C_{11})$	1.67990	π *	$(C_4 - C_5)$	0.39139	18	0.3	0.066
π	$(C_7 - C_{11})$	1.67990	π *	$(C_6 - C_9)$	0.34219	19	0.3	0.069
π	$(C_{14} - C_{15})$	1.64735	π *	$(C_{16} - C_{19})$	0.34219	20	0.29	0.067
π	$(C_{14} - C_{15})$	1.64735	π *	$(C_{17} - C_{21})$	0.35984	19	0.29	0.067
π	$(C_{16} - C_{19})$	1.69021	π *	$(C_{14} - C_{15})$	0.39031	22	0.28	0.07
π	$(C_{16} - C_{19})$	1.69021	π *	$(C_{17} - C_{21})$	0.35984	21	0.29	0.071
π	$(C_{17} - C_{21})$	1.64735	π *	$(C_{14} - C_{15})$	0.39031	22	0.27	0.069
π	$(C17 - C_{21})$	1.64735	π *	$(C_{16} - C_{19})$	0.34219	20	0.28	0.067
σ	$(C_{29} - H_{38})$	1.84834	π *	$(C_{17} - C_{21})$	0.35984	12	0.46	0.07
σ	$(C_{29} - H_{38})$	1.84834	σ*	$(C_{30} - H_{34})$	0.01601	6	0.86	0.063
σ	$(C_{39} - S_{41})$	1.97925	σ*	$(N_{25} - C_{42})$	0.05277	8	1.43	0.096
π	$(C_{39} - C_{45})$	1.73334	π *	$(S_{41} - C_{42})$	0.63064	29	0.22	0.079
σ	$(C_{40} - N_{43})$	1.97841	σ*	$(N_{25} - C_{42})$	0.05277	6	1.16	0.077
π	$(C_{40} - O_{44})$	1.91434	LP (2)	N_{43}	1.92042	12	0.17	0.063
π	$(C_{40} - O_{44})$	1.91434	π *	$(C_{39} - C_{45})$	0.28300	9	0.27	0.047
π	$(S_{41} - C_{42})$	1.84834	LP (2)	N_{43}	1.92042	12	0.24	0.072
π	$(S_{41} - C_{42}))$	1.84834	π*	$(C_{39} - C_{45})$	0.28300	27	0.34	0.089

π	$(C_{46} - C_{48})$	1.65062	π*	$(C_{47} - C_{49})$	0.29371	19	0.29	0.067
π	$(C_{46} - C_{48})$	1.65062	π *	$(C_{51} - C_{53})$	0.37039	22	0.28	0.07
π	$(C_{47} - C_{49})$	1.64135	π*	$(C_{46} - C_{48})$	0.35121	23	0.28	0.071
π	$(C_{47} - C_{49})$	1.64135	π*	$(C_{51} - C_{53})$	0.37039	21	0.27	0.069
π	$(C_{51} - C_{53})$	1.65616	π*	$(C_{46} - C_{48})$	0.35121	19	0.29	0.066
π	$(C_{51} - C_{53})$	1.65616	π *	$(C_{47} - C_{49})$	0.29371	21	0.29	0.07
LP (1)	N_{43}	1.99948	σ*	$(C_{39} - C_{40})$	0.09788	6	0.79	0.064
LP (2)	N_{43}	1.92042	π*	(C ₄₀ - O ₄₄)	0.35013	77	0.16	0.112
LP (2)	N_{43}	1.24797	π *	$(S_{41} - C_{42})$	0.63064	144.68	0.1	0.112
LP (2)	O_{44}	1.97959	σ*	$(C_{39} - C_{40})$	0.09788	18	0.67	0.099
LP (2)	O_{44}	1.88072	σ*	$(C_{40} - N_{43})$	0.06721	22	0.65	0.108
LP (1)	N_{58}	1.96668	σ*	$(C_{53} - C_{57})$	0.03752	11	0.85	0.088
π*	$(C_1 - N_2)$	0.25467	π *	$(C_4 - C_5)$	0.39139	39	0.04	0.064
π*	$(C_7 - C_{11})$	0.39379	π *	$(C_4 - C_5)$	0.39139	215.88	0.02	0.084
π *	$(C_7 - C_{11})$	0.39379	π *	$(C_6 - C_9)$	0.29426	141.93	0.02	0.079
π*	$(C_{39} - C_{45})$	0.28300	σ*	(C ₄₀ - O ₄₄)	0.02004	32	0.06	0.07
π*	$(S_{41} - C_{42})$	0.63064	σ*	$(N_{24} - Ns_{25})$	0.03320	5	0.34	0.064

Table 4.6: Antibiotic and antifungal inhibition zone levels of CPTBN

SAMPLE	DMSO Extract 100 µl added and Zone of inhibition (mm/ml)							
SAMFLE	25 μl	50 μl	75 µl	100 μl	Control			
Bacillus subtilis	12	14	16	19	20			
Staphylococcus aureus	14	17	20	24	25			
E.coli	10	12	14	16	20			
Pseudomonas	11	12	14	16	20			
Candida albicans	13	15	17	20	22			
A.niger	12	14	16	19	20			

Table 4.7: Molecular docking performance results of the compound CPTBN against selective potential protein inhibitors (PDB)

					Inhibition		
Ligand name	PDB ID	Bond distance (Å)	Amino acid (residues)	Bond	Constant (Micromolar-	Binding Energy (kcal/mol)	Inter- molecular energy (kcal/mol)
		3.5	Glutamine (GLN)	van der Waals	IIIII))		
IBN	2gom	3.6	Lysine (LYS)	Pi-Cation	1.42 μΜ	-7.98	-9.47
(CP)	2gom	2.1	Tyrosine (TYR)	van der Waals			
rile (1.8	Isoleucine (ILE)	van der Waals			
onit	Arrid o				16.35nm	-10.62	-12.11
.) enz	4ydo	2.4	Leucine (LEU)	Pi-Alkyl			
enyl 1y1]b		2.9	Tyrosine (TYR)	Pi-Pi T-shaped			
l)ph neth		2.7	Proline (PRO)	Pi-Alkyl			
-2-y] ne}r		2.1	Leucine (LEU)	Conventional	404.34	7.27	0.74
pan lide	5i76	2.0	g : (GDD)	hydrogen bond	4.84 μΜ	-7.25	-8.74
(pro H)-y		2.9	Serine (SER)	van der Waals			
-(4-) -5(4)		2.9	Glutamine (GLN)	van der Waals			
yl)-5 azol		1.9	Isoleucine (ILE)	van der Waals			
heny -thia		2.4	Glycine (GLY)	van der Waals			
rop] -1,3	4d7o	2.9	Tryptophan (TRP)	Amide-Pi stacked	1.63 μM	-7.85	-9.34
4-Chlo]-4-oxo		3.3	Phenylalanine (PHE)	van der Waals			
$4-[\{2-[3-(4-Chlorophenyl)-5-(4-(propan-2-yl)phenyl) \\ azol-1-yl]-4-oxo-1, 3-thiazol-5(4H)-ylidene\} methyl] beginner a sol-1-yll-1-$		2.1	Phenylalanine (PHE)	Pi-Pi T-shaped			
4 pyra	1bdc	2.7	Asparagine(ASN)	van der Waals			
1111-]		2.8	Leucine(LEU)	Alkyl	428.64nm	-8.69	-10.18
$4-[\{2-[3-(4-Chlorophenyl)-5-(4-(propan-2-yl)phenyl)\\-4,5-dihydro-1H-pyrazol-1-yl]-4-0x0-1,3-thiazol-5(4H)-ylidene\}methyl]benzonitrile~(CPTBN)$		2.9	Serine(SER)	Conventional hydroden bond			
4,5 -d		2.8	Glycine(GLY)	van der Waals			

Spectroscopic identification, structural features and molecular docking studies on 5-(4-Propoxybenzylidene)-2-[3-(4-chlorophenyl)-5-[4(propan-2-yl) phenyl-4,5-dihydro-1H-pyrazol-1-yl]-1,3-thiazol-4(5H)-one using Pim-1 kinase cancer protein

Abstract

A comprehensive investigation of the molecular structure, electronic properties and vibrational spectra of 5-(4-Propoxybenzylidene)-2-[3-(4-chlorophenyl)-5-[4-(propan-2-yl) phenyl]-4,5-dihydro-1*H*-pyrazol-1-yl]-1,3-thiazol-4(5*H*)-one have been studied. Thiazol is one of the leading heterocyclic five-member ring compounds that contain one nitrogen and one sulphur atom. Many natural and/or synthetic compound contain thiazol which are attractive compounds found in the building of numerous natural products and certain pharmaceutical agents. To understand the molecular-orbital interaction and structural investigation of the title compound, the density functional theory (DFT) calculation has been imposed using the B3LYP/ 6-31G and 6-311G basis sets combination. The experimental FT-IR, FT-Raman spectral data along with theoretical quantum chemical calculation were investigated. For potential energy distributions (PED) analysis, the VEDA 4 program is utilized to do comparative frequency assignments. With the optimized structure, the highest occupied molecular orbital (HOMO) - the lowest unoccupied molecular orbital (LUMO) energies and Natural Bond Orbital (NBO) were applied to describe the chemical reactivity. The electron density interactions distributed in space, which exist within these compound is analyzed by different topological methods namely, atom in molecule (AIM), localized orbital locator (LOL), electron localization function (ELF) and the reduced gradient of the density(RDG). Finally, the molecular docking studies of the title compound for potent Pim-1 kinase cancer PDB ID: 3a99, 1gj8, 1xqz was investigated using the Auto Dock program.

CHAPTER - 5

Spectroscopic identification, structural features and molecular docking studies on 5-(4-Propoxybenzylidene)-2-[3-(4-chlorophenyl)-5-[4(propan-2-yl) phenyl-4,5-dihydro-1H-pyrazol-1-yl]-1,3-thiazol-4(5H)-one using Pim-1 kinase cancer protein

5.1 Introduction

Heterocyclic aromatic compounds containing nitrogen andsulphur are important molecules in organic chemistry synthesis [130,131]. Susithra et al. [132] reported when heterocycles are supposed to have hetero-nuclear atoms, they can be acted as an ideal ligand that can delocalize and thereby stimulate resonance hybridization to interact with strong intermediate to produce the anti-malarial drugs. The geometrical parameters such as bond lengths and bond angles of 5-(4-Propoxybenzylidene)-2-[3-(4-chlorophenyl)-5-[4-(propan-2-yl) phenyl]-4,5-dihydro-1*H*-pyrazol-1-yl]-1,3-thiazol-4(5*H*)-one have been obtained from B3LYP/6-31G and 6-311G basis sets. The global reactivity descriptors (ionization potential, electron affinity, electronegativity, electrophilicity index, global hardness, global softness, and chemical potential) have been predicted with the help of HOMO/LUMO energy values. Experimental FT-IR, FT-Raman spectra of the title compound were recorded and compared with the computed values obtained by the same levels of DFT with B3LYP functional.

Chemically interactive regions in the molecule have been concentrated through Aim in Molecule (AIM), Localized Orbital Locator (LOL), Electron Localization Function (ELF) and Reduced Density Gradient (RDG). Natural bond orbital (NBO) analysis have been performed to explain the conjugative interaction, donor, acceptor, and second-order perturbation of the compound. Also, based on a key factor in PASS online data allows to define a variety of medicinal potential. Attract attention by repetition in listening data and

then provide content of Pim-1 kinase inhibitors. The proto-oncogene proviral integration site for Moloney murine leukemia virus (PIM) kinases (PIM-1, PIM-2, and PIM-3) are serine/threonine kinases that are involved in several signalling pathways important in cancer cells [133-135]. This investigation aimed to evaluate the role of the Pim kinase inhibitor in ligand progression using molecular docking.

5.2 Experimental profile

The synthesized compound 5-(4-Propoxybenzylidene)-2-[3-(4-chlorophenyl)-5-[4-(propan-2-yl) phenyl]-4,5-dihydro-1*H*-pyrazol-1-yl]-1,3-thiazol-4(5*H*)-one has been taken without any further purification as per the procedure reported by V. V. Salian et al. [87] and spectroscopic grade for acquiring spectra. The FT-IR spectrum of the compound was recorded in a Perkin-Elmer spectrometer fitted with a KBr beam splitter covering 4000-0 cm⁻¹ region at a resolution of ±1 cm⁻¹. The FT-Raman spectrum of the chosen compound was measured using the Bruker RFS 27 model. The spectrum was captured in the 3500-0 cm⁻¹ Stokes region using the 1064 nm line of a Nd:YAG laser for the excitation operating at 200 mW power.

5.3 Computational details

The DFT computational method is widely used to describe the quantum states of many-electron systems of the molecule. The Gaussian 09W [20] program package was utilized to proceed with DFT calculations on the title compound through B3LYP/6-31G and B3LYP/6-311G basis sets to characterize the structure electronic and other properties. The geometrical parameters bond length and bond angles have been obtained using B3LYP/6-31G and 6-311G basis sets [15]. Further, the optimized ground state geometry of the title compound to study the different properties like FT-IR, FT-Raman, MEP surface mapping, and NBO analysis. Potential energy distribution (PED percent) calculations using VEDA4

software are used to analyze the theoretical vibrational wavenumber obtained for the molecule. [88] Frontier molecular orbital (FMOs) analysis (HOMO-LUMO) and molecular electrostatic potential (MEP) with contour map have been accomplished by GaussView 5.0 [31, 89] to obtain the electronic properties of the title compound. Multiwfn software [54] has also been utilized to obtain topology analysis (AIM, RDG, LOL, and ELF). To find out the various interactions amidst the filled and the vacant orbitals, NBO analysis [90] has been done using the NBO 3.1 program available in Gaussian 09 package at DFT /6-311G level of theory. Besides, molecular docking observations were visualized using pymol and Discovery studio software [57, 136]. The interactions of the title molecule with a Pim-1 kinase inhibitor PDB ID: 3a99, 1gj8, 1xqz receptors.

5.4 Results and discussion

5.4.1 Molecular geometry

Density functional theory is used to get optimized structure with bond length and angle values. The optimized geometrical parameters of the compound has been calculated by DFT-B3LYP functional method with 6-311G and 6-31G basis sets and atom numbering of title compound has been shown in Fig.5.1. The detailed experimental [87] and calculated bond length and bond angle were listed in Tables 5.1 and 5.2. According to optimized structure, the C-H bond length is observed at 1.08 -1.10 Å for phenyl ring and 1.09 Å for pyrazol ring using a theoretical approach by B3LPY/6-31G and B3LPY/6-311G. Experimentally, the C-H bond in phenyl ring has a bond length range of 0.93Å and 0.97-0.98 Å in pyrazol ring. This difference might be attributed to that low scattering factor of the hydrogen atom involved in the diffraction method [137]. The C-C bond lengths in all rings lie between the normal C-C single and C=C double bond lengths indicating the conjugation of electron density in all the rings [138]. It showed that the C-C bond lengths varied from 1.36 Å to 1.55 Å in B3LPY/6-31G/6-31IG and 1.29 Å to 1.52 Å in XRD, respectively.

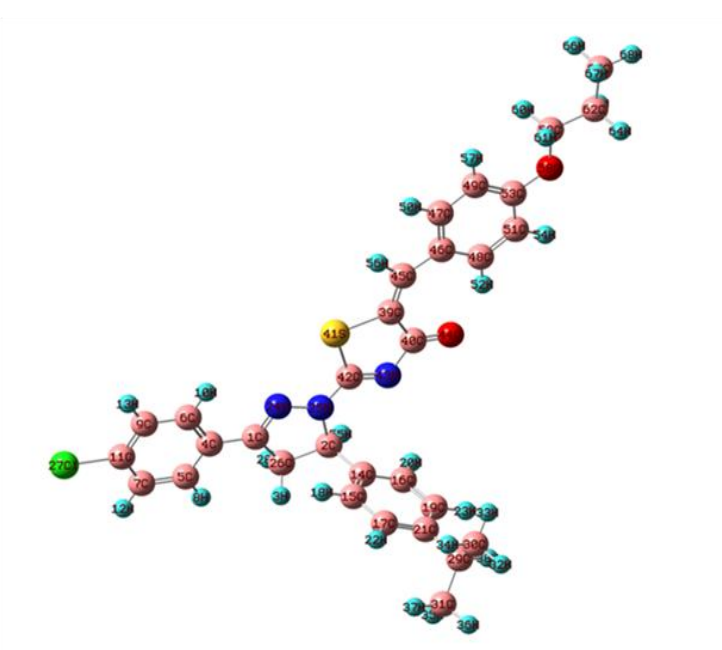


Fig. 5.1 Optimized structure of 5-(4-Propoxybenzylidene)-2-[3-(4-chlorophenyl)-5-[4(propan-2-yl) phenyl-4,5-dihydro-1H-pyrazol-1-yl]-1,3-thiazol4(5H)-one

The intermolecular distance of C_2 - C_{26} (1.56 Å /DFT, 1.54 Å /XRD) is higher than the other C-C atoms. This is because of the existence of a nitrogen atom (N₂₅) that is attached to the C₂ atom. The C-N bond length of pyrazol ring is C_2 -N₂₅ = 1.51 Å [DFT], 1.47 Å [XRD]. The C-N values in the thiazol ring, showed that the bond lengths for C_{42} -N₄₃ is 1.30 Å in both DFT/XRD, and C_{40} -N₄₃ are 1.41 Å in DFT and 1.38 Å in XRD. The bond length between carbon and sulphur atoms of the title molecule is found to be C_{39} -S₄₁₌1.87 Å and S₄₁-C₄₂= 1.84 Å, respectively. These values are suggesting that some multiple bond character is present in the thiazol ring [139]. Y.S. Mary reported that the C=O bond lengths (DFT/XRD) in the carbonyl group are 1.26 Å [140]. Similarly, the C_{40} =O₄₄ bond showed double bond character, with a bond length value of 1.25 Å by both basis sets B3LYP/6-31G/B3LYP/6-311G and 1.22 Å in XRD. The bond lengths of propoxybenzylidenein the title compound are, C_{62} - C_{65} =1.65 Å DFT, O_{58} - C_{59} =1.46 Å /DFT, C_{53} - O_{58} =1.39 Å /DFT which is well agree with reported values [141].

Normally, C-Cl bond length indicates a considerable increase in its length when compared with the C-H bond length [142]. From this observation, it is clear that the C_{11} - Cl_{27}

bond length of the title compound found at 1.82 Å and 1.83 Å using B3LYP/6-31G and 6-311G. The comparative analysis revealed that, except for a few values observed in DFT, calculated bond lengths are in good agreement with the literature values.

5.4.2 Vibrational assignments

In recent years, FT-IR and FT-Raman have been mostly used as vibrational spectroscopy for structural characterization of molecular systems through DFT calculations. The title compound is constituted by N=68 atoms and hence it has 3N-6= 198 normal modes of vibration. The observed and calculated wavenumber and potential energy distributions are discussed below. The fundamental modes of vibration were carried out and are depicted in Table 5.2. The theoretical and experimental FT-IR and FT-Raman spectra are given in Figs. 5.2 and 5.3, respectively.

C-H vibrations

Usually a C-H stretching vibration of the hetero-aromatic structure exits C-H stretching vibrations in the region of 3100-3000 cm⁻¹ [142]. The characteristic zone for the identification of the C-H stretching vibration is affected by the nature of substituent group interaction. In the present study, the C-H stretching vibrations are spotted at 3070 cm⁻¹ and 3040 cm⁻¹ in the FT-IR spectrum. The scaled frequency of C-H stretching bands have been obtained in the range of 3091-3018 cm⁻¹ in B3LYP/6-31G and 3082-3014cm⁻¹ in B3LYP/6-31IG basis sets. The hetero-aromatic configuration reveals the presence of C-H stretching, in-plane and out-of-plane bending vibrations in the range of 3200-3000 cm⁻¹, 1200-900 cm⁻¹ and 980-700 cm⁻¹ [142, 143]. In the title compound, the medium strong bands at 1264 cm⁻¹ in the FT-IR spectrum and at 1125 cm⁻¹ in the FT-Raman spectrum were assigned as C-H in-plane-bending vibrations. Corresponding computed wavenumbers for this modes were

Fig. 5.2 Observed FT-IR and simulated spectra of 5-(4-Propoxybenzylidene)-2-[3-(4-chlorophenyl)-5-[4(propan-2-yl) phenyl-4,5-dihydro-1H-pyrazol-1-yl]-1,3-thiazol4(5H)-one

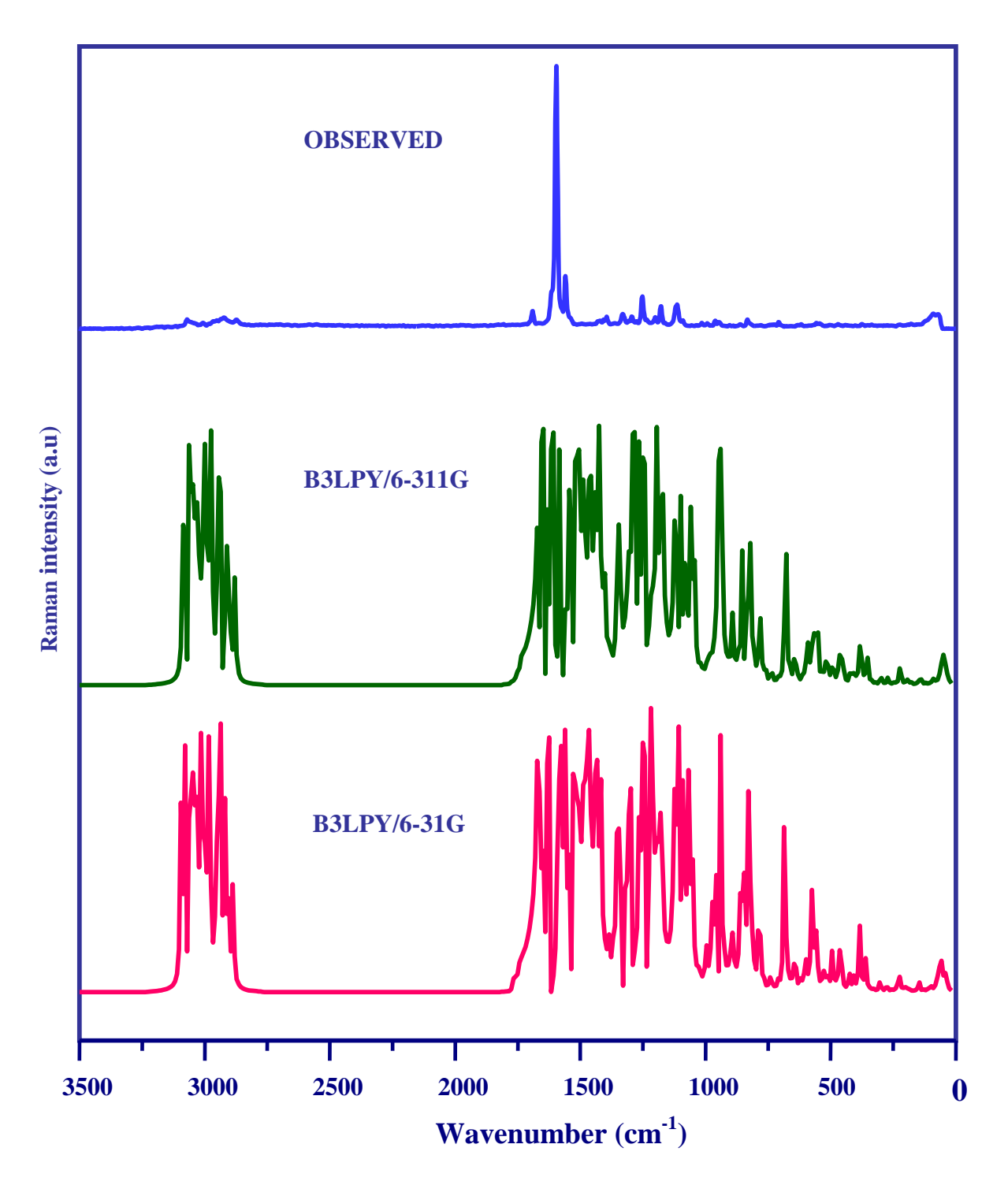


Fig. 5.3 Observed FT-Raman and simulated spectra of 5-(4-Propoxybenzylidene)-2-[3-(4-chlorophenyl)-5-[4(propan-2-yl) phenyl-4,5-dihydro-1H-pyrazol-1-yl]-1,3-thiazol4(5H)-one

1263, 1257, 1203, 1190, 1118, 1153, 1144, 1139 and 1127 cm⁻¹ by B3LYP/6-311G. The C–H out-of-plane bending vibrations are observed as a weak bands at 994, 860, 618, 569 and 536 cm⁻¹ in FT-IR spectrum and at 1000 and 950 cm⁻¹ in FT-Raman spectrum. Thus, the theoretically evaluated values for C–H vibrational modes are in good agreement with the experimental data.

CH₃ vibrations

In the title compound, there are three -CH₃ groups (two attached to the phenyl and one oxybenzylidene ring). Generally, there are nine fundamental modes of vibrations in CH₃ they are symmetrical stretching, asymmetrical stretching, in-plane stretching, out-of-plane stretching, symmetric deformations, asymmetrical deformations, in-plane rocking, out-ofplane rocking and twisting [3, 109]. In the present case, the stretching vibration of the CH₃ group in FT-IR spectrum at 2961 (ms) cm⁻¹was classified as asymmetric, while vibration found at 2929 cm⁻¹ were assigned as symmetric stretching vibration. Theoretically assigned, asymmetric stretching vibration of the title compound calculated in the range of 3012-2970 cm⁻¹ in (B3LYP/6-31G) and 3008-2963 cm⁻¹(B3LYP/6-311G). The CH₃ symmetric stretching mode appeared in the region 2930-2909 cm⁻¹(B3LYP/6-31G) and 2924-2903 cm⁻¹ (B3LYP/6-311G). The in-plane bending vibrations of the CH₃ group were experimentally obtained at 1494 cm⁻¹ in FT-IR spectrum and 1440 cm⁻¹ in FT-Raman spectrum, which are well agree with a literature value [144]. The calculated out-of-plane and in-plane bending vibrations of the title compound were identified in the region 1521-1438 cm⁻¹ (B3LYP/6-31G) and 1519-1435 cm⁻¹ (B3LYP/6-311G). The two in-plane rocking deformations of the -CH₃ group was calculated at 908, 895cm⁻¹ by B3LYP/ 6-31G and 903, 891 cm⁻¹ by B3LYP/ 6-311G, respectively, corresponding experimental values are found 904 cm⁻¹ in FT-IR spectrum and 900 cm⁻¹ FT-Raman spectrum.

CH₂ vibrations

There are six fundamental modes of vibrations in CH₂ group. They are asymmetric stretching, symmetric stretching, scissoring, rocking, wagging and twisting [137]. V.Arjunan et al. [145], reported that the symmetric methylene group stretching vibration observed at 2922 cm⁻¹ in FT-IR spectrum. In our investigation, the CH₂ symmetric stretching mode observed at 2936 cm⁻¹ in FT-IR spectrum, 2941 cm⁻¹ in B3LYP/ 6-31G and 2938 cm⁻¹ in B3LYP/ 6-311G. Asymmetric stretch ν_{ass} CH₂ was predicted theoretically at 3000, 2990 cm⁻¹ in B3LYP/ 6-31G and 2996, 2985 cm⁻¹ in B3LYP/ 6-311G basis sets. The rocking (σ_{rock}) mode is assigned at 1288 cm⁻¹ in both FT-IR spectrum and FT-Raman spectrum, and the corresponding theoretical value at 1294 cm⁻¹ (B3LYP/6-31G), 1290 cm⁻¹ (B3LYP/6-311G).

The CH_2 wagging (γ_{wagg}) mode is observed at 1175 cm⁻¹ in both FT-IR and FT-Raman spectra. The twisting vibrations of CH_2 is identified at 1180 cm⁻¹ in FT-IR spectrum, 1245 cm⁻¹ in FT-Raman spectrum and 1245, 1186cm⁻¹ in B3LYP/6-31G and 1233, 1182cm⁻¹ in B3LYP/6-311G basis sets.

C-C vibrations

The phenyl ring carbon-carbon stretching vibrations usually occur in the region 1625–1100 cm⁻¹ [146]. In present case, C–C vibrations found at 1596(vs) cm⁻¹ in the FT-Raman spectrum and at 1599(s), 1233(s) cm⁻¹ in the FT-IR spectrum and theoretically it was found in the range of 1631-1585 cm⁻¹, 1234 cm⁻¹ using B3LYP/6-31G and 1625-1581 cm⁻¹, 1235 cm⁻¹ using B3LYP/6-311G basis set. The in-plane and out-of-plane C-C-C bends are reported as 651-509 cm⁻¹ and 477-282 cm⁻¹ respectively [147]. Likewise, the in-plane theoretical values are obtained at 494, 475 cm⁻¹ (B3LYP/6-31G) and 490, 472 cm⁻¹ (B3LYP/6-311G). The experimental out-of-plane C-C bending vibrations are found at 78 cm⁻¹ in FT-IR spectrum. Here in this study, the observed theoretical frequencies

were assigned in 89-9 cm⁻¹ from B3LYP/6-31G and 80-6 cm⁻¹ from B3LYP/6-311G. Further, the ring C-C bending vibrations of theoretical scaled frequency have been mixed with other vibrations. These modes have widely appeared below the 600 cm⁻¹ wavenumber range. The band at 827(w) cm⁻¹ in FT-IR and 832(w) cm⁻¹ in FT-Raman was assigned as C-C ring breathing vibrations and DFT wavenumbers are computed to be 834 cm⁻¹ and 830 cm⁻¹, these are compatible with reported data [148].

C=O and C-O vibrations

In the present investigation oxygen substitution were observed with C4(C₄₀) position of thiazole and aromatic substitution at the *para* position of benzene (oxybenzylidene). The measurement of the C-O band is difficult due to the interfering with many other vibrations. The C=O stretching vibration exhibits a strong band in the region 1600–1750 cm⁻¹ and C –O stretching vibrations are in the region 1300-100 cm⁻¹ [149]. On comparing the present investigation with the above literature, the medium strong band stretching mode of C=O is assigned at 1692 cm⁻¹ and C-O is assigned at 1017 cm⁻¹ in the FT-IR spectrum. The theoretical frequencies by B3LYP/6-31G are 1650, 1024 cm⁻¹ and 1643, 1016 cm⁻¹ by B3LYP/6-311G. Experimentally, C=O out-of-plane vibration modes were observed at 756 cm⁻¹ in FT-IR spectrum. The corresponding computedvibrations were assigned at 769, 763, 446, 214, 183 and 148 cm⁻¹ by B3LYP/6-31G and 765, 759, 441, 208, 175, 140 cm⁻¹ by B3LYP/6-311G.

C-Cl vibrations

Generally, the C-Cl in-plane ($_{\delta}$) and out-of-plane ($_{\gamma}$) bending vibrations appears in the lower frequency region. Because the chlorine atom has a higher electronegativity than the carbon atom, the bonding electrons in the C-Cl bond will be closer to the chlorine than the carbon, increasing the force constant and causing a frequency shift [148]. In the present study, the predicted in-plane ($_{\delta}$) bending vibration is assigned at 648 cm⁻¹ for B3LYP/6 31G

and 643 cm⁻¹ for B3LYP/6-311G. The out-of-plane (γ) bending vibrations have been assigned at 818, 373 cm⁻¹ for B3LYP/6-31G and 815, 372 cm⁻¹ for B3LYP/6-311G by theoretically.

C-S vibrations

Identification of C –S stretching vibrational mode of amoleculeis a difficult task. The absorption of this group is of variable intensity which can be found in a wide range of 1035–245 cm⁻¹ in both aliphatic and aromatic sulphides [150]. In the title compound, the experimentally (FT-IR) vibration at 950 cm⁻¹ found was assigned as C-S stretching vibration. Theoretical the stretching of the C-S band in the thiazole ring was found at 995 cm⁻¹ in B3LYP/6-31G and 950 cm⁻¹ in B3LYP/6-311G. The C-S out-of-plane bending vibration was observed at 809, 796 cm⁻¹ in B3LYP/6-31G and 806, 792 cm⁻¹ in B3LYP/6-311G basis sets.

C-N, C=N and N-N vibrations

In general, identifying C=N and C-N vibrations was challenging because mixing of several bands appeared. Silverstain et al. [151] reported that the C-N stretching absorption is appeared in the region of 1689-1417 cm⁻¹ for aromatic compounds. The C=N stretching vibrations is found experimentally at 1400cm⁻¹ in FT-Raman spectum, theoretically assigned at 1403 cm⁻¹ in the B3LYP/6-31G and 1400 cm⁻¹ B3LYP/6-31IG basis sets. The N-N stretching vibration of the title compound was calculated at 1091cm⁻¹ in B3LYP/6-31G, 1085 cm⁻¹ in B3LYP/6-31G basis sets [152], respectively.

5.4.3 Global reactivity descriptors

The highest occupied molecular orbital (HOMO) and lowest unoccupied molecular orbital (LUMO) are fundamental standard parameter in quantum chemical calculation, They are also, called as frontier molecular orbitals (FMOs). The FMOs portray the moleculestability, and it plays a significant role in computing the molecular electrical

transport properties. E_{HOMO} and E_{LUMO} are frequently illustrating negative pictorial stabilization of the compoundsby green-red isosurface which clearly explain the charge transfer mechanism.

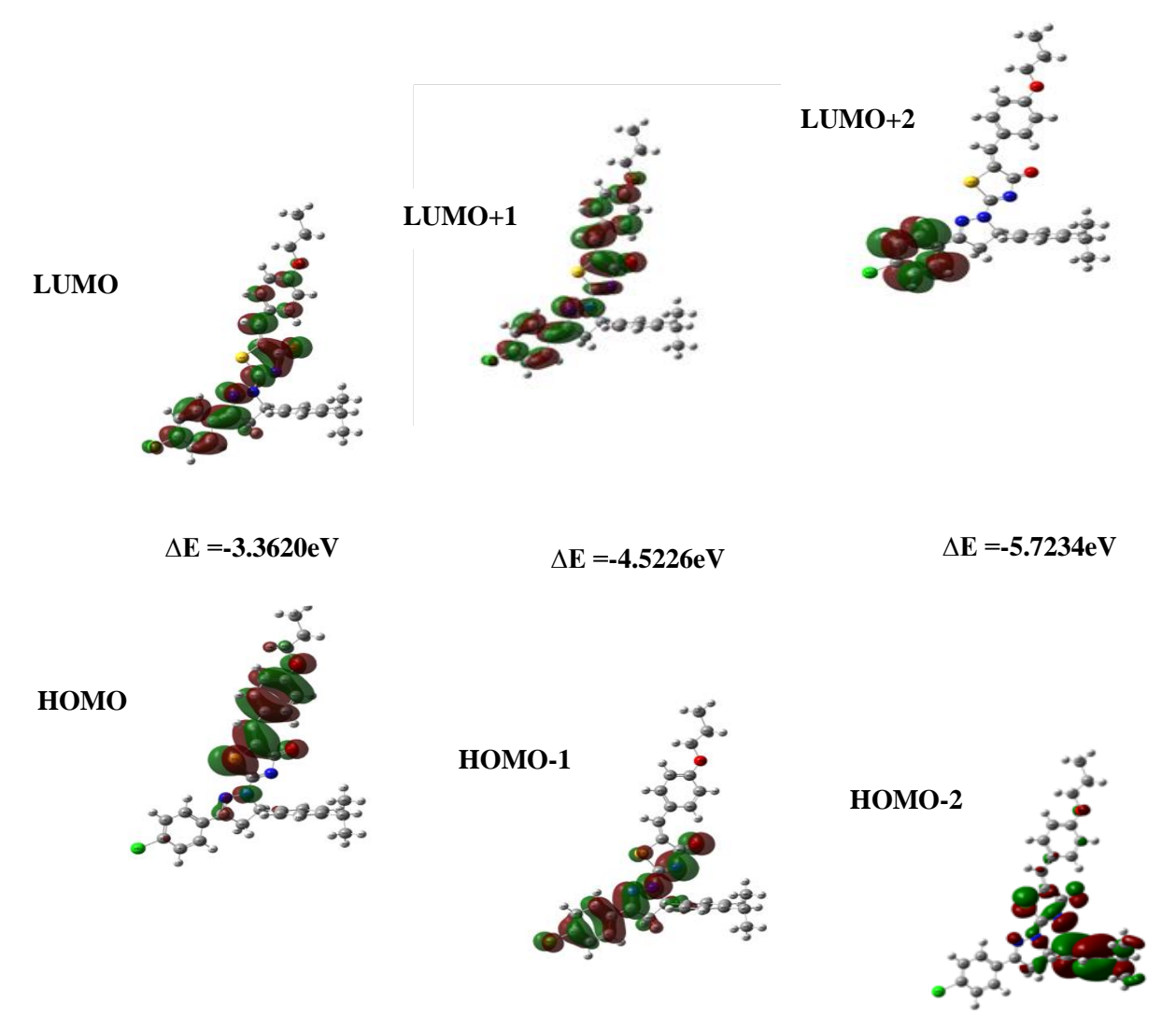


Fig. 5.4 HOMO - LUMO energy gap distribution plots of 5-(4-Propoxybenzylidene)-2-[3-(4-chlorophenyl)-5-[4(propan-2-yl) phenyl-4,5-dihydro-1H-pyrazol-1-yl]-1,3-thiazol4(5H)-one at DFT/B3LPY/6-311G basis set

The combination between these orbitals are important in various responses to describe the kinetic stability and chemical reactivity of amolecule. In our analysis, we found that the title compound has a total of 600 orbitals out of which 143 are occupied and the remaining 457 are virtual orbitals. The orbitals numbered 143 and 144 account for HOMO and LUMO orbitals. From the basis set B3LYP/6-31G the FMO energy gap of studied

molecule is HOMO= -5.5198 eV, LUMO= -2.1701 eV, energy gap ΔE =-3.3497 eV and B3LYP / 6-311G basis set is HOMO= -5.7563 eV, LUMO= -2.3943 eV, energy gap ΔE =-3.3620 eV. Bandgap energy values (H-1 \rightarrow L+1, H-2 \rightarrow L+2) of compound are found to be -4.5226 eV and -5.7234 eV (Fig. 5.4), respectively. The ionization potential $I = -E_{HOMO}$ with electron affinity $A = -E_{LUMO}$, electro-negativity $\chi = (I + A)/2$, chemical potential $\mu = -(I + A)/2$ with hardness $\eta = (I - A)/2$, softness $\sigma = 1/\eta$, electrophilicity index $\omega = \mu^2/2\eta$ of the title compound have been estimated theoretically [14] and the corresponding values are tabulated in Table 5.4.

5.4.4 Molecular electrostatic potential (MEP)

MEP is used to the visualize electron density of the molecule and is a very useful tool in recognizing sites for electrophilic and nucleophilic reactions. The electrostatic potential V(r) is identified as the energy collaborated between the charges formed by protons, electrons and nuclei existing in a given dimension [153, 154].

Using the Gaussian 09 programme, we reported and showed the MEP surface mapping, alpha density, and total density of the title molecule [20]. Potential increases in the following sequence: red, orange, yellow, green, blue, green. Electrophilic regions were associated to the negative (red and yellow) sectors of MEP, however nucleophilic regions are correlated to the positive (green and blue) parts. In present case, the negative charge covers the carbonyl group on the thiazole ring and propoxybenzylidene, the positive charge occupies all hydrogen atoms in the molecule, and the neutral zone encompasses the remaining groups, Fig. 5.5 illustrates the MEP and alpha density of the title molecule.

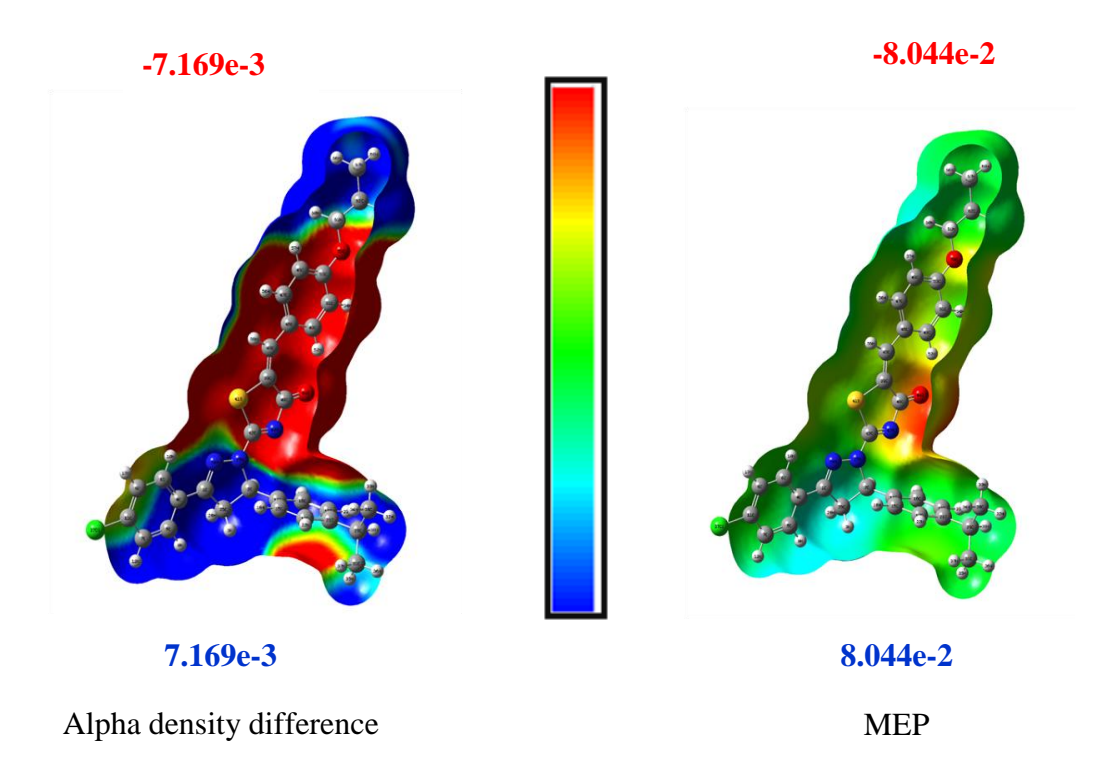


Fig. 5.5 Alpha density difference(e-3), and MEP(Molecular electrostatic potential surface) of 5-(4-Propoxybenzylidene)-2-[3-(4-chlorophenyl)-5-[4(propan-2-yl) phenyl-4,5-dihydro-1H-pyrazol-1-yl]-1,3-thiazol4(5H)-one

5.4.5 NBO analysis

Natural Bond Orbital analysis [54] is used to understand the intermolecular and intramolecular interactions of atomic bonds leading to the stability of the molecule. This study examines all conceivable interactions between "full" (donor) Lewis-type NBOs and "empty" (acceptor) non-Lewis NBOs, and uses second-order perturbation theory to quantify their energy significance. The hybridization of atoms involved in bonding orbitals and atomic lone pairs can really be accessed via NBO analysis. For each donor (i) and acceptor (j), the stabilization energy E (2) associated with the delocalization $i \rightarrow j$ is estimated as equation 5.1: $E(2) = \Delta E_{ij} = q_i \frac{(F_{i,j})^k}{(E_{ij} - E_i)}$ (5.1)

where q_i is the donor orbital occupancy, E_i and E_j are diagonal elements and $F\left(i,j\right)$ is the off-diagonal NBO element. The intramolecular charge transfer interactions for the most

significant stabilization energies E (2) were obtained from the NBO calculations. The larger the E (2) value shows the intensive interaction between electron-donors, electron-acceptors, and the greater extent of conjugation [155, 156] of the whole system are presented in Table 5.5. The most important hyper conjugative interaction of the title compound is bonding to lone pair π (C39-C45) \rightarrow LP (2) S41 showed the stabilization energy of 540.23 kcal/mol. The delocalization of π * electron from anti-bonding distributed to anti-bonding showed the high stabilization energy between π *(C7-C11) \rightarrow π *(C4-C5) with 195.69 kcal/mol energies. Lone pair of sulphur LP (2) S41 is distributed to antibonding π *(C42- N43) showed the stabilization energy of 99.8 kcal/mol. This electron distributed energy has been observed and listed in Table 5.5 as a result of occupational interaction.

5.4.6 Topology analysis

Atoms in molecules (AIM)

The quantum theory of atoms in molecules (AIM) is a useful tool for the characterization of hydrogen bonding, intra- inter molecular interactions within the molecule [157, 158]. The chemical structure of an element is identified using critical point's (CP's). The type of critical point described as: (3, -3) nuclear critical point (NCP); (3, -1) bond critical point (BCP); (3, +1) ring critical point (RCP); and (3,+3) cage critical point (CCP). The number and type of critical points that can coexist in a molecule or crystal follow a strict topological relationship which states equation (5.2) that:

$$n_{NCP} - n_{BCP} + n_{RCP} - n_{CCP} = \begin{cases} 1(Isolated-molecules) \\ 0(Infinite-crystals) \end{cases}$$
 (5.2)

where 'n' denotes the number of the subscripted type of CP. The topology relationship of anisolated system is known as the Poincare –Hopf relationship (PH). The topology analysis of the compound displays 68 (3,-3) nuclear critical points, 73 (3,-1) bond critical points (BCPs) between attractive pairs and 6 (3,+1) ring critical points corresponding to π - π

interactions. One bond critical point is associated with a very weak (O44-C40-C39-C45-C45-C48-H52) hydrogen bonding interaction. When these lines showed that the Poincare-Hopf relationship is satisfied, we can see all expected CPs are presented, hence we can confirm that all CPs have been found.

$$(3, -3)$$
: $68, (3, -1)$: $73, (3, +1)$: $6, (3, +3)$: 0
 $68 - 73 + 6 - 0 = 1$

From Multiwfn we can calculate the energy of the hydrogen bond by a relationship between bond energy E_{HB} (equation 5.3) and potential energy density $V(r_{BCP})$ at corresponding BCP as

$$E_{HR} = V(r_{RCP})/2 \tag{5.3}$$

The energy of the hydrogen bond O44-C40-C39-C45-C46-C48 -H52 was calculated to be 46.60 kcal/mol. Magenta, orange, and yellow spheres correspond to (3,-3), (3,-1), and (3,+1) critical points and bond path is pictured in Fig.5.6 (a). The indices of CPs are labeled by cyan numbers. The yellow sphere and line denoted between the green colour bond path showed that the index 117 corresponds to the bond critical point (BCP) of O-C----H hydrogen bond, respectively. AIM maps of the hydrogen bond region are presented in Fig. 5.6 (b).

Localized orbital locator (LOL) and electron localization function (ELF)

The topologies of the localized orbital locator (LOL) and electron localization function (ELF) are investigated by electron density to elucidate cores and the valence shell of the atoms. To define Fermi hole curvature Becke and Edgecombe proposedthat the local scalar function V(r) showed the excess kinetic energy of the Pauli repulsion regions (absence of LOL). Extensively, Savin and Silvi [42,158] explained the two main types of

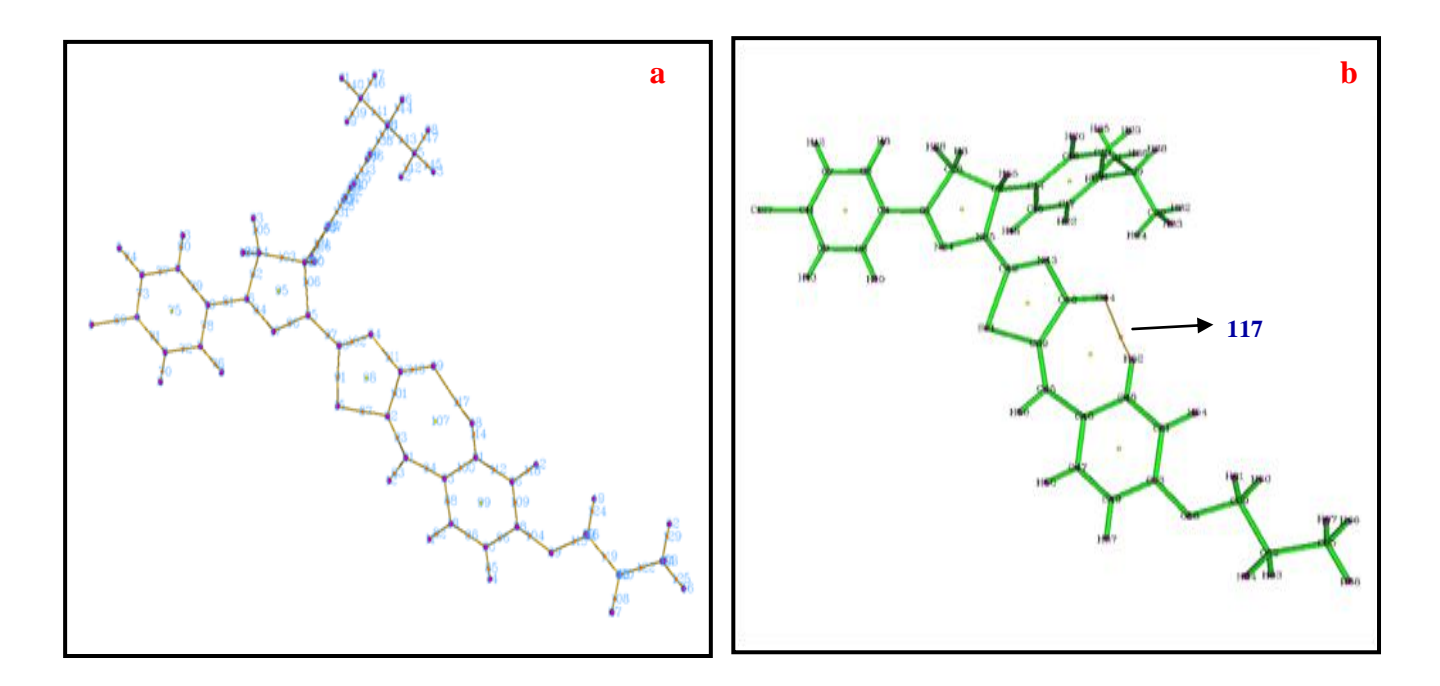


Fig. 5.6 AIM critical point maps of the 5-(4-Propoxybenzylidene)-2-[3-(4-chlorophenyl)-5-[4(propan-2-yl) phenyl-4,5-dihydro-1H-pyrazol-1-yl]-1,3-thiazol4(5H)-one bonding region

localized orbital locator (LOL) showed the surface topology of the interaction bond path. The carbon and nitrogen core present in the compound is represented by the red-dot blue ring, inner shell is represented by red-dot yellow ring and the path electrons' delocalization is represented by greenish-yellowcolour which is shown in Fig. 5.7 (a). The axis's of the LOL limits from 0.00 to 1.00. Fig.5.7 (b) ELF isosurface showed the relation between LOL and ELF regions of the title compound. From electron localization function (ELF) analysis, it finds the positions of isosurface, shared and unshared in space where ELF is maximum, and to use the value of ELF in these points. By defining the electron localization (ELF) gradient in terms of η by the mapping its values are between $0 \le \eta \le 1$:The value of ELF and $\eta(r)$ ranges from 0.0 to 1.00, the values in the interval 1.00to 0.5 indicates regions containing bonding and anti-bonding localized electrons, whereas the values less than 0.5 describe the domains where electrons are expected to be delocalized. High electron

localization zones between core and lone pairtovalence atoms are revealed by the red ring-like region around each hydrogen, chlorine (LP) and oxygen (LP) atoms. Colour shade maps or contour maps of bonding regions are present in Fig.5.7 (c). High ELF values (approximately 0.600 to 1.00 Bohr unit) are coloured red; the colour range from yellow to green are middle denoted region 0.60 to 0.40 Bohr unit and the lower end regions below 0.4 Bohr unit are represented by blue.

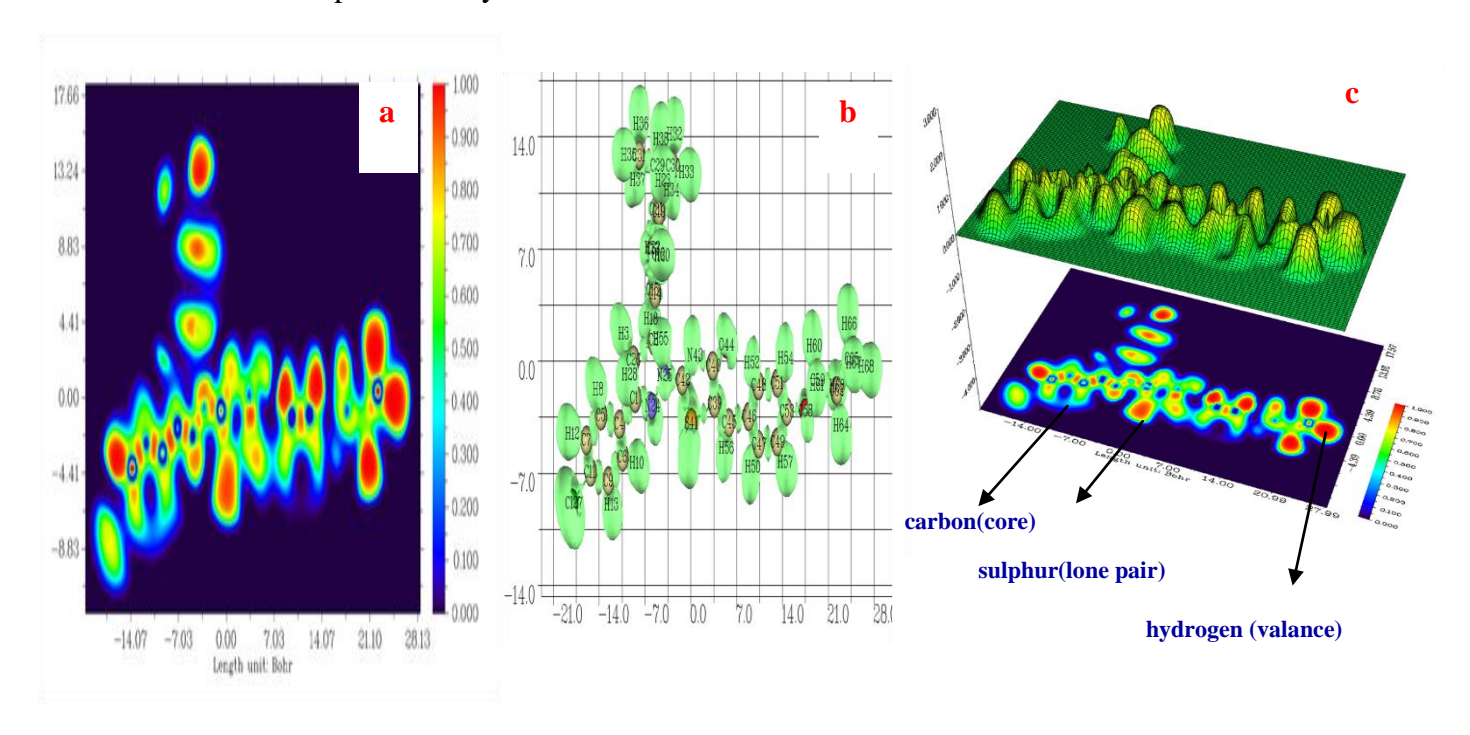


Fig.5.7 a) LOL b) ELFisosurface and c) ELFregion of 5-(4-Propoxybenzylidene)-2-[3-(4-chlorophenyl)-5-[4(propan-2-yl) phenyl-4,5-dihydro-1H-pyrazol-1-yl]-1,3-thiazol4(5H)-one

Reduced density gradient analysis (RDG)

The non-covalent interactions (NCI) method is used to detect NCI in real space [159]. This method enables the identification of NCI as isosurfaces of the reduced density gradient RDG (r) in equation 5.4:

$$RDG(r) = \frac{1}{2(3\pi r^2)^{1/2}} \frac{|\nabla \rho(r)|}{\rho(r)^{4/3}}$$
 (5.4)

These isosurfaces expand over large regions of space containing interacting atoms. This approach recovers a more intuitive picture of van der Waals's interactions, hydrogen bonds, and steric repulsions than other local pairwise approaches, such as atoms in molecules (AIM) theory, or the electron localization function (ELF). The application of the reduced density gradient to visualize interacting regions was motivated by the deviations from the exponential behaviour observed when RDGis plotted versus $\rho(r)$ for interacting systems [160]. The value of Hessian matrix of electron density is used to find the nature of an interaction. [$\lambda_2 > 0$, for non bondedand $\lambda_2 < 0$ for bonded].

In this graph, blue colour indicate the hydrogen bonding interaction, the green colours are van der Waals interactions and the red colours are identified as strong repulsion. From Fig.5.8, the van der Waals interaction is the predominant factor as electrostatic interaction in the molecule. The isosurface of the title compound mixed system displays very strong van der Waals interaction with strong steric effect as repulsive interaction and weak hydrogen bonding interaction. Moreover, hydrogen and van der Waals regions are more impacted by the presence of propoxybenzylidene moiety.

5.4.7 Molecular docking

To explore the biological activity of the title molecule, molecular docking simulations have been performed using Auto Dock/Vina software [66]. Docking has become a standard technology in drug discovery to virtually screen libraries of existing or hypothetical chemicals to identify new active chemo-types that bind to predict the target

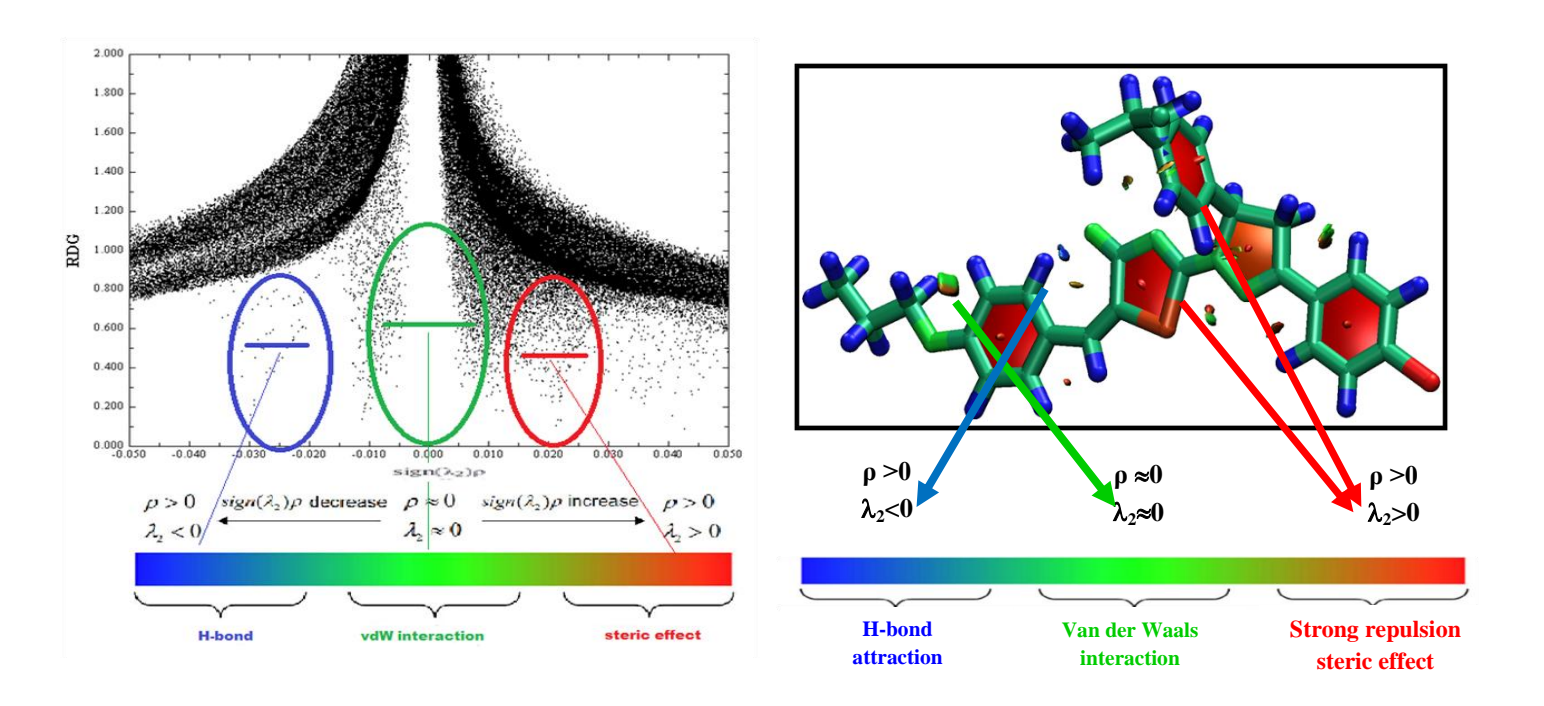


Fig. 5.8 Reduced density gradient 2D and 3D of 5-(4-Propoxybenzylidene)-2-[3-(4-chlorophenyl)-5-[4(propan-2-yl) phenyl-4,5-dihydro-1H-pyrazol-1-yl]-1,3-thiazol4(5H)-one

binding modes of protein and to point out the active site of ligands. PASS [161] is an online tool that predicts different types of activities based on the compound structure. PASS analysis of the title compound predicts several activities, amongst other activities choosing Pim-1 kinase inhibitor activity with Pa (probability to be active) and Pi (probability to be inactive) values are listed in Table 5.6. Pim kinases are emerging as important mediators of cytokine signaling pathways in hematopoietic cells, and they contribute to the progression of certain leukemias and solid tumors [162]. Based on this, we decided to carry the molecular docking simulation of the title compound bind with the human Pim-1 kinase enzyme. The 3D structure of proteins obtained from Protein Data Bank (PDB ID: 3a99, 1gj8, 1xqz) has a good resolution. Auto Dock Tools (ADT) graphical user interface was used to add polar hydrogen and to calculate atomic charges by Kollman method. Water molecules and co-crystallized ligands were removed. The optimized structures of ligands PDB were obtained using the DFT (B3LYP) theory with the 6-311G basis set on Gaussian 09. Partial charges were calculated by the Geistenger method. The active site to the energies was defined to add residues of the active sites with the use of grid sizes 126Å×126Å×126Å

using Auto grid [62]. AutoDock binding affinity (kcal/mol), inhibition constants, and nature of the bond with residues were computed and the best lowest energy docked positions of the ligand with target protein are illustrated in Table 5.7 and Figs. 5.9 (a) and 5.9 (b).

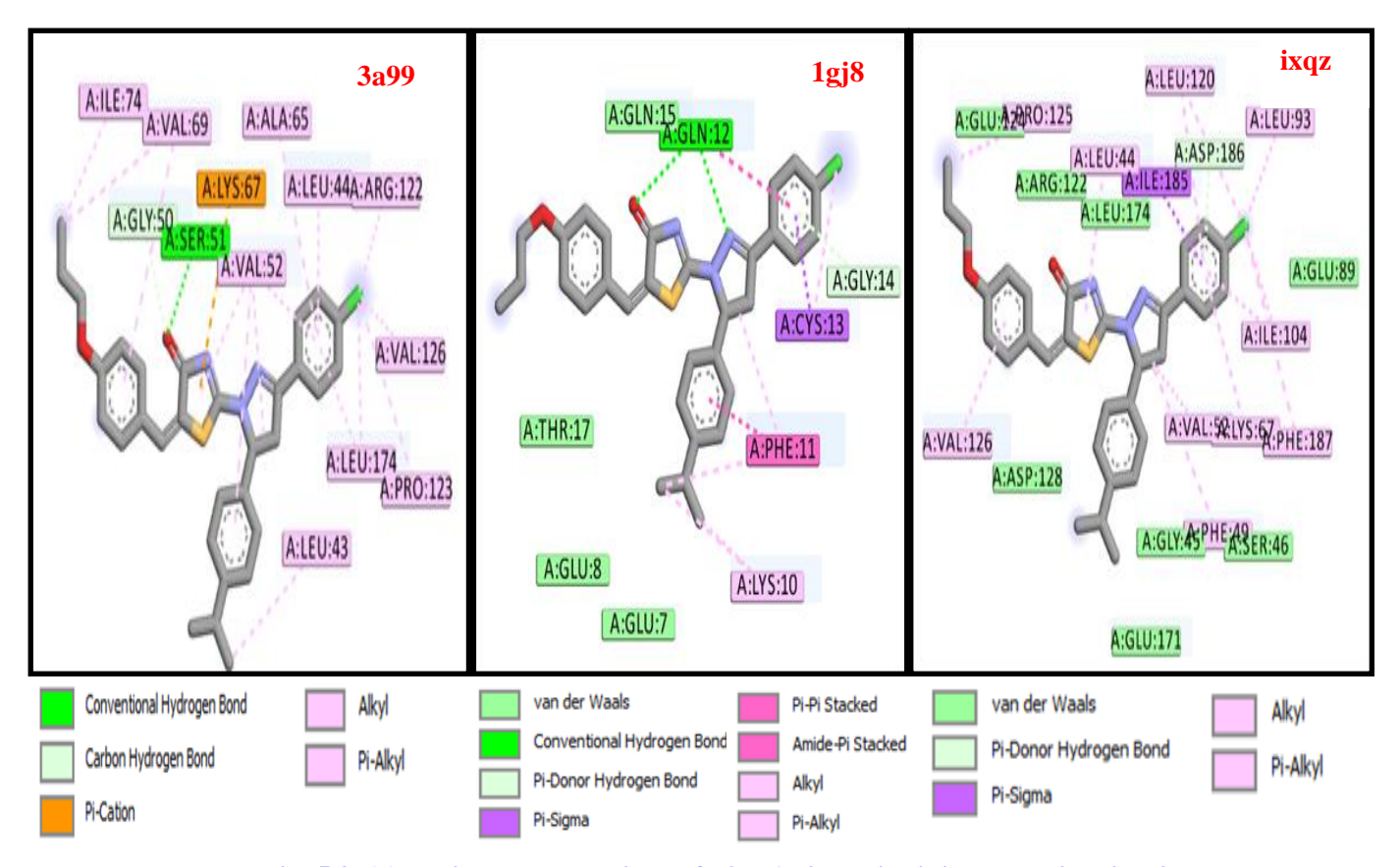


Fig. 5.9. (a) Residues Interactions of Pim-1 kinase inhibitor protein with ligand (PCPPT)

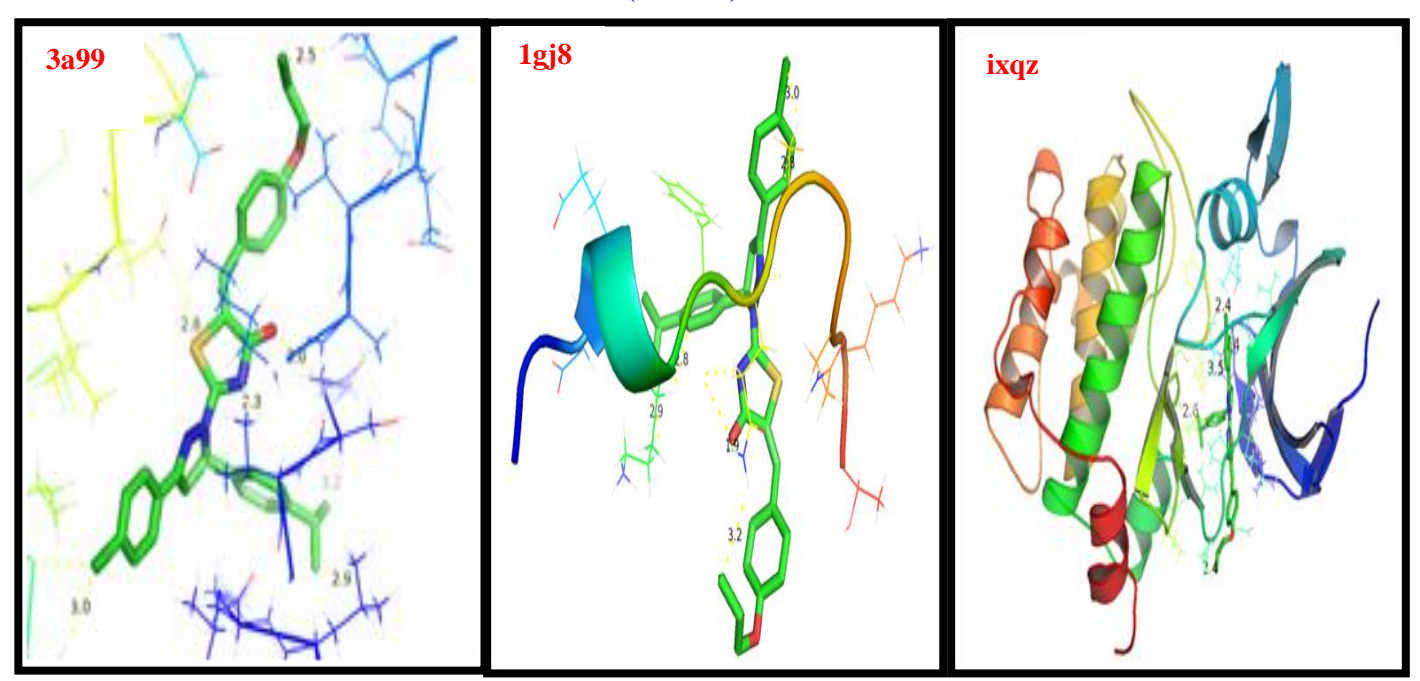


Fig. 5. 9. (b) Docked position values of Pim-1 kinase inhibitor protein with ligand (PCPPT)

The bond interactions present in the title compound are Pi-alkyl, carbon-hydrogen bond, conventional hydrogen bond and Pi-cation. 3a99 interaction with amino acid forms Alkyl (2.5 Å; ILE A:74, 3.0 Å; VAL A:174) having various binding energies of -9.23, -9.13 and -9.01 kcal/mol. The inhibition constant values are identified as 170.15 nM, 201.86 nM, 248.98 nM and RMSD value are 81.47 Å, 83.69 Å and 82.21 Å. The result of 1gj8 encircled by residues Pi-sigma (2.8 Å, CYS A:13), conventional hydrogen bond (1.9 Å, GLN A:12), and Alkyl (2.9 Å, LYS A:10). It has a docking score of -6.98, -6.95, -6.90 kcal/mol respectively. The inhibition constant values are identified as 7.65 μM, 19.13 μM, and 12.09 μM and RMSD value are 26.16 Å, 26.28 Å and 26.31 Å, respectively. The prediction of 1xqz insight the potent of Pim kinase inhibitor docked with ligand shows van der Waals (2.6 Å, GLN A:171), Alkyl (2.4 Å, PRO A:125; 2.4 Å, LEU A: 93; 2.4 Å, LYS A: 67) interactions which can provide some binding energies of -9.14, -9.01 and -7.83 kcal/mol. The inhibition constant values are identified as 201.35 nM, 249.97 nM, and 1.82 μM. The RMSD values are 77.89 Å, 79.25 Å, and 55.22 Å, respectively.

5.8 Conclusion

FT-IR and FT-Raman spectrum of 5-(4-Propoxybenzylidene)-2-[3-(4-chlorophenyl)-5-[4-(propan-2-yl) phenyl]-4,5-dihydro-1*H*-pyrazol-1-yl]-1,3-thiazol-4(5*H*)-one were recorded and studied by both experimentally and theoretically. The vibrational wavenumber was computed using B3LYP/6-31G and B3LYP/6-31IG basis sets. The HOMO and LUMO analysis are used to determine the charge transfer and the chemical activity of the molecule. From the molecular electrostatic potential, it is evident that the negative charge covers the carbonyl group, positive charge covers hydrogen atoms in the propoxybenzylidene, the neutral region is covered over the remaining groups and showed the more electronegativity in the carbonyl group makes it most reactive part of the compound. The stability of the molecule arising from hyper-conjugative interaction and charge delocalization has been

studied using NBO analysis. AIM analysis confirmed the presence of an intramolecular hydrogen bond between O44-H27---N14 with energy of 46.60 kcal/mol. The surface electron density core, lone pair and valence findings were confirmed by electron localization function (ELF) and localized orbital locator (LOL) studies. Intra- and intermolecular non-covalent and weak interactions (van der Waals forces) of thiazole and pyrazole were explored using the reduced density gradient (RDG) methods. The anticancer protein 3a99 has higher binding energy, inhibition constant and RMSD values. From these results, the title compound may be observed as an effective Pim-1 kinase drug.

Table 5.1: Optimized geometrical parameters (Bond lengths) of 5-(4-Propoxybenzylidene)-2-[3-(4-chlorophenyl)-5-[4-(propan-2-yl) phenyl]-4,5-dihydro-1*H*-pyrazol-1-yl]-1,3-thiazol-4(5*H*)-one.

	Bond length(Å)			Bond length(Å)				Bond length(Å)			
Parameter	B3LYP/ 6-31G	B3LYP/ 6-311G	XRD*	Parameter	B3LYP/ 6-31G	B3LYP/ 6-311G	XRD*	Parameter	B3LYP/ 6- 31G	B3LYP/ 6- 311G	XRD*
C_1 - C_4	1.46	1.46	1.46	C ₁₆ -H ₂₀	1.08	1.08	0.93	C ₄₂ -N ₄₃	1.30	1.30	1.30
C_1-N_{24}	1.31	1.30	1.29	C_{17} - C_{21}	1.41	1.41	1.38	C_{45} - C_{46}	1.46	1.46	1.45
C_1 - C_{26}	1.52	1.52	1.50	C_{17} - H_{22}	1.09	1.08	0.93	C_{45} - H_{56}	1.09	1.09	0.93
C_2 - C_{14}	1.52	1.52	1.51	C_{19} - C_{21}	1.40	1.40	1.39	C_{46} - C_{47}	1.42	1.41	1.39
C_2-N_{25}	1.51	1.51	1.51	C ₁₉ -H23	1.09	1.08	0.98	C_{46} - C_{48}	1.42	1.42	1.39
C_2 - C_{26}	1.56	1.56	1.47	C_{21} - C_{29}	1.53	1.53	1.52	C_{47} - C_{49}	1.39	1.39	1.38
C_2 - H_{55}	1.09	1.09	0.98	N_{24} - N_{25}	1.39	1.39	1.38	C_{47} - H_{50}	1.09	1.08	0.93
H_3 - C_{26}	1.09	1.09	0.97	N_{25} - C_{42}	1.35	1.35	1.34	C_{48} - C_{51}	1.39	1.39	1.37
C_4 - C_5	1.41	1.41	1.38	C_{26} - H_{28}	1.10	1.09	0.97	C_{48} - H_{52}	1.08	1.08	0.93
C_4 - C_6	1.41	1.41	1.40	C_{29} - C_{30}	1.55	1.54	1.41	C_{49} - C_{53}	1.40	1.40	1.38
C_5 - C_7	1.40	1.40	1.37	C_{29} - C_{31}	1.55	1.54	1.41	C_{49} - H_{57}	1.08	1.08	0.93
C_5 - H_8	1.08	1.08	0.93	C_{29} - H_{38}	1.10	1.09	0.96	C_{51} - C_{53}	1.41	1.40	1.36
C_6 - C_9	1.39	1.39	1.37	C_{30} - H_{32}	1.10	1.09	0.96	C_{51} - H_{54}	1.08	1.08	0.93
C_6 - H_{10}	1.08	1.08	0.93	C_{30} - H_{33}	1.10	1.09	0.96	C_{53} - O_{58}	1.38	1.39	1.37
C_7-C_{11}	1.39	1.39	1.36	C_{30} - H_{34}	1.10	1.09	0.96	O_{58} - C_{59}	1.46	1.46	

C ₇ -H ₁₂	1.08	1.08	0.93	C ₃₁ -H ₃₅	1.10	1.09	0.96	C ₅₉ -H ₆₀	1.10	1.09
C_9 - C_{11}	1.40	1.39	1.38	C_{31} - H_{36}	1.10	1.09	0.96	C_{59} - H_{61}	1.10	1.09
C_9 - H_{13}	1.08	1.08	0.93	C_{31} - H_{37}	1.10	1.09	0.96	C_{59} - C_{62}	1.52	1.52
C_{11} - Cl_{27}	1.82	1.83	1.78	C_{39} - C_{40}	1.49	1.49	1.50	C_{62} - H_{63}	1.10	1.09
C_{14} - C_{15}	1.41	1.40	1.37	C_{39} - S_{41}	1.87	1.87	1.75	C_{62} - H_{64}	1.10	1.09
C_{14} - C_{16}	1.40	1.40	1.37	C_{39} - C_{45}	1.36	1.36	1.34	C_{62} - C_{65}	1.54	1.54
C_{15} - C_{17}	1.40	1.39	1.38	C_{40} - N_{43}	1.41	1.41	1.38	C_{65} - H_{66}	1.09	1.09
C_{15} - H_{18}	1.09	1.08	0.93	C_{40} - O_{44}	1.25	1.25	1.22	C_{65} - H_{67}	1.10	1.09
C_{16} - C_{19}	1.40	1.40	1.39	S_{41} - C_{42}	1.84	1.84	1.76	C_{65} - H_{68}	1.10	1.09

^{*-} Taken from Ref.[87]

Table 5.2: Optimized geometrical parameters (Bond angles) of 5-(4-Propoxybenzylidene)-2-[3-(4-chlorophenyl)-5-[4-(propan-2-yl) phenyl]-4,5-dihydro-1*H*-pyrazol-1-yl]-1,3-thiazol-4(5*H*)-one.

Bond angle	B3LYP/	B3LYP/	Bond angle	B3LYP/	B3LYP/
(degree)	6-31G	6-311G	(degree)	6-31G	6-311G
C4-C1-N24	121.71	121.63	C29-C30H-33	111.11	111.08
C4-C1-C26	125.17	125.27	C29-C30-H34	111.10	111.20
N24-C1-C26	113.11	113.10	H32-C30-H33	108.31	108.24
C14-C2-N25	112.36	112.29	H32C-30-H34	107.82	107.82
C14-C2-C26	115.13	115.18	H33-C30-H34	107.87	107.89
C14-C2-H55	109.27	109.19	C29-C31-H35	111.17	111.13
N25-C2-C26	100.19	100.23	C29-C31-H36	110.51	110.49
N25-C2-H55	107.27	107.37	C29-C31-H37	111.12	111.20
C26-C2-H55	112.12	112.11	H35-C31-H36	108.26	108.20
C1-C4-C5	120.62	120.65	H35-C31-H37	107.89	107.91
C1-C4-C6	120.62	120.72	H36-C31-H37	107.76	107.77
C5-C4-C6	118.75	118.63	C40-C39-S41	108.95	108.92
C4-C5C-7	120.90	120.96	C40-C39-C45	132.92	133.05
C4-C5-H8	120.25	120.33	S41-C39-C45	118.13	118.03
С7-С5-Н8	118.85	118.71	C39-C40-N43	113.47	113.46
C4-C6-C9	120.75	120.80	C39-C40-O44	124.81	124.72
C4-C6-H10	119.05	119.08	N43-C40-O44	121.72	121.82
C9-C6-H10	120.20	120.12	C39-S41-C42	86.31	86.21
C5-C7-C11	118.79	118.73	N25-C42-S41	119.67	119.88
C5-C7-H12	120.73	120.72	N25-C42-N43	122.87	122.70
C11-C7-H12	120.48	120.55	S41-C42-N43	117.45	117.41
C6-C9-C11	118.97	118.93	C40-N43-C42	113.81	114.00
C6-C9-H13	120.71	120.70	C39-C45-C46	135.13	135.18
C11-C9-H13	120.33	120.36	C39-C45-H56	113.74	113.71
C7-C11-C9	121.84	121.95	C46-C45-H56	111.13	111.11
C7-C11-Cl27	119.10	119.06	C45-C46-C47	116.05	116.15
C9-C11-Cl27	119.06	118.99	C45-C46-C48	126.50	126.45
C2-C14-C15	121.39	121.36	C47-C46-C48	117.45	117.40
C2-C14-C16	119.99	120.11	C46-C47-C49	122.18	122.17
C15-C14-C16	118.61	118.53	C46-C47-H50	119.09	119.13
C14-C15-C17	120.64	120.69	C49-C47-H50	118.73	118.70

 C14-C15-H18	120.15	120.21	C46-C48-C51	120.65	120.69
C17-C15-H18	119.21	119.10	C46-C48-H52	118.99	119.03
C14-C16-C19	120.54	120.60	C51-C48-H52	120.35	120.29
C14-C16-H20	119.55	119.57	C47-C49-C53	119.12	119.15
C19-C16-H20	119.88	119.81	C47-C49-H57	119.62	119.60
C15-C17-C21	121.04	121.07	C53-C49-H57	121.26	121.25
C15-C17-H22	119.11	119.05	C48-C51-C53	120.75	120.75
C21-C17-H22	119.85	119.88	C48-C51-H54	120.93	120.98
C16-C19-C21	121.24	121.28	C53-C51-H54	118.32	118.26
C16-C19-H23	119.39	119.36	C49-5C3-C51	119.84	119.85
C21-C19H-23	119.36	119.36	C49-C53-O58	124.27	124.34
C17-C21-C19	117.92	117.83	C51-C53-O58	115.89	115.82
C17-C21-C29	121.36	121.38	C53-O58-C59	119.75	119.98
C19-C21-C29	120.73	120.78	O58-C59-H60	109.49	109.45
C1-C24-N25	108.73	108.72	O58-C59-H61	109.53	109.47
C2-N25-N24	113.52	113.40	O58-C59-C62	107.03	107.02
C2-N25-N42	124.76	124.72	H60-C59-H61	108.45	108.73
N24-N25-C42	121.65	121.78	H60-C59-C62	111.17	111.09
C1-C26C-C2	103.58	103.63	H61C-59-C62	111.14	111.06
C1-C26-H3	112.34	112.37	C59-C62-H63	108.57	108.50
C1-C26-H28	110.54	110.54	C59-C62-H64	108.56	108.49
C2-C26-H3	111.19	111.21	C59-C62-C65	112.05	112.22
C2-C26-H28	111.78	111.67	H63-C62-H64	106.77	106.79
H3-C26-H28	107.48	107.48	H63-C62-C65	110.37	110.33
C21-C29-C30	111.70	111.80	H64-C62-C65	110.36	110.32
C21-C29-C31	111.89	111.95	C62-C65-H66	110.74	111.50
C21-C29-H38	107.05	106.94	C62-C65-H67	111.43	111.50
C30-C29-C31	110.93	111.06	C62-C65-H68	111.43	110.72
C30-C29-H38	107.47	107.38	H66-C65-H67	107.63	107.80
C31-C29-H38	107.51	107.41	H66-C65-H68	107.63	107.56
C29-C30-H32	110.51	110.48	H67-C65-H68	107.81	107.57

Table 5.3: Vibrational assignments, observed and calculated wave numbers of 5-(4-Propoxybenzylidene)-2-[3-(4-chlorophenyl)-5-[4-(propan-2-yl) phenyl]-4,5-dihydro-1H-pyrazol-1-yl]-1,3-thiazol-4(5H)-one at B3LYP method with 6-31G and 6-311G basis sets

Observed		Calcı	ılated		
S.No.	wavenui	mbers (cm ⁻¹)	wavenumbers	(cm ⁻¹) (Scaled)	Vibrational
S.1NO.	FT-IR	FT-Raman	B3LYP/	B3LYP/	assignments (PED%)
	I 1-1IX	r 1-Kaman	6-31G	6-311G	
			3091	3082	<i>^U</i> СН(99)
	3070w		3075	3070	υ CH(99)
			3070	3066	υ CH(98)
			3066	3060	υ CH(98)
			3061	3054	υ CH(98)
			3053	3049	υ CH(99)
	3040w		3045	3042	υ CH(98)
			3040	3036	υ CH(98)
			3037	3031	υ CH(99)
			3031	3028	^U СН(99)
			3027	3023	υ CH(98)
			3024	3019	υ CH(98)
			3018	3014	υ CH(99)
	2936w		3012	3008	$v_{\rm ass}$ CH ₃ (97)
			3009	3002	$v_{\rm ass}$ CH ₃ (97)
			3000	2996	$v_{\rm ass}$ CH ₂ (98)
			2996	2991	$v_{\rm ass}$ CH ₃ (97)
			2990	2985	$v_{\rm ass~CH_2(97)}$
			2981	2977	$v_{\rm ass}$ CH ₃ (97)
			2975	2970	υ CH(98)
	2961ms		2970	2963	$v_{\rm ass}$ CH ₃ (97)
			2951	2945	$v_{\rm ass}$ CH ₃ (97)
	2936w		2942	2938	$v_{\rm SS}$ CH ₂ (98)
			2933	2930	$v_{\rm ass}$ CH ₃ (97)
		2929w	2930	2924	$v_{\rm SS}$ CH ₃ (98)
			2925	2919	$v_{\rm SS}$ CH ₃ (98)
			2918	2912	$v_{\rm SS}$ CH ₃ (98)
			2909	2903	$v_{\rm SS}$ CH ₃ (98)
			2901	2896	υ CH(97)
	2875m		2882	2875	$v_{\rm SS}{ m CH}_2(98)$
	1692ms		1650	1643	$^{\upsilon}$ CO (71), $^{\upsilon}$ CN (21)
			1631	1625	v CC (68), δ CH (19)
			1619	1614	$^{\upsilon}$ CC (68), $^{\delta}$ CH (20)

		1606	1604	v CC (68), δ CH (20)
1599s		1599	1599	$^{\upsilon}$ CC (67), $^{\upsilon}$ CN (15), $^{\delta}$ CH (12)
	1596vs	1596	1592	$^{\upsilon}$ CC (67), $^{\upsilon}$ CN (15), $^{\delta}$ CH (10)
		1585	1581	v CC (68), δ CH (13), δ CC (10)
		1579	1576	$^{\upsilon}$ CN (66), $^{\upsilon}$ CO (13), $^{\upsilon}$ CC (12)
		1572	1570	U CC (68), $^{\delta}$ CO (16), U CN (10),
	1560s	1566	1564	U CN (69), U CO (19)
1542vs		1551	1551	δ CH (72), U CC (10)
		1540	1542	$\rho_{\text{SCISS}}, \text{CH}_2(76)$
		1534	1535	δ CH (73), $^{\upsilon}$ CC (12)
		1530	1527	δ CH (65), U CC (17)
		1521	1519	δ opbCH ₃ (6a)
		1514	1511	δ opbCH ₃ (69)
		1506	1503	δ opbCH ₃ (68)
1494ms		1496	1495	$\delta_{\text{ipbCH}_3 (68)}$
		1494	1490	$\rho_{\rm SCISS}$ CH ₂ (75)
		1485	1483	δ ipbCH ₃ (68)
		1475	1475	δ ipbCH ₃ (68)
		1466	1462	$\rho_{\text{SCISS}} \text{CH}_2(75)$
		1456	1456	δ CH (68), U CC (10)
		1453	1450	δ CH (68), U CC (12)
	1440w	1445	1441	δ sb CH ₃ (76)
		1438	1435	$\delta_{\mathrm{sb}\mathrm{CH}_{\mathrm{3}}\mathrm{(76)}}$
		1431	1426	δ CH (68)
1423ms		1420	1417	δ CH (68)
		1413	1408	$\delta_{\rm sb}{\rm CH_3}$ (75)
	1400m	1403	1400	v CN (66), δ CH (14)
		1389	1389	σ rock CH ₂ (67), U CC (16)
		1380	1381	δ CH (65), v CCC (12)
		1376	1375	$^{\upsilon}$ CC (65), $^{\delta}$ CH (10)
		1370	1368	δ CH (66), v CCC (12)
		1355	1353	δ CH (66)
		1348	1344	σ rock (65), ν CCC (10)
	1330m	1336	1335	δ CH (65), v CCC (12)
		1330	1327	v CC (63), δ CH (12)
		1316	1313	v CC (68), δ CH (13)
		1304	1302	δ CH (66)

1288ms	1288m	1294	1290	σ rock CH ₂ (67), U CC (12)
		1285	1283	$\tau_{\text{CH}_2(59)}$
		1275	1271	v CC (63), δ CH (23)
1264ms		1266	1263	δ CH (68)
		1261	1257	σ rock CH ₂ (67)
		1253	1250	δ CH (68)
	1245ms	1245	1243	$\tau_{\rm CH_2(58)}$
1233s		1234	1235	v CC (66), δ CH (14)
		1232	1228	δ CH (63), v CCC (16)
		1223	1220	δ CH (65)
		1216	1212	δ CH (65), v CCC (12)
		1205	1203	δ CH (66)
		1194	1190	δ CH (65)
		1190	1188	δ CH (66)
1180ms		1186	1182	$\tau \text{ CH}_2(57)$
1175ms	1175ms	1175	1171	$\gamma \text{ wagg CH}_2(55)$
		1166	1160	δ CO (61)
		1156	1153	δ CH (66)
		1147	1144	δ CH (64)
		1143	1139	δ CH (64)
	1125ms	1132	1127	δ CH (64)
		1115	1112	υ CCH ₃ (67)
		1099	1096	δ ring (60)
1092ms		1094	1092	v CCH ₃ (66)
		1091	1085	v_{NN} (72), δ CN (14), δ CO (10)
		1086	1081	v CC (67), δ ring (16)
		1080	1075	$^{\upsilon}$ CC (68), $^{\upsilon}$ CO (14)
		1071	1066	γ CH(59)
		1064	1060	δ ring (61)
1050w		1055	1051	δ ring (61)
		1050	1042	$\delta \operatorname{ring}(61)$
		1036	1030	δ ring (60)
		1029	1023	γ CH(58)
1017ms		1024	1016	U CO (69), U CC (12)
		1014	1009	γ CH(59)
	1000w	1006	1002	γ CH(59)
994w		1003	998	γ CH(60)
		983	982	γ CH(60)

975w		979	973	γ (11 (62)
913W		979 965	973 961	γ opr CH ₃ (62)
	050			γ CH(58)
	950vw	955 946	950 943	v CS(74)
		940	938	γ opr CH ₃ (62)
		939	936 925	$^{\gamma}$ CH (58)
				$\delta \operatorname{ring}(61)$
004	000	921	917	γ CH ₃ (60)
904w	900	908	903	δ rock CH ₃ (61)
		895	891	δ rock CH ₃ (61)
		886	882	γ CH (58)
		878	875	γ CH (58)
		870	866	γ CH (58)
860w		868	860	γ CH (58)
		856	854	$^{\gamma}$ CH (57)
		845	841	γ CH (58)
827w	832w	834	830	Ring breathing(60)
		818	815	$^{\gamma}$ CCl (71)
		809	806	$^{\gamma}$ CS (75)
		796	792	$^{\gamma}$ CS (74)
		790	785	δ ring (64)
		782	778	$\delta_{\text{wagg CH}_2(61)}$
		769	765	δ CO(70)
756w		763	759	$^{\gamma}$ CO(68)
		750	743	γ ring (56)
		725	721	γ ring (55)
720w		720	716	δ ring (61)
		706	702	$\gamma \operatorname{ring}(55)$
		692	689	υ CC(66)
		666	662	$\delta_{\rm iprCH_3(59)}$
		648	643	$\delta_{\rm ccl(57)}$
		629	626	γ _{CH(58)}
618w		620	617	γ CH(58)
010**		600	596	γ CH(59)
		585	581	γ CH(58)
569w		579	572	γ CH(58)
20711		566	560	γ _{CH(58)}
		554	551	Ring breathing (60)
536w		538	535	γ CH(59)
- 2 2		531	525	$\gamma \operatorname{ring}(54)$
		517	513	$\delta_{\rm ring}$ (55)

504w	505	501	$\delta_{\rm ring}$ (55)
	494	490	δ CC (61)
	475	472	δ CC (60)
	461	453	γ CC (52)
	446	441	$\gamma CO (50)$
	440	438	γ CH (54)
	435	430	$\gamma \operatorname{ring}(54)$
	422	419	$^{\gamma}$ ring (54)
406vw	412	408	$^{\gamma}$ ring (54)
	406	400	$^{\gamma}$ CC (55)
	388	385	$^{\gamma}$ ring (49)
	373	372	$^{\gamma}$ CCl (51)
	364	360	$\delta_{\rm ring}$ (50)
	350	345	$^{\gamma}$ CC (48)
	339	333	$^{\gamma}$ CCH ₃ (49)
	320	316	$\delta_{\text{CC (54)}}$
	306	301	δ CC (55)
	284	280	δ ring (60)
	279	274	δ CC (58)
	256	252	τ CCH ₃ (54)
	250	246	δ CC (58)
	248	241	τ CH ₃ (48)
	235	230	τ CH ₃ (48)
	229	225	$\tau_{\mathrm{CH}_3(48)}$
	222	217	δ ring (57)
	214	208	$^{\gamma}$ CO (61)
	206	202	δ ring (59)
	200	196	$\delta \operatorname{ring}(60)$
	183	175	$\gamma CO (57)$
	174	168	$\delta_{\rm ring}$ (58)
	161	155	$\gamma \text{ CC } (49)$
	148	140	$\gamma CO (48)$
	135	130	γ CN (48)
	125	119	$\delta_{\rm ring}$ (53)
	106	98	$\delta_{\rm ring}$ (55)
	95	87	$\tau \frac{\text{CO}(49)}{\text{CO}(49)}$
78vw	89	80	γ CC (49)
	83	73	γ CC (48)
	75	67	γ CC (49)

62	56	δ _{CC (58)}
55	49	δ CC (58)
49	40	$^{\gamma}$ ring (48)
45	36	γ CC (48)
39	31	γ CC (47)
35	28	γ CC (48)
31	25	γ CC (48)
26	22	γ CC (48)
21	19	γ CC (45)
16	14	γ CC (45)
9	6	γ CC (48)

s-strong, ms-medium strong, vs-very strong, w-weak, vw-very weak, v-stretching, ν_{ss} -symmetric stretching, ν_{ass} - asymmetric stretching, δ -in-plane pending, γ -out-of-plane bending, ρ -scissoring, ω -wagging, σ -rocking, τ -twisting.

Table 5.4: Calculated E-HOMO, E-LUMO (H-1 \rightarrow L+1, H-2 \rightarrow L+2), energy gap (E_L–E_H), ionization potential (i), electron affinity (a), global hardness (η), electronegativity (χ), chemical softness (σ), chemical potential (μ) and global electrophilicity (ω)

Molecular	Energy	Energy	(I) (eV)	(A) (eV)	(ŋ) (eV)	(χ)	(σ) (eV)	(μ) (eV)	(ω) (eV)
properties	(eV)	gap (eV)				(eV)			
E _{HOMO}	-5.7563								
$\mathbf{E}_{\mathbf{LUMO}}$	-2.3943	3.3620	5.7563	2.3943	1.6810	4.753	0.5949	-4.0753	4.9399
$\mathbf{E}_{\text{HOMO-1}}$	6.3539								
$\mathbf{E}_{\mathrm{LUMO+1}}$	1.8313	4.5226	6.3539	1.8313	2.2613	4.0926	0.4422	-4.0926	3.7035
$\mathbf{E}_{\text{HOMO-2}}$	6.7645								
$E_{LUMO+2} \\$	1.0411	5.7234	6.7645	1.0411	2.8617	3.9028	0.3494	-3.9028	2.6613

Table 5.5: Second order perturbation theory analysis of fock matrix on NBO for 5-(4-Propoxybenzylidene)-2-[3-(4-chlorophenyl)-5-[4-(propan-2-yl) phenyl]-4,5-dihydro-1*H*-pyrazol-1-yl]-1,3-thiazol-4(5*H*)-one.

Donar	Donar		Acceptor			E(2) ^a	E(i)-	
(i)	Type	ED/e	(j)	Type	ED/e(q _i)	Kcal/mol	$\mathbf{E}(\mathbf{j})^{\mathbf{b}}$	$\mathbf{F}(\mathbf{i},\mathbf{j})^{\mathbf{c}}$
π	C1-N24	1.923	π*	C4-C5	0.390	7.93	0.32	0.049
σ	C1-C26	1.973	σ^*	C2-C14	0.040	5.08	1.09	0.067
σ	C2-H55	1.894	σ^*	H3-C26	0.048	8.32	0.91	0.079
π	C4-C5	1.645	π^*	C1-N24	0.255	16.67	0.24	0.058
π	C4-C5	1.645	π^*	C6-C9	0.297	19.66	0.28	0.068
π	C4-C5	1.645	π^*	C7-C11	0.392	22.43	0.26	0.069
σ	C6-C9	1.645	σ^*	C11-C127	0.032	4.95	0.81	0.057
π	C6-C9	1.667	π^*	C4-C5	0.390	20.57	0.28	0.068
π	C6-C9	1.667	π^*	C7-C11	0.392	21.12	0.26	0.067
π	C7-C11	1.680	π^*	C4-C5	0.390	17.84	0.3	0.066
π	C7-C11	1.680	π^*	C6-C9	0.297	19.15	0.3	0.068
π	C14-C15	1.673	π^*	C16-C19	0.343	19.55	0.28	0.067
π	C14-C15	1.673	π^*	C17-C21	0.359	18.95	0.29	0.067
π	C16-C19	1.693	π^*	C14-C15	0.388	21.07	0.27	0.069
π	C16-C19	1.693	π^*	C17-C21	0.359	21.11	0.28	0.07
π	C17-C21	1.650	π^*	C14-C15	0.388	21.43	0.27	0.069
π	C17-C21	1.650	π^*	C16-C19	0.343	20.03	0.28	0.066
σ	C29-H38	1.910	π^*	C17-C21	0.359	10.97	0.47	0.069
σ	C29-H38	1.910	σ^*	C30-H34	0.015	6.13	0.93	0.069
σ	C29-H38	1.910	σ^*	C31-H37	0.015	6.13	0.93	0.069
σ	C39-S41	1.978	σ^*	N25-C42	0.053	9	1.44	0.102
π	C39-C45	1.727	LP (2)	S41	1.998	540.23	0.01	0.119
π	C39-C45	1.727	π^*	C40-O44	0.358	29.54	0.28	0.083
σ	C40-N43	1.980	σ^*	N25-C42	0.053	6.25	1.17	0.077
π	C40-O44	1.916	π^*	C39-C45	0.284	8.91	0.27	0.046
π	C40-O44	1.916	π^*	C42-N43	0.517	6.73	0.28	0.044
σ	S41-C42	1.982	σ^*	C39-C45	0.035	7.14	1.39	0.089
σ	C42-N43	1.980	σ^*	S41-C42	0.046	1.15	1.29	0.035
π	C42-N43	1.839	LP (2)	S41	1.998	102.39	0.05	0.102
π	C42-N43	1.839	π^*	C40-O44	0.358	27.11	0.31	0.087
π	C46-C48	1.669	π^*	C47-C49	0.316	20.72	0.29	0.069
π	C46-C48	1.669	π^*	C51-C53	0.355	19.28	0.28	0.066

π	C47-C49	1.665	π^*	C46-C48	0.368	20.58	0.27	0.068
π	C47-C49	1.665	π^*	C51-C53	0.355	22.37	0.27	0.07
π	C51-C53	1.650	π^*	C46-C48	0.368	21.42	0.28	0.07
π	C51-C53	1.650	π^*	C47-C49	0.316	19.26	0.29	0.067
LP (1)	N24	2.000	σ^*	C2-N25	0.044	4.81	0.82	0.056
LP (1)	N25	1.999	π^*	C1-N24	0.255	26.7	0.24	0.072
LP (1)	N25	1.999	σ^*	S41-C42	0.046	6.95	0.75	0.068
LP (1)	N25	1.999	σ^*	C42-N43	0.062	13.04	0.68	0.088
LP (3)	C127	2.000	π^*	C7-C11	0.392	12.39	0.32	0.061
LP (1)	S41	2.000	σ^*	C39-C40	0.097	7.95	0.99	0.08
LP (1)	S41	2.000	σ^*	C42-N43	0.062	8.55	0.94	0.08
LP (2)	S41	1.998	π^*	C39-C45	0.035	65.6	0.2	0.112
LP (2)	S41	1.998	π^*	C42-N43	0.517	99.8	0.21	0.133
LP (1)	N43	1.999	σ^*	C39-C40	0.097	5.99	0.81	0.062
LP (1)	N43	1.999	σ^*	S41-C42	0.046	5.63	0.84	0.062
LP (2)	O44	1.877	σ^*	C39-C40	0.097	18.59	0.69	0.102
LP (2)	O44	1.877	σ^*	C40-N43	0.062	22.97	0.65	0.111
LP (1)	O58	1.945	σ^*	C49-C53	0.029	6	0.97	0.069
π^*	C1-N24	0.255	π^*	C4-C5	0.390	37.71	0.04	0.063
π^*	C7-C11	0.392	π^*	C4-C5	0.390	195.69	0.02	0.083
π^*	C7-C11	0.392	π^*	C6-C9	0.297	131.61	0.02	0.078
π^*	C39-C45	0.035	π^*	C40-O44	0.358	30.02	0.06	0.069
π^*	C42-N43	0.517	π^*	C40-O44	0.358	53.08	0.05	0.072

Table 5.6: PASS prediction for the activity spectrum of title compound, Pa represents probability to be active and Pi represents probability to be inactive.

Pa	Pi	Activityname
0,260	0,102	Antimetastatic
0,189	0,036	Pim-1 kinase inhibitor
0,177	0,031	Protein-tyrosine phosphatase inhibitor
0,153	0,012	Bcl2 antagonist
0,192	0,054	Vascular adhesion protein 1 inhibitor
0,133	0,008	Pim-2 kinase inhibitor
0,242	0,121	Atherosclerosis treatment
0,246	0,131	Antineurogenic pain
0,101	0,005	CDC25B inhibitor
0,107	0,018	Autotaxin inhibitor
0,128	0,039	Lipoxygenase inhibitor
0,292	0,205	APOA1 expression enhancer
0,207	0,120	Antiobesity
0,132	0,049	Vasculitis treatment
0,082	0,010	Bcl-xL inhibitor
0,126	0,061	Sodium/bile acid cotransporter inhibitor
0,093	0,030	5-Lipoxygenase inhibitor
0,260	0,199	CDK9/cyclin T1 inhibitor
0,078	0,024	Protein-tyrosine phosphatase 2C inhibitor
0,205	0,157	Antidiabetic
0,092	0,044	Peroxisome proliferator-activated receptor gamma antagonist
0,240	0,195	Vanilloid 1 agonist

Table 5.7: Molecular docking parameters of 5-(4-Propoxybenzylidene)-2-[3-(4-chlorophenyl)-5-[4-(propan-2-yl) phenyl]-4,5-dihydro-1*H*-pyrazol-1-yl]-1,3-thiazol-4(5*H*)-one bind with human pim-1 kinase enzyme.

Protein	PDB	Bond Amino distance acid		Bond	Binding affinity (kcal/mol)			Inhibition Constant Ki (µM or nM)			RMSD (Å)		
name	ID	(Å)	(residues)		1	2	3	1	2	3	1	2	3
m-2-		2.5	ILE A 74	Pi-alkyl	-9.23	-9.13	-9.01	170.15 nM	201.86 nM	248.98 nM	81.47	83.69	82.21
5-(4-Propoxybenzylidene)-2-[3-(4-chlorophenyl)-5-[4-(propan-2-yl)] phenyl]-4,5-dihydro-1 H -pyrazol-1-yl]-1,3-thiazol-4(5 H)-one	3a99	2.9	GLY A 48	carbon- hydrogen bond									
		3.0	SER A 50	conventional hydrogen bond									
		3.0	VAL A 174	Pi-alkyl									
chle zol-1		2.8	CYS A 13	Pi-sigma	-6.98	-6.95	-6.90	7.65 μM	19.13 μΜ	12.09 μΜ	26.16	26.28	26.31
e)-2-[3-(4	1gj8	1.9	GLN A 12	conventional hydrogen bond				·	·	·			
den dro-		2.9	LYS A 10	Ailkyl									
ropoxybenzylic enyl]-4,5-dihyc		2.6	GLN A 171	vander Waals	-9.14	-9.01	-7.83	201.35 nM	249.97 nM	1.82 μM	77.89	79.25	55.22
		2.4	PRO A 125	Pi-alkyl									
	1xqz	2.4	LEU A 93	Pi-alkyl									
(4-P		2.4	LYS A 67	Pi-alkyl									
5-(3.5	ILE A 185	Pi-sigma									

Exploration mechanism of spectral characterization, biological activity and molecular docking studies of 5-(4-Hydrobenzylidene)-2-[3-(4-chlorophenyl)-5- [4-(propan-2-yl) phenyl]-4, 5- dihydro-1 *H*-pyrazol-1-yl]-1, 3-thiazol-4(5*H*)-one

Abstract

Thiazole is a well-established heterocyclic compound having a broad range of structural and spectroscopic properties. In the present work, the experimental FT-IR (4000-0 cm⁻¹) and FT-Raman (3500-0 cm⁻¹) absorption data of the 5-(4-Hydrobenzylidene)-2-[3-(4chlorophenyl)-5- [4-(propan-2-yl) phenyl]-4, 5- dihydro-1*H*-pyrazol-1-yl]-1, 3-thiazol-4(5H)-one (HCPPT) were combined with a theoretical quantum chemical calculation. For the theoretical computations, the optimized geometrical parameters and the vibrational assignment of the HCPPT were determined by density functional theory (DFT) calculation using B3LYP functional cc-pVDZ and 6-311G basis sets. The charge transfer inside the molecule is easily identified by density plots across the highest occupied molecular orbital and lowest unoccupied molecular orbital energy surfaces. It also provides information about the chemical activity of the compound. A molecular electrostatic potential surface was plotted to assess the molecular electrophilic and nucleophilic reactivity. The charge delocalization and stability of the (HCPPT) title molecule was carried out using natural bond orbital (NBO) analysis. Non covalent interactions, topology, two- and threedimension finger-print plots were also studied using reduced density gradient analysis. In addition, anti-microbial activity of the (HCPPT) title compound are evaluated against bacterial: gram-positive organisms (staphylococcus aureus, Bacillus subtilis), bacterial: gram- negative organisms (Escherichia coli, Pseudomonas aeruginosa) and fungal organisms (candida albicans and Aspergillus Niger) to investigate its biological action. Furthermore, molecular docking studies of the title compound revealed that it may exhibit antineoplastic (solid tumours), anti-cancerous and anti-inflammatory activities.

CHAPTER - 6

Exploration mechanism of spectral characterization, biological activity and molecular docking studies of 5-(4-Hydrobenzylidene)-2-[3-(4-chlorophenyl)-5- [4-(propan-2-yl) phenyl]-4, 5- dihydro-1*H*-pyrazol-1-yl]-1, 3-thiazol-4(5*H*)-one

6.1 Introduction

The thiazole structure is an important pharmacophore in science, because of its ubiquitous occurrence in a difference of physical, chemical, and biological properties. Reactivity and endurance of the sulphur and nitrogen contains heterocycles gives the impressive application of the researcher's in current decades [86, 163]. Thiazole-pyrazole is a common core structure in a broad range of compounds with essential agricultural and pharmacological properties. Besides, numerous thiazole hybrids have been identified as potential in antibacterial [164–166], anticancer [167], anti-inflammatory [168], antitubercular [169], antioxidant [170]. B3LYP method was utilised with the cc-pVDZ and 6-311G basis sets for the current work (4-Hydrobenzylidene) -2-[3-(4-chlorophenyl) [4-(propan-2-yl) phenyl] -5- [4-(propan-2-yl) phenyl] dihydro-1H-pyrazol-1-yl]-4, 5-dihydro-1H-pyrazol-1-yl (HCPPT). The molecular geometries, vibrational frequencies and frontier molecular orbital (HOMO-LUMO) energies of HCPPT were investigated. Experimental FT-IR and FT-Raman spectra were analyzed and compared with estimated vibrational assignments based on potential energy distribution (PED). Global chemical reactivity characteristics such as ionisation potential (I), electron affinity (A), electro-negativity (γ) , chemical potential (μ) , hardness (η) , softness (σ) , and electrophilicity index (ω) were predicted from HOMO/LUMO energy values. The possibility of electrophilic, nucleophilic and bonding interactions within the electron density distribution was shown using a molecular electrostatic potential map (MEP). The topological analysis was used to

determine the atoms in molecules (AIM), electron localization function (ELF), and localization orbital locator (LOL) and a reduced density gradient (RDG). In HCPPT, the stabilizing energy is provided by the E(2) form in NBO due to the hyper-conjugation influence on inter- and intramolecular interactions. Antimicrobial activities of thiazole compound were successfully tested using the disc diffusion method with standard strains of bacteria: gram-positive (staphylococcus aureus, Bacillus subtilis), bacteria: gram-negative (Escherichia coli, Pseudomonas aeruginosa), and fungal organisms (Candida albicans and Aspergillus Niger). Finally, a molecular docking study suggested that interactions between the ligand and specific targets of antineoplastic (solid tumours), anti-cancerous and anti-inflammatory proteins are exploring as drugs towards their futuristic applications.

6.2 Experimental details

The synthesized compound HCPPT was taken without further purification and used for characterization techniques:

- A Perkin-Elmer spectrometer was used to create an FT-IR spectrum with a covering field of 4000-0 cm⁻¹.
- In a Bruker RFS 27 Raman module, a Nd: YAG laser in the 3500-0 cm⁻¹
 range was employed to record FT-Raman spectrum.
- To measure the antibacterial activity of the HCPPT, the disc diffusion method was performed.

6.3 Computational details

The density functional theory (DFT) was used to do all quantum chemistry computations using Gaussian 09 program [20]. Geometric optimizations on the title compound were executed using B3LYP/cc - pVDZ and B3LYP/6-311G basis sets. The VEDA 4 program [88] performs vibrational assignments for FT-IR and FT-Raman

frequencies spanning from 4000 to 0 cm⁻¹. The accuracy of the method was evaluated by comparing the optimized structure with the experimental data. GaussView 5.0 [31] was used to visualize the molecular electrostatic potential (MEP) and Frontier molecular orbital's (FMOs)

The global reactivity characteristics such as ionization potential (I), electron affinity (A), electro- negativity (χ), chemical potential (μ), hardness (η), softness (σ), and electrophilicity index (ω) were determined [171]. This global reactivity has recently been used to explain the nature of pharmacological activities in biological molecules. To explore inter- and intra-molecular delocalization, the second order perturbation technique was used with the NBO 3.1 program [90].

The Multiwfn program [54] was used to determine the atoms in molecules (AIM), electron localization function (ELF), and localization orbital locator (LOL). Reduced density gradient (RDG) or non-covalent interaction (NCI) can be used to compute 2D and 3D interactions between atoms. The computations were done by Multiwfn, and the results were plotted by the VMD program [118]. The primary goal of this research is to learn more about the biological properties and molecular interactions of the title compound. The disc diffusion method [172] was used to screen antimicrobial activity. The optimized structure of the title compound was docked with a suitable protein using Autodock Tools (ADT) [91].

6.4 Results and discussion

6.4.1 Molecular geometric properties

The geometrical characteristics of the HCPPT in the ground state were optimized using the cc-pVDZ and 6-311G basis sets at the DFT-B3LYP level of theory. Fig. 6.1 shows the compound's optimized structure of the compound with numbering of atoms. Gaussian 09W [20] conceivably used to compute the bond length and bond angle between atoms. The

following results were compared to the closely related crystallographic data [87] and tabulated in Tables 6.1 and 6.2.

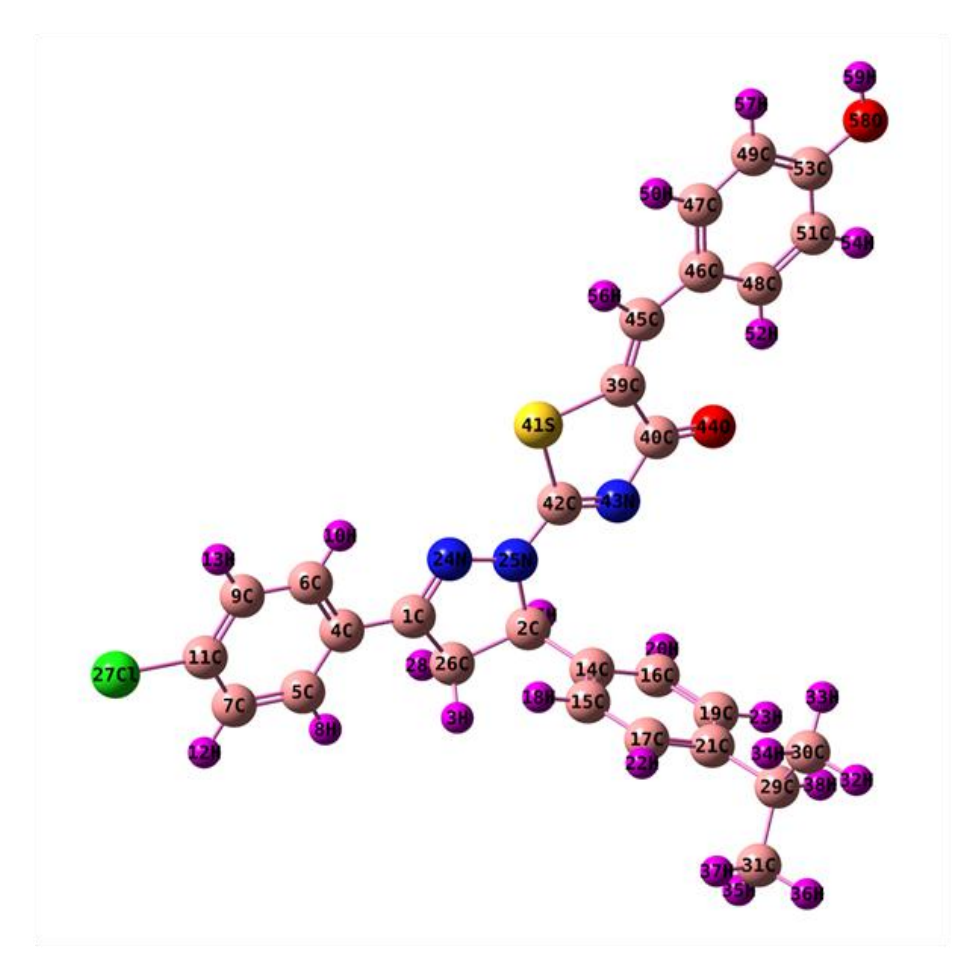


Fig. 6.1 Optimized structure of HCPPT

In thiazole ring, the different bond length and bondangle of carbon, sulphur and nitrogen atom were computed. The bond length of C₃₉-C₄₀-1.51/1.49 Å, C₃₉-S₄₁-1.80 Å/1.87 Å, C₄₂-N₄₃-1.30 Å/1.30 Å and bond angle of C₄₀-C₃₉-S₄₁-108.78°/108.92°, S₄₁-C₄₂-N₄₃-118.84°/117.38°, C₄₀-C₃₉-C₄₅- 132.64°/133.03° were reported using B3LYP/cc-pVDZ//6-311G basis sets, respectively. These values are well agreed with the data reported by Bourakadi et al. [173]. The shorter angle C₃₉-S₄₁-C₄₂ has clearly indicated the presence of sulphur bond as 87.64° (cc-pVDZ) and 86.22° (6-311G). Substituent of oxygen in thiazol form C₄₀=O₄₄ bond is 1.22 Å (cc-pVDZ) and 1.24 Å (6-311G) which shows electronegative properties present in the title molecule.

In pyrazole ring, the two nitrogens with a carbon atom in the ring show C₁-N₂₄- $1.30/1.30\ \mathring{A},\ N_{24}\text{-}N_{25}\text{-}\ 1.37/1.39\ \mathring{A},\ C_{1}\text{-}C_{26}\text{-}\ 1.52/1.52\ \mathring{A},\ C_{2}\text{-}C_{26\text{-}}\ 1.55\ \mathring{A}/1.56\ \mathring{A},\ respectively.$ The bond angle was found to be C_1 - C_{26} - C_2 - $102.99^{\circ}/103.62^{\circ}$, C_1 - C_{24} - N_{25} - $108.87^{\circ}/108.69^{\circ}$, C_2 - N_{25} - N_{24} - 114.01°/ 113.33° using B3LYP/cc-pVDZ/6-311G basis set. The C-H bond length of the phenyl linked to the pyrazole ring was determined to be between 1.08 and 1.09 Å. For the C-C-H bond angle, computed values were determined between 118°-120° in phenyl ring and lower than the 110° in methyl at phenyl ring and pyrazol ring. This is similar to the report [174, 175]. The optimized C-C bond lengths were calculated in the range 1.55- 1.38 Å and experimentally noticed in the range 1.51- 1.35 Å [176]. Whereas, the optimized C-C-C bond angles were calulated in the range of the above 125° due the electron donors (CH₃), acceptors (Cl) and below 120° due to the heterocyclic bond ring. The occurrence of the hydroxyl bond O₅₈-H₅₉ is specifically stated by shorter bond distance (0.96 Å/PVDZ, 0.972 Å/6-311G and 0.96 Å/XRD). The longer bond length is found in C-Cl = 1.76 Å/cc-pVDZ, 1.83 Å /6-311G and 1.78 Å/XRD detected due to the electronegative nature of chlorine. These bond lengths values are generally compatible with similar structures in literature [177, 178], respectively.

6.4.2 Vibrational frequency assignments

The vibrational frequency calculation made in this study reveals that the title compound belongs to C1 point group symmetry. It is a nonlinear molecule, there are 59 atoms with 171 normal mode of vibration. The optimized molecular structure of HCPPT and corresponding vibrational frequencies are calculated at DFT/B3PLY/cc-pVDZ and DFT/B3PLY/6-311G basis sets to interpretation of experimental spectroscopic data. The calculated vibrational wavenumbers, measured FT-IR and FT-Raman band positions and the calculated PED for each normal mode are presented in Table 6.3. The experimental and theoretically predicted FT-IR spectra in the region 4000-0 cm⁻¹ and the corresponding FT-Raman spectra in the 3500-0 cm⁻¹ are given in Figs. 6.2 and 6.3 respectively.

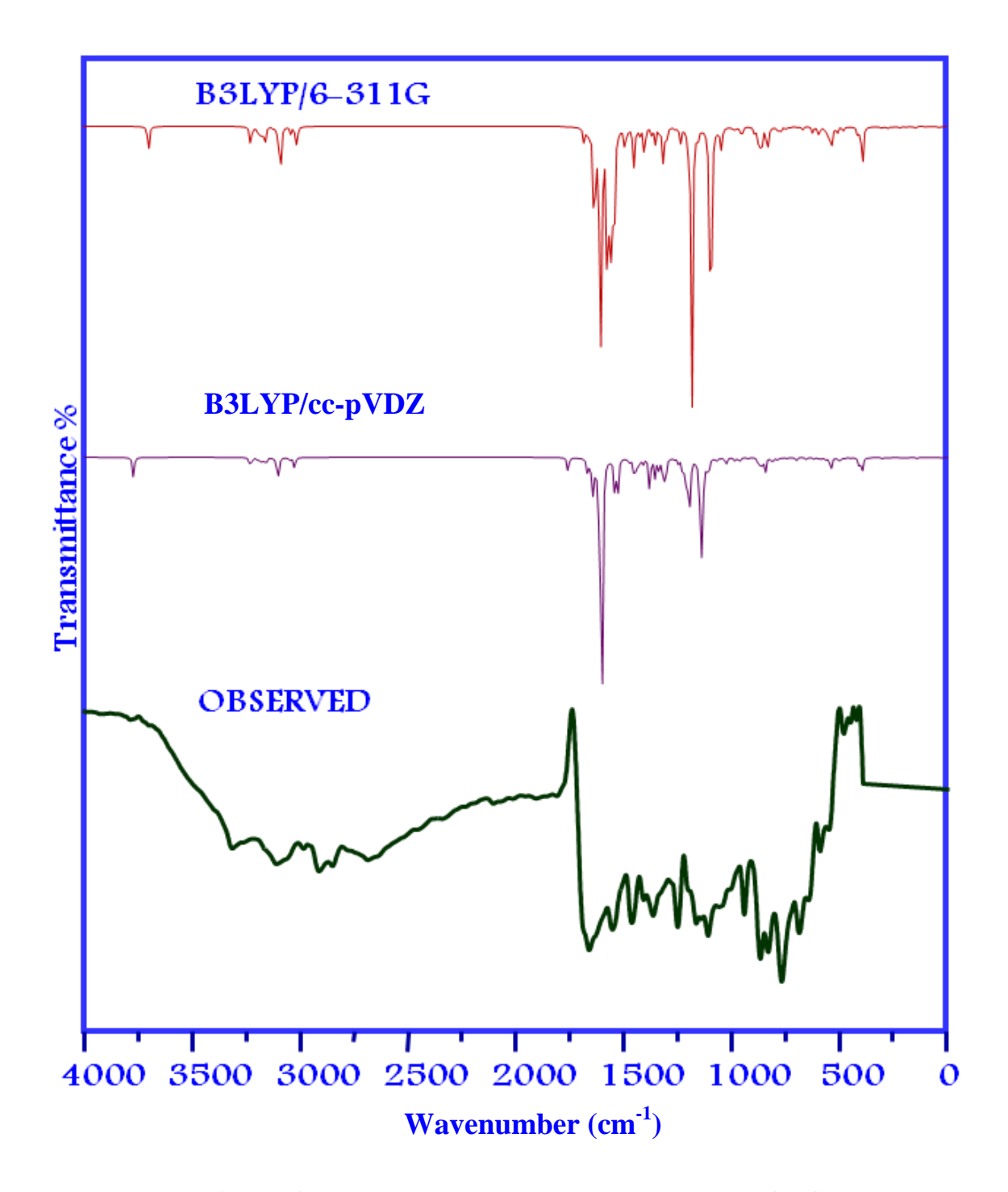


Fig. 6.2 Observed and calculated FT-IR spectrum of HCPPT

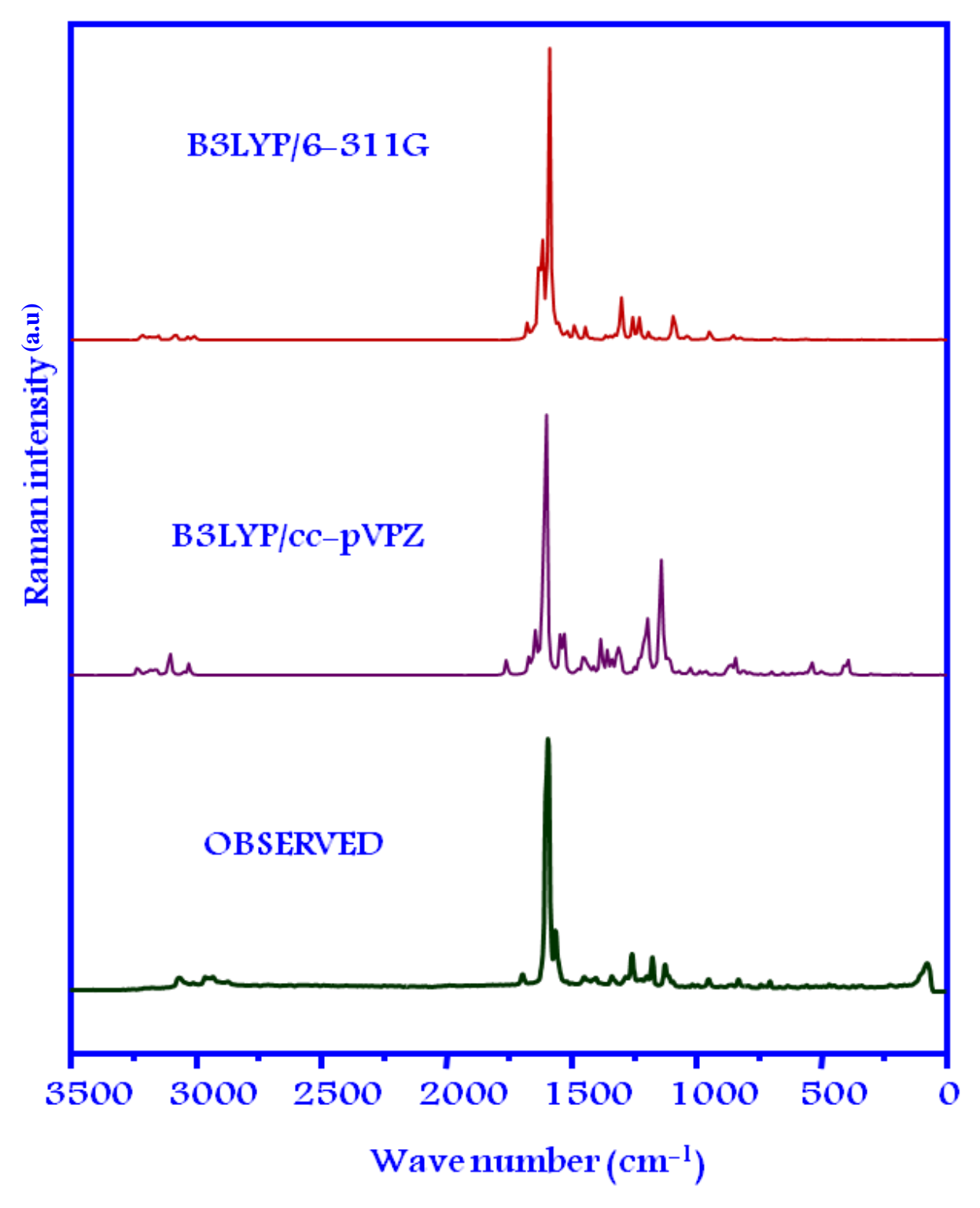


Fig. 6.3 Observed and calculated FT-Raman spectrum of HCPPT.

Hydroxyl vibration

The hydroxyl group induces vibrations in stretching, in-plane bending and out-of-plane bending vibrational modes. Usually stretching vibrations of O-H occurred in the range 3590 - 3400 cm⁻¹ [179]. In the present investigation, the hydrogen bond defines the precise position of the O-H bond in the title compound. This hydrogen bonding produces a significant hydroxyl stretching vibrations of the title molecule at 3314 cm⁻¹ in FT-IR, 3317 cm⁻¹ inB3LYP/cc-PVDZ and 3318 cm⁻¹ B3LYP/6-311G basis sets, respectively. The O-H in-plane bending vibrations appear between 1250 cm⁻¹ and 1150 cm⁻¹, and it is not significantly affected by intermolecular hydrogen bonding unlike the stretching and out-of-plane bending vibrations [180]. In present case, the theoretical calculated O-H in-plane vibrations are found at 1140, 1092, 1073 cm⁻¹ in B3LYP/cc-pVDZ and 1141, 1106, 1085 cm⁻¹ in B3LYP/6-311G. The computed O-H out-of-plane bending of the title molecule is found at 348 cm⁻¹ and 350 cm⁻¹, respectively.

C-H vibrations

C-H stretching vibrations of hetero-aromatic compounds and their derivatives typically exhibit multiple weak modes in the range 3100-3000 cm⁻¹ [asymmetric] and 2990-2900 cm⁻¹ [symmetric] stretching range [181]. The experimental counter parts in this investigation were found at 3114, 2985, 2851 cm⁻¹ in FT-IR and 3065, 3001 cm⁻¹ in FT-Raman spectra, corresponding theoretical peaks found between 3112-2948 cm⁻¹ [B3LYP/6-311G].

Several medium to moderate intensity modes of C-H in-plane bending vibrations have been found in the range of 1300-1000 cm⁻¹. The C-H out-of-plane bending vibrations produces powerful modes in the range of 1000 to 650 cm⁻¹ [182]. In this study the computed frequencies for C-H in-plane and out-of-plane bending vibrations are 1370, 1196, 1065 cm⁻¹ [B3LYP/cc- pVDZ] and 1372, 1196 cm⁻¹ [B3LYP/6-311G] basis sets, which are well agree

with experimental frequencies 1369, 1116, 1195, 1109 cm⁻¹ (FT-IR) and 1066 cm⁻¹ (FT-Raman), respectively. In the title compound, benzene substituted C-H out-of-plane bending vibrations are observed as a strong and very strong intense modes at 875, 836 and 776 cm⁻¹ in FT-IR spectrum. The medium and weak intense modes are observed at 831 and 741 cm⁻¹ in FT- Raman spectrum. Similarly, the theoretical value of C-H out-of-plane bending vibrations appear at 876, 836, 777, 744 cm⁻¹ in B3LYP/cc-pVDZ and 875, 834, 775, 740 cm⁻¹ in B3LYP/6-311G.

Methyl group vibration

The asymmetric and symmetric stretching vibration of CH₃ are reported in the range 2900-3000 cm⁻¹ and 2900-2840 cm⁻¹ [183, 184]. In the present study, CH₃ asymmetric vibrations in the FT-IR and FT-Raman spectra were found at 2913 (m) and 2929 (w) cm⁻¹. These modes are calculated in B3LYP/cc-pVDZ at 2935, 2915 cm⁻¹ and B3LYP/6-311G at 2932, 2915 cm⁻¹. The symmetric stretching modes of the methyl group are calculated at 2875, 2863 cm⁻¹ in B3LYP/cc-pVDZ and 2874, 2863 cm⁻¹ in B3LYP/6-311G, respectively, whereas their experimental FT-Raman values have been observed as a medium peak at 2870 cm⁻¹. The CH₃ in-plane and out-of-plane bending vibrations seen at 1399 cm⁻¹ in the FT-Raman spectrum and 1413 cm⁻¹ in the FT-IR spectrum. Corresponding to theoretical values of in-plane bending vibrations are 1404, 1395 cm⁻¹ in B3LYP/cc-pVDZ and 1402, 1396 cm⁻¹ in B3LYP/6-311G. The out-of -plane bending vibrations are 1423, 1415 cm⁻¹ in B3LYP/cc-pVDZ and 1423, 1415 cm⁻¹ in B3LYP/6-311G. The out-of-plane rocking bands are found in FT-Raman at 1015 and 993 cm⁻¹, respectively. Generally, twisting vibrations of methyl group are identified below 500 cm⁻¹ [185, 186]. The calculated values of this mode are 230, 219 cm⁻¹ in B3LYP/cc-pVDZand 229, 217 cm⁻¹ in B3LYP/6-311G and experimentally at 183(w) cm⁻¹ in FT-Raman spectrum.

CH₂ vibrations

Mostly, CH₂ asymmetric and CH₂ symmetric stretching vibrations were identified in the range 3000 -2900 cm⁻¹ [109]. In the present investigation, the CH₂ asymmetric and symmetric stretching vibrations were computed at 2923, 2881 cm⁻¹ in B3LYP/6-311G, 2925 and 2880 cm⁻¹ in B3LYP/cc-pVDZ. The CH₂ rocking band observed in FT-IR spectrum at 1147 cm⁻¹ and FT-Raman spectrum at 1173 cm⁻¹, corresponding theoretical vibrations are identified at 1172,1146 cm⁻¹ in B3LYP/6-311G and 1175,1148 cm⁻¹ in B3LYP/cc-pVDZ. The in-plane scissoring vibration is found at 1390 cm⁻¹ in B3LYP/6-311G and 1392 cm⁻¹ in B3LYP/cc-pVDZ, and the twisting vibration of the title compound is calculated at 1103 cm⁻¹ B3LYP/6-311G and 1106 cm⁻¹ in B3LYP/cc-pVDZ basis sets.

Carbon ring vibrations

The aromatic ring C-C and C=C stretching vibrations are usually expected to be in the range of 1650-1200 cm⁻¹ [186]. In present case, C=C stretching band observed in FT-Raman at 1598(vs) and 1447(w) cm⁻¹. Corresponding theoretical values showed an excellent agreement with experimental data. C-C-C in-plane and out-of-plane bending modes are expected in the region 900-640 cm⁻¹ and 580-475 cm⁻¹ [187]. In this study, in-plane bending vibration was observed at 949 cm⁻¹ in FT-IR and 950 cm⁻¹ in FT-Raman spectrum. The C-C-C in-plane bending modes were calculated in the range of 950- 921 cm⁻¹ [B3LYP/6-311G] and 698-655 cm⁻¹ [B3LYP/cc-pVDZ].

C-O vibrations

The C-O group in the title compound produces three vibrations (stretching, in-plane bending and out-of-plane bending vibrations) [188]. The very strong band in FT-IR at 1664 cm⁻¹ and 1665 cm⁻¹ in both B3LYP/cc-pVDZ and B3LYP/6-311G are assigned to C-O stretching vibration of the title molecule. The computed values were at 1665 cm⁻¹ [B3LYP/6-311G] and 1666 cm⁻¹ [B3LYP/cc-pVDZ], respectively. The calculated band at

1568 cm⁻¹ in B3LYP/6-311G and 1570 cm⁻¹ in B3LYP/cc-pVDZ are assigned as C-O inplane bending vibration.

C-N and C-S vibrations

Identification of C-N and C-S stretching vibrations is a difficult task because it occurs in a complicated region of the vibrational spectrum [189, 190]. In this study, the C-N stretching vibration creates a prominent band in the FT-IR spectrum at 1557 (vs), 1256 (ms) cm⁻¹ and in the FT-Raman spectrum at 1561, 1447, 1255 cm⁻¹. The computed wavenumbers are at 1559, 1445, 1253 cm⁻¹ in B3LYP/6-311G and 1560, 1445, 1256 cm⁻¹ in B3LYP/cc-pVDZ. The C-S stretching vibration produce a medium band at 596(m) cm⁻¹ in FT-IR spectrum, 595 cm⁻¹ in B3LYP/6-311G and 598 cm⁻¹ in B3LYP/cc-pVDZ.

C-Cl vibrations

Generally, stretching, in-plane and out-of-plane vibration modes were used to identify the halogen band [178]. The stretching vibration mode of C₁₁- Cl₂₇ was noted in the FT-IR spectrum at 1007 cm⁻¹. The corresponding theoretical values are found at 1008 cm⁻¹ (B3LYP/6-311G) and 1010 cm⁻¹ (B3LYP/cc-pVDZ). The in-plane and out-of-plane bending frequencies for C-Cl vibrations are 649, 422 cm⁻¹ (B3LYP/6-311G) and 650, 427 cm⁻¹ (B3LYP/cc-pVDZ), respectively.

6.4.3 Frontier molecular orbital analysis

The highest occupied molecular orbital (HOMO), which carries electrons, has a tendency to give electrons and operates as an electron donor. On the other hand the lowest unoccupied molecular orbital (LUMO) is an orbital that can accept electrons. HOMO and LUMO are also known as frontier molecular orbitals (FMOs) because they generate greened isosurface circles, which are spotted in Fig. 6.4.

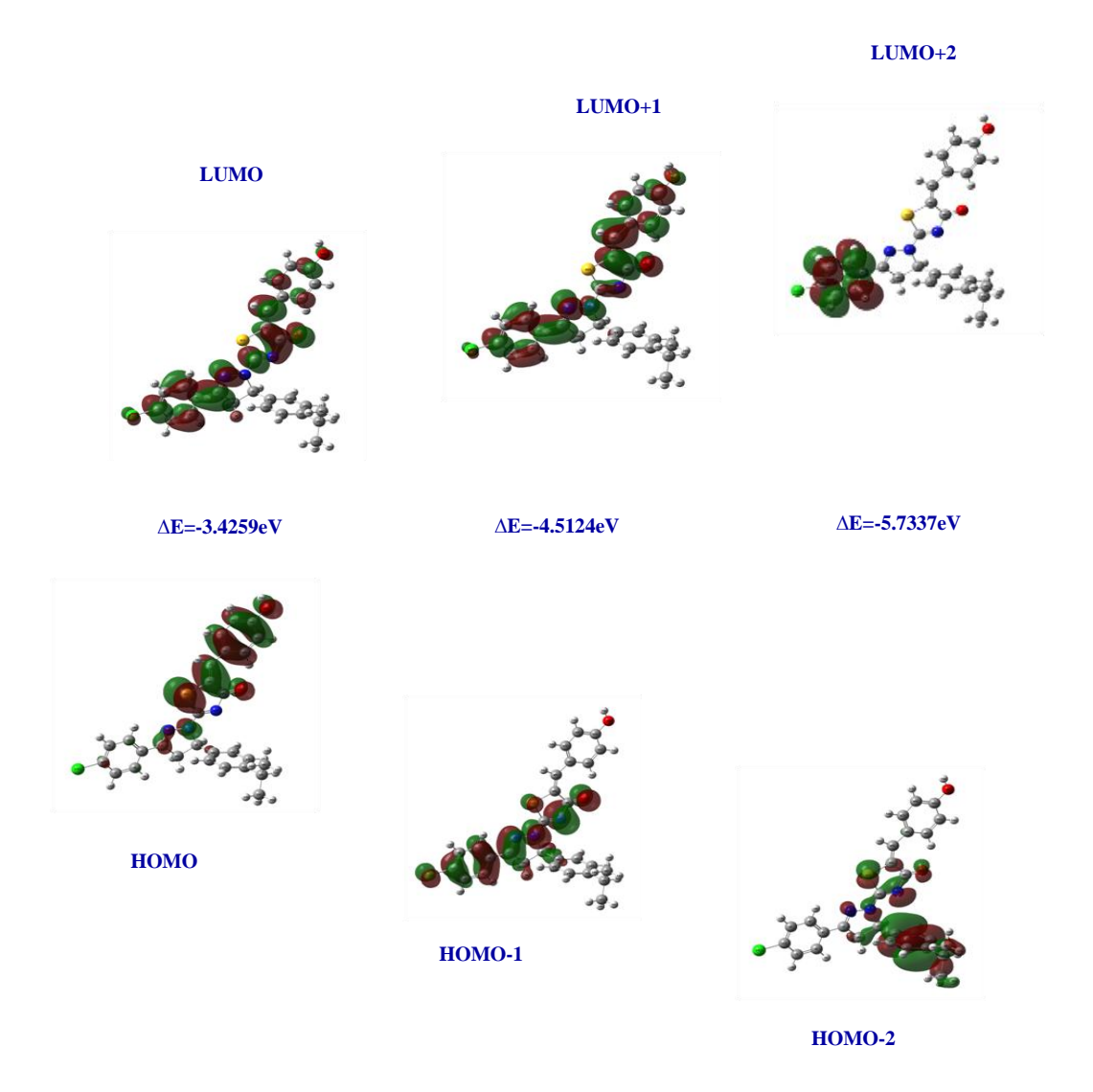


Fig. 6.4 HOMO - LUMO energy gap distribution of HCPPT at B3LYP/6-311G basis set

The positive surface is indicated by red colour and the negative surface is represented by green colour. In our analysis, FMOs energies and the corresponding energy gap was calculated for different energy distribution by B3LYP / cc-pVDZ basis set is reported as E_{HOMO} = -5.5005 eV , E_{LUMO} = -2.1189 eV, Energy gap (ΔE)= HOMO-LUMO = -3.3816 eV and B3LYP / 6-311G basis set is reported as E_{HOMO} = -5.8703 eV, E_{LUMO} = -2.4444 eV and energy gap ΔE =- 3.4259 eV. The HCPPT has a total of 543 orbits out of which 131 are occupied and the remaining 412 are virtual orbitals.

6.4.4 Global reactivity descriptors

HOMO and LUMO energy values (Frontier molecular orbital) can be used to calculate global chemical reactivity descriptors of organic molecules such as hardness, chemical potential, softness, electro negativity, and electrophilicity index [37, 191]. According to simple molecular orbital theory approaches; the HOMO energy is related to the ionization potential (I) and the LUMO energy has been used to estimate the electron affinity (A) respectively by the following relations

Ionization potential (I) =
$$-E_{HOMO}$$
 (6.1)

Electron affinity (A) = -
$$E_{LUMO}$$
 (6.2)

Electro- negativity
$$\chi = (I + A)/2$$
 (6.3)

Chemical potential
$$\mu = -(I + A)/2$$
 (6.4)

Hardness
$$\eta = (I - A)/2$$
 and (6.5)

Softness
$$\sigma = 1/\eta$$
 (6.6)

Electrophilicity index
$$\omega = \mu^2 / 2\eta$$
 (6.7)

The calculated values of the global reactivity descriptors for the title molecule are collected in Table 5.5.

6.4.5 Molecular Electrostatic Potential

The molecular electrostatic potential (MEP) map aids to predict the probable reactive region for electrophile-nucleophile interactions. Maximum negative regions that are electron rich are represented by the red colour, and this red represents the region of electrophilic attack. The maximum positive region is depicted by a deep blue colour and this blue represents the region of nucleophilic attack. [192]. Using the computer software Gauss view, a mapped electrostatic potential surface for the title molecule was plotted and shown in Fig.6.5.

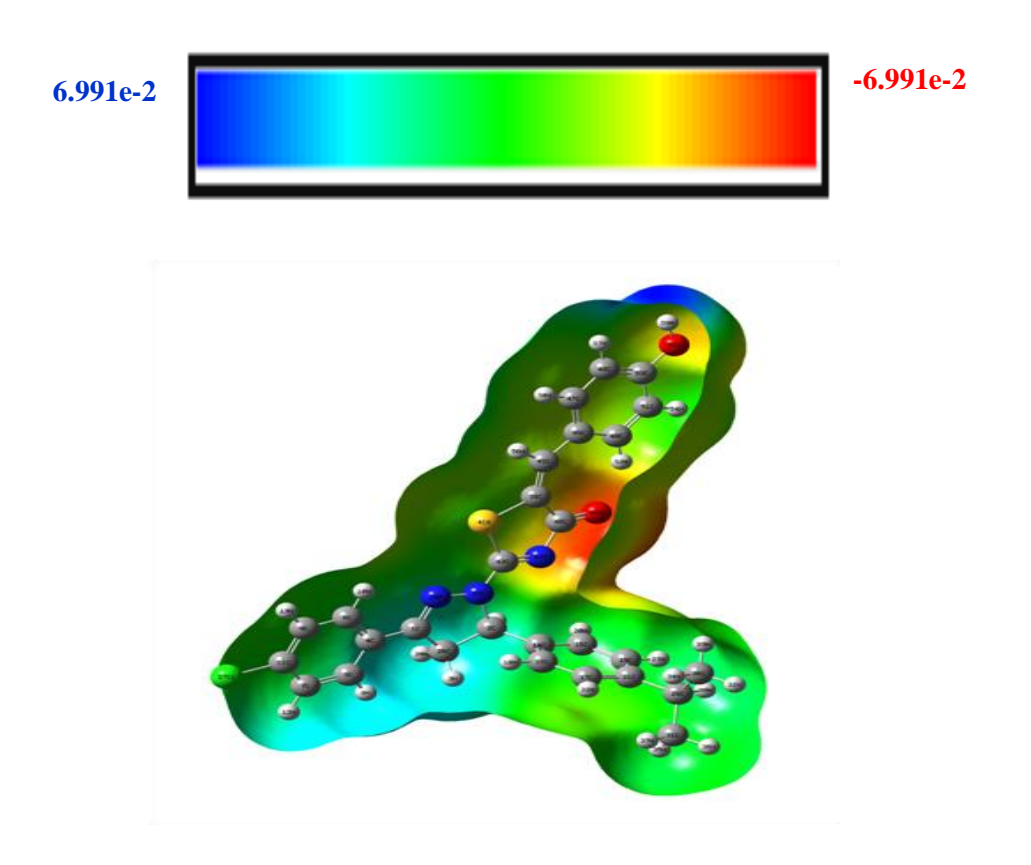


Fig. 6.5 Molecular electrostatic potential surface (MEP) of HCPPT

6.4.6 NBO analysis

NBO analysis is a helpful tool for understanding electronic charge transfer and intramolecular interactions takes place inside a molecule [193]. To explore various second-order interactions, the computation was performed using NBO at the DFT/B3LYP level. This is a measure of the delocalization (or) hyper conjugation of the title compound. The stabilization energy E(2) associated with the delocalization $i \rightarrow j$ are expressed as the equation (6.8).

$$E(2) = \Delta E_{ij} = q_{i} \frac{(F_{i,j})^{2}}{(E_{i} - E_{i})}$$
(6.8)

where q_i is the donor orbital occupancy, E_i and E_j are diagonal elements and F (i, j) is the off-diagonal NBO element. From the second order perturbation analysis of Fock Matrix, NBO shows the delocalization of electron density between occupied Lewis-type (bond or

lone pair) and unoccupied Non- Lewis-type. The identified results have been tabulated in Table 6.5. The most important hyper conjugative interactions are

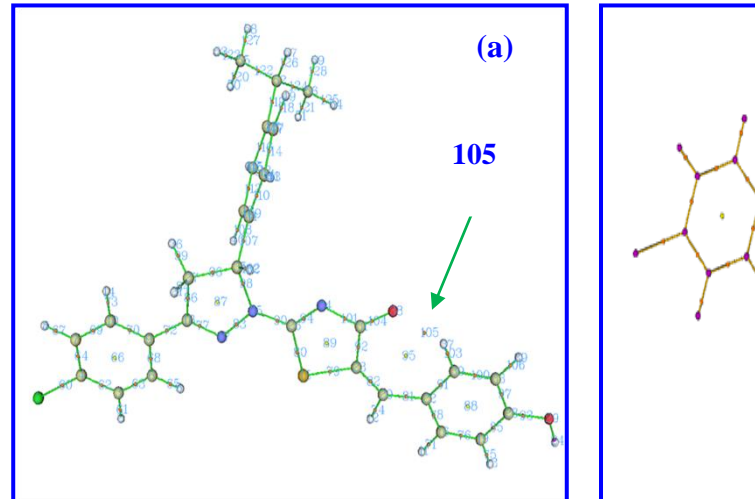
- $ightharpoonup \pi C_{39}$ - C_{45} \rightarrow LP(2) S_{41} leading to the stabilization energy is 533.9 kcal/mol.
- $\rightarrow \pi^*C_7-C_{11} \rightarrow \pi^*C_4-C_5$ stabilization energy is 196.05 kcal/mol.
- $ightharpoonup \pi^*C_7\text{-}C_{11} \to \pi^*C_6\text{-}C_9$ stabilization energy is 131.65 kcal/mol.
- $ightharpoonup \pi C_{42}$ -N₄₃ \rightarrow LP(2) S41 stabilization energy is 102.44 kcal/mol.
- ightharpoonup LP(2) S₄₁ $\rightarrow \pi$ *C₄₂- N₄₃ stabilization energy is 99.74 kcal/mol.
- ightharpoonup LP(2) S₄₁ $\rightarrow \pi^*$ C₃₉-C₄₅ stabilization energy is 65.79 kcal/mol.
- \rightarrow π^*C_{42} - $N_{43} \rightarrow \pi^*C_{40}$ - O_{44} stabilization energy is 53.08 kcal/mol.

Above results clarify the lone pair of sulphur atom (LP(2) S_{41}) interacts with nearby carbon, nitrogen, and oxygen atoms in a hyper conjugative manner.

6.4.7 Topology analysis

Atoms in molecules

Atoms in molecule analysis are presented in Fig. 6.6 (a).



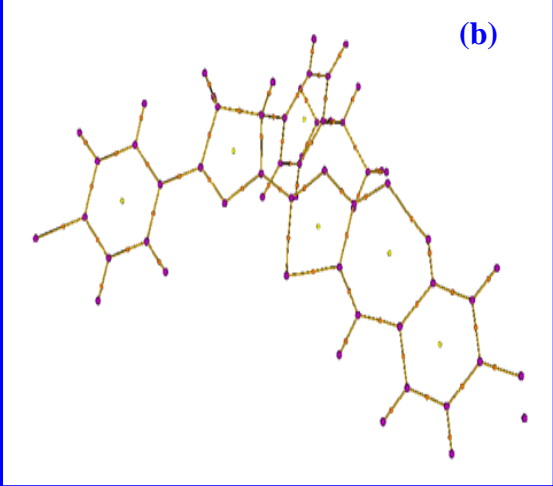


Fig. 6.6 AIM map and bond critical point map of the HCPPT bonding region

It is a scalar field in three dimensions. The number of critical points are the best ways to summarize the topological characteristics of a scalar field. Four types of critical points

exist: (3,-3) nuclear critical point (NCP); (3,-1) bond critical point (BCP); (3,+1) ring critical point (RCP); and (3,+3) cage critical point (CCP). In the form of AIM [41], the following topological equation states that of molecules:

$$n_{NCP} - n_{BCP} + n_{RCP} - n_{CCP} = \begin{cases} {}^{1(Isolated-molecules)} \\ {}^{0(Infinite-crystals)} \end{cases}$$

$$(6.9)$$

$$(3,-3): 59, (3,-1): 63, (3,+1): 6, (3,+3): 0$$

$$59 - 63 + 6 - 0 = 1$$

where n is the number of the critical point (CP) subscripted type. In the field of topographic analysis, Poincare-Hopf relationship is well known CP represents isolated state of the compound HCPPT. The molecular graph shows magenta sphere as (3,-3) - nuclear critical point, orange sphere as (3,-1) - bond critical point, and yellow sphere as (3,+1) - ring critical point. This result describes the relationship between bond energy E_{HB} (6.10) and potential energy density V(r) corresponding BCP as

$$E_{HB} = V(r_{BCP})/2 (6.10)$$

One bond critical point (105) is associated with a very weak (O44-C40-C39-C45-C46-C48 -H52) hydrogen bonding interaction. The intramolecular interaction of hydrogen bond energy (E_{HB}) at bond critical point (BCP) output indicates E_{HB} =-(0.035288)/2*2625.5=-46.32 KJ/mol. The topological model of bond is presented in Fig. 6.6 (b).

Localized orbital locator (LOL) and electron localization function (ELF)

The electron density properties can be used to analyze covalent bonds, electron lone pairs, and atomic shell structure using the localization orbital locator (LOL) and electron localization function (ELF). The surface analysis based on covalent bonds offers the ELF and LOL maps, which show the regions of molecular space with a high possibility of detecting an electron pair. [45, 194]. Based on Pauli repulsion a complete LOL is denoted by $\tau(r)$ and ELF is denoted by $\eta(r)$ resulting in an kinetic energy density using Multiwfn

programme. LOL simply displays the gradients of the localized orbitals and is maximized when axis of the limits from 0.00 to 0.800. The localized over the regions are presented in Fig.6.7.

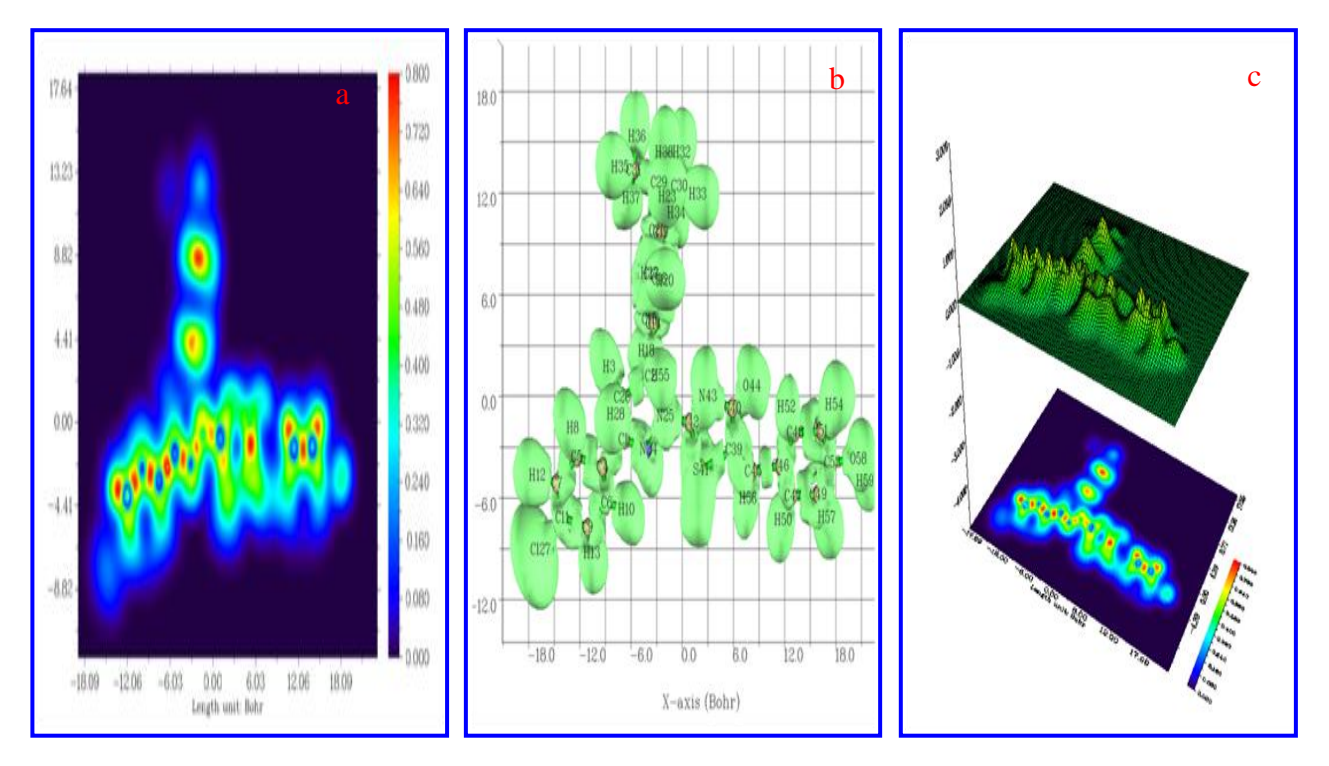


Fig. 6. 7 (a) Localized orbital locator (LOL) for HCPPT obtained in xy plane, (b) Electron localization function (ELE) with isosurface and (c) ELE shaded surface map with projection effect.

Localized orbital locator (LOL) plane map has been shown in Fig.6.7 (a), in this the thiazol - pyrazol core bonding with benzene ring is shown by a blue colour circle and BCP (Bond Critical Point) has been shown by red with yellow colour circle in XY. Electron localization function (ELE) isosurface of the title molecule shown in Fig 6.7 (b) which shows the relation between LOL and ELF regions. From electron localization function (ELF) analysis, it is need to find the positions of shared and unshared isosurface. By defining the value of ELF, $\eta(r)$ ranges from 0.0 to 0.800, where relatively high values in the interval 0.800 to 0.5 indicate regions containing bonding and anti-bonding localized electrons. The high values in the range from 0.800 to 0.5 represent regions containing bonding and anti-bonding centralized electrons, and lower values (>0.5) indicates the

domains where electrons are delocalized. Next, high electron localization zones between core and lone pair to valence atoms are revealed by the red ring like region around each hydrogen, chlorine (LP) and oxygen (LP) atoms of the title compound. Colour shade maps or contour maps of bonding regions are presented in Fig.6.7 (c).

Reduced density gradient analysis (RDG)

The reduced density gradient is a key quantity in the density functional theory coming from density $\rho(r)$, and used to give the details of the homogeneous distribution of the electron. This is a non-dimensional quantity written in the following form (6.11):

$$RDG(r) = \frac{1}{2(3\pi r^2)^{1/2}} \frac{|\nabla \rho(r)|}{\rho(r)^{4/3}}$$
(6.11)

Johnson et al.[52] found that low-value RDG isosurface provides a simple description of the interaction zones. As a result, the low-gradient isosurface (RDG) is able to detect and visualize weak interactions by specific non-covalent interactions (NCI). In the current study three types of interacting regions are identified by NCI: a strong attraction (blue) in hydrogen, a steric repulsion (red) in the ring centers, and a weakly attraction (green) in π -stacking between the rings. From the Fig. 6.8, it is seen that the non-bonded overlap ring found in the thiazol ring, chlorine atom is identified as a steric interaction (red colour) and the strong isosurfaces. Secondly, within the methyl bond and the non-covalent thiazol-pyrazol core, the reactive green isosurfaces (semi- red and green colour) reveal a mildly attractive vanderWaals interaction. Lastly, a hydrogen bond is indicated by the blue dot closer between thiazol and hydroxybenzylidene of the compound.

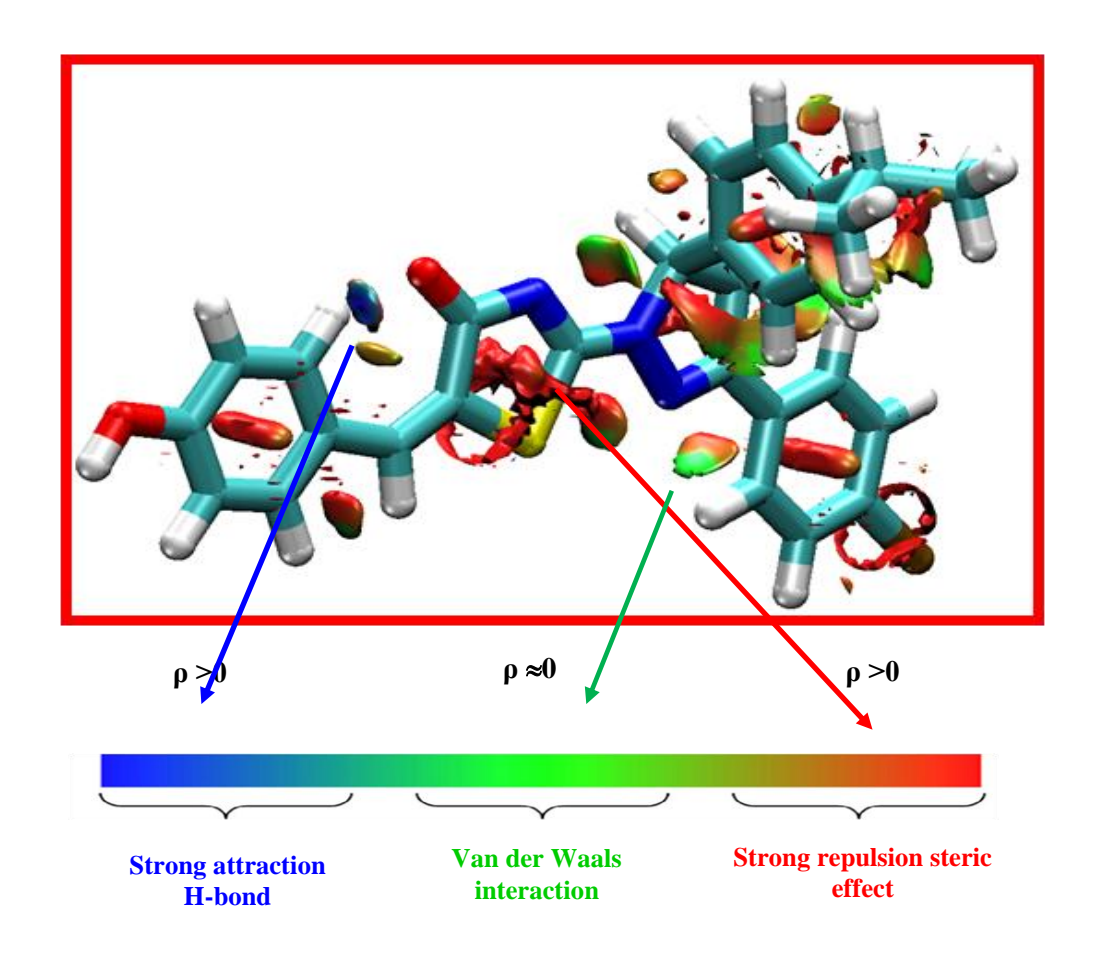


Fig. 6.8 RDG 3D colour scaling of non-covalent interaction in HCPPT

6.4.8. Antimicrobial activity

Microorganisms are the agents of many diseases. Different antimicrobial agents kill microorganisms and inhibitor or arrest their growth. Antimicrobial activity can be detected using a variety of screening methods. Among them, antimicrobial activity is used to perform the disk-diffusion method [195]. In this method, the agar plate surface is inoculated by spreading a volume of the microbial inoculum over the entire agar surface. Then, a hole with a diameter of 5 to 8 mm is punched aseptically with a sterile cork borer or a tip. DMSO standard is diluted (1:100) of the antimicrobial solution with different concentration (25 μg/ml, 50 μg/ml, 75 μg/ml, 100 μg/ml) is introduced into the well. Then, agar plates are incubated under suitable conditions depending upon the test microorganism. The activity in contact with bacterial and fungal pathogens was photographed and shown in Fig. 6.9 (a).

HCPPT was screened for its in vitro antibacterial activity against two Gram-positive bacteria: *Staphylococcus aureus, Bacillus subtilis*, two Gram-negative bacteria: *Escherichia coli, Pseudomonas aeruginosa*, two fungal strains: *Candida albicans and Aspergillus Niger*. Results revealed that the compound showed zone of inhibition which is plotted in the form of bar graph [Fig. 6.9 (b)] and tabulated in Table 6.6. The bar graph pictured the different concentrations values. According to the range of concentration 25 μg/ml-violet colour, 50 μg/ml-red colour, 75 μg/ml -green colour, 100 μg/ml-pink colour inhibition, compared with controls concentration, respectively. The results of an inhibition zone are lies between 12-25 mm. A standardized bar graph of zone size and antibacterial strains reveals good antibacterial activity against Escherichia coli at 100 μg/ml and good antifungal activity against Candida albicans at control concentration μg/ml.

6.4.9. Molecular Docking

PASS (prediction of activity spectra for substance) [161] is a web- based tool that reveals a new biological target for the most possible active sites of ligand (Table.6.7). Molecular docking simulations were performed using an Auto Dock/tool [57]. This biological, computational research started with the examination of known protein data bank (PDB) structure. The optimized structure of the ligand was obtained from DFT/B3LYP/ 6-311G basis set as a (ligand*. pdb) input file format. PASS Selective disease inhibition proteins are downloaded from the Research Collaboratory for structural Bioinformatics (RCSB) protein data bank [64]. The native protein site is removed from the active site and the new binding site are taken in the format. Moreover, docking area is selected by constructing a grid box of size $120 \times 120 \times 120$ points centered at x, y, and z coordinates, using Auto Grid. The Auto dock parameters, a Lamarckian genetic algorithm (LGA) explore the binding modes of the protein [62]. The conformational docking trials based on searches: 100, population size: 150, maximum number of energy evaluations: 250000, maximum

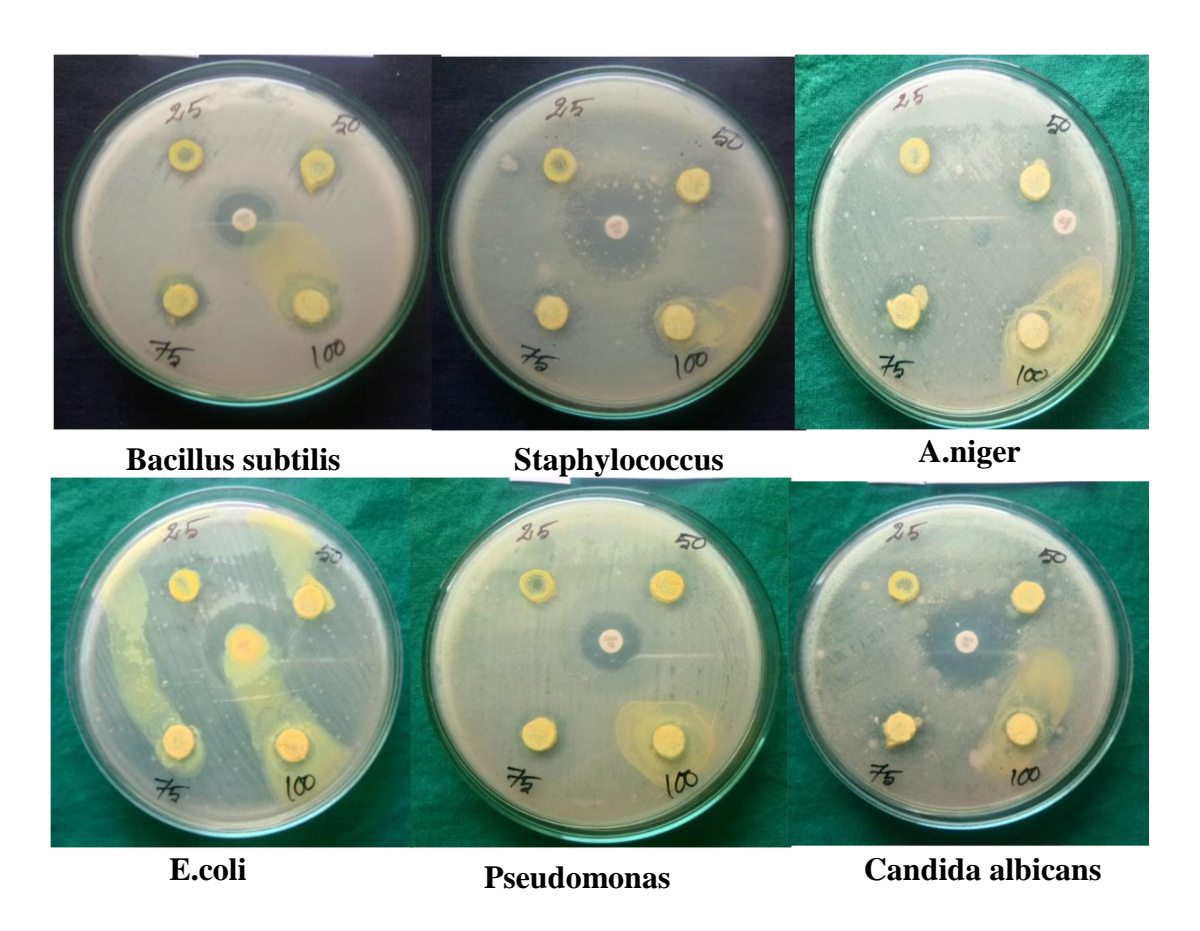


Fig.6.9 (a) Anti bacterial study and anti-fungal Study

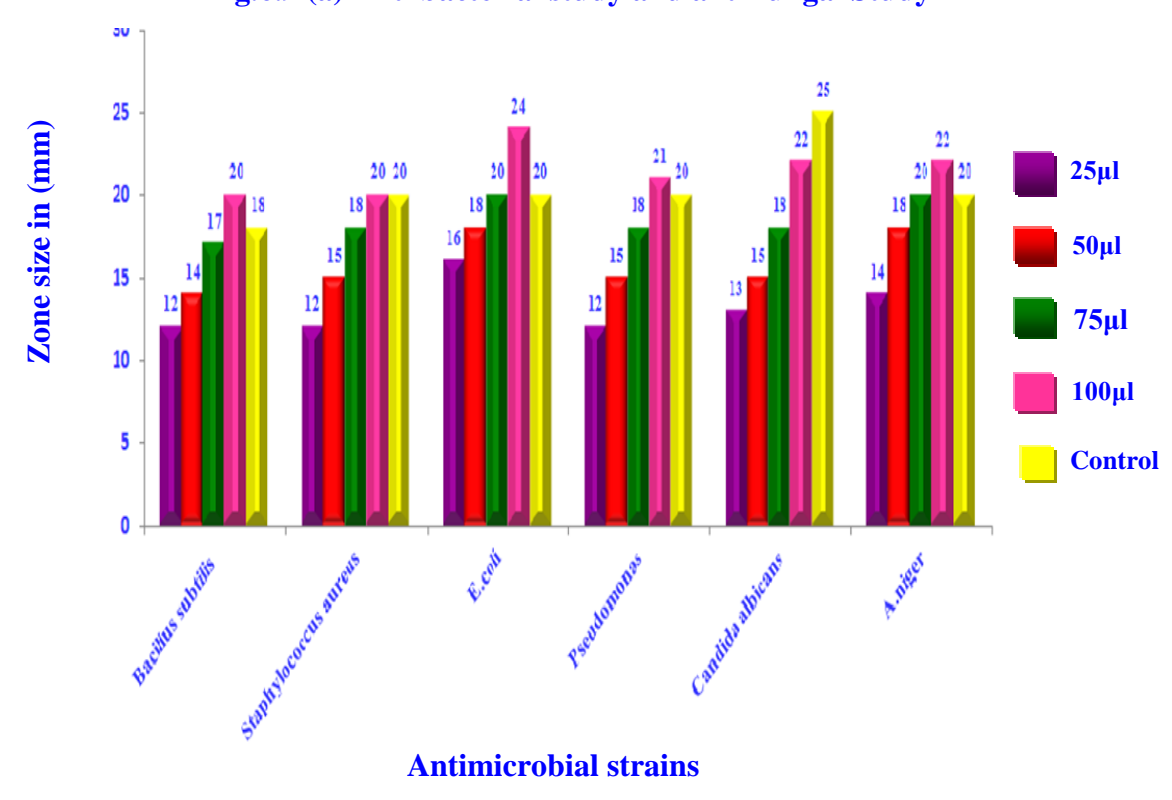


Fig. 6.9 (b) Bar graph of anti bacterial study and anti-fungal Study of HCPPT

number of retries: 10000, and root-mean-square (RMS) cluster tolerance: 2.0 Å, respectively. Figs. 6.10 (a, b, c, d, e, f) show the validate lowest binding affinity of the compound was constructed and visualized using PYMOL. The dotted lines show the minimum docking energy of residual interactions. The values were investigated and tabulated in Table 6.8.

From the best lowest energy (or) docked position of the ligand with target protein (6iap, 1uhp, 6pgp, 5zxi, 1jei, 4zbr) the Auto Dock binding affinity (kcal/mol), inhibitory constants (nM or pM or μ M), and nature of the bond with residues were evaluated as follow:

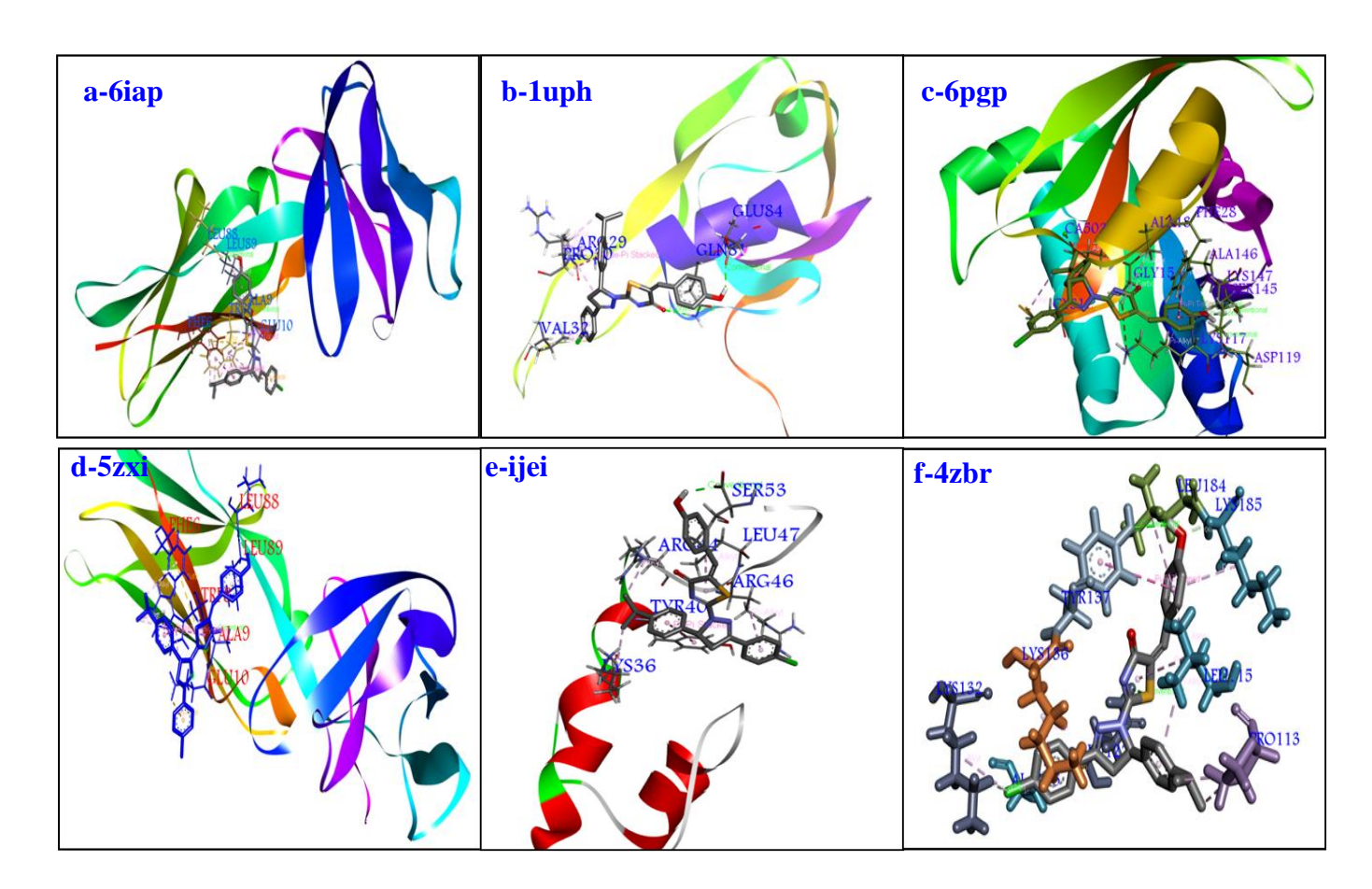


Fig. 6.10 The molecular docking results of the HCPPT compound with antineoplastic proteins a-6iap, b-1uph, c-6pgp, Anti-cancer proteins d-5zxi, e- 1jei, anti-inflammatory proteins f-4zbr

Ligand active interaction with Antineoplastic (solid tumors)

The binding mechanism of the ligand to the target with protein 6iap (antibody) Fig.6.10 (a) is discussed below: The amino acid bond interaction of 6iap with HPCPT are conventional hydrogen bond interaction with residue (2.0; LEU A: 88), van der Waals bond interaction with residue (2.1; ASP A: 90) and Pi-sigma bond interaction with residue (1.7; TRP A: 80). The binding affinity of its protein-ligand interactions are - 8.10, -7.61, -6.94 kcal/mol, respectively. The inhibition constants are 1.15 μ M, 2.63 μ M, and 8.25 μ M, with RMSD values of 26.964 Å, 38.622 Å, and 27.304 Å.

Ligand active interaction with solid tumors

To illustrate the ligand binding mechanism to the target protein 1uhp, 6pgp Figs.6.10 (b, c) as follows: The docked 1uhp from bond interaction were evaluated from the amino acid. The conventional hydrogen bond interaction with residue (2.1; GLU A:84 and 2.0; GLN A 81), and Pi-alkyl bond interaction with residue (2.5; PRO A 30). The binding affinity, RMSD values and corresponding inhibition constants are -7.27, -7.07, -7.03 kcal/mol, 14.866, 15.016, 11.534 Å, and 4.67, 6.56, 7.03 μM, respectively. The amino acid bond interaction of 6PGP with the title compound are conventional hydrogen bond interaction with residue (2.5; ALA A:146), Pi-alkyl bond interaction with residue (2.2; LYS A:147) and carbon hydrogen bond with residue (1.8; ASP A: 119). The value of -10.49, -10.47, -9.59 kcal/mol is the binding affinity of the protein-ligand interaction. With RMSD values of 15.494 Å, 10.167 Å, and 11.118 Å, the inhibition constants are 20.46 nM, 20.99 nM, and 93.32 nM, respectively.

Ligand active interaction with Anti-cancer

Figs.6.10 (d, e) show the illustration of the ligand binding mechanism to the target protein 5zxi, 1jei. The amino acid bond interaction of 5zxi with the title compound are conventional hydrogen bond interaction with residue (2.1; GLU A:22), Pi- Donor hydrogen

bond interaction with residue (3.0; THR A: 252) and Alkyl bond interaction with residue (2.3; LEU A: 294). The protein-ligand interaction shown the resultant binding affinity is -12.39, -7.73, -7.54 kcal/mol. The inhibition constant values are identified as 823.92 pM, 2.16 μM, 2.95 μM, and RMSD value is 50.441 Å, 45.109 Å, and 57.650Å. Further, The protein interaction of 1JEI amino acid bonds with the title compound is a conventional hydrogen bond interaction with residue (2.0; SER A: 53), Alkyl interaction with residue (2.9; ARG A: 46), and Pi- Pi Stacked interaction with residue (3.5; TYP A: 40). In the protein-ligand binding, -8.68, -7.68, -7.48 kcal/mol are observed binding energies and 434.57 nM, 2.35 μM, 3.27 μM are the inhibition constants, with RMSD values of 11.451 Å, 8.628 Å, and 8.667 Å. This low value of binding energy (Pico size) shows that this molecule is a good anti-cancer drug.

Ligand active interaction with anti-inflammatory

The target protein 4zbr interact with ligand shown in Fig.6.10 (f) as follows: The amino acid bond interaction of 4zbr involved with the HCPPT is two conventional hydrogen bond interaction with residue (2.3; TRY A: 137, 2.8; LYS A: 132) and Pi-cation bond interaction with residue (3.2; LYS A: 130). The binding affinity of the protein-ligand interaction is shown by the docking results of -8.59, -7.90, -7.41 kcal/mol. The inhibition constant values are 504.42 nM, 1.62 μ M, 3.71 μ M, and RMSD value is 77.419 Å, 77.418 Å, and 76.601 Å.

6.5 Conclusion

Quantum chemical techniques are being more widely employed in computational chemistry calculations to investigate the mechanism of simulations and interactions. The following conclusions are obtained for the HCPPT.

A comprehensive vibrational analysis of 5-(4-Hydroxybenzylidene)-2-[3-(4-chlorophenyl)-5-[4-(propan-2-yl) phenyl]-4, 5-dihydro-1*H*- -1-yl]-1,3-thiazol-4(5*H*)-one

- (HCPPT) was obtained experimentally using FT-IR and FT-Raman. Similarly, using the DFT/B3LYP/cc-PVDZ, 6-311G basis set, they are theoretically computed. The measured and predicted vibrational frequencies have an excellent correlation with literature values.
- ➤ B3LYP/6-311G approach was used to find the HOMO and LUMO electronic charge density as well as the energy band gap. The charge density shows the localized active site of FMOs excitation. The energy gap between HOMOs and LUMOs shows that the HCPPT molecule has significant charge mobility with increasing excitation energy.
- ➤ MEP map indicates that the oxygen atom related to electrophilic reactivity and hydrogen bonded with oxygen atom related to nucleophilic reactivity.
- ➤ NBO analysis shows that the different Lewis and non-Lewis interactions of energies are due to the presence of sulphur, nitrogen atoms, and OH.
- AIM analysis confirms the presence of an intramolecular interaction with an energy of 46.32 KJ/mol in the hydrogen bond O44-H27---N14.
- ➤ Electron localization function (ELF) and localised orbital locator (LOL) studies confirmed the surface electron density core, lone pair, and valance findings.
- ➤ The RDG isosurface of HCPPT displays a intra-, inter-molecular non-covalent and weak interactions (van der Waals forces) in thiazol and pyrazol rings.
- ➤ The antimicrobial activity inhibition was plotted in the form of bar graph to display biological activity of HCPPT.
- Finally, Molecular docking simulations are used to explore the Antineoplastic (solid tumors) Anticancer and anti-inflammatory interaction mechanism of HCPPT. Most of the protein -ligand interaction shows that inhibition constants are nano in size, especially anti-cancerous protein 5zxi having higher Pico-size.

Table 6.1: Molecular geometry [bond length (Å)] of HCPPT by B3LYP/cc-pVDZ and B3LYP/6-311G basis sets with XRD

	Bond lengt	th (Å)			Bond length	ı (Å)		Bond length (Å)			
Parameter	B3LYP/ cc-PVDZ	B3LYP/ 6-311G	XRD*	Parameter	B3LYP/ cc-PVDZ	B3LYP/ 6-311G	XRD	Parameter	B3LYP/ cc-PVDZ	B3LYP/ 6-311G	XRD*
C_1 - C_4	1.46	1.46	1.46	C_{15} - H_{18}	1.09	1.08	0.93	C ₃₉ -C ₄₅	1.36	1.36	1.34
C_1-N_{24}	1.29	1.30	1.29	C_{16} - C_{19}	1.40	1.40	1.39	C_{40} - N_{43}	1.40	1.41	1.38
C_1 - C_{26}	1.52	1.52	1.50	C_{16} - H_{20}	1.09	1.08	0.93	C_{40} - O_{44}	1.22	1.25	1.22
C_2 - C_{14}	1.52	1.52	1.51	C_{17} - C_{21}	1.41	1.41	1.38	S_{41} - C_{42}	1.78	1.84	1.76
C_2-N_{25}	1.49	1.51	1.51	C_{17} - H_{22}	1.09	1.08	0.93	C_{42} - N_{43}	1.30	1.30	1.30
C_2 - C_{26}	1.55	1.56	1.47	C_{19} - C_{21}	1.40	1.40	1.39	C_{45} - C_{46}	1.46	1.46	1.45
C_2 - H_{55}	1.10	1.09	0.98	C_{19} - H_{23}	1.09	1.08	0.98	C_{45} - H_{56}	1.10	1.09	0.93
H_3 - C_{26}	1.10	1.09	0.97	C_{21} - C_{29}	1.52	1.53	1.52	C_{46} - C_{47}	1.41	1.42	1.39
C_4 - C_5	1.41	1.41	1.38	N_{24} - N_{25}	1.37	1.39	1.38	C_{46} - C_{48}	1.42	1.42	1.39
C_4 - C_6	1.41	1.41	1.40	N_{25} - C_{42}	1.35	1.35	1.34	C_{47} - C_{49}	1.39	1.39	1.38
C_5 - C_7	1.40	1.40	1.37	C_{26} - H_{28}	1.10	1.09	0.97	C_{47} - H_{50}	1.09	1.08	0.93
C_5 - H_8	1.09	1.08	0.93	C_{29} - C_{30}	1.54	1.55	1.41	C_{48} - C_{51}	1.39	1.39	1.37
C_6 - C_9	1.39	1.39	1.37	C_{29} - C_{31}	1.54	1.54	1.41	C_{48} - H_{52}	1.09	1.08	0.93
C_6 - H_{10}	1.09	1.08	0.93	C_{29} - H_{38}	1.10	1.09	0.96	C_{49} - C_{53}	1.40	1.40	1.38

C ₇ -C ₁₁	1.40	1.39	1.36	C ₃₀ -H ₃₂	1.10	1.09	0.96	C ₄₉ -H ₅₇	1.09	1.08	0.93
C_7 - H_{12}	1.09	1.08	0.93	C_{30} - H_{33}	1.10	1.09	0.96	C_{51} - C_{53}	1.40	1.40	1.36
C_4 - C_6	1.41	1.41	1.40	N_{25} - C_{42}	1.35	1.35	1.34	C_{47} - C_{49}	1.39	1.39	1.38
C_5-C_7	1.40	1.40	1.37	C_{26} - H_{28}	1.10	1.09	0.97	C_{47} - H_{50}	1.09	1.08	0.93
C_5 - H_8	1.09	1.08	0.93	C_{29} - C_{30}	1.54	1.55	1.41	C_{48} - C_{51}	1.39	1.39	1.37
C_6 - C_9	1.39	1.39	1.37	C_{29} - C_{31}	1.54	1.54	1.41	C_{48} - H_{52}	1.09	1.08	0.93
C_6 - H_{10}	1.09	1.08	0.93	C_{29} - H_{38}	1.10	1.09	0.96	C_{49} - C_{53}	1.40	1.40	1.38
C_7 - C_{11}	1.40	1.39	1.36	C_{30} - H_{32}	1.10	1.09	0.96	C_{49} - H_{57}	1.09	1.08	0.93
C_7 - H_{12}	1.09	1.08	0.93	C_{30} - H_{33}	1.10	1.09	0.96	C_{51} - C_{53}	1.40	1.40	1.36
C_9 - C_{11}	1.40	1.39	1.38	C_{30} - H_{34}	1.10	1.09	0.96	C_{51} - H_{54}	1.09	1.08	0.93
C_9 - H_{13}	1.09	1.08	0.93	C_{31} - H_{35}	1.10	1.09	0.96	C_{53} - O_{58}	1.36	1.39	1.37
C ₁₁ -Cl ₂₇	1.76	1.83	1.78	C_{31} - H_{36}	1.10	1.09	0.96	O_{58} - H_{59}	0.97	0.97	0.96
C_{14} - C_{15}	1.40	1.40	1.37	C_{31} - H_{37}	1.10	1.09	0.96				
C_{14} - C_{16}	1.40	1.40	1.37	C_{39} - C_{40}	1.51	1.49	1.50				
C_{15} - C_{17}	1.39	1.39	1.38	C_{39} - S_{41}	1.79	1.85	1.75				

^{*-} Taken from Ref.[87]

Table 6.2: Molecular geometry [bond angle (°)] of HCPPT by B3LYP/cc-pVDZ and B3LYP/6-311G basis sets

В	Sond angle (°)		В	ond angle (°)		Bond angle (°)			
Domomoton	B3LYP/	B3LYP/	Downwoton	B3LYP/	B3LYP/	Danamatan	B3LYP/	B3LYP/	
Parameter	cc-PVDZ	6-311G	Parameter	cc-PVDZ	6-311G	Parameter	cc-PVDZ	6-311G	
C ₄ -C ₁ -N ₂₄	121.66	121.59	C_{15} - C_{17} - C_{21}	121.19	121.09	C_{40} - C_{39} - S_{41}	108.78	108.92	
C_4 - C_1 - C_{26}	125.23	125.32	C_{15} - C_{17} - H_{22}	118.88	119.03	C_{40} - C_{39} - C_{45}	132.64	133.03	
N_{24} - C_1 - C_{26}	113.09	113.08	C_{21} - C_{17} - H_{22}	119.93	119.88	S_{41} - C_{39} - C_{45}	118.59	118.05	
C_{14} - C_2 - N_{25}	112.22	112.10	C_{16} - C_{19} - C_{21}	121.38	121.29	C_{39} - C_{40} - N_{43}	112.76	113.46	
C_{14} - C_2 - C_{26}	115.14	115.37	C_{16} - C_{19} - H_{23}	119.24	119.34	C_{39} - C_{40} - O_{44}	124.89	124.67	
C_{14} - C_2 - H_{55}	108.86	109.18	C_{21} - C_{19} - H_{23}	119.38	119.37	N_{43} - C_{40} - O_{44}	122.36	121.87	
N_{25} - C_2 - C_{26}	100.16	100.16	C_{17} - C_{21} - C_{19}	117.64	117.81	C_{39} - S_{41} - C_{42}	87.64	86.22	
N_{25} - C_2 - H_{55}	107.69	107.36	C_{17} - C_{21} - C_{29}	121.54	121.42	N_{25} - C_{42} - S_{41}	119.19	119.89	
C_{26} - C_2 - H_{55}	112.36	112.18	C_{19} - C_{21} - C_{29}	120.81	120.76	N_{25} - C_{42} - N_{43}	121.97	122.72	
C_1 - C_4 - C_5	120.75	120.67	C_1 - C_{24} - N_{25}	108.87	108.69	S_{41} - C_{42} - N_{43}	118.84	117.38	
C_1 - C_4 - C_6	120.78	120.68	C_2 - N_{25} - N_{24}	114.01	113.33	C_{40} - N_{43} - C_{42}	111.99	114.02	
C_5 - C_4 - C_6	118.47	118.65	C_2 - N_{25} - C_{42}	124.63	124.80	C_{39} - C_{45} - C_{46}	135.20	135.13	
C_4 - C_5 - C_7	121.06	120.94	N_{24} - N_{25} - C_{42}	121.15	121.79	C_{39} - C_{45} - H_{56}	113.62	113.73	
C_4 - C_5 - H_8	120.27	120.34	C_1 - C_{26} - C_2	102.99	103.62	C_{46} - C_{45} - H_{56}	111.19	111.14	
C_7 - C_5 - H_8	118.67	118.72	C_1 - C_{26} - H_3	112.41	112.48	C_4 - C_{46} - C_{47}	116.30	116.09	
C_4 - C_6 - C_9	120.93	120.80	C_1 - C_{26} - H_{28}	110.27	110.44	C_{45} - C_{46} - C_{48}	126.37	126.38	
C_4 - C_6 - H_{10}	118.99	119.08	C_2 - C_{26} - H_3	111.76	111.28	C_{47} - C_{46} - C_{48}	117.33	117.53	

C ₉ -C ₆ -H ₁₀	120.09	120.12	C_2 - C_{26} - H_{28}	112.12	111.62	C_{46} - C_{47} - C_{49}	121.93	121.79
C_5 - C_7 - C_{11}	119.23	118.74	H_3 - C_{26} - H_{28}	107.36	107.46	C_{46} - C_{47} - H_{50}	119.25	119.25
C_5 - C_7 - H_{12}	120.69	120.72	C_{21} - C_{29} - C_{30}	111.73	111.79	C_{49} - C_{47} - H_{50}	118.83	118.97
C_{11} - C_7 - H_{12}	120.08	120.54	C_{21} - C_{29} - C_{31}	111.99	112.03	C_{46} - C_{48} - C_{51}	120.97	120.81
C_6 - C_9 - C_{11}	119.41	118.92	C_{21} - C_{29} - H_{38}	106.73	106.93	C_{46} - C_{48} - H_{52}	118.64	118.94
C_6 - C_9 - H_{13}	120.70	120.71	C_{30} - C_{29} - C_{31}	111.18	111.04	C_{51} - C_{48} - H_{52}	120.39	120.25
C_{11} - C_9 - H_{13}	119.89	120.37	C_{30} - C_{29} - H_{38}	107.45	107.36	C_{47} - C_{49} - C_{53}	119.67	119.31
C_7 - C_{11} - C_9	120.90	121.95	C_{31} - C_{29} - H_{38}	107.45	107.38	C_{47} - C_{49} - H_{57}	120.18	120.24
C_7 - C_{11} - Cl_{27}	119.61	119.07	C_{29} - C_{30} - H_{32}	110.63	110.47	C_{53} - C_{49} - H_{57}	120.15	120.45
C_9 - C_{11} - Cl_{27}	119.49	118.98	C_{29} - C_{30} - H_{33}	111.28	111.10	C_{48} - C_{51} - C_{53}	120.63	120.33
C_2 - C_{14} - C_{15}	121.43	121.50	C_{29} - C_{30} - H_{34}	111.36	111.20	C_{48} - C_{51} - H_{54}	120.79	121.02
C_2 - C_{14} - C_{16}	120.20	119.99	H_{32} - C_{30} - H_{33}	108.15	108.23	C_{53} - C_{51} - H_{54}	118.58	118.65
C_{15} - C_{14} - C_{16}	118.37	118.50	H_{32} - C_{30} - H_{34}	107.56	107.80	C_{49} - C_{53} - C_{51}	119.47	120.24
C_{14} - C_{15} - C_{17}	120.74	120.70	H_{33} - C_{30} - H_{34}	107.70	107.91	C_{49} - C_{53} - O_{58}	122.80	122.69
C_{14} - C_{15} - H_{18}	120.26	120.29	C_{29} - C_{31} - H_{35}	111.35	111.13	C_{51} - C_{53} - O_{58}	117.73	117.07
C_{17} - C_{15} - H_{18}	118.99	119.01	C_{29} - C_{31} - H_{36}	110.62	110.45	C_{53} - O_{58} - H_{59}	108.86	112.19
C_{14} - C_{16} - C_{19}	120.67	120.60	C_{29} - C_{31} - H_{37}	111.43	111.25			
C_{14} - C_{16} - H_{20}	119.52	119.51	H_{35} - C_{31} - H_{36}	108.07	108.20			
C_{19} - C_{16} - H_{20}	119.80	119.86	H_{35} - C_{31} - H_{37}	107.72	107.93			

 $\textbf{Table 6.3:} \ \ \textbf{Observed and calculated wavenumbers along with vibrational assignments for -HCPPT using B3LYP/6-311G and B3LY3/cc-pVDZ$

	Observed wavenumbers (cm ⁻¹)		Calculate wavenuml (cm ⁻¹)		Vibrational assignments
	FT-IR	FT-Raman	B3LYP/6-311G	B3LYP/ cc-pVDZ	(PED%)
1.	3314m		3317	3318	υ OH (99)
2.	3114m		3310	3112	v CH (98)
3.			3093	3095	v CH (98)
4.			3081	3085	v CH (98)
5.		3065m	3068	3071	v CH (99)
6.			3056	3060	v CH (98)
7.			3045	3045	v CH (98)
8.		3008w	3027	3031	v CH (98)
9.			3010	3013	v CH (99)
10.			3003	3005	v CH (98)
11.			2995	2995	v CH (99)
12.	2985m		2982	2983	v CH (98)
13.		2960m	2962	2962	v CH (98)
14.			2955	2958	v CH (97)
15.			2947	2948	v CH (98)
16.		2929w	2932	2935	v _{ass} CH ₃ (98)
17.			2923	2925	v _{ass} CH ₂ (98)
18.	2913m		2915	2915	v _{ass} CH ₃ (98)
19.			2902	2905	v _{ass} CH ₃ (98)
20.			2897	2898	v _{ass} CH ₃ (98)
21.			2881	2880	υ _{ss} CH ₂ (97)
22.		2870m	2874	2875	v _{ss} CH ₃ (97)
23.			2863	2863	v _{ss} CH ₃ (97)
24.	2851m		2853	2855	v CH (98)
25.	1664vs		1665	1666	υ CO (80), υ CN (12)
26.			1632	1630	υ CC (76), δ CH (18)
27		1589vs	1590	1592	υ CC (75), δ CH (20)
28.			1581	1581	υ CC (76), δ CH (18)
29.			1568	1570	δ CO (81), υ CC (16)
30.	1557s	1561vs	1559	1560	υ CN (73), δ CH (16)
31.			1522	1525	υ CC (80), δ CH (15)

32.						
34. 1445 1445 υ CN (70), υ CO (15), υ CC (12) 35. 1437 1439 δ CH (69), υ CC (18) 36. 1430 1430 δ CH (71), υ CO (15) 37. 1423 1425 δ opb CH3 (72) 38. 1413m 1415 1416 δ opb CH3 (72) 39. 1409 1410 δ CH (72), ρ siss CH2 (13) 40. 1402 1404 δ ipb CH3 (82) 41. 1396 1395 δ ipb CH3 (82) 42. 1399w 1390 1392 ρ sciss CH2 (86) 43. 1350 δ CH (79), δ OH (16) 6 44. 1369m 1370 1372 δ CH (80) 45. 1312 1315 δ CH (75) 47. 1285 1286 δ CH (76) 48. 1260 1262 δ b CH3 (73) 49. 1256ms 1255m 1255 126 υ CN (67), δ CH (13) 50. 1242 1244 δ CH (78) 51. 1230 1231 δ CH (78) 53. 126 1208	32.			1496	1497	υ CC (80), δ CH (16)
35.	33.	1467m	1447w	1470	1472	υ CC (68), υ CH (14), υ OCH (10)
36. 1430 1430 δ CH (71), v CO (15) 37. 1423 1425 δ cpb CH3 (73) 38. 1413m 1415 1416 δ cpb CH3 (72) 39. 1409 1410 δ CH (72), ρ sciss. CH2 (13) 40. 1402 1404 δ ipb CH3 (82) 41. 1396 1395 δ ipb CH3 (82) 42. 1399w 1390 1392 ρ sciss. CH2 (86) 43. 1384 1385 δ CH (79), δ OH (16) 44. 1369m 1370 1372 δ CH (80) 45. 1347 1346 δ b CH (75) 46. 1312 1315 δ CH (75) 47. 1285 1286 δ CH (76) 48. 1260 1262 δ b CH (78) 50. 1242 1244 δ CH (78) 51. 1230 1231 δ CH (78) 52. 1217 1218 δ CH (81) 54. 1195w 1196 1196 δ CH (80) 55. 1188 1191 v CC (72), δ CH (12)	34.			1445	1445	υ CN (70), υ CO (15), υ CC (12)
$\begin{array}{cccccccccccccccccccccccccccccccccccc$	35.			1437	1439	δ CH (69), υ CC (18)
38. 1413m 1415 1416 δ_{opb} CH ₃ (72) 39. 1409 1410 δ CH (72), ρ sciss, CH ₂ (13) 40. 1402 1404 δ ipb CH ₃ (82) 41. 1396 1395 δ ipb CH ₃ (82) 42. 1399w 1390 1392 ρ sciss, CH ₂ (86) 43. 1384 1385 δ CH (79), δ OH (16) 44. 1369m 1370 1372 δ CH (80) 45. 1347 1346 δ sb CH ₃ (72) 46. 1312 1315 δ CH (75) 47. 1285 1286 δ CH (76) 48. 1260 1262 δ sb CH ₃ (73) 49. 1256ms 1255m 1253 1256 ν CN (67), δ CH (13) 50. 1242 1244 δ CH (78) 51. 1230 1231 δ CH (78) 52. 1217 1218 δ CH (80) 54. 1195w 1196 1196 δ CH (80) 55. 1188 1191 ν CC (72), δ CH (12)	36.			1430	1430	δ CH (71), υ CO (15)
39.	37.			1423	1425	$\delta_{\text{opb}} \text{CH}_3 (73)$
40.	38.	1413m		1415	1416	$\delta_{\mathrm{opb}} \mathrm{CH}_3 (72)$
41.	39.			1409	1410	δ CH (72), $ρ$ sciss. CH ₂ (13)
42. 1399w 1390 1392 ρ sciss CH2 (86) 43. 1384 1385 δ CH (79), δ OH (16) 44. 1369m 1370 1372 δ CH (80) 45. 1347 1346 δ sb CH3 (72) 46. 1312 1315 δ CH (75) 47. 1285 1286 δ CH (76) 48. 1260 1262 δ sb CH3 (73) 49. 1256ms 1255m 1253 1256 υ CN (67), δ CH (13) 50. 1242 1244 δ CH (78) 51. 1230 1231 δ CH (78) 52. 1217 1218 δ CH (78) 53. 1206 1208 δ CH (80) 55. 1188 1191 υ CC (72), δ CH (12) 56. 1180 1182 δ CH (80) 57. 1170m 1173m 1172 1175 δ rock CH2 (73) 58. 1166 1166 υ CC (75), υ CH (16) 59. 1161 1164 υ CC (76), δ CH (12) 60. 1152 1151 δ CH (68), υ CC (12) 61. 1147ms 1146 1148 σ rock CH2 (69) 62. 1140 1141 υ CO (67), δ OH (17), δ CH (12) 63. 1133 1135 υ CC (70) 64. 1123m 1125 1130 υ CC (72) 65. 1116ms 1118 1124 δ CH (68) 66. 1116 116 δ CH (68) 67. 1110m 1110 1114 δ CH (68) 68. 1107 1111 δ CH (68) 69. 1103 1106 τ CH2 (68) 70. υ CC (71)	40.			1402	1404	δ_{ipb} CH ₃ (82)
43.	41.			1396	1395	δ_{ipb} CH ₃ (82)
$\begin{array}{c ccccccccccccccccccccccccccccccccccc$	42.		1399w	1390	1392	ρ_{sciss} .CH ₂ (86)
45.	43.			1384	1385	δ CH (79), δ OH (16)
46. 1312 1315 δ CH (75) 47. 1285 1286 δ CH (76) 48. 1260 1262 δ_{sb} CH ₃ (73) 49. 1256ms 1255m 1253 1256 v CN (67), δ CH (13) 50. 1242 1244 δ CH (78) 51. 1230 1231 δ CH (78) 52. 1217 1218 δ CH (81) 54. 1195w 1196 1196 δ CH (80) 55. 1188 1191 v CC (72), δ CH (12) 56. 1180 1182 δ CH (80) 57. 1170m 1173m 1172 1175 δ_{rock} CH ₂ (73) 58. 1166 1166 v CC (75), v CH (16) 59. 1161 1164 v CC (76), δ CH (12) 60. 1152 1151 δ CH (68), v CC (12) 61. 1147ms 1146 1148 σ rock CH ₂ (69) 62. 1140 1141 v CO (67), δ OH (17), δ CH (12) 63. 11133 1135 v CC (70) <	44.	1369m		1370	1372	δ CH (80)
47.	45.			1347	1346	δ_{sb} CH ₃ (72)
48.	46.			1312	1315	δ CH (75)
49. 1256ms 1255m 1253 1256 υ CN (67), δ CH (13) 50. 1242 1244 δ CH (78) 51. 1230 1231 δ CH (78) 52. 1217 1218 δ CH (78) 53. 1206 1208 δ CH (81) 54. 1195w 1196 1196 δ CH (80) 55. 1188 1191 υ CC (72), δ CH (12) 56. 1180 1182 δ CH (80) 57. 1170m 1173m 1172 1175 δ rock CH2 (73) 58. 1166 1166 υ CC (75), υ CH (16) 59. 1161 1164 υ CC (76), δ CH (12) 60. 1152 1151 δ CH (68), υ CC (12) 61. 1147ms 1146 1148 σ rock CH2 (69) 62. 1140 1141 υ CO (67), δ OH (17), δ CH (12) 63. 1133 1135 υ CC (70) 64. 1123m 1125 1130 υ CC (72) 65. 1116ms 1118 1124 δ CH (68) 67.	47.			1285	1286	δ CH (76)
50. 1242 1244 δ CH (78) 51. 1230 1231 δ CH (78) 52. 1217 1218 δ CH (78) 53. 1206 1208 δ CH (81) 54. 1195w 1196 1196 δ CH (80) 55. 1188 1191 v CC (72), δ CH (12) 56. 1180 1182 δ CH (80) 57. 1170m 1173m 1172 1175 δ rock CH2 (73) 58. 1166 1166 v CC (75), v CH (16) 59. 1161 1164 v CC (76), δ CH (12) 60. 1152 1151 δ CH (68), v CC (12) 61. 1147ms 1146 1148 σ rock CH2 (69) 62. 1140 1141 v CO (67), δ OH (17), δ CH (12) 63. 1133 1135 v CC (70) 64. 1123m 1125 1130 v CC (72) 65. 1116ms 1118 1124 δ CH (68) 66. 1115 1119 δ CH (68) 67. 1109m 1110 <	48.			1260	1262	δ_{sb} CH ₃ (73)
51. 1230 1231 δ CH (78) 52. 1217 1218 δ CH (78) 53. 1206 1208 δ CH (81) 54. 1195w 1196 1196 δ CH (80) 55. 1188 1191 v CC (72), δ CH (12) 56. 1180 1182 δ CH (80) 57. 1170m 1173m 1172 1175 δ rock CH2 (73) 58. 1166 1166 1166 v CC (75), v CH (16) 59. 1161 1164 v CC (76), δ CH (12) 60. 1152 1151 δ CH (68), v CC (12) 61. 1147ms 1146 1148 σ rock CH2 (69) 62. 1140 1141 v CO (67), δ OH (17), δ CH (12) 63. 1133 1135 v CC (70) 64. 1123m 1125 1130 v CC (72) 65. 1116ms 1118 1124 δ CH (68) 66. 1115 1119 δ CH (68) 67. 1109m 1110 1114 δ CH (68) 68. <	49.	1256ms	1255m	1253	1256	υ CN (67), δ CH (13)
52. 1217 1218 δ CH (78) 53. 1206 1208 δ CH (81) 54. 1195w 1196 1196 δ CH (80) 55. 1188 1191 v CC (72), δ CH (12) 56. 1180 1182 δ CH (80) 57. 1170m 1173m 1172 1175 δ rock CH ₂ (73) 58. 1166 1166 v CC (75), v CH (16) 59. 1161 1164 v CC (76), δ CH (12) 60. 1152 1151 δ CH (68), v CC (12) 61. 1147ms 1146 1148 σ rock CH ₂ (69) 62. 1140 1141 v CO (67), δ OH (17), δ CH (12) 63. 1133 1135 v CC (70) 64. 1123m 1125 1130 v CC (72) 65. 1116ms 1118 1124 δ CH (68) 67. 1109m 1110 1114 δ CH (68) 68. 1107 1111 δ CH (68) 69. 1103 1106 τ CH ₂ (68) 70. 1096	50.			1242	1244	δ CH (78)
$\begin{array}{cccccccccccccccccccccccccccccccccccc$	51.			1230	1231	δ CH (78)
54. 1195w 1196 1196 δ CH (80) 55. 1188 1191 υ CC (72), δ CH (12) 56. 1180 1182 δ CH (80) 57. 1170m 1173m 1172 1175 δ rock CH₂ (73) 58. 1166 1166 υ CC (75), υ CH (16) 59. 1161 1164 υ CC (76), δ CH (12) 60. 1152 1151 δ CH (68), υ CC (12) 61. 1147ms 1146 1148 σ rock CH₂ (69) 62. 1140 1141 υ CO (67), δ OH (17), δ CH (12) 63. 1133 1135 υ CC (70) 64. 1123m 1125 1130 υ CC (72) 65. 1116ms 1118 1124 δ CH (68) 66. 1115 1119 δ CH (68) 67. 1109m 1110 1114 δ CH (68) 68. 1107 1111 δ CH (68) 69. 1103 1106 τ CH₂ (68) 70. 1096 1110 υ CC (71)	52.			1217	1218	δ CH (78)
55. 1188 1191 υ CC (72), δ CH (12) 56. 1180 1182 δ CH (80) 57. 1170m 1173m 1172 1175 δ rock CH₂ (73) 58. 1166 1166 υ CC (75), υ CH (16) 59. 1161 1164 υ CC (76), δ CH (12) 60. 1152 1151 δ CH (68), υ CC (12) 61. 1147ms 1146 1148 σ rock CH₂ (69) 62. 1140 1141 υ CO (67), δ OH (17), δ CH (12) 63. 1133 1135 υ CC (70) 64. 1123m 1125 1130 υ CC (72) 65. 1116ms 1118 1124 δ CH (73) 66. 1115 1119 δ CH (68) 67. 1109m 1110 1114 δ CH (68) 68. 1107 1111 δ CH (69) 69. 1103 1106 τ CH₂ (68) 70. 1096 1110 υ CC (71)	53.			1206	1208	δ CH (81)
56. 1180 1182 δ CH (80) 57. 1170m 1173m 1172 1175 δ rock CH2 (73) 58. 1166 1166 υ CC (75), υ CH (16) 59. 1161 1164 υ CC (76), δ CH (12) 60. 1152 1151 δ CH (68), υ CC (12) 61. 1147ms 1146 1148 σ rock CH2 (69) 62. 1140 1141 υ CO (67), δ OH (17), δ CH (12) 63. 1133 1135 υ CC (70) 64. 1123m 1125 1130 υ CC (72) 65. 1116ms 1118 1124 δ CH (68) 66. 1115 1119 δ CH (68) 67. 1109m 1110 1114 δ CH (68) 68. 1107 1111 δ CH (69) 69. 1103 1106 τ CH2 (68) 70. 1096 1110 υ CC (71)	54.		1195w	1196	1196	δ CH (80)
57. 1170m 1173m 1172 1175 δ rock CH2 (73) 58. 1166 1166 υ CC (75), υ CH (16) 59. 1161 1164 υ CC (76), δ CH (12) 60. 1152 1151 δ CH (68), υ CC (12) 61. 1147ms 1146 1148 σ rock CH2 (69) 62. 1140 1141 υ CO (67), δ OH (17), δ CH (12) 63. 1133 1135 υ CC (70) 64. 1123m 1125 1130 υ CC (72) 65. 1116ms 1118 1124 δ CH (73) 66. 1115 1119 δ CH (68) 67. 1109m 1110 1114 δ CH (68) 68. 1107 1111 δ CH (69) 69. 1103 1106 τ CH2 (68) 70. 1096 1110 υ CC (71)	55.			1188	1191	υ CC (72), δ CH (12)
58. 1166 1166 υ CC (75), υ CH (16) 59. 1161 1164 υ CC (76), δ CH (12) 60. 1152 1151 δ CH (68), υ CC (12) 61. 1147ms 1146 1148 σ rock CH2 (69) 62. 1140 1141 υ CO (67), δ OH (17), δ CH (12) 63. 1133 1135 υ CC (70) 64. 1123m 1125 1130 υ CC (72) 65. 1116ms 1118 1124 δ CH (73) 66. 1115 1119 δ CH (68) 67. 1109m 1110 1114 δ CH (68) 68. 1107 1111 δ CH (69) 69. 1103 1106 τ CH ₂ (68) 70. 1096 1110 υ CC (71)	56.			1180	1182	δ CH (80)
$\begin{array}{cccccccccccccccccccccccccccccccccccc$	57.	1170m	1173m	1172	1175	$\delta_{\text{rock}} \text{ CH}_2 (73)$
$\begin{array}{cccccccccccccccccccccccccccccccccccc$	58.			1166	1166	υ CC (75), υ CH (16)
61. 1147ms 1146 1148 σ rock CH2 (69) 62. 1140 1141 υ CO (67), δ OH (17), δ CH (12) 63. 1133 1135 υ CC (70) 64. 1123m 1125 1130 υ CC (72) 65. 1116ms 1118 1124 δ CH (73) 66. 1115 1119 δ CH (68) 67. 1109m 1110 1114 δ CH (68) 68. 1107 1111 δ CH (69) 69. 1103 1106 τ CH2 (68) 70. 1096 1110 υ CC (71)	59.			1161	1164	υ CC (76), δ CH (12)
62. 1140 1141 υ CO (67), δ OH (17), δ CH (12) 63. 1133 1135 υ CC (70) 64. 1123m 1125 1130 υ CC (72) 65. 1116ms 1118 1124 δ CH (73) 66. 1115 1119 δ CH (68) 67. 1109m 1110 1114 δ CH (68) 68. 1107 1111 δ CH (69) 69. 1103 1106 τ CH ₂ (68) 70. 1096 1110 υ CC (71)	60.			1152	1151	δ CH (68), υ CC (12)
63. 1133 1135 υ CC (70) 64. 1123m 1125 1130 υ CC (72) 65. 1116ms 1118 1124 δ CH (73) 66. 1115 1119 δ CH (68) 67. 1109m 1110 1114 δ CH (68) 68. 1107 1111 δ CH (69) 69. 1103 1106 τ CH ₂ (68) 70. 1096 1110 υ CC (71)	61.	1147ms		1146	1148	$\sigma_{rock} CH_2(69)$
64. 1123m 1125 1130 υ CC (72) 65. 1116ms 1118 1124 δ CH (73) 66. 1115 1119 δ CH (68) 67. 1109m 1110 1114 δ CH (68) 68. 1107 1111 δ CH (69) 69. 1103 1106 τ CH ₂ (68) 70. 1096 1110 υ CC (71)	62.			1140	1141	υ CO (67), δ OH (17), δ CH (12)
65. 1116ms 1118 1124 δ CH (73) 66. 1115 1119 δ CH (68) 67. 1109m 1110 1114 δ CH (68) 68. 1107 1111 δ CH (69) 69. 1103 1106 τ CH ₂ (68) 70. 1096 1110 υ CC (71)	63.			1133	1135	v CC (70)
66. 1115 1119 δ CH (68) 67. 1109m 1110 1114 δ CH (68) 68. 1107 1111 δ CH (69) 69. 1103 1106 τ CH ₂ (68) 70. 1096 1110 υ CC (71)	64.		1123m	1125	1130	v CC (72)
67. 1109m 1110 1114 δ CH (68) 68. 1107 1111 δ CH (69) 69. 1103 1106 τ CH ₂ (68) 70. 1096 1110 υ CC (71)	65.	1116ms		1118	1124	δ CH (73)
68. 1107 1111 δ CH (69) 69. 1103 1106 τ CH ₂ (68) 70. 1096 1110 υ CC (71)	66.			1115	1119	δ CH (68)
69. 1103 1106 τ CH ₂ (68) 70. 1096 1110 υ CC (71)	67.		1109m	1110	1114	δ CH (68)
69.11031106τ CH2 (68)70.10961110υ CC (71)	68.			1107	1111	δ CH (69)
	69.			1103	1106	
71. 1092 1106 δ OH (74). δ CH (12)	70.			1096	1110	v CC (71)
(· · /) (/	71.			1092	1106	δ ΟΗ (74), δ СΗ (12)

72.			1086	1094	υ CN (67), δ CO (14)
73.			1073	1085	υ CC (71), δ OH (17)
74.	1066m		1065	1073	δ CH (68)
75.			1026	1062	δ CH (68)
76.		1015w	1016	1025	^γ oprCH ₃ (62)
77.	1007m		1008	1010	υ CCL (75), δ CH (11)
78.		993w	991	993	^γ _{opr} CH ₃ (62)
79.			982	985	υ NN (75), δ CN (16)
80.			969	970	v CC (68)
81.			961	961	⁷ СН (63)
82.	949ms	950w	950	952	$\delta_{\rm ring}$ (67)
83.			941	945	$\delta_{\rm ring}$ (67)
84.			932	934	$\delta_{\rm ring}$ (67)
85.			921	920	$\delta_{\rm ring}$ (65)
86.			916	916	⁷ CH (66)
87.			910	914	^ү СН (63)
88.			904	905	^ү СН (63)
89.			898	900	^ү СН (63)
90.			893	896	⁷ CH (65)
91.			886	888	$\delta_{ipr}CH_3$ (62)
92.	875s		875	876	^ү СН (63)
93.			862	866	υ CS (71), δ CC (14)
94.			855	856	$\delta_{ipr}CH_3$ (62)
95.			840	845	$\delta_{\rm ring}$ (62)
96.	836s	831m	834	836	^ү СН (63)
97.			813	814	δ CC (70)
98.		790w	793	795	^ү СН (64)
99.	776vs		775	777	^ү СН (64)
100.			764	765	^ү СН (64)
101.			758	760	^ү СН (62)
102.			749	750	$\delta_{\rm ring}$ (63)
103.		741w	740	744	^γ CH (63)
104.			734	735	Ring breathing (68)
105.			729	730	$\delta_{\rm ring}$ (63)
106.			722	722	γ CH (61)
107.			713	715	$\delta_{\rm ring}$ (65)
108.		705m	708	711	$\delta_{\rm ring}$ (65)
109.	695ms		696	698	γ _{ring} (60)
110.			675	677	γ _{ring} (61)
111.			662	663	γ _{ring} (60)

112.	651ms		653	655	γ _{ring} (61)
113.			649	650	δ CCL (67), δ ring (11)
114.			645	647	$^{\gamma}$ ring (60)
115.		635w	637	640	$\delta_{\rm ring}$ (63)
116.	596m		595	598	v CS (70)
117.			575	577	$\delta_{\rm ring}$ (63)
118.			569	569	$\delta_{\rm ring}$ (63)
119.	557m	557w	556	557	$\delta_{\rm ring}$ (64)
120.			522	524	γ CC (58)
121.			506	509	$\gamma_{\rm ring}$ (59)
122.	488w		489	490	γ CC (58)
123.			480	483	γ CC (58)
124.		469w	472	476	⁷ CC (57)
125.			465	467	δ CC (62)
126.			459	461	^γ CO (59), ^γ CH (10)
127.	457w	449w	451	455	$\delta_{\rm ring}$ (61)
128.			443	445	$\gamma_{\rm ring}$ (58)
129.			436	439	$\delta_{\rm ring}$ (63)
130.	431w		430	432	δ CCC (60)
131.			422	427	γ CCL (57)
132.		412w	415	418	δ CC (60)
133.			402	405	$\gamma_{\rm ring}$ (58)
134.			395	396	$\gamma_{\rm ring}$ (58)
135.			381	383	$\gamma_{\rm ring}$ (55)
136.		372w	370	375	$\gamma_{\rm ring}$ (55)
137.			362	366	δ СОН (53)
138.			355	358	δ CCH ₃ (55)
139.			348	350	^ү ОН (57)
140.		337w	340	345	$\gamma_{\rm ring}$ (57)
141.			327	331	δ CC (58)
142.			316	320	⁷ CC (56)
143.			302	308	δ CCC (58)
144.			285	289	⁷ CCC (58)
145.		223w	272	275	δ CCC (57)
146.			263	266	δ CCC (57)
147.			248	250	⁷ CCC (52)
148.			229	230	$\tau \text{ CH}_3 (58)$
149.		183w	217	219	$\tau \text{ CH}_3 (58)$
150.			206	206	⁷ CCC (52)
151.			188	193	τ CCC (52)

152.		180	182	τ CCC (52)
153.		173	175	δ CCC (54)
154.	167w	166	169	δ CCC (54)
155.		149	150	δ CCC (55)
156.		135	136	⁷ CCC (53)
157.		120	124	⁷ CN (51)
158.		104	105	⁷ CC (48)
159.		94	95	γ _{ring} (50)
160.		89	93	γ _{ring} (51)
161.		80	84	τ CCC (49)
162.	75m	75	77	γ _{ring} (50)
163.		55	56	γ _{ring} (50)
164.		46	51	$\delta_{\rm ring}$ (53)
165.		36	40	$\delta_{\rm ring}$ (55)
166.		30	32	τ CCC (53)
167.		25	29	τ CCC (53)
168.		24	26	γ _{ring} (51)
169.		20	21	⁷ CC (51)
170.		12	13	⁷ CC (50)
171.		10	12	^γ CC (51)

s-strong, m-medium, ms-medium strong, vs-verystrong, w-weak, ν -stretching, ν_{ss} -symmetric stretching, ν_{ass} -asymmetric stretching, δ - in-plane bending, γ - out-of-plane bending, ρ - scissoring, ω - wagging, σ - rocking, τ - twisting

Table 6.4: Energy gap values of HCPPT calculate the global reactivity descriptors (E_{HOMO} - E_{LUMO}), $E_L \rightarrow E_H$, $E_{H-1} \rightarrow E_{L+1}$, $E_{H-2} \rightarrow E_{L+2}$) using the 6-311G levels of theory

Molecular	Energy	Energy	(I)	(A)	(η)	(X)	(σ)	(μ) (eV)	(ω)
properties	(eV)	gap (eV)	(eV)	(eV)	(eV)	(eV)	(eV)		(eV)
E _{HOMO}	-5.8703								
$\mathbf{E}_{\mathbf{LUMO}}$	-2.444	3.4259	5.8703	2.444	1.7130	4.1574	0.5838	-4.1574	5.0450
$E_{\text{HOMO-1}}$	-6.3998								
$E_{LUMO+1} \\$	-1.8874	4.5124	6.3998	1.8874	2.2562	4.1436	0.4432	-4.1436	3.8049
$E_{\text{HOMO-2}}$	-6.8031								
$E_{LUMO+2} \\$	-1.0690	5.7337	6.8031	1.0690	2.8669	3.9363	0.3488	-3.9363	2.7023

Table 6.5: Second order perturbation theory analysis of Fock matrix in NBO basis of the HCPPT

Donar	T D	ED/	Acceptor	T	ED/:()	E(2) ^a	E(i)-	E/: •\C
(i)	Type	ED/e	(j)	Type	$ED/e(q_i)$	Kcal/mol	$\mathbf{E}(\mathbf{j})^{\mathbf{b}}$	$\mathbf{F}(\mathbf{i},\mathbf{j})^{\mathbf{c}}$
π	C4 - C5	1.64507	π^*	C1 - N24	0.25495	16.67	0.24	0.058
π	C4 - C5	1.64507	π^*	C6 - C9	0.29683	19.66	0.28	0.068
π	C4 - C5	1.64507	π^*	C7 - C11	0.39228	22.42	0.26	0.069
π	C6 - C9	1.66673	π^*	C4 - C5	0.39	20.57	0.28	0.068
π	C6 - C9	1.66673	π^*	C7 - C11	0.39228	21.12	0.26	0.067
π	C7 - C11	1.67968	π^*	C6 - C9	0.29683	19.15	0.3	0.068
π	C14 - C15	1.67258	π^*	C16 - C19	0.3434	19.55	0.28	0.067
π	C14 - C15	1.67258	π^*	C17 - C21	0.35905	18.94	0.29	0.067
π	C16 - C19	1.69335	π^*	C14 - C15	0.38843	21.07	0.27	0.069
π	C16 - C19	1.69335	π^*	C17 - C21	0.35905	21.1	0.28	0.07
π	C17 - C21	1.64955	π^*	C16 - C19	0.3434	20.03	0.28	0.066
σ	C26 - H28	1.95701	π^*	C1 - N24	0.25495	5.55	0.5	0.05
σ	C29 - H38	1.90956	π^*	C17 - C21	0.35905	10.97	0.47	0.069
σ	C39 - S41	1.9775	σ^*	N25 - C42	0.05341	9	1.44	0.102
π	C39 - C45	1.72741	LP (2)	S41	1.93756	533.9	0.01	0.119
π	C39 - C45	1.72741	π^*	C40 - O44	0.35748	29.49	0.28	0.083
σ	C40 - N43	1.98023	σ^*	N25 - C42	0.05341	6.25	1.17	0.077
π	C40 - O44	1.91548	π^*	C39 - C45	0.28459	8.94	0.27	0.046
π	C40 - O44	1.91548	π^*	C42 - N43	0.51656	6.73	0.28	0.044
σ	S41 - C42	1.98222	σ^*	C39 - C45	0.03531	7.14	1.39	0.089
π	C42 - N43	1.83932	LP (2)	S41	1.93756	102.44	0.05	0.102
π	C42 - N43	1.83932	π^*	C40 - O44	0.35748	27.11	0.31	0.087
π	C46- C48	1.66863	π^*	C47 - C49	0.31568	20.73	0.28	0.069
π	C46- C48	1.66863	π^*	C51 - C53	0.35881	19.55	0.28	0.066
π	C47 - C49	1.6654	π^*	C46- C48	0.36742	20.55	0.27	0.068
π	C47 - C49	1.6654	π^*	C51 - C53	0.35881	22.17	0.27	0.07
π	C51 - C53	1.6515	π^*	C46- C48	0.36742	21.06	0.28	0.069
π	C51 - C53	1.6515	π^*	C47 - C49	0.31568	19.51	0.29	0.067
LP (1)	N25	1.74889	π^*	C1 - N24	0.25495	26.68	0.24	0.072

-	LP (2)	S41	1.93756	π*	C39 - C45	0.28459	65.79	0.2	0.112
	LP (2)	S41	1.93756	π^*	C42 - N43	0.51656	99.74	0.21	0.133
	LP (1)	N43	1.92198	σ^*	C39 - C40	0.09668	6	0.81	0.062
	LP (2)	O44	1.87712	σ^*	C40 - N43	0.06812	22.97	0.65	0.111
	LP (1)	O58	1.96986	σ^*	C49 - C53	0.02884	7.12	0.88	0.07
	π^*	C1 - N24	0.25495	π^*	C4 - C5	0.39	37.65	0.04	0.063
	π^*	C7 - C11	0.39228	π^*	C4 - C5	0.39	196.05	0.02	0.083
	π^*	C7 - C11	0.39228	π^*	C6 - C9	0.29683	131.65	0.02	0.078
	π^*	C39 - C45	0.28459	π^*	C40 - O44	0.35748	30	0.06	0.069
	π^*	C42 - N43	0.51656	π^*	C40 - O44	0.35748	53.08	0.05	0.072

a→E(2) means energy of hyper conjugative interaction (stabilization energy).

Table 6.6: Antimicrobial inhibition level with different concentration level of HCPPT

SAMPLE	DMSO	Extract 100 µl	added an	d Zone of inhib	oition (mm/ml)
SAMIFLE	25 μl	50 μl	75 μl	100 μl	Control
Bacillus subtilis	12	14	17	20	18
Staphylococcus aureus	12	15	18	20	20
E.coli	16	18	20	24	20
Pseudomonas	12	15	18	21	20
Candida albicans	13	15	18	22	25
A.niger	14	18	20	22	20

 $b \rightarrow$ Energy difference between donor and acceptor i and j NBO orbitals.

 $c \rightarrow\!\! F(i,j)$ is the Fock matrix element between i and j NBO orbitals.

Table 6.7: PASS prediction for the activity spectrum of title compound, Pa represents probability to be active and Pi represents probability to be inactive

Pa	Pi	Activity name
0,674	0,005	Mcl-1 antagonist
0.651	0,003	Alkaline phosphatase inhibitor
0,609	0,030	Antiinflammatory
0,560	0,007	PfA-M1 aminopeptidase inhibitor
0,556	0,034	Insulysin inhibitor
0,558	0,070	Phosphatase inhibitor
0,484	0,013	Thiol protease inhibitor
0,445	0,004	Dual specificity phosphatase inhibitor
0,439	0,024	Antineoplastic (solid tumors)
0,418	0,004	HCV NS3-helicase inhibitor
0,414	0,020	Non-steroidal antiinflammatory agent
0,432	0,084	HIF1A expression inhibitor
0,340	0,006	Cyclooxygenase inhibitor
0,336	0,007	Dual specificity phosphatase 1 inhibitor
0,341	0,015	Amyloid beta precursor protein antagonist
0,397	0,074	APOA1 expression enhancer
0,370	0,051	Myc inhibitor
0,437	0,006	Nicotinic alpha4beta4 receptor agonist
0,319	0,123	Antineurogenic pain

Table 6.8: The lowest binding bonds with a distance value of various proteins docked ligand (HCPPT) show the binding affinity, inhibition constant, and RMSD

		Bond			Binding	Inhibition	
Ligand name	PDB ID	distance (Å)	Amino acid (residues)	Bond	affinity (kcal/mol)	Constant Ki (µM or nM orpM)	RMSD (Å)
zol-1-	біар	2.0	LEU A 88	conventional hydrogen bond	-8.10	1.15 μΜ	26.964
yra		2.1	ASP A 90	van der Waals	-7.61	2.63 μΜ	38.622
-1 <i>H</i> -p		1.7	TRP A 80	Pi-sigma	-6.94	8.25 μΜ	27.304
dihydro	1uhp	2.1	GLU A 84	conventional hydrogen bond	-7.27	4.67 μΜ	14.866
/1]-4, 5-		2.0	GLN A 81	conventional hydrogen bond	-7.07	6.56 μΜ	15.016
neny		2.5	PRO A 30	Pi-alkyl	-7.03	7.03 μM	11.534
.2-yl) pl CPPT)	брдр	2.5	ALA A 146	conventional hydrogen bond	-10.49	20.46 nM	15.494
ropan		2.2	LYS A 147	Pi-alkyl	-10.47	20.99 nM	10.167
5-[4-(p 4(5 <i>H</i>)-(1.8	ASP A 119	carbon hydrogen bond	-9.59	93.32 nM	11.118
chlorophenyl)-5-[4-(propan-2-yl) _F yl]-1,3-thiazol-4(5 <i>H</i>)-one (HCPPT)	5zxi	2.1	GLU A 22	conventional hydrogen bond	-12.39	823.92 pM	50.441
orop 1,3-1		2.3	LEU A 294	Alkyl	-7.73	2.16 μΜ	45.109
4-chlc yl]-		3.0	THR A 252	Pi- Donor hydrogen bond	-7.54	2.95 μΜ	57.650
1-2-[3-(1 jei	2.0	SER A 53	conventional hydrogen bond	-8.68	434.57 nM	11.451
ene)		2.9	ARG A 46	Alkyl	-7.68	2.35 μΜ	8.628
ylid		3.5	TYP A 40	Pi- Pi Stacked	-7.48	3.27 μΜ	8.667
$5-(4-\mathrm{Hydroxybenzylidene})-2-[3-(4-\mathrm{chlorophenyl})-5-[4-(\mathrm{propan-}2-\mathrm{yl}) \ \mathrm{phenyl}]-4, 5-\mathrm{dihydro-}1H-\mathrm{pyrazol-}1-1, 3-\mathrm{thiazol-}4(5H)-\mathrm{one} \ (\mathrm{HCPPT})$	4zbr	2.3	TRY A 137	conventional hydrogen bond	-8.59	504.42 nM	77.419
t-Hydro		2.8	LYS A 132	conventional hydrogen bond	-7.90	1.62 μΜ	77.418
·2-(¢		3.2	LYS A 130	Pi-cation	-7.41	3.71 μΜ	76.601

Spectral investigations, Topology, combining DFT computations with molecular docking studies of 5-(4-Methoxybenzylidene)-2-[3-(4-chlorophenyl)-5-[4-(propan-2-yl) phenyl]-4,5-dihydro-1H-pyrazol-1-yl]-1,3-thiazol-4(5H)-one

Abstract

In this work, 5-(4-Methoxybenzylidene)-2-[3-(4-chlorophenyl)-5-[4-(propan-2-yl) phenyl]-4, 5-dihydro-1H-pyrazol-1-yl]-1,3-thiazol-4(5H)-one (MCPPT) molecule was optimized geometrically and vibrational wavenumbers were obtained with the aid of density functional theory (DFT) along with B3LYP/6-31G and 6-311G hybrid functions. For the experimental calculation, the vibrational spectrum was obtained in the region of 4000–0 cm⁻¹ and 3500–0 cm⁻¹ for FT-IR and FT-Raman spectrum, respectively. Moreover, frontier molecular orbitals (HOMO-LUMO), MEP, and NBO were performed for the optimized structure. Various inter and molecular interactions in the MCPPT have been thoroughly investigated using topological approaches such as localized orbital locator (LOL), electron localization function (ELF) analysis, and the non-covalent interactions (NCI) approach. Finally, the molecular docking analysis reveals that the interaction between the title compound (ligand) and protein-anti neurogenic pain (5pbe), anti-inflammatory (4x7s), myeloid cell leukemia-1 (6dm8), myeloblastin (1fuj) and naproxen (4ot2) was investigated. This ligand-enzyme interaction was carried out to find the drugs nature of the compound.

CHAPTER - 7

Spectral investigations, Topology, combining DFT computations with molecular docking studies of 5-(4-Methoxybenzylidene)-2-[3-(4-chlorophenyl)-5-[4-(propan-2-yl) phenyl]-4,5-dihydro-1H-pyrazol-1-yl]-1,3-thiazol-4(5H)-one

7.1 Introduction

In recent years, heterocycles have fascinated researchers as a vital scaffold of natural products of note, incorporation of small heterocyclic moieties especially a five-membered sulfur- and nitrogen-containing thiazole ring is an enthralling area of research in enhancing the potency of the drug candidate [196, 197]. According to several reports, thiazole-pyrazole derived compounds are the most privileged structures that are widely stimulated for their wide range of pharmacological activities, such as anti-diabetic [198, 199], antitumor [200], anti antimicrobial [201], anti-inflammatory [202], capabilities. The current study is focused on a structural investigation of 5-(4-Methoxybenzylidene)-2-[3-(4-chlorophenyl)-5-[4-(propan-2-yl) phenyl]-4,5-dihydro-1H-pyrazol-1-yl] -1,3-thiazol-4(5H)-one (MCPPT). Geometric parameters, in particular bond lengths and bond angles, have been acquired. The FT-IR and FT-Raman spectra were recorded experimentally and computed theoretically. Theoretical investigation of the structural and vibrational properties of the MCPPT molecule was carriedout with the help of density functional theory (DFT). The molecular electrostatic potential (MEP) was analysed to recognize the most reactive regions for electrophilic and nucleophilic attacks. HOMO-LUMO analysis has been used to elucidate information regarding charge transfer within the molecule. The redistribution of electron density (ED) in various bonding, anti-bonding orbit's and E(2) energies had been calculated by natural bond orbital (NBO) analysis to give clear evidence of stabilization originating from the hyper conjugation of various intra-molecular interactions. Topological parameters are used to identify an extended theoretical study on structural features such as localized orbital locator (LOL), electron localization function (ELF), and non-covalent interactions (NCI). Molecular docking were performed to identity the binding energies, and inhibition constant of the title compound with neurogenic pain (5pbe), anti-inflammatory (4x7s), myeloid cell leukemia-1 (6dm8), myeloblastin (1fuj) andnaproxen (4ot2) proteins.

7.2 Experimental details

The spectroscopic characteristics of MCPPT were investigated by FT-IR and FT-Raman spectroscopic techniques. The FT-IR spectrum was documented in the range of 4000–0 cm⁻¹ by the KBr pellet method on the Perkin-Elmer Spectrum spectrometer. The FT-Raman spectrum of the compound was also documented in the range of 3500–0 cm⁻¹ by the 1064 nm Nd: YAG laser method on the Bruker RFS27 Multi-RAM FT-Raman spectrometer.

7.3 Computational techniques

All computational calculations are computed using the Gaussian 09W [20] programme with the density functional theory (DFT) method. The optimized structure parameters and frequencies were computed using B3LYP/6-31G and B3LYP/6-311G basis sets levels. For visualization of the molecule, spectrum simulation and iso-density plots, Gauss View 5.0 has been used [31]. VEDA software [10] calculates the potential energy distributions (PEDs) or fundamental modes of vibration using vibration spectral computations. The natural bonding orbital (NBO) calculations [90] were accomplished using the NBO 3.1 program as implemented in the Gaussian 09W package at the abovementioned level in order to figure out various second order interactions into the middle of the filled orbital of one subsystem and the vacant orbital of one more subsystem, that is a measure of the intermolecular and intra-molecular delocalization or hyper conjugation.

Topological analysis of the electron localization function (ELF), localization orbital locator (LOL) and reduced density gradient (RDG) were performed using the Multiwfn program [57]. Molecular docking studies have been undertaken in order to address the most important biological reactive properties of MCPPT using Pymol and the Autodock tool [62].

7.4 Results and discussion

7.4.1 Molecular geometrical optimization

The optimized structural parameters (bond lengths and bond angles) of MCPPT were investigated at the DFT level using the B3LYP/6-31G and 6-311G basis sets. The optimized structure along with atomic numbers are shown in Fig.7.1. The optimized parameters data are tabulated in Tables 7.1 and 7.2.

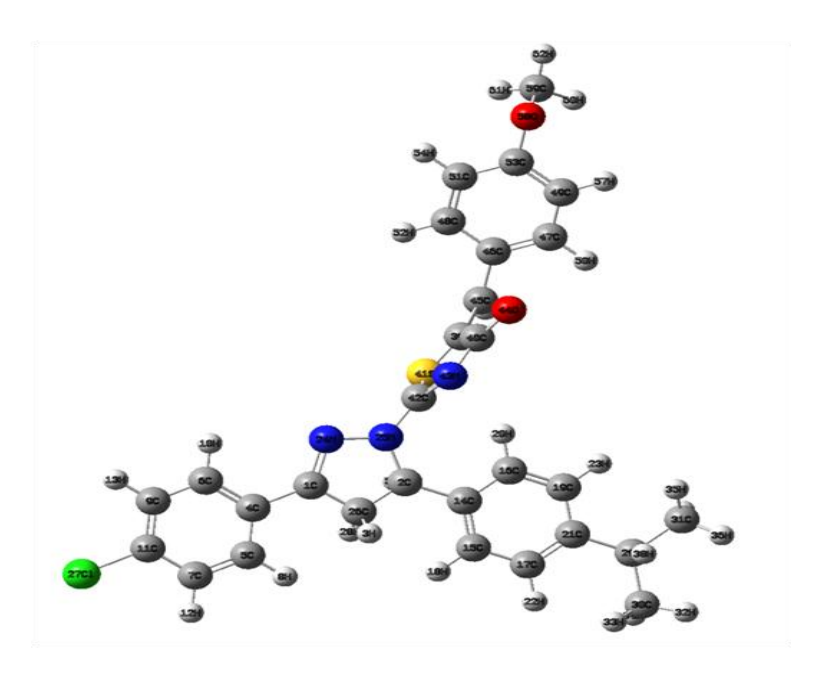


Fig. 7.1 Optimized structure of MCPPT

The optimized structural parameters are now compared with the related experimental data [87]. For the phenyl ring, the carbon–carbon single bond lengths lie between 1.39 Å and 1.40 Å, double bond lengths lie between 1.40 Å and 1.41 Å. The carbon–hydrogen bond lengths lie between 1.08 and 1.09 Å. The C-C bond lengths in the five member rings are in

the range of 1.49 Å to 1.56 Å. The C-S bond lengths of thiazole are 1.84 Å (S_{41} - C_{42}) and 1.87 Å (C_{39} - S_{41}). The C-C and C-N bonds in the ring are approximately calculated at 1.49 Å, 1.41 Å, respectively. The bond length C_{40} = O_{44} of the title molecule is found to be 1.22 Å (6-31G), 1.24 Å (6-311G) basis sets. The calculated bond angle of MCPPT are C_{40} - C_{39} - C_{45} =133°, C_{40} - C_{39} - S_{41} =108°, S_{41} - C_{39} - C_{45} =118°, S_{25} - S_{41} =119°. The shorter bond angle found in thiazole ring at C39-S41-C42, 87.64° (6-31G), and 86.22° (6-311G) has clearly indicated the presence of a sulphur bond. The nitrogen atom formed different bond angle with adjustent carbon-hydrogen atoms are S_{24} - S_{25} - S_{42} =121°, S_{25} - S_{25} - S_{26} =100°, and S_{25} - S_{27} - S_{27} - S_{26} =100°, respectively. The bond length of methoxy benzylidene ring is 1.39 Å

7.4.2 Vibrational Analysis

The title molecule MCPPT consists of 62 atoms, which have 180 normal modes of vibration. This compound belongs to the C1 symmetry group. Scale factors are used to fit the calculated wavenumbers with those of the observed ones. All the experimental and theoretical vibrational frequencies of the title compound, along with corresponding vibrational assignments are given in Table 7.3. The experimental and simulated FT-IR and FT-Raman spectra are depicted in Fig. 7.2 and 7.3, respectively.

Phenyl ring vibrations

According to the literature [149, 203] in infrared spectra, most mononuclear and polynuclear aromatic compounds have three or four peaks in the region of 3100-2900 cm⁻¹. These are due to the stretching vibrations of the ring C-H bands. In the present study, the C-H stretching vibrations are noticed at 3056 cm⁻¹ in FT-IR, 3069, 3014, 2954 cm⁻¹ in FT-Raman, corresponding theoretical values are assigned at 3075, 3058, 3045, 3034, 3025, 3021, 2985, 2972, 2955, 2951, 2944 cm⁻¹ in B3LYP/6-31G and 3070, 3055, 3041, 3030, 3016, 3008, 2982, 2969, 2953, 2945, 2940 cm⁻¹ in B3LYP/6-311G basics sets, respectively. Socrates et al. [149] reported that the ring C=C and C-C vibrations are semicircle stretching vibrations that produce strong peaks, usually in the region of

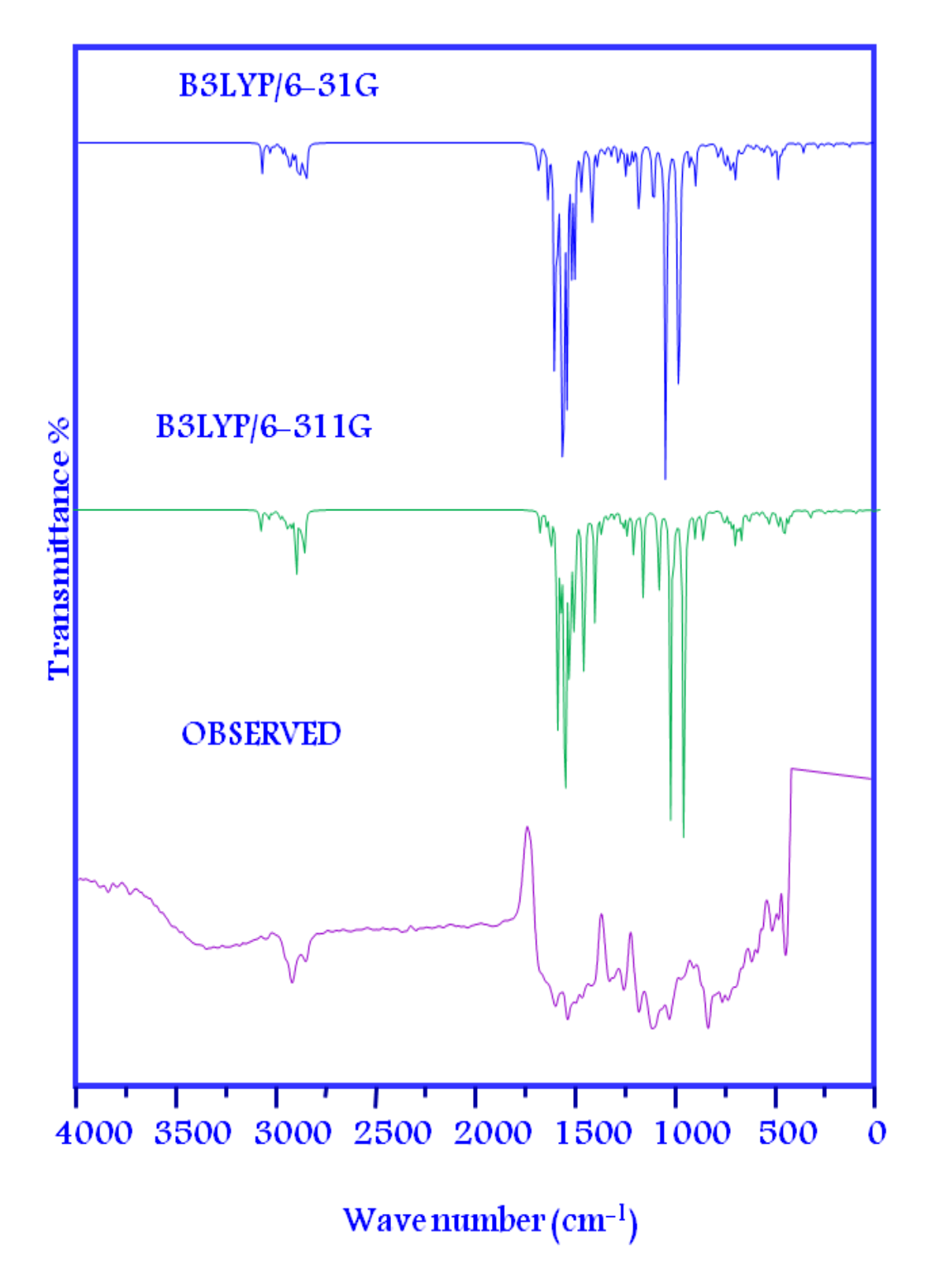


Fig.7.2 Experimental and calculated FT-IR spectra of MCPPT

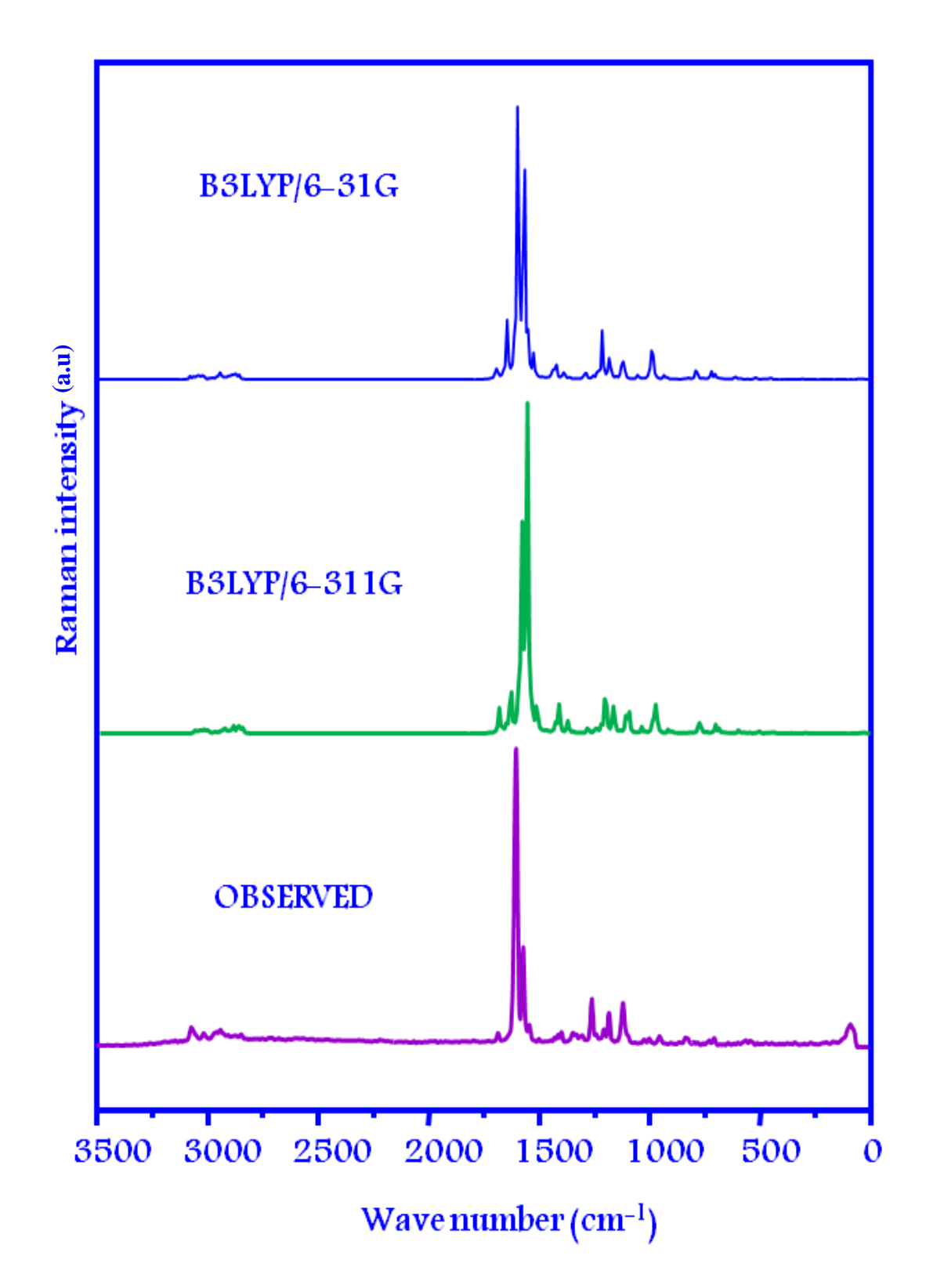


Fig.7.3 Experimental and calculated FT-Raman spectra of MCPPT

1625–1400 cm⁻¹. In the present case, the corresponding modes were observed at 1649, 1495 cm⁻¹ in FT-IR and at 1494 cm⁻¹ in FT-Raman. These vibrations theoretically computed at 1653, 1499 cm⁻¹ and 1650, 1495 cm⁻¹ for B3LYP/6-31G and B3LYP/6-31IG basis set, respectively. Fatmah et al. [204] reported that the FT-IR spectrum observed at 988 cm⁻¹ are assigned as C-H in-plane bending modes of the phenyl ring. In the present case, the in-plane C-H vibration modes are observed at 1105 (ms) cm⁻¹ in FT-IR and 1112 (s) cm⁻¹ in FT-Raman. The out-of-plane C-H deformations of the phenyl rings with the highest wave numbers have a weaker intensity than those absorbing at lower wave numbers. These γ CH modes are observed between 1000-700 cm⁻¹ [15]. In the present case, out-of-plane bending vibrations are observed at 821(vs), 720 (vs) cm⁻¹ in FT-IR and 828 (ms) cm⁻¹ in FT-Raman. The corresponding computed values were assigned at the range of 882-717 cm⁻¹ in B3LYP/6-31G and 872 -709 cm⁻¹ in B3LYP/6-311G.

Thiazole-Pyrazole ring vibrations

Ring stretching modes (C-N, N-C, C-S, N-N) were observed in a narrow spectral region at 1342–1066 cm⁻¹ for C-N, 590–380 cm⁻¹ for C-S in thiazole [205, 206], and 1150–925 cm⁻¹ for N-C and N-N in pyrazole [174]. The C-N stretching vibrations are identified in the current case at 1535 (vs) cm⁻¹ in FT-IR spectra and at 1688 (m) and 1539 (m) cm⁻¹ in FT-Raman spectra. The theoretically computed values were assigned at 1686, 1540 cm⁻¹ [B3LYP/6-31G] and at 1685, 1536 cm⁻¹ [B3LYP/6-311G]. The stretching vibrations of N-C and N-N are calculated at 1042, 976 cm⁻¹ in B3LYP/6-31G and 1036, 969 cm⁻¹ in B3LYP/6-31IG, respectively. The C-S stretching vibrations are computed using B3LYP/6-31G at 812, 708, 599 cm⁻¹ and B3LYP/6-311G at 795, 701, 593 cm⁻¹.

The asymmetric stretching $\upsilon_{ass}CH_2$, symmetric stretching $\upsilon_{ss}CH_2$, scissoring vibration ρ siss CH_2 , present in the region of 2945 \pm 45, 2885 \pm 45 and 1445 \pm 35 cm⁻¹, respectively [109, 207]. In the present study, the DFT calculations give $\upsilon_{ass}CH_2 = 2905$ cm⁻¹

in B3LYP/6-31G, 2899 cm⁻¹ in B3LYP/6-311G and υ_{ss} CH₂=2879 cm⁻¹ in B3LYP/6-31G, 2875 cm⁻¹ in B3LYP/6-311G, which are assigned as the stretching modes of the CH₂ group. The scissoring mode of CH₂ was observed at 1426 cm⁻¹ in the FT-Raman spectrum and computed at 1429 cm⁻¹ in B3LYP/6-31G, 1425 cm⁻¹ in B3LYP/6-311G. The CH₂ twisting and wagging vibrations are recognized in the regions 1180–1390 cm⁻¹, 1065-740 cm⁻¹ [3]. In the present case, the wagging and twisting modes are assigned at ω CH₂=1245, 1203 cm⁻¹, τ CH₂= 1065 cm⁻¹ in B3LYP/6-31G, ω CH₂= 1240, 1200 cm⁻¹, τ CH₂=1059 cm⁻¹ in B3LYP/6-311G and experimental bands were observed at ω CH₂=897 (w) cm⁻¹, τ CH₂= 1057(ms) cm⁻¹ in FT-IR spectra and ω = 1239 (w), 1198 (m), 895 (ms) cm⁻¹ in FT-Raman spectra.

O-CH₃ vibration

The wavenumbers of the methoxy group vibrational modes are generally influenced by a variety of interesting interactions such as electronic effects, inter-molecular hydrogen bonding and Fermi resonance [208]. Electronic effects such as back donation and induction, mainly caused by the existence of oxygen atoms adjacent to the CH₃ group, can shift the place of the C–H stretching and bending modes [209-211]. The symmetrical stretching mode υ_{ss}CH₃ is looked for in the range of 2920 ± 80 cm⁻¹ in which all the three C–H bonds extend and of contract in phase. In accordance with the above, asymmetric and symmetric vibration have been noticed at 2954 cm⁻¹ in the FT-Raman spectrum. The theoretically estimated values were assigned 2955, 2939, 2870 cm⁻¹ in B3LYP/6-31G and 2953, 2935, 2866 cm⁻¹ in B3LYP/6-311G. Balachandran et al. [210] reported that the O-CH₃ stretching mode is assigned as a strong band in FT-Raman at 1617 cm⁻¹ and a medium weak band at 1275 cm⁻¹. Similar to the literature, very strong band at 1173 cm⁻¹ in FT-IR and medium strong band at 1688 cm⁻¹ and 1170 cm⁻¹ in FT-Raman are assigned as O-CH₃ stretching mode. The corresponding theoretical values are found at 1686, 1176 cm⁻¹ in B3LYP/6-31G and 1685, 1172 cm⁻¹ in B3LYP/6-311G. Castaneda et al. [212] reported that in the methyl

group, two bending vibrations and rocking wavenumbers are found in the range 1100 ± 95 and 1080 ± 80 cm⁻¹. In the current study, the bands calculated at $\delta_{ipr}O$ -CH₃=1079, 1072, $\gamma_{opr}O$ -CH₃= 1025, 1018 cm⁻¹ (MCPPT), 1018 cm⁻¹ (FT-IR) and 1019 cm⁻¹ (FT-Raman) are assigned as rocking modes of the methyl groups. Venkkatram Reddy and co-workers [213] have proposed assignment for O-CH₃ bending mode in the region 300–670 cm⁻¹ for anisole and its derivatives. Krishnakumar and John Xavier [214] asssigned C-O-CH₃ angle bending mode at 341, 382 and 430 cm⁻¹ for the o-, m- and p-methoxybenzaldehydes, respectively. Based on the above literature the band observed at 428 cm⁻¹ in FT-Raman spectrum attributes to C-O-CH₃ angle bending vibrations of MCPPT. The theoretically computed values at 435, 360, 349 cm⁻¹ in B3LYP/6-31G and 430, 355, 342 cm⁻¹ in B3LYP/6-311G basis sets, respectively.

Other vibration

Methyl group vibrations are found mainly around nine fundamentals in the aromatic ring system. It can be related to each of the CH₃ groups, particularly CH₃ ν_{asss} -asymmetric and, ν_{ss} -symmetrical; CH₃ips- in-plane stretch; δ_{ipb} CH₃- in-plane-bending and δ_{opb} CH₃- out-of-plane-bending; CH₃sb-symmetric bending; δ_{ipr} CH₃-in-plane rocking; δ_{opr} CH₃- out-of-plane rocking and τ CH₃-twisting modes of CH₃ group [215, 216]. The CH₃ asymmetric and symmetric stretching mode of MCPPT appears in FT-IR at 2925, 2858 and 2936 cm⁻¹ in FT-Raman spectra. Theoretical asymmetric and symmetric stretching vibration of MCPPT are assigned in the range 2939-2855 cm⁻¹ [B3LYP/6-31G] and 2935-2853 cm⁻¹ [B3LYP/6-311G]. The out-of-plane and in-plane-bending are observed at δ_{opb} CH₃= 1463ms cm⁻¹ in FT-IR, δ_{opb} CH₃= 1471w, δ_{ipb} CH₃= 1442w cm⁻¹ in FT-Raman. The corresponding computed values are δ_{opb} CH₃= 1485, 1473, 1465 cm⁻¹, δ_{ipb} CH₃= 1459, 1450, 1437 cm⁻¹ in B3LYP/6-31G, δ_{opb} CH₃= 1481, 1470, 1463 cm⁻¹, δ_{ipb} CH₃=1452, 1445, 1433 cm⁻¹ in B3LYP/6-311G. The symmetric bending modes of CH₃ assigned at 1423, 1394, 1363 cm⁻¹

(B3LYP/6-31G) and 1418, 1385, 1359 cm⁻¹ (B3LYP/6-311G). The out-of-plane rocking modes are identified in FT-IR bands at 1018 (vs), 750 (vs) cm⁻¹ and in the FT-Raman bands at 1019 (w) cm⁻¹. The calculated bending modes found at 1025, 798, 758cm⁻¹ for B3LYP/6-31G and at 1018, 789, 750 cm⁻¹ for B3LYP/6-311G. The methyl bending modes are observed at δ_{ipr} CH₃= 1092, 1079, 985 cm⁻¹, τ CH₃=255, 231, 225 cm⁻¹[B3LYP/6-31G] and at δ_{ipr} CH₃= 1085, 1072, 975 cm⁻¹, τ CH₃=247, 227, 219 cm⁻¹ [B3LYP/6-311G]. Mooney et al. [217, 218] reported that the vibrations of C-Cl, Br, and I are assigned in the wavenumber range of 1129-480 cm⁻¹. For the title compound, the bands at 989, 922 cm⁻¹ in the B3LYP/6-31G and at 983, 914 cm⁻¹ in the B3LYP/6-311G are assigned as C-Cl stretching modes. The in-plane bending vibration are assigned at 1276 cm⁻¹ in B3LYP/6-31G and 1269 cm⁻¹ in B3LYP/6-311G. The deformation bands are observed at 266 in FT-Raman, theoretically reported at 275 cm⁻¹ in B3LYP/6-31G and 265 cm⁻¹ in B3LYP/6-311G.

7.4.3 Frontier Molecular Orbital Analysis

The highest occupied molecular orbital (HOMO) and the lowest unoccupied molecular orbital (LUMO) are entitled as frontier molecular orbitals (FMOs) predict the excitation properties and the ability of electron transport within the molecule and give the chemical stability of the molecule. The FMOs play an essential role to assign the electronic properties of the materials [219- 221]. In general, the chemical tendency of the molecule is determined by the energy values of HOMOand LUMO, and their energy gap. The calculated energy values of the title compound are HOMO=-5.5528eV, LUMO =-2.1869eV, energy gap =3.3658eV in B3LYP/6-31G and HOMO=-5.7813eV, LUMO =-2.4076eV, energy gap=3.3737eV in B3LYP/6-311G basis sets, respectively. Theisosurface of HOMO and LUMO of the title compound are shown in Fig.7.4.

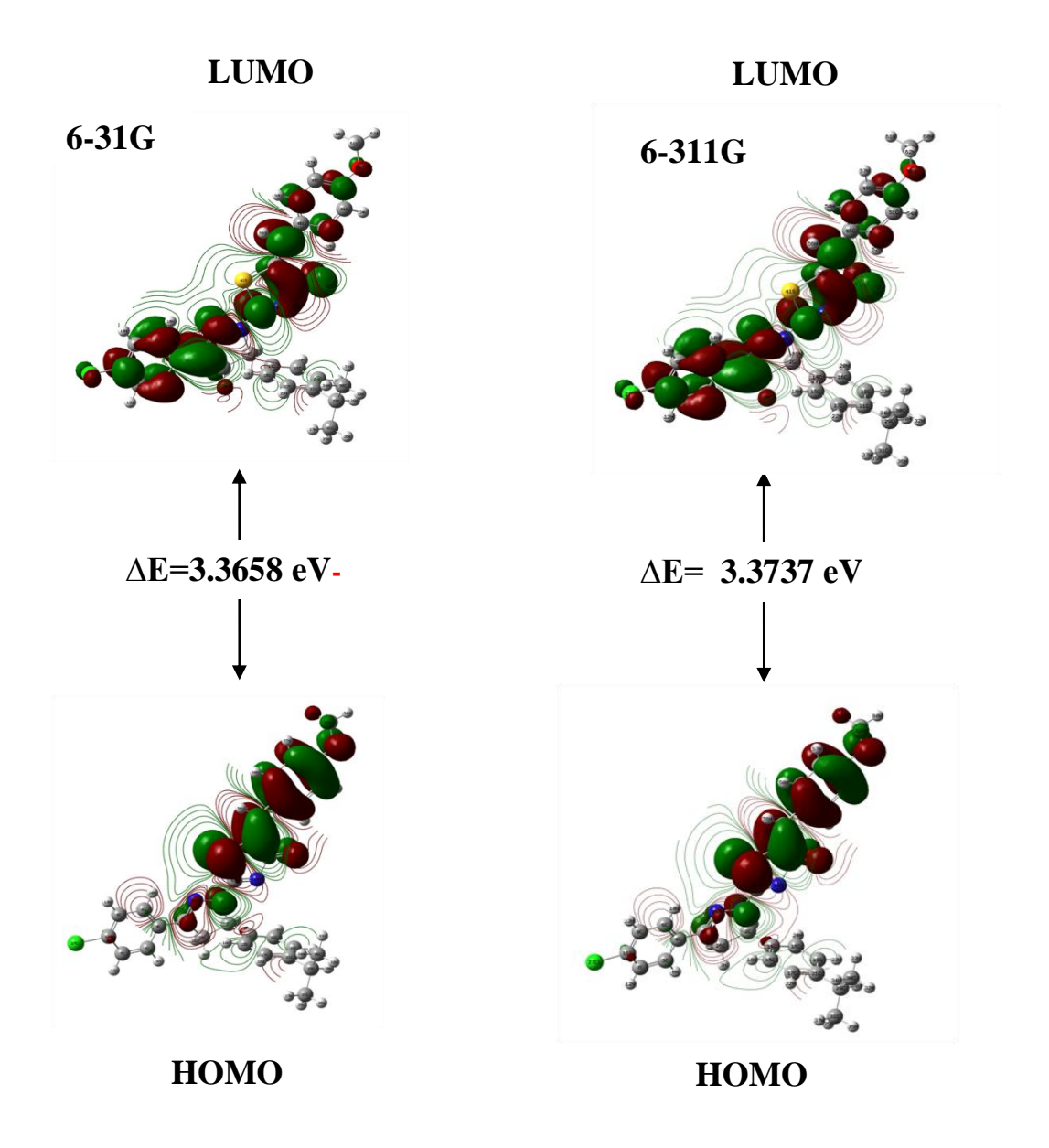


Fig. 7.4 HOMO - LUMO energy gap plots of MCPPT in B3LYP/6-31G and 6-311G basis sets

Global reactivity descriptors, electronegativity (χ), chemical potential (μ), chemical hardness (η), global softness (σ), global electrophilicity index (ω) are defined by equations 7. 1 to 7.7 [37, 191, 20].

Ionization potential (I) =
$$-E_{HOMO}$$
 (7.1)

Electron affinity (A) = -
$$E_{LUMO}$$
 (7.2)

Electro- negativity
$$\chi = \frac{(l+A)}{2}$$
 (7.3)

Chemical potential
$$\mu = -(I + A)/2$$
 (7.4)

Hardness
$$\eta = (I - A)/2$$
 and (7.5)

Softness
$$\sigma = 1/\eta$$
 (7.6)

Electrophilicity index
$$\omega = \mu^2/2\eta$$
 (7.7)

The calculated values of global reactivity descriptors of the title compound are tabulated in the Table 7.4.

7.4.4 Molecular Electrostatic Potential (MEP)

The electrostatic potential that is generated in the space throughout a molecule by its nuclei and electrons (treated as static distributions of charge) is a very beneficial property for analysing and molecular reactive behaviour. This is useful parameter to indicate the sites or regions of electrophilic and nucleophilic. The reactive sites can be identified by different colour codes. The potential decreases in the order of blue > green > yellow > orange > red. The red colour in the MEP graphic indicates an electron-rich site which is a negative region showing electrophilic reactivity. The blue colour in the MEP graph indicates an electron-deficient site, which is a positive region showing nucleophilic reactivity, and the Green colour in the MEP graph indicates the neutral, zero electrostatic potential interaction region, respectively [222].

The electrophilic and nucleophilsites of MCPPT, is shown in Fig.7.5. The negative charge covered by methoxy group, shown in yellow colour and negative charge surrounded by oxygen atom, shown in red colour are noted as nucleophilic region of the title compound. The maximum positive region is covered by hydrogens, which are shown in blue colour and green occupy over the remaining portions of the title molecule represents electrophilic region.

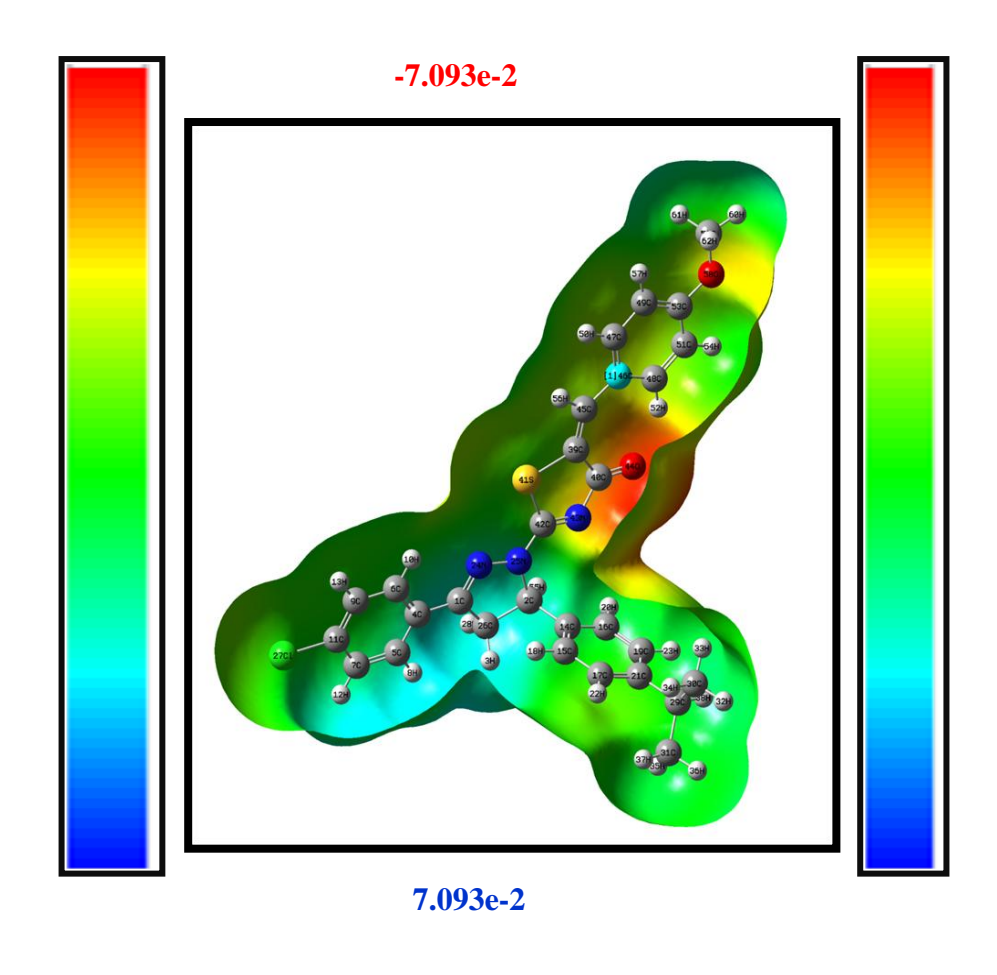


Fig. 7.5 Molecular electrostatic potential surface (MEP) map of MCPPT

7.4.5 Donor-acceptor interaction

The NBO technique was an effective method to provide an information on interactions between filled Lewis-type NBOs (donor) and vacant non-Lewis NBOs (acceptor) orbitals of two subsystems. In order to interpret the inter-, and intramolecular electron density inside the molecule and estimate their stabilisation energy using second order perturbation theory, an NBO analysis was performed on MCPPT at the B3LYP/6-311G level of theory. The charge was transferred between two subsystems' unoccupied (antibonding or Rydgberg) and full (bonding or lone pair) orbitals as a result of hyperconjugative contact or intermolecular delocalization. The stabilization energy E(2), which is associated with electron delocalization amidst electron donor orbital 'i' and electron acceptor orbital 'j' reflects the extent of conjugation of the whole system. Larger

E(2) means a stronger electron donor-acceptor interaction. According to NBO analysis, the stabilization energy (E2) is computed by the formula [223]:

$$E(2) = \Delta E_{ij} = q_{i} \frac{(F_{i,j})^{2}}{(E_{j} - E_{i})}$$
 (7.8)

where q_i is the donor orbital occupancy, E_j and E_i are diagonal elements and F (i, j) is the off diagonal NBO Fock matrix element. Donor-acceptor interactions having stabilization energy E(2) higher than 4 kcal/mol were reported as most significant regions which are tabulated in table 7.5. According to the NBO analysis, the large electron density interactions between the π -bonding C_{39} - C_{45} and C_{42} - N_{42} are distributed to lone pair LP (2) sulphur S_{41} with stabilisation energies of about 635.75 and 105.63 kcal/mol, respectively. Whereas, π^* - antibonding C_{42} - N_{43} , C_1 - N_{24} , C_7 - C_{11} , C_7 - C_{11} is distributed to π^* - antibonding C40 - O_{44} , C_4 - C_5 , C_4 - C_5 , C_6 - C_9 with stabilization energy of about 51.96, 39.62, 209.01, 140.63 kcal/mol.

7.4.6 Topology analysis

Localized orbital locator (LOL) and electron localization function (ELF)

The Localized Orbital Locator (LOL) is a unique descriptor to know chemical bonding between atoms in molecules. It's an electron density XY Plane map filled with LOL colours that explains the chemically significant regions (electron pair in a space region) of MCPPT atoms. The Electron Localization Function (ELF) is a shaded map visualizer that appears at the top of the topology image (isosurface) as a green map. Several colours are represented on this surface, as shown in Fig.7.6. The colours red and orange denote a strong electronic localization. A depletion region between the inner and valence shells is represented by the blue colour circle. The localised orbital locator has the minimum values in the hydrogen and carbon regions. In this work, the O-CH₃ atoms have clearly shown lone pair at O and blue colour circle around the carbon atoms denote a low electron

localization value. This core, valance and lone pair region are visualized through isosurface and the shaded surface maps with projection effect [224, 225].

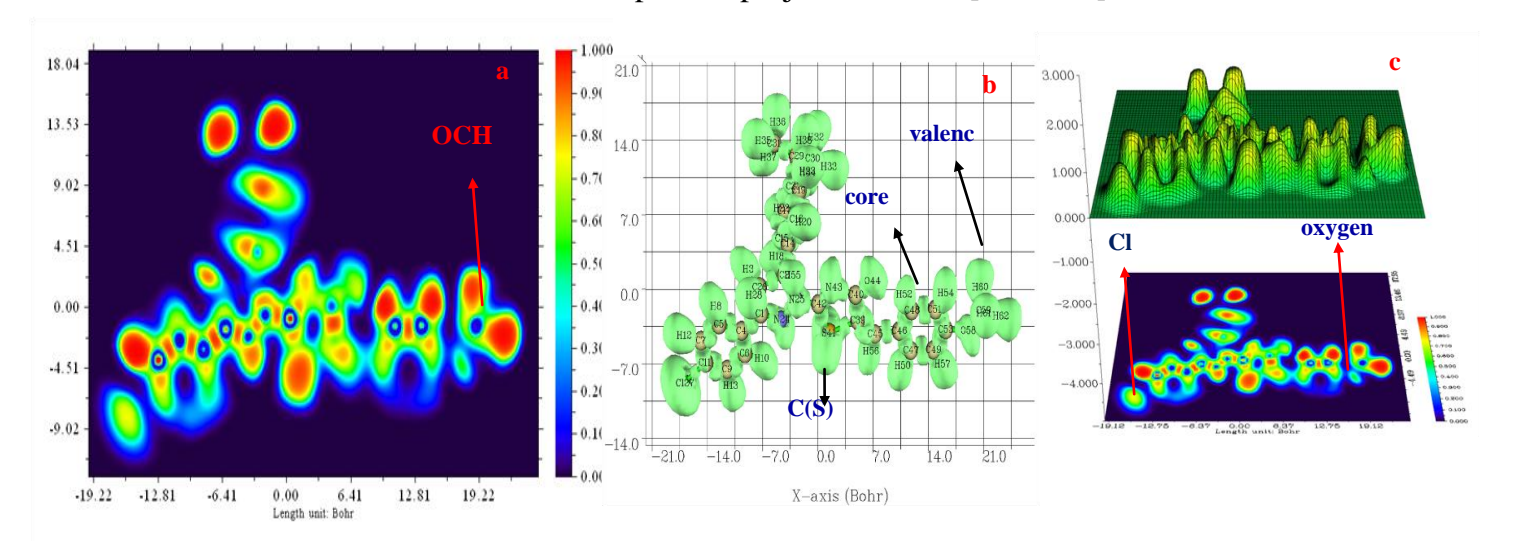


Fig. 7.6 a) Localized orbital locator (LOL) for MCPPT obtained in xy plane, b) Electron localization function (ELE) with isosurface and c) Electron localization function (ELE) shaded surface map with projection effect

Reduced density gradient analysis (RDG)

A reduced density gradient characteristic has been developed as a tool for exposing non-covalent interactions. Interactions develop between weak to strong in conjunction with reactions, and RDG is the backbone of reactivity research [52, 118]. RDG analysis is used to forecast real-space weak couplings based on electron density. It is a dimensionless quantity that is first derived by equation.

RDG(r) =
$$\frac{1}{2(3\pi r^2)^{1/2}} \frac{|\nabla \rho(r)|}{\rho(r)^{4/3}}$$
 (7.9)

In the present work (Fig.7.7), the blue colour signifies greater attraction, the red colour reflects the ring system which is responsible for the steric effect. This compound emits the green colour that reflects the contact between van der Walls, i.e.,non-covalent interaction that might have been liable for the labelled compound stabilization.

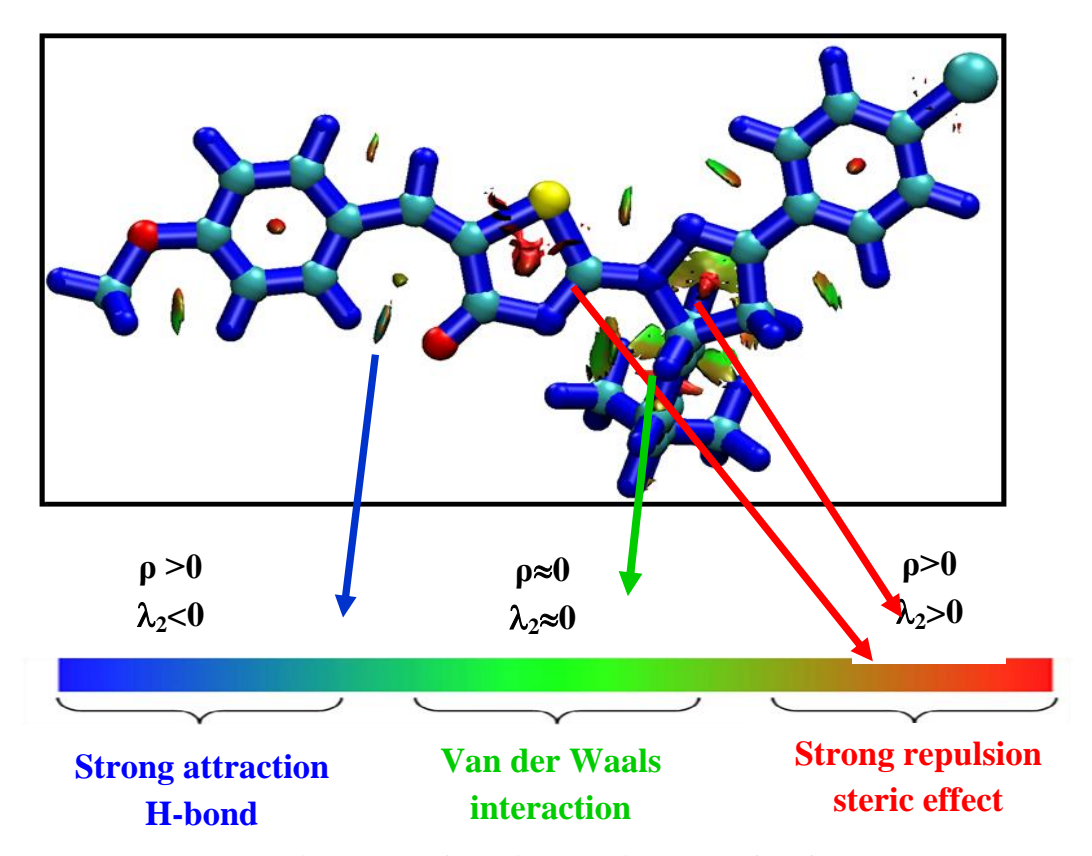


Fig. 7.7 RDG 3D interaction plot of MCPPT

7.4.7 Molecular Docking

PASS (prediction of activity spectra for substance) [161] is a web- based tool to predict the activity of a compound. PASS analysis (Table7.6) of the MCPPT predicts Mcl-1 antagonist, non-steroidal anti-inflammatory agent and Anti-inflammatory activity with Pa (probability to be active) value of (0,647), (0,472) and (0,592). The structure of anti-neurogenic pain (5pbe), anti-inflammatory (4x7s), meloid cell leukemia-1(6dm8), myeloblastin-I (1fuj), naproxen (4ot2) proteins are downloaded from the PDB data base. To evaluate the inhibitory essence of the compound with above enzymes, molecular docking observations were carried out. Molecular docking calculations were done by the Auto Dock 4.2 and Discover studio visualizer [57] softwares. The dotted lines (Fig.7.8) represent a residual interaction of the minimum docking energy. The obtained results are examined and tabulated in Table 7.7.

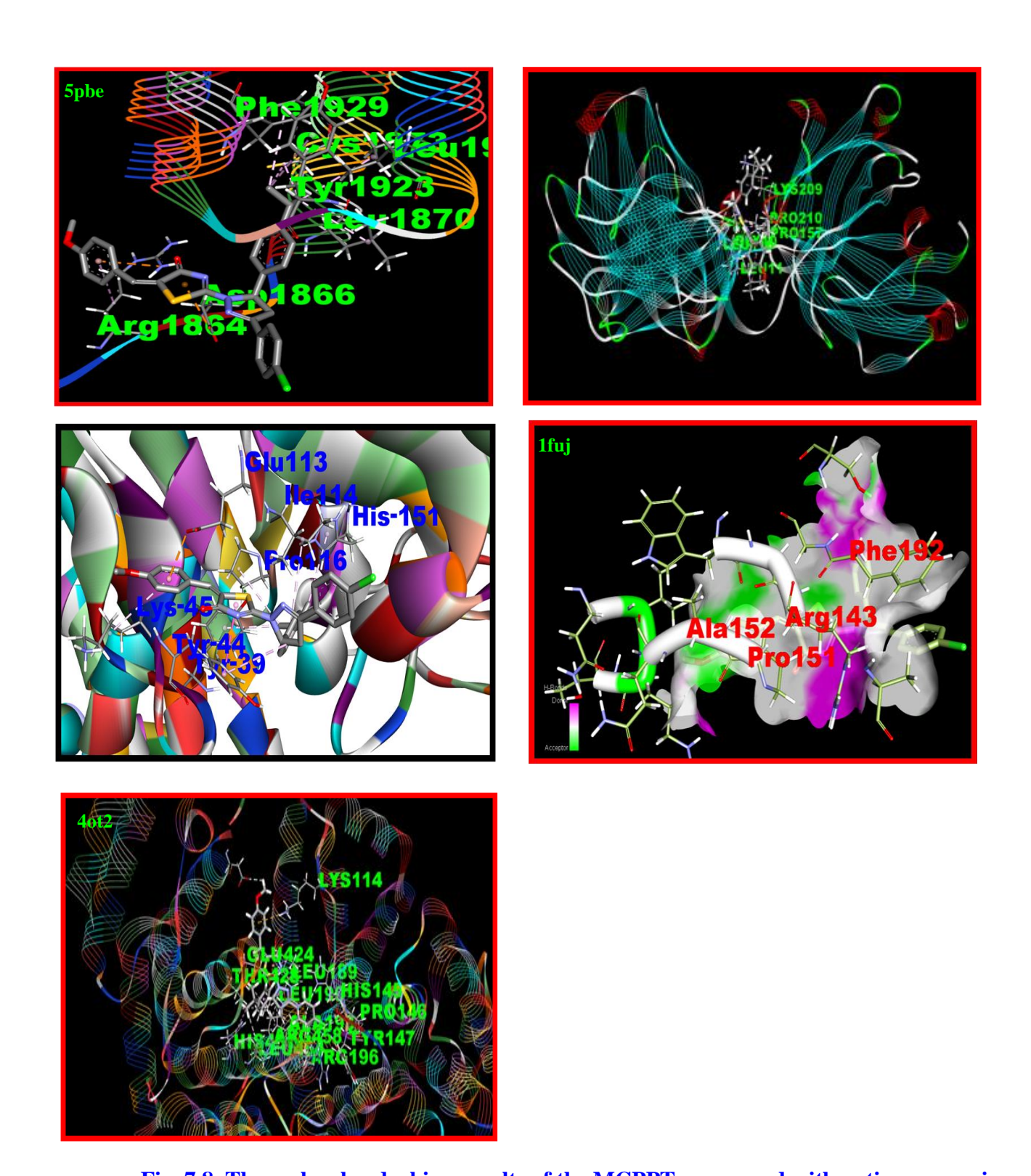


Fig. 7.8 The molecular docking results of the MCPPT compound with anti-neurogenic pain (5pbe), anti-inflammatory (4x7s), meloid cell leukemia-1 (6dm8), myeloblastin I (1fuj), naproxen (4ot2)

Ligand active interaction with anti-neurogenic pain (5pbe)

5pbe crystal structure of a anti-neurogenic pain protein interacts with ligand from conventional hydrogen bond with residue - 2.2 Å: ARG: A:1864, Pi-Cation bond with residue - 2.4 Å: ASP: A:1866 and Pi-sigma bond with residue - 2.4 Å: PHE: A:1929. The binding affinity of its protein-ligand interactions are - 7.25, -6.37, -6.27 kcal/mol, respectively. The inhibition constants are 4.85 μ M, 21.47 μ M, and 25.47 μ M, with RMSD values of 40.12 Å, 42.75 Å, and 42.35 Å.

Ligand active interaction with anti-inflammatory (4x7s)

4x7s crystal structure of a anti-inflammatory protein interacts with ligand from Pialkyl bond with residue - 2.4 Å: PRO:H:210, van der Waals bond with residue - 2.6 Å: GLY:H:10, Pi-sigma bond with residue - 3.2 Å: LYS:H:209. The binding affinity of its protein-ligand interactions are - 7.84, -7.60, -7.50 kcal/mol, respectively. The inhibition constants are 1.80 μ M, 2.69 μ M, and 3.19 μ M, with RMSD values of 29.68 Å, 27.80 Å, and 30.10 Å.

Ligand active interaction with myeloid cell leukemia-1(6dm8)

6dm8 crystal structure of a myeloid cell leukemia-1 protein interacts with ligand from conventional hydrogen bond with residue - 2.8 Å: TYR: A:39, Pi-alkyl bond with residue - 2.5 Å: LYS: A:45 and Pi-Pi stacked bond with residue - 2.6 Å: TYR: A:45. The binding affinity of its protein-ligand interactions are -8.61, -8.24, -7.78 kcal/mol, respectively. The inhibition constants are 484.62 nM, 906.81 nM, and 1.97 μM, with RMSD values of 174.06 Å, 178.17 Å, and 180.11 Å.

Ligand active interaction with myeloblastin I (1fuj)

1fuj crystal structure of a myeloblastin- I protein interacts with ligand from carbon hydrogen bond with residue - 2.0 Å: VAL: A:73, Pi-Alkyl with residue - 1.5 Å: PRO: A:151 and conventional hydrogen bond with residue - 2.4 Å: ARG: A:143. The value of -8.94,

-8.39, -7.98 kcal/mol is the binding affinity of the protein-ligand interaction,with RMSD values of 40.99 Å, 41.56 Å, and 36.14 Å, the inhibition constants are 281.69 nM, 707.67 nM, and 1.42 nM, respectively.

Ligand active interaction with naproxen (4ot2)

4ot2 crystal structure of a naproxen protein interacts with ligand from Amide-Pistacked bond with residue - 2.8 Å: LEU: A:189, Pi-Anion bond with residue - 3.0 Å: GLU: A:424 and Pi-Cation bond with residue - 3.0 Å: LYS: A:114. The binding affinity, RMSD values and corresponding inhibition constants are -8.96, -8.90, -8.36 kcal/mol, 73.00, 74.298, 92.79 Å, and 268.89, 298.11, 749.69 nM, respectively.

7.5 Conclusion

With the support of density functional theory, the vibrational spectra of 5-(4-Methoxybenzylidene)-2-[3-(4-chlorophenyl)-5-[4-(propan-2-yl) phenyl]-4, 5-dihydro-1H-pyrazol-1-yl]-1,3-thiazol-4(5H)-one (MCPPT) were discussed in detail. FT-IR and FT-Raman spectra have been recorded and evaluated. The molecular geometry, vibrational wavenumbers of the title compound were determined and analyzed both at B3LYP/6-31G and B3LYP/6-311G basis sets. The energy gap between the HOMO and LUMO revealed that the charge transfer takes within the molecule from the ring methoxybenzylidene, thiazol to pyrazole. MEP surface graph indicates, the negative potential sites were presented on the electronegative atoms, while the positive potential sites were around the hydrogen atom. The strong intramolecular interactions are revealed by natural bond orbital analysis. The XY Plane map filled, shaded map with projection effect and non-covalent interaction was obtained from topological analysis. In addition, combining DFT calculations with molecular docking results reveals MCPPT compound drugs nature of different biological activities such asantineurogenic pain (5pbe), anti-inflammatory (4x7s), myeloid cell leukemia-1(6dm8), myeloblastin (1fuj) and naproxen (4ot2).

Table 7.1: Optimized geometrical parameters (Bond lengths) of MCPPT

D	B3LYP/	B3LYP/	D	B3LYP/	B3LYP/	D4	B3LYP/	B3LYP/
Parameter	6-31G	6- 311G	Parameter	6-31G	6- 311G	Parameter	6-31G	6- 311G
C1-C4	1.46	1.46	C15-H18	1.09	1.08	C39-C45	1.36	1.36
C1-N24	1.31	1.30	C16-C19	1.40	1.40	C40-N43	1.41	1.41
C1-C26	1.52	1.52	C16-H20	1.08	1.08	C40-O44	1.25	1.25
C2-C14	1.52	1.52	C17-C21	1.41	1.41	S41-C42	1.84	1.84
C2-N25	1.51	1.51	C17-H22	1.09	1.08	C42-N43	1.30	1.30
C2-C26	1.56	1.56	C19-C21	1.40	1.40	C45-C46	1.46	1.46
C2-H55	1.09	1.09	C19-H23	1.09	1.08	C45-H56	1.09	1.09
H3-C26	1.09	1.09	C21-C29	1.53	1.53	C46-C47	1.42	1.41
C4-C5	1.41	1.41	N24-N25	1.39	1.39	C46-C48	1.42	1.42
C4-C6	1.41	1.41	N25C-42	1.35	1.35	C47C-49	1.39	1.39
C5C-7	1.40	1.40	C26-H28	1.10	1.09	C47-H50	1.09	1.08
C5-H8	1.08	1.08	C29-C30	1.55	1.55	C48-C51	1.39	1.39
C6-C9	1.39	1.39	C29-C31	1.55	1.54	C48-H52	1.08	1.08
C6-H10	1.08	1.08	C29-3H8	1.10	1.09	C49-C53	1.40	1.40
C7-C11	1.39	1.39	C30-H32	1.10	1.09	C49-H57	1.08	1.08
C7-H12	1.08	1.08	C30-H33	1.10	1.09	C51-C53	1.40	1.40
C9-C11	1.40	1.39	C30H-34	1.10	1.09	C51-H54	1.08	1.08
C9-H13	1.08	1.08	C31-H35	1.10	1.09	C53-O58	1.39	1.39
C11-C127	1.82	1.83	C31-H36	1.10	1.09	O58-C59	1.45	1.45
C14-C15	1.41	1.40	C31-H37	1.10	1.09	C59-H60	1.10	1.08
C14-C16	1.40	1.40	C39-C40	1.49	1.49	C59-H61	1.10	1.09
C15-C17	1.40	1.39	C39-S41	1.87	1.87	С59-Н62	1.09	1.09

Table 7.2: Optimized geometrical parameters (Bond angle) of MCPPT

D	B3LYP/	B3LYP/	D	B3LY/	B3LYP/	Danisanistani	B3LYP/	B3LYP/
Parameter	6-31G	6- 311G	Parameter	6-31G	6- 311G	Parameter	6-31G	6- 311G
C4-C1-N24	121.68	121.60	C21-C17-H22	119.85	119.87	C39-C40-N43	113.47	113.46
C4-C1-C26	125.21	125.30	C16-C19-C21	121.24	121.27	C39-C40-O44	124.79	124.70
N24-C1-C26	113.10	113.09	C16-C19-H23	119.39	119.36	N43-C40-O44	121.74	121.84
C14-C2-N25	112.32	112.24	C21-C19H-23	119.37	119.36	C39-S41-C42	86.32	86.22
C14-C2-C26	115.19	115.24	C17-C21-C19	117.91	117.83	N25-C42-S41	119.65	119.86
C14-C2-H55	109.26	109.17	C17-C21-C29	121.37	121.41	N25-C42-N43	122.90	122.73
N25-C2-C26	100.17	100.21	C19-C21-C29	120.71	120.76	S41-C42-N43	117.45	117.41
N25-C2-H55	107.27	107.37	C1-C24-N25	108.72	108.72	C40-N43-C42	113.82	114.00
C26-C2-H55	112.15	112.13	C2-N25-N24	113.49	113.38	C39-C45-C46	135.11	135.17
C1-C4-C5	120.65	120.68	C2-N25-c42	124.82	124.79	C39-C45-H56	113.75	113.72
C1-C4-C6	120.59	120.68	N24-N25-C42	121.61	121.74	C46-C45-H56	111.14	111.11
C5-C4-C6	118.76	118.64	C1-C26C-C2	103.57	103.63	C45-C46-C47	116.04	116.15
C4-C5C-7	120.89	120.95	C1-C26-H3	112.34	112.37	C45-C46-C48	126.47	126.42
C4-C5-H8	120.25	120.33	C1-C26-H28	110.51	110.52	C47-C46-C48	117.49	117.43
С7-С5-Н8	118.86	118.72	C2-C26-H3	111.24	111.24	C46-C47-C49	122.16	122.14
C4-C6-C9	120.75	120.80	C2-C26-H28	111.75	111.65	C46-C47-H50	119.10	119.13
C4-C6-H10	119.05	119.08	H3-C26-H28	107.48	107.48	C49-C47-H50	118.75	118.72
C9-C6-H10	120.20	120.12	C21-C29-C30	111.66	111.75	C46-C48-C51	120.64	120.68
C5-C7-C11	118.79	118.73	C21-C29-C31	111.99	112.05	C46-C48-H52	118.96	118.99
C5-C7-H12	120.73	120.72	C21-C29-H38	107.05	106.93	C51-C48-H52	120.39	120.33
C11-C7-H12	120.48	120.55	C30-C29-C31	110.93	111.06	C47-C49-C53	119.08	119.11
C6-C9-C11	118.96	118.93	С30-С29-Н38	107.46	107.36	C47-C49-H57	119.60	119.58
C6-C9-H13	120.71	120.71	C31-C29-H38	107.48	107.38	C53-C49-H57	121.32	121.30
C11-C9-H13	120.33	120.36	C29-C30-H32	110.51	110.48	C48-C51-C53	120.68	120.70
C7-C11-C9	121.84	121.95	C29-C30H-33	111.11	111.08	C48-C51-H54	120.97	121.03
C7-C11-Cl27	119.10	119.07	C29-C30-H34	111.09	111.19	C53-C51-H54	118.34	118.27
C9-C11-Cl27	119.05	118.98	H32-C30-H33	108.31	108.25	C49-5C3-C51	119.94	119.94

_									
_	C2-C14-C15	121.44	121.41	H32C-30-H34	107.82	107.82	C49-C53-O58	124.28	124.33
	C2-C14-C16	119.95	120.06	H33-C30-H34	107.88	107.89	C51-C53-O58	115.78	115.73
	C15-C14-C16	118.61	118.53	C29-C31-H35	111.17	111.14	C53-O58-C59	119.09	119.36
	C14-C15-C17	120.64	120.68	C29-C31-H36	110.48	110.47	O58-C59-H60	111.20	105.04
	C14-C15-H18	120.18	120.23	C29-C31-H37	111.17	111.25	O58-C59-H61	111.21	111.18
	C17-C15-H18	119.18	119.08	H35-C31-H36	108.25	108.19	O58-C59-H62	105.11	111.19
	C14-C16-C19	120.54	120.60	H35-C31-H37	107.91	107.92	H60-C59-H61	109.68	109.71
	C14-C16-H20	119.53	119.55	H36-C31-H37	107.73	107.75	H60-C59-H62	109.78	109.71
	C19-C16-H20	119.91	119.83	C40-C39-S41	108.95	108.92	H61-C59-H62	109.78	109.90
	C15-C17-C21	121.04	121.08	C40-C39-C45	132.93	133.07	C39-C40-N43	113.47	113.46
	C15-C17-H22	119.11	119.04	S41-C39-C45	118.12	118.01	C39-C40-O44	124.79	124.70

Table 7.3: Experimental and calculated wavenumbers along with vibrational assignments for MCPPT using B3LYP/6-31G and B3LYP/6-311G

	Observed frequencies		Calculated	frequencies	
S.No		(cm ⁻¹)		n ⁻¹)	Vibrational againments (DED) (1000/)
5.110	ET ID	ET DANZANI	B3LYP/	B3LYP/	Vibrational assignments (PED) (100%)
	FT-IR	FT-RAMAN	6-31G	6-311G	
1		3069	3075	3070	υ CH(99)
2	3056		3058	3055	υ CH(99)
3			3045	3041	υ CH(98)
4			3034	3030	υ CH(99)
5			3025	3023	υ CH(98)
6		3014	3021	3016	υ CH(99)
7			3012	3008	υ CH(99)
8			2985	2982	υ CH(98)
9			2972	2969	υ CH(98)
10		2954	2955	2953	$v_{ass}CH_3(99)$
11			2951	2945	υ CH(98)
12			2944	2940	υ CH(98)
13			2939	2935	$v_{ass}CH_3(98)$
14			2934	2930	υ CH(99)
15	2925		2932	2925	$v_{ass}CH_3(97)$
16			2921	2917	υ CH(99)
17			2914	2906	υ CH(99)
18			2905	2899	$v_{ass}CH_2(98)$

19			2895	2893	$v_{ass}CH_3(97)$
20			2894	2890	$v_{ass}CH_3(97)$
21			2883	2881	$v_{ass}CH_3(97)$
22			2879	2875	$v_{\rm ss} CH_2(98)$
23			2870	2866	$v_{ss}CH_3(98)$
24	2858		2862	2860	$v_{ss}CH_3(97)$
25			2855	2853	$v_{ss}CH_3(97)$
26		2845	2850	2847	υ CH(98)
27		1688m	1686	1685	υ CO(98), υ CC(98), υ CN(98)
28			1676	1672	υ CC(72), δ CH(21)
29	1649		1653	1650	υ CC(70), δ CH(23)
30			1635	1631	υ CC(72), δ CH(19)
31	1596vs	1598vs	1601	1597	υ CC(66), $υ$ CN(12), $δ$ CH(10)
32			1586	1582	δ CH(68), υ CC(12), υ CN(10)
33			1581	1578	δ CH(72), υ CC(18)
34		1560vs	1566	1562	υ CC(65), υ CO(12), υ CN(12), δ CH(10)
35			1557	1555	υ CC(72),δ CH(19)
36	1535vs	1539m	1540	1536	υ CN(67), υ CO(13), δ CH(10)
37			1527	1523	δ CH(74), υ CCC(10),
38			1515	1512	δ CH(74), υ CCC(12),
39	1495ms	1494w	1499	1495	δ CH(74), υ CCC(12),
40			1485	1481	$\delta_{\rm opb}$ CH ₃ (72)
41		1471w	1473	1470	$\delta_{\mathrm{opb}} \mathrm{CH}_3(72)$
42	1463ms		1465	1463	$\delta_{\rm opb}$ CH ₃ (73)
43			1459	1452	$\delta_{\rm ipb}$ CH ₃ (73)
44		1442w	1450	1445	δ_{ipb} CH ₃ (73)
45			1437	1433	δ_{ipb} CH ₃ (73)
46		1426w	1429	1425	ρ_{sciss} CH ₂ (73)
47			1423	1418	δ_{sb} CH ₃ (78)
48		1409w	1414	1410	δCH(73)
49		1398w	1406	1399	δ CH (72), υ CC(13)
50			1394	1385	δ_{sb} CH ₃ (80)
51			1387	1379	δ CH (75)
52		1369	1376	1370	δ CH (75)
53			1363	1359	$\delta_{sb}CH_3$ (80)
54			1351	1345	δ CH (73)
55			1343	1337	δ CH (72)
56	1323m	1323w	1331	1325	δ CH (73)
57			1318	1313	δ CH (75)
58	1300m	1297w	1304	1298	δ CH (75)
59			1287	1283	δ CH (72), δ CO (10)
60			1280	1275	δ CH (72), δ CC (15)

					22 (52) 2 27 (12) 2 27 (13)
61			1276	1269	υCC (68), δ CH (12), δCCl (10)
62	1250ms	1254ms	1260	1252	δ CH (68)
63		1239w	1245	1240	$\omega_{\text{wag}} \text{CH}_2 (72)$
64			1232	1227	υCC (66), δ CH (18), δ CC (12)
65			1224	1218	δ CH (68), υCN (18), υCS (10)
66		1198m	1203	1200	$\omega_{\text{wag}} \text{CH}_2 (70)$
67	1173vs	1170s	1176	1172	υ CO (64), δ CH (16), δ CH ₃ (10)
68			1169	1162	υCC (64), δ CH (19)
69			1155	1151	δ CH (64), υCC (20)
70			1140	1133	δ CH (64), υCC (20)
71		1112s	1122	1115	δ CH (64), υCC (20)
72	1105ms		1112	1106	δ CH (68)
73			1103	1094	δ CH (72)
74			1092	1085	δ_{ipr} CH ₃ (61), δ CH (21)
75			1079	1072	δ_{ipr} CH ₃ (60), δ CH (20)
76	1057ms		1065	1059	$\tau CH_2(75)$
77			1042	1036	ν CN (68), δ CH (11), δ CO (10)
78			1034	1029	δ CH (67)
79	1018vs	1019w	1025	1018	$\gamma_{\rm opr}$ CH ₃ (62)
80			1019	1011	δ CH (68)
81			1015	1004	δ CH (68)
82		996m	1003	995	υCC (62), δ CC (22)
83			989	983	υCCl (72), δ CH (14)
84			985	975	δ_{ipr} CH ₃ (61), δ CH (20)
85			976	969	υΝΝ (60), ν CN (14), δ CO (12)
86	960ms		966	962	δ CC (63), δ_{rock} (21)
87			963	959	γ CH (74)
88		946m	958	950	δ_{ring} (67), δ CH (12)
89			941	932	δ_{ring} (67), δ CH (12)
90			922	914	δ_{ring} (66), δ CH (12), υ CCl (10)
91	895ms	897w	909	896	$\gamma_{\text{ring}}(59), \omega_{\text{wag}} \text{CH}_2 (10)$
92			894	880	υ CO (76)
93			882	872	γ CH (63)
94			875	863	γ CH (63)
95			862	855	γ CH (63)
96			853	847	γ CH (63)
97		828ms	840	831	γ CH (65)
98	821vs		829	820	γ CH (64), γ _{ring} (12)
99			823	818	γ CH (62)
100			812	795	υCS(62), δ CC (16), δ CH (10)
101			798	789	γ_{opr} CH ₃ (58)
					10hr2 ()

102			784	775	γ CH (62)
103			776	762	$\delta_{\rm ring}$ (64)
104	750vs		758	750	γ _{opr} CH ₃ (58)
105			749	744	γ CH (60)
106			744	738	γ CH (62)
107			737	729	γ CH (62)
108	720vs		726	721	γ CH (62)
109			723	715	γ CH (62)
110			717	709	γ CH (62)
111			708	701	$\delta_{\rm ring}$ (66), $vCS(12)$
112		694ms	699	695	γ CH (62)
113	683ms		690	685	$\delta_{\rm ring}$ (64)
114			675	671	$\delta_{\rm ring}$ (62)
115			667	660	$\delta_{\rm ring}$ (62)
116			656	652	γ CO (60), γ _{ring} (14)
117	646ms		649	645	γ _{ring} (61)
118			642	637	δ CO (59), δ_{ring} (21)
119			635	629	γ CH (62)
120			628	622	γ CH (64), γ CO (16)
121			617	613	δ_{ring} (60), $vCCl(18)$
122	600m		605	602	$vCC(68)$, δ_{ring} (18)
123			599	593	$vCS(66)$, δ_{ring} (20)
124			586	581	$\delta_{\rm ring}$ (61)
125	571ms		578	570	$\delta_{\rm ring}$ (62)
126			573	564	$\delta_{\rm ring}$ (62)
127		558w	566	560	γ CN (61), γ _{ring} (17)
128			550	547	γ _{ring} (58)
129		537w	542	539	δ CC (66)
130			525	520	δ CO (68)
131			510	506	$\gamma_{\rm ring}$ (59)
132	497m		503	498	δ CH (68)
133			490	484	$\gamma_{\rm ring}$ (58)
134			474	471	$\delta_{\rm ring}$ (65)
135	464w		470	464	δCC (66)
136			458	453	$\gamma_{\rm ring}$ (58)
137			450	445	γ_{ring} (58)
138			442	438	δ_{ring} (62), $vCCl(14)$
139	428ms		435	430	δ_{ring} (62), δ CO (15)
140			417	411	γ _{ring} (58)
141			389	385	δCC (64)
142			380	376	γ _{ring} (58)

143		371	368	γ _{ring} (58)
144		360	355	γ CC (62), γ CO (12)
145		349	342	δ CO (60), δ CH ₃ (13)
146	335w	341	335	γ _{ring} (55), γ CN (17)
147		327	322	γ _{ring} (56), γ CC (17)
148		310	304	γ _{ring} (56), γ CN (16)
149		294	288	$\delta_{ m ring}$ (55)
150		278	272	δ CO (67)
151	266w	275	265	δ CCl (61)
152		266	256	δ O CH $_3$ (50)
153		255	247	τCCH ₃ (46)
154		249	242	τ CC (45)
155		244	238	τ CC (45)
156		238	232	γ CC (49)
157		231	227	$\tau \text{CH}_3(57)$
158		225	219	$\tau \text{CH}_3 (58)$
159		209	205	γ CC (47)
160		196	191	δ CC (49)
161		185	180	$\tau \text{CH}_3 (58)$
162		172	169	γ CN (58), γ CO (21)
163		168	160	δ CO (61)
164		157	151	γ CC (50)
165		140	132	γ CC (49)
166		135	128	τ CC (51)
167		117	114	γ CO (52)
168		90	84	τ CC (55)
169	79s	87	80	τ CN (52)
170		75	71	τ CC (52)
171		68	64	τ CO (51)
172		55	53	τ CC (52)
173		46	42	τ CC (50)
174		40	33	τ CC (52)
175		36	28	τ CC (51)
176		30	25	τ CC (51)
177		26	23	τ CC (52)
178		21	16	τ CC (52)
179		18	14	τ CC (51)
180		13	10	γ CC (49)

s-strong, m-medium, ms-medium strong, vs-very strong, w-weak, υ -stretching, υ_{ss} -symmetric stretching, υ_{ass} -asymmetric stretching, δ -in-plane bending, γ -out-of-plane bending, ρ -scissoring, ω -wagging, σ -rocking, τ -twisting

 Table 7.4: Calculated (HOMO-LUMO) energy values of MCPPT

Frontier molecular orbitals parameters	Energy values	Energy values
Frontier molecular orbitals parameters	B3LYP/6-31G	B3LYP/6-311G
E _{HOMO} (ev)	-5.5527	-5.7813
E _{LUMO} (ev)	-2.1870	-2.4076
Energy Gap (ev)	3.3658	3.3737
Ionization Energy (I) (ev)	5.5527	5.7813
Electron Affinity (A) (ev)	2.1870	2.4076
Chemical potential (µ)	-3.8699	-4.0945
Hardness of the molecule (η)	1.6829	1.6869
Softness of the molecule (σ)	0.5942	0.5928
Electronegativity of the molecule (χ) (ev)	3.8699	4.0945
Electrophilicity index of the molecule (ω)	4.4495	4.9692

 Table 7.5: Second order perturbation theory analysis of Fock matrix in NBO for MCPPT

Donor(i)	Туре	ED/e	Acceptor (j)	Type	ED/e	E(2) ^a Kcal/mol	E(j)- E(i) ^b a.u	F(i,j) ^c a.u
π	C1 - N24	1.9167	π*	C4 - C5	0.39123	8.2	0.32	0.05
σ	C2 - H55	1.89317	σ^*	H3 - C26	0.05106	7.24	0.85	0.071
σ	C2 - H55	1.89317	π^*	C14 - C15	0.39019	12.12	0.48	0.073
σ	H3 - C26	1.96003	π^*	C1 - N24	0.25636	6.25	0.48	0.052
π	C4 - C5	1.64584	π^*	C1 - N24	0.25636	17.01	0.24	0.059
π	C4 - C5	1.64584	π^*	C6 - C9	0.29464	19.73	0.28	0.068
π	C4 - C5	1.64584	π^*	C7 - C11	0.39472	22.59	0.27	0.07
π	C6 - C9	1.66347	π^*	C4 - C5	0.39123	21.03	0.28	0.069
π	C6 - C9	1.66347	π^*	C7 - C11	0.39472	21.54	0.26	0.068
π	C7 - C11	1.68127	π^*	C4 - C5	0.39123	17.71	0.3	0.066
π	C7 - C11	1.68127	π^*	C6 - C9	0.29464	19.42	0.3	0.069
π	C14 - C15	1.67209	π^*	C16 - C19	0.34098	19.84	0.29	0.067
π	C14 - C15	1.67209	π^*	C17 - C21	0.36081	18.97	0.29	0.067
π	C16 - C19	1.68928	π^*	C14 - C15	0.39019	21.55	0.27	0.07
π	C16 - C19	1.68928	π^*	C17 - C21	0.36081	21.58	0.28	0.071
π	C17 - C21	1.64899	π^*	C14 - C15	0.39019	21.48	0.27	0.069
π	C17 - C21	1.64899	π^*	C16 - C19	0.34098	20.18	0.28	0.067
σ	C39 - S41	1.97929	σ^*	N25 - C42	0.03356	7.94	1.43	0.096
π	C39 - C45	1.72704	LP (2)	S41	1.38494	635.75	0.01	0.118

π	C39 - C45	1.72704	π*	C40 - O44	0.35426	29.75	0.28	0.083
π	C40 - O44	1.91611	π^*	C39 - C45	0.27813	8.89	0.27	0.046
π	C40 - O44	1.91611	π^*	C42 - N43	0.5143	6.45	0.28	0.043
π	C42 - N43	1.83937	LP (2)	S41	1.38494	105.63	0.05	0.101
π	C42 - N43	1.83937	π^*	C40 - O44	0.35426	27.43	0.31	0.087
LP (1)	N25	1.74692	π^*	C1 - N24	0.25636	26.09	0.25	0.072
LP (3)	C127	1.99187	π^*	C7 - C11	0.39472	12.64	0.32	0.062
LP (2)	S41	1.38494	π^*	C39 - C45	0.27813	62.78	0.2	0.111
LP (2)	S41	1.38494	π^*	C42 - N43	0.5143	98.47	0.21	0.133
LP (2)	O44	1.88003	σ^*	C39 - C40	0.0979	18.04	0.67	0.099
LP (2)	O44	1.88003	σ^*	C40 - N43	0.06712	22.08	0.65	0.108
π^*	C1 - N24	0.25636	π^*	C4 - C5	0.39123	39.62	0.04	0.064
π^*	C7 - C11	0.39472	π^*	C4 - C5	0.39123	209.01	0.02	0.084
π^*	C7 - C11	0.39472	π^*	C6 - C9	0.29464	140.63	0.02	0.079
π^*	C39 - C45	0.27813	π^*	C40 - O44	0.35426	31.71	0.06	0.07
π^*	C42 - N43	0.5143	π^*	C40 - O44	0.35426	51.96	0.05	0.071

Table 7.6: PASS prediction for the activity spectrum of title compound, Pa represents probability to be active and Pi represents probability to be inactive.

Pa	Pi	Activity name			
0,647	0,005	Mcl-1 antagonist			
0,592	0,033	Antiinflammatory			
0,553	0,003	Alkaline phosphatase inhibitor			
0,534	0,008	PfA-M1 aminopeptidase inhibitor			
0,472	0,015	Non-steroidal antiinflammatory agent			
0,462	0,015	Thiol protease inhibitor			
0,498	0,051	Insulysin inhibitor			
0,464	0,018	Antineoplastic (solid tumors)			
0,443	0,004	Dual specificity phosphatase inhibitor			
0,407	0,005	HCV NS3-helicase inhibitor			
0,365	0,005	Cyclooxygenase inhibitor			
0,346	0,015	Amyloid beta precursor protein antagonist			
0,511	0,192	Gluconate 2-dehydrogenase (acceptor) inhibitor			

Table 7.7: Molecular interaction data of ligand MCPPTduring docking in the active site of enzymes

Ligand name	PDB ID	Bond distance (Å)	Amino acid (residues)	Bond	Binding affinity (kcal/mol)	Inhibition Constant Ki (µM or nM orpM)	RMSD (Å)
l]-4,5-	Antinneuro genic pain (50be)	2.3	ARG:A:1864	conventional hydrogen bond	-7.25	4.85μΜ	40.123
eny	Antinneuro genic pain (50be)	2.4	ASP:A:1866	Pi-Cation	-6.37	21.47 μM	42.745
qd .	Ar ge	2.4	PHE:A:1929	Pi-sigma	-6.27	$25.47 \mu M$	42.350
ın-2-yl) one	Antiinflammato ry (4x7s)	2.4	PRO:H:210	Pi-alkyl	-7.84	1.80 μΜ	29.680
(propa 4(5H)-	iinflamn ry (4x7s)	2.6	GLY:H:10	Vander Waals	-7.60	2.69 μΜ	27.803
-[4- zol-	Ant	3.2	LYS:H:209	Pi-sigma	-7.50	3.19 µM	30.108
5-(4-Methoxybenzylidene)-2-[3-(4-chlorophenyl)-5-[4-(propan-2-yl) phenyl]-4,5-dihydro-1H-pyrazol-1-yl]-1,3-thiazol-4(5H)-one	Myeloid cell leukemia-1(6dm8)	2.8	TYR:A:39	conventional hydrogen bond	-8.61	484.62 nM	174.066
ılorop -1-yl]-	Myeloid cell kemia-1(6dn	2.5	LYS:A:45	Pi-alkyl	-8.24	906.81 nM	178.173
3-(4-ch yrazol	My	2.6	TYR:A:45	Pi-Pi stacked	-7.78	1.97 μΜ	180.119
ne)-2-[o-1H-p	astin)I	2.0	VAL:A:73	Carbon hydrogen bond	-8.94	281.69 nM	40.989
lide) ydr	eloblas (1fuj)I	1.5	PRO:A:151	Pi-Alkyl	-8.39	707.67 nM	41.558
/benzyl dihy	Myeloblastin (1fuj)I	2.4	ARG:A:143	conventional hydrogen bond	-7.98	1.42 μΜ	36.141
Aethox ,	Naproxen (40t2)	2.8	LEU:A:189	Amide-Pi- stacked	-8.96	268.89 nM	73.002
4-A	lapı (40	3.0	GLU:A:424	Pi-Anion	-8.90	298.11 nM	74.298
Ņ	Z	3.0	LYS:A;114	Pi-Cation	-8.36	749.69 nM	92.793

Spectroscopic investigation (FT-IR, FT-Raman), vibrational assignments, topology evaluation and molecular docking study of 5-Chloro-1-(4-chlorobenzyl)-3-[2-(3-(4-chlorophenyl)-5-[4-(propan-2-yl) phenyl]-4,5-dihydro-1H-pyrazol-1-yl) -4-oxo- 4,5-dihydro-1,3-thiazol-5(4H)-ylidene]-2,3-dihydro-1H-indol-2-one

Abstract

The FTIR and FT-Raman spectra of 5-Chloro-1-(4-chlorobenzyl)-3-[2-(3-(4-chlorophenyl)-5-[4-(propan-2-yl) phenyl]-4,5-dihydro-1H-pyrazol-1-yl) -4-oxo- 4,5-dihydro-1,3-thiazol-5(4H)-ylidene]-2,3-dihydro-1H-idole-2-one were measured in the range of 4000–400 cm⁻¹ and 3500–0 cm⁻¹ ranges, respectively. Using the 6-31G and 6-311G basis sets, the density functional theory was used to optimize the geometry, frequency, and vibrational bands of the title molecule. Optimized geometric parameters such as bond length and bond angles were computed. The scaled values were compared to experimental FTIR and FT-Raman spectra. The HOMO-LUMO and MEP surface investigation, along with their essential chemical parameters reveal the reactivity of electrophilic, nucleophilic and electrical properties of the compound. The natural bond orbital method was used to study the molecular stability and bond strength. Topology studies were conducted to identify critical points in the molecule. Molecular docking analysis was used to assess its activity against COVID-19, HIV, insulin, and anti-inflammatory proteins. Among these, the highest binding affinity was observed against the HIV target protein 2m8n with a docking score of 10.83 kcal/mol.

CHAPTER - 8

Spectroscopic investigation (FT-IR, FT-Raman), vibrational assignments, topology evaluation and molecular docking study of 5-Chloro-1-(4-chlorobenzyl)-3-[2-(3-(4-chlorophenyl)-5-[4-(propan-2-yl) phenyl]-4,5-dihydro-1H-pyrazol-1-yl) -4-oxo- 4,5-dihydro-1,3-thiazol-5(4H)-ylidene]-2,3-dihydro-1H-indol-2-one

8.1 Introduction

Thiazole and its derivatives are widely used in the manufacturing of synthetic drugs, fungicides and dyes. The derivatives of thiazole like phenylthiazolyl, iso-thiazole are found to have a potent local anaesthetic, anti-inflammatory, analgesic and antipyretic activities [226-228]. Thiazoles are one of the most intensively investigated classes of aromatic five-membered heterocyclic and containing three carbons, one sulphur, and one nitrogen atom. Thiazole and its derivatives are also very useful compounds in different fields of chemistry including medicine and agriculture [229]. It has an important component effect of the pharmacophores of a large number of medicinal significance molecules and the evaluation of their biological activity, such as antibacterial, antiprotozoal, antitubercular, antifungal, and anthelmintic, with emphasis on their potential medicinal applications [230].

To the best of our knowledge, the literature survey implies that no study has been made on this molecule. From the above-enlightened findings, we were motivated to study spectroscopic properties and use the computational molecular modelling techniques to correlate the observed results. In the present work, structural and biological properties of the compound 5-Chloro-1-(4-chlorobenzyl)-3-[2-(3-(4-chlorophenyl)-5-[4-(propan-2-yl) phenyl]-4,5-dihydro-1H-pyrazol-1-yl) -4-oxo- 4,5-dihydro-1,3-thiazol-5(4H)-ylidene]-2,3-dihydro-1H-indole-2-one (5CPPTI) were investigated. The FT-IR and FT-Raman spectra of the (5CPPTI) were reported both experimentally and theoretically. The study of frontier

molecular orbitals (HOMO-LUMO) has been used to represent how the charge transfer takes place in the molecule. Global reactivity descriptors also computed. Molecular electrostatic potential (MEP) has been inspected to understand the correlation between molecular structure and biological activity.

The natural bond orbital method was used to study the molecular stability and bond strength. Topological studies were investigated to identify critical points in the molecule.

8.2 Experimental details

The structure of CPTBN along with the synthesis procedure was screened by Salian et al. [87]. In the present work, technical studies were carried out as follows:

- Fourier transform infrared spectrum was recorded between 4000-400 cm⁻¹ using the
 Perkin Elmer spectrometer, which was calibrated using an MCT (Mercury-Cadmium-Telluride) detector with KBr (potassium bromide) pellet technique.
- FT-Raman spectrum was obtained within the interval of 3500-0 cm⁻¹ using a Bruker RFS27V the 1064 nm line of a Nd: YAG laser device for excitation controlled at 200 mWpower. At room temperature, the spectrum was recorded at a scanning speed of 10cm^{-1} and a spectral resolution of 1.0 cm^{-1} .

8.3 Computational details

The molecular structure of the title compound carried out using the Gaussian 09 program [20]. The electronic structure of the molecule has to prove with the density functional theory. The Gaussian 09 program performed with Becke's three-parameter hybrid model and the Lee-Yang-Parr correlation was a useful functional (B3LYP) in DFT technique. The potential energy distributions predicted by VEDA program. The visual representations for fundamental modes are also checked by the GaussView program [31]. The Lamarckian genetic algorithm [62] applied to search for protein-ligand interactions, for

visualization performed using PyMol [63]. The molecular docking performed by the AutoDock 4.0.1 software [57], which was also applied to detect the docking input files and analyze the docking result.

8.4. Results and discussion

8.4.1. Molecular geometry

The optimized molecular structure of 5-Chloro-1-(4-chlorobenzyl)-3-[2-(3-(4-chlorophenyl)-5-[4-(propan-2-yl) phenyl]-4,5-dihydro-1H-pyrazol-1-yl) -4-oxo- 4,5-dihydro-1,3-thiazol-5(4H)-ylidene]-2,3-dihydro-1H-indole-2-one (5CPPTI) with atom numbering is shown in Fig. 8.1. By allowing all parameters to be unperturbed, the equations converge to maximise geometries that conform to the true energy minimum, as seen by the absence of imaginary frequencies in the estimation of the vibration mode. Both the DFT (B3LYP/6-31G) and (B3LYP/6-311G) methods are used to measure the most optimised bond lengths and bond angles of this compound, as set out in Tables 8.1 and 8.2. In the case of B3LYP measurement about DFT computation, the aromatic C-C bond lengths of the title compound are observed to have higher values.

8.4.2 Vibrational analysis

The title compound consists of 73 atoms, which has 213 normal modes. This compound belongs to C1 point group symmetry. The computed vibrational wavenumbers and the atomic displacements corresponding to the different normal modes are used for identifying the vibrational modes unambiguously. The calculated vibrational wavenumbers, measured infrared and Raman band positions and their assignments are given in Table 8.3. The observed (FT-IR and FT-Raman) and simulated spectra are shown in Figs. 8.2 and 8.3, respectivly

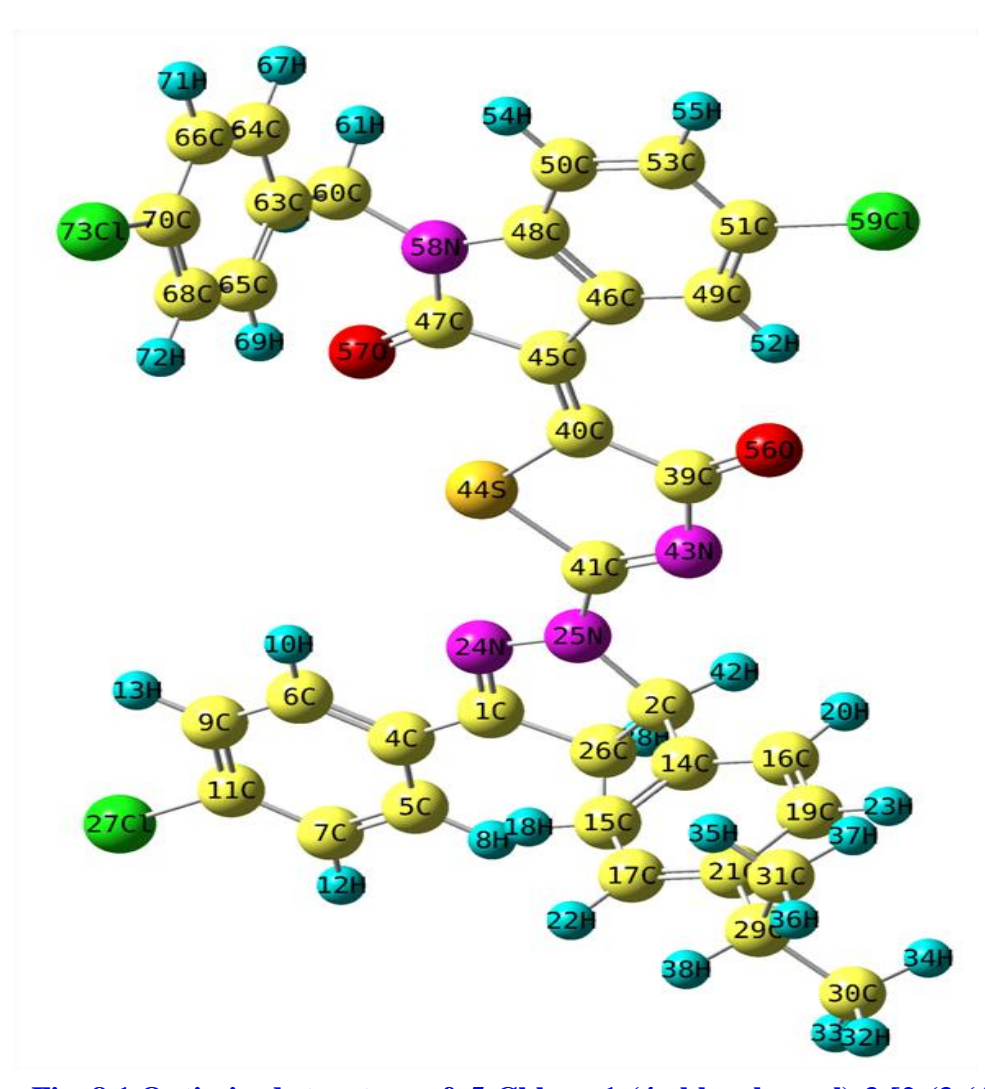


Fig. 8.1 Optimized structure of 5-Chloro-1-(4-chlorobenzyl)-3-[2-(3-(4-chlorophenyl)-5-[4-(propan-2-yl) phenyl]-4,5-dihydro-1H-pyrazol-1-yl) -4-oxo-4,5-dihydro-1,3-thiazol-5(4H)-ylidene]-2,3-dihydro-1H-indole-2-one (5CPPTI)using B3LYP/6-311G basis set

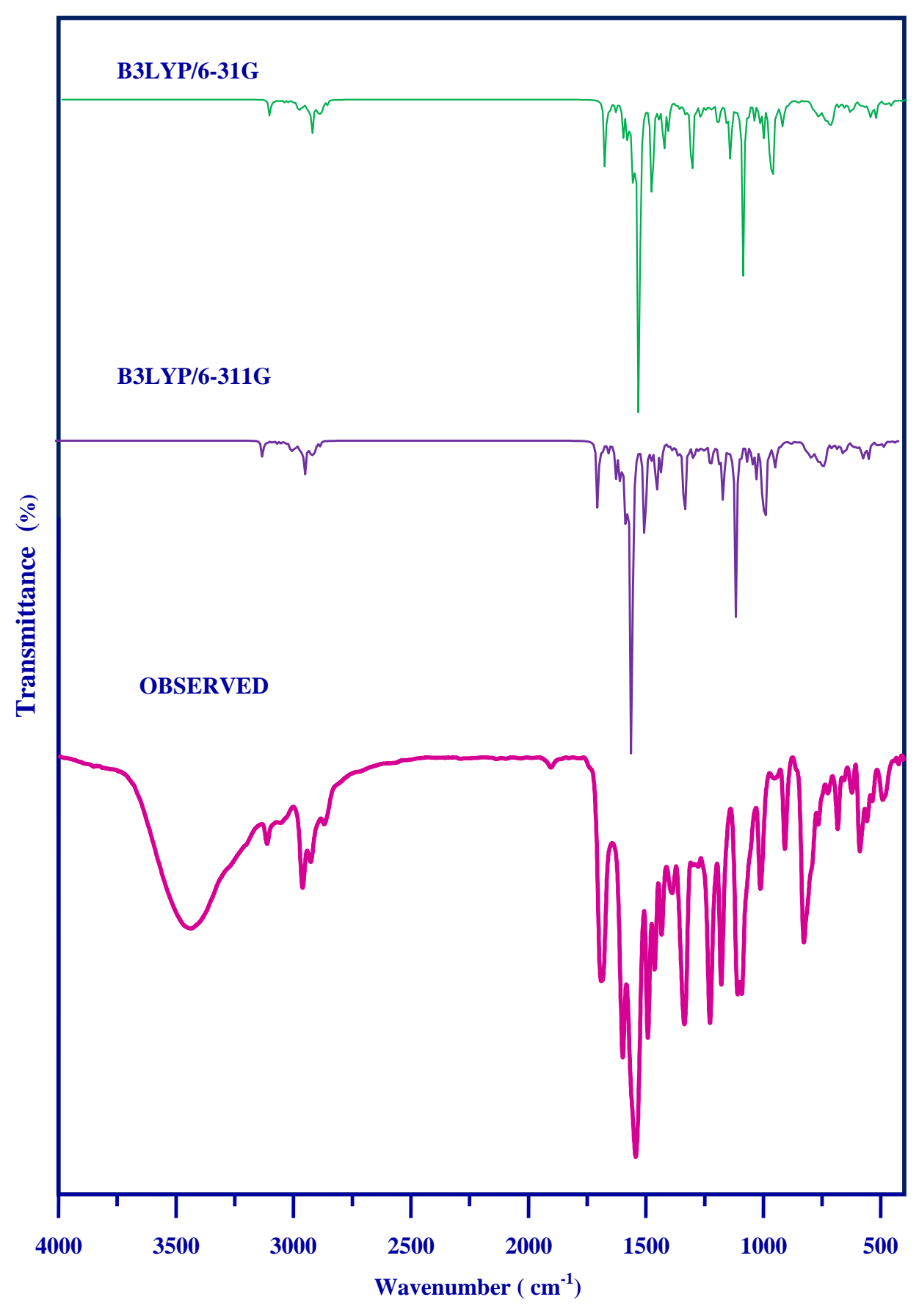


Fig. 8.2. Observed FT-IR and simulated spectra of 5CPPTI

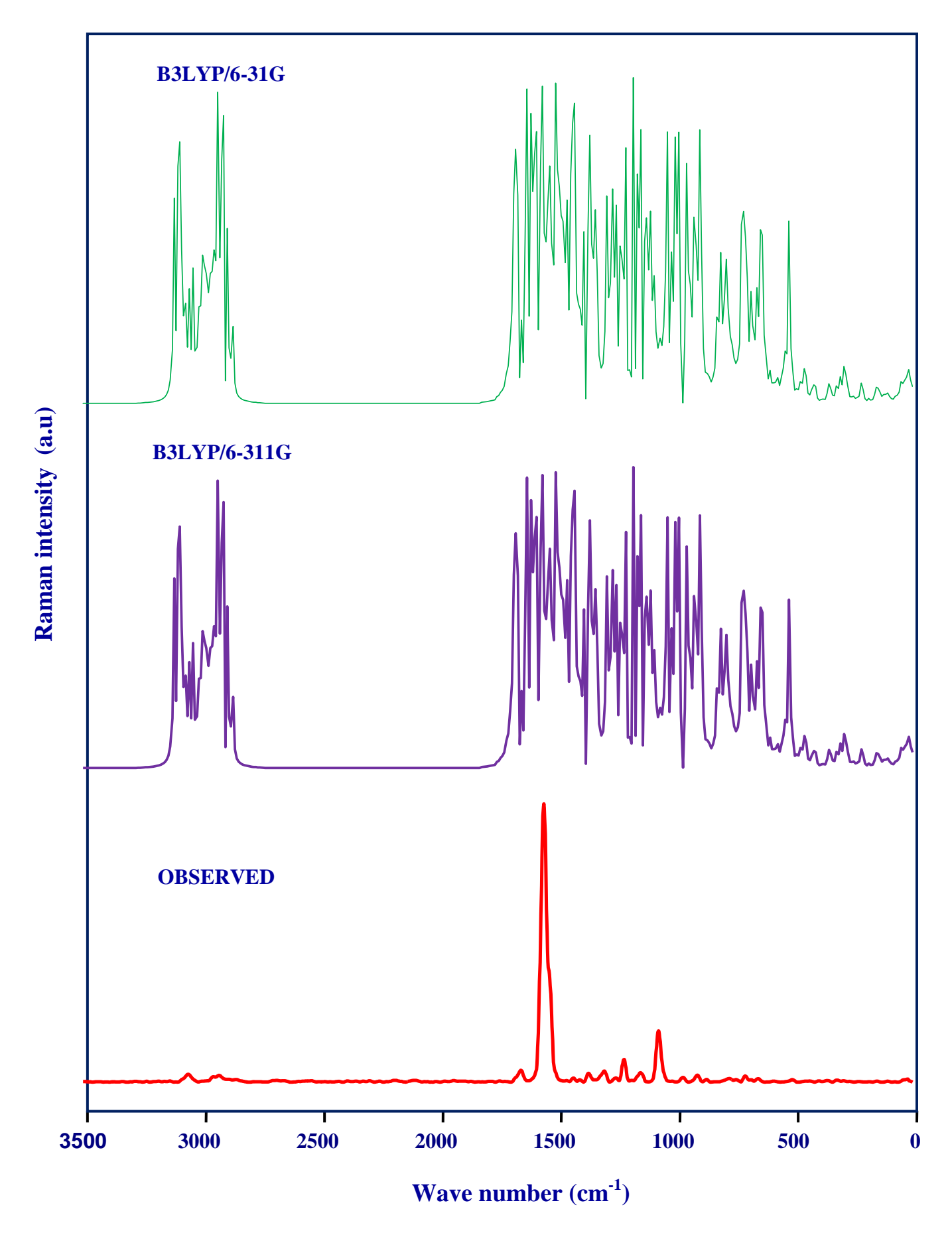


Fig.8.3 Observed FT-Ramanand simulated spectra of 5CPPTI

CH₃ vibrations

For the assignments of CH₃ group frequencies, nine fundamentals can be associated to each CH₃ group namely, CH₃ symmetrical stretch, CH₃ in-plane stretch (i.e., in-plane hydrogen stretching modes), CH₃ in-plane bending (i.e., hydrogen deformation modes), CH₃ symmetrical bending, CH₃ in-plane rocking, CH₃ out-of-plane rocking and CH₃ twisting. In addition to that, CH₃ out-of-plane stretch and CH₃ out-of-plane bending modes of the CH₃ group would be expected to be depolarized for a symmetry species. The C–H stretching in CH₃ occurs at lower frequencies than those of aromatic ring (2925–3000 cm⁻¹). The vibrations of methyl group are observed in the typical range reported earlier [231- 234]. The CH₃ symmetric stretching frequencies are established at 2965, 2960 and 2953 cm⁻¹ whereas CH₃ asymmetric frequencies are assigned at 2936 and 2903 cm⁻¹ in FT Raman and 2982 cm⁻¹ in FT-IR spectrum. The asymmetric deformation of CH₃ group is usually observed at around 1450 cm⁻¹ for methyl substituted aromatic rings [235-237].

In this study, the observed FT-IR band at 2925 cm⁻¹ is assigned as CH₃ asymmetric stretching mode and corresponding calculated wavenumbers are 2958, 2952, 2945, 2937, 2932, 2902, 2892 cm⁻¹ (6-31G) and 2952, 2947, 2940, 2930, 2927, 2897, 2888 (6-311G) . The CH₃ in-plane bending vibrations are appeared at 1458 cm⁻¹in FT-IR and 1463 cm⁻¹ in FT-Raman. The computed wavenumbers are δ_{opb} = 1510, 1499 cm⁻¹, δ_{ipb} = 1505, 1492 cm⁻¹, δ_{sb} = 1413, 1376 cm⁻¹ predicted by B3LYP/ 6-31G basis setand δ_{opb} = 1505, 1492 cm⁻¹, δ_{ipb} = 1466, 1460 cm⁻¹, δ_{Sb} = 1407, 1370 cm⁻¹ predicted by B3LYP/ 6-311G basis set. The band observed at 1007 cm⁻¹ in FT-Raman the corresponding theoretical value bound at 1009, 989 cm⁻¹ in B3LYP/6-31G and in 1004, 985 cm⁻¹ B3LYP/6-311G are assigned as a CH₃ out-of-plane bending vibration of the title compound.

C-H vibrations

Aromatic compounds commonly exhibit multiple weak C-H stretching bands in the region 3100-3000 cm⁻¹ [238]. Accordingly, in the present study the C-H stretching

vibrations of the title compound is computed at 3119, 3114, 3107, 3099, 3092, 3075, 3069, 3055, 3040, 3019, 3011, 3003, 2996, 2986, 2979, 2970, 2873 cm⁻¹ [6-31G] and 3115, 3109, 3103, 3095, 3088, 3072, 3065, 3051, 3034, 3015, 3006, 2995, 2988, 2982, 2975, 2967, 2869 cm⁻¹ [6-311G].

The bands due to C-H in-plane and out-of plane bending vibration interacting somewhat with C-C stretching vibration are observed as a number of medium weak intensity sharp bands in the region 1300-1000 cm⁻¹ and 1000-750 cm⁻¹ [238]. In title compound, the C-H in-plane bending vibrations are attributed at 1423, 1381, 1337, 1277, 1108 cm⁻¹ in FT-IR spectrum and 1432, 1399, 1334, 1287, 1252, 1109 cm⁻¹ in FT-Raman spectrum. The corresponding wavenumber are theoretically predicted in the range 915-567 cm⁻¹ (6-31G) and 911-561 cm⁻¹ (6-311G).

C-C vibrations

The ring carbon-carbon (C-C) stretching vibrations usually occur in the region 1625–1400 cm⁻¹ [239]. The C-C stretching vibrations at 1659 cm⁻¹ in FT-IR, 1616, 1577, 1470, 1376 cm⁻¹ in FT-Raman spectrum were assigned by Amul et al. [240]. In this study, carbon-carbon stretching vibrations are assigned at 1593, 1222, 1172 cm⁻¹ in FT-IR spectrum. Prabhu et al. [241] observed that the C-C in-plane deformation vibrations were assigned at 670, 630, 620, 570, 500 and 490 cm⁻¹. In this study, the computed values by B3LYP/6-31G and 6-311Gare well agree with reported values.

C=O vibrations

All carbonyl compounds have a very intense and narrow peak in the range of 1800-1600 cm⁻¹ [242]. The multiple bonded groups are highly polar and therefore give rise to an intense infrared absorption band in the region 1700-1800 cm⁻¹. The carbon-oxygen double bond is formed by π - π bonding between carbon and oxygen. Because of the different electro negativities of the carbon and oxygen atoms, the bonding electrons are not equally

distributed between the atoms [243]. In the present study, the C=O stretching vibration is observed at 1682 cm⁻¹ as a strong band in FT-IR, and the computed wavenumbers at 1687 and 1682 cm⁻¹ with PED contributions of 68% and 70%. Both the experimentally observed FT-IR and FT-Raman bands show excellent agreement with theoretical values.

8.4.3 Frontier molecular orbitals

The frontier orbital gap helps to characterize the chemical reactivity and the kinetic stability of the molecule. The HOMO (Highest Occupied Molecular Orbital) which can be consider as the outer orbital containing electrons tends to give these electrons as an electron donor and hence the ionization potential is directly related to the energy of the HOMO. On the other hand, LUMO (Lowest Unoccupied Molecular Orbital) can accept electrons and the LUMO energy is directly related to electron affinity. The calculated energy values of HOMO = 6.3158 eV and LUMO = 3.1891 eV and the energy gapvalue ΔE is 3.1267 eV. The energy gap explains which influences the biological activity of the molecule which are given in Fig. 8.4.

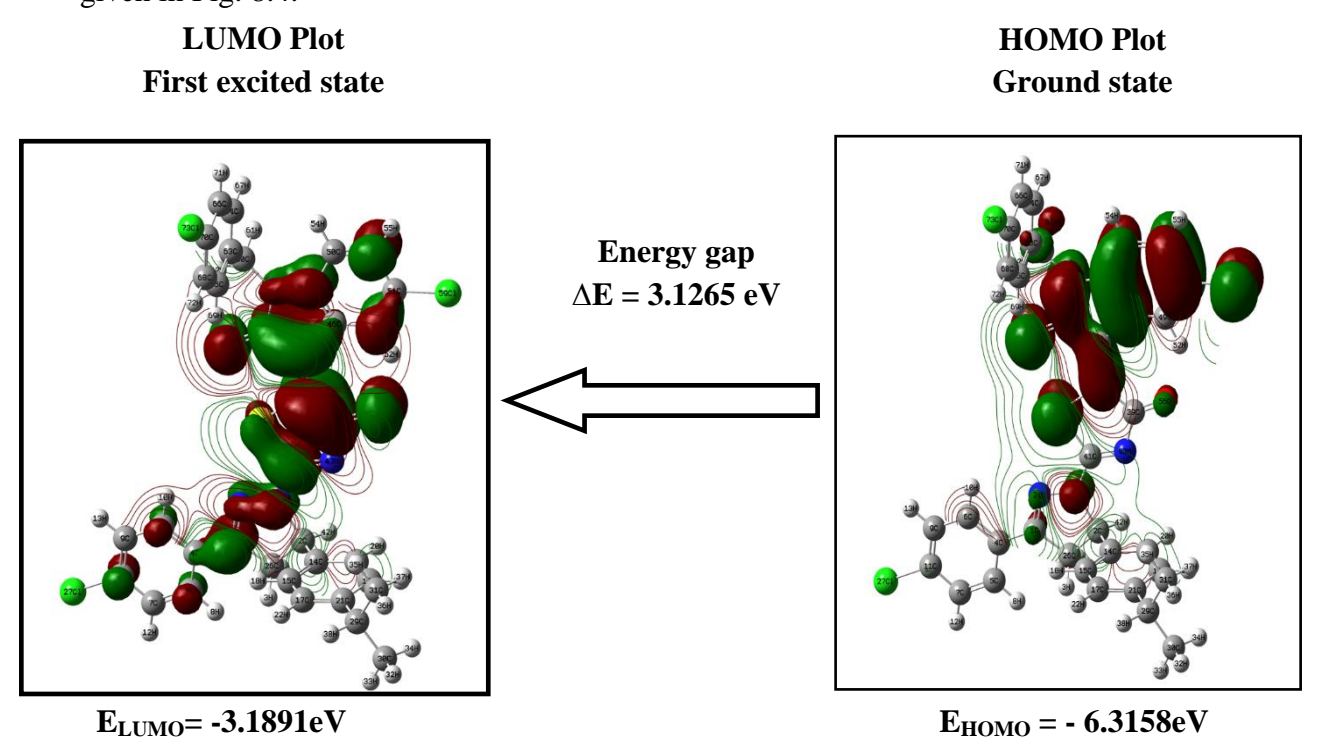


Fig. 8.4 HOMO - LUMO energy gap plots of 5CPPTI

The chemical potential, global hardness and electrophilicity [244] will pave the way to understand the structure and reactivity of the molecule, with the aid of DFT based descriptors.

Parr et al. [14] proposed the global electrophilicity power of a ligand as $\omega = \mu^2/2\eta$. This index measures the stabilization in energy when the system acquired an additional electronic charge from the environment. Electrophilicity encompasses both the ability of an electrophile to acquire additional electronic charge and the resistance of the system to exchange electronic charge with the environment. The Table 8.4, it contains information about both electron transfer (chemical potential) and stability (hardness) and is a better descriptor of global chemical reactivity.

8.4.4 Molecular electrostatic potential (MEP)

Molecular electrostatic Potentialis is a very useful descriptor to understandthe electrophilic and nucleophilic reaction sites [245]. Different colours represent the different values of the electrostatic potential at the surface; red represents the regions with the most electrostatic potential, blue represents the regions with the most positive electrostatic potential. MEP plays an important role in the interaction between drug-receptor and enzyme substrate, which predicts the recognition of one molecule by another. According to the MEP map study of the title molecule, oxygen and nitrogen atoms (red coded region) are found in the negative regions which are shown in Fig. 8.5.

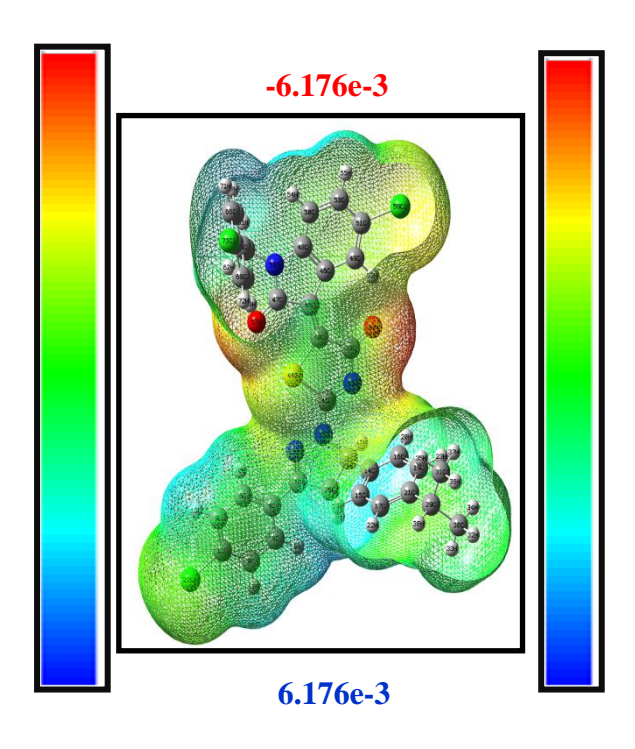


Fig. 8.5 Molecularelectrostatic potential (MEP) surface of 5CPPTI

8.4.5 NCI surface analysis

The real space weak interaction, supported on electron density and derivatives is approached by RDG analysis and it is improved by Johnson et al. [52]. It is a dimensionless extent and the first gradient found in the literature. The leading intention of this portion is to study the non-covalent interactions between the dissimilar entities and to appraise their consequence in the steadiness of the crystal formation. The graphical visualization of non-covalent interactions locations is succeeding by NCI-RDG analysis. It is examined as a resolve and helpful technique of characterizing repellent steric interaction van der Waals interactions and hydrogen bonds using a simple colour code. The quality of the strength of the interaction can be investigated through RDG surface analysis. Red, green and blue colour codes are used to describe destabilizing steric interactions, van der Waals and stabilizing hydrogen bonding respectively.

$$RDG(r) = \frac{1}{2(3\pi r^2)^{1/2}} \frac{|\nabla \rho(r)|}{\rho(r)^{4/3}}$$
(8.1)

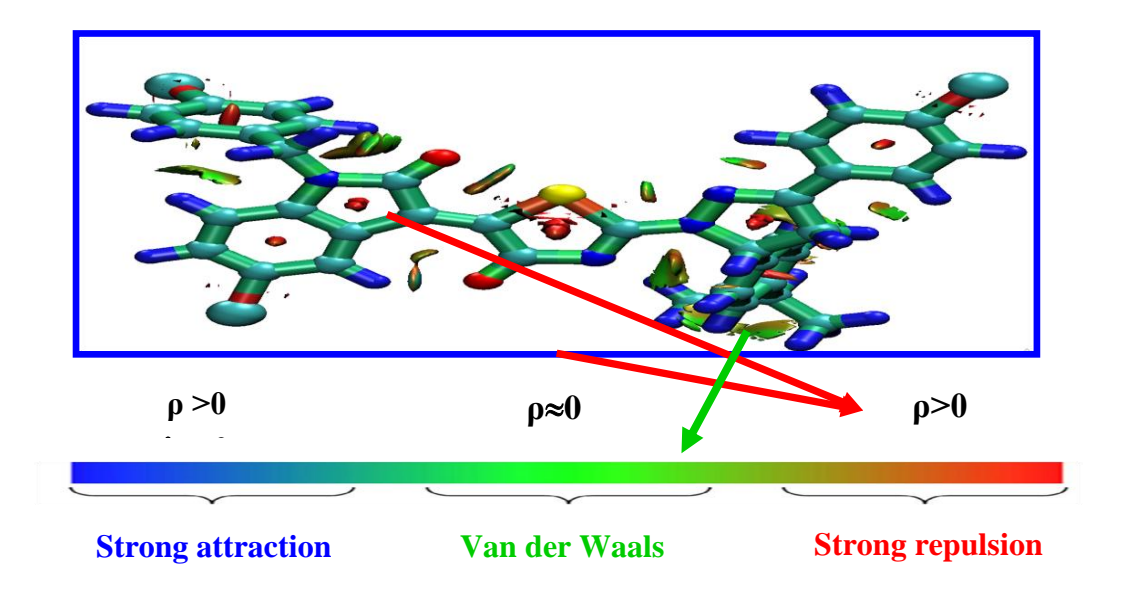


Fig. 8.6 RDG 3D colour scaling of non-covalent interaction in 5CPPTI

The plot of v(r) against 12 sign will help to comprehend the quality and strength of the interaction. The sign of 12, the second greatest value of the Hessian matrix of electron density, is used to find the nature of an interaction. If 12 > 0, for non bonded and if 12 < 0 for bonded. The RDGisosurface of the title compound was drawn with isosurface value 0.5 as illustrated in Fig. 8.6. The software and it was plotted by Multiwfn and VMD program [118]. The red colour in scale in the figure depicts a forcible repulsion that seems in all centralized of the ring system. While a strong van der Waals interaction took place between the amide group and one of the propane phenyl as well as one hydrogen atom in the chloro substituted phenyl ring.

8.4.6 ELF and LOL analysis

The ELF (electron localization function) and LOL (localized orbital locator) maps were topology analysis performed based on the covalent bonds. These maps reveal the regions where the probability of finding an electron pair is high [246]. ELF and LOL share a similar interpretation depending on the kinetic energy density [247]. Colour shade maps of the ELF and LOL for the title molecule were presented in Figs. 8.7 and 8.8, respectively. The electron localization function is the estimation of electron localization in atomic and

molecule system. Pauli repulsion existing among two like—spin electrons was used as a measure of electron localization. Region with strongest Pauli repulsion corresponds to highly localized electrons. ELF studies give description of the bonding, reactivity and chemical structure [248]. The upper limit for ELF is 0.8 and the lower limit is 0. Two dimensional graphical data employing colourgradiation is used to characterize the ELF values for the title compound. Red colour corresponds to high values of ELF while blue represents the region with low end of ELF value. For the title compound the maximum Pauli repulsion was around hydrogen with single electron depicted by the red region.

The regions with chlorine nitrogen having similar spin electrons close together where depicted by the blue region, whereas electron depletion regions (blue region) are identified at Nitrogen and oxygen atom. ELF and LOL analysis provides the description of the chemical structure, molecular bonding and reactivity with extensive prominence on their use for the quantitative analysis of aromaticity.

8.4.7 NBO analysis

In quantum chemistry, a natural bond orbital (NBO) is a computed bonding orbital with maximum electron density. Natural bond orbital are used in computational chemistry to calculate bonds, bond order, donor-acceptor interactions and the distribution of electron density between atoms. The NBO also analysis the bonding in terms of the natural hybrid orbital. NBO calculations of the title compound were completed utilizing NBO 3.1 program [90] and the summary of important results are accounted in Table 8.5. The greater the E(2) value, the more grounded is the association between e⁻ contributors and e⁻acceptors and uncovers an all the more giving inclination from electron donors to electron acceptors and a more prominent level of conjugation of the entire framework.

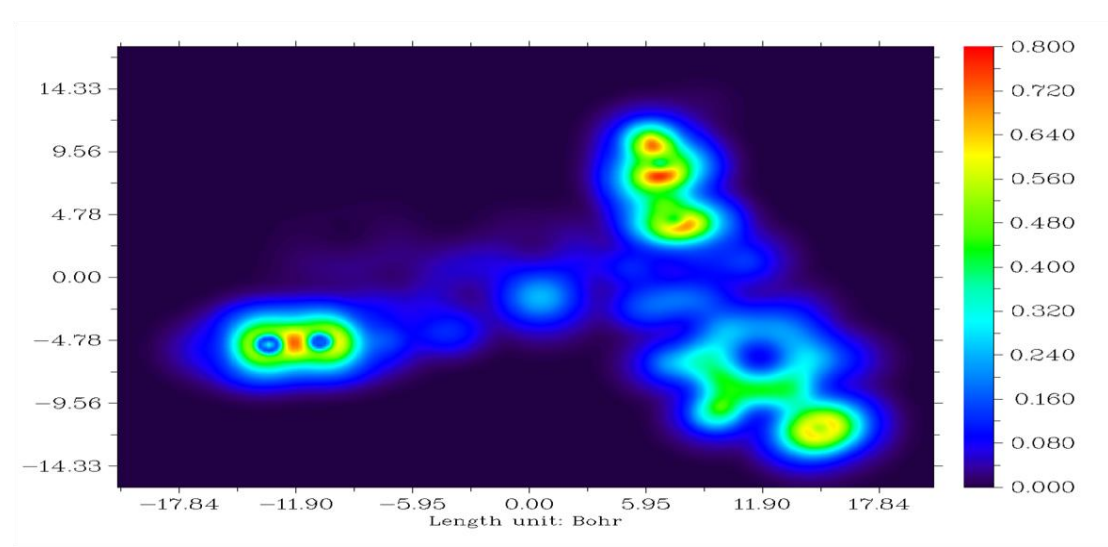


Fig. 8.7 localized orbital locator (LOL) for 5CPPTI obtained in xy plane

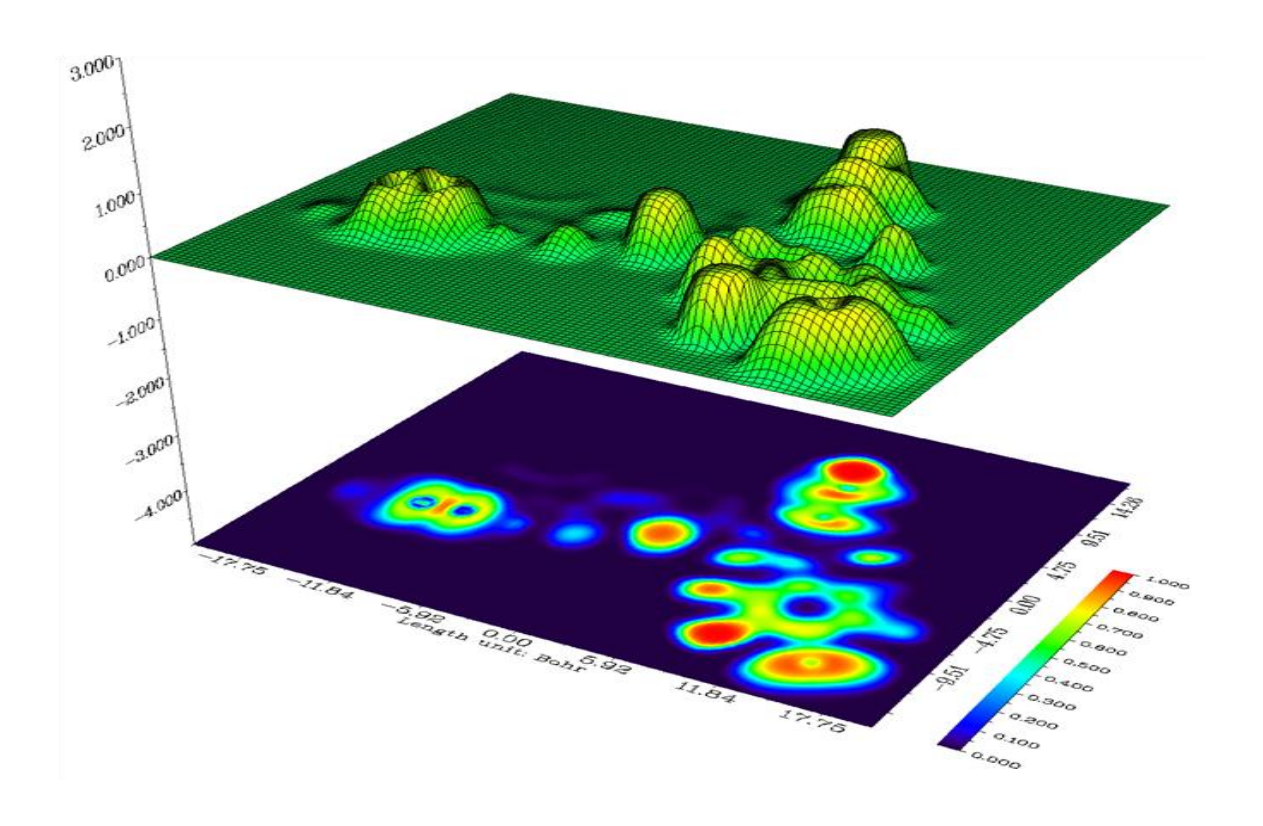


Fig. 8.8 Electron localization function (ELF) or shaded surface map with projection effect of 5CPPTI

8.4.8 Molecular docking study

The protein-drug interaction was studied by automated docking to determine the orientation of inhibitors bound to the active site of target protein. A genetic algorithm method, implemented in the program Autodock 4.2 was employed [62]. The 2D structures (.mol) of the 5CPPTI are converted to 3D structure (.pdb). The protein structure file was downloaded from the protein data bank [59]. For docking calculations, Gasteinger partial charges were assigned to the inhibitors and non-polar hydrogen atoms were assigned to the inhibitors. All torsions were allowed to rotate during docking. The grid map was centered at the residues of the protein. The number of docking run was 50, the population in the genetic algorithm was 250, and the number of energy evaluation was 1000. The docking results for inhibitors against protein, showed minimum docking energy, inhibition constant, with RMSD as noted. The molecular docking of the protein with 5CPPTI yielded best possible conformations with parameters including the docking energy, binding energy, intermolecular energy, inhibition constant and RMSD (Table 8.6). Molecular docking studies were performed using Auto dock tool software. The target protein from antiviral activity drugs against a) covid-19 (6xm4) b) HIV (2m8n) c) Anti-inflammatory (6hgf) and d) Insulin (3tuv) was downloaded from Protein Data Bank and the active sites were chosen.

Fig 8.9 shows the active site of three dimensional structure of a target receptor molecule protein. Among the all active sites, the pocket found to be best active contains 58 amino acids. The minimum docking energy was found in the protein 6xm4–ligand is 8.95 kcal/mol, RMSD (root mean square deviation) is 305.24 Å, and estimated inhibition constant is 277.03 nM. The minimum docking energy was found in the 2m8n–ligand is 10.83 kcal/mol and RMSD (root mean square deviation) 14.866 Å, and estimated inhibition constant is 11.50 nM. The minimum docking energy was found in the 6hgf–ligand is 9.41 kcal/mol and RMSD (root mean square deviation) is 15.494 Å, and estimated inhibition

constant is 127.45 nM. The minimum docking energy was found in the 3tuv–ligand is 3.73 kcal/mol and RMSD (root mean square deviation) is 33.31 Å, and estimated inhibition constant is 1.84 mM.

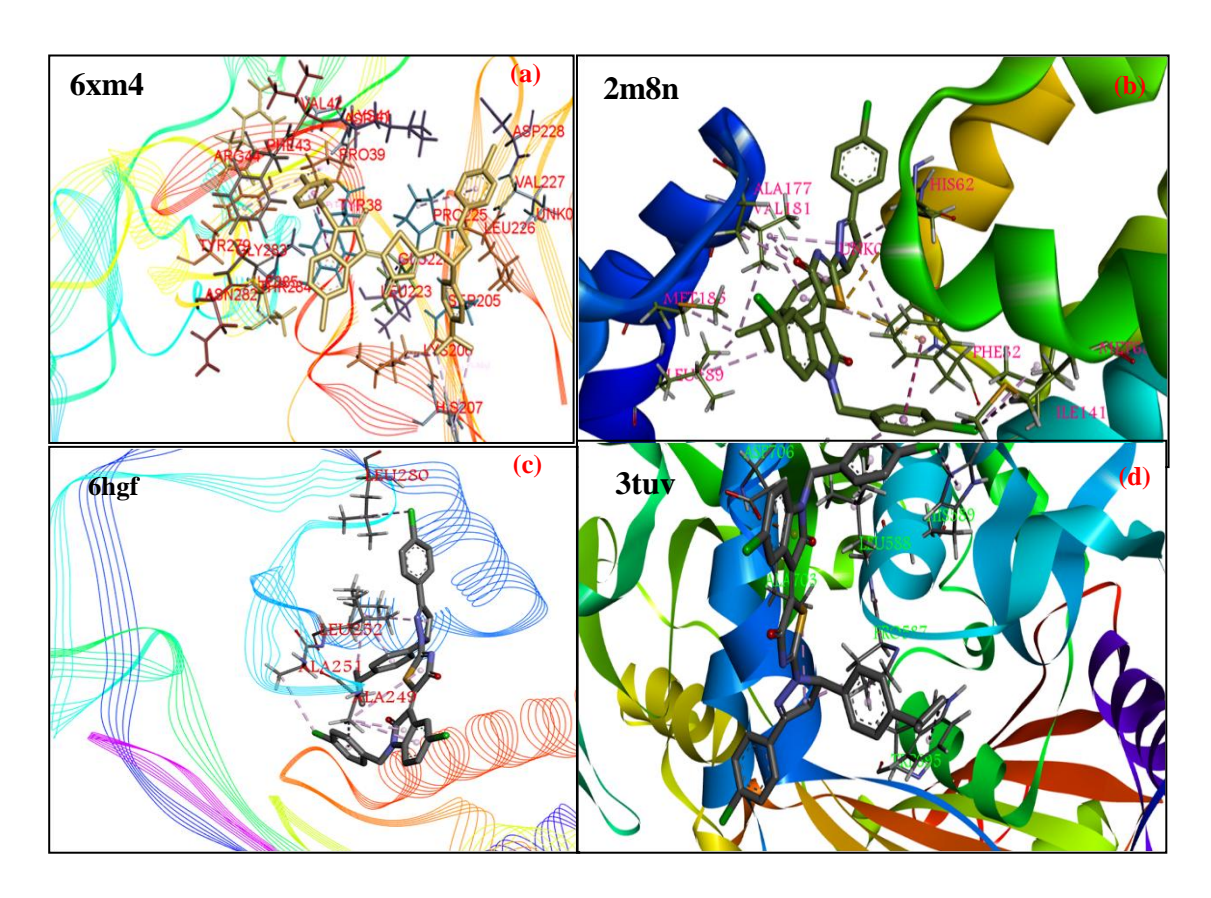


Fig .8.9 a) covid-19 (6xm4) b) HIV (2m8n) c) Anti-inflammatory (6hgf) d) Insulysin (3tuv)

8.5 Conclusion

In the present study, an elaborate vibrational spectral analysis and quantum chemical calculation of 5-Chloro-1-(4-chlorobenzyl)-3-[2-(3-(4-chlorophenyl) -5-[4-(propan-2-yl) phenyl]-4,5-dihydro-1H-pyrazol-1-yl) -4-oxo- 4,5-dihydro-1,3-thiazol-5(4H)-ylidene]-2,3-dihydro-1H-indole-2-one (5CPPTI) was discussed. The geometrical parameters hold from DFT was in line with the experimental data. The vibrational analysis and PED were calculated to assure the presence of a variable functional block. MEP predicts that the most reactive part in the molecule and intermolecular interaction. The natural bond orbital

analysis transacts in this study gives information about the molecular species which are equitable for more chemical stability. The value of HOMO–LUMO energy gap depicts the presence of biological activity of the title derivative. The molecular docking results refer to the inhibitory activity against COVID-19 (6xm4), HIV (2m8n), Insulin (3tuv) and Anti-inflammatory (6hgf) protein.

Table 8.1: Optimized structural parameters (bond length) of 5CPPTI calculated by DFT/B3LYP method with 6-31G and 6-311G basis sets

Bond Length (Å)	6-31G	6-311G	Bond Length (Å)	6-31G	6-311G
C1-C4	1.460	1.461	C31-H36	1.097	1.092
C1-C24	1.306	1.305	C31-H37	1.097	1.092
C1-C26	1.522	1.520	C39-C40	1.511	1.510
C2-C14	1.518	1.518	C39-N43	1.395	1.395
C2-N25	1.511	1.509	C39-O56	1.245	1.242
C 2-C26	1.556	1.554	C40-S44	1.840	1.844
C2-H42	1.092	1.088	C40-C45	1.360	1.357
H 3-C26	1.093	1.089	C41-N43	1.308	1.306
C4-C5	1.408	1.407	C41-S44	1.861	1.866
C4-C6	1.412	1.410	C45-C46	1.472	1.471
C5-C7	1.398	1.396	C45-C47	1.504	1.502
С5-Н8	1.084	1.081	C46-C48	1.424	1.422
C6-C9	1.393	1.391	C46-C49	1.401	1.399
C6-H10	1.084	1.080	C47-O57	1.251	1.249
C7-C11	1.392	1.389	C47-N58	1.386	1.384
C7-H12	1.083	1.079	C48-C50	1.389	1.387
C9-C11	1.396	1.393	C48-N58	1.409	1.410
C9-H13	1.083	1.079	C49-C51	1.395	1.393
C11-Cl27	1.822	1.825	C49-H52	1.080	1.076
C14-C15	1.404	1.402	C50-C53	1.404	1.402
C14-C16	1.403	1.400	C50-H54	1.083	1.079
C15-C17	1.397	1.395	C51-C53	1.393	1.389
C 15-H18	1.087	1.083	C51-C159	1.829	1.833
C16-C19	1.396	1.394	C53-H55	1.083	1.079
C16-H20	1.085	1.081	N58-C60	1.465	1.464
C17-C21	1.405	1.403	C60-H61	1.095	1.092
C17-H22	1.086	1.083	C60-H62	1.095	1.091
C19-C21	1.406	1.404	C60-C63	1.520	1.520
C19-H23	1.086	1.082	C63-C64	1.402	1.400
C21-C29	1.526	1.525	C63-C65	1.406	1.403
N24-N25	1.396	1.398	C64-C66	1.401	1.399
N25-C41	1.341	1.340	C64-H67	1.087	1.083

C26	5-H28	1.097	1.092	C65-C68	1.398	1.395
C29	9-C30	1.546	1.545	C65-H69	1.086	1.082
C29	9-C31	1.546	1.545	C66-C70	1.391	1.388
C29	9-Н38	1.100	1.095	C66-H71	1.083	1.079
C30)-Н32	1.096	1.092	C68-C70	1.395	1.391
C30)-Н33	1.096	1.091	C68-H72	1.083	1.079
C30)-Н34	1.097	1.092	C70-C173	1.827	1.830
C31	-H35	1.095	1.091			

Table 8.2: Optimized structural parameters (bond angle) of 5CPPTI calculated by DFT/B3LYP method with 6-31G and 6-311G basis sets

Bond angle			Bond angle		
(degree)	6-31G	6-311G	(degree)	6-31G	6-311G
C4 -C1 -N24	121.61	121.49	C29 -C31 -H36	110.45	110.44
C 4 -C1 -C26	125.16	125.29	C29 -C31 -H37	111.15	111.23
N24 -C1 -C26	113.22	113.21	H35 -C31 -H36	108.31	108.24
C14 -C2 -N25	112.25	112.14	H35 -C31 -H37	107.82	107.83
C14 -C2 -C26	115.35	115.44	H36 -C31 -H37	107.82	107.83
C14 -C2 -H42	109.35	109.27	C40 -C39 -N43	113.58	113.59
N25 -C2 -C26	100.11	100.14	C40 -C39 -O56	123.40	123.34
N25 C-2 -H42	107.10	107.20	N43 -C39 -O56	123.02	123.07
C26 -C2 -H42	112.15	112.13	C39 -C40 -S44	109.79	109.82
C1 -C4 -C5	120.60	120.65	C39 -C40 -C45	128.13	128.17
C1 -C4 -C6	120.55	120.62	S44 -C40 -C45	122.08	122.01
C5 -C4 -C6	118.85	118.73	N25 -C41 -N43	122.95	122.92
C4 -C5 -C7	120.84	120.90	N25 -C41 -S44	119.15	119.34
C4 -C5 -H8	120.29	120.38	N43 -C41 -S44	117.89	117.74
C7 -C5 -H8	118.87	118.72	C39 -N43 -C41	113.02	113.25
C4 -C6 -C9	120.69	120.74	C40 -S44 -C41	85.72	85.60
C4 -C6 -10	119.13	119.17	C40 -C45 -C46	134.52	134.43

C9 -C6 -10	120.17	120.09	C40 -C45 -C47	119.99	120.13
C5 -C7 -C11	118.79	118.73	C46 -C45 -C47	105.50	105.44
C5 -C7 -H12	120.75	120.74	C45 -C46 -C48	107.06	107.12
C11 -C7 -H12	120.46	120.53	C45 -C46 -C49	133.87	133.88
C6 -C9 -C11	118.96	118.93	C48 -C46 -C49	119.06	119.00
C6 -C9 -H13	120.69	120.68	C45 -C47 -O57	127.49	127.38
C11 -C9 -H13	120.35	120.39	C45 -C47 -N58	107.53	107.61
C7 -C11 -C9	121.86	121.97	O57 -C47 -N58	124.98	125.00
C7 -C11 -C127	119.07	119.05	C46 -C48 -C50	122.28	122.30
C9 -C11 -C127	119.06	118.98	C46 -C48 -N58	109.66	109.64
C2 -C14 -C15	121.55	121.53	C50 -C48 -N58	128.06	128.07
C2 -C14 -C16	119.81	119.92	C46 -C49 -C51	117.88	117.86
C15 -C14 -C16	118.64	118.54	C46 -C49 - H52	120.27	120.24
C14 -C15 -C17	120.48	120.53	C51 -C49 - H52	121.85	121.90
C14 -C15 -H18	120.34	120.40	C48 -C50 -C53	118.16	118.20
C17 -C15 -H18	119.18	119.07	C48 -C50 -H54	121.62	121.65
C14 -C16 -C19	120.67	120.72	C53 -C50 -H54	120.21	120.14
C14 -C16 -H20	119.44	119.46	C49 -C51 -C53	123.12	123.26
C19 -C16 -H20	119.87	119.80	C49 -C51 -C159	118.47	118.33
C15 -C17 -C21	121.22	121.26	C53 -C51 -Cl59	118.42	118.41
C15 -C17 -H22	119.46	119.43	C50 -C53 -C51	119.50	119.39
C21 -C17 -H22	119.31	119.31	C50 -C53 -H55	120.26	120.27
C16 -C19 -C21	121.08	121.12	C51 -C53 -H55	120.24	120.34
C16 -C19 -H23	119.01	118.94	C47 -N58 -C48	110.25	110.19
C21 -C19 -H23	119.90	119.94	C47 -N58 -C60	122.95	123.03
C17 -C21 -C19	117.91	117.82	C48 -N58 -C60	126.80	126.76
C17 -C21 -C29	120.68	120.72	N58 -C60 -H61	108.58	108.80

C19 -C21 -C29	121.41	121.46	N58 -C60 -H62	105.48	105.51
C1 -N24 -N25	108.55	108.55	N58 -C60 -C63	114.03	114.07
C2 -N25 -N24	113.40	113.26	H61 -C60 -H62	107.91	107.71
C2 -N25 -C41	125.16	125.14	H61 -C60 -C63	110.36	110.29
N24 -N25 -C41	121.39	121.54	H62 -C60 -C63	110.20	110.18
C1 -C26 -C2	103.67	103.72	C60 -C63 -C64	120.81	120.75
C1 -C26 -H3	112.34	112.39	C60 -C63 -C65	120.20	120.37
C1 -C26 -H28	110.41	110.42	C64 -C63 -C65	118.98	118.86
C2 -C26 -H3	111.25	111.27	C63 -C64 -C66	120.98	121.04
C2 -C26 -H28	111.71	111.60	C63 -C64 -H67	119.89	119.92
H3 -C26 -H28	107.51	107.50	C66 -C64 -H67	119.12	119.04
C21 -C29 -C30	111.74	111.85	C63 -C65 -C68	120.73	120.82
C21 -C29 -C31	111.78	111.83	C63 -C65 -H69	119.66	119.78
C21 -C29 -H38	107.09	106.98	C68 -C65 -H69	119.61	119.40
C30 -C29 -C31	110.94	111.08	C64 -C66 -C70	118.57	118.52
C30 -C29 -H38	107.51	107.41	C64 -C66 -H71	120.89	120.89
C31 -C29 -H38	107.51	107.40	C70 -C66 -H71	120.54	120.59
C29 -C30 -H32	110.48	110.46	C65 -C68 -C70	118.81	118.75
C29 -C30 -H33	111.19	111.16	C65 -C68 -H72	120.79	120.79
C29 -C30 -H34	111.09	111.19	C70 -C68 -H72	120.40	120.46
H32 -C30 -H33	108.27	108.21	C66 -C70 -C68	121.93	122.01
H32 -C30 -H34	107.78	107.77	C66 -C70 -C173	119.05	119.02
H33 -C30 -H34	107.90	107.92	C68 -C70 -C173	119.02	118.97
C29 -C31 -H35	111.17	111.14			

Table 8.3: Vibration assignments, observed and calculated wave numbers of 5CPPTI at B3LYP method with 6-31G and 6-311Gbasis sets

Obser		served	Color	lotod	
Mode	wavei	numbers	Calcu wavenuml		
.No	(0	cm ⁻¹)	wavenum	ocis (cm)	Vibrational assignments (PED%)
.110	FT-IR	FT-	B3LYP/6-	B3LYP/6-	-
F1-IK		RAMAN	31G	311G	
1	3113		3119	3115	υ CH(99)
2			3114	3109	υ CH(99)
3			3107	3103	υ CH(98)
4			3099	3095	υ CH(98)
5			3092	3088	υ CH(99)
6		3064	3075	3072	υ CH(98)
7			3069	3065	υ CH(99)
8			3055	3051	υ CH(98)
9			3040	3034	υ CH(99)
10			3019	3015	υ CH(98)
11			3011	3006	υ CH(97)
12			3003	2995	υ CH(98)
13			2996	2988	υ CH(98)
14			2986	2982	υ CH(99)
15			2979	2975	υ CH(98)
16			2970	2967	υ CH(97)
17	2959	2962	2966	290	$v_{ass}CH_2$ (96)
18			2958	2952	$v_{ass}CH_3$ (96)
19			2952	2947	$v_{ass}CH_2$ (96)
20		2936	2945	2940	$v_{ass}CH_3$ (96)
21			2937	2930	$v_{ass}CH_3$ (96)
22	2925		2932	2927	$v_{ass}CH_3$ (97)
23			2917	2913	$v_{ss}CH_2$ (96)
24			2910	2905	$v_{ss}CH_2$ (96)
25			2902	2897	$v_{ss}CH_3$ (97)
26			2892	2888	υ _{ss} CH ₃ (97)

27	2864		2873	2869	υCH (98)
28	1687	1682	1687	1682	υCO (62), υCN (16), υCC (14)
29	100,	1002	1666	1663	υCO (66), υCC (17), υCN (10)
30			1652	1647	υCC (74), δ CH (22)
31			1638	1635	υCC (75), δ CH (19)
32			1619	1613	υCC (75), δ CH (18)
33			1608	1603	υCC (74), δ CH (20)
34	1593		1596	1592	υCC (76), δ CH (18)
35		1586	1587	1584	υCN (66), υCC (14), δ CH (12)
36			1575	1571	υCC (74), δ CH (22)
37			1564	1563	υCC (74), δ CH (14)
38			1561	1557	υCC (75), υCO (18)
39	1542		1552	1545	υCN (67), υCC (15), δ CH (10)
40			1541	1537	υCN (72), υCO (21)
41			1525	1521	δ CH (88)
42			1510	1505	δ _{OPB} CH ₃ (79)
43	1491	1492	1499	1492	$\delta_{\text{OPB}} \text{ CH}_3 (80)$
44			1488	1483	δCH (88)
45			1479	1475	δ CH (86), δ_{sciss} CH ₂ (10)
46		1463	1472	1466	$\delta_{\text{IPB}} \text{ CH}_3 (79)$
47	1458		1463	1460	$\delta_{\text{IPB}} \text{ CH}_3 (79)$
48			1456	1454	δ_{sciss} CH ₂ (86)
49			1450	1447	δ_{sciss} CH ₂ (86)
50		1432	1435	1431	δ CH (74), υCC (18)
51	1423		1425	1420	δ CH (80)
52			1414	1411	δ CH (82)
53			1413	1407	δ_{SB} CH ₃ (82)
54		1399	1409	1402	δ CH (84)
55	1381		1385	1380	δ CH (84)
56			1376	1370	δ_{SB} CH ₃ (83)
57			1367	1362	$\rho_{ROCK} CH_2(80)$
58			1355	1351	$\rho_{ROCK} CH_2(80)$
59			1350	1345	δ CH (80)

60	1337	1334	1342	1336	δ CH (68), υCC (18)
61			1329	1325	δ CH (68), υCC (20)
62			1314	1311	δ CH (66), υCC (18)
63			1302	1299	δ CH (66), υCCC (18)
64		1287	1294	1290	δ CH (66), υCCC (18)
65	1277		1281	1275	δ CH (60), υCC (16), δ CN (12),
66			1270	1266	υCC (61), δ CH (18), δ CCl (11)
67			1267	1260	υCC (61), δ CH (18), δ CCl (10)
68		1252	1256	1251	δ CH (72), δ CC (21)
69			1248	1244	γ_{wag} CH ₂ (62), δ CH (12), υ CC (10)
70			1235	1231	υCC (71), δ CH (12), δ CCl (10)
71	1222		1225	1220	υCC (70), δ CH (12), δ CC (11)
72			1207	1203	δ CH (80)
73			1201	1197	δ CH (80)
74		1184	1190	1185	γ _{wag} CH ₂ (78), γCH(12)
75	1172		1182	1179	υCC (69), δ CH (13)
76			1173	1170	δ CH (82), υCC (10)
77			1165	1161	υCC (66), δ CN (16), δ CH (10)
78			1157	1150	υCC (68), δ CH (12)
79			1151	1145	δ CH (71), υCC (18),
80			1137	1133	δ CH (82)
81			1125	1121	δ CH (82)
82	1110	1109	1115	1110	δ CH (82)
83			1109	1101	$\delta_{IPR} CH_3 (69), \delta CH (18)$
84			1103	1097	$\Gamma \mathrm{CH}_2 (72)$
85	1086		1095	1092	υ CN (61), υ NN (11), δ CO (10)
86			1090	1088	δ CH (82)
87			1075	1070	$\delta_{IPR}CH_3$ (68), δ CH (18)
88			1067	1062	δ CH (82)
89			1050	1044	δ CH (82)
90			1035	1031	ν CC (68), δ_{IPR} CH ₃ (16)
91			1027	1022	υCCl (74), δ CH (19)
92	1012		1020	1013	υCCl (74), δ CH (19)

93		1007	1009	1004	γ _{OPR} CH ₃ (68), γ CH (12)
94			989	985	γ _{OPR} CH ₃ (68), γ CH (12)
95			983	979	υNN(62), υCC (11), δ CN (10)
96			970	967	$\delta_{RING}(62)$, $vCN(18)$
97	951	948	957	950	$\delta_{RING}(62)$, vCC (17)
98			945	941	$\delta_{RING}(66)$, δCC (12)
99			940	935	$\delta_{RING}(66)$, ν CCl (12)
100			933	927	$\delta_{RING}(65)$, vCCl (14)
101			923	920	$\delta_{RING}(66)$, vCC (12)
102	910	910	915	911	γ CH (61), γ CH ₂ (16)
103			900	897	γ CH (68)
104			891	888	γ CH (68)
105			880	878	γ CH (68)
106			874	870	γ CH (68)
107			867	863	γ CH (68)
108			859	855	γ CH (68)
109			845	841	γ CH (69)
110			837	833	γ CH (64)
111	827		830	826	γ CH (64)
112			822	820	γ CC (66)
113			817	813	γ CH (68)
114			812	809	γ CC (66)
115		802	806	801	$\delta_{ m RING}(66)$
116			799	794	γ CC (68)
117			791	788	υ CC (69), δ CC (20)
118			785	783	$\delta_{\text{RING}}(67)$
119			781	775	γ CH (64)
120			779	770	γ CH (64)
121	760	763	772	766	γ CH (64)
122			767	761	γ CH (64)
123		748	760	756	γ CH (64)
124			755	750	γ CH (64)
125			747	743	γ CH (64)

126			740	735	γ CH (64)
127			731	727	$\delta_{\text{RING}}(62)$, ν CC (18)), ν CC1 (10)
128	725	724	725	720	$\delta_{\mathrm{RING}}(60)$
129			720	713	$\delta_{\text{RING}}(62)$
130			714	709	γ CH (64), γ CC (18)
131			708	703	$\gamma_{RING}(58), \gamma \text{ CH } (22)$
132		696	702	693	$\gamma_{RING}(58)$, γ CH (20)
133	682		690	685	$\gamma_{RING}(58), \gamma \text{ CH } (20)$
134			686	680	γ CO (60), $\gamma_{RING}(21)$
135			679	672	$δ_{RING}(58)$, $δ$ CH (17), $ν$ CCl (11)
136			675	669	$\gamma_{ m RING}(60)$
137			668	663	$\gamma_{RING}(58)$, vCCl (18)
138			660	657	δ _{RING} (58), υ CCl (22)
139	654		655	650	$\delta_{RING}(58)$, $\delta CC(56)$
140			644	640	$\delta_{RING}(58)$
141			633	632	$\delta_{RING}(58)$, vCCl (24)
142	628	626	630	626	$\delta_{RING}(58)$, vCCl (25)
143			621	617	$\delta_{\mathrm{RING}}(56)$
144			605	602	$\delta_{ m RING}(58)$
145			598	594	$\delta_{\mathrm{RING}}(58)$
146			592	588	$\delta_{RING}(60)$, vCCl (19)
147	583		583	580	$\gamma_{ m RING}(58)$
148			575	570	γ CH (59), γ CCL (14)
149			567	561	γ CH (59), γ CC (19)
150	555		560	557	$\delta_{RING}(66)$
151		549	555	550	γ CO (62), γ CCL (16)
152			546	542	γ CC (58)
153	532		539	535	$\delta_{\mathrm{RING}}(60)$
154			524	522	$\delta_{RING}(60)$
155			510	507	$\gamma_{RING}(58)$
156	491		493	490	γ CCL (55)
157			484	481	$\gamma_{RING}(58)$
158			475	473	γ CC (55)

159		464	461	γ CC (55)	
160		456	450	$\gamma_{RING}(55)$	
161		435	432	$\gamma_{RING}(52)$	
162	421	427	423	$\gamma_{RING}(53)$	
163		415	411	$\gamma_{RING}(53)$	
164		408	401	$\gamma_{RING}(55)$	
165		389	384	δ CC (58)	
166		380	376	$\delta_{RING}(58)$	
167		364	358	$\delta_{ring}(62)$	
168		353	349	γ CC (55)	
169		345	340	γ CCH ₂ (55))
170		332	325	γ CCH ₂ (55))
171		317	313	δ CC (60)	
172		312	306	δ CCl (62)	
173		297	294	δ CC (62)	
174		292	287	γ CC (54)	
175		282	275	δ CC (60)	
176		271	263	γ CC (54)	
177		260	255	γ CC (53)	
178		251	247	γ CC1 (52)	
179		245	239	γ CC1 (52)	
180		240	232	γ CC (53)	
181		227	220	γ CCl (55)	
182		216	211	γ CC (54)	
183		207	200	$\tau \mathrm{CH_3} (60)$	
184		195	186	$\tau \mathrm{CH_3} (60)$	
185		184	179	$\gamma_{ring}(54)$	
186		175	168	γ CCH ₃ (52)	ı
187		167	160	γ CC (52)	
188	15	55 158	153	γ CC (52)	
189		154	148	γ CC (50)	
190		150	142	$\gamma_{ring}(52)$	
191		144	138	$\gamma_{ring}(52)$	

192		138	131	δ CC (62)
193		132	127	γ CC (54)
194		125	122	$\gamma_{\rm ring}(54)$
195		115	111	δ CC (59)
196		109	104	γCN (53)
197		101	96	$\gamma_{\rm ring}(55)$
198		84	80	$\gamma_{\rm ring}(55)$
199	74	79	74	$\gamma_{\rm ring}(55)$
200		71	66	$\delta_{ring}(61)$
201		63	58	$\delta_{ring}(60)$
202		59	53	$\gamma_{ring}(55)$
203		56	50	$\delta_{ring}(60)$
204		45	40	δ CC (64)
205		42	35	δ CC (61)
206		39	32	δ CC (60)
207		33	26	γ CC (55)
208		30	23	γ CC (52)
209		27	21	δ CC (60)
210		20	16	δ CC (60)
211		17	12	$\gamma_{ring}(51)$
212		10	8	$\gamma_{ring}(50)$
213		9	6	$\gamma_{ring}(48)$

s-strong, ms-medium strong, w-weak, vw-very weak, vs-very strong, v-stretching, v_{sym}-sym stretching, v_{ass}-asymstretching, δ -in-plane, δ _{inb}-in-plane bending. δ _{inr}-in-plane rocking, γ -out-of-plane, γ _{opb}-out-of-plane bending, γ _{ring}- out-of-plane ring, scis-scissoring, ρ _{scis}-in plane scissoring, w-wagging, rock-rocking, Γ -twisting, δ ring-ring vibration.

Table 8.4: Calculated E-HOMO, E-LUMO), energy gap (E_{LUMO} – E_{HOMO}), Ionization potential (I), Electron affinity (A), global hardness (η), electronegativity (χ), Chemical softness (σ), chemical potential (μ) and global electrophilicity (ω) using the 6-311G levels of theory

Molecular properties	Energy (eV)	Energy gap (eV)	(I) (eV)	(A) (eV)	(η) (eV)	(χ) (eV)	(σ) (eV)	(μ) (eV)	(ω) (eV)
E _{HOMO}	6.3158	3.1267	6.3158	3.1891	1.5634	4.7525	0.6397	- 4.7525	7.2235
E _{LUMO}	3.1891	3.1207	0.3130	3.1071	1.5051	1.7525	0.0377	1.7323	7.2233

Table 8.5: Second order perturbation theory analysis of Fock matrix on NBO of 5CPPTI

Donor(i)	Туре	ED/e	Acceptor (j)	Туре	ED/e	E(2) ^a Kcal/mol	E(j)- E(i) ^b a.u	F(i,j) ^c a.u
σ	C2 - H42	1.87007	π*	C14 - C15	0.39569	12.11	0.48	0.073
π	C4 - C5	1.64536	π^*	C1 - N24	0.25178	17.55	0.24	0.059
π	C4 - C5	1.64536	π^*	C6 - C9	0.2919	19.74	0.29	0.068
π	C4 - C5	1.64536	π^*	C7 - C11	0.3924	22.22	0.27	0.069
π	C6 - C9	1.65977	π^*	C4 - C5	0.39225	21.04	0.28	0.069
π	C6 - C9	1.65977	π^*	C7 - C11	0.3924	21.74	0.26	0.068
π	C40 - S44	1.83215	π^*	C41 - N43	0.56694	27.69	0.34	0.097
π	C41 - N43	1.82144	π^*	C39 - O56	0.49038	27.83	0.27	0.085
π	C41 - N43	1.82144	π^*	C40 - S44	0.66732	19.43	0.26	0.073
π	C45 - C46	1.50119	π^*	C47 - O57	0.36579	30.41	0.23	0.077
π	C45 - C46	1.50119	π^*	C48 - C50	0.34117	23.84	0.27	0.075
π	C45 - C46	1.50119	π^*	C49 - C51	0.35598	28.04	0.27	0.08
π	C48 - C50	1.6886	LP (1)	C53	0.95002	48.39	0.15	0.093
π	C48 - C50	1.6886	π^*	C45 - C46	0.50004	13.49	0.27	0.057
π	C49 - C51	1.6494	LP (1)	C53	0.95002	60.1	0.14	0.099
π	C49 - C51	1.6494	π^*	C45 - C46	0.50004	19.38	0.26	0.066
π	C63 - C64	1.66478	π^*	C65 - C68	0.31246	20.11	0.28	0.068
π	C63 - C64	1.66478	π*	C66 - C70	0.38852	22.72	0.27	0.07
LP (3)	C127	1.99993	π*	C7 - C11	0.3924	12.8	0.32	0.062
LP (1)	S44	2	σ^*	C39 - C40	0.07623	7.25	0.96	0.075

LP (1)	C53	1.99896	π*	C48 - C50	0.34117	58.57	0.14	0.1
LP (1)	C53	1.99896	π^*	C49 - C51	0.35598	59.91	0.14	0.1
LP (2)	O56	1.92239	σ^*	C39 - N43	0.04329	12.91	0.64	0.082
LP (2)	O57	1.88386	σ^*	C47 - N58	0.08456	25.23	0.64	0.114
LP (1)	N58	1.65564	π^*	C47 - O57	0.01473	61.68	0.24	0.108
LP (1)	N58	1.65564	π^*	C48 - C50	0.34117	34.63	0.28	0.087
π^*	C1 - N24	0.25178	π^*	C4 - C5	0.39225	36.98	0.04	0.064
π^*	C7 - C11	0.3924	π^*	C4 - C5	0.39225	229.69	0.02	0.084
π^*	C7 - C11	0.3924	π^*	C6 - C9	0.2919	140.54	0.02	0.079
π^*	C14 - C15	0.39569	π^*	C17 - C21	0.35863	258.02	0.01	0.081
π^*	C40 - S44	0.66732	π^*	C39 - O56	0.49038	423.56	0.01	0.085
π^*	C40 - S44	0.66732	π^*	C45 - C46	0.50004	54.63	0.06	0.064
π^*	C41 - N43	0.56694	π^*	C39 - O56	0.49038	287.71	0.01	0.075
π^*	C45 - C46	0.50004	π^*	C48 - C50	0.34117	115.22	0.02	0.066
π^*	C45 - C46	0.50004	π^*	C49 - C51	0.35598	223.76	0.02	0.084
π^*	C47 - O57	0.36579	π^*	C45 - C46	0.50004	194.63	0.02	0.086
π^*	C66 - C70	0.38852	π^*	C63 - C64	0.35484	186.42	0.02	0.084
π^*	C66 - C70	0.38852	π^*	C65 - C68	0.31246	171.67	0.02	0.08

 $a \rightarrow E(2)$ means energy of hyper conjugative interaction (stabilization energy).

 $b{\rightarrow}$ Energy difference between donor and acceptor i and j NBO orbitals.

 $c \to F(i,j)$ is the Fock matrix element between i and j NBO orbitals.

Table 8.6: The lowest binding bonds with a distance value of various proteins docked ligand 5CPPTI show the binding affinity, inhibition constant, and RMSD

Ligand name	PDB ID	Bond distance (Å)	Amino acid (residues)	Bond	Binding affinity (kcal/mol)	Inhibition Constant Ki (µM or nM ormM)	RMSD (Å)
pan- 1,3-	6xm4	2.4	LYS A 206	Pi-alkyl	-8.95	277.03 nM	305.24
4(proj tydro- ne		2.7	TYR A 38	Pi-Pi T-shaped	-8.22	946.51M	306.66
o-1-(4-chlorobenzyl)-3-[2-(3-(4-chlorophenyl)-5-[4(] enyl]-4,5-dihydro-1H-pyrazol-1-yl)-4-oxo- 4,5-dihye thiazol-5(4H)-ylidene]-2,3-dihydro-1H- indol-2-one		3.1	GLU A 224	Pi-sigma	-7.78	1.99 μΜ	289
pheny oxo- 4 I- inde	2m8n	2.0	PHE A 32	Pi-Sulfur	-10.83	11.50 nM	14.866
hloroj yl)-4-c ro-1H		3.2	GLUA175	vanderWaals	-10.41	23.44 nM	15.016
3-(4-c zol-1- dihyd		3.2	ALA A 31	Pi-alkyl	-9.87	58.03 nM	11.534
3-[2-(-pyra]-2,3-	6hgf	2.6	ASN A248	vanderWaals	-9.41	127.45nM	15.494
nzyl)- .o-1H idene		2.2	LEU A 252	Pi-alkyl	-7.97	1.44 μΜ	10.167
orobe Jihyd 4H)-yl		3.1	ALA A 251	Pi-alkyl	-7.45	$3.49 \mu M$	11.118
(4-chlo]-4,5-0 zol-5(4	3tuv	2.2	GLU A 699	vanderWaals	-3.73	1.84 mM	33.31
ro-1-(henyl thiaz		2.9	ASP A 706	Pi-Anion	-3.58	2.39 mM	9.60
5-Chloro-1-(4-chlorobenzyl)-3-[2-(3-(4-chlorophenyl)-5-[4(propan-2-yl) phenyl]-4,5-dihydro-1H-pyrazol-1-yl)-4-oxo- 4,5-dihydro-1,3-thiazol-5(4H)-ylidene]-2,3-dihydro-1H- indol-2-one		3.7	LEU A588	alkyl	-1.47	83.27 mM	47.78

SUMMARY OF CONCLUSION

As said earlier, a concept of molecular spectroscopy was introduced to describe the properties of chemical substances. In principle, the stated goal can be reached by known theoretical methods. It would be obviously be desirable if the quantum mechanical calculation could be done. The quantum mechanical computations were applied suitable computed aided software (GAUSSIAN 09) with appropriate basis sets.

Utilizing experimental spectroscopic techniques and quantum chemical calculations, a thorough investigation of the structural and spectral properties of all the Thaizole-Pyrazole molecule has been carried out. FT-IR and FT-Raman spectra of the molecule are experimentally recorded and analyzed. The calculated vibrational frequencies of the title molecules have been found in good agreement with IR and Raman experimental data. This shows results presented in this work indicate that this level of theory is reliable for the prediction of both infrared and Raman spectra of the compounds.

The molecular optimized geometrical parameters such as bond length and bond angle were calculated and compared with the earlier experimental literatures. Moreover, Frontier molecular orbitals (HOMO-LUMO) analysis, molecular electrostatic potential and Natural bond orbital (NBO) interpretation were carried out. The calculated HOMO-LUMO energies show that all compounds have band gap lesser than 4.00 eV. Particularly, compound

5-Chloro-1-(4-chlorobenzyl)-3-[2-(3-(4-chlorophenyl)-5-[4-(propan-2-yl) phenyl]-4,5-dihydro-1H-pyrazol-1-yl)

-4-oxo- 4,5-dihydro-1,3-thiazol-5(4H)-ylidene]-2,3-dihydro-1H-indole-2-one (5CPPTI) have the lowest band gap (3.1265 eV) comparing other. By mapping the electron density subsurface, the chemical reactivity of the molecule was obtained. Natural bond orbital (NBO) analysis is used to contemplate the hyperconjugative interaction of the molecular stability and stability and charge delocalization.

NBO analysis shows that, in these all compounds the strongest bond formed between donor π^*C_{39} -O₄₅ \rightarrow LP(2)S₄₁ which have maximum stabilization energy in 635.75 kcal/mol for 5-(4-Methoxybenzylidene)-2-[3-(4-chlorophenyl)-5-[4-(propan-2-yl) phenyl]-4,5-dihydro-1H-pyrazol-1-yl] -1,3-thiazol-4(5H)-one (MCPPT). This stabilization energy has been calculated from second order perturbation theory.

Topology analysis show that the AIM calculations intimate that the character of the hydrogen bonds personate in the all the entitle molecule. The electron distribution and localization on the surface of the compounds were analyzed using ELF and LOL. Weak interaction of the molecules has been studied by using reduced density gradient (RDG) 2D and 3D graphed by Multiwfn. These studies proved that weak interaction like steric effect and van der Waal's effect were present in all compounds.

Molecular docking studies reveal that Thaizole-Pyrazole derivatives play a vital role in drug discovery and results reveals that these compounds have good biological activities.

REFERENCES

- [1] F.A. Settle, Hand book of instrumental techniques for analytical chemistry, New Jersey, Prentice, Inc, 21(1997).
- [2] Y.R. Sharma, Elementary organic spectroscopy, S. Chand & Company Pvt. Ltd, fifthRevised Edition, (2013).
- [3] N.B. Colthup, L.H. Daly, S.E. Wiberley, Introduction to infrared and Raman spectroscopy, Third Edition, Academic Press, New York, (1990).
- [4] F. Iachello, R. D. Levine, Algebraic theory of molecules, Oxford University Press, New York, (1995).
- [5] Stefano Oss, Algebraic Models in Molecular Spectroscopy, Adv. Chem. Phys., 93(1996).
- [6] S.L. Gupta, V. Kumar, H.V. Sharma, Elements of spectroscopy, Pragati Prakashan Publications, Twenty-fifth Revised Edition, Meerut, (2012).
- [7] G. Herzberg, Molecular Spectra and Molecular Structure: II, Infrared and Raman Spectra of Polyatomic Molecules, Van Nostrand Reinhold, New York, 1 (1966).
- [8] C. N. Banwell, Fundamentals of Molecular Spectroscopy, Fifth Edition, Tata McGraw-Hill, New Delhi, 5 (2013).
- [9] L.A. Woodward, Introduction to the theory of molecular vibrations and vibrational spectroscopy, Oxford Clarendon Press, (1972).
- [10] J.B. Foresman and A.E. Frisch, Exploring Chemistry with Electronic Structure Methods, second Edition, Gaussian, Inc., Pittsburgh, PA, (1996).
- [11] M. Castella-Ventura, E. Kassab, G. Buntinx, O. Poizat, Structure of the anion radical of 2,2'-bipyridine in solution, Phys. Chem. Chem. Phys., 20 (2000).
- [12] D.N. Shin, J.W. Hahn, K.H. Jung, T.K. Ha, Study of the cis and trans conformers of 2-halophenols using coherent anti-Stokes Raman spectroscopic and quantum chemical methods J. Raman Spectrosc. 29 (1998) 245-249.
- [13] B. Giese, D. Mc. Naughton, Density functional theoretical (DFT) and surface-enhanced Raman spectroscopic study of guanine and its alkylated derivatives, Phys. Chem. Chem. Phys, 20 (2002).
- [14] R.G. Parr, W. Yang, Density Functional Theory of Atoms and Molecules, Oxford University Press, New York, (1989).

- [15] A.D. Becke, Density-functional thermochemistry.III. The role of exact exchange, J. Chem. Phys., 98 (1993) 5643.
- [16] C. Lee, W. Yang, R.G. Parr, Development of the Colle-Salvetti correlation-energy formula into a functional of the electron density, Phys. Rev. B., 37(1988) 785-789.
- [17] Yu. N. Panchenko, R.A. Munoz, N.F. Stepanov, Kinematic models of a force field, J. Mol. Struct., 12 (1972) 289-297.
- [18] Yu. N. Panchenko, Methods of scaling quantum mechanical molecular force fields, J. Mol. Struct., 410 (1997) 327-329.
- [19] Yu. N. Panchenko, Scaling of quantum-mechanical molecular force fields, Russ. Chem. Bull., (Russian Chemical Bulletin), 45 (1996) 735-760.
- [20] M. J. Frisch, G. W. Trucks, H. B. Schlegel, G. E. Scuseria, M. A. Robb, J. R. Cheeseman, G. Scalmani, V. Barone, B. Mennucci, G. A. Petersson, H. Nakatsuji, M. Caricato, X. Li, H. P. Hratchian, A. F. Izmaylov, J. Bloino, G. Zheng, J. L. Sonnenberg, M. Hada, M. Ehara, K. Toyota, R. Fukuda, J. Hasegawa, M. Ishida, T. Nakajima, Y. Honda, O. Kitao, H. Nakai, T. Vreven, J. A. Montgomery, Jr., J.E. Peralta, F. Ogliaro, M. Bearpark, J. J. Normand, K. Raghavachari, A. Rendell, J. C. Burant, S. S. Iyengar, J. Tomasi, M. Cossi, N. Rega, J. M. Millam, M. Klene, J. E. Knox, J. B. Cross, V. Bakken, C. Adamo, J. Jaramillo, R. Gomperts, R. E. Stratmann, O. Yazyev, A. J. Austin, R. Cammi, C. Pomelli, J. W. Ochterski, R. L. Martin, K. Morokuma, V. G. Zakrzewski, G. A. Voth, P. Salvador, J. J. Dannenberg, S. Dapprich, A. D. Daniels, Ö. Farkas, J. B. Foresman, J. V.Ortiz, J. Cioslowski, D. J. Fox, Gaussian 09, B.01 Revision, Gaussian Inc., Wallingford, CT, (2010).
- [21] P. Hohenberg, W. Kohn, Density functional theory (DFT), Phys. Rev. 136, (1964).
- [22] A. Hesselmann, A.Gorling, Random phase approximation correlation energies withexact Kohn-Sham exchange, Molecular Physics, 108 (2010).
- [23] V. Mourik, V. Tanja, G. danitz, J. Robert, A critical note on density functional theory studies on rare-gas dimers, J. Chem. Phys., 116 (2002).
- [24] J. Vondrasek, L. Bendova, V. Klusak, Hobza Pavel, Correlated *Ab Initio* quantum chemical calculations, J. Am. Chem. Soc., 8 (2005).
- [25] J.A. Pople, Modern Theoretical Chemistry, H.F. Schaefer, III Ed., Plenum, New York, (1976)

- [26] W.J. Hehre, R.F. Stewart, J. A. Pople, Self- consistent molecular-orbital methods. Use of gaussian expansions of Slater-Type atomic orbitals. J. Chem, Phys.51 (1969).
- [27] W.J. Hehre, R.F. Stewart, J. A. Pople, Small Gaussian expansion of Slater-Type orbitals. J. Chem, Phys., 52 (1970) 2769.
- [28] W.J. Pietro, B.A. Levi, W.J. Hehre, R.F. Stewart, Molecular orbital theory of the properties of inorganic and organometallic compounds. 1. STO-NG basis sets for third-row main-group elements. In org. Chem. 19 (1980) 2225-2229.
- [29] W.J. Pietro, E.S. Blurock, R.S Hout, W.J. Hehre, R.F. Stewart, Molecular orbital theory of the properties of inorganic and organometallic compounds. 2. STO-NG basis sets for fourth-row main-group element. In org. Chem., 20 (1981) 3650-3654.
- [30] W.J. Pietro, W.J. Hehre, Molecular orbital theory of the properties of inorganic and organometallic compounds. 3. STO-3G basis sets for first- and second-row transition metals, J. Comput. Chem., 4(1983) 241-251.
- [31] M.J. Frisch, A.B. Neilson, A.J. Holder, Gauss View Molecular Visualization Program. User manual, Gaussian Inc, Pittsburgh, PA, (2000).
- [32] K. I. Ramachandran, G. Deepa, K.Namboori, Computational Chemistry and Molecular Modeling: Principles and Applications, Springer, Heidelberg, (2008) 224.
- [33] J.B. Foresman, Ab initio techniques in chemistry interpretation and visualization ACS Books, Washington, D.C., (1996).
- [34] A. A. Altaf, S. Kausar, A. Badshah, Spectral Calculations with DFT, intechopen., (2018).
- [35] D.B. Cook, Handbook of computational quantum chemistry, New York, Oxford University, Press, Oxford, UK, (1997).
- [36] Ira N. Levine, Quantum Chemistry, Allyn and Baron Inc. Boston, 1970.
- [37] T.A. Koopmans, Uber die Zuordnung von wellenfunktionen and Eigen werten zu den einzelnen Elektronen Eines Atoms, Physica, 1 (1934) 104-113.
- [38] P. Thul, V.P. Gupta, V.J. Ram, P. Tandon, Structural and spectroscopic studies on 2-pyranones, Spectrochim. Acta A.,75 (2010) 251-260.

- [39] P. Bultinck, R.C. Dorca, Negative and Infinite Fukui Functions: The Role of Diagonal Dominance in the Hardness Matrix, J. Math. Chem., 34 (2003) 67-74.
- [40] F. Weinhold, C. R. Landis, Valancy and Bonding: A Natural Bond Orbital Donor-Acceptor Perspective, Cambridge University Press, Cambridge, 2005.
- [41] R.F.W. Bader, Atoms in Molecules, a Quantum Theory, Oxford University Press, Oxford, (1990).
- [42] B.Silvi, I. Fourré and M.E. Alikhani,. The Topological Analysis of the Electron Localization Function. A Key for a Position Space Representation of Chemical Bonds. Monatshefte Für Chemie Chemical Monthly, 136 (2005).
- [43] G. Saleh, C.Gatti, L.L.Presti, Energetics of non-covalent interactions from electron and energy density distributions, J.Comptc.,1053 (2015) 53-59.
- [44] J. Cerny, P. Hobza, Non-covalent interactions in biomacromolecules., Phys.Chem. Chem. Phys., 39 (2007) 5291-5303.
- [45] G.R. Desiraju, Crystal Engineering. from molecules to materials, 656 (1989) 5-15.
- [46] N. Krishnamoorthy, M.H. Yacoub, S.N. Yaliraki, A computational modeling approach for enhancing self-assembly and biofunctionalisation of collagen biomimetic peptides, Biomaterials, 32 (2011) 7275-7285.
- [47] A. Dutta, A.D. Jana, S. Gangopadhyay, K.K. Das, J. Marek, R. Marek, Unprecedented π···π interaction between an aromatic ring and a pseudo-aromatic ring formed through intramolecular H-bonding in a bidentate Schiff baseligand: crystal structure and DFT calculations, Phys. Chem. Chem.Phys., 35 (2011) 15845-15853.
- [48] G.M. Day, T.G. Cooper, A.J. Cruz-Cabeza, K.E. Hejczyk, H.L. Ammon, S.X.M. Boerrigter, Significant progress in predicting the crystal structures of small organic molecules, Acta Crystallogr, Sect. B: Struct. Sci., 65 (2009) 107-125.
- [49] T.S. Koritsanszky, P. Coppens, Chemical Applications of X-ray Charge-Density Analysis, Chem. Rev., 101 (2001) 1583-1628.
- [50] C. Gatti, Chemical bonding in crystals: new directions, Z. Kristallogr., 220 (2005).
- [51] C. Gatti, P. Macchi, Modern charge density analysis, Springer, Dordrecht-Heidelberg-London-New York, (2012).
- [52] E.R. Johnson, S. Keinan, P. Morisanchez, J. Contreras Garcia, A.J. Cohen,W.Yang, Revealing Noncovalent Interactions, J. Am. Chem. Soc. 132., 2010.

- [53] C. Garcia, W. Yang, E.R. Johnson, Analysis of Hydrogen-Bond Interaction Potentials from the Electron Density: Integration of Noncovalent Interaction Regions, J. Phys. Chem. A., 115 (2011) 12983-12990.
- [54] T. Lu, F. Chen, Multiwfn: A multifunctional wavefunction analyzer, J. Comput. Chem. 33., (2012).
- [55] W. Humphray, A. Dalke, K. Schulten, VMD: Visual molecular dynamics, J. Mol. Graph., 14 (1996) 33-38.
- [56] https://www.pymol.org/
- [57] S. Diego, Cailf, Discovery studio modeling environment, Accelry software Release 4.0.USA, (2013).
- [58] V Temml, T Kaserer, Z Kutil, P Landa, Pharmacophore modeling for COX-1 and-2 inhibitors with LigandScout in comparison to Discovery Studio, Future Medicinal Chemistry, 6 (2014) 1869-1881.
- [59] N.K. Sharma, K.K. Priyanka, Benzothiazole: the molecule of diverse biological activities, Inter J Curr Pharm Res.,1 (2010).
- [60] J.Bajorath, Integration of virtual and high-throughput screening, Nat. Rev. Drug. Discov., 11 (2002) 882-894.
- [61] D. Kuntz, J.M. Blaney, S.J. Oatley, R. Langridge, T.E. Ferrin, A geometric approach to interactions macromolecule-ligand., J. Mol. Biol., 161 (1982).
- [62] G.M. Morris, D.S. Goodsell, R.S. Halliday, R. Huey, W.E. Hart, R.K. Belew, A.J.Olson, Automated docking using a Lamarckian genetic algorithm and an empirical binding free energy function, J. Comput. Chem., 19 (1998).
- [63] O. Trott, A.J. Olson, AutoDock Vina: improving the speed and accuracy of docking with a new scoring function, efficient optimization, and multithreading, J. Comput. Chem., 31 (2010) 455-461.
- [64] http://www.rcsb.org/pdb/home/home.do.
- [65] D.N. Sathyanarayana, Vibrational Spectroscopy: Theory and Applications, New AgeInternational Publishers, New Delhi, (2007).
- [66] J. Chamberain, J.E. Gibbs, H.E Gebbie, The determination of refractive index spectra by fourier spectrometry, Infrared Physics, (1969).
- [67] D. A. Skoog, F. J. Holler, T. A. Nieman, Principles of Instrumental Analysis, HarcourtAsia PTE Ltd, Singapore, (1998).

- [68] D. Robert Braun, Introduction to Instrumental Analysis, Infrared Spectroscopy, Pharma. Book Syndicate, Hyderabad, (2006).
- [69] Thermonikcolt, Introduction to Fourier Transform Infrared Spectrometry, (2001).
- [70] B.C. Smith, Fundamentals of Fourier Transform Infrared Spectroscopy, CRC Press, Boca Raton, (1996).
- [71] H. Kaur, Instrumental Methods of Chemical Analysis, Pragathi Prakashan, India, (2003).
- [72] B.Stuart, Infrared Spectroscopy: Fundamentals and Applications, John Wiley & Sons, Ltd., (2004).
- [73] L.J. Bellamy, the Infrared Spectra of Compound Molecules, Chapman and Hall, London,(1975).
- [74] J. R. Durig, S. M. Craven, W. C. Harris, Vibrational Spectra and Structure, Marcel Dekker, Inc, New York, (1972).
- [75] G.M. Howell, Fourier Transform Raman Instrumentation, Encyclopedia of AnalyticalChemistry John Wiley & Sons, (2003)
- [76] R. John Ferraro, Kazuo Nakamoto and W. Chris Brown, Introductory Raman Spectroscopy, 2nd Ed., Elsevier, (2003).
- [77] D.Bruce Chase, Fourier Transform Raman Spectroscopy, J. Am.Chem , AnalyticalChemistry, (1987).
- [78] P.B. Norton, J.J. Esposito, The new encyclopedia, britannica. 15th edition. USA; 3 (1994).
- [79] R.L. McCreery, Raman spectrocopy for chemical analysis, analytical science.wiley.com., 157 (2000).
- [80] B. Gadhiya, M. Rajput, A. Bapodra, K. Ladva, Design, synthesis, and evaluation of antimicrobial activities of some novel thiazole and thiadiazole derivatives clubbed with 1H-Benzimidazole, RasayanJ.chem. 9 (2016) 355-372.
- [81] https://wikimili.com/en/imidazole.
- [82] A. Viji, V. Balachandran, S. Babayan, B. Narayana, V.V. Saliyan, FT-IR and FT-Raman investigation, quantum chemical studies, molecular docking study and antimicrobial activity studies on the novel bioactive drug of 1-(2,4-Chlorobenzyl)-3- [2-(3-(4-chlorophenyl)-5-(4-(propan-2-ly)phenyl-4,5-dihydro-1H-pyrazol-1-yl]-

- 4 oxo -4 ,5-dihydro -1,3-thiazol-5(4H)-ylidence]-2,3-dihydro-1H-indol-2-one, J. Mol. Struct., 1215 (2020) 12822244.
- [83] E. Nour. A. Abdel-Sattar, A.M. E1-Naggar, M.S.A. Abdel-Mottaleb, Novel Thiazole Derivatives of Medicinal Potential: Synthesis and Modeling, J. Chem. (Hindawi), (2017) 1-11.
- [84] R.N. Phalen, W.K. Wong, Integrity of disposable nitrile exam gloves exposes to simulated movement, J. Occup. Environ. Hyg., 8(5) (2011) 289-299.
- [85] A.R. Krishnan, H. Saleem, S. Subashchandrabose, N. Sundaraganesan, S. Sebastian, Molecular structure, vibrational spectroscopic (FT-IR, FT-Raman), UV and NBO analysis of 2-chlorobenzonitrile by density functional method, Spectrochim. Acta., 78 (2011) 582-589.
- [86] A. Ayati, S.Emami, A. Asadipour, A. Shadier, a. Foroumadi, Recent application of 1,3-thiazole core structure in the identification of new lead compounds and drug discovery, Eur.J.Med.Chem., 97 (2015) 699-728.
- [87] Vinutha V. Salian, B. Narayana, B.k. Sarojini, M.S. Kumar, A.G. Lobo, Tailormade heterocyclic pyrazoline- thiazolidinones as effective inhibitors of Escherichia coli FabH: Design, synthesis and structural studies, J. Mol. Struct., 1192 (2019) 91-104.
- [88] M.H. Jamroz, Vibrational Energy Distribution Analysis VEDA 4, (2004).
- [89] R. Dennington, T. Kerth, J. Millam Gauss View, Version 5, Semi cham. Inc., Shawnee Mission KS, (2009).
- [90] E.D. Glendening, A.E. Reed, J.E. Carpenter, F. Weinhold, NBO version 3.1, Pittsburg, Theoretical chemistry institute and department of chemistry, University of Wisconsin, Madison, (1988) and Comput. Mol. Sci., 2 (2012) 1.
- [91] S.K. Gill, A.F. Christopher, V. Gupta, P. Bansal, Emerging role of bioinformatics tools and software in evolution of clinical research Perspect. Clin. Res., 7 (2016) 115-122
- [92] D. Seeliger, B.L. De Groot, Ligand docking and binding site analysis with Pymol and Auto dock/Vina, J. Comput. Aided Mol. Des., 24 (2010) 417–442.
- [93] S Parveen, M.A. Al-Alshaikh, C.Y Panicker, A.A. El-Emam., Vinutha V. Salian,B. Narayana, Spectroscopic investigations and molecular docking study of (2 E)-

- 1-(4- Chlorophenyl)-3-[4-(propan-2-yl)phenyl]prop-2-en-1-one using quantum chemical calculations. J. Mol. Struct.,1120 (2016) 317–326.
- [94] Mustafa Er, Arif Ozer, S.Direkel, T. Karakurt, H. Tahtaci, Novel substituted benzothiazole and Imidazo[2,1-b] [1,3,4] thiadiazole derivatives: synthesis, characterization, molecular docking study, and investigation of their in vitro antileishmanial and antibacterial activities, J. Mol. Struct., 1194 (2019) 284-296.
- [95] K. Vanasundari, V. Balachandran, M. Kavimani, B. Narayana, Spectroscopic investigation, vibrational assignments, Fukui functions, HOMO-LUMO, MEP and molecular docking evaluation of 4-[(3,4 –dichlorophenyl) amino] 2- methylidene 4 oxo butanoic acid by DFT method, J. Mol. Struct., 1147 (2017) 136-147.
- [96] Priyanka Singh, S. S. Islam, A. Prabaharan, Spectroscopic investigation (FT-IR, FT- Raman), HOMO-LUMO, NBO, and molecular docking analysis of N-ethyl-N- ntrosourea, a potential anticancer agent, J. Mol. Struct.,1154 (2019) 39-50.
- [97] M. Sathish, G. Meenakshi, S. Xavier, S. Sebastain, S.Periandy, N.A. Ahmad, J. Jamalis, M.M. Rosli, H. Kun-Fun, Synthiesis, molecular structure, hirshfeld surface, spectral investigation and molecular study of 3-(5-bromo-2-thienyl)-1-(4-fluorophenyl)-3-acetyl-2-pyrazoline(2) by DFT method J. Mol. Struct. 1164., 2018.
- [98] S. Beegum, Y. Sheena Mary, C.Y. Panicker, S. Armakovic, S.J. Armakovic, M. Arisoy, O. Temiz-Arpaci, C.V. Alsenoy, Spectroscopic, tantimicrobial and computational study of novel benzoxazole derivative, J. Mol. Struct.,1176 (2019) 881-894.
- [99] F. R. Dollish, Characteristic Raman frequencies of organic compounds, in: W. G. Fateley, F. F. Bentley (Eds.), New York, Wiley, (1974).
- [100] R.M. Silverstein, G.C. Bassler, T.C. Morrill, Spectrometric Identification of Organic compounds, John Wiley & Sons, New York, (1981).
- [101] S. Fatma, A. Bishnoi, A. K. Verma, Synthesis, spectral analysis (FT-IR, 1 HNMR, 13CNMR and UV-visible) and quantum chemical studies on molecular geometry, NBO, NLO, chemical reactivity and thermodynamic properties of novel 2-amino-4- (4-(dimethylamino)phenyl)-5-oxo-6-phenyl-5, 6-dihydro-4H-pyrano [3, 2-c] quinoline-3-carbonitrile, J. Mol. Struct., 1095 (2015) 112–124.

- [102] F. Bardak, Experimental and DFT analysis of structural and spectroscopic features of nitroterephthalic acid, and computational insights into its molecular interactions with hER-a via molecular docking, J. Mol. Struct., 1175 (2019) 458-470.
- [103] G.P. Sheeja Mol, D. Aruldas, I.H. joe, S. Balachandran, A.R. Anuf, J. George, Spectroscopic investigation, fungicidal activity and molecular dynamics simulation on benzimidazol-2-yl carbamate derivatives, J. Mol. Struct., 1176 (2019) 226-237.
- [104] S.S. Khemalapure, V.S. Katti, C.S. Hiremath, M. Basanagouda, S.M. Hiremath, S.J. Armakovic, Molecular structure, optoelectronic properties, spectroscopic (FT-IR,FT- Raman and UV-Vis), H-BDE, NBO and drug likeness investigations on 7,8- benzocoumarin-4-acetic acid(7BAA), J. Mol. Struct., 1195 (2019) 815-826.
- [105] T.K. Kuruvilla, S. Muthu, J.C. Prasana, J. George, S. Seyyanthi, Spectroscopic(FT-IR, FT-Raman), quantum mechanical and docking studies in methyl[(3s)-3- (naphthalene-1-yloxy)-3-(thiophen-2-yl)propy1]amine J. Mol. Struct., 1175 (2019)163-174.
- [106] S.C. Jevaseelan, R. Premkumar, K. Kaviyarasu, A. Milton Franklin Benial, Spectroscopic, quantum chemical, molecular docking and in-vitro,anti-cancer activity studies on 5-methoxyindole-3- carboxaldehyde. J. Mol. Struct. 1197 (2019) 134-46.
- [107] A.S. E1-Azab, Y. Sheena Mary, C. Yohannan Panicker, Alaa A.M. Abdel-Aziz, Ibrahim A. A1- Suwaidn, C.V. Alsenov, FT-IR, FT-Raman and molecular docking studyofethyl-4-(2(4-oxo-3-phenethyl-3,4-dihydroquinazolin-2ylthio)acetamido)benzoate, J. Mol. Struct., 111 (2016) 9-18.
- [108] V. Madhavan, H.T. Varghese, S. Mathew, J. Vinsova, C.Y. Panicker, FT-IR, FTRamanand DFT calculations of 4-chloro-2-(3, 4-dichlorophenylcarbamoyl) phenyl acetate, Spectrochim. Acta., 72 (3) (2009) 547-553.
- [109] N.P. Roeges, A Guide to the Complete Interpretation of Infrared Spectra of Organic Structures, Wiley, (1994).
- [110] E. Mooney, The infra-red spectra of chloro-and bromobenzene derivatives II. Nitro benzenes, Spectrochim. Acta. 20 (6) (1964) 1021-1032.
- [111] V. Sortur, J. Yenagi, J. Tonannavar, V.B. Jadhav, M.V. Kulkarni, Spectrochim. Acta A 71 (2008) 688–694.

- [112] M. Govindarajan, M. Karabacak, Analysis of vibrational spectra (FT-IR and FT-Raman) and nonlinear optical properties of organic 2-chloro-p-xylene, Spectrochim. Acta. 94 (2012) 36-47.
- [113] S. Fatma, A. Bishnoi, V. Singh, Fatmah A. M. A1-Omary, Ali A. E-Emam, S. Pathak, R.Srivastava, O. Prasad, L. Sinha, Spectroscopic and 1-(2,6-bis (4-methoxyphenyl)- 3,3-dimethylpiperidine-4-ylidene)-2-(3-(3, 5-dimethyl-1 H pyrazol-1-yl)pyrazin-2- yl)hydrazine by DFT method, J. Mol. Struct. 1106 (2016) 277-285.
- [114] Y.S. Mary, C.Y. Panicker, M. Sapna Kumari, B. Narayana, J.A. War, FT-IR, NBO, HOMO-LUMO, MEP analysis and molecular docking study of 1-[3-(4Fluorophenyl)-5-phenyl-4, 5-dihydro-1H-pyrazol-1-yl] ethanone, Spectrochim. Acta. 5 (2015) 483-493.
- [115] Marzieh Miar, A. Shiroudi, K. Pourshamsian, Theoretical investigations on the HOMO–LUMO gap and global reactivity descriptor studies, natural bond orbital, and nucleus-independent chemical shifts analyses of 3-phenylbenzo[d]thiazole-2(3H)- imine and its para-substituted derivatives: Solvent and substituent effects, 45 (2021) 147-158.
- [116] R.G. Parr, L.V. Szentpaly, S. Liu, Electrophilicity Index, J. Am. Chem. Soc, 121(9) (1999) 1922-1924.
- [117] M. Karabacak, L. Sinha, O. Prasad, Z. Cinar, M. Cinar, The spectroscopic (FT-Raman, FT-IR, UV and NMR), molecular electrostatic potential, polarizability and hyperpolarizability, NBO and HOMO–LUMO analysis of monomeric and dimeric structures of 4-chloro-3,5-dinitrobenzoic acid, Spectrochimica Acta A Mol. Biomol. Spectrosc. 93 (2012) 33-46.
- [118] W. Humphrey, A. Dalke, K. Schulten, VMD: visual molecular dynamics, J. Mol. Graph. 14 (1996) 33-38.
- [119] A. D. Becker, K. E. Edgecombe, A simple measure of electron localization in atomic and molecular systems, J. Chem. Phys. 92 (1990) 5397-5403.
- [120] S. Noury, F. Colonna, A. Savin, B. Silvi, Analysis of the delocalization in the topological theory of chemical bond, J. Mol. Struct. 450 (1998) 59–68.
- [121] K. Jayasheela, Lamya H. Al-Wahaibi, S. Periandy, Hanan M. Hassan, S. Sebastian, S.Xavier, J. C. Daniel, Ali A. El-Emam, M. I. Attia, Probing vibrational

- activities, electronic properties, molecular docking, and hirshfeld surfaces analysis of 4- chlorophenyl({[(1E)-3-(1Himidazol-1-yl)-1-phenyl propylidene] amino}oxy) methanone: Apromising anti-Candida agent J. Mol. Struct. 1159 (2018) 83-95.
- [122] A. Savin, The electron localization function (ELF) and its relatives: interpretations and difficulties. J. Mol. Struct, 727 (1-3) (2005)., 127–131.
- [123] N. Salih, J. Salimon, E. Youif, Synthesis and antimicrobial activities of 9H-carbazole derivatives, Arab. J. Chem.9 (2016) 781-786.
- [124] E. Yousif, E. Rentschler, N. Salih, J. Salimaon, A. Hameed, M. Katan, Sythesis and antimicrobial screening of tetra schiff bases of 1,2,4,5-tetra (5-amino-1,3,4-thiadiazole-2-yl)benzene, J. Saudi chem.soc.18 (2014) 269-275.
- [125] D.B. Kitchen, H.Decornez, J.R.Furr, J.Bajorath, Docking and scoring in virtual screening for drug discovery: methods and applications, Nat. Rev. Drug Discov, 3(2004) 935-949
- [126] M. Hammel, G. Sfyroera, D. Ricklin, P. Magotti, J. D. Lambris and B. V. Geisbrecht, A structural basis for complement inhibition by staphylococcus aureus, Nature Immunology, (2007) 430–437.
- [127] S. Kumar, M. F.Mabanglo, M. A. Hast, Y. Shi, L. S. Beese, Crystal Structure of Candida Albicans Protein Farnesyltransferase in Apo form, Wiley, 2013.
- [128] T. L. Poulos, H. Li, J. K. Holden, S. Kang, F.C. Beasley, M.A. Cinelli, S.G. Roy, Nitric oxide synthase as a target for Methicillin- resistant Staphylococcus aureus, J. Chem biol. 22 (2015) 785-792.
- [129] H. Gouda, H. Torigoe A. Saito, M. Sato, Y.J. Arata, I. Shimada, Three-Dimensional Solution Structure of the B Domain of Staphylococcal Protein A: Comparisons of the Solution and Crystal Structures, Biochemistry, 31(1992) 199.
- [130] P. Blum, A. Sagner, A. Tiehm, P. Martus, T. Wendel, P. Grathwohl, Importance of heterocylic aromatic compounds in monitored natural attenuation for coal tar contaminated aquifers: a review, J. Contam. Hydrol. 126 (2011) 181-194.
- [131] Y. Sheena Mary, C. Yohannan Panicker, M. Sapnakumari, B. Narayana, B.K. Sarojini, Abdulaziz A. Al-Saadi, C.V Alsenoy, J. A. War, FT-IR, NBO, HOMO–LUMO, MEP analysis and molecular docking studyof 1-[3-(4-Fluorophenyl)-5-phenyl-4,5-dihydro-1H-pyrazol-1-yl]ethanone,Spectrochimica Acta A Mol. Biomol. Spectrosc. 136 (2015) 483–493.

- [132] G. Susithra, S. Ramalingam ,S. Periandy , R. Aarthi , Molecular structure investigation towardspharmacodynamic activity and QSAR analysis on hypoxanthine using experimental and computational tools Egyp. Jour. Bas. App. Sci. (2018).
- [133] S. Aayisha, T. S. R. Devi, S.Janani, , S. Muthu, M. Raja, , S. Sevvanthi and R. Hemamalini, .Molecular Docking, Quantum chemical computational and Vibrational studies on bicyclic heterocycle –6-nitro-2,3-dihydro-1,4-benzodioxinel: Anti-cancer agent. Computational Biology and Chemistry, (2020). 107226.or J. compbiolchem.2020.107226.
- [134] I. Wayne Cheney, Shunqi Yan, Todd Appleby, Heli Walker, Todd Vo, NanhuaYao,RobertHamatake, Zhi Hong and Jim Z. Wu. Identification and structure— activity relationships of substitutedpyridones as inhibitors of Pim-1 kinaseBioorganic & Medicinal Chemistry Letters 17 (2007) 1679–1683.
- [135] Daisuke Morishita, Miho Takami, Seiko Yoshikawa, Ryohei Katayama, Shigeo Sato, Mutsuko Kukimoto-Niino, Takashi Umehara, Mikako Shirouzu, Kazuhisa Sekimizu, Shigeyuki Yokoyama, and Naoya Fujita Cell-permeable Carboxylterminal p27Kip1 Peptide Exhibits Anti-tumor Activity by Inhibiting Pim-1 Kinase, THE JOURNALOF BIOLOGICAL CHEMISTR, (2011) 2681–2688.
- [136] Biovia discovery studio 4.5; https://discover.3ds.com
- [137] S. Parveen, M.A. Al-Alshaikh, C. Y. Panicker, A. A. El-Emam, B. Narayana, V. V., Saliyan, C. Van Alsenoy., Vibrational and structural observations and molecular docking study on 1-{3-(4-chlorophenyl)-5-[4-(propan-2-yl)phenyl]-4,5-dihydro-1H-pyrazol-1-yl}-ethanone, J. Mol. Struct., 1112(2016)136–146.
- [138] A. Sarau Devi, V.V. Aswathy, Y. Sheena Mary, C.Yohannan Panicker, S.Armakovic, S.J. Armakovic, C. Van Alsenoy, Synthesis, XRD single crystal structure analysis, vibrational spectral analysis, molecular dynamics and molecular docking studies of 2-(3-methoxy-4-hydroxyphenyl) benzothiazole. , J. Mol. Struct., 1148(2017) 282–292
- [139] K. Venil, A. Lakshmi, V. Balachandra, B. Narayana, Vinutha V. Salian,FT-IR and FT-Raman investigation, quantum chemical analysis and molecular docking studies of 5-(4-Propan-2-yl)benzylidene)-2-[3-(4-chlorophenyl)-5[4-(propan-2-yl)benzylidene)-2-[3-(4-chlorophenyl)-5]-[4-(propan-2-yl)benzylidene)-2-[3-(4-chlorophenyl)-5]-[4-(propan-2-yl)benzylidene)-2-[3-(4-chlorophenyl)-5]-[4-(propan-2-yl)benzylidene)-2-[3-(4-chlorophenyl)-5]-[4-(propan-2-yl)benzylidene)-2-[3-(4-chlorophenyl)-5]-[4-(propan-2-yl)benzylidene)-2-[3-(4-chlorophenyl)-5]-[4-(propan-2-yl)benzylidene)-2-[3-(4-chlorophenyl)-5]-[4-(propan-2-yl)benzylidene)-2-[3-(4-chlorophenyl)-5]-[4-(propan-2-yl)benzylidene)-2-[3-(4-chlorophenyl)-5]-[4-(propan-2-yl)benzylidene)-2-[3-(4-chlorophenyl)-5]-[4-(propan-2-yl)benzylidene)-2-[3-(4-chlorophenyl)-5]-[4-(propan-2-yl)benzylidene)-2-[3-(4-chlorophenyl)-5]-[4-(propan-2-yl)benzylidene)-2-[3-(4-chlorophenyl)-5]-[4-(propan-2-yl)benzylidene)-2-[3-(4-chlorophenyl)-5]-[4-(propan-2-yl)benzylidene)-2-[3-(4-chlorophenyl)-5]-[4-(propan-2-yl)benzylidene)-2-[3-(4-chlorophenyl)-5]-[4-(propan-2-yl)benzylidene)-2-[3-(4-chlorophenyl)-5]-[4-(4-chlorophenyl)-5]-[4-(4-chlorophenyl)-2-[4-(

- yl)phenyl-4,5- dihydro -1H-pyrazol-1-yl]-1,3-thiazol-4(5 H)-one, J. Mol. Struct 1225 (2021)129070.
- [140] Y.S. Mary, C.Y. Panicker, S. Armakovic, S.J. Armakovic, B. Narayana, B.K. Sarojini, C. Van Alsenoy, Investigation of reactive and spectroscopic properties of oxobutanoic acid derivative: Combined spectroscopic, DFT, MD and docking study, J.Mol. Struct, 1148 (2017) 266-275.
- [141] R.A. Sheakh Mohamad, W. M. Hamad and H. J. Aziz, Acta Cryst., 76, 920 (2020).
- [142] H. Behbehani and H. M Ibrahim4-Thiazolidinones in Heterocyclic Synthesis: Synthesis of Novel Enaminones, Azolopyrimidines and 2-Arylimino-5-arylidene-4-thiazolidinones. Molecules, 17 (2012)., 6362–6385.
- [143] S. Alturk, D. Avcı, O. Tamer, Y. Atalay, Comparison of different hybrid DFT methods on structural, spectroscopic, electronic and NLO parameters for a potential NLO material, j.comptc 1100 (2017) 34-45.
- [144] S. Janani, Hemamalini Rajagopal, S. Muthu, S. Aayisha, M. Raja, Molecular structure, Spectroscopic (FT-IR, FT-Raman, NMR), HOMO-LUMO, Chemical reactivity, AIM, ELF, LOL and Molecular docking studies on 1-Benzyl-4-(N-Bocamino) piperidine, J. Mol. Struct, 129657(2020) 31970-0.
- [145] V. Arjunan, R. Anitha, S.Thirunarayanan, S. Mohan, Simulations on the structure, vibrations and electronic properties of 1,2–epoxy–3–phenoxy propane and 1,2–epoxy–3–(p –tolyloxy)propane by FT–IR, FT–Raman, FT–NMR and DFT methods. Chemical Data Collections, 11-12 (2017). 139–167.
- [146] S. M. Hiremath, A. Suvitha, N. R. Patil, C. S. Hiremath, S.S. Khemalapure, S. K. Pattanayak, V. S. Negalurmath, K. Obelannavar, Molecular structure, vibrational spectra, NMR, UV, NBO, NLO, HOMO-LUMO and molecular docking of 2-(4, 6-dimethyl-1-benzofuran-3-yl) acetic acid (2DBAA): Experimental and theoretical approach, J. Mol. Struct, 1171 (2018) 362-374.
- [147] Y.B. Shankar Rao, M.V.S. Prasad, N. Udaya Sri, V. Veeraiah, Vibrational (FT-IR, FTRaman) and UV-Visible spectroscopic studies, HOMO–LUMO, NBO, NLO and MEP analysis of Benzyl (imino (1H-pyrazol 1-yl) methyl) carbamateusing DFT Calculaions, J.Mol. Struct, 1108 (2016) 567-582.
- [148] C. Sivakumar, V.Balachandran, B.Narayana, Vinutha V. Salian, B. Revathi,N. Shanmugapriya, K. Vanasundari, Molecular spectroscopic investigation,

- quantum chemical, moleculardocking and biological evaluation of 2-(4-Chlorophenyl)-1-[3-(4-chlorophenyl)-5-[4-(propan-2-yl) phenyl-3,5-dihydro-1H-pyrazole-yl] ethanone, J.Mol. Struct, 1224 (2021) 129010.
- [149] Socrates George, Infrared and Raman Characteristic Group Frequencies, Tables and Charts, thirded., Wiley, New York, 2001. J. Chem. Educ. ,72, 4 (1995) A93
- [150] M. Kaur, Y.S. Mary, C.Y. Panicker, H.Y. Varghese, H. Yathirajan, K. Byrappa, C.Van Alsenoy, Vibrational spectroscopic (FT-IR, FT-Raman) and quantum chemical calculations of 1-(5, 5-dioxido-10H-phenothiazin-10-yl) ethanone,. Spectrochim. ActaA Mol. Biomol. Spectrosc., 120 (2014), 445-455.
- [151] R.M. Silverstein. F.X. Webster, Spectroscopic Identification of Organic Compounds.7th ed., Wiley, New York, 2005.
- [152] Yusuf Sert, Mehmet Gumus, Halil Gokce, Ibrahim Kani, Irfan Koca, Molecular docking, Hirshfeld surface, structural, spectroscopic, electronic, NLO and thermodynamic analyses on novel hybrid compounds containing pyrazole and coumarin cores, J. Mol. Struct. 1171 (2018) 850-866.
- [153] W. Coats, J. P. Redfern, Nature 1964, 201, 68. and 2.E. Temel, C. Alas, alvar, H. Gcokçe, A. Güder, Ç. Albayrak, Y.B. Alpaslan, G. Alpaslan, N. Dilek, DFT calculations, spectroscopy and antioxidant activity studies on (E)-2-nitro-4-[(phenylimino) methyl] phenol, Spectrochim. Acta A Mol. Biomol. Spectrosc. 136 (2015) 534-546.
- [154] P. Kolandaivel, V. Nirmala, Study of proper and improper hydrogen bonding using Bader's atoms in molecules (AIM) theory and NBO analysis, J. Mol. Struct. 694 (1-3)(2004) 33-38.
- [155] A.E. Reed, L.A. Curtiss, F. Weinhold, Intermolecular interactions from a natural bondorbital, donor-acceptor viewpoint, Chem. Rev. 88 (6) (1988) 899-926.
- [156] R. Mohamed Asath, R. Premkumar, T. Mathavan, A. Milton Franklin Benial, Spectrochim Acta A Mol BiomolSpectrosc., 175, 51 (2017).
- [157] G.L. Sosa, N.M. Peruchena, R.H. Contreras, E.A. Castro, Topological and NBO analysis of hydrogen bonding interactions involving C-H/O bonds, J. Mol. Struct., 577 (2-3) (2002) 219-228.
- [158] A. Savin, R. Nesper, S. Wengert, T.F. Fassler, ELF: the electron localization function, Angew. Chem., Int. Ed. Engl. 36 (17) (1997) 1808-1832.

- [159] M. Latha Beatricea, S. Mary Delphine, M.Amalanathan, Molecular structure, spectroscopic, Fukui function, RDG, anti-microbial and molecular docking analysis of higher concentration star anise content compound methyl 4-methoxybenzoate-DFT study, J.Mol.Struc., 1238 (2021) 130381.
- [160] I. Rozas, I. Alkorta, J. Elguero, Behavior of Ylides Containing N, O, and C Atoms as Hydrogen Bond Acceptors, J. Am. Chem. *Soc.*, 122 (45), (2000) 11154-11161.
- [161] A. Lagunin, A. Stepanchikova, D. Filimonov, V. Poroikov, PASS: prediction of activity spectra for biologically active substances, Bioinformatics 16, (2000) 747-748.
- [162] A.N. Bullock, J. Debreczeni, A.L. Amos, S. Knapp, Benjamin, Structure and substratespecificity of the Pim-1 kinase, J. Biol. Chem, (2005) 41675–41682.
- [163] V.A. Adole, T.B. Pawar, and B.S. Jagdale, DFT computational insights into structural, electronic and spectroscopic parameters of 2-(2-Hydrazineyl) thiazole derivatives: a concise theoretical and experimental approach, J. Sulphur Chem. (2020)1–18.
- [164] P.Makam, R. Kankanala and A Prakash, 2-(2-Hydrazinyl) thiazole derivatives: Design, synthesis and in vitro antimycobacterial studies, Eur J Med Chem., 69 (2013) 564–576.
- [165] L.J. Piddock. Understanding drug resistance will improve the treatment of bacterial infections. Nat Rev Microbiol.,15 (2017) 639–640.
- [166] S. Bondock, A.M. Fouda, Synthesis and evaluation of some new 5-(hetaryl) thiazolesas potential antimicrobial agents, Synth Commun., 48 (2018) 561–573.
- [167] B. Parrino, A. Attanzio, V. Spano, S.Cascioferro, A. Montalbano, P. Barraja, L. Tesoriere, P. Diana, G. Cirrincione, A. Carbone, Synthesis, antitumor activity and CDK1 inhibiton of new thiazole nortopsentin analogues, Eur J Med Chem.,138 (2017)371–383.
- [168] M.H.M. Helal, M.A. Salem, M.S.A. El-Gaby, M.Aljahdali, Synthesis and biological evaluation of some novel thiazole compounds as potential anti-inflammatory agents, Eur J Med Chem., 65 (2013) 517–526.
- [169] V.U. Jeankumar, J. Renuka, P. Santosh, V.SoniJ.PadmaSridevi, P. Suryadevara, P.Yogeeswari, D. Sriram, Thiazole-aminopiperidine hybrid analogues: Design

- and synthesis of novelMycobacterium tuberculosis GyrB inhibitors, Eur J Med Chem., 70 (2013) 143–153.
- [170] B.F. Abdel-Wahab, H. Abdel-Gawad, G.E.A. Awad, F.A.Badria, Synthesis, antimicrobial, antioxidant, antiinflammatory, and analgesic activities of some new 3- (2-thienyl) pyrazole-based heterocycles, Med Chem Res., 21(2012) 1418–1426.
- [171] B. Vijayakumar, V. Kannappan, and V. Sathyanarayanamoorthi, DFT analysis and spectral characteristics of Celecoxib a potent COX-2 inhibitor. J.Molstruc., 1121 (2016) 16–25.
- [172] M. Sertcelik, Synthesis, spectroscopic properties, crystal structures, DFT studies, and the antibacterial and enzyme inhibitory properties of a complex of Co(II) 3,5-difluorobenzoate with 3-pyridinol, J.Chem.Res., (2020) 1-7.
- [173] K. El Bourakadi, M. El Mehdi, R. T. Boere, El Kacem, A. Qais, R. Bouhfid,. Synthesis, characterization and DFT studies of 6-bis(2-(thiazol-4-yl)-benzimidazol-1- yl) hexane hemihydrate crystal: Experimental and theoretical investigation. J.Molstruc., 1202 (2020)127253.
- [174] V. Krishnakumar, N. Jayamani, R Mathammal, Molecular structure, vibrational spectral studies of pyrazole and 3,5-dimethyl pyrazole based on density functional calculations, j.saa., 79(5) (2011) 1959–1968.
- [175] Y.Sert, H. Gokce, Chandra, M. Mahendra, N. Srikantamurthy, Molecular docking and vibrational spectroscopy studies of (E)-N'-hydroxy-1,3-diphenyl-4,5-dihydro-1H- pyrazole-5-carboximidamide J.Molstruc., 1184 (2019) 79-91.
- [176] Y. Sert, G.A. El-Hiti, H Gokce, F Ucun, B.F. Abdel-Wahab, B.M Kariuki, DFT, molecular docking and experimental FT-IR, laser-Raman, NMR and UV investigations on a potential anticancer agent containing triazole ring system, J. Mol. Struct.,1211 (2020) 128077.
- [177] N. Prabavathi, A. Nilufer, V. Krishnakumar, Spectroscopic (FT-IR, FT-Raman, UV and NMR) investigation, conformational stability, NLO properties, HOMO–LUMO and NBO analysis of hydroxyquinoline derivatives by density functional theory calculations, j.saa., 114(2013) 449–474.
- [178] P. Devi, S. Fatma, S. Shukla, R. Kumar, V. Singh, A. Bishnoi, Synthesis, spectroscopic investigation, molecular docking and DFT studies of novel (2Z,4Z)-

- 2,4- bis(4-chlorobenzylidene)-5-oxo-1-phenylpyrrolidine-3-carboxylic acid (BCOPCA), J.heliyon., 4(12) (2018) 01009.
- [179] G. Fogarasi, P. Pulay, Vibrational Spectra and Structure, Elsevier, Amsterdam, 14 (1985) 125–219.
- [180] A.K. Srivastava, B Narayana, B.K. Sarojini, N. Misra, Vibrational, structural and hydrogen bonding analysis of N'-[(E)-4-Hydroxybenzylidene]-2- (naphthalen-2-yloxy) acetohydrazide: combined density functional and atoms-in-molecule based theoretical studies. Indian Journal of Physics, 88(6) (2014) 547–556.
- [181] A. Fu, D. Du, Z. Zhou, Density functional theory study of vibrational spectra of acridine and phenazine, Spectrochim. Acta Mol. Biomol. Spectrosc., 59 (2003) 245–253.
- [182] V.Krishnakumar, N. Surumbarkuzhali, Analysis of structure and vibrational spectra of 2,5-dihydroxybenzoicacid based on density functional theory calculations, J. Raman Spectrosc., 41(4), (2009) 473-478.
- [183] K. Thirunavukkarasu, P. Rajkumar, S. Selvaraj, et al., Vibrational (FT-IR and FT-Raman), electronic (UV-vis), NMR (¹H and ¹³C) spectra and molecular docking analyses of anticancer molecule 4-hydroxy-3-methoxycinnamaldehyde, J. Mol. Struct., 1173(2018) 307-320.
- [184] C.S. Hiremath, J. Yenagi, J. Tonannavar, FT-Raman and infrared spectra and vibrational assignments for 3-chloro-4-methoxybenzaldehyde, as supported by *ab initio*, hybrid density functional theory and normal coordinate calculations., J.saa.,68 (2007) 710-717.
- [185] K. Govindarasu, E. Kavitha, Structural, vibrational spectroscopic studies and quantum chemical calculations of n-(2,4-dinitrophenyl)-1-alanine methyl ester by density functional theory, J. Mol. Struct., 1088 (2015) 70-84.
- [186] K. Nourah Z. Alzoman, Y. Sheena Mary, C. Yohannan Panicker, A. Ibrahim, Al-Swaidan, Ali A. El-Emam, Omar A. Al-Deeb, Abdulaziz A. Al-Saadi, Christian Van Alsenoy, Javeed Ahmad War, Spectroscopic investigation (FTIR and FT-Raman), vibrational assignments, HOMO-LUMO, NBO, MEP analysis and molecular docking study of 2-[(4-chlorobenzyl)sulfanyl]-4-(2- methylpropyl)-6-(phenylsulfanyl)- pyrimidine-5-carbonitrile, a potential chemotherapeutic agent, Spectrochim. Acta A Mol. Biomol. Spectrosc., 139 (2015) 413-424.

- [187] Jacob George, Johanan Christian Prasana, S. Muthu, Tintu K. Kuruvilla, S. Sevanthi, Rinnu Sara Saji, Spectroscopic (FT-IR, FT Raman) and quantum mechanical study on N-(2,6-dimethylphenyl)-2-{4-[2-hydroxy-3-(2-methoxyphenoxy) propyl]piperazin-1-yl}acetamide, J. Mol. Struct., 1171 (2018) 268-278.
- [188] N. Sudharsana, V. Krishnakumar, R. Nagalakshmi, Bis (3-methoxy-4-hydroxy-benzaldehyde-2,4,6-trinitrophenol) organic cocrystal: Synthesis and physicochemical properties. Eur. Phys. J. Plus.,131 (2016) 348.
- [189] Y. Megrouss, F.T. Baara, N. Boukabcha, A. Chouaih, A. Hatzidimitriou, A. Djafri, F. Hamzaoui, Synthesis, X-ray structure determination and related physical properties of thiazolidinone derivative by DFT quantum chemical method, Acta Chim. Slov., 66 (2019) 490–500.
- [190] M. El, M. Mekhzoum, K. El Bourakadi, E.M. Essassi, A. Qaiss, R. Bouhfid, Synthesis, crystal and DFT studies of N-(carboxyethyl)-2-methylbenzothiazolium bromide, J. Mol. Struct., 1193 (2019) 303-309.
- [191] R.S. Mulliken, A new electroaffinity scale; together with data on valence states and on valence ionization potentials and electron affinities, J. Chem. Phys., 2 (11) (1934) 782-793.
- [192] Y.S. Mary, H.T. Varghese, C.Y. Panicker, M. Girisha, B.K. Sagar, H.S. Yathirajan, A.A. Al-Saadi, C. VanAlsenoy, Vibrational spectra, HOMO, LUMO, NBO, MEP analysis and molecular docking study of 2,2-diphenyl-4-(piperidine-1-yl) butanamide, Spectrochim. Acta., 150 (2015) 543–556.
- [193] V. Balachandran, V. Karunakaran, Quantum mechanical study of the structure and vibrational spectroscopic (FT-IR and FT-Raman), first-order hyperpolarizability, NBO and HOMO-LUMO studies of 4-bromo-3-nitroanisole, Spectrochim. Acta Part A., 106 (2013) 284-298.
- [194] R. Chauvin, C. Lepetit, B. Silvi, E. Alikhani, Applications of Topological Methods in Molecular Chemistry, Springer International Publishing, 22(2016).
- [195] M. Balouiri, M. Sadiki, & S. K Ibnsouda, Methods for in vitro evaluating antimicrobial activity: A review, J. Pharm. Anal., 6 (2) (2016) 71–79.
- [196] A. Gomtsyan, Heterocycles in drugs and drug discovery, Chem. Heterocycl. Compd., 48 (2012) 7-10.

- [197] Mahima Bhat, P. M. Gurubasavaraja Swamy, Boja Poojary, B. C.Revanasiddappa, M. Vijay Kumar, Vasantha Kumar, Biological evaluation and in silico molecular docking study of a new series of thiazol-2-yl-hydrazone conglomerates, Research on ChemicalIntermediates, 44 (2018) 2779–2805.
- [198] M.J. Nanjan, M. Mohammed, B.R. Prashantha Kumar, M.J.N. Chandrasekar, Thiazolidinediones as antidiabetic agents: a critical review, Bio.org. Chem., 77 (2018) 548–567.
- [199] Karmen Szabo, Rosanna Maccari, Rosaria Ottana, GyongyiGyemant, Extending the investigation of 4-thiazolidinone derivatives as potential multi-target ligands of enzymes involved in diabetes mellitus and its long-term complications: A study with pancreatic α-amylase, Carbohydrate Research, 499 (2021) 108220.
- [200] N.S. El-Gohary, M.I. Shaaban, Design, Synthesis, antimicrobial, antiquorumsensing and antitumor evaluation of new series of pyrazolopyridine derivatives, Eur. J. Med. Chem., 157 (2018) 729-742.
- [201] N. Marepu, S. Yeturu, M. Pal, 1,2,3-Triazole fused with pyridine/pyrimidine asnew template for antimicrobial agents: regioselective synthesis and identification of potent N-heteroarenes, Bio. org. Med. Chem. Lett., 28 (2018) 3302-3306.
- [202] Deepika Sharma, Sanjiv Kumar, Balasubramanian Narasimhan, Kalavathy Ramasamy, Siong Meng Lim, Syed Adnan Ali Shah, Vasudevan Mani, 4-(4-Bromophenyl)-thiazol-2-amine derivatives: synthesis, biological activity and molecular docking study with ADME profile, BMC Chem., 60 (2019) 1-16.
- [203] V. Krishnakumar, V. Balachandran, Structures and vibrational frequencies of 2-hydroxy-3-methoxy-5-nitrobenzaldehyde and 2-methoxy-1-naphthaldehyde based on density functional theory calculations, Spectrochim. Acta A., 63 (2006) 464–476.
- [204] A.M.Fatmah. Al-Omary, Asha Raj, K. Raju, C. Yohannan Panicker, Nadia G. Haress, Ali A. El-Emam, Mahmoud B. El-Ashmawy, Abdulaziz A. Al-Saadi, Christian Van Alsenoy, Javeed Ahmad War, Spectroscopic investigation (FT-IR, FT-Raman), HOMO–LUMO, NBO analysis and molecular docking studyof 2-[(4-chlorobenzyl)sulfanyl]-4-(2-methylpropyl)-6-[3-trifluoromethyl)-anilino] pyrimidine-5-carbonitrile, a potential chemotherapeutic agent,

- Spectrochimica Acta Part A: Molecular and Biomolecular Spectroscopy, 136 (2015) 520–533
- [205] P. Ladwa, G. Dhuda, B. Godhaniya, J.J. Modha, Synthesis of thiazolylazomethine substituted pyrazole derivative using conventional and one pot multicomponent synthetic routes, 134(2) (2019) 242-257.
- [206] S. Muthu, E. Elamuruguporchelvi, Anitha Varghese, DFT electronic structure calculations, spectroscopic studies, and normalcoordinate analysis of 2-[(5-nitro-1,3-thiazol-2-yl)carbamoyl]phenylacetate, Spectrochimica Acta Part A: Molecular andBiomolecular Spectroscopy 138 (2015) 743–752.
- [207] G.Varsanyi, Assignments of Vibrational Spectra of Seven Hundred Benzenen Derivatives, Wiley, New York, 1974.
- [208] S.K. Kurtz, T.T. Perry, A Powder Technique for the Evaluation of Nonlinear Optical Materials.J. Appl. Phys. 39 (1968) 3798–3813.
- [209] M. Gussoni, C. Castiglioni, Infrared intensities. Use of the CH-stretching band intensity as a tool for evaluating the acidity of hydrogen atoms in hydrocarbons, J. Mol. Struct. 521 (2000) 1–8.
- [210] V. Balachandran, G. Santhi, V. Karpagam, A. Lakshmi, DFT computation and spectroscopic analysis of N-(p-methoxybenzylidene) aniline, a potentially useful NLO material, J. Mol. Struct. 1047 (2013) 249-261.
- [211] K.B. Benzon, H.T. Varghese, C.Y. Panicker, K. Pradhan, B. Tiwary, A.K. Nanda, C. Van Alsenoy, Spectroscopic and theoretical characterization of 2-(4-methoxyphenyl)- 4,5-dimethyl-1H-imidazole 3-oxide, Spectrochimica Acta Part A: Molecular and Biomolecular Spectroscopy 151 (2015) 965–979.
- [212] I.C.H. Castaneda, J.L. Jios, O.E. Piro, G.E. Tobon, C.O.D. Vedova, Spectroscopic (FT-IR, FT-Raman), first order hyperpolarizability, NBO analysis, HOMO and LUMO analysis of 2,4-bis(2-methoxyphenyl)-1-phenylanthracene-9,10-dione by ab initio HF and density functional methods, J. Mol. Struct. 842 (2007) 46–54.
- [213] B. Venkkatram Reddy, G. Ramana Rao, Molecular structure, NBO analysis of the hydrogen-bonded interactions, spectroscopic (FT–IR, FT–Raman), drug likeness and molecular docking of the novel anti COVID-2 molecule (2E)-N-methyl-2-[(4-oxo-4H-chromen-3-yl)methylidene]-hydrazinecarbothioamide (Dimer) quantum chemical approach, Vib. Spectrosc. 6 (1994) 231–250.

- [214] V. Krishnakumar, R. John Xavier, FT Raman and FT-IR Spectral Studies of 3-Mercapto-1,2,4-Triazole, Spectrochim. Acta 61A (2005) 253–258.
- [215] M. Gussoni, C. Castiglioni, G. Zerbi, Nonlinear optical and vibrational properties of conjugated polyaromatic molecules, J. Phys. Chem. 88 (1994) 600–604.
- [216] V. KrishnaKumar, D. Barathi, R. Mathammal, Quantum mechanical study of the structure and spectroscopic (FT-IR, FT-Raman, 13C, and 1H) and HOMO–LUMO analysis of 2,4-dimethoxy benzaldehyde(DMBA) and 4-methoxy-3-methyl benzaldehyde (MMBA), Journal of Molecular Structure 1035 (2013) 145–156.
- [217] E.F. Mooney, The infra-red spectra of chloro- and bromobenzene derivatives—II. Nitrobenzenes, Spectrochim. Acta., 20 (1964) 1021–1032.
- [218] E.F. Mooney, The infrared spectra of chloro- and bromobenzene derivatives—I: Anisoles and phenetoles, Spectrochim. Acta., 19 (6) (1963) 877–887.
- [219] I. Fleming, Frontier Orbitals and Organic Chemical Reactions, John Wiley and Sons, New York, 1976.
- [220] T. Karakurt, M. Dincer, A. Cetin, M. Sekerci, Molecular structure and vibrational bands and chemical shift assignments of 4-allyl-5-(2-hydroxyphenyl)-2,4-dihydro-3H-1,2,4-triazole-3-thione by DFT and ab initio HF calculations, Spectrochim. Acta 77A (2010) 189–198.
- [221] Madiha Kazmi, Aliya Ibrar, Hafiz Saqib Ali, Mehreen Ghufran, Abdul Wadood, Ulrich Fleorke, Jim Simpson, Aamer Saeed, Antonio Frontera, Imtiaz Khan, A combined experimental and theoretical analysis of the solid-state supramolecular self-assembly of N-(2,4-dichlorophenyl)-1-naphthamide: synthesis, anticholinesterase potential and molecular docking analysis, J. Mol.Struct. 1197 (2019) 458-470.
- [222] C. Sivakumar, B. Revathi, V. Balachandran, B.Narayana, Vinutha V. Salian, N. Shanmugapriya, K. Vanasundari, Molecular structure, spectroscopic, quantum chemical, topological, molecular docking and antimicrobial activity of 3-(4-Chlorophenyl)-5-[4-propan-2-yl) phenyl-4, 5-dihydro-1 *H* -pyrazol-1-yl] (pyridin-4-yl) methanone, J. Mol. Struct, 1244 (2021) 129-286.
- [223] V. Karunakaran, V. Balachandran, FT-IR, FT-Raman spectra, NBO, HOMO– LUMO and thermodynamic functions of 4-chloro-3-nitrobenzaldehyde based on

- ab initio HF and DFT calculations, Spectrochimica Acta Part A: Molecular and BiomolecularSpectroscopy 98 (2012) 229–239.
- [224] D. Shoba, S. Periandy, S. Boomadevi, S. Ramalingam, E. Fereduni, FT-IR, FT-Raman,UV, NMR spectra, molecular structure, ESP, NBO and HOMO–LUMO investigation of2-methylpyridine 1-oxide: A combined experimental and DFT study, Spectrochim. Acta A.,118 (2014)438-447.
- [225] Michal Michalski, Agnieszka J.Gordon, Slawomir, Berski, Topological analysis of the electronlocalization function (ELF) applied to the electronic structure of oxaziridine: the nature of N-O bond, Structural Chemistry, 30(2019) 2181-2189.
- [226] N. Klose, K. Niedbolla, K. Schwartz, I. Bottcher, 4,5Bis(4-methoxyphenyl)2-cycloalkylthioimiddazole mitantiphlogistischerWirkung, Arch.Pharm. 316 (1983) 941-951.
- [227] R.K.Satsangi,S.M. Zaidi,V.C. Misra, 1-(4-substituted-thiazol-20yl) hydantoins as anti-inflammatory and CNS-active agents, Pharmazie 38 (1983) 341-342.
- [228] E. Daniel Lynch, Ian McClenaghan, E. Mark Light, L. Simon Coles, The Hydrogenbonding networks of 2- amino-4-phenyl-1,3-thi zolederivatives, Cryst. Eng. 5 (2002) 123-136.
- [229] Muhammad Adeel, A.C.Ataualpa Braga, Muhammad Nawaz Tahir, FazalHaq, Muhammad Khalid, Mohammad A. Halim, J. Mol. Struct. 1131 (2017) 136-148.
- [230] Jain, Shweta, Pattnaik, satyanarayana, Pathak, Devender, Anticancer potential of Thiazole derivatives: A retrospective review, 18 (2018) 640-655.
- [231] V. Arjunan, R. Santhanam, T. Ravi, H, Rosi, S. Mohan, Synthesis and characterization of an anticoagulant 4-hydroxy-1-thiocoumarin by FTIR, FT-Raman, NMR, DFT, NBO and HOMO–LUMO analysis, *Spectrochim. Acta Part A* 1037(2013) 305-316.
- [232] K. Rastogi, M.A. Palafox, R.P. Tanwar, L. Mittal, 3,5-Difluorobenzonitrile: ab initio calculations, FTIR and Raman spectra, Spectrochimica Acta A., 58 (2002) 1987-2004.
- [233] M. Dien, Introduction to Modern Vibrational Spectroscopy, Wiley, New York,1993.

- [234] P.B. Nagabalasubramanian, S. Periandy, S. Mohan, Synthesis and Characterization of Cr(III) & Fe(II) Bis (2-Methoxybenzylidene) Biphenyl-4,4'-Diamine Complexes, Spectrochimica Acta A 74 (2009) 277-280.
- [235] J.H.S. Green, D.J. Harison, W. Kynoston, Vibrational spectra of benzene derivatives—XII 1,2,4-trisubstituted compounds Spectrochimica Acta A 27 (1971) 807-815.
- [236] K. Bahgat, N. Jasem, Talaat El-Emary, Theoretical and experimental investigations on the structure and vibrational spectra of 6-amino-3-methyl-1-phenyl-1H-pyrazolo-[3,4-b]pyridine-5-carboxylic acid and 6,7-dihydro-3-methyl-6-oxo-1-phenyl-1H-pyrazolo[3,4-b]pyridine-5-carboni trile, J. Serb. Chem. Soc. 74 (2009) 555.
- [237] R. Ditchfield, Molecular Orbital Theory of Magnetic Shielding and Magnetic Susceptibility, J. Chem. Phys. 56 (1972) 5688.
- [238] O. Hernandez, K.S.Knight, W. Van Beek, A. Boucekkine, A. Boudjada, W. Paulus, J. Meinnel, Phases II and IV of 1,3,5-trichloro-2,4,6-trimethylbenzene: Ab initio crystal structure determination by high-resolution powder diffraction, J. Mol. Struct. 791 (2006) 41-52.
- [239] V. Krishnakumar, N. Surumbarkuzhali, S. Muthunatesan, Scaled quantum chemical studies on the vibrational spectra of 4-bromo benzonitrile, Spectrochim. Acta 71 (2009) 1810–1813.
- [240] B. Amul, S. Muthu, M. Raja, S. Sevvanthi, Spectral, DFT and molecular docking investigations on Etodolac J. Mol. Struct. 791 (15) (2020) 1248040.
- [241] M.D. Prabhu, T.Yenagi, Vinayak.Tonannavar, XRD structure and vibrational analysis of DL-β-Leucine, as aided by DFT tetramer model and characterized by NBO, AIM and NCI calculations, 1218(15) (2020) 128495.
- [242] A.J. Bowles, W.O. George, D.B. Cunliffe-Jones, Conformations of some αβ-unsaturated carbonyl compounds. Part II. Infrared and Raman spectra of methyl and ethyl acrylates and trans-crotonates, J. Chem. Soc. B, (1971) 01-02.
- [243] M.C. Gupta, Atomic and Molecular Spectroscopy, New Age International Private Limited, Publishers, New Delhi, (2001).

- [244] R. Mathammal, N. Jayamani, and N. Geetha, Molecular Structure, NMR, HOMO, LUMO, and Vibrational Analysis of O-Anisic Acid and Anisic Acid Based on DFT Calculations (2013).
- [245] I. Rozas, I. Alkorta, J. Elguero, Behavior of Ylides Containing N, O, and C Atoms as Hydrogen Bond Acceptors, J. Am. Chem. Soc. 122 (2000) 11154–11161.
- [246] H. Jacobsen, Localized-orbital locator (LOL) profiles of chemical bonding, Can. J. Chem. 86 (2008) 695–702.
- [247] J. Poater, M. Duran, M. Sola, B. Silvi, Theoretical Evaluation of Electron Delocalization in Aromatic Molecules by Means of Atoms in Molecules (AIM) and Electron Localization Function (ELF) Topological Approaches, Chem. Rev. 105 (2005) 3911–3947.
- [248] D. Aruldas, I. Hubert Joe, S.D.D. Roy, S. Balachandran, DFT computation and experimental analysis of vibrational and electronic spectra of phenoxy acetic acid herbicides, Spectrochim. Acta A., 108 (2013) 89.

金

Sources

Title	~	Enter titl	le			Fir	nd sources			
Title: Heliyon x										
which provides an i calculation of CiteS	he Ci indic core, value	teScore me ation of reso , as well as r es have beer	earch impact, etroactively fo	ensure a more robust, earlier. The updated r r all previous CiteSco I are no longer availal	nethodology will re years (ie. 2018	be applied to	the		-	
ter refine list			1 result		<u>.</u>	Download S	Scopus Source List	(i) Learn r	nore about Sc	opus Source L
			☐ All ∨	Export to Excel	Save to sour	ce list		View met	rics for year:	2020
isplay options		^	Sou	rce title ↓		CiteScore ↓	Highest percentile ↓	Citations 2017-20 ↓	Documents 2017-20 ↓	% Cited ↓
Display only Open Access journals				Ones Assess		2.1	750/	11 427	E 430	F2
unts for 4-year timeframe			Ш г неп	yon <i>Open Access</i>		2.1	75% 27/110	11,427	5,410	53
No minimum selected										
Minimum citations		*	∧ Тор	of page						
Minimum documents										
escore highest quartile										
Show only titles in top 10 percent										
1st quartile										
2nd quartile										
3rd quartile										
4th quartile										
eurce type		^								
Journals										
Book Series										
Conference Proceedings										
Trade Publications				elle .	. Dron	ng	22		Thh	1+1/22
oply Clear filters	1	ll	2	ASS	r. K. RENU	KA DEV	I			31131

Dr. V. BALACHANDRAN Assistant Professor Research Department of Physics A. A. Government Arst College Wusirt Tirchirappalli - 621 211

PG & Research Dept. of Physics Govt. Arts College for Women (A) Pudukkottai - 622 001.



Contents lists available at ScienceDirect

Heliyon

journal homepage: www.cell.com/heliyon



Research article

Quantum chemical calculation, performance of selective antimicrobial activity using molecular docking analysis, RDG and experimental (FT-IR, FT-Raman) investigation of 4-[{2-[3-(4-chlorophenyl)-5-(4-propan-2-yl) phenyl)-4, 5-dihydro- 1H- pyrazol-1-yl]-4-oxo-1, 3- thiazol-5(4H)-ylidene} methyl] benzonitrile



N. Shanmugapriya ^a, V. Balachandran ^{a,*}, B. Revathi ^a, B. Narayana ^b, Vinutha V. Salian ^b, K. Vanasundari ^a, C. Sivakumar ^a

ARTICLE INFO

Keywords:
Thiazole
DFT
RDG
ELF
Docking
Antimicrobial activity

ABSTRACT

The research received a great deal of worldwide attention due to the nature of interpretation before the experimental process. Based on the systematic process the structure of thiazole -pyrazole compound 4-[{2-[3-(4-chlorophenyl)-5-(4-propan-2-yl) phenyl)-4, 5-dihydro- 1H- pyrazol-1-yl]-4-oxo-1, 3- thiazol-5(4H)-ylidene} methyl] benzonitrile [CPTBN] was investigated. In the first level, the spectral statistics on experimental FT-IR and FT-Raman was reported. At the next level, geometrical parameters was theoretically acquired from density functional theory (DFT) using B3LPY/6-31G and 6-311G basis set. The computed Wavenumber were collected and compared with the experimental data. The vibrational modes were interpreted in terms of potential energy distribution (PED) results. The FMO, MEP, and NBO analysis further validated the electrophilic and nucleophilic interaction in the molecular systems. Two grams-positive bacteria: staphylococcus aureus, Bacillus subtilis and two gram-negative bacteria: Esherichia coli, Pseudomonas aeruginosa was performed for antibacterial activity. Two fungal strain Candida albicans and Aspergillus Niger was carried out against a ligand using anti-fungal activity. The molecular docking analysis explores the antimicrobial and selective potential inhibitory nature of the binding molecule. Besides, RDG and ELF analysis were also performed to show the nature of interactions between the molecule.

1. Introduction

Recently, the investigation of vibrations of substituent azoles compounds was an incredible arrangement of enthusiasm among the spectroscopists because of their physical and chemical properties. Thiazole is one of the most intensively studied classes of aromatic amalgamation that was initially outlined by Hantzsch and Weber in 1887 [1]. It belongs to the family of azoles, the heterocyclic five-membered compounds containing sulphur and nitrogen atoms at 1,3 positions in their fragrant ring structure [2]. Thiazole core occupies a very important position among the heterocyclic compounds which is naturally bioactive. Attached to various active elements like pyrazole, phenyl, nitrile contains compounds were synthesized in a laboratory environment and were eventually

introduced to be used to treat various diseases and varieties of industrial purposes such as fungicides, dye, and paint production [3, 4]. Consistently, the active elements nitrile are a common choice as both a chemical and physical barrier to these hazards, especially nitrile gloves were useful to a huge number of human services and industry laborers who are exposed to chemical and organic risks [5]. Benzonitrile often plays a key role in the inhibition of hydrogen absorption [6]. The present work involves the study of comprehensive molecular geometry and vibrational modes of CPTBN using quantum chemical computations. It has a molecular formula $C_{29}H_{23}ClN_4OS$. The global reactivity descriptors like highest occupied molecular orbital (HOMO), lowest unoccupied molecular orbital (LUMO), and molecular electrostatic potential (MEP) analysis were interpreted with the theoretical value. The energy gap values (ΔE)

E-mail address: brsbala@rediffimail.com (V. Balachandran).

a Centre for Research, Department of Physics, Arignar Anna Government Arts College (Affiliated to Bharathidasan University), Tiruchirappalli, Musiri, 621 211, India

b Department of Studies in Chemistry, Mangalore University, Mangalagangotri, 574 199, India

^{*} Corresponding author.

have been calculated using B3LYP/6-31G and 6-311G basis sets and reported as a result of the molecular transitions. The investigation of natural bond orbital (NBO) provides information on the chemical features such as intra and intermolecular charge transfer, second-order perturbation characteristic relationships between the Lewis (donor) and non-Lewis (acceptor) [6, 7]. The title molecule's reduced density gradient (RDG) and electron localization function (ELF) were investigated using Multiwfn software. The disc diffusion method was used to successfully evaluate anti-microbial activity of the compound at 25, 50, 75, and 100 μg/ml concentration levels with established bacterial and fungus strains. To explore the potential biological activity of the thiazole (CPTBN) compound, few studies included in the molecular docking analysis and report on the drug-like behaviors of the title compound. The anti-microbial, monoclonal antibodies, Nitric oxide synthase inhibitor, and Staphylococcal protein A protein structural activity observed were consistent with the results of docking pose providing key insight of selective antimicrobial and medical potential inhibitors. The above findings are opening up new avenues of medicinal chemistry and important for clinical manifestation.

2. Experimental details

The structure of CPTBN along with the synthesis procedure was screened by Salian et al. [8] intrinsically and were used for spectral measurements. For the compound characterization,

- Fourier transform infrared spectrum was recorded between 4000-0 cm⁻¹ using a Perkin Elmer spectrometer, which was calibrated using an MCT Mid-IR range detector with KBr (potassium bromide) pellets technique.
- FT-Raman spectrum were obtained within the interval of 3500-0 cm⁻¹ using a Bruker RFS27 the 1064 nm line of a Nd: YAG laser device for excitation controlled at 200 mW power. At room temperature, the spectrum was recorded at a scanning speed of 10 cm⁻¹ and a spectral resolution of 1.0 cm⁻¹.
- Using the disc diffusion method, the title compound with four concentrations of 25, 50, 75, and 100 μg/ml in distilled DMSO was prepared and tested against antimicrobial strains were maintained on agar medium at 4 °C. Antimicrobial cultures such as Staphylococcus aureus, Bacillus subtilis, Esherichia coli, Pseudomonas aeruginosa, Candida albicans and Aspergillus Nige were tested.

3. Computational details

In the present work, geometry optimizations and electronic structure calculation of the CPTBN were first performed for B3LYP functional with 6-31G and 6-311G basis sets using the Gaussian 09 program [9]. The correlation function is used to predict the molecular structure of the CPTBN. The potential energy distribution (PEDs) is done with the help of (VEDA) program [10]. GAUSSVIEW program [11] provided a visual presentation of vibrational modes.

Screening the calculations exposed that, the density functional theory (DFT) computations with the promising vibrational properties, molecular geometry, and orbital energy of CPTBN. Besides natural bond orbital (NBO) calculations were carried out using the NBO program implemented in Gaussian 09 [12]. Multi-wfn software provides a route for a consistent description of interactions between the atoms in terms of the topological properties of the electron density $\rho(r)$. Electron localization function (ELF) map and Reduced Density Gradient (RDG) were calculated using the Multi-wfn program [13]. Molecular docking studies were performed with the help of an Auto dock [14] software. Discovery Studio Visualizer 4.1 [15] and Pymol software [16].

4. Results and discussions

4.1. Molecular geometry

The density functional theory is one of the most reliable computational approaches for the theoretical investigation of the structure of the molecule. The Gaussian 09 shows an optimized molecular form of CPTBN computed by B3LYP/6-31G, B3LYP/6-311G, and visualized through the Gauss view program shown in Figure 1. The optimized bond lengths and angles of the title compound are tabulated in Tables 1 and 2, respectively. The optimized structure is found to be with C1 point group symmetry having its ground state energy of 2271.46 a.u with a dipole moment of 8.9529 Debye. Elaboration of the collected data is as follows.

The optimized geometrical structure of the title molecule benzonitrile substituent in the thiazole ring system, chain with pyrazol bounds by two phenyl rings (one is chlorophenyl - PhI and the other is 4-(Propan-2-yl) phenyl - PhII. Normally, the C-C bond lengths of aromatic rings formed by the phenyl ring are greater than range 1.3900 Å, although the computed value falls in the range $C_4-C_6 = 1.4102/1.4120 \text{ Å}, C_9-C_{11} =$ 1.3933/1.3964 Å, C_5 – $C_7 = 1.3959/1.3977$ Å. for PhI and C_{14} – $C_{15} =$ $1.4038/1.405\text{Å}, C_{16}-C_{19} = 1.3964/1.3982\text{Å}, C_{17}-C_{21} = 1.4056/1.4076$ Å for PhII. The title compound is somewhat regular and the spread of C-C bond distance is 1.3900-1.5500 Å in (phenyl ring I) PhI and 1.3900–1.4500 Å in (phenyl ring II) PhII, which is similar to the report by Parveen et al. [17]. The computed bond lengths of the C=C double bond values are $C_4-C_5 = 1.4067/1.4083\text{Å}$, $C_6-C_9 = 1.3907/1.3931\text{Å}$, C_7-C_{11} = 1.3886/1.3922Å for PhI and C_{14} – C_{16} = 1.3981/1.4009Å, C_{15} – C_{17} = 1.3934/1.3957Å, C_{19} – $C_{21} = 1.4011/1.4036\text{Å}$ for PhII. This observation reveals that the C-C atoms in both rings are between the conventional C-C single and C=C double bond lengths, indicating that the electron density is conjugated on all rings. The outer shell carbon-hydrogen bond length values are experimentally falling in the range of 0.90 Å to 1.09 Å, whereas the calculated C-H (ring) and C-H (methyl) values are 1.0800 Å and 1.0900 Å, respectively. The C-H length in both phenyl rings is found almost equal to around 1.08 Å, is very close to the experimental value 1.09 Å, which indicates that C-H bond lengths remain unaffected by the substitution in rings. Generally, the thiazole ring has a difference in bond length is due to the presence of a sulphur and nitrogen atom. The theoretical value of the C₃₉-S₄₁ bond length is 1.8653/1.8592Å and the experimental value is found to be 1.86 Å [3]. The $C_{40} = O_{44}$ carbonyl moiety present in thiazole has a double bond character, as evidenced by the compound's estimated bond length (DFT) of 1.2450/1.2472 Å. The shortening of these C-N bonds reveals the effect of resonance in this part of the molecule. It attempts to draw the electron density of the neighbouring atoms which as a result move closer together to share the electrons more easily. The literature value of C-N, C=N, C=N bond length (XRD) is 1.3000 Å, 1.31 Å and 1.1600 Å [17]. In the current studies $C_1-N_{24} = 1.3046/1.3061\text{Å}, C_2-N_{25} = 1.5079/1.5097\text{Å}$ present in pyrazole ring, $C_{42} = N_{43} = 1.3051/1.3059$ Å present in thiazole ring, and C_{57} $\equiv N_{58} = 1.1682/1.1748 \text{Å}$ present in benzonitrile ring indicating that π -electron in the molecules are delocalized in the C–C of the molecule which is similar in reported by Mustafa Er et al. [18]. The chlorine is extremely electronegative, it strives to get more electron density, and the computed value is 1.825 Å, that is found near the phenyl ring PhI. The experimental values are taken from similar C-Cl bond length is observed in 1.8200 Å by Vanasundari et al. [19]. The magnitude of the length N-N bond is described in 1.38 Å assigned by Priyanka Singh et al. [20] and is found in the center to be 1.3963/1.3946Å for the CPTBN molecule. The angle formed between two adjacent bonds shows the internal bond angles $N_{25}\text{--}C_{42}\text{--}N_{43},\,C_1\text{--}N_{24}\text{--}N_{25},\,C_{39}\text{--}C_{40}\text{--}O_{44}$ and $N_{43}\text{--}C_{40}\text{--}O_{44}$ are found around the range to be 123°, 108°, 124°, and 122° in the CPTBN respectively. This shortest bond angle is formed between thiazol is C_{39} - S_{41} - C_{42} in 86°.

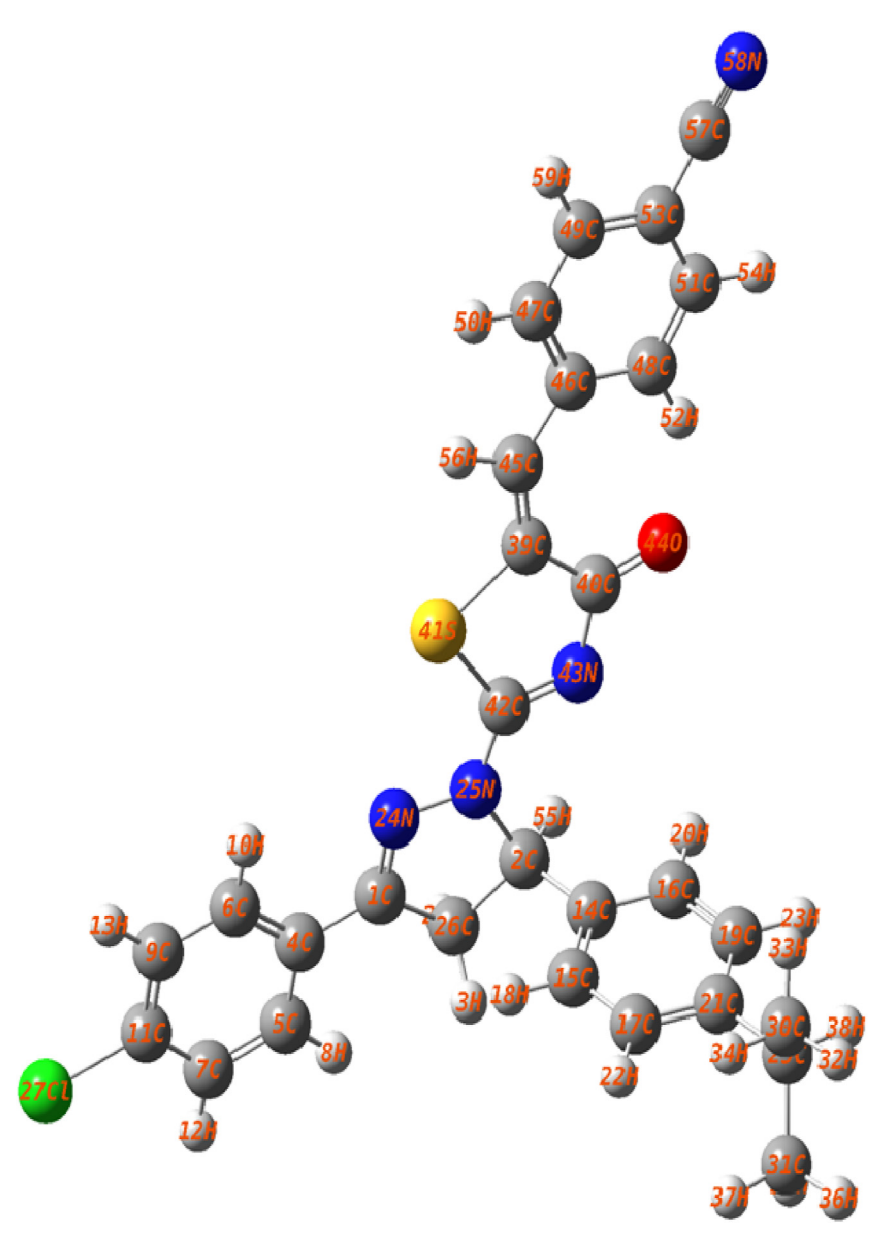


Figure 1. Optimized structure of CPTBN using B3LYP/6-311G basis set.

4.2. Vibrational assignments

The main aim of this vibrational calculation is to provide a clear interpretation of both experimental and theoretical results. The experimental calculation was carried out using IR and Raman (Figures 2 and 3). Comparative theoretical calculations were performed using the B3LYP method with 6–31 G and 6-311G basis sets were reported in Table 3. Generally, the vibrational modes of a compound with N atoms are more complex, with 3N 5 vibrational modes for a linear compound and 3N 6 modes for a nonlinear compound. On specifying three rotational and one translational degrees of freedom (3N-6) of CPTBN under (C1) point group symmetry has 59 atoms and 171 fundamental vibrational modes. Based on the optimized structure, the detailed spectral information is interpreted as follows.

4.2.1. C– H vibrations

The spectrum of a compound represents its energy absorption pattern is represented by the regions. In the present study, there are three different benzene rings attached to the combination of thiazole with pyrazol. The occurrence of benzene C–H stretching vibration extends

often above 3000 cm⁻¹ for aromatic composition and less than 3000 cm⁻¹ for non-aromatic composition. In the FT-IR, FT-Raman spectra, aromatic compounds predominantly have a C-H vibration of 3000-3100 cm⁻¹. The essence and location of the replacement are affected in this region by the band. Because of their high polarization, these C-H detention modes typically appear with Raman strength. A spectrum of FT-Raman, its aromatic stretching mode C-H was used for the observation of the observed band 3074 cm⁻¹ and 3053 cm⁻¹ by Sathish et al. [21]. In the case of the title compound, it exhibits multiple weak band's shoulders on the stronger C- H stretching vibration in the region 3067 cm^{-1} , 3013 cm^{-1} , 2957 cm^{-1} and 2868 cm^{-1} vibrational magnitude by B3LYP/6-311G. Normally, the C-H in-plane vibrational bending mode occurs in the region 1530- $1000~{\rm cm}^{-1}$. Spectrum of C–H in-plane vibrational bending mode observed at 1424 cm⁻¹ (w), 1396 cm⁻¹ (ms), and 1114 cm⁻¹ (ms) in FT-IR spectrum and 1285 cm⁻¹ (ms), 1251 cm⁻¹ (s), 1173 cm⁻¹ (ms) in FT-Raman spectrum, the computed wavenumbers for this mode were coincident with 1429, 1394, 1290, 1251, 1120 cm⁻¹ for B3LYP/6-31G and 1425, 1395, 1286, 1250, 1116 cm⁻¹ for B3LYP/6-311G. The out-of-plane C-H bending mode of the phenyl ring are observed at 804 cm⁻¹(IR), 928, 832, 806 cm⁻¹ (FT-Raman) and

Table 1. Optimized structural parameters (bond length) of CPTBN calculated by DFT/B3LYP method with 6-31G and 6-311G basis sets.

S.No	Bond Length (Å)	B3LYP/6-31G	B3LYP/6-311G	S.No	Bond Length (Å)	B3LYP/6-31G	B3LYP/6-3110
1	C1-C4	1.4607	1.4604	33	C26-H28	1.0923	1.0968
2	C1-N24	1.3046	1.3061	34	C29-C30	1.5450	1.5465
3	C1-C26	1.5198	1.5219	35	C29-C3I	1.5446	1.5461
4	C2-C14	1.5176	1.5182	36	C29-H38	1.0949	1.0993
5	C2-N25	1.5079	1.5097	37	C30-H32	1.0923	1.0965
6	C2-C26	1.5552	1.5570	38	C30-H33	1.0910	1.0953
7	C2-H55	1.0875	1.0918	39	C30-H34	1.0925	1.0968
8	H3-C26	1.089	1.0934	40	C31-H35	1.0913	1.0956
9	C4-C5	1.4067	1.4083	41	C31-H36	1.0922	1.0964
10	C4-C6	1.4102	1.4120	42	C31-H37	1.0925	1.0968
11	C5-C7	1.3959	1.3977	43	C39-C40	1.5001	1.5028
12	C5-H8	1.0810	1.0844	44	C39-S41	1.8653	1.8592
13	C6-C9	1.3907	1.3931	45	C39-C45	1.3535	1.3576
14	C6-H10	1.0799	1.0835	46	C40-N43	1.4008	1.4006
15	C7-C11	1.3886	1.3922	47	C40-O44	1.2450	1.2472
16	C7-H12	1.0792	1.0828	48	S41-C42	1.8449	1.8442
17	C9-C11	1.3933	1.3964	49	C42-N43	1.3051	1.3059
18	C9-H13	1.0793	1.0829	50	C45-C46	1.4644	1.4649
19	C11-CL27	1.8250	1.8222	51	C45-H56	1.0864	1.0896
20	C14-C15	1.4038	1.4059	52	C46-C47	1.4165	1.4184
21	C14-C16	1.3981	1.4009	53	C46-C48	1.4123	1.4146
22	C15-C17	1.3934	1.3957	54	C47-C49	1.3868	1.389
23	C15-H18	1.0832	1.0866	55	C47-H50	1.0824	1.0858
24	C16-C19	1.3964	1.3982	56	C48-C51	1.3905	1.3927
25	C16-H20	1.0814	1.0850	57	C48-H52	1.0776	1.0815
26	C17-C21	1.4056	1.4076	58	C49-C53	1.4073	1.4098
27	C17-H22	1.0823	1.0858	59	C49-H59	1.0806	1.084
28	C19-C21	1.4011	1.4036	60	C51-C53	1.4067	1.4092
29	C19-H23	1.0827	1.0861	61	C51-H54	1.0807	1.0842
30	C21-C29	1.5251	1.5260	62	C53-C57	1.4301	1.4303
31	N24-N25	1.3963	1.3946	63	C57-N58	1.1682	1.1748
32	N25-C42	1.3427	1.3433				

computed values in the range 932- $810~\rm{cm}^{-1}$ (DFT) by Begum et al. [22]. The correlated scale vibrations observed at wavenumbers 896 (w), 829 (ms), $811~\rm{cm}^{-1}$ (w) (FT-IR) and $945~\rm{cm}^{-1}$ (m) (FT-Raman) are coincident with 933, 900, 833, $814~\rm{cm}^{-1}$ for B3LYP/6-31G and 932, 898, 829, 810 cm $^{-1}$ for B3LYP/6-311G.

4.2.2. Methyl group vibrations

For the assignments of benzene ring has a methyl CH₃ group was expected in nine fundamental modes, namely symmetrical stretch, asymmetrical stretch, symmetric deformations, asymmetrical deformations, in-plane (δ), out-of-plane (γ), in-plane rocking (δ rock), out-of-plane rocking (γ rock), and twisting bending (Γ CH₃) [23]. From the structure of the title molecule possesses two CH₃ (5-(4-Propan-2-yl) phenyl)) group substitutions in the pyrazole ring chain. The symmetric and asymmetric methyl group stretching band can be observed in the region 2942-2879 cm⁻¹.

Naturally, the CH $_3$ group related to electron-donating substitutions that bind to the same ring systems. These vibrations attain amplitude of 3000-2840 cm $^{-1}$. The CH $_3$ asymmetric stretching vibration is recorded in the FT-IRs spectrum at 2929 (w) cm $^{-1}$ FT-Raman spectrum at 2947 (w) cm $^{-1}$, 2933 (w) cm $^{-1}$. Theoretically computed mode having wavenumber at 2952, 2936, 2934 cm $^{-1}$ for B3LYP/6-31G and 2948, 2932, 2930 cm $^{-1}$ for B3LYP/6-31G. The aromatic ring has a weak symmetric stretching vibration value that appears in the region 2903, 2881 cm $^{-1}$ for B3LYP/6-31G and 2900, 2879 cm $^{-1}$ for B3LYP/6-311G. The in-plane vibrations ($\delta_{\rm iph}$) bending mode has been calculated at 1390, 1385, 998 cm $^{-1}$ (6-31G), and

1389, 1382, 998 cm $^{-1}$ (6-311G). The out-of-plane bending vibrations of title compound occur in medium peak (γ_{opb}) 1409 (ms) cm $^{-1}$ FT-Raman is assigned and deformation is predicted at a range (γ_{opb}) 1420, 1415, 1025 cm $^{-1}$ for B3LYP/6-31G and 1418, 1410, 1021 cm $^{-1}$ for B3LYP/6-311G. The rocking mode of the CH $_3$ group is computed at 1103, 1025 cm $^{-1}$ for B3LYP/6-31G and 1100, 1021 cm $^{-1}$ for B3LYP/6-311G well in agreement with a recorded value of 1099 cm $^{-1}$ in the FT-Raman spectrum. Moreover, the twisting vibration of Γ CH $_3$ falls below 500 cm $^{-1}$. In the present study twisting CH $_3$ deformations vibrations possessed at 181 (w) in FT-Raman spectrum, at 185 cm $^{-1}$ B3LYP/6-31G and 180cm $^{-1}$ in B3LYP/6-311G in with the PED contribution is 58 %.

4.2.3. CH₂ vibrations

Methylene (CH₂) vibration is formed due to the presence of pyrazole in the title molecule which creates four fundamental frequencies out of six and follows an anti-symmetric stretching mode- ν_{ass} (CH₂), asymmetric stretching mode- $\nu(CH_2)$, a scissoring mode-sis (CH₂), twisting mode- Γ (CH₂) and a rocking mode- $\rho(CH_2)$. According to the literature, CH₂ symmetric and asymmetric vibration fall in the range around 3000-2800 cm⁻¹ [24]. The CH₂ asymmetric stretching modes are computed at 2955, 2915 cm⁻¹ for B3LYP/6-31G and 2953, 2912 cm⁻¹ for B3LYP/6-311G, but no peak can be seen in this region on a recorded spectrum. The bending mode, which involves a hydrogen atom attached to the core carbon, is between 1450 and 875 cm⁻¹, although there is a coupling of vibration modes that generally occurs, especially CH₂ scissoring and rocking, which are more sensitive to the molecular

Table 2. Optimized structural parameters (bond angle) of CPTBN calculated by DFT/B3LYP method with 6- 31Gand6-311G basis sets.

1 C4-C1-N24 121.66 125.75 54 C2-C26-H28 111.73 2 C4-C1-C26 125.16 125.26 55 H3-C26-H28 107.50 3 N24-C1-C26 113.17 113.16 56 C21-C29-C30 111.67 4 C14-C2-N25 112.28 112.16 57 C21-C29-C31 111.97 5 C14-C2-C26 115.28 115.36 58 C21-C29-H38 107.05 6 C14-C2-H55 109.32 109.24 59 C30-C29-H38 107.76 8 N25-C2-C26 100.08 100.12 60 C30-C29-H38 107.46 8 N25-C2-H55 107.21 107.31 61 C31-C29-H38 107.48 9 C26-C2-H55 112.16 112.15 62 C29-C30-H32 110.48 10 C1-C4-C5 120.62 120.67 64 C29-C30-H33 111.13 11 C1-C4-C6 120.57 120.67 64 C29-C30-H33 111.11	111.63 107.49 111.74 112.07 106.93 111.07 107.36 107.37 110.46 111.11 111.21 108.22 107.81 107.91 111.16 110.43 111.29
3 N24-C1-C26 113.17 113.16 56 C21-C29-C30 111.67 4 C14-C2-N25 112.28 112.16 57 C21-C29-C31 111.97 5 C14-C2-C26 115.28 115.36 58 C21-C29-H38 107.05 6 C14-C2-H55 109.32 109.24 59 C30-C29-H38 107.46 8 N25-C2-E65 100.08 100.12 60 C30-C29-H38 107.46 8 N25-C2-H55 107.21 107.31 61 C31-C29-H38 107.48 9 C26-C2-H55 112.16 112.15 62 C29-C30-H32 110.48 10 C1-C4-C5 120.62 120.65 63 C29-C30-H33 111.13 11 C1-C4-C6 120.57 120.67 64 C29-C30-H33 111.11 12 C5-C4-C6 118.81 118.69 65 H32-C30-H34 107.81 14 C4-C5-H8 120.86 120.29 66 H32-C30-H34 107.91	111.74 112.07 106.93 111.07 107.36 107.37 110.46 111.11 111.21 108.22 107.81 107.91 111.16 110.43
4 C14-C2-N25 112.28 112.16 57 C21-C29-C31 111.97 5 C14-C2-C26 115.28 115.36 58 C21-C29-H38 107.05 6 C14-C2-H55 109.32 109.24 59 C30-C29-C31 110.93 7 N25-C2-C26 100.08 100.12 60 C30-C29-H38 107.46 8 N25-C2-H55 107.21 107.31 61 C31-C29-H38 107.48 9 C26-C2-H55 112.16 112.15 62 C29-C30-H32 110.48 10 C1-C4-C5 120.62 120.65 63 C29-C30-H32 110.48 11 C1-C4-C6 120.57 120.67 64 C29-C30-H34 111.11 12 C5-C4-C6 118.81 118.69 65 H32-C30-H34 107.81 14 C4-C5-H8 120.29 120.37 67 H33-C30-H34 107.91 15 C7-C5-H8 118.86 118.71 68 C29-C31-H35 111.19 16 C4-C6-C9 120.73 120.78 69 C29-C31-H35 111.19 17 C4-C6-H10 119.09 119.12 70 C29-C31-H36 110.45 17 C4-C6-H10 120.18 120.10 71 H35-C31-H36 108.24 19 C5-C7-C11 118.80 118.74 72 H35-C31-H37 107.92 20 C5-C7-H12 120.73 120.72 73 H36-C31-H37 107.92 21 C11-C7-H12 120.47 120.53 74 C40-C39-C41 118.24 24 C11-C9-H13 120.71 120.71 76 S41-C39-C45 118.24 25 C7-C11-C9 121.84 121.95 78 C39-C40-N43 113.46 26 C7-C11-C27 119.06 118.99 80 C39-C40-N43 113.46 27 C9-C11-C127 119.06 118.99 80 C39-C40-N43 113.46 28 C2-C14-C15 121.47 121.46 81 N25-C42-N43 123.19 30 C15-C14-C16 118.63 118.54 83 S41-C42-N43 117.33 31 C14-C15-C17 120.62 120.07 84 C40-N43-C42 113.91 32 C14-C15-H18 119.15 119.03 86 C39-C45-H56 114.89	112.07 106.93 111.07 107.36 107.37 110.46 111.11 111.21 108.22 107.81 107.91 111.16 110.43
5 C14-C2-C26 115.28 115.36 58 C21-C29-H38 107.05 6 C14-C2-H55 109.32 109.24 59 C30-C29-C31 110.93 7 N25-C2-C26 100.08 100.12 60 C30-C29-H38 107.46 8 N25-C2-H55 100.21 107.31 61 C31-C29-H38 107.48 9 C26-C2-H55 112.16 112.15 62 C29-C30-H32 110.48 10 C1-C4-C5 120.62 120.65 63 C29-C30-H33 111.13 11 C1-C4-C6 120.57 120.67 64 C29-C30-H33 111.11 12 C5-C4-C6 118.81 118.69 65 H32-C30-H34 111.11 12 C5-C4-C6 118.81 118.69 65 H32-C30-H34 107.81 14 C4-C5-C7 120.86 120.92 66 H32-C30-H34 107.81 15 C7-C5-H8 118.86 118.71 68 C29-C31-H35 111.19	106.93 111.07 107.36 107.37 110.46 111.11 111.21 108.22 107.81 107.91 111.16 110.43
6 C14-C2-H55 109.32 109.24 59 C30-C29-C31 110.93 7 N25-C2-C26 100.08 100.12 60 C30-C29-H38 107.46 8 N25-C2-H55 107.21 107.31 61 C31-C29-H38 107.48 9 C26-C2-H55 112.16 112.15 62 C29-C30-H32 110.48 10 C1-C4-C5 120.62 120.65 63 C29-C30-H33 111.13 11 C1-C4-C6 120.57 120.67 64 C29-C30-H34 111.11 12 C5-C4-C6 118.81 118.69 65 H32-C30-H33 108.29 13 C4-C5-C7 120.86 120.92 66 H32-C30-H34 107.81 14 C4-C5-H8 120.29 120.37 67 H33-C30-H34 107.81 15 C7-C5-H8 118.86 118.71 68 C29-C31-H35 111.19 16 C4-C6-C9 120.73 120.78 69 C29-C31-H36 110.45 17 C4-C6-H10 119.09 119.12 70 C29-C31-H36 110.45 17 C4-C6-H10 119.09 119.12 70 C29-C31-H36 110.45 19 C5-C7-C11 118.80 118.74 72 H35-C31-H36 108.24 19 C5-C7-C11 118.80 118.74 72 H35-C31-H37 107.92 20 C5-C7-H12 120.73 120.72 73 H36-C31-H37 107.92 21 C11-C7-H12 120.73 120.72 73 H36-C31-H37 107.92 22 C6-C9-C11 118.80 118.74 72 H35-C31-H37 107.92 23 C6-C9-C11 118.96 118.93 75 C40-C39-S41 108.92 24 C11-C9-H13 120.71 120.71 76 S41-C39-C45 132.84 25 C7-C11-C9 121.84 121.95 78 C39-C40-O44 124.41 26 C7-C11-C27 119.10 119.07 79 N43-C40-O44 124.41 26 C7-C11-C27 119.10 119.07 79 N43-C40-O44 124.41 26 C7-C11-C127 119.10 119.07 79 N43-C40-O44 124.41 27 C9-C11-C127 119.06 118.99 80 C39-S41-C42 86.38 28 C2-C14-C15 121.47 121.46 81 N25-C42-S41 119.48 29 C2-C14-C16 118.63 118.54 83 S41-C42-N43 117.33 11 C14-C15-C17 120.62 120.67 84 C40-N43-C42 113.91 31 C14-C15-C17 120.62 120.67 84 C40-N43-C42 113.91 32 C14-C15-H18 120.23 120.30 85 C39-C45-C46 134.89 33 C17-C15-H18 119.15 119.03 86 C39-C45-C46 134.89	111.07 107.36 107.37 110.46 111.11 111.21 108.22 107.81 107.91 111.16 110.43
7 N25-C2-C26 100.08 100.12 60 C30-C29-H38 107.46 8 N25-C2-H55 107.21 107.31 61 C31-C29-H38 107.48 9 C26-C2-H55 112.16 112.15 62 C29-C30-H32 110.48 10 C1-C4-C5 120.62 120.65 63 C29-C30-H33 111.13 11 C1-C4-C6 120.57 120.67 64 C29-C30-H34 111.11 12 C5-C4-C6 118.81 118.69 65 H32-C30-H34 107.81 13 C4-C5-C7 120.86 120.92 66 H32-C30-H34 107.91 15 C7-C5-H8 118.86 118.71 68 C29-C31-H36 111.19 16 C4-C6-C9 120.73 120.78 69 C29-C31-H36 110.45 17 C4-C6-H10 119.09 119.12 70 C29-C31-H37 111.19 18 C9-C6-H10 120.18 120.10 71 H35-C31-H37 107.92	107.36 107.37 110.46 111.11 111.21 108.22 107.81 107.91 111.16 110.43
8 N25-C2-H55 107.21 107.31 61 C31-C29-H38 107.48 9 C26-C2-H55 112.16 112.15 62 C29-C30-H32 110.48 10 C1-C4-C5 120.62 120.65 63 C29-C30-H33 111.13 11 C1-C4-C6 120.57 120.67 64 C29-C30-H33 111.11 12 C5-C4-C6 118.81 118.69 65 H32-C30-H34 111.11 12 C5-C4-C6 118.81 118.69 65 H32-C30-H34 107.81 14 C4-C5-H8 120.29 120.37 67 H33-C30-H34 107.91 15 C7-C5-H8 118.86 118.71 68 C29-C31-H35 111.19 16 C4-C6-C9 120.73 120.78 69 C29-C31-H35 111.19 18 C9-C6-H10 119.09 119.12 70 C29-C31-H36 110.45 19 C5-C7-C11 118.80 118.74 72 H35-C31-H37 107.72 20 C5-C7-H12 120.73 120.72 73 H36-C31-H37 <td>107.37 110.46 111.11 111.21 108.22 107.81 107.91 111.16 110.43</td>	107.37 110.46 111.11 111.21 108.22 107.81 107.91 111.16 110.43
9 C26-C2-H55 112.16 112.15 62 C29-C30-H32 110.48 10 C1-C4-C5 120.62 120.65 63 C29-C30-H32 111.13 11 C1-C4-C6 120.57 120.67 64 C29-C30-H34 111.11 12 C5-C4-C6 118.81 118.69 65 H32-C30-H33 108.29 13 C4-C5-C7 120.86 120.92 66 H32-C30-H34 107.81 14 C4-C5-H8 120.29 120.37 67 H33-C30-H34 107.90 15 C7-C5-H8 118.86 118.71 68 C29-C31-H35 111.19 16 C4-C6-C9 120.73 120.78 69 C29-C31-H35 111.19 16 C4-C6-H10 119.09 119.12 70 C29-C31-H37 111.19 18 C9-C6-H10 120.18 120.10 71 H35-C31-H36 108.24 19 C5-C7-C11 118.80 118.74 72 H35-C31-H37 107.92 20 C5-C7-H12 120.73 120.72 73 H36-C31-H37 107.92 21 C11-C7-H12 120.47 120.53 74 C40-C39-S41 108.92 22 C6-C9-C11 118.96 118.93 75 C40-C39-C45 132.84 23 C6-C9-H13 120.71 120.71 76 S41-C39-C45 118.24 24 C11-C9-H13 120.32 120.36 77 C39-C40-N43 113.46 25 C7-C11-C9 121.84 121.95 78 C39-C40-N43 113.46 26 C7-C11-C127 119.10 119.07 79 N43-C40-044 122.14 27 C9-C11-C127 119.06 118.99 80 C39-S41-C42 86.38 28 C2-C14-C15 121.47 121.46 81 N25-C42-S41 119.48 29 C2-C14-C16 119.90 120.00 82 N25-C42-N43 123.19 30 C15-C14-C16 118.63 118.54 83 S41-C42-N43 117.33 31 C14-C15-C17 120.62 120.67 84 C40-N43-C42 113.91 32 C14-C15-H18 120.23 120.30 85 C39-C45-C46 134.89 33 C17-C15-H18 119.15 119.03 86 C39-C45-H56 113.98	110.46 111.11 111.21 108.22 107.81 107.91 111.16 110.43
10	111.11 111.21 108.22 107.81 107.91 111.16
11	111.21 108.22 107.81 107.91 111.16 110.43
12 C5-C4-C6 118.81 118.69 65 H32-C30-H33 108.29 13 C4-C5-C7 120.86 120.92 66 H32-C30-H34 107.81 14 C4-C5-H8 120.29 120.37 67 H33-C30-H34 107.90 15 C7-C5-H8 118.86 118.71 68 C29-C31-H35 111.19 16 C4-C6-C9 120.73 120.78 69 C29-C31-H36 110.45 17 C4-C6-H10 119.09 119.12 70 C29-C31-H37 111.19 18 C9-C6-H10 120.18 120.10 71 H35-C31-H36 108.24 19 C5-C7-C11 118.80 118.74 72 H35-C31-H37 107.92 20 C5-C7-H12 120.73 120.72 73 H36-C31-H37 107.92 21 C11-C7-H12 120.73 120.72 73 H36-C31-H37 107.72 21 C11-C7-H12 120.47 120.53 74 C40-C39-S41 108.92 22 C6-C9-C11 118.96 118.93 75 C40-C39-C45 132.84 23 C6-C9-H13 120.71 120.71 76 S41-C39-C45 118.24 24 C11-C9-H13 120.32 120.36 77 C39-C40-N43 113.46 25 C7-C11-C9 121.84 121.95 78 C39-C40-O44 124.41 26 C7-C11-C127 119.10 119.07 79 N43-C40-O44 122.14 27 C9-C11-C127 119.06 118.99 80 C39-S41-C42 86.38 28 C2-C14-C15 121.47 121.46 81 N25-C42-S41 119.48 29 C2-C14-C16 119.90 120.00 82 N25-C42-N43 123.19 30 C15-C14-C16 118.63 118.54 83 S41-C42-N43 117.33 31 C14-C15-C17 120.62 120.67 84 C40-N43-C42 113.91 32 C14-C15-H18 120.23 120.30 85 C39-C45-C46 134.89 33 C17-C15-H18 119.15 119.03 86 C39-C45-C46 134.89	108.22 107.81 107.91 111.16 110.43
13	107.81 107.91 111.16 110.43
14 C4-C5-H8 120.29 120.37 67 H33-C30-H34 107.90 15 C7-C5-H8 118.86 118.71 68 C29-C31-H35 111.19 16 C4-C6-C9 120.73 120.78 69 C29-C31-H36 110.45 17 C4-C6-H10 119.09 119.12 70 C29-C31-H37 111.19 18 C9-C6-H10 120.18 120.10 71 H35-C31-H36 108.24 19 C5-C7-C11 118.80 118.74 72 H35-C31-H37 107.92 20 C5-C7-H12 120.73 120.72 73 H36-C31-H37 107.72 21 C11-C7-H12 120.47 120.53 74 C40-C39-S41 108.92 22 C6-C9-C11 118.96 118.93 75 C40-C39-C45 132.84 23 C6-C9-H13 120.71 120.71 76 S41-C39-C45 118.24 24 C11-C9-H13 120.32 120.36 77 C39-C40-N43 113.46 25 C7-C11-C9 121.84 121.95 78 C39-C40-	107.91 111.16 110.43
15 C7-C5-H8 118.86 118.71 68 C29-C31-H35 111.19 16 C4-C6-C9 120.73 120.78 69 C29-C31-H36 110.45 17 C4-C6-H10 119.09 119.12 70 C29-C31-H37 111.19 18 C9-C6-H10 120.18 120.10 71 H35-C31-H36 108.24 19 C5-C7-C11 118.80 118.74 72 H35-C31-H37 107.92 20 C5-C7-H12 120.73 120.72 73 H36-C31-H37 107.72 21 C11-C7-H12 120.47 120.53 74 C40-C39-S41 108.92 22 C6-C9-C9-C11 118.96 118.93 75 C40-C39-C45 132.84 23 C6-C9-H13 120.71 120.71 76 S41-C39-C45 118.24 24 C11-C9-H13 120.32 120.36 77 C39-C40-O44 124.41 26 C7-C11-C9 121.84 121.95 78 C39-C40-O44 124.41 27 C9-C11-C127 119.06 118.99 80 C3	111.16 110.43
16 C4-C6-C9 120.73 120.78 69 C29-C31-H36 110.45 17 C4-C6-H10 119.09 119.12 70 C29-C31-H37 111.19 18 C9-C6-H10 120.18 120.10 71 H35-C31-H36 108.24 19 C5-C7-C11 118.80 118.74 72 H35-C31-H37 107.92 20 C5-C7-H12 120.73 120.72 73 H36-C31-H37 107.72 21 C11-C7-H12 120.47 120.53 74 C40-C39-S41 108.92 22 C6-C9-C11 118.96 118.93 75 C40-C39-C45 132.84 23 C6-C9-H13 120.71 120.71 76 S41-C39-C45 118.24 24 C11-C9-H13 120.32 120.36 77 C39-C40-N43 113.46 25 C7-C11-C9 121.84 121.95 78 C39-C40-O44 124.41 26 C7-C11-C127 119.10 119.07 79 N43-C40-O44 122.14 27 C9-C11-C127 119.06 118.99 80 C3	110.43
17 C4-C6-H10 119.09 119.12 70 C29-C31-H37 111.19 18 C9-C6-H10 120.18 120.10 71 H35-C31-H36 108.24 19 C5-C7-C11 118.80 118.74 72 H35-C31-H37 107.92 20 C5-C7-H12 120.73 120.72 73 H36-C31-H37 107.72 21 C11-C7-H12 120.47 120.53 74 C40-C39-S41 108.92 22 C6-C9-C11 118.96 118.93 75 C40-C39-C45 132.84 23 C6-C9-H13 120.71 120.71 76 S41-C39-C45 118.24 24 C11-C9-H13 120.32 120.36 77 C39-C40-N43 113.46 25 C7-C11-C9 121.84 121.95 78 C39-C40-O44 124.41 26 C7-C11-CL27 119.10 119.07 79 N43-C40-O44 122.14 27 C9-C11-CL27 119.06 118.99 80 C39-S41-C42 86.38 28 C2-C14-C15 121.47 121.46 81 N	
18 C9-C6-H10 120.18 120.10 71 H35-C31-H36 108.24 19 C5-C7-C11 118.80 118.74 72 H35-C31-H37 107.92 20 C5-C7-H12 120.73 120.72 73 H36-C31-H37 107.72 21 C11-C7-H12 120.47 120.53 74 C40-C39-S41 108.92 22 C6-C9-C11 118.96 118.93 75 C40-C39-C45 132.84 23 C6-C9-H13 120.71 120.71 76 S41-C39-C45 118.24 24 C11-C9-H13 120.32 120.36 77 C39-C40-N43 113.46 25 C7-C11-C9 121.84 121.95 78 C39-C40-O44 124.41 26 C7-C11-CL27 119.10 119.07 79 N43-C40-O44 122.14 27 C9-C11-CL27 119.06 118.99 80 C39-S41-C42 86.38 28 C2-C14-C15 121.47 121.46 81 N25-C42-S41 119	111 20
19 C5-C7-C11 118.80 118.74 72 H35-C31-H37 107.92 20 C5-C7-H12 120.73 120.72 73 H36-C31-H37 107.72 21 C11-C7-H12 120.47 120.53 74 C40-C39-S41 108.92 22 C6-C9-C11 118.96 118.93 75 C40-C39-C45 132.84 23 C6-C9-H13 120.71 120.71 76 S41-C39-C45 118.24 24 C11-C9-H13 120.32 120.36 77 C39-C40-N43 113.46 25 C7-C11-C9 121.84 121.95 78 C39-C40-O44 124.41 26 C7-C11-CL27 119.10 119.07 79 N43-C40-O44 122.14 27 C9-C11-CL27 119.06 118.99 80 C39-S41-C42 86.38 28 C2-C14-C15 121.47 121.46 81 N25-C42-S41 119.48 29 C2-C14-C16 119.90 120.00 82 N25-C42-N43 123.19 30 C15-C14-C16 118.63 118.54 83 S41-C42-N43 17.33 31 C14-C15-C17 120.62 120.67 84 C40-N43-C42 113.91 32 C14-C15-H18 120.23 120.30 85 C39-C45-C46 134.89 33 C17-C15-H18 119.15 119.03 86 C39-C45-H56 113.98	111.29
20 C5-C7-H12 120.73 120.72 73 H36-C31-H37 107.72 21 C11-C7-H12 120.47 120.53 74 C40-C39-S41 108.92 22 C6-C9-C11 118.96 118.93 75 C40-C39-C45 132.84 23 C6-C9-H13 120.71 120.71 76 S41-C39-C45 118.24 24 C11-C9-H13 120.32 120.36 77 C39-C40-N43 113.46 25 C7-C11-C9 121.84 121.95 78 C39-C40-O44 124.41 26 C7-C11-CL27 119.10 119.07 79 N43-C40-O44 122.14 27 C9-C11-CL27 119.06 118.99 80 C39-S41-C42 86.38 28 C2-C14-C15 121.47 121.46 81 N25-C42-S41 119.48 29 C2-C14-C16 119.90 120.00 82 N25-C42-N43 123.19 30 C15-C14-C16 118.63 118.54 83 S41-C42-N43 117.33 31 C14-C15-C17 120.62 120.67 84	108.17
21 C11-C7-H12 120.47 120.53 74 C40-C39-S41 108.92 22 C6-C9-C11 118.96 118.93 75 C40-C39-C45 132.84 23 C6-C9-H13 120.71 120.71 76 S41-C39-C45 118.24 24 C11-C9-H13 120.32 120.36 77 C39-C40-N43 113.46 25 C7-C11-C9 121.84 121.95 78 C39-C40-O44 124.41 26 C7-C11-CL27 119.10 119.07 79 N43-C40-O44 122.14 27 C9-C11-CL27 119.06 118.99 80 C39-S41-C42 86.38 28 C2-C14-C15 121.47 121.46 81 N25-C42-S41 119.48 29 C2-C14-C16 119.90 120.00 82 N25-C42-N43 123.19 30 C15-C14-C16 118.63 118.54 83 S41-C42-N43 117.33 31 C14-C15-C17 120.62 120.67 84 C40-N43-C42 113.91 32 C14-C15-H18 120.23 120.30 85	107.94
22 C6-C9-C11 118.96 118.93 75 C40-C39-C45 132.84 23 C6-C9-H13 120.71 120.71 76 S41-C39-C45 118.24 24 C11-C9-H13 120.32 120.36 77 C39-C40-N43 113.46 25 C7-C11-C9 121.84 121.95 78 C39-C40-O44 124.41 26 C7-C11-CL27 119.10 119.07 79 N43-C40-O44 122.14 27 C9-C11-CL27 119.06 118.99 80 C39-S41-C42 86.38 28 C2-C14-C15 121.47 121.46 81 N25-C42-S41 119.48 29 C2-C14-C16 119.90 120.00 82 N25-C42-N43 123.19 30 C15-C14-C16 118.63 118.54 83 S41-C42-N43 117.33 31 C14-C15-C17 120.62 120.67 84 C40-N43-C42 113.91 32 C14-C15-H18 120.23 120.30 85 C39-C45-C46 134.89 33 C17-C15-H18 119.15 119.03 86	107.72
23 C6-C9-H13 120.71 120.71 76 S41-C39-C45 118.24 24 C11-C9-H13 120.32 120.36 77 C39-C40-N43 113.46 25 C7-C11-C9 121.84 121.95 78 C39-C40-O44 124.41 26 C7-C11-CL27 119.10 119.07 79 N43-C40-O44 122.14 27 C9-C11-CL27 119.06 118.99 80 C39-S41-C42 86.38 28 C2-C14-C15 121.47 121.46 81 N25-C42-S41 119.48 29 C2-C14-C16 119.90 120.00 82 N25-C42-N43 123.19 30 C15-C14-C16 118.63 118.54 83 S41-C42-N43 117.33 31 C14-C15-C17 120.62 120.67 84 C40-N43-C42 113.91 32 C14-C15-H18 120.23 120.30 85 C39-C45-C46 134.89 33 C17-C15-H18 119.15 119.03 86 C39-C45-H56 113.98	108.90
24 C11-C9-H13 120.32 120.36 77 C39-C40-N43 113.46 25 C7-C11-C9 121.84 121.95 78 C39-C40-O44 124.41 26 C7-C11-CL27 119.10 119.07 79 N43-C40-O44 122.14 27 C9-C11-CL27 119.06 118.99 80 C39-S41-C42 86.38 28 C2-C14-C15 121.47 121.46 81 N25-C42-S41 119.48 29 C2-C14-C16 119.90 120.00 82 N25-C42-N43 123.19 30 C15-C14-C16 118.63 118.54 83 S41-C42-N43 117.33 31 C14-C15-C17 120.62 120.67 84 C40-N43-C42 113.91 32 C14-C15-H18 120.23 120.30 85 C39-C45-C46 134.89 33 C17-C15-H18 119.15 119.03 86 C39-C45-H56 113.98	132.96
25 C7-C11-C9 121.84 121.95 78 C39-C40-O44 124.41 26 C7-C11-CL27 119.10 119.07 79 N43-C40-O44 122.14 27 C9-C11-CL27 119.06 118.99 80 C39-S41-C42 86.38 28 C2-C14-C15 121.47 121.46 81 N25-C42-S41 119.48 29 C2-C14-C16 119.90 120.00 82 N25-C42-N43 123.19 30 C15-C14-C16 118.63 118.54 83 S41-C42-N43 117.33 31 C14-C15-C17 120.62 120.67 84 C40-N43-C42 113.91 32 C14-C15-H18 120.23 120.30 85 C39-C45-C46 134.89 33 C17-C15-H18 119.15 119.03 86 C39-C45-H56 113.98	118.14
26 C7-C11-CL27 119.10 119.07 79 N43-C40-O44 122.14 27 C9-C11-CL27 119.06 118.99 80 C39-S41-C42 86.38 28 C2-C14-C15 121.47 121.46 81 N25-C42-S41 119.48 29 C2-C14-C16 119.90 120.00 82 N25-C42-N43 123.19 30 C15-C14-C16 118.63 118.54 83 S41-C42-N43 117.33 31 C14-C15-C17 120.62 120.67 84 C40-N43-C42 113.91 32 C14-C15-H18 120.23 120.30 85 C39-C45-C46 134.89 33 C17-C15-H18 119.15 119.03 86 C39-C45-H56 113.98	113.45
27 C9-C11-CL27 119.06 118.99 80 C39-S41-C42 86.38 28 C2-C14-C15 121.47 121.46 81 N25-C42-S41 119.48 29 C2-C14-C16 119.90 120.00 82 N25-C42-N43 123.19 30 C15-C14-C16 118.63 118.54 83 S41-C42-N43 117.33 31 C14-C15-C17 120.62 120.67 84 C40-N43-C42 113.91 32 C14-C15-H18 120.23 120.30 85 C39-C45-C46 134.89 33 C17-C15-H18 119.15 119.03 86 C39-C45-H56 113.98	124.31
28 C2-C14-C15 121.47 121.46 81 N25-C42-S41 119.48 29 C2-C14-C16 119.90 120.00 82 N25-C42-N43 123.19 30 C15-C14-C16 118.63 118.54 83 S41-C42-N43 117.33 31 C14-C15-C17 120.62 120.67 84 C40-N43-C42 113.91 32 C14-C15-H18 120.23 120.30 85 C39-C45-C46 134.89 33 C17-C15-H18 119.15 119.03 86 C39-C45-H56 113.98	122.24
29 C2-C14-C16 119.90 120.00 82 N25-C42-N43 123.19 30 C15-C14-C16 118.63 118.54 83 S41-C42-N43 117.33 31 C14-C15-C17 120.62 120.67 84 C40-N43-C42 113.91 32 C14-C15-H18 120.23 120.30 85 C39-C45-C46 134.89 33 C17-C15-H18 119.15 119.03 86 C39-C45-H56 113.98	86.28
29 C2-C14-C16 119.90 120.00 82 N25-C42-N43 123.19 30 C15-C14-C16 118.63 118.54 83 S41-C42-N43 117.33 31 C14-C15-C17 120.62 120.67 84 C40-N43-C42 113.91 32 C14-C15-H18 120.23 120.30 85 C39-C45-C46 134.89 33 C17-C15-H18 119.15 119.03 86 C39-C45-H56 113.98	119.70
31 C14-C15-C17 120.62 120.67 84 C40-N43-C42 113.91 32 C14-C15-H18 120.23 120.30 85 C39-C45-C46 134.89 33 C17-C15-H18 119.15 119.03 86 C39-C45-H56 113.98	123.01
31 C14-C15-C17 120.62 120.67 84 C40-N43-C42 113.91 32 C14-C15-H18 120.23 120.30 85 C39-C45-C46 134.89 33 C17-C15-H18 119.15 119.03 86 C39-C45-H56 113.98	117.29
32 C14-C15-H18 120.23 120.30 85 C39-C45-C46 134.89 33 C17-C15-H18 119.15 119.03 86 C39-C45-H56 113.98	114.08
33 C17-C15-H18 119.15 119.03 86 C39-C45-H56 113.98	134.95
	113.95
34 C14-C16-C19 120.53 120.59 87 C46-C45-H56 111.13	111.10
35 C14-C16-H20 119.55 119.56 88 C45-C46-C47 115.75	115.85
36 C19-C16-H20 119.90 119.82 89 C45-C46-C48 126.30	126.28
37 C15-C17-C21 121.06 121.10 90 C47-C46-C48 117.96	117.87
38 C15-C17-H22 119.11 119.04 91 C46-C47-C49 121.69	121.70
39 C21-C17-H22 119.84 119.86 92 C46-C47-H50 119.20	119.23
40 C16-C19-C21 121.24 121.28 93 C49-C47-H50 119.11	119.07
41 C16-19-H23 119.38 119.35 94 C46-C48-C51 120.52	120.58
42 C21-C19-H23 119.37 119.37 95 C46-C48-H52 119.11	119.14
43 C17-C21-C19 117.91 117.82 96 C51-C48-H52 120.37	120.29
44 C17-C21-C29 121.37 121.41 97 C47-C49-C53 119.75	119.80
45 C19-C21-C29 120.71 120.76 98 C47-C49-H59 120.49	120.42
45 C19-C21-C29 120.71 120.70 98 C47-C49-H59 120.49 46 C1-N24-N25 108.58 108.59 99 C53-C49-H59 119.77	119.78
	120.87
	119.66
49 N24-N25-C42 121.46 121.62 102 C53-C51-H54 119.43	119.47
50 C1-C26-C2 103.65 103.71 103 C49-C53-C51 119.24	119.17
51 C1-C26-H3 112.34 112.39 104 C49-C53-C57 120.26	120.29
52 C1-C26-H28 110.44 110.44 105 C51-C53-C57 120.50	120.54
53 C2–C26–H3 111.23 111.25	140.04

environment. The twisting mode of the CH $_2$ group is computed at 1196 cm $^{-1}$ (6-31G) and 1194 cm $^{-1}$ (6-311G) agree with the recoded value of 1195 cm $^{-1}$ FT-IR and 1196 cm $^{-1}$ FT-Raman. The mode scissoring value 1375 cm $^{-1}$ (w) in FT-Raman spectrum compared with computed wavenumber 1379 cm $^{-1}$ for B3LYP/6-31G and 1376 cm $^{-1}$ for B3LYP/6-311G.

4.2.4. Nitrile vibrations

Nitrogen compounds with cumulated double bonds or triple bonds, such as nitrile and cyanates, have a specific spectrum, typically with a single, usually intense absorption peak at 2280–2200 ${\rm cm}^{-1}$ [6,25]. The saturated cyclic nitrile is detected by the presence of a band near 2250 ${\rm cm}^{-1}$ while their aromatic counterparts absorb at lower frequencies near

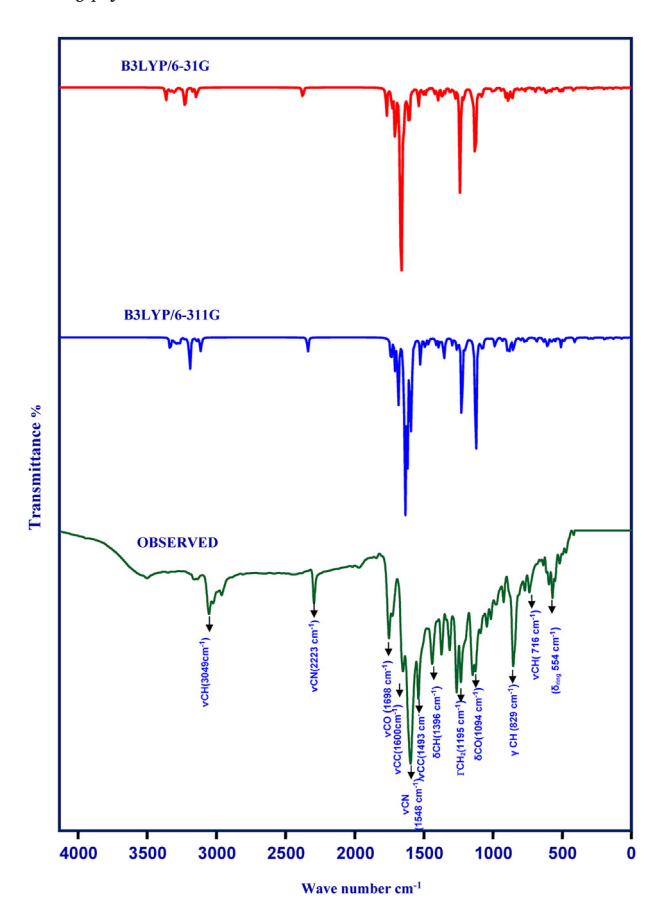


Figure 2. Observed FT-IR and simulated spectra of CPTBN.

2230 cm $^{-1}$. Generally, the IR and Raman spectrum exhibits $C\equiv N$ is stretching vibrations at 2235 cm $^{-1}$ and 2290 cm $^{-1}$. Similarly, the large range that has been reported against or appearance of $C\equiv N$ is 2223 (w) cm $^{-1}$ for FT-IR and 2222 (m) cm $^{-1}$ for FT-Raman, but also supported by the appearance of medium-strong stretching bands. Around 1738 cm $^{-1}$ and 1698 cm $^{-1}$ for a cyclic ring in the compounds, that confirm the formation of [3 + 2] ring condensation product reported by Bardak et al. [26] The correlated scale vibrations of PED contribution observed in 1300, 1550 cm $^{-1}$ at 6-31G, 1296,1548 cm $^{-1}$ at 6-311G and experimental at 1548 cm $^{-1}$ (vs) cm $^{-1}$ in FT-IR spectrum.

4.2.5. C–C vibrations

In general, the stretching vibration of heterocyclic aromatic compounds C-C bond occurs in the region 1650-1200 cm⁻¹ reported by Sheeja Mol et al. [27]. In the present study, a medium-strong band is observed in 1493 (ms) cm⁻¹ at FT-IR spectrum and 1441(w), 1551(m) cm⁻¹ at FT-Raman spectrum, the strong band is observed in the corresponding computed DFT value is 1442, 1552 cm⁻¹ for 6-31G and 1440, 1550 cm⁻¹ for 6-311G. The title molecule has five rings with C-C stretching vibrations and form peaks arising in the array at 1631-1025 cm⁻¹ [28]. A combination of C–H vibration present in stretching C–C bond locate the very strong frequency in 1600 cm⁻¹ near FT-IR and 1594, 1561 cm⁻¹ near FT-Raman. The predicted corresponding value lie at 1600, 1564 cm⁻¹ in 6-31G and 1598, 1562 cm⁻¹ in 6-311G. The combination of stretching C-C and in-plane C-C vibration locate the very strong frequency in both FT-IR and FT-Raman is 1225 cm⁻¹. The ring carbon-carbon stretching vibration occur in the region 1625-1400 cm⁻¹ routed by Fatma et al. [25] is compared with the values. The C-C stretching at 1428 cm^{-1} , 1235 cm^{-1} , 1002 cm^{-1} in the IR spectrum and $1579\,\mathrm{cm}^{-1}$, $1531\,\mathrm{cm}^{-1}$, $1439\,\mathrm{cm}^{-1}$, $1380\,\mathrm{cm}^{-1}$, $1123\,\mathrm{cm}^{-1}$ in the Raman spectrum are assigned by Kuruvilla et al. [29]. In the present case, bending and ring vibration of C–C falls below 1000 cm⁻¹ and are shown in Table 3. The C–C in-plane bending medium band occurs between 1000-600 cm $^{-1}$ [28]. A medium intense FT-Raman band is identified at 823 cm $^{-1}$, which corresponds to the calculated value lies at 826 cm $^{-1}$ in 6-31G and 821 cm $^{-1}$ in 6-311G. From the FT-Raman spectrum the values predicted at $\delta_{ring}=945 {\rm ms}$, $631 {\rm m}$, $551 {\rm vw}$, $353 {\rm ms}$ cm $^{-1}$ that confirms the formation of δ ring in the range 632, 671, 622, 339, 332, 327, 310, 81, 76, 71, 23 cm $^{-1}$ for B3LYP/6-311G and δ ring in the range 684, 675, 625, 340, 334, 331, 314, 84, 75, 25 23 cm $^{-1}$ for B3LYP/6-31G. The C–C in-plane bending vibration mode calculated at δ_{ipb} 695, 440, 390, 345 cm $^{-1}$ for B3LYP/6-31G, and δ_{ipb} 694, 396, 388, 343 cm $^{-1}$ for B3LYP/6-311G. The out-of-plane C–C bending modes of γ_{opb} in the range 850, 844, 622, 405, 375, 310, 298, 35, 29, 23, 18, 14, 8 cm $^{-1}$ for B3LYP/6-311G and γ_{opb} in the range 855, 847, 625, 444, 379, 314, 300, 38, 30, 20, 15, 10 cm $^{-1}$ for B3LYP/6-31G.

4.2.6. C=O vibrations

The C=O stretching of the carbonyl group is identical large dipole moment and intense stretching vibration whose peak is, generally expected in the region 1740-1660 cm⁻¹. In the present study, a moderate band was observed within the FT-IR spectrum at 1698 (ms) cm⁻¹ is assignable. The C=O stretching vibrations deviate from the B3LYP/6-311G predicted value by 1659cm⁻¹. The strong band in the FT-IR and FT-Raman, near 1750- 1655 cm⁻¹ confirm the possibility of a carbonyl group in an aromatic compound [30]. The C=O in-plane bending vibration occurs in the range of 820-630 cm⁻¹. El-Azab et al. reported that C=O in-plane bending vibration was appearing at 694 cm⁻¹ [31]. For this compound vibration mode was observed as a weak intense peak at 694 (w) cm⁻¹ in the FT-IR spectrum. The corresponding in-plane C=O occurs modes in the 695 cm⁻¹ for B3LYP/6-31G and 694 cm⁻¹ for B3LYP/6-311G. Based on the absorption and emission, the prominent absorptions in the combination of $\delta C = O$, δCC , the medium-strong peak is observed in the magnitude of FT-IR is 1094 (ms) cm⁻¹, the corresponding value lies in 1095 cm⁻¹ at both B3LYP/6-31G and B3LYP/6-311G.

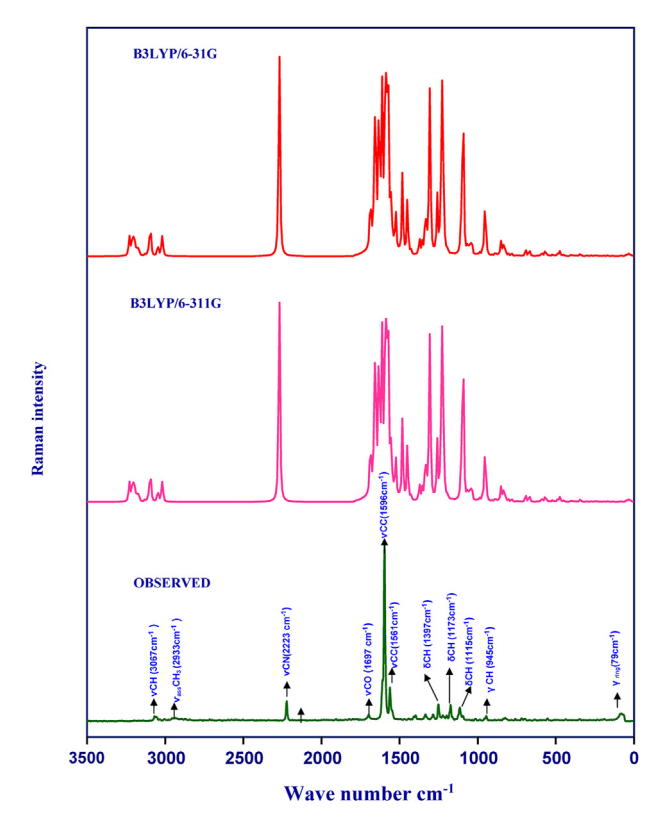


Figure 3. Observed FT-Raman and simulated spectra of CPTBN.

Table 3. Vibrational assignments, observed and calculated wavenumbers (scaled) CPTBN at B3LYP method with 6-31G and 6-311G basis sets.

Mode No.	Observed wavenur	nbers (cm ⁻¹)	Calculated wavenumb	Vibrational assignments (PED %)		
	FT-IR	FT-RAMAN	B3LYP/6-31G	B3LYP/6-311G		
1		3067m	3075	3067	νCH(98)	
2			3060	3061	νCH(98)	
3	3049w		3054	3050	νCH(99)	
4			3036	3027	νCH(98)	
5		3013w	3018	3012	νCH(98)	
6			3010	3008	νCH(98)	
7			3002	3001	νCH(97)	
8			2999	2997	νCH(97)	
9			2995	2994	νCH(97)	
10			2994	2990	νCH(98)	
11			2988	2986	νCH(98)	
12			2982	2979	νCH(99)	
13			2975	2972	νCH(98)	
14	2957w		2966	2960	ν CH(99)	
15			2955	2953	$\nu_{\rm ass}$ CH ₂ (88)	
16		2947w	2952	2948	$\nu_{\rm ass}$ CH ₃ (89)	
17			2928	2924	$\nu_{\rm ass}$ CH ₃ (89)	
18		2933w	2936	2932	ν _{ass} CH ₃ (89)	
19	2929w		2934	2930	$\nu_{\rm ass}$ CH ₃ (89)	
20			2915	2912	$\nu_{\rm ass}$ CH ₂ (96)	
21			2903	2900	$\nu_{\rm ass}$ CH ₃ (96)	
22			2881	2879	ν _{ass} CH ₃ (89)	
23	2868w	2868w	2870	2868	νCH(97)	
24	2223w	2222ms	2228	2223	νCN(98)	
25	1698ms	1697w	1702	1699	νCO(82),δCC(14)	
26			1655	1653	νCC(75), δCH(15)	
27	1600ms	1596vs	600	1598	νCC(74), δCH(16)	
28		1561vs	1564	1562	νCC(74), δCH(15)	
29		1551m	1552	1550	νCC(72), δCH(14)	
30	1548vs		1550	1548	νCN(72), νCC(12), δCH(10)	
31			1525	1522	νCC(88), δCH(16)	
32	1493ms	1493w	1498	1495	νCC(78), δCH(10), νCO(10)	
33			1455	1453	νCN(72), νCO(14), δCH(10),	
34		1441w	1442	1440	νCC(70), νCN(15), νCO(12)	
35			1440	1436	δCH(69), νCC(18)	
36	1424w		1429	1425	δCH(68), νCC(18)	
37			1420	1418	δ _{opb} CH ₃ (72)	
38		1409m	1415	1410	δ _{opb} CH ₃ (72)	
39	1396ms	1397ms	1394	1395	δCH(68), νCCl(20)	
40			1390	1389	δ _{ipb} CH ₃ (82)	
41			1385	1382	δ _{ipb} CH ₃ (82)	
42		1375w	1379	1376	ρ _{scis} CH ₂ (80)	
43	1370ms	24, 211	1370	1368	δCH(69), νCC(10)	
44			1345	1343	δCH(68), νCC(12)	
45	1331ms	1334ms	1333	1330	δ _{sb} CH ₃ (69)	
46	10011115	100 11110	1325	1322	δCH(62)	
47			1314	1312	δCH(66)	
48	1306w		1304	1305	δ _{sb} CH ₃ (72)	
49	1300W		1300	1296	δCH(67), νCN(10)	
50			1293	1290	δCH(69)	
51		1285ms	1290	1286	δCH(09)	
52		1 2001115	1290	1280	δCH(70)	
	1974				δCH(70)	
53	1274ms		1278	1275		
54		1051.	1265	1262	γCH(59)	
55		1251s	1253	1250	δCH(63)	
56			1250	1246	δCH(64)	
57			1245	1241	δCH(69)	

(continued on next page)

Table 3 (continued)

Mode No.	Observed wavenum	nbers (cm ⁻¹)	Calculated wavenumb	Vibrational assignments (PED %	
	FT-IR	FT-RAMAN	B3LYP/6-31G	B3LYP/6-311G	
58			1240	1237	νCC(70)
59	1225s	1225s	1230	1226	νCC(70), δCC(12)
50			1205	1203	δCH(72)
51	1195ms	1196ms	1196	1194	Г CH ₂ (69)
52			1192	1189	δCH(64)
53			1185	1182	δCH(64)
54		1173ms	1178	1175	δCH(64)
65			1154	1151	δCH(63)
66			1140	1137	δCH(63)
57	1114ms	1115ms	1120	1116	δCH(62)
58			1114	1110	νCC(71), δCH(12)
69			1107	1107	Γ CH ₂ (68)
70		1099ms	1103	1100	δ _{ipr} CH ₃ (62)
71	1094ms		1095	1095	δCO(66), δCC(22)
72	1058w		1061	1056	δCH(69)
73		1033w	1035	1033	δCH(63)
74			1030	1028	δCH(62)
75			1025	1021	δ _{Opr} CH ₃ (62)
76	1014w	1012w	1015	1014	νCCL(78)
77	1017W	1012W	998	998	δ _{ipr} CH ₃ (70)
78	985w		995	993	νCN(68), νNN(12)
79	903W	980w	980	981	γ CH(66)
80		900W		973	· · · · · · · · · · · · · · · · · · ·
			975		δ _{ipr} CH ₃ (69)
81			966	965	δ_{ring} (58)
82			958	957	δ _{ring} (56)
83	949w		951	949	δ _{ring} (57)
84			948	945	$\delta_{\rm ring}$ (60)
85		945m	933	932	γ CH(58)
86			928	925	γ CH(57)
87			920	918	γ CH(58)
88			910	906	γ CH(58)
89	896w		900	898	γ CH(58)
90		889w	893	890	νCH(59)
91			878	875	νCS(78),
92			870	866	νCH(59)
93		850w	853	850	γ CC(68)
94			847	844	γ CC(68)
95		837w	840	838	γ CS(78), νCN(12)
96	829ms		833	829	γ CH(68)
97		823w	826	821	γ CC(68)
98			820	816	γ CH(58)
99	811w		814	810	γ CH(56)
100			793	790	γ CH(58)
101			784	781	γ CH(58),
102			770	767	$\delta_{\rm ring}$ (60)
103	748w		753	750	νCH(55)
104			740	738	$\delta_{\rm ring}$ (58), ν CS(12)
105		720w	724	720	δ_{ring} (60), ν CS(12)
106	716w		718	715	δ_{ring} (59)
107	7.20	694w	695	694	δ CC(62), δ CO(17)
107	685vw	OJTW	684	682	γ _{ring} (62)
108	OOOVW	668vw	675	671	
	662	UUOVW			γ ring (63)
110	662vw		663	660	γ CO(72)
111			650	647	δ _{ring} (68)
112		***	641	638	γ CH(58)
113		631m	632	630	δ _{ring} (59)
114	619vw		625	622	γ CC(58), γ ring (20)
115			605	602	$\delta_{\rm ring}$ (57), δ CN(18)

(continued on next page)

Table 3 (continued)

Mode No.	Observed wavenu	mbers (cm ⁻¹)	Calculated wavenumb	Vibrational assignments (PED %)	
	FT-IR	FT-RAMAN	B3LYP/6-31G	B3LYP/6-311G	
116	579w		582	580	δ CN(58), δ _{ring} (17)
117			566	564	δCN(58), δ _{ring} (20)
118	554ms	551vw	554	552	$\delta_{\rm ring}$ (60)
119			530	528	γ CH(62)
120			520	517	γ CH(60)
121	504w		505	503	γ CH(60)
122	494vw		498	495	γ CH(61)
123	1511		481	479	δ _{ring} (58)
124	460vw		465	462	νCCL(53), δCC(19)
125	100711	440w	444	440	δCC(52)
126		440W	430	427	
	406vw		408		δ_{ring} (58), δ CC(12)
127	400vW			405	γ CC(56)
128			400	396	δCC(60)
129			390	388	δCC(60)
130			379	375	γ CC(58)
131			365	363	γ CCH ₃ (57)
132		353ms	358	355	$\delta_{\rm ring}$ (58)
133			345	343	δCC(58)
134			340	339	γ _{ring} (53)
135			334	332	γ _{ring} (54)
136		325w	331	327	γ _{ring} (54)
137			320	319	δCCH ₃ (56)
138			314	310	γ CC(52), γ _{ring} (21)
139		297w	300	298	γ CC(53)
140			280	275	δCCC(58)
141			255	253	δCCC(60)
142		233w	236	233	γ CCC(52)
143			215	212	δCCC(60)
144			207	202	Γ CH ₃ (58)
145			190	188	γ CCC(58)
146		181w	185	180	Γ CH ₃ (58)
147			172	169	γ CCC(53)
148			166	162	Γ CCCC(52)
149			153	151	Γ CCCC(52)
150			148	145	γ CCH ₃ (62)
151			140	138	
152		129w	133	130	δ _{ring} (63) δCCC(67)
		129W			
153			128	122	γ CCN(62)
154			125	117	δCCC(63)
155			116	111	γ CCC(60)
156			105	103	δCCC(60)
157		92	97	93	γ CCC(62)
158			95	89	δCCC(60)
159		79s	84	81	γ _{ring} (56)
160			80	76	γ _{ring} (55)
161			75	71	γ _{ring} (55)
162		64s	68	65	γ CCC(54)
163			62	59	γ CCC(54)
164			53	51	γ CCC(50)
165			45	42	γ CCC(52)
166			38	35	γ CC(54)
167			30	29	γ CC(54)
168			25	23	γ ring (52)
169			20	18	γ cC(52)
170			15	14	γ CC(52)
171			10	8	γ CC(52)

s-strong, ms-medium strong, w-weak, vw-very weak, vs-very strong, v-stretching, ν_{sym} -sym stretching, ν_{ass} -asym stretching, δ -in-plane, δ_{inb} -in-plane bending, δ_{inr} -in-plane rocking, γ -out-of-plane, γ_{opb} -out-of-plane bending, γ_{ring} -out-of-plane ring, scis-scissoring, ρ_{scis} -in plane scissoring, w-wagging, rock-rocking, Γ -twisting, δ -ring ring vibration.

4.2.7. C-Cl vibrations

The vibrations assignments of the benzene ring belong to C–Halogen (F, Cl, Br) bonds, which are formed between the ring and the halogen atoms are particularly important. Because of the lowering of molecular symmetry and the presence of heavy atoms, vibrations indeed be mixed [32, 33, 34, 35]. In the FT-Raman spectrum, a strong band is observed due to the presence of Cl, Br, and F atoms. Reporting in the FT-Raman spectrum, bands at 720vs cm⁻¹ are assigned to C–Cl is stretching vibration observer by Govindarajan et al. [36]. For simple organic chlorine compounds, C–Cl absorptions are in the region between 750–700 cm⁻¹. Sundaraganesan et al. [37] reported C–Cl is stretching at 704 cm⁻¹ (IR), 705 cm⁻¹ (Raman), and 715 cm⁻¹ (DFT) and the deformation bands at 250 cm⁻¹ and 160 cm⁻¹. The C–Cl stretching vibration is observed at 460 (vw) cm⁻¹ in FT-IR, and the corresponding computed value is 465 cm⁻¹ in B3LYP/6-31G and 462 cm⁻¹ in 6-311G.

4.2.8. C-S vibrations

The characteristic frequency for the C–S stretching appears as a weak band in the region 800-600 cm $^{-1}$. In the current study, FT-Raman spectrum with very low intensity is assigned to C–S symmetric stretching vibrations and agreement with the literature value. The C–S stretching modes are reported at 783, 632 cm $^{-1}$ in FT-IR, 633 cm $^{-1}$ in FT-Raman, and 785, 635 cm $^{-1}$ theoretically found by E1-Azab et al. [31]. The C–S stretching vibrations are reported as 770 cm $^{-1}$ in the FT-IR spectrum, and at 770, 636 cm $^{-1}$ theoretically assigned by Fatima et al. [38]. Our FT-Raman shows bands at 720(w) cm $^{-1}$. The calculated values of C–S stretching vibrations in the thiazole ring are corresponding to 878, 740, 724 cm $^{-1}$ for B3LYP/6-31G and 875, 738, 720 cm $^{-1}$ for B3LYP/6-311G.

4.3. Local reactivity properties of MEP

The molecular electrostatic potential (MEP) plot is a visual illustration of the foremost reactive sites during a molecule and mapped with the rainbow colour scheme (electron made regions represent with red colour, whereas poor lepton regions represent with blue colour and inexperienced shows of zero potential) [39]. Potential will increase within the order red < orange < yellow < green < blue. Using the Gaussian 09 program, we tracked and plotted the alpha density (e-4), density difference (e-3), and MEP (e-2) surface mapping. Surface analysis diagram of title compound net electrostatic effect produced at that point by total charge distribution (electron + proton) of the molecule and correlates

with electronegativity, partial charges, and chemical reactivity of the molecules. It provides a visual method to understand the relative step-by-step polarity of the molecule.

Based on the three electrostatic potential surfaces deepest red potential value in this molecule ranges from-4.055e⁻⁴ a.u, -6.088e⁻³ a.u and $-7.960e^{-2}$ a.u, deepest blue potential value in this molecule ranges from $4.055e^{-4}$ a.u, $6.088e^{-3}$ a.u and $7.960e^{-2}$ a.u. Alpha density represents the full electrophilic region (blue colour). Density difference shows the region energy difference between alpha density and MEP. In the reactive properties of MEP, the nucleophilic reactive site (red colour) shows the molecule's negative regions, and is located on the thiazole ring and partly above the benzonitrile. The other site is the electrophilic reactive site (blue colour) which indicates the positive regions of the molecule and is located on all hydrogen atoms in the molecule. The more dominant green colour over the MEP surface indicates that the electrostatic potential is midway between the vicinity of the red and blue regions. Therefore intermolecular interaction of the compound was confirmed by the reactive site region, the electrostatic potential surface along with the Alpha density, and complete title compound density is shown in Figure 4.

4.4. HOMO-LUMO energy and global reactivity descriptors

The energies of the highest occupied molecular orbital (HOMO), the outermost orbital containing electrons, tend to give electrons and act as an electron donor. On the other hand lowest unoccupied molecular orbital (LUMO), the innermost orbital containing is vacant and can accept electrons. HOMO and LUMO energy gaps between orbits are called frontier molecular orbital (FMOs). In a simple molecule, orbital theory approaches HOMO and LUMO can offer a reasonable qualitative prediction of the excitation properties and the ability of electron transport. The positive surface indicated by red colour and the negative surface is represented by green colour. The energies of the HOMO and LUMO orbital for the possible excitations were carried as 3.57 eV for B3LYP/6-31G and 3.58 eV for B3LYP/6-311G. Based on the root density functional descriptors, global reactivity descriptors of the title molecule described the ionization potential (I), electron affinity (A), chemical potential (μ), electro-negativity (γ), global hardness (η), global softness (σ) and global electrophilicity (ω) value, according to the equations given below [40]. Using HOMO and LUMO orbital energies, the ionization energy (I) and electron affinity (A) can be expressed as Eqs. (1) and (2)

Ionization potential
$$I = -E_{HOMO}(E_H)$$
 (1)

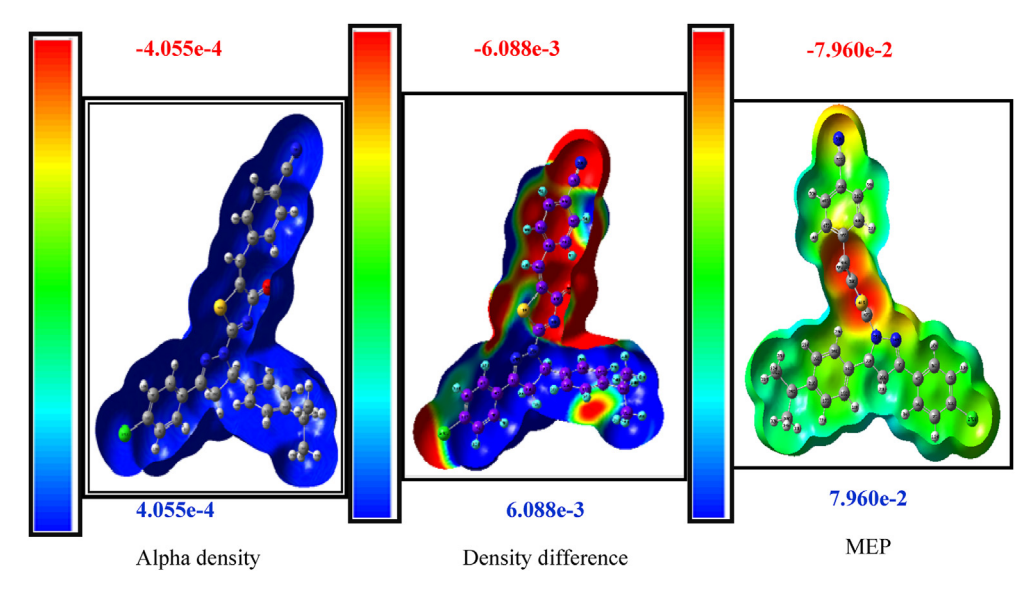


Figure 4. Alpha density (e-4), density difference (e-3), and MEP (Molecular electrostatic potential surface) of CPTBN.

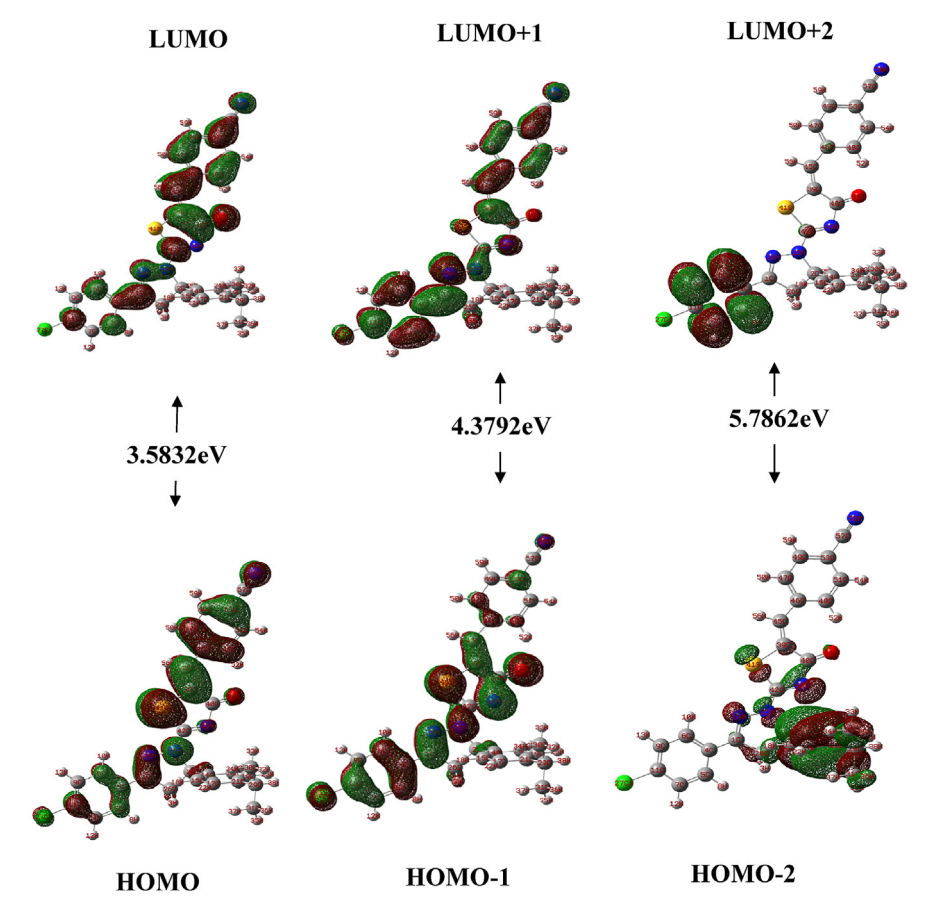


Figure 5. HOMO - LUMO energy distribution plots of CPTBN at DFT/B3LYP/6-311G basis set.

Electron affinity
$$A = -E_{LUMO}(E_L)$$
 (2)

Conforming the Koopman's statement that the negative energies of E_{HOMO} were 6.46 eV, 6.70 eV, 6.99 eV and E_{LUMO} were 2.88 eV, 2.32 eV, 1.21 eV. Moreover, the energy gap is calculated with the occurrence of orbital diagram HOMO-LUMO, HOMO-1-LUMO+1, HOMO-2-LUMO+2, and the most significant higher orbital energy gaps were determined in 6-311G at 3.58 eV, 4.37 eV, 5.78 eV (Figure 5). Predict the molecular electronic transitions properties results based on the finding the orbital energy gaps. In a series of E_{HOMO} and E_{LUMO} , it calculates the resistance to change in the electron distribution was defined by

Global hardness
$$\eta = (I - A)$$
 (3)

Reactive side of the compound show $\eta=1.79$ eV, 2.18 eV, 2.89 eV. which was find from the Eq. (3). The global softness Eq. (4) was the inverse of global hardness:

Global softness
$$\sigma = 1/\eta$$
 (4)

Value was $\sigma=0.55$ eV, 0.45 eV, 0.34 eV. Generally, the electron in solids has a chemical potential expressing (negative value of electronegativity - $\chi)$ the ability of an uncharged atom or molecule of a chemical system by Eq. (5)

$$\mu = -(I + A)/2$$
 (5)

The power of an atom in a molecule to attract electrons towards it. Value is $\chi = 4.6757$ eV, 4.5107 eV, 4.1059 eV has taken from the Eq. (6)

Electro-negativity is
$$\chi = (I + A)/2$$
 (6)

Global electrophilicity, according to Parr et al. [41], evaluates the stabilization energy when the system acquires an additional electronic charge from the environment. The relationship between electrochemical potential and global or chemical hardness can be computed using the following formula (7):

Global electrophilicity index
$$\omega = \mu 2/2\eta$$
 (7)

The electrophilicity index of the CPTBN, $\omega=6.1013$ eV, 4.6461 eV, 2.9136 eV. From the result ω , it measures the maximum electron flow

Table 4. Calculated E-HOMO, E-LUMO(H-1 \rightarrow L+1, H-2 \rightarrow L+2), energy gap (E_L-E_H), Ionization potential (I), Electron affinity (A), global hardness (η), electronegativity (χ), chemical softness (σ), chemical potential (μ) and global electrophilicity (ω) using the 6-311G levels of theory.

**				-		*			
Molecular properties	Energy (eV)	Energy gap (eV)	(I) (eV)	(A) (eV)	(ŋ) (eV)	(χ) (eV)	(σ) (eV)	(μ) (-eV)	(ω) (eV)
Еномо	-6.4673								
E _{LUMO}	-2.8841	3.5832	6.4673	2.8841	1.7916	4.6757	0.558	-4.6757	6.1013
E _{HOMO-1}	-6.7003								
E_{LUMO+1}	-2.3211	4.3792	6.7003	2.3211	2.1896	4.5107	0.457	-4.5107	4.6461
E _{HOMO-2}	-6.9990								
E_{LUMO+2}	-1.2128	5.7862	6.9990	1.2128	2.8931	4.1059	0.346	-4.1059	2.9136

between donor and acceptor orbits with lower energy transitions. These values of global reactive descriptor are computed and listed in Table 4, which ensures the molecule's indisputable biological activity.

4.5. Fock matrix for bonds

Calculations of the NBO [12] were made using the Gaussian 09 [10] program to interpret the many second-order perturbation interactions between the full orbits of one subsystem and the empty orbits of another subsystem, which is a measure of hyperconjugation intermolecular delocalization. The donor-acceptor interactions in the NBO basis were

evaluated using the second-order Fock matrix [42]. The interactions result in a loss of occupancy from the localized NBO of the idealized Lewis structure in an empty non-Lewis orbital. For each donor (i) and acceptor (j), the stabilization energy in the Eq. (8) E (2) associated with the delocalization $[i\rightarrow j]$ is estimated at

$$E(2) = \Delta Eij = qi \frac{\left(F_{ij}\right)^2}{\left(E_j - E_i\right)} \tag{8}$$

where q_i is the orbital occupancy of the donor, E_i and E_j are diagonal elements and F (i,j) is the off-diagonal NBO Fock matrix element. The

Table 5. Second-order perturbation theory analysis of Foci matrix in NBO basis corresponding to the intramolecular bonds of the title compounds.

Donor(i)	Type	ED/e	Acceptor (j)	Type	ED/e	E (2) ^a Kcal/mol	E(j)-E(i) ^b a.u	F (i,j) ^c a.u
π	(C ₆ –C ₉)	1.66281	π *	(C ₄ –C ₅)	0.39139	21	0.28	0.069
π	(C_6-C_9)	1.66281	π *	(C ₇ –C ₁₁)	0.39379	22	0.26	0.068
σ	(C_6-H_{10})	1.97641	σ*	(C ₄ –C ₅)	0.02245	5	1.06	0.064
π	(C ₇ –C ₁₁)	1.67990	π *	(C ₄ –C ₅)	0.39139	18	0.3	0.066
π	(C ₇ –C ₁₁)	1.67990	π *	(C_6-C_9)	0.34219	19	0.3	0.069
π	$(C_{14}-C_{15})$	1.64735	π *	$(C_{16}-C_{19})$	0.34219	20	0.29	0.067
π	(C ₁₄ -C ₁₅)	1.64735	π *	$(C_{17}-C_{21})$	0.35984	19	0.29	0.067
π	$(C_{16}-C_{19})$	1.69021	π *	$(C_{14}-C_{15})$	0.39031	22	0.28	0.07
π	$(C_{16}-C_{19})$	1.69021	π *	$(C_{17}-C_{21})$	0.35984	21	0.29	0.071
π	$(C_{17}-C_{21})$	1.64735	π *	$(C_{14}-C_{15})$	0.39031	22	0.27	0.069
π	$(C17 - C_{21})$	1.64735	π *	$(C_{16}-C_{19})$	0.34219	20	0.28	0.067
σ	(C ₂₉ -H ₃₈)	1.84834	π *	(C ₁₇ -C ₂₁)	0.35984	12	0.46	0.07
σ	(C ₂₉ -H ₃₈)	1.84834	σ*	$(C_{30}-H_{34})$	0.01601	6	0.86	0.063
σ	(C ₃₉ -S ₄₁)	1.97925	σ*	(N ₂₅ -C ₄₂)	0.05277	8	1.43	0.096
π	(C ₃₉ -C ₄₅)	1.73334	π *	(S ₄₁ -C ₄₂)	0.63064	29	0.22	0.079
σ	(C ₄₀ -N ₄₃)	1.97841	σ*	(N ₂₅ -C ₄₂)	0.05277	6	1.16	0.077
π	(C ₄₀ -O ₄₄)	1.91434	LP (2)	N ₄₃	1.92042	12	0.17	0.063
π	(C ₄₀ -O ₄₄)	1.91434	π *	(C ₃₉ -C ₄₅)	0.28300	9	0.27	0.047
π	$(S_{41}-C_{42})$	1.84834	LP (2)	N ₄₃	1.92042	12	0.24	0.072
π	$(S_{41}-C_{42}))$	1.84834	π *	(C ₃₉ -C ₄₅)	0.28300	27	0.34	0.089
π	(C ₄₆ -C ₄₈)	1.65062	π *	(C ₄₇ –C ₄₉)	0.29371	19	0.29	0.067
π	(C ₄₆ -C ₄₈)	1.65062	π *	(C ₅₁ -C ₅₃)	0.37039	22	0.28	0.07
π	(C ₄₇ -C ₄₉)	1.64135	π *	(C ₄₆ -C ₄₈)	0.35121	23	0.28	0.071
π	(C ₄₇ –C ₄₉)	1.64135	π *	(C ₅₁ -C ₅₃)	0.37039	21	0.27	0.069
π	$(C_{51}-C_{53})$	1.65616	π *	(C ₄₆ -C ₄₈)	0.35121	19	0.29	0.066
π	$(C_{51}-C_{53})$	1.65616	π *	(C ₄₇ –C ₄₉)	0.29371	21	0.29	0.07
LP (1)	N_2	1.99953	σ*	(C ₂ -N ₂₅)	0.03916	5	0.81	0.06
LP (1)	N ₂₅	1.99913	π *	(C ₁ -N ₂₄)	0.01741	26	0.25	0.071
LP (1)	N ₂₅	1.99913	σ*	(C ₂ -H ₅₅)	0.03916	6	0.61	0.056
LP (1)	N ₂₅	1.99913	σ*	(S ₄₁ -C ₄₂)	0.04831	7	0.74	0.07
LP (1)	N ₂₅	1.74932	σ*	(C ₄₂ -N ₄₃)	0.63064	13	0.67	0.087
LP (3)	Cl ₂₇	1.92589	π *	(C ₇ –C ₁₁)	0.39379	13	0.32	0.062
LP (1)	S ₄₁	2.00000	σ*	(C ₃₉ -C ₄₀)	0.09788	7	0.95	0.074
LP (1)	S ₄₁	1.94182	σ*	(C ₄₂ -N ₄₃)	0.05976	7	0.93	0.072
LP (1)	N ₄₃	1.99948	σ*	(C ₃₉ -C ₄₀)	0.09788	6	0.79	0.064
LP (2)	N ₄₃	1.92042	π *	(C ₄₀ -O ₄₄)	0.35013	77	0.16	0.112
LP (2)	N ₄₃	1.24797	π *	(S ₄₁ -C ₄₂)	0.63064	144.68	0.1	0.112
LP (2)	O ₄₄	1.97959	σ*	(C ₃₉ -C ₄₀)	0.09788	18	0.67	0.099
LP (2)	O ₄₄	1.88072	σ*	(C ₄₀ -N ₄₃)	0.06721	22	0.65	0.108
LP (1)	N ₅₈	1.96668	σ*	(C ₅₃ –C ₅₇)	0.03752	11	0.85	0.088
π *	(C ₁ -N ₂)	0.25467	π *	(C ₄ –C ₅)	0.39139	39	0.04	0.064
π *	(C ₇ –C ₁₁)	0.39379	π *	(C ₄ –C ₅)	0.39139	215.88	0.02	0.084
π *	(C ₇ –C ₁₁)	0.39379	π *	(C ₆ –C ₉)	0.29426	141.93	0.02	0.079
π *	(C ₃₉ –C ₄₅)	0.28300	σ*	(C ₄₀ –O ₄₄)	0.02004	32	0.06	0.07
π*	(S ₄₁ -C ₄₂)	0.63064	σ*	(N ₂₄ - Ns ₂₅)	0.03320	5	0.34	0.064

^a E (2) means energy of hyper conjugative interaction (stabilization energy).

^b Energy difference between donor and acceptor i and j NBO orbitals.

 $^{^{}c}\,$ F (i,j) is the Fock matrix element between i and j NBO orbitals.

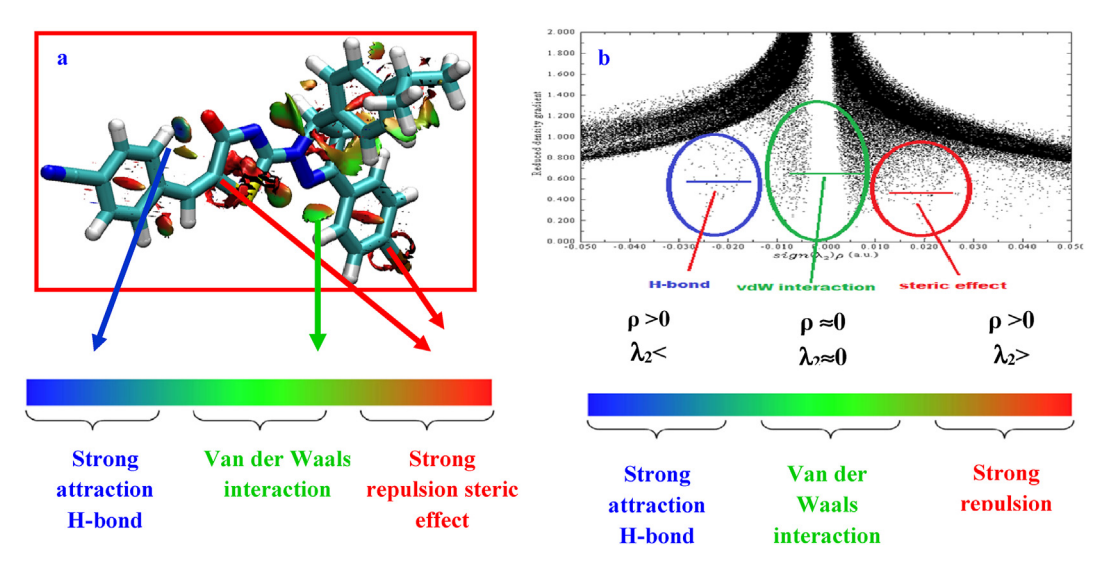


Figure 6. RDG a) 3D colour scaling of non-covalent interaction and b) 2D scatter graph of the electron densityp versus RDG interaction in CPTBN.

transmission of this electron to electron from a bonding orbital (donor- σ , π) with depreciation in its occupancy [41], an anti-bonding orbital (acceptor - σ^* , π^*) and Lone pair (LP) can be defined as charge transfer. Several other types of valuable data, such as directionality, hybridization, and partial loading, have been analyzed from the NBO results.

The strong intra-molecular hyperconjugation interaction of the π^* electrons from $C_7\text{--}C_{11}$ to the π^* anti-bonding orbital's of $S_{41}\text{--}C_{42}$ bond shows leading to the stabilization of 215.88 kcal/mol. This enhanced $\pi^*(C_7\text{--}C_{11})$ NBO further conjugates with $\pi^*(C_4\text{--}C_5)$, $\pi^*(C_6\text{--}C_9)$, resulting in enormous stabilization energy of 215.88, 141.93 Kcal/mol, as shown in Table 5. The interaction between π^* and π^* shows $(C_6\text{--}C_9)$, $(C_7\text{--}C_{11})$, and $(S_{41}\text{--} C_4)_2$ the electrons is heavy intermolecular. It allows the equilibrium of α kcal/mol, in the $(C_6\text{--}C_9)$ to the anti-bonding orbits of $(C_{11}\text{--}Cl_{27})$, $(C_4\text{--}C_5)$, and $(C_7\text{--}C_{11})$. In addition to these interactions, there is also a strong lone pair show stabilization capacity, such as LP (1)N $_{25}$ - $\pi^*(C_1\text{--}N_{24})$ 26 kcal/mol, LP (2)N $_{43}$ - $\pi^*(S_{41}\text{--}C_{42})$ 144.68 kcal/mol using 6-311G respectively. These charge transfers are responsible for the structure-activity of the system.

4.6. Reduced density gradient (RDG)

The RDG method is a powerful way to analyze non-covalent intermolecular interactions. The RDG function is a fundamental dimensionless quantity used to describe the deviation from a homogeneous electron distribution, which succeeding Eq. (9) was developed by E. R. Johnson et al. [43].

$$RDG(r) = \frac{1}{2(3\pi r^2)^{\frac{1}{2}}} \frac{|\nabla \rho(r)|}{\rho(r)^{\frac{4}{3}}}$$
(9)

where $\rho(r)$ and RDG (r) are the electron density and its first derivative, respectively. The gradient subsurface plots of RDG versus the electron density $\rho(r)$ multiplied by the sign of the second Hessian eigenvalue sign [k2(r)] were rendered by the VMD 1.9.2 program [44] based on outputs of Multiwfn software 4.1 program [45], shown in Figure 6. The RDG surface blue indicates that a stronger interactive hydrogen bond interacts between benzonitrile and thiazole ring, green colour can be identified as van der Waals (VDW) interaction region placed partial half elliptical slab present in the outer part of the title compound and red colour represent the strong repulsion that appears in the centre of the ring system and the strong region or interaction is located in the C–Cl, and thiazole ring atom. The methyl hydrogen-carbon with a hydrogen atom in the ring system as shown in the Figure 6(a).

The density values of the low-gradient spikes (the RDG versus plot) appear to be a good indicator of the strength of the interaction. When 2D

is plotting RDG values versus ρ it is more meaningful to use the sign of λ_2 is utilized to distinguish the bonded ($\lambda_2 < 0$) from nonbonding ($\lambda_2 > 0$) interactions, plotted in Figure 6(b).

4.7. Localized orbital locator (LOL) and electron localization function (ELF)

The localized orbital locator (LOL) and electron localization function (ELF) is one of the most powerful methods for understanding chemical bonding because it allows the identification of chemically relevant locations in the molecular space where electrons concentrate, such as a bonding, non-bonding and lone pair. This analysis was defined by LOL $[\gamma(r)]$ and ELF $[\eta(r)]$ which is related with Fermi hole curvature [46]. And it is defined as a measure of excess Kinetic energy density due to Pauli repulsion. The shaded surface map of electron localization function and localized orbital locator -LOL are drawn using Multi-wfn software [47], they are presented in Figures 7 and 8 respectively. Basins are divided into two categories. On the one hand, core basins are clustered around nuclei (with Z > 2), whereas valence basins occupy the remaining area. The inner atomic shell structure is quite similar to the structure provided by the core basins and a valence basin is characterized by a number of the core is connected [48, 49]. In our description, the localization colour code (Figure 7) used for the domain are: red-dot blue ring show the carbon core, red-dot yellow ring show the joining bond between core atoms or inner shell (C-C, C-N) bond and white shell rounded with rings of red, yellow, green show the valence shell (i.e., hydrogen bonding). Next, an electron localization function shows the shaded surface map obtained from localization orbits. Depending upon the density of electron it notify the boundary region are highly localized with board peak (hydrogen regions nearer to 1), the ring bond region is middle localized with a sharp peak (like water droplet) and C≡N region are low localized with small dens peak. shown in Figure 8.

4.8. Antibiotic and antifungal activity

Microbial is killed and ruled out from reproduction by antimicrobial drugs. Nevertheless, these microorganisms are caused by improper and unnecessary use of antibiotics to develop resistance to these substances [3, 50]. Thiazole compound was assayed at a concentration range of 25 μ g/ml-violet colour, 50 μ g/ml-red colour, 75 μ g/ml -green colour, 100 μ g/ml-pink colour and total control - blue colour range shown in bar chart Figure 9 against two Gram-positive bacteria: *Bacillus subtilis*, *Staphylococcus aureus* and two Gram-negative bacteria: *Escherichia coli*, *Pseudomonas aeruginosa* Figure 10. The anti-fungal activity was carried

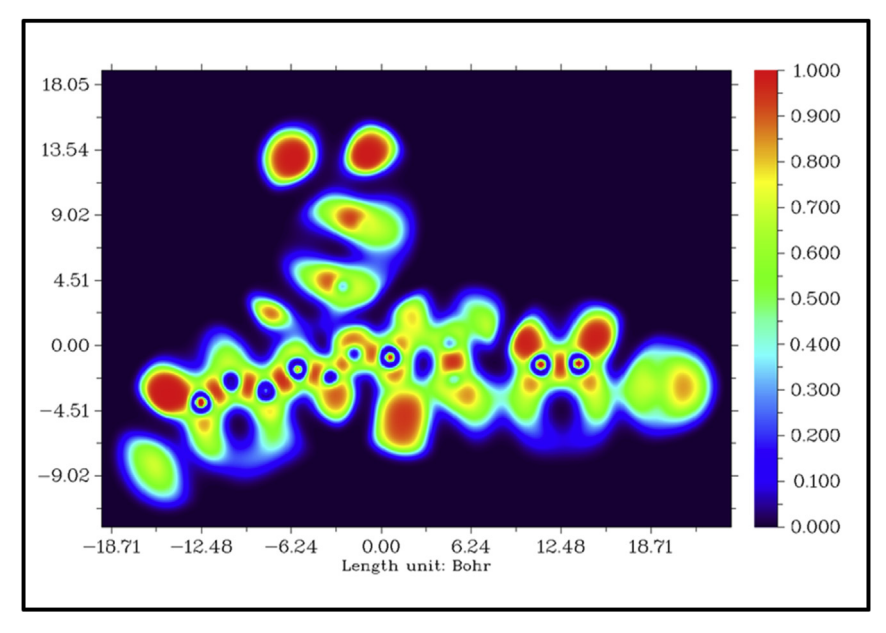


Figure 7. Localized orbital locator (LOL) for CPTBN obtained in xy plane.

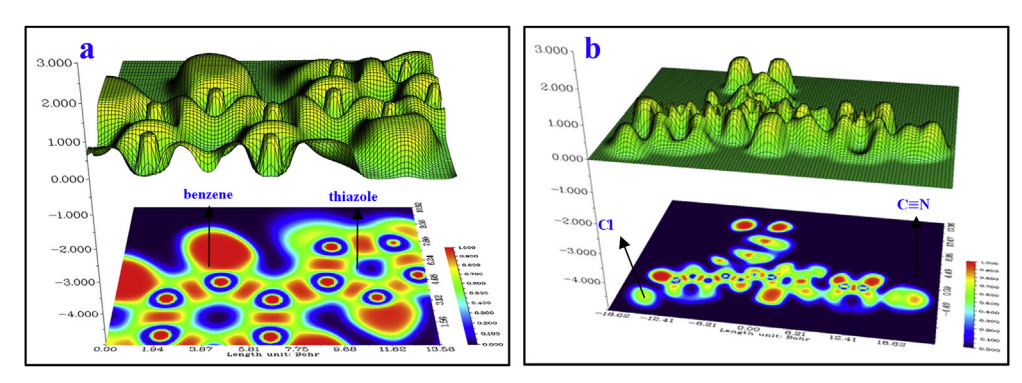


Figure 8. Electron localization function (ELF) or shaded surface map with projection effect of a) thiazole and benzene ring and b) full CPTBN.

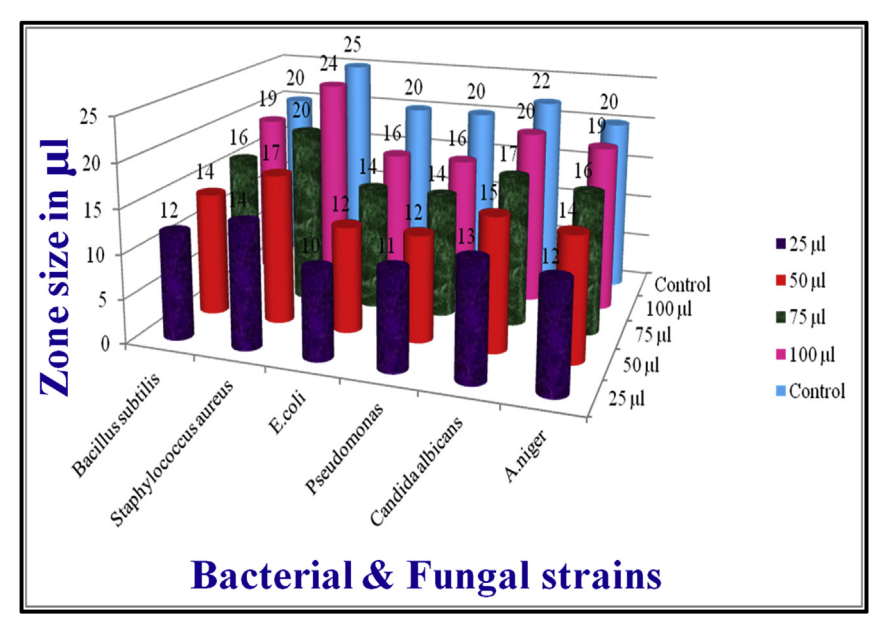


Figure 9. Bar chart for antibacterial and antifungal of CPTBN.

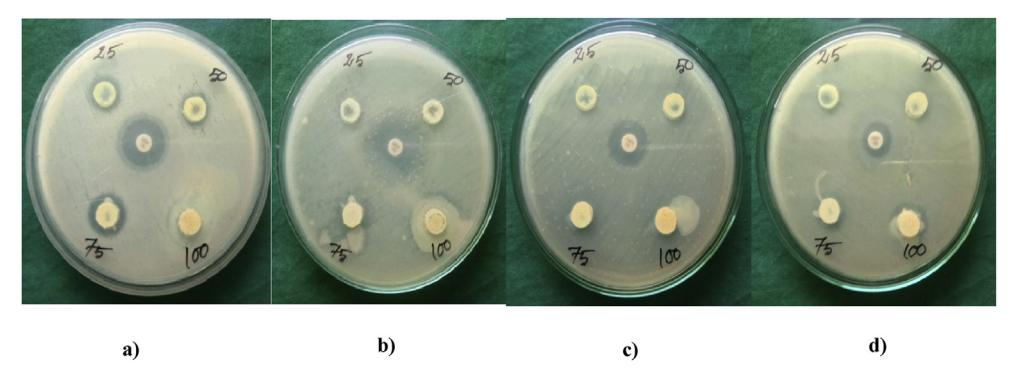


Figure 10. CPTBN microbial tests against bacterial microorganisms a) Bacillus subtilis, b) Staphylococcus aureus, c) Escherichia coli and d) Pseudomonas aeruginosa using disk-diffusion method.

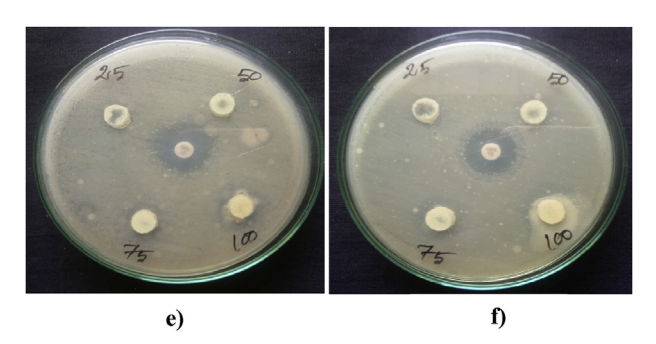


Figure 11. CPTBN microbial testing of fungal microorganism e) Candida albicans and f) Aspergillus Niger using Disk-diffusion method.

out against a well-known fungal strain *Candida albicans and Aspergillus Niger* (Figure 11) by the disc diffusion method [51]. Bacterial and fungal pathogens standardized using the DMSO standard were diluted (1:100) and added to an aliquot into respective wells. The plates were incubated in a static incubator at 37 °C for 18–24 h and the determined zone of inhibitory concentration values are listed in Table 6. Results revealed that the compound showed varying zone of inhibition against the test panel of pathogens were plotted in the form of bar graph Figure 9. Notably, the compound showed the highest inhibition against bacterial strains *Staphylococcus aureus*, whereas 24µl respectively at 100 µg/ml. Furthermore, significant inhibition against fungi strains *Candida* Aabicans whereas 20μ l showed inhibition at 100μ g/ml against A. Niger is shown in Figures.10 and 11.

4.9. Molecular docking

Molecular docking is a computational technique that tries to predict the sub-region or binding composites from multi-dimensional images of the macromolecule (protein) non-covalent bonding and a small molecule (ligands) [52]. Multiple views of the visualization are a useful way of extending 3D, the 2D display shows dimensional limitations. To collect such views directly from the PDB (protein data bank). Based on the antibiotics, antifungal and biological behaviors of the CPTBN, different types of protein activities such as high-resolution antibacterial, antifungal, Monoclonal antibodies, Nitric oxide synthase inhibitor, Staphylococcal protein A. Taken protein structure has been downloaded from the RCSB [53] PDB ID website of the database 2GOM, 4YDO, 5I76, 4D7O and 1BDC. Initially, the title molecule was minimized as a pdb file based on the DFT method and bind with downloaded protein Finding 3D structures with the lowest binding energy of the compound were constructed using auto dock tools and minimum docking energy values were investigated. The dotted lines show the bond formation between the ligand and targeted proteins. The docking runs were analyzed for the predicted binding interactions, including binding energy, inhibition constant, and intermolecular energy, between the receptors and ligand in the best scoring pose, which was listed in Table 7. Discovery studio [15] generates the binding position of a ligand-protein dock in 3D view (Figures 12a, 12c, 12e, 12g and 12i) and 2D represent (Figures 12b, 12d, 12f, 12h and 12j) represent a residual interaction energy conformation.

4.9.1. Antibacterial activity

Antibacterial activity and virtual screening by molecular docking of staphylococcus aureus is a protein tied to its complementary target to provide bacterial suppression of structure. Staphylococcus aureus (PDB ID -2GOM) protein resolution is 1.25 Å having unit cell length a = 59.59Å, b = 59.59Å, c = 45.63Å, and angle $\alpha=90^\circ,\,\beta=90^\circ,\,\gamma=90^\circ$ [54]. The docking result of CPTBN ligand interaction has shown (Figures 12a and 12b) a binding affinity to the target protein 2GOM, as indicated by the bonding interaction between the ligand and catalytic site amino acids. Glutamine (GLN) from a van der Waals interaction was found near benzonitrile and Lysine (LYS) forms a Pi-Cation interaction near the thiazole ring. Binding energy and inhibition constant are -7.913 kcal/mol and 1.42 μ M.

4.9.2. Antifungal activity

Antifungal of a medication used to treat a fungus infection medicine that contains a fungicide. One of the antifungal protein target *Candida*

Table 6. Antibiotic and Antifungal inhibition zone levels of CPTBN.

SAMPLE	DMSO Extract 10	DMSO Extract 100 μ l added and Zone of inhibition (mm/ml)									
	25 μl	50 μl	75 μl	100 μl	Control						
Bacillus subtilis	12	14	16	19	20						
Staphylococcus aureus	14	17	20	24	25						
E.coli	10	12	14	16	20						
Pseudomonas	11	12	14	16	20						
Candida albicans	13	15	17	20	22						
A.niger	12	14	16	19	20						

Heliyon	
7	
(2021)	
e07634	

Ligand name	PDB ID	Bond distance (Å)	Amino acid (residues)	Bond	Inhibition Constant (Micromolar-µM/ Nanomolar- nm))	Binding Energy (kcal/mol)	Inter-molecular energy (kcal/mol)
4-[{2-[3-(4-Chlorophenyl)-5-(4-(propan-2-yl)phenyl)-	2GOM	3.5	Glutamine (GLN)	van der Waals	1.42 μΜ	-7.98	-9.47
I,5-dihydro-1 <i>H</i> -pyrazol-1-yl]-4-oxo-		3.6	Lysine (LYS)	Pi-Cation			
1,3-thiazol-5(4 <i>H</i>)-ylidene}methyl]benzonitrile (CPTBN)	4YDO	2.1	Tyrosine (TYR)	van der Waals	16.35nm	-10.62	-12.11
		1.8	Isoleucine (ILE)	van der Waals			
		2.4	Leucine (LEU)	Pi-Alkyl			
		2.9	Tyrosine (TYR)	Pi-Pi T-shaped			
	5176	2.7	Proline (PRO)	Pi-Alkyl	4.84 μΜ	-7.25	-8.74
		2.1	Leucine (LEU)	Conventional hydrogen bond			
		2.9	Serine (SER)	van der Waals			
		2.9	Glutamine (GLN)	van der Waals			
	4D7O	1.9	Isoleucine (ILE)	van der Waals	1.63 μΜ	-7.85	-9.34
		2.4	Glycine (GLY)	van der Waals			
		2.9	Tryptophan (TRP)	Amide-Pi stacked			
		3.3	Phenylalanine (PHE)	van der Waals			
	1BDC	2.1	Phenylalanine (PHE)	Pi-Pi T-shaped	428.64nm	-8.69	-10.18
		2.7	Asparagine (ASN)	van der Waals			
		2.8	Leucine (LEU)	Alkyl			
		2.9	Serine (SER)	Conventional hydroden bond			
		2.8	Glycine (GLY)	van der Waals			

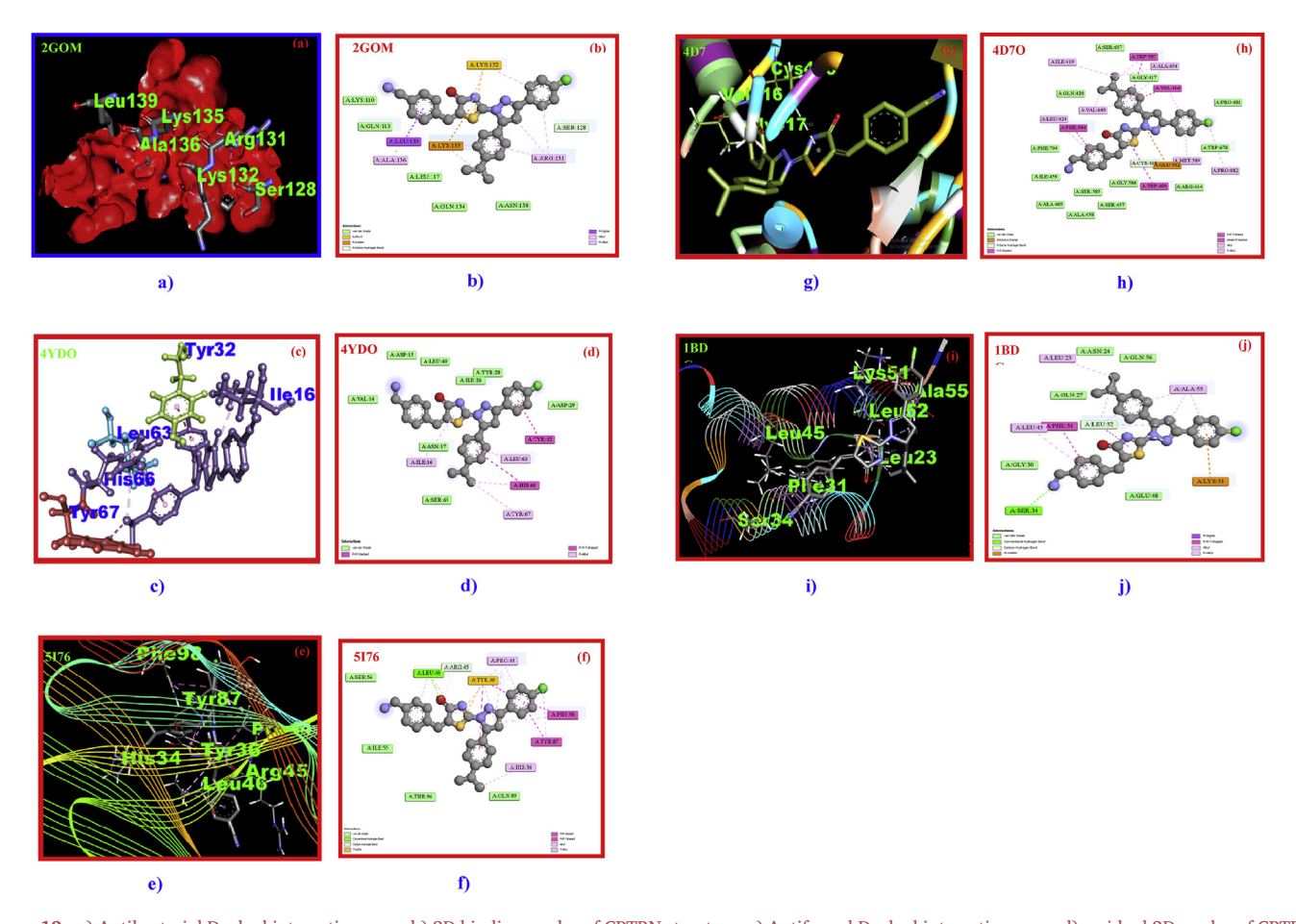


Figure 12. a) Antibacterial Docked interaction pose, b) 2D binding modes of CPTBN structure, c) Antifungal Docked interaction pose, d) residual 2D modes of CPTBN structure, e) Monoclonal antibodies Docked interaction pose, f) targeting 2D modes of CPTBN structure, g) Nitric oxide synthase inhibitor docked interaction pose, h) 2D amino acid bonding modes of CPTBN structure, i) Staphylococcal Protein A docked interaction pose and j) 2D protein interaction modes of CPTBN structure.

Albicans PDB ID: 4YDO are examined ligand (CPTBN) using molecular docking studies. Our aim to verified amino acid (residue) interaction of protein 4YDO are Crystal Structure (Figures 12c and 12d) of Candida Albicans Protein Farnesyl transferase in Apo form has a resolution 3.00 Å having a unit cell length a=96.824 Å, b=96.824 Å, c=183.082 Å, and angle $\alpha=90^\circ, \beta=90^\circ, \gamma=90^\circ$ [55]. The binding interaction between the ligand and catalytic site amino acids Tyrosine (TYR) and Isoleucine (ILE) forms a Van der Waals interaction near Thiazol ring, Leucine (LEU) forms a Pi-Alkyl interaction and Tyrosine (TYR) forms a Pi-Pi T-shaped interaction. Binding energy and inhibition constant are -10.62 kcal/mol and 16.35 Nanomolar.

4.9.3. Monoclonal antibodies

To develop highly efficient therapeutic and diagnostic agents. Monoclonal antibodies (mAbs) structure of the protein PDB ID: 5176 is used to simulate the ligand were performed by Auto Dock-Vina Software [56]. 5176 protein has a resolution 1.922Å having unit cell length $a=72.482\, \text{Å},\, b=68.037\text{Å},\, c=97.689\, \text{Å},\, \text{and angle}\, \alpha=90^\circ,\, \beta=101.85^\circ,\, \gamma=90^\circ.$ Examination of the binding energy (-7.85) kcal/mol, inhibition constant (1.76µM) and shown in Figures.12e and 12f. CPTBN ligand bind at the active site of protein by lower amino acid (residue) interaction. Amino acid Leucine (LEU) forms a conventional hydrogen bond with carbonyl present in the thiazole ring. Van der Waals interaction Serine (SER):, Glutamine (GLN): was found near both benzonitrile and propane-2-yl. Proline (PRO) residual alkyl and Pi-alkyl bind with O atom and interaction with the core of the chlorophenyl ring, thiazole ring, and pyrazole ring.

4.9.4. Nitric oxide synthase inhibitor

PDB ID - 4D7O protein (Figure 12g and 12h) [57] has a resolution 1.78 Å had a unit cell length $a=51.77 \mathring{A},\, b=110.58 \mathring{A},\, c=165.16 \mathring{A}$ and angle $\alpha=90^\circ,\, \beta=90^\circ,\, \gamma=90^\circ.$ Amino acid Tryptophan (TRP) and Phenylalanine (PHE) forms Amide-Pi stacked and van Der Waals interaction with a CH $_3$ atom in the propan group. Most of the core rings are interactive with alkyl Pi-Pi, T-Shaped, and amide Pi stacked presented in protein. Two van Der Waals interactions with Isoleucine (ILE) and Glycine (GLY) bound with benzonitrile ring. Binding energy and inhibition constants were -7.85 kcal/mol and 1.63 μM .

4.9.5. Staphylococcal Protein A

Staphylococcal Protein A (PDB ID -1BDC) receptor is a persistent human pathogen that causes a variety of diseases, both in clinical appearance and in severity found in normal human flora, located on the skin and mucous membranes. To investigate nanomolar bacterial binding targets for complementary ligand interaction. Staphylococcal Protein A interaction protein [58] shows (Figures 12i and 12j)the existence of many conventional bonds, which are as follows: Benzonitrile ring form three residual interaction at the same time are Phenylalanine (PHE) form Pi-Pi T-shaped, Serine (SER) form conventional hydrogen bond, Glycine (GLY) form VanderWaals interaction. Leucine (LEU) form carbon-hydrogen bond interaction with the core thiazole ring. Asparagine (ASN) form a van der Waals interaction was found near CH₃. The inhibition constant was 428.64 Nanomolar and the observed binding energy was -8.69 kcal/mol.

5. Conclusion

In the integrating work, analysis of 4-[{2-[3-(4-chlorophenyl)-5-(4propan-2-yl) phenyl)-4, 5-dihydro- 1H- pyrazol-1-yl]-4-oxo-1, 3thiazol-5(4H)-ylidene} methyl] benzonitrile [CPTBN] molecule through the first level of the spectral statistics on experimental FT-IR, and FT-Raman are recorded and at the next level, detailed vibrational assignments using DFT/B3LYP/6-31G and B3LYP/6-311G basis level were computed. The geometry of the title molecule is analyzed theoretically. The three different zone mapped surfaces provide a visual plot to understand the atoms in an intermolecular polarity. Positive and negative regions of the MEP map that are localized around the title compound indicate possible sites of nucleophilic and electrophilic reactivity of the molecule. The energy flow from the gap is generally low to high, and Gaussian diagrams have been used to visualize it. The reactive nature of the CPTBN is hypothetically dissected using techniques for the quantum system and addressed by electronic properties, such as hardness, chemical potential, electro-negativity, global hardness, and global softness. The NBO interprets the conjugate relationship of the orbital donor and the unoccupied orbital acceptor in the molecular system. RDG generates the colourful illustration, hydrogen bond, van der Waals and steric effects depict the interaction of the atoms inside the molecule. The electron localization of the region in the molecular space at which identified chemically significant regions as a bond and lone pair. Antimicrobial inhibitory activity against the compound was explored through the tests. Utilizing the molecular restraining nature of the particle was seen as the most vulnerable restricting ligand to a catalyst and the most grounded hydrogen authoritative. The title molecule is docked with receptors highresolution antibacterial (2GOM), antifungal (4YDO), Monoclonal antibodies (5I76), Nitric oxide synthase inhibitor (4D70), Staphylococcal protein A (1BDC) and gives good binding affinity values. Acceptable and delicate antibacterial effect against all screened pathogens and the definitive medicine support the docking results. The nature of the molecules shows the binding activity of thiazole with biological targets were examined and discussed in terms of interaction energy. The inclusion of antimicrobial resistance raises to the development of new antibiotics through a direct further rational work mode of action.

Declarations

Author contribution statement

- N. Shanmugapriya: Conceived and designed the experiments; Performed the experiments; Analyzed and interpreted the data; Wrote the paper.
- V. Balachandran, B. Revathi: Contributed reagents, materials, analysis tools or data.
 - B. Narayana, Vinutha V. Salian: Performed the experiments.
 - K. Vanasundari, C. Sivakumar: Analyzed and interpreted the data.

Funding statement

Badiadka Narayana was supported by University Grants Commission (SR/S/Z/-23/2010/32).

Data availability statement

No data was used for the research described in the article.

Declaration of interests statement

The authors declare no conflict of interest.

Additional information

No additional information is available for this paper.

References

- [1] B. Gadhiya, M. Rajput, A. Bapodra, K. Ladva, Design, synthesis, and evaluation of antimicrobial activities of some novel thiazole and thiadiazole derivatives clubbed with 1H-Benzimidazole, Rasayan J. Chem. 9 (2016) 355–372.
- [2] https://wikimili.com/en/imidazole.
- [3] A. Viji, V. Balachandran, S. Babayan, B. Narayana, V.V. Saliyan, FT-IR and FT-Raman investigation, quantum chemical studies, molecular docking study and antimicrobial activity studies on the novel bioactive drug of 1-(2,4-Chlorobenzyl)-3-[2-(3-(4-chlorophenyl)-5-(4-(propan-2-ly)phenyl-4,5-dihydro-1H-pyrazol-1-yl]-4 oxo -4,5-dihydro-1,3-thiazol-5(4H)-ylidence]-2,3-dihydro-1H-indol-2-one, J. Mol. Struct. 1215 (2020) 12822244.
- [4] E. Nour, A. Abdel-Sattar, A.M. E1-Naggar, M.S.A. Abdel-Mottaleb, Novel thiazole derivatives of medicinal potential: synthesis and modeling, J. Chem (Hindawi) (2017) 1–11.
- [5] R.N. Phalen, W.K. Wong, Integrity of disposable nitrile exam gloves exposes to simulated movement, J. Occup. Environ. Hyg. 8 (5) (2011) 289–299.
- [6] A.R. Krishnan, H. Saleem, S. Subashchandra bose, N. Sundaraganesan, S. Sebastian, Molecular structure, vibrational spectroscopic (FT-IR, FT-Raman), UV and NBO analysis of 2-chlorobenzonitrile by density functional method, Spectrochim. Acta 78 (2011) 582–589.
- [7] A. Ayati, S. Emami, A. Asadipour, A. Shadier, A. Foroumadi, Recent application of 1,3-thiazole core structure in the identification of new lead compounds and drug discovery, Eur. J. Med. Chem. 97 (2015) 699–728.
- [8] Vinutha V. Salian, B. Narayana, B.k. Sarojini, M.S. Kumar, A.G. Lobo, Tailor-made heterocyclic pyrazoline- thiazolidinones as effective inhibitors of Escherichia coli FabH: design, synthesis and structural studies, J. Mol. Struct. 1192 (2019) 91–104.
- [9] M.J. Frisch, G.W. Trucks, D.J. Fox, Gaussian 09, Revision E.01, Gaussian, Inc., Wallingford CT, 2009.
- [10] M.H. Jamroz, Vibrational Energy Distribution Analysis VEDA, 4, Warsaw.S, 2004.
- [11] R. Dennington, T. Kerth, J. Millam, Gauss View, Version 5, Semi cham. Inc., Shawnee Mission KS, 2009.
- [12] E.D. Glendening, A.E. Reed, J.E. Carpenter, F. Weinhold, NBO Version 3.1, Pittsburg, Theoretical chemistry institute and department of chemistry, University of Wisconsin, Madison, 1988. E.D. Glendening, C.R. Landis, F. Weinhold, Comput. Mol. Sci. 2 (2012) 1.
- [13] T. Lu, F. Chen, Multiwfn: a multifunctional wave function analyzer, J. Chem. Inf. Comput. Chem. 33 (2012) 580–592.
- [14] G.M. Morris, R. Huey, W. Lindstrom, M.F. Sanner, R.K. Belew, D.S. Goodsell, A.J. Olson, AutoDock4 and AutoDockTools4: automated docking with selective receptor flexibility, J. Comput. Chem. 30 (2009) 2785–2791.
- [15] S. Diego, Cailf, Discovery Studio Modeling Environment, Accelry software Release 4.0, USA, 2013.
- [16] D. Seeliger, B.L. De Groot, Ligand docking and binding site analysis with Pymol and Auto dock/Vina, J. Comput. Aided Mol. Des. 24 (2010) 417–442.
- [17] S. Parveen, M.A. Al-Alshaikh, C. Y Panicker, A.A. El-Emam, Vinutha V. Salian, B. Narayana, Spectroscopic investigations and molecular docking study of (2 E)-1-(4-Chlorophenyl)-3-[4-(propan-2-yl)phenyl]prop-2-en-1-one using quantum chemical calculations, J. Mol. Struct. 1120 (2016) 317–326.
- [18] Mustafa Er, Arif Ozer, S. Direkel, T. Karakurt, H. Tahtaci, Novel substituted benzothiazole and Imidazo[2,1-b][1,3,4] thiadiazole derivatives: synthesis, characterization, molecular docking study, and investigation of their in vitro antileishmanial and antibacterial activities, J. Mol. Struct. 1194 (2019) 284–296.
- [19] K. Vanasundari, V. Balachandran, M. Kavimani, B. Narayana, Spectroscopic investigation, vibrational assignments, Fukui functions, HOMO-LUMO, MEP and molecular docking evaluation of 4-[(3,4 –dichlorophenyl) amino] 2- methylidene 4 oxo butanoic acid by DFT method, J. Mol. Struct. 1147 (2017) 136–147.
- [20] Priyanka Singh, S.S. Islam, A. Prabaharan, Spectroscopic investigation (FT-IR, FT-Raman), HOMO-LUMO, NBO, and molecular docking analysis of N-ethyl-N-ntrosourea, a potential anticancer agent, J. Mol. Struct. 1154 (2019) 39–50.
- [21] M. Sathish, G. Meenakshi, S. Xavier, S. Sebastain, S. Periandy, N.A. Ahmad, J. Jamalis, M.M. Rosli, H. Kun-Fun, Synthiesis, molecular structure, hirshfeld surface, spectral investigation and molecular study of 3-(5-bromo-2-thienyl)-1-(4fluorophenyl)-3-acetyl-2-pyrazoline(2) by DFT method, J. Mol. Struct. 1164 (2018) 420–437.
- [22] S. Beegum, Y. Sheena Mary, C.Y. Panicker, S. Armakovic, S.J. Armakovic, M. Arisoy, O. Temiz-Arpaci, C.V. Alsenoy, Spectroscopic, tantimicrobial and computational study of novel benzoxazole derivative, J. Mol. Struct. 1176 (2019) 881–894.
- [23] F.R. Dollish, in: W.G. Fateley, F.F. Bentley (Eds.), Characteristic Raman Frequencies of Organic Compounds, Wiley, New York, 1974.
- [24] R.M. Silverstein, G.C. Bassler, T.C. Morrill, Spectrometric Identification of Organic Compounds, John Wiley & Sons, New York, 1981.
- [25] S. Fatma, A. Bishnoi, A.K. Verma, Synthesis, spectral analysis (FT-IR, 1 HNMR, 13CNMR and UV-visible) and quantum chemical studies on molecular geometry, NBO, NLO, chemical reactivity and thermodynamic properties of novel 2-amino-4-(4-(dimethylamino)phenyl)-5-oxo-6-phenyl-5, 6-dihydro-4H-pyrano [3, 2-c] quinoline-3-carbonitrile, J. Mol. Struct. 1095 (2015) 112–124.
- [26] F. Bardak, Experimental and DFT analysis of structural and spectroscopic features of nitroterephthalic acid, and computational insights into its molecular interactions with hER-a via molecular docking, J. Mol. Struct. 1175 (2019) 458–470.
- [27] G.P. Sheeja Mol, D. Aruldas, I.H. joe, S. Balachandran, A.R. Anuf, J. George, Spectroscopic investigation, fungicidal activity and molecular dynamics simulation on benzimidazol-2-yl carbamate derivatives, J. Mol. Struct. 1176 (2019) 226–237.
- [28] S.S. Khemalapure, V.S. Katti, C.S. Hiremath, M. Basanagouda, S.M. Hiremath, S.J. Armakovic, Molecular structure, optoelectronic properties, spectroscopic (FT-

- IR,FT-Raman and UV-Vis), H-BDE, NBO and drug likeness investigations on 7,8-benzocoumarin-4-acetic acid(7BAA), J. Mol. Struct. 1195 (2019) 815–826.
- [29] T.K. Kuruvilla, S. Muthu, J.C. Prasana, J. George, S. Seyyanthi, Spectroscopic(FT-IR, FT-Raman), quantum mechanical and docking studies in methyl[(3s)-3-(naphthalene-1-yloxy)-3-(thiophen-2-yl)propyl]amine, J. Mol. Struct. 1175 (2019) 163–174.
- [30] S.C. Jevaseelan, R. Premkumar, K. Kaviyarasu, A. Milton Franklin Benial, Spectroscopic, quantum chemical, molecular docking and in-vitro, anti-cancer activity studies on 5-methoxyindole-3- carboxaldehyde, J. Mol. Struct. 1197 (2019) 134-146.
- [31] A.S. E1-Azab, Y. Sheena Mary, C. Yohannan Panicker, Alaa A.M. Abdel-Aziz, Ibrahim A. A1- Suwaidn, C.V. Alsenov, FT-IR, FT-Raman and molecular docking study of ethyl4-(2(4-oxo-3-phenethyl-3,4-dihydroquinazolin-2-ylthio)acetamido) benzoate, J. Mol. Struct. 111 (2016) 9–18.
- [32] V. Madhavan, H.T. Varghese, S. Mathew, J. Vinsova, C.Y. Panicker, FT-IR, FTRamanand DFT calculations of 4-chloro-2-(3, 4-dichlorophenylcarbamoyl) phenyl acetate, Spectrochim. Acta 72 (3) (2009) 547–553.
- [33] N.P. Roeges, A Guide to the Complete Interpretation of Infrared Spectra of Organic Structures, Wiley, 1994.
- [34] E. Mooney, The infra-red spectra of chloro-and bromobenzene derivatives II. Nitro benzenes, Spectrochim. Acta. 20 (6) (1964) 1021–1032.
- [35] V. Sortur, J. Yenagi, J. Tonannavar, V.B. Jadhav, M.V. Kulkarni, Spectrochim. Acta A 71 (2008) 688–694.
- [36] M. Govindarajan, M. Karabacak, Analysis of vibrational spectra (FT-IR and FT-Raman) and nonlinear optical properties of organic 2-chloro-p-xylene, Spectrochim. Acta 94 (2012) 36–47.
- [37] N. Sundaraganesan, S. Ayyappan, H. Umamaheswari, B. Dominic Joshua, FTIR, FTRaman Spectra and ab initio, DFT vibrational analysis of 2,4-dinitrophenylhydrazine, Spectrochim. Acta 66 (2007) 17–27.
- [38] S. Fatma, A. Bishnoi, V. Singh, Fatmah A.M. A1-Omary, Ali A.E. Emam, S. Pathak, R. Srivastava, O. Prasad, L. Sinha, Spectroscopic and 1-(2,6-bis (4-methoxyphenyl)-3,3-dimethylpiperidine-4-ylidene)-2-(3-(3, 5-dimethyl-1 H pyrazol-1-yl)pyrazin-2-yl)hydrazine by DFT method, J. Mol. Struct. 1106 (2016) 277–285.
- [39] Y.S. Mary, C.Y. Panicker, M. Sapna Kumari, B. Narayana, J.A. War, FT-IR, NBO, HOMO-LUMO, MEP analysis and molecular docking study of 1-[3-(4Fluorophenyl)-5-phenyl-4, 5-dihydro-1H-pyrazol-1-yl] ethanone, Spectrochim. Acta 5 (2015) 483–493.
- [40] T.A. Koopmans, Uber die Zuordnung von wellen funktionen and Eigenwerten zu den einzelnen Elektronen Eines Atoms, Physica 1 (1934) 104–113.
- [41] R.G. Parr, L.V. Szentpaly, S. Liu, Electrophilicity index, J. Am. Chem. Soc. 121 (9) (1999) 1922–1924.
- [42] M. Karabacak, L. Sinha, O. Prasad, Z. Cinar, M. Cinar, The spectroscopic (FT-Raman, FT-IR, UV and NMR), molecular electrostatic potential, polarizability and hyperpolarizability, NBO and HOMO–LUMO analysis of monomeric and dimeric

- structures of 4-chloro-3,5-dinitrobenzoic acid, Spectrochimica Acta A Mol. Biomol. Spectrosc. 93 (2012) 33–46.
- [43] E.R. Johnson, S. Keinan, P. Mori-Sanchez, J. Contreras-Garcia, A.J. Cohen, W. Yang, Revealing non-covalent interactions, J. Am. Chem. Soc. 132 (18) (2010) 6498-6506
- [44] W. Humphrey, A. Dalke, K. Schulten, VMD: visual molecular dynamics, J. Mol. Graph. 14 (1996) 33–38.
- [45] T. Lu, F. Chen, A multifunctional wave function analyzer, J. Comput. Chem. 33 (2012) 580–592.
- [46] A.D. Becker, K.E. Edgecombe, A simple measure of electron localization in atomic and molecular systems, J. Chem. Phys. 92 (1990) 5397–5403.
- [47] S. Noury, F. Colonna, A. Savin, B. Silvi, Analysis of the delocalization in the topological theory of chemical bond, J. Mol. Struct. 450 (1998) 59–68.
- [48] K. Jayasheela, Lamya H. Al-Wahaibi, S. Periandy, Hanan M. Hassan, S. Sebastian, S. Xavier, J.C. Daniel, Ali A. El-Emam, M.I. Attia, Probing vibrational activities, electronic properties, molecular docking, and hirshfeld surfaces analysis of 4-chlorophenyl({[(1E)-3-(1Himidazol-1-yl)-1-phenyl propylidene] amino}oxy) methanone: apromising anti-Candida agent, J. Mol. Struct. 1159 (2018) 83–95.
- [49] A. Savin, The electron localization function (ELF) and its relatives: interpretations and difficulties, J. Mol. Struct. 727 (1-3) (2005) 127–131.
- [50] N. Salih, J. Salimon, E. Youif, Synthesis and antimicrobial activities of 9H-carbazole derivatives, Arab. J. Chem. 9 (2016) 781–786.
- [51] E. Yousif, E. Rentschler, N. Salih, J. Salimaon, A. Hameed, M. Katan, Sythesis and antimicrobial screening of tetra schiff bases of 1,2,4,5-tetra (5-amino-1,3,4thiadiazole-2-yl)benzene, J. Saudi Chem.Soc. 18 (2014) 269–275.
- [52] D.B. Kitchen, H. Decornez, J.R. Furr, J. Bajorath, Docking and scoring in virtual screening for drug discovery: methods and applications, Nat. Rev. Drug Discov. 3 (2004) 935–949.
- [53] RCSB. http://www.rcsb.org/pdb-structure.
- [54] M. Hammel, G. Sfyroera, D. Ricklin, P. Magotti, J.D. Lambris, B.V. Geisbrecht, A structural basis for complement inhibition by staphylococcus aureus, Nat. Immunol. (2007) 430–437.
- [55] S. Kumar, M.F. Mabanglo, M.A. Hast, Y. Shi, L.S. Beese, Crystal Structure of Candida Albicans Protein Farnesyltransferase in Apo Form, Wiley, 2013.
- [56] O. Trott, A.J. Olson, Software news and update Auto Dock-Vina: improving the speed and accuracy of docking with a new scoring function, efficient optimization, and multithreading, J. Comput. Chem. 31 (2010) 455–461.
- [57] T.L. Poulos, H. Li, J.K. Holden, S. Kang, F.C. Beasley, M.A. Cinelli, S.G. Roy, Nitric oxide synthase as a target for Methicillin- resistant Staphylococcus aureus, J. Chem Biol. 22 (2015) 785–792.
- [58] H. Gouda, H. Torigoe, A. Saito, M. Sato, Y.J. Arata, I. Shimada, Three-dimensional solution structure of the B domain of staphylococcal protein A: comparisons of the solution and crystal structures, Biochemistry 31 (1992) 199.

盒

Sources

Title	~	Enter ti	tle			Fir	nd sources				
Title: Asian Journal Of Che	emist	try ×									
which provides an i calculation of CiteS	ne Ci ndic core, value	iteScore me ation of re , as well as es have bee	search impact, retroactively fo	ensure a more robust, stab earlier. The updated methor or all previous CiteScore ye d are no longer available.	odology will be app	olied to	the				
ter refine list			1 result		业 Dow	nload :	Scopus Source List	(i) Learn n	nore about Sc	opus Source	Lis
pply Clear filters			☐ All ∨	Export to Excel	Save to source list			View met	rics for year:	2020	~
isplay options		^	Sou	rce title 🗸	CiteSo	core 🗸	Highest percentile ↓	Citations 2017-20 ↓	Documents 2017-20 ↓	% Cited ↓	>
Display only Open Access journals unts for 4-year timeframe No minimum selected			1 Asia	in Journal of Chemistry	0.7		17% 327/398 General Chemistry	1,459	2,085	32	
⁾ Minimum citations			H								
Minimum documents			^ Тор	of page							
escore highest quartile											
Show only titles in top 10 percent											
1st quartile											
2nd quartile											
3rd quartile											
4th quartile											
ource type		^									
Journals											
Book Series											
Conference Proceedings											
Trade Publications) 100		12/22 D	K. RENUK	A I	31 3 2 ² DEVI		Tf.42	3/15/2	מע
pply Clear filters	1	Le	3	Ass	ociate Profesi	sor &	Head				

Dr. V. BALACHANDRAN Assistant Professor Research Department of Physics A. A. Government Aret College Niueiri, Tirchirappalli - 021 211

Associate Professor & Head PG & Research Dept. of Physics Govt. Arts College for Women (A) Pudukkottai - 622 001.



ASIAN JOURNAL OF CHEMISTRY



https://doi.org/10.14233/ajchem.2022.23565

Spectroscopic Identification, Structural Features and Molecular Docking Studies on 5-(4-Propoxybenzylidene)-2-[3-(4-chlorophenyl)-5-[4(propan-2-yl) phenyl-4,5-dihydro-1*H*-pyrazol-1-yl]-1,3-thiazol-4(5*H*)-one using Pim-1 Kinase Cancer Protein

N. Shanmugapriya^{1,6}, K. Vanasundari^{1,6}, V. Balachandran^{1,*,6}, B. Revathi^{1,6}, C. Sivakumar^{1,6} and A. Viji^{2,6}

¹Centre for Research, Department of Physics, Arignar Anna Government Arts College (Affiliated to Bharathidasan University), Tiruchirappalli, Musiri-621211, India

²KongunaduCollege of Engineering and Technology (Autonomous), Thottiam, Tiruchirappalli-621215, India

*Corresponding author: E-mail: brsbala@rediffmail.com

Received: 3 October 2021; Accepted: 14 December 2021; Published online: 10 March 2022; AJC-20726

A comprehensive investigation of the molecular structure, electronic properties and vibrational spectra of 5-(4-propoxybenzylidene)-2-[3-(4-chlorophenyl)-5-[4-(propan-2-yl)phenyl]-4,5-dihydro-1*H*-pyrazol-1-yl]-1,3-thiazol-4(5*H*)-one have been studied. Many natural and/ or synthetic compounds contain, thiazole which are attractive compounds found in the building of numerous natural products and certain pharmaceutical agents. To understand the molecular-orbital interaction and structural investigation of the title compound, the density functional theory (DFT) calculation has been carried out using B3LYP/6-31G and 6-311G basis sets combination. The experimental FT-IR, FT-Raman spectral data along with theoretical quantum chemical calculation were investigated. For potential energy distributions (PED) analysis, the VEDA 4 program is utilized to do comparative frequency assignments. With the optimized structures, the highest occupied molecular orbital (HOMO), the lowest unoccupied molecular orbital (LUMO) energies, molecular electrostatic potential (MEP) and natural bond orbital (NBO) were applied to describe the chemical reactivity. The electron density interactions distributed in space, which exist within these compounds are analyzed by different topological methods namely, atom in molecule (AIM), localized orbital locator (LOL), electron localization function (ELF) and the reduced density gradient (RDG). Finally, the molecular docking studies of the title compound for potent Pim-1 kinase cancer PDB ID: 3A99, 1GJ8, 1XQZ was investigated using the Auto Dock program.

Keywords: Thiazole, DFT, Atom in molecule, Reduced density gradient, Electron localization function, Pim kinase inhibitor.

INTRODUCTION

Heterocyclic aromatic compounds containing nitrogen and sulphur are the important molecules in organic chemistry synthesis [1,2]. Susithra *et al.* [3] reported when heterocycles are supposed to have hetero-nuclear atoms, they can be acted as an ideal ligand, which can delocalize and thereby stimulate resonance hybridization to interact with strong intermediate to produce the antimalarial drugs. The geometrical parameters such as bond length of 5-(4-propoxybenzylidene)-2-[3-(4-chlorophenyl)-5-[4-(propan-2-yl) phenyl]-4,5-dihydro-1*H*-pyrazol-1-yl]-1,3-thiazol-4(5*H*)-one have been obtained from B3LYP/6-31G and 6-311G basis sets. The global reactivity descriptors (ionization potential, electron affinity, electronegativity, electrophilicity index, global hardness, global soft-

ness and chemical potential) has been predicted with the help of HOMO/LUMO energy values. Experimental FT-IR, FT-Raman spectra of the title compoundwere recorded and compared with the computed values obtained by the same level of DFT with B3LYP functional.

Chemically interactive regions in the molecule have been concentrated through aim in molecule (AIM), localized orbital locator (LOL), electron localization function (ELF) and reduced density gradient (RDG) [3]. Natural bond orbital (NBO) analysis has been performed to explain the conjugative interaction, donor, acceptor and second-order perturbation of the compound. Also, based on a key factor in PASS online data allows to define a variety of medicinal potential. Attract attention by repetition in listening data and then provide content of Pim-1 kinase inhibitors. The proto-oncogene proviral integration site for

This is an open access journal, and articles are distributed under the terms of the Attribution 4.0 International (CC BY 4.0) License. This license lets others distribute, remix, tweak, and build upon your work, even commercially, as long as they credit the author for the original creation. You must give appropriate credit, provide a link to the license, and indicate if changes were made.

Moloney murine leukemia virus (PIM) kinases (PIM-1, PIM-2 and PIM-3) are serine/threonine kinases that are involved in several signalling pathways important in cancer cells [4-6]. This investigation aimed to evaluate the role Pim kinase inhibitor in ligand progression using molecular docking.

EXPERIMENTAL

The synthesized compound 5-(4-propoxybenzylidene)-2-[3-(4-chlorophenyl)-5-[4-(propan-2-yl)phenyl]-4,5-dihydro-1H-pyrazol-1-yl]-1,3-thiazol-4(5H)-one has been taken without any further purificationas per the procedure reported by Salian et al. [7] and spectroscopic grade for acquiring spectra. The FT-IR spectrum of the compound were recorded in Perkin-Elmer spectrometer fitted with a KBr beam splitter covering $4000-400 \text{ cm}^{-1}$ region at a resolution of $\pm 1 \text{ cm}^{-1}$. The FT-Raman spectrum of the chosen compound was measured using Bruker RFS 27 model. The spectrum was recorded in the region 3500-0 cm⁻¹ Stokes region using the 1064 nm line of a Nd:YAG laser for the excitation operating at 200 mW power.

Computational details

The DFT computational method is widely used to describe the quantum states of many-electron systems of the molecule. The Gaussian 09W [8] program package was utilized to proceed with DFT calculations on the title compound through, B3LYP/ 6-31G and B3LYP/6-311G basis sets to characterize the structure electronic and other properties. The geometrical parameter bond length has been obtained using B3LYP/6-31G and 6-311G basis sets [9]. Further, we have used the optimized ground state geometry of the title compound to study the different properties

like FT-IR, FT-Raman, MEP surface mapping and NBO analysis. The theoretical vibrational wavenumber obtained for compound is interpreted by means of potential energy distribution (PED %) calculations using VEDA4 software [10] Frontier molecular orbital (FMOs) analysis (HOMO-LUMO) and molecular electrostatic potential (MEP) with contour map have been performed by Gauss View 5.0 to obtain the electronic properties of the title compound. Multiwfn software [11] has also been utilized to obtain topology analysis (AIM, RDG, LOL and ELF). NBO analysis [12] provides an investigation of charge transfer or conjugative interactions in molecular systems, has been done using NBO 3.1 program available in Gaussian 09 package at DFT/6-311G level of theory. Besides, molecular docking studies were visualized using pymol and Discovery studio software [13,14]. The interactions of the title molecule with a Pim-1 kinase inhibitors PDB ID: 3A99, 1GJ8, 1XQZ receptors were studied.

RESULTS AND DISCUSSION

Molecular geometry: The optimized molecular structure of the title compound is shown in Fig. 1. The bond lengths of the title compound compared with a closely related crystallographic data available in literature [7] are presented in Table-1.

According to it, the C-H bond length observed at 1.08-1.10 Å for phenyl ring and 1.09 Å for pyrazol ring using a theoretical approach by B3LPY/6-31G and B3LPY/6-311G. Experimentally, the C-H bond in phenyl ring has a bond length range of 0.93 Å and 0.97-0.98 Å in pyrazol ring. This difference might be attributed due to fact that low scattering factor of hydrogen atom involved in the diffraction method [15]. The

TABLE-1 OPTIMIZED GEOMETRICAL PARAMETERS (BOND LENGTHS, Å) OF 5-(4-PROPOXYBENZYLIDENE)-2-[3-(4-CHLOROPHENYL)-5-[4-(PROPAN-2-YL)PHENYL]-4,5-DIHYDRO-1*H*-PYRAZOL-1-YL]-1,3-THIAZOL-4(5*H*)-ONE

Parameter	B3LYP/ 6-31G	B3LYP/ 6-311G	XRD	Parameter	B3LYP/ 6-31G	B3LYP/ 6-311G	XRD	Parameter	B3LYP/ 6-31G	B3LYP/ 6-311G	XRD
C_1 - C_4	1.46	1.46	1.46	C ₁₆ -H ₂₀	1.08	1.08	0.93	C_{42} - N_{43}	1.30	1.30	1.30
C_1-N_{24}	1.31	1.30	1.29	C_{17} - C_{21}	1.41	1.41	1.38	C_{45} - C_{46}	1.46	1.46	1.45
C_{1} - C_{26}	1.52	1.52	1.50	C ₁₇ -H ₂₂	1.09	1.08	0.93	C_{45} - H_{56}	1.09	1.09	0.93
C_2 - C_{14}	1.52	1.52	1.51	C_{19} - C_{21}	1.40	1.40	1.39	C_{46} - C_{47}	1.42	1.41	1.39
C_2 - N_{25}	1.51	1.51	1.51	C ₁₉ -H23	1.09	1.08	0.98	C_{46} - C_{48}	1.42	1.42	1.39
C_2 - C_{26}	1.56	1.56	1.47	C_{21} - C_{29}	1.53	1.53	1.52	C_{47} - C_{49}	1.39	1.39	1.38
C_2 - H_{55}	1.09	1.09	0.98	N ₂₄ -N ₂₅	1.39	1.39	1.38	C_{47} - H_{50}	1.09	1.08	0.93
H_3-C_{26}	1.09	1.09	0.97	N_{25} - C_{42}	1.35	1.35	1.34	C_{48} - C_{51}	1.39	1.39	1.37
C_4 - C_5	1.41	1.41	1.38	C_{26} - H_{28}	1.10	1.09	0.97	C_{48} - H_{52}	1.08	1.08	0.93
C_4 - C_6	1.41	1.41	1.40	C_{29} - C_{30}	1.55	1.54	1.41	C_{49} - C_{53}	1.40	1.40	1.38
C_5 - C_7	1.40	1.40	1.37	C_{29} - C_{31}	1.55	1.54	1.41	C_{49} - H_{57}	1.08	1.08	0.93
C_5 - H_8	1.08	1.08	0.93	C_{29} - H_{38}	1.10	1.09	0.96	C_{51} - C_{53}	1.41	1.40	1.36
C_6 - C_9	1.39	1.39	1.37	C_{30} - H_{32}	1.10	1.09	0.96	C_{51} - H_{54}	1.08	1.08	0.93
C_6 - H_{10}	1.08	1.08	0.93	C_{30} - H_{33}	1.10	1.09	0.96	C_{53} - O_{58}	1.38	1.39	1.37
C_{7} - C_{11}	1.39	1.39	1.36	C_{30} - H_{34}	1.10	1.09	0.96	O_{58} - C_{59}	1.46	1.46	_
C_7 - H_{12}	1.08	1.08	0.93	C_{31} - H_{35}	1.10	1.09	0.96	C_{59} - H_{60}	1.10	1.09	_
$C_9 - C_{11}$	1.40	1.39	1.38	C_{31} - H_{36}	1.10	1.09	0.96	C_{59} - H_{61}	1.10	1.09	_
C_9 - H_{13}	1.08	1.08	0.93	C_{31} - H_{37}	1.10	1.09	0.96	C_{59} - C_{62}	1.52	1.52	_
C_{11} - Cl_{27}	1.82	1.83	1.78	C_{39} - C_{40}	1.49	1.49	1.50	C_{62} - H_{63}	1.10	1.09	-
C_{14} - C_{15}	1.41	1.40	1.37	C_{39} - S_{41}	1.87	1.87	1.75	C_{62} - H_{64}	1.10	1.09	_
C_{14} - C_{16}	1.40	1.40	1.37	C_{39} - C_{45}	1.36	1.36	1.34	C_{62} - C_{65}	1.54	1.54	-
C_{15} - C_{17}	1.40	1.39	1.38	C_{40} - N_{43}	1.41	1.41	1.38	C_{65} - H_{66}	1.09	1.09	-
C_{15} - H_{18}	1.09	1.08	0.93	C_{40} - O_{44}	1.25	1.25	1.22	C_{65} - H_{67}	1.10	1.09	-
C_{16} - C_{19}	1.40	1.40	1.39	S_{41} - C_{42}	1.84	1.84	1.76	C_{65} - H_{68}	1.10	1.09	_

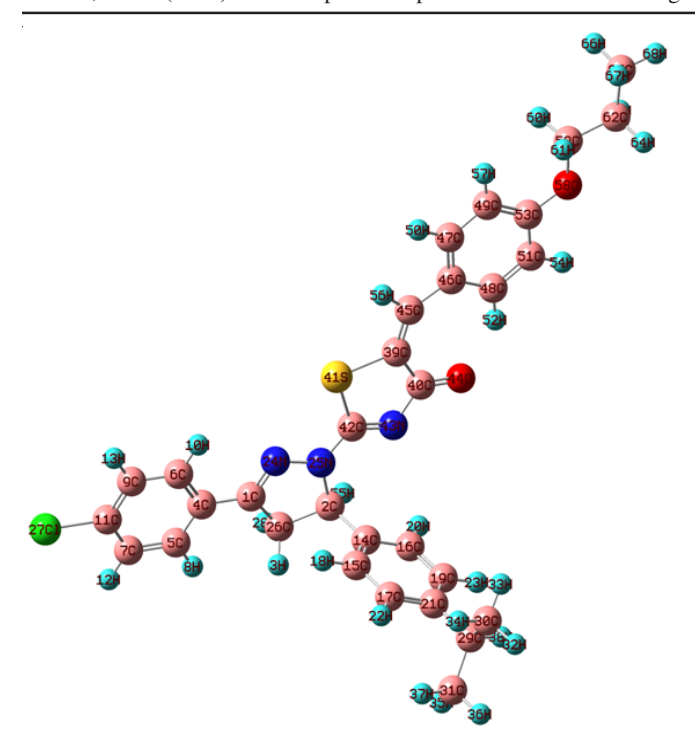


Fig. 1. Optimized structure of 5-(4-propoxybenzylidene)-2-[3-(4-chlorophenyl)-5-[4(propan-2-yl)phenyl-4,5-dihydro-1*H*-pyrazol-1-yl]-1,3-thiazol-4(5*H*)-one

C-C bond lengths in all rings lie between the normal C-C single and C=C double bond lengths indicating the conjugation of electron density in all the ring [16]. It shows that the varied range of C-C bond length of 1.36 Å to 1.55 Å for B3LPY/6-31G/6-311G and 1.29 Å to 1.52 Å for XRD, respectively.

The intermolecular distance of C₂-C₂₆ (1.56 Å/DFT, 1.54 Å/ XRD) is higher than the other C-C atoms. This is due to the presence of a nitrogen atom (N_{25}) that attached to the C_2 atom. The pyrazol ring C-N bond lengths are C_2 - $N_{25} = 1.51 \text{ Å}$ /DFT, 1.47 Å/XRD. The C-N values in the thiazol ring, show that the bond lengths for C₄₂-N₄₃ is 1.30 Å in both DFT/XRD and C₄₀- N_{43} are 1.41 Å/DFT and 1.38 Å/XRD. Likewise, C-S values of thiazole ring C_{39} - S_{41} and S_{41} - C_{42} bond lengths are 1.87 Å and 1.84 Å, respectively. These values suggest that some multiple bond character is present in the thiazole ring [17]. The C=O bond lengths (DFT/XRD) in the carbonyl group are 1.26 Å (C-O) reported by Mary [18]. Similarly, the $C_{40}=O_{44}$ bond showed double bond character, with a bond length value of 1.25 Å by both B3LYP/6-31G/B3LYP/6-311G and 1.22 Å in XRD. The bond lengths of propoxybenzylidene in the title compound are C_{62} - $C_{65} = 1.65 \text{ Å/DFT}$, O_{58} - $C_{59} = 1.46 \text{ Å/DFT}$, C_{53} - O_{58} = 1.39 Å/DFT comparable to that reported value [19].

Normally, the C-Cl bond length indicates a considerable increase in its length when compared with the C-H bond length [15]. Experimental value relates to the chlorine atom substituted phenyl ring shown the bond length 1.78 Å. From this observation, it is clear that the C_{11} - Cl_{27} bond length of the title compound falls at 1.82 Å and 1.83 Å using B3LYP/6-31G and 6-311G. The comparative analysis reveals that except of few values observed in DFT, calculated bond lengths are good agreement with literature values.

Vibrational assignments: In recent years, FT-IR and FT-Raman have been mostly used as vibrational spectroscopy for structural characterization of molecular systems through DFT calculations. The title compound is constituted by N=68 atoms and hence has 3N-6=198 normal modes of vibration. The observed and calculated wavenumber and potential energy distributions are discussed below. The fundamental modes of vibration were carried out and are depicted in Table-2. The simulated and experimental FT-IR and FT-Raman spectra are given in Figs. 2 and 3, respectively.

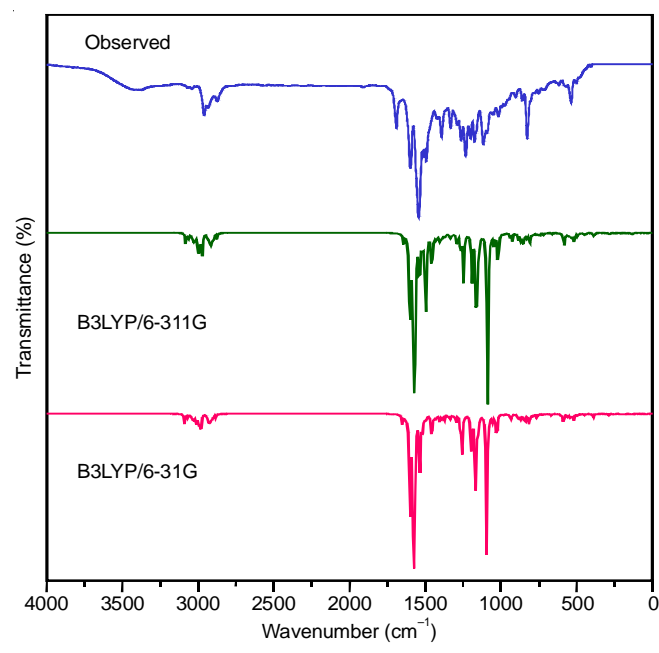


Fig. 2. FT-IR simulated spectra of 5-(4-propoxybenzylidene)-2-[3-(4-chlorophenyl)-5-[4(propan-2-yl)phenyl-4,5-dihydro-1*H*-pyrazol-1-yl]-1,3-thiazol-4(5*H*)-one

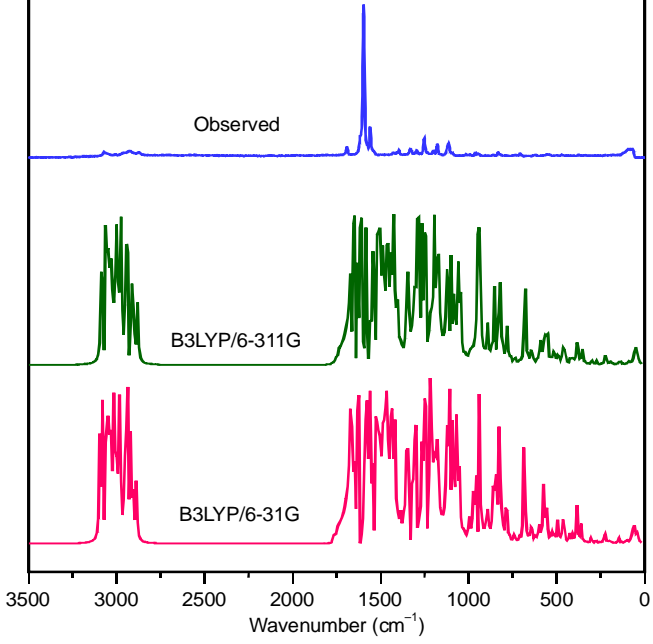


Fig. 3. FT-Raman simulated spectra of 5-(4-propoxybenzylidene)-2-[3-(4-chlorophenyl)-5-[4(propan-2-yl)phenyl-4,5-dihydro-1*H*-pyrazol-1-yl]-1,3-thiazol-4(5*H*)-one

860 Shanmugapriya et al. Asian J. Chem.

TABLE-2
VIBRATIONAL ASSIGNMENTS, OBSERVED AND CALCULATED WAVENUMBERS (cm⁻¹) OF 5-(4-PROPOXYBENZYLIDENE)-2-[3-(4-CHLOROPHENYL)-5-[4-(PROPAN-2-YL) PHENYL]-4,5-DIHYDRO-1*H*-PYRAZOL-1-YL]-1,3-THIAZOL-4(5*H*)-ONE AT B3LYP METHOD WITH 6-31G AND 6-311G BASIS SETS

Obse wavenu (cm	ımbers	wavenum	ulated bers (cm ⁻¹) iled)	Vibrational assignments (PED%)	Obse wavenum	erved bers (cm ⁻¹)	wavenum	ulated bers (cm ⁻¹) aled)	Vibrational assignments (PED%)
FT-IR	FT- Raman	B3LYP/ 6-31G	B3LYP/ 6-311G	- (FED%)	FT-IR	FT- Raman	B3LYP/ 6-31G	B3LYP/ 6-311G	assignments (PED%)
		3091	3082	νCH(99)	1050w		1055	1051	δring (61)
3070w		3075	3070	vCH(99)			1050	1042	δring (61)
		3070	3066	vCH(98)			1036	1030	δring (60)
		3066	3060	νCH(98)			1029	1023	γCH(58)
		3061	3054	νCH(98)	1017ms		1024	1016	vCO (69), vCC (12)
		3053	3049	vCH(99)			1014	1009	γCH(59)
3040w		3045	3042	vCH(98)		1000w	1006	1002	γCH(59)
		3040	3036	vCH(98)	994w		1003	998	γCH(60)
		3037	3031	vCH(99)			983	982	γCH(60)
		3031	3028	vCH(99)	975w		979	973	γopr CH ₃ (62)
		3027	3023	vCH(98)			965	961	γCH(58)
		3024	3019	vCH(98)		950vw	955	950	vCS(74)
		3018	3014	vCH(99)			946	943	γopr CH ₃ (62)
2936w		3012	3008	$v_{ass}CH_{3}(97)$			939	938	γCH (58)
		3009	3002	v _{ass} CH ₃ (97)			929	925	δring (61)
		3000	2996	$v_{ass}CH_2(98)$			921	917	γCH ₃ (60)
		2996	2991	$v_{ass}CH_3(97)$	904w	900	908	903	δrock CH ₃ (61)
		2990	2985	$V_{ass}CH_2(97)$			895	891	δrock CH ₃ (61)
		2981	2977	v _{ass} CH ₃ (97)			886	882	γCH (58)
		2975	2970	vCH(98)			878	875	γCH (58)
2961ms		2970	2963	v _{ass} CH ₃ (97)			870	866	γCH (58)
		2951	2945	$v_{ass}CH_3(97)$	860w		868	860	γCH (58)
2936w		2942	2938	$v_{ass}CH_{2}(98)$			856	854	γCH (57)
2,00		2933	2930	$V_{ass}CH_{3}(97)$			845	841	γCH (58)
		2930	2924	$V_{ass}CH_3(98)$	827w	832w	834	830	Ring breathing (60)
		2925	2919	v _{ss} CH ₃ (98)	02711	032**	818	815	γCCl (71)
		2918	2912	$V_{ss}CH_3(98)$			809	806	γCS (75)
		2909	2903	$v_{ss}CH_3(98)$			796	792	γCS (74)
		2901	2896	vCH(97)			790	785	δring (64)
2875m		2882	2875	ν _{ss} CH ₂ (98)			782	778	δwagg CH,(61)
1692ms		1650	1643	$v_{ss}CI_{2}(70)$ vCO(71), vCN(21)			769	765	$\delta CO(70)$
10921118		1631	1625	vCC (71), vCN (21) vCC (68), δCH (19)	756w		763	759	γCO(68)
		1619	1614	vCC (68), δCH (20)	750W		750	743	• • • •
		1606	1604	vCC (68), δCH (20)			725	721	γring (56)
1599s		1599	1599	vCC (67), vCN (15), &CH (12)	720w		720	716	γring (55)
13998	1596vs	1596	1592	vCC (67), vCN (15), δCH (12)	720W		706	702	δring (61)
	139008	1585	1592				692	689	γring (55)
		1579	1576	vCC (68), δCH (13), δCC (10)			666	662	vCC(66)
				vCN (66), vCO (13), vCC (12)					δipr CH ₃ (59)
	1560a	1572	1570	vCC (68), δCO (16), vCN (10)			648 629	643	δccl(57)
1540	1560s	1566	1564	vCN (69), vCO (19)	(10			626	γCH(58)
1542vs		1551	1551	δCH (72), vCC (10)	618w		620	617	γCH(58)
		1540	1542	$\rho_{\text{sciss}} \text{CH}_2 (76)$			600	596	γCH(59)
		1534	1535	δCH (73), vCC (12)	7.00		585	581	γCH(58)
		1530	1527	δCH (65), vCC (17)	569w		579	572	γCH(58)
		1521	1519	δορbCH ₃ (6a)			566	560	γCH(58)
		1514	1511	δopbCH ₃ (69)	506		554	551	Ring breathing (60)
1404		1506	1503	δopbCH ₃ (68)	536w		538	535	γCH(59)
1494ms		1496	1495	δipbCH ₃ (68)			531	525	γring (54)
		1494	1490	$\rho_{\text{scissc}}H_2$ (75)	50.4		517	513	δring (55)
		1485	1483	δipbCH ₃ (68)	504w		505	501	δring (55)
		1475	1475	δipbCH ₃ (68)			494	490	δCC (61)
		1466	1462	$\rho_{\text{SCISSC}} H_2(75)$			475	472	δCC (60)
		1456	1456	δCH (68), vCC (10)			461	453	γCC (52)
		1453	1450	δCH (68), vCC (12)			446	441	γCO (50)
	1440w	1445	1441	δsb CH ₃ (76)			440	438	γCH (54)
		1438	1435	$\delta \text{sb CH}_{_3}$ (76)			435	430	γring (54)
		1431	1426	δCH (68)			422	419	γring (54)

1423ms		1420	1417	δCH (68)	406vw	412	408	γring (54)
		1413	1408	δsb CH ₃ (75)		406	400	γCC (55)
	1400m	1403	1400	νCN (66), δCH (14)		388	385	γring (49)
		1389	1389	σrock CH,(67), vCC (16)		373	372	γCCl (51)
		1380	1381	δCH (65), vCCC (12)		364	360	δring (50)
		1376	1375	νCC (65), δCH (10)		350	345	γCC (48)
		1370	1368	δCH (66), vCCC (12)		339	333	γCCH ₃ (49)
		1355	1353	δCH (66)		320	316	δCC (54)
		1348	1344	σrock (65), vCCC (10)		306	301	δCC (55)
	1330m	1336	1335	δCH (65), vCCC (12)		284	280	δring (60)
		1330	1327	vCC (63), δCH (12)		279	274	δCC (58)
		1316	1313	νCC (68), δCH (13)		256	252	τCCH ₃ (54)
		1304	1302	δCH (66)		250	246	δCC (58)
1288ms	1288m	1294	1290	σrock CH ₂ (67), vCC (12)		248	241	τCH ₃ (48)
		1285	1283	τCH ₂ (59)		235	230	τCH ₃ (48)
		1275	1271	vCC (63), δCH (23)		229	225	τCH ₃ (48)
1264ms		1266	1263	δCH (68)		222	217	δring (57)
		1261	1257	orock CH ₂ (67)		214	208	γCO (61)
		1253	1250	δCH (68)		206	202	δring (59)
	1245ms	1245	1243	τCH, (58)		200	196	δring (60)
1233s		1234	1235	νCC (66), δCH (14)		183	175	γCO (57)
		1232	1228	δCH (63), vCCC (16)		174	168	δring (58)
		1223	1220	δCH (65)		161	155	γCC (49)
		1216	1212	δCH (65), vCCC (12)		148	140	γCO (48)
		1205	1203	δCH (66)		135	130	γCN (48)
		1194	1190	δCH (65)		125	119	δring (53)
		1190	1188	δCH (66)		106	98	δring (55)
1180ms		1186	1182	τCH ₂ (57)		95	87	τCO(49)
1175ms	1175ms	1175	1171	γ wagg CH ₂ (55)	78vw	89	80	γCC (49)
		1166	1160	δCO (61)		83	73	γCC (48)
		1156	1153	δCH (66)		75	67	γCC (49)
		1147	1144	δCH (64)		62	56	δCC (58)
		1143	1139	δCH (64)		55	49	δCC (58)
	1125ms	1132	1127	δCH (64)		49	40	γring (48)
		1115	1112	vCCH ₃ (67)		45	36	γCC (48)
		1099	1096	δring (60)		39	31	γCC (47)
1092ms		1094	1092	νCCH ₃ (66)		35	28	γCC (48)
		1091	1085	νΝΝ (72), δCN (14), δCO (10)		31	25	γCC (48)
		1086	1081	νCC (67), δring (16)		26	22	γCC (48)
		1080	1075	νCC (68), νCO (14)		21	19	γCC (45)
		1071	1066	γCH(59)		16	14	γCC (45)
		1064	1060	δring (61)		9	6	γCC (48)

C–H vibrations: The hetero-aromatic structure shows the presence of C-H stretching vibrations in the region of 3100-3000 cm⁻¹ [20]. The characteristic region for the identification of the C-H stretching vibration is affected by the nature of substituent group interaction. In present study, the C-H stretching vibrations are observed at 3040 cm⁻¹ and 3070 cm⁻¹ in the FT-IR spectrum. The scaled frequency of C-H stretching bands have been obtained from 3091-3018 cm⁻¹ using B3LYP/6-31G and 3082-3014 cm⁻¹ using B3LYP/6-311G basis set. The heteroaromatic configuration reveals the presence of C-H stretching, in-plane and out-of-plane bending vibrations in the range 3200-3000 cm⁻¹, 1200-900 cm⁻¹ and 980-700 cm⁻¹. Substitution sensitive C-H in-plane-bending vibrations are in the range of 1300-1000 cm⁻¹ [21]. In the title compound, the medium strong bands at 1264 cm⁻¹ in the FT-IR spectrum and at 1125 cm⁻¹ in the FT-Raman spectrum were assigned as C-H in-plane-bending vibrations. The theoretically computed wavenumbers for this mode were 1266, 1261, 1205, 1194, 1190, 1156, 1147, 1143

and 1132 cm⁻¹ using B3LYP/6-31G and at 1263, 1257, 1203, 1190, 1118, 1153, 1144,1139 and 1127 cm⁻¹ using B3LYP/6-311G. The C–H out-of-plane bending vibrations are observed as a weak band at 994, 860, 618, 569 and 536 cm⁻¹ in FT-IR and at 1000 and 950 cm⁻¹ in FT-Raman spectra, respectively. The calculated frequencies of these modes are in the range of 1014- 983 cm⁻¹, 886-845 cm⁻¹ and 629-538 cm⁻¹ using B3LYP/6-31G and at 1009-982 cm⁻¹, 882-841 cm⁻¹ and 626-535 cm⁻¹ using a B3LYP/6-311G basis set. Thus, the theoretically evaluated values for C–H vibrational modes are in good agreement with the experimental data.

CH₃ vibrations: Generally, there are nine fundamental modes of vibrations associated in CH₃ groups such as symmetrical stretch, two asymmetrical stretch, in-plane bending, out-of-plane bending, symmetric bending, in-plane rocking, out-of-plane rocking and twisting [22]. Asymmetric and symmetric stretching modes of a methyl groupattached to the benzene ring are usually downshifted because of electronic effects and

are expected near 2925 and 2865 cm⁻¹ for asymmetric and symmetric stretching vibrations. The CH₃ stretching modes are reported at 2980, 2917, 2895 cm⁻¹ in the IR spectrum, 2987, 2980, 2916, 2899 cm⁻¹ in the Raman spectrum are assigned by Viji et al. [23]. In the title compound, the CH₃ asymmetric and symmetric stretching modes appear in the range 3012-2920 cm⁻¹; 2930-2909 cm⁻¹ by B3LYP/6-31G and 3008-2963 cm⁻¹ and 2924-2903 cm⁻¹ by B3LYP/6-311G method. The inplane bending vibrations of the CH₃ group were experimentally obtained at 1494 cm⁻¹ FT-IR spectrum and 1440 cm⁻¹ in FT-Raman spectrum and these values are in good agreement with the literature [24]. In the present study, the calculated out-ofplane and in-plane bending vibration were located in the region 1521-1438 cm⁻¹ (6-31G) and 1519-1435 cm⁻¹ (6-311G). Out of three, only two in-plane rocking deformations at 904 cm⁻¹ in FT-IR and 900 cm⁻¹ in FT-Raman spectra are in agreement with theoretical values 908, 895 cm⁻¹ by B3LYP/6-31G and 903,891 cm⁻¹ by B3LYP/6-311G, respectively. The computed twisting τCH_3 values by B3LYP/6-31G method are predicted at $\tau = 256, 248, 235, 229 \text{ cm}^{-1}$ and 252, 241, 230, 225 cm⁻¹ by B3LYP/6-311G level of theory (Table-2).

CH₂ vibrations: There are six fundamental modes of vibrations can be associated with the CH₂ group, namely asymmetric and symmetric stretching, scissoring and rocking (inplane bending), wagging and twisting (out-of-plane bending). Arjunan *et al.* [25] reported the symmetric methylene group stretching vibration observed at 2922 cm⁻¹. In this investigation, the CH₂ symmetric stretching mode observed at 2936 cm⁻¹ in FT-IR spectrum and the theoretical value appears at 2942 cm⁻¹ by B3LYP/6-31G and 2938 cm⁻¹ by B3LYP/6-311G method. For, asymmetric stretch v_{ass} CH₂ was predicted theoretically at 3000, 2990 cm⁻¹ by B3LYP/6-31G and 2996, 2985 cm⁻¹ by B3LYP/6-311G. The rocking (σ_{rock}) mode is assigned at 1288 cm⁻¹ in both FT-IR sand FT-Raman spectra and at 1294 (6-31G), 1290 (6-311G) cm⁻¹ theoretically (B3LYP).

The CH_2 wagging (γ_{wagg}) mode is observed at 1175 cm⁻¹ in both FT-IR and FT-Raman spectra and theoretically the values obtained at 1175(6-31G), 1171(6-311G) cm⁻¹. The twisting mode of CH_2 vibrationis identified at 1180 cm⁻¹ in the FT-IR spectrum and 1245 cm⁻¹ in FT-Raman spectrum. The DFT calculated frequencies are observed at 1245, 1186 cm⁻¹ by B3LYP/6-31G and at 1233, 1182 cm⁻¹ by B3LYP/6-311G.

C–C vibrations: In phenyl ring, carbon-carbon stretching vibrations are usually appear in the interval of 1625–1400 cm⁻¹ [26-28]. In the present study, the DFT calculated frequencies are observed in the range 1631-1585 cm⁻¹ using B3LYP/6-31G and 1625-1581 cm⁻¹ using B3LYP/6-311G basis set. The same modes strong peaksare observed in FT-Raman spectrum at 1596 (vs) cm⁻¹ and in FT-IR spectrum at 1599(s) cm⁻¹. Normally, the ring deformation modes are observed below the frequency 1000 cm⁻¹. Shankar Rao *et al.* [27] calculated the in-plane C-C-C deformation bands occur in the region at 651-509 cm⁻¹ while the out-of-plane C-C-C deformation bands occur in the region 477-282 cm⁻¹. Likewise, the C-C in-plane bending vibrations are obtained at 494, 475 cm⁻¹ by B3LYP/6-31G and 490, 472 cm⁻¹ by B3LYP/6-311G. The frequencies observed in the out-of-plane C-C bending vibration are experimentally at 78

cm⁻¹ in FT-IR spectra. Here, the theoretical frequencies are assigned at in the region 89-90 cm⁻¹ using B3LYP/6-31G and 80-86 cm⁻¹ using B3LYP/6-311G.

C=O and C-O vibrations: In present investigation, the oxygen substitution were observed with $C4(C_{40})$ position of thiazole and aromatic substitution at the para-position of benzene (oxybenzylidene). The measurement of the C-O band is difficult due to the interfering with many other vibrations. Although there is a high absorption peak for CO vibrations when combined with C-C stretching, C-N stretching and C-H bending vibrations, the contribution of PED is only 20%. The C=O stretching vibration exhibits a strong band in the region 1750-1600 cm⁻¹ and C–O stretching vibrations are in the region 1300-100 cm⁻¹ [29]. On comparing the present investigation with the above literature, the medium strong band stretching mode of C=O is assigned at 1692 cm⁻¹ and C-O is assigned at 1017 cm⁻¹ in the FT-IR spectrum. The theoretical frequencies (B3LYP/6-31G) are 1650, 1024 cm⁻¹ and 1643, 1016 cm⁻¹ for B3LYP/6-311G.

C-Cl vibrations: Generally, the C-Cl in-plane (δ) and out-of-plane (γ) bending vibrations appears in the lower frequency region. Because the chlorine atom has a higher electronegativity than the carbon atom, the bonding electrons in the C-Cl bond will be closer to the chlorine than the carbon, increasing the force constant and causing a frequency shift [28]. In present study, the predicted in-plane (δ) bending vibrations is assigned at $\delta = 648$ cm⁻¹ for B3LYP/6-31G and $\delta = 643$ cm⁻¹ for B3LYP/6-31G. The out-of-plane (γ) bending vibrations have been assigned at $\gamma = 818$, 373 cm⁻¹ for B3LYP/6-31G and $\gamma = 815$, 372 cm⁻¹ for B3LYP/6-311G by theoretically.

C-S vibrations: The assignment of the molecular identification in C–S stretching vibrational mode is a difficult task. The absorption of this grouphaving variable intensity, which can be found in a wide range of 1035-245 cm⁻¹ in both aliphatic and aromatic sulphides [30]. The title compound were detected experimentally at 950 cm⁻¹ in FT-Raman. Theoretically, the stretching of C-S band in the thiazol ring at 995 cm⁻¹ in B3LYP/6-31G and 950 cm⁻¹ in B3LYP/6-311G. The C-S out-of-plane bending vibration was observed at 809, 796 cm⁻¹ by B3LYP/6-31G and 806, 792 cm⁻¹ in B3LYP/6-311G.

C–N, C=N and N-N vibrations: In general, identifying C=N and C-N vibrations was particularly challenging because mixing of several bands appeared possible in this region. Silverstain *et al.* [31] reported the C-N stretching absorption in the region 1689-1417 cm⁻¹ for aromatic compound. Similarly, computed value is agreeing with the literature. When C=N stretching band is found experimentally at 1400 cm⁻¹ in FT-Raman, theoretically assignment at 1403 cm⁻¹ in the B3LYP/6-31G and 1400 cm⁻¹ B3LYP/6-311G. The theoretically computed N-N stretching vibration combined with C-N in-plane bending vibration has been calculated at 1091(6-31G) cm⁻¹, 1085(6-31G) cm⁻¹ [32], respectively.

Global reactivity descriptors: The highest occupied molecular orbitals (HOMO) and lowest unoccupied molecular orbitals (LUMO) are fundamentally standard in quantum estimation; also, orbitals are called frontier molecular orbitals (FMOs). The FMOs portrays the molecular stability and it plays

a significant role in computing the molecular electrical transport properties. The E_{HOMO} and E_{LUMO} are frequently illustrating contour stabilization of the compounds by green-red isosurface circles, which clearly explain the charge transfer mechanism. The combination between these orbitals is important in various responses to describe the kinetic stability and chemical reactivity for the examined compounds. In present analysis, it is found that the title compound has a total of 600 orbitals out of which 143 are occupied and the remaining 457 are virtual orbitals. The orbitals numbered 143 and 144 account for HOMO and LUMO orbitals. The FMOs energy gap of studied molecule of B3LYP/6-31G basis set is reported as HOMO = -5.5198 eV, LUMO = -2.1701 eV, energy gap ΔE = -3.3497 eV and B3LYP/

6-311G basis set is reported as HOMO = -5.7563 eV, LUMO= -2.3943 eV, energy gap ΔE =- 3.3620 eV. Taking higher basis set B3LYP/6-311G band gap energy values (H-1 \rightarrow L+1, H-2 \rightarrow L+2) of compound are found to be -4.5226 eV and -5.7234 eV (Fig. 4), respectively. The ionization potential I= -E_{HOMO} with electron affinity A= - E_{LUMO} , electro-negativity χ = (I + A)/2, chemical potential $\mu = -(I + A)/2$ with hardness $\eta = (I - A)/2$ A)/2, softness $\sigma = 1/\eta$, electrophilicity index $\omega = \mu^2/2\eta$ of the title compound have been estimated theoretically [33] and the corresponding values are shown in Table-3.

Molecular electrostatic potential (MEP): MEP is related to the visualized map of electron density and is a very useful tool in understanding sites for electrophilic and nucleophilic

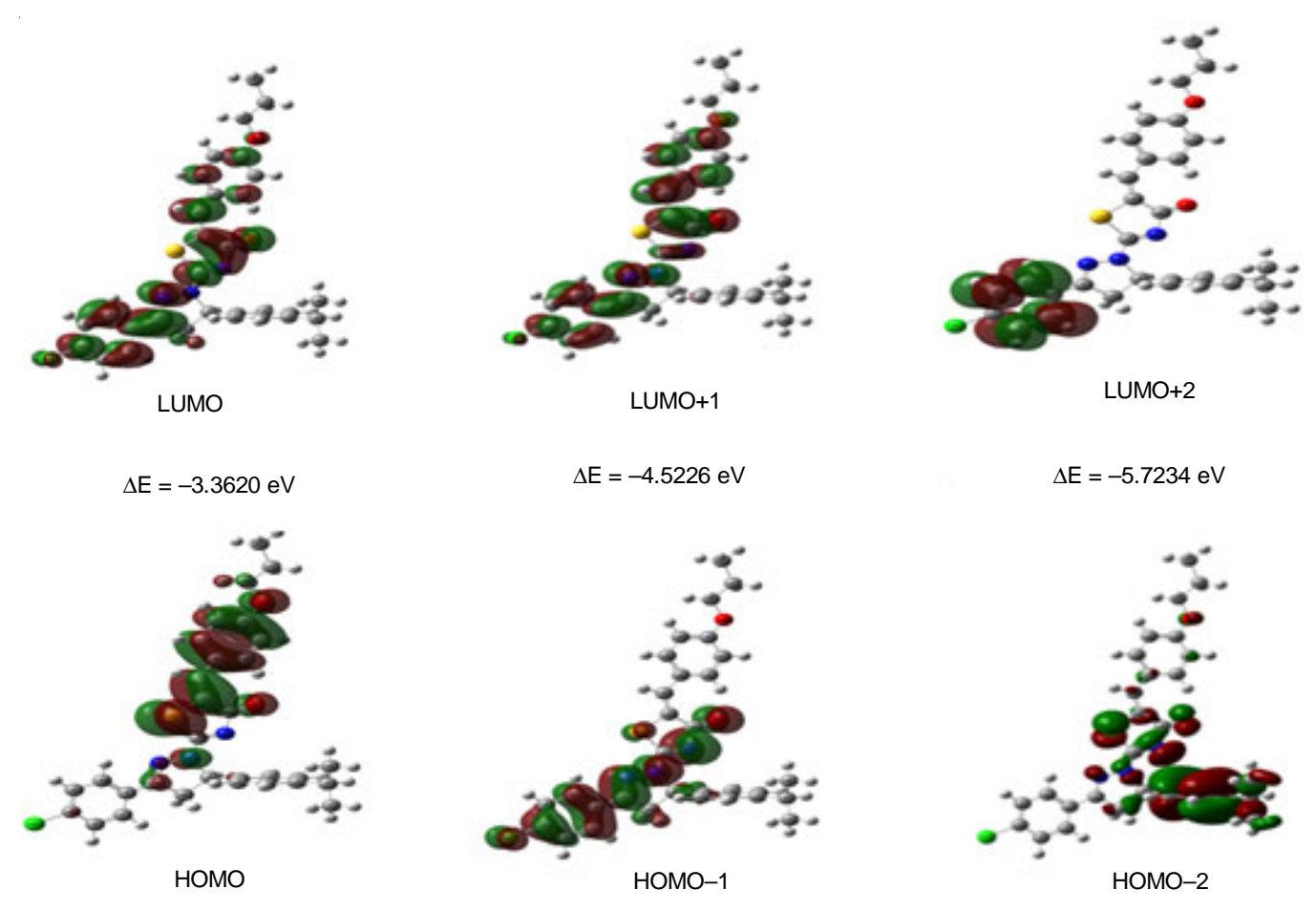


Fig. 4. HOMO-LUMO energy distribution plots of 5-(4-propoxybenzylidene)-2-[3-(4-chlorophenyl)-5-[4(propan-2-yl)phenyl-4,5-dihydro-1H-pyrazol-1-yl]-1,3-thiazol-4(5H)-one at DFT/6-311G basis set

TABLE-3
CALCULATED E-HOMO, E-LUMO(H-1 \rightarrow L+1, H-2 \rightarrow L+2), ENERGY GAP (E ₁ –E ₁), IONIZATION POTENTIAL (I),
ELECTRON AFFINITY (A), GLOBAL HARDNESS (η), ELECTRONEGATIVITY (χ), CHEMICAL SOFTNESS (σ),
CHEMICAL POTENTIAL (μ) AND GLOBAL ELECTROPHILICITY (ω) USING THE 6-311G LEVELS OF THEORY

Molecular properties	Energy (eV)	Energy gap (eV)	I (eV)	A (eV)	η (eV)	χ (eV)	σ(eV)	μ (eV)	ω(eV)
E _{HOMO}	-5.7563								
E_{LUMO}	-2.3943	3.3620	5.7563	2.3943	1.6810	4.753	0.5949	-4.0753	4.9399
$E_{\text{HOMO-1}}$	6.3539								
E_{LUMO+1}	1.8313	4.5226	6.3539	1.8313	2.2613	4.0926	0.4422	-4.0926	3.7035
E _{HOMO-2}	6.7645								
E _{LUMO+2}	1.0411	5.7234	6.7645	1.0411	2.8617	3.9028	0.3494	-3.9028	2.6613

864 Shanmugapriya et al. Asian J. Chem.

reactions. The electrostatic potential V(r) is identified as the energy collaborated between the charges formed by protons, electrons and nuclei existing in a given dimension [34,35]. We have reported and plotted the MEP surface mapping density of the title compound using Gaussian 09 program [8]. Potential increases in the order red < orange < yellow < green < blue. The negative (red and yellow) regions of MEP were related to electrophilic reactivity and the positive (green and blue) regions to nucleophilic reactivity. From the MEP, it is evident that the negative charge covers the carbonyl group is located on the thiazol ring and propoxybenzylidene, positive charge coversall hydrogen atoms in the molecule andthen the neutral region is located over the remaining groups. The molecular electrostatic potential surface of the title compound is shown in Fig. 5.

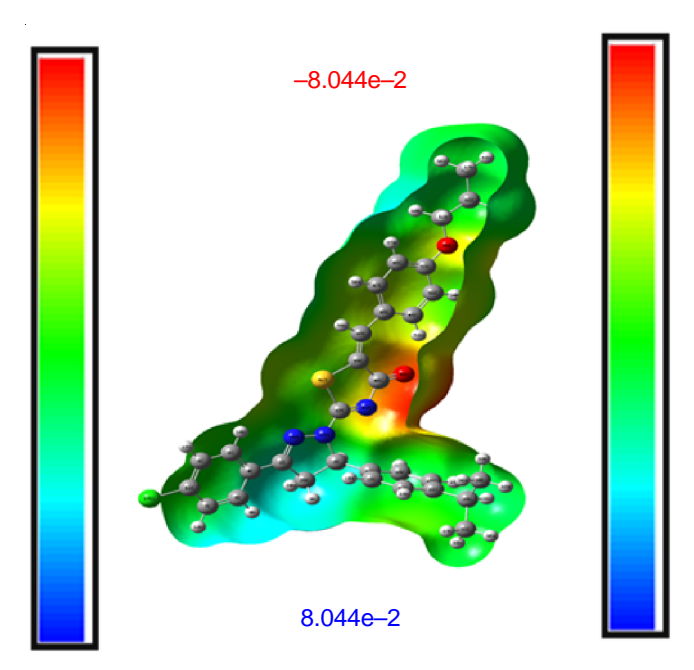


Fig. 5. MEP (molecular electrostatic potential surface) of 5-(4-propoxybenzylidene)-2-[3-(4-chlorophenyl)-5-[4(propan-2-yl)phenyl-4,5-dihydro-1*H*-pyrazol-1-yl]-1,3-thiazol-4(5*H*)-one

NBO analysis: Natural bond orbital analysis [11] gives an understanding of the intermolecular and intramolecular interactions of atomic bonds leading to the stability of the molecule. This analysis is carried out by examining all possible interactions between "fille \leq (donor) Lewis-type NBOs and "empty" (acceptor) non-Lewis NBOs, estimating their energetic importance by second-order perturbation theory. The NBO analysis allows the measuring of the hybridization of atoms involved in bonding orbitals and of the atomic lone pairs. Moreover, this type gives as BD (1) for 1-center bond, BD (2) for 2-center bond, LP (1) for 1-center valence lone pair and BD*(1) for 1-center anti-bond, BD*(2) for 2-center anti-bond labels corresponding to Lewis and non-Lewis NBOs, respectively. For each donor (i) and acceptor (j), the stabilization energy E(2) associated with the delocalization $i \rightarrow j$ is estimated as eqn. 1:

$$E(2) = \Delta E_{ij} = q_i \frac{(F_{i,j})^2}{(E_i - E_i)}$$
 (1)

where q_i is the donor orbital occupancy, E_i and E_i are diagonal elements and F (i,j) is the off-diagonal NBO element. The intramolecular charge transfer interactions for the most significant stabilization energies E(2) were obtained from the NBO calculations. The larger the E(2) value shows the intensive interaction between electron-donors, electron-acceptors and the greater extent of conjugation [36,37] of the whole system are presented in Table-4. The most important hyper conjugative interaction of the title compound isbonding to lone pair BD (2) C39-C45→LP (2) S41 shows the leading stabilization energy of 540.23 kcal/mol. The delocalization of BD*(2) electron from anti-bonding distributed to anti-bonding show the high stabilization energy is BD*(2) C7-C11 \rightarrow BD*(2) C6-C9 for 131.61 kcal/mol and BD*(2) C7-C11 \rightarrow BD*(2) C4-C5 for 195.69 kcal/mol. Lone pair of sulphur LP (2)S41 is distributed to antibonding BD*(1) C42- N43 and BD*(1) C39-C45 show the stabilization energy of 99.8 kcal/mol and 65.6 kcal/mol. This electron energy has been observed and listed in Table-4 as a result of occupational interaction.

Topology analysis

Atoms in molecules (AIM): The quantum theory of atoms in molecules (AIM) is a useful tool for the characterization of hydrogen bonding, and intrainter molecular interactions within the molecule [38,39]. The chemical structure of an element is identified using critical point's (CP's). The type of critical point described as: (3, -3) nuclear critical point (NCP); (3, -1) bond critical point (BCP); (3, +1) ring critical point (RCP); and (3,+3) cage critical point (CCP). The number and type of critical points that can coexist in a molecule or crystal follow a strict topological relationship which states eqn. 2 as:

$$n_{\text{NCP}} - n_{\text{BCP}} + n_{\text{RCP}} - n_{\text{CCP}} = \begin{cases} {}^{\text{l(Isolated-molecules)}} \\ {}^{\text{0(Infinite-crystals)}} \end{cases}$$
 (2)

where n denotes the number of the subscripted type of CP. The topology relationship of anisolated systemsis known as the Poincare-Hopf (PH) relationship. The topology analysis of the compound displays 68 (3,-3) nuclear critical points, 73 (3,-1) bond critical points (BCPs) between attractive pairs and 6 (3,+1) ring critical points corresponding to π - π interactions. One bond critical point is associated with a very weak (O44-C40-C39-C45-C45-C48-H52) hydrogen bonding interaction. When these lines show that the Poincare-Hopf relationship is satisfied, we can see all expected CPs are presented, hence we can confirmed that all CPs have been found.

$$(3, -3)$$
: 68, $(3, -1)$: 73, $(3, +1)$: 6, $(3, +3)$: 0
68 - 73 + 6 - 0 = 1

From Multiwfn, the energy of hydrogen bond is calculated by a relationship between bond energy E_{HB} (eqn. 3) and potential energy density $V(r_{BCP})$ at corresponding BCP as:

$$E_{HB} = \frac{V(r_{BCP})}{2} \tag{3}$$

The energy of the hydrogen bond O44-C40-C39-C45-C46-C48-H52 was calculated to be 46.60 kcal/mol. Magenta, orange and yellow spheres corresponds to (3, -3), (3, -1) and (3, +1) critical points and bond path Fig. 6(A). The indices of CPs are labelled by cyan numbers. The yellow sphere and line

 $TABLE-4\\ SECOND ORDER PERTURBATION THEORY ANALYSIS OF FOCK MATRIX ON NBO OF THE 5-(4-PROPOXYBENZYLIDENE)-2-[3-(4-CHLOROPHENYL)-5-[4-(PROPAN-2-YL)PHENYL]-4,5-DIHYDRO-1<math>H$ -PYRAZOL-1-YL]-1,3-THIAZOL-4(5H)-ONE

Donar (i)	Туре	ED/e	Acceptor (j)	Туре	$ED/e(q_i)$	E(2) ^a (Kcal/mol)	$E(i)-E(j)^{b}$	$F(i,j)^{c}$
BD (2)	C1-N24	1.92317	BD*(2)	C4-C5	0.38999	7.93	0.32	0.049
BD (1)	C1-C26	1.97344	BD*(1)	C2-C14	0.03967	5.08	1.09	0.067
BD (1)	C2-H55	1.89423	BD*(1)	H3-C26	0.04766	8.32	0.91	0.079
BD (2)	C4-C5	1.64504	BD*(2)	C1-N24	0.2551	16.67	0.24	0.058
BD (2)	C4-C5	1.64504	BD*(2)	C6-C9	0.29685	19.66	0.28	0.068
BD (2)	C4-C5	1.64504	BD*(2)	C7-C11	0.39233	22.43	0.26	0.069
.BD (1)	C6-C9	1.64504	BD*(1)	C11-Cl27	0.03193	4.95	0.81	0.057
.BD (2)	C6-C9	1.66679	BD*(2)	C4-C5	0.38999	20.57	0.28	0.068
.BD (2)	C6-C9	1.66679	BD*(2)	C7-C11	0.39233	21.12	0.26	0.067
BD (2)	C7-C11	1.67977	BD*(2)	C4-C5	0.38999	17.84	0.3	0.066
BD (2)	C7-C11	1.67977	BD*(2)	C6-C9	0.29685	19.15	0.3	0.068
BD (2)	C14-C15	1.67260	BD*(2)	C16-C19	0.34331	19.55	0.28	0.067
BD (2)	C14-C15	1.67260	BD*(2)	C17-C21	0.35910	18.95	0.29	0.067
BD (2)	C16-C19	1.69329	BD*(2)	C14-C15	0.38842	21.07	0.27	0.069
BD (2)	C16-C19	1.69329	BD*(2)	C17-C21	0.35910	21.11	0.28	0.07
BD (2)	C17-C21	1.64966	BD*(2)	C14-C15	0.38842	21.43	0.27	0.069
BD (2)	C17-C21	1.64966	BD*(2)	C16-C19	0.34331	20.03	0.28	0.066
BD (1)	C29-H38	1.90958	BD*(2)	C17-C21	0.35910	10.97	0.47	0.069
BD (1)	C29-H38	1.90958	BD*(1)	C30-H34	0.01540	6.13	0.93	0.069
BD (1)	C29-H38	1.90958	BD*(1)	C31-H37	0.01540	6.13	0.93	0.069
BD (1)	C39-S41	1.97750	BD*(1)	N25-C42	0.05342	9	1.44	0.102
BD (2)	C39-C45	1.72685	LP (2)	S41	1.99791	540.23	0.01	0.119
BD (2)	C39-C45	1.72685	BD*(2)	C40-O44	0.35800	29.54	0.28	0.083
BD (1)	C40-N43	1.98023	BD*(1)	N25-C42	0.05342	6.25	1.17	0.077
BD (2)	C40-O44	1.91570	BD*(2)	C39-C45	0.28406	8.91	0.27	0.046
BD (2)	C40-O44	1.91570	BD*(2)	C42-N43	0.51724	6.73	0.28	0.044
BD (1)	S41-C42	1.98222	BD*(1)	C39-C45	0.03534	7.14	1.39	0.089
BD (1)	C42-N43	1.97971	BD*(1)	S41-C42	0.04637	1.15	1.29	0.035
BD (2)	C42-N43	1.83934	LP (2)	S41 C40-O44	1.99791	102.39	0.05 0.31	0.102 0.087
BD (2)	C42-N43 C46-C48	1.83934 1.66946	BD*(2) BD*(2)	C40-O44 C47-C49	0.35800 0.31590	27.11 20.72	0.31	0.087
BD (2) BD (2)	C46-C48	1.66946	BD*(2)	C47-C49 C51-C53	0.31390	19.28	0.29	0.066
BD (2) BD (2)	C40-C48 C47-C49	1.66513	BD*(2)	C31-C33 C46-C48	0.35490	20.58	0.28	0.068
BD (2) BD (2)	C47-C49 C47-C49	1.66513	BD*(2)	C40-C48 C51-C53	0.35490	22.37	0.27	0.008
BD (2)	C51-C53	1.65032	BD*(2)	C46-C48	0.36800	21.42	0.28	0.07
BD (2)	C51-C53	1.65032	BD*(2)	C40-C40 C47-C49	0.31590	19.26	0.29	0.067
LP (1)	N24	1.99950	BD*(1)	C2-N25	0.04392	4.81	0.82	0.056
LP (1)	N25	1.99906	BD*(2)	C1-N24	0.25510	26.7	0.24	0.072
LP (1)	N25	1.99906	BD*(1)	S41-C42	0.04637	6.95	0.75	0.068
LP (1)	N25	1.99906	BD*(1)	C42-N43	0.06186	13.04	0.68	0.088
LP (3)	C127	1.99995	BD*(2)	C7-C11	0.39233	12.39	0.32	0.061
LP (1)	S41	2.00000	BD*(1)	C39-C40	0.09667	7.95	0.99	0.08
LP (1)	S41	2.00000	BD*(1)	C42-N43	0.06186	8.55	0.94	0.08
LP (2)	S41	1.99791	BD*(2)	C39-C45	0.03534	65.6	0.2	0.112
LP (2)	S41	1.99791	BD*(2)	C42-N43	0.51724	99.8	0.21	0.133
LP (1)	N43	1.99941	BD*(1)	C39-C40	0.09667	5.99	0.81	0.062
LP (1)	N43	1.99941	BD*(1)	S41-C42	0.04637	5.63	0.84	0.062
LP (2)	O44	1.87708	BD*(1)	C39-C40	0.09667	18.59	0.69	0.102
LP (2)	O44	1.87708	BD*(1)	C40-N43	0.06186	22.97	0.65	0.111
LP (1)	O58	1.94538	BD*(1)	C49-C53	0.02868	6	0.97	0.069
BD*(2)	C1-N24	0.25510	BD*(2)	C4-C5	0.38999	37.71	0.04	0.063
BD*(2)	C7-C11	0.39233	BD*(2)	C4-C5	0.38999	195.69	0.02	0.083
BD*(2)	C7-C11	0.39233	BD*(2)	C6-C9	0.29685	131.61	0.02	0.078
BD*(2)	C39-C45	0.03534	BD*(2)	C40-O44	0.35800	30.02	0.06	0.069
BD*(2)	C42-N43	0.51724	BD*(2)	C40-O44	0.35800	53.08	0.05	0.072

866 Shanmugapriya et al. Asian J. Chem.

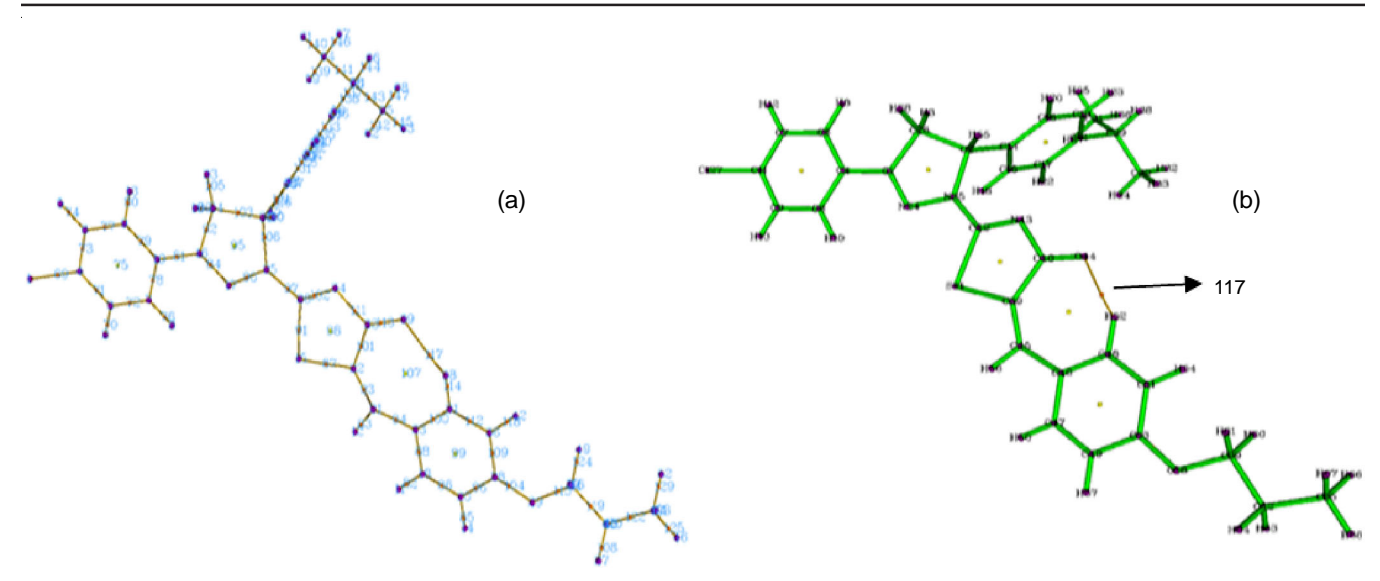


Fig. 6. AIM critical point maps of the 5-(4-propoxybenzylidene)-2-[3-(4-chlorophenyl)-5-[4(propan-2-yl)phenyl-4,5-dihydro-1*H*-pyrazol-1-yl]-1,3-thiazol-4(5*H*)-one bonding region

denote between the green colour bond path show the index 117 corresponds to the bond critical point (BCP) of O-C----H hydrogen bond, respectively. AIM map of the hydrogen bonding region are presented in Fig. 6b.

Localized orbital locator (LOL) and electron localization function (ELF): The topologies of the localized orbital locator (LOL) and electron localization function (ELF) are investigated electron density (gradient) in an attempt to elucidate cores and the valence shell of the atoms. To define Fermi hole curvature Becke & Edgecombe [40] proposed a local scalar function V(r) and show the excess kinetic energy of the Pauli repulsion regions (absence of LOL) of space. Extensively, Savin & Silvi [41] explained the two main types of basins in a molecule: core and valence. Core basins engulf centre nuclei present in the molecule and valence basins identifies the boundaries shared by the cores and lone pair. The localized orbital locator (LOL) shows the surface topology of interaction bond path. The carbon and nitrogen core present in compound is represented by the red-dot blue ring, inner shell is represented by red-dot yellow ring and the path electrons delocalization is

represented by greenish-yellow colour shown in Fig. 7a. The axis's of the LOL limits from 0.00 to 1.00. ELF isosurface explains the relation between LOL and ELF regions of the title compound is shown in Fig. 7b. From electron localization function (ELF) analysis, it finds the positions of isosurface, shared and unshared in space where ELF is maximal and to use the value of ELF in these points. By defining the electron localization (ELF) gradient in terms of η by the mapping its values on to range $0 \le \eta \le 1$: The value of ELF, $\eta(r)$ ranges from 0.0 to 1.00, where relatively high values in the interval 1.00 to 0.5 indicates regions containing bonding and antibonding localized electrons, whereas lower values (> 0.5) describe domains where electrons are expected to be delocalized. Very low electron localization zones between valence and inner shells revealed by the blue ring like region around each carbon and nitrogen atoms. Next, high electron localization zones between core and lone pair to valence atoms are revealed by the red ring like region around each hydrogen, chlorine (LP) and oxygen (LP) atoms. Colour shade maps or contour maps of bonding region are present in Fig. 7c. High ELF values

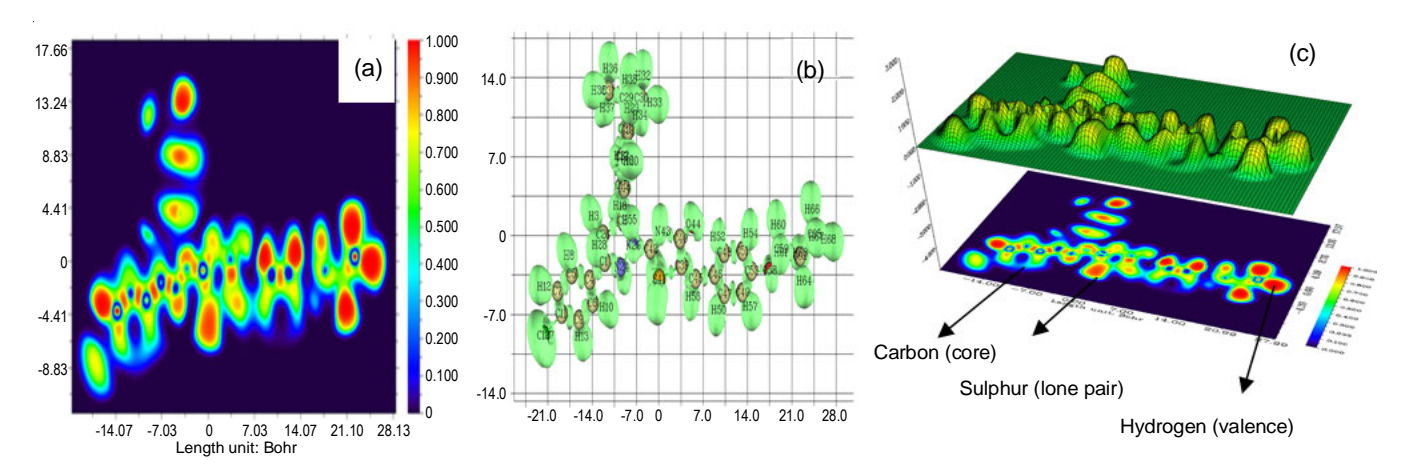


Fig. 7. (a) LOL, (b) ELF isosurface and (c) ELF region of 5-(4-propoxybenzylidene)-2-[3-(4-chlorophenyl)-5-[4(propan-2-yl)phenyl-4,5-dihydro-1*H*-pyrazol-1-yl]-1,3-thiazol-4(5*H*)-one

(\sim 0.600 to 1.00 Bohr unit) are coloured red; the series descends through yellow to green for middle (0.60 to 0.40Bohr unit) and the lower end (below 0.4 Bohr unit) of the scale is represented by blue.

Reduced density gradient analysis (RDG): Recently developed the non-covalent interactions (NCI) method to detect NCI in real space [42]. This method enables the identification of NCI as isosurfaces of the reduced density gradient RDG (r) in eqn. 4:

RDG(r) =
$$\frac{1}{2(3\pi r^2)^{1/2}} \frac{|\nabla \rho(r)|}{\rho(r)^{4/3}}$$
 (4)

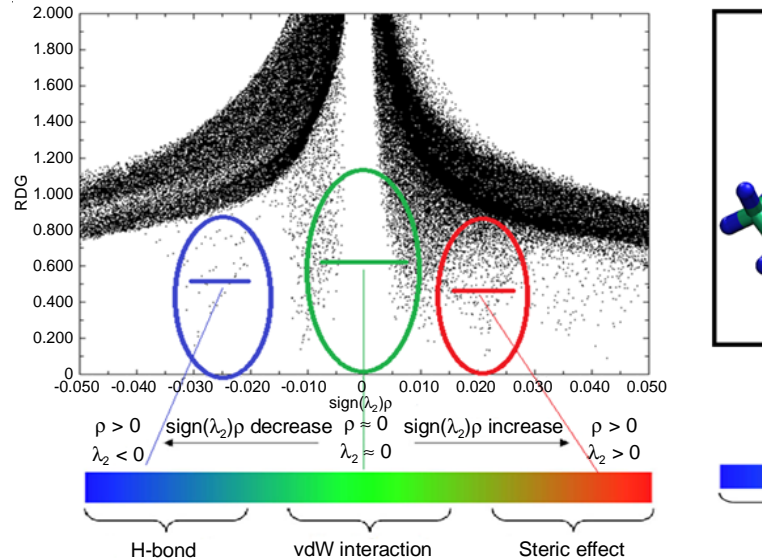
These isosurfaces expand over large regions of space containing interacting atoms. This approach recovers a more intuitive picture of van der Waals interactions, hydrogen bonds and steric repulsions than other local pair wise approaches, such as atoms in molecules (AIM) theory, or the electron localization function (ELF). The application of the reduced density gradient is to visualize interacting regions was motivated by the deviations from the exponential behaviour observed when RDG is plotted versus $\rho(r)$ for interacting systems [43]. Value of Hessian matrix of electron density is used to find the nature of an interaction. If $\lambda_2 > 0$, for non-bonded and if $\lambda_2 < 0$ for bonded. The blue colour indicates the hydrogen bonding interaction, the green colour represents van der Waals interactions and the red colour is identified as strong repulsion. From Fig. 8, the van der Waals interaction is the predominant factor as electrostatic interaction in the molecule. The isosurface of the title compound displays very strong van der Waals interact with strong steric effect as repulsive interaction and weak hydrogen bonding (one only) interaction. Moreover, hydrogenic and van der Waals regions are more impacted in the presence of propoxybenzylidene moiety in the structure pyrazole and thiazole.

Molecular docking: To explore the biological activity of the title molecule, molecular docking simulations have been performed using Auto Dock/Vina software [44]. Docking has

become a standard technology in drug discovery to virtually screen hypothetical chemicals to identify new active chemotypes, which predicts the target binding modes of protein and to point out the active site of ligands. PASS [45] is an online tool that predicts different types of activities based on the compound structure. From PASS analysis of title compound predicts several activities, amongst other activities choosing Pim-1 kinase inhibitor activity with Pa (probability to be active) and Pi (probability to be inactive) values are listed in Table-5. In light of their oncogenic potential, the Pim kinase family is

TABLE-5
PASS PREDICTION FOR THE ACTIVITY SPECTRUM OF TITLE
COMPOUND, Pa REPRESENTS PROBABILITY TO BE ACTIVE
AND PI REPRESENTS PROBABILITY TO BE INACTIVE

AND	FIKEFKES	ENTS FRODABILITY TO BE INACTIVE
Pa	Pi	Activity name
0.260	0.102	Antimetastatic
0.189	0.036	Pim-1 kinase inhibitor
0.177	0.031	Protein-tyrosine phosphatase inhibitor
0.153	0.012	Bc12 antagonist
0.192	0.054	Vascular adhesion protein 1 inhibitor
0.133	0.008	Pim-2 kinase inhibitor
0.242	0.121	Atherosclerosis treatment
0.246	0.131	Antineurogenic pain
0.101	0.005	CDC25B inhibitor
0.107	0.018	Autotaxin inhibitor
0.128	0.039	Lipoxygenase inhibitor
0.292	0.205	APOA1 expression enhancer
0.207	0.120	Antiobesity
0.132	0.049	Vasculitis treatment
0.082	0.010	Bcl-xL inhibitor
0.126	0.061	Sodium/bile acid cotransporter inhibitor
0.093	0.030	5-Lipoxygenase inhibitor
0.260	0.199	CDK9/cyclin T1 inhibitor
0.078	0.024	Protein-tyrosine phosphatase 2C inhibitor
0.205	0.157	Antidiabetic
0.092	0.044	Peroxisome proliferator-activated receptor
		gamma antagonist
0.240	0.195	Vanilloid 1 agonist



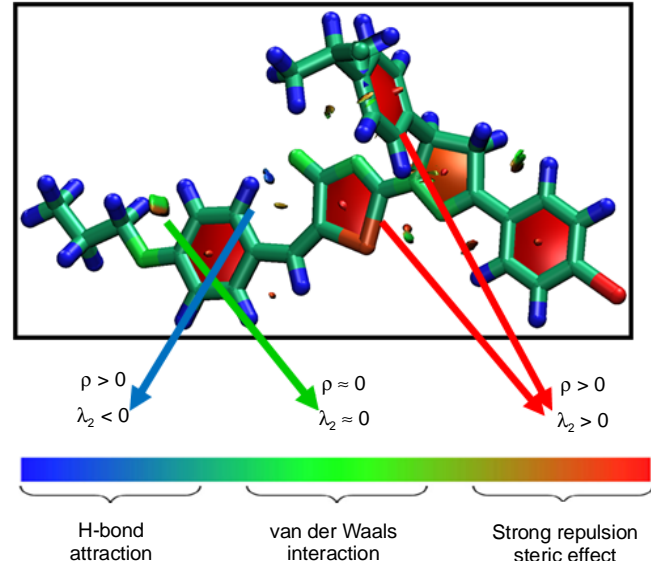


Fig. 8. Reduced density gradient 2D and 3D of 5-(4-propoxybenzylidene)-2-[3-(4-chlorophenyl)-5-[4(propan-2-yl)phenyl-4,5-dihydro-1*H*-pyrazol-1-yl]-1,3-thiazol-4(5*H*)-one

Asian J. Chem. 868 Shanmugapriya et al.

emerging as an important new target for drug discovery efforts. Pim kinases are emerging as important mediators of cytokine signaling pathways in hematopoietic cells and they contribute to the progression of certain leukemias and solid tumors [46]. Based on this, molecular docking simulation was carried out for the title compound bind with the human Pim-1 kinase enzyme. The 3D structure of proteins was obtained from Protein Data Bank (PDB ID: 3A99, 1GJ8, 1XQZ) has a good resolution. Auto Dock Tools (ADT) graphical user interface was used to add polar hydrogen and to calculate atomic charges by Kollman method. Water molecules and co-crystallized ligands were removed. The optimized structures of ligands PDB were obtained using the DFT (B3LYP) theory with the 6-311G basis set on Gaussian 09. Partial charges were calculated by Geistenger method. The active site to the energies was defined to add residues of the active site with the use of grid size 126 $\text{Å} \times$ $126 \text{ Å} \times 126 \text{ Å}$ using Auto grid [47]. The Auto Dock binding affinity (kcal/mol), inhibition constants (nM or µM) and nature of the bond with residues were computed (Table-6) and the best lowest energy docked position of the ligand with target protein are shown in Figs. 9a-b. The bond interactions present in the title compound are pi-alkyl, carbon-hydrogen bond,

2.4

3.5

LYS A 67

ILE A 185

Pi-alkyl

Pi-sigma

conventional hydrogen bond and pi-cation, 3A99 interaction with amino acid forms alkyl (2.5 Å; ILE A:74, 3.0 Å; VAL A:174) having various binding energies of -9.23, -9.13 and -9.01 kcal/mol. The inhibition constant values are identified as 170.15 nM, 201.86 nM, 248.98 nM and RMSD value are 81.47 Å, 83.69 Å and 82.21 Å. The result of 1GJ8 encircled by residues pi-sigma (2.8 Å, CYS A:13), conventional hydrogen bond (1.9 Å, GLN A:12) and alkyl (2.9 Å, LYS A:10). They have a docking score of -6.98, -6.95, -6.90 kcal/mol, respectively. The inhibition constant values are identified as $7.65 \mu M$, $19.13 \mu M$ and 12.09 µM and RMSD value are 26.16 Å, 26.28 Å and 26.31 Å. The prediction of 1XQZ insight the potent of Pim kinase inhibitor docked with ligand shows van der Waals (2.6 Å, GLN A:171), alkyl (2.4 Å, PRO A:125; 2.4 Å, LEU A: 93; 2.4 Å, LYS A: 67), which can provide some binding energies of -9.14, -9.01 and -7.83 kcal/mol. The inhibition constant values are identified as 201.35 nM, 249.97 nM and 1.82 µM. The RMSD value is 77.89 Å, 79.25 Å and 55.22 Å.

Conclusion

The FT-IR and FT-Raman spectra of 5-(4-propoxybenzylidene)-2-[3-(4-chlorophenyl)-5-[4-(propan-2-yl)phenyl]-4,5-

249.97 n

		MOLECULAR DOCKING PARAMETERS OF 5-(4-PROPOXYBENZYLIDENE)-2-[3-(4-CHLOROPHENYL)-5-[4-(PROPAN-2-YL) PHENYL]-4,5-DIHYDRO-1 <i>H</i> -PYRAZOL-1-YL]-1,3-THIAZOL-4(5 <i>H</i>)-ONE BIND WITH HUMAN PIM-1 KINASE ENZYME												
	PDB ID	Bond distance	Amino acid (residues)	Bond	Binding affinity Bond (kcal/mol)				ion const ıM or nM		F	RMSD (Å)		
		(Å)	(residues)		1	2	3	1	2	3	1	2	3	
		2.5	ILE A 74	Pi-alkyl				nM	Z	Σ				
	3A99	2.9	GLY A 48	Carbon-hydrogen bond	-9.23	-9.13	9.01	5 n	201.86 nM	248.98 nM	81.47	83.69	82.21	
	3A33	3.0 SER A 50	Conventional hydrogen bond	-9.	-9.	-9.	70.15	8.1.	6.8	81.	83.	82.		
		3.0	VAL A 174	Pi-alkyl				17	70	24				
		2.8	CYS A 13	Pi-sigma	~	10	6.90	M	Μμ	MM	9	∞	1	
	1GJ8	1.9	GLN A 12	Conventional hydrogen bond	6.98	-6.98		.65 µM	13	19.13 µM 12.09 µM	26.16	26.28	26.31	
		2.9	LYS A 10	Ailkyl	Î.	1	1	7.6	19.	12.	2	2	2	
		2.6	GLN A 171	Van der Waals										
	1XQZ	2.4	PRO A 125	Pi-alkyl	4	_	~	ПМ	пМ	Σ	6	ν.	7	
		2.4	LEU A 93	Pi-alkyl	9.1	-9.01	7.83	35	.97	.82 µM	77.89	79.25	55.22	
		2.4	LYS A 67	Pi-alkyl	7	1	1	21	49	3.	7	7	S	

TABLE-6

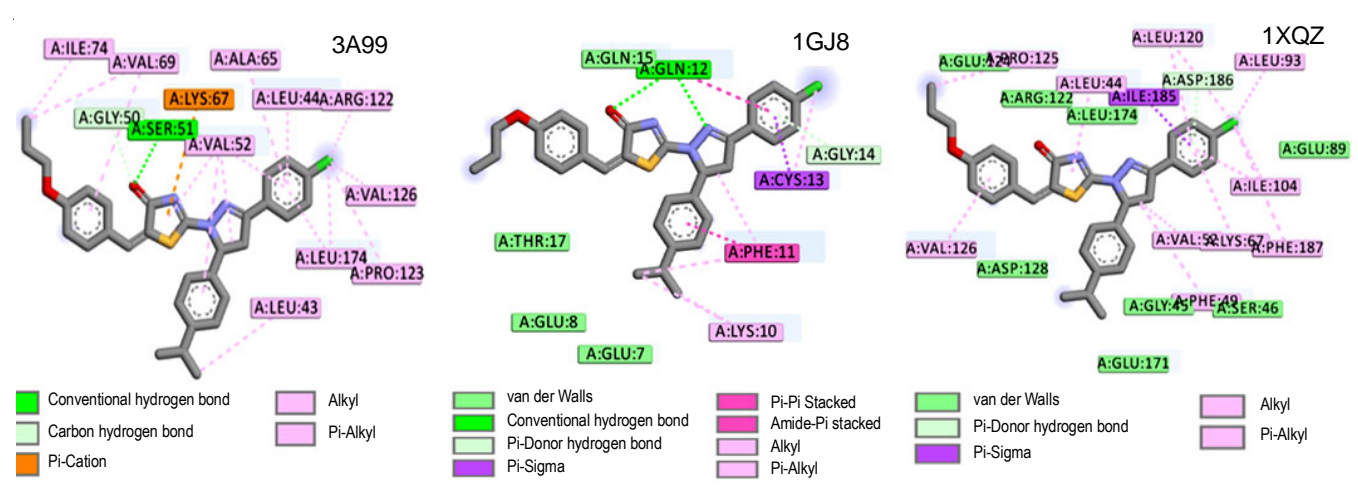


Fig. 9a. Residues interactions of Pim-1 kinase inhibitor protein with ligand (PCPPT)

Fig. 9b. Docked position values of Pim-1 kinase inhibitor protein with ligand (PCPPT)

dihydro-1*H*-pyrazol-1-yl]-1,3-thiazol-4(5*H*)-one was studied by both experimentally and theoretically. The vibrational wavenumber was computed using B3LYP/6-31G and B3LYP/6-311G basis sets DFT methods are assigned with the help of potential energy distribution analysis. The HOMO and LUMO analysis are used to determine the charge transfer and the chemical activity of molecule. From the molecular electrostatic potential, it is evident that the negative charge covers the carbonyl group, positive charge covers hydrogen atoms in the propoxybenzylidene, the neutral region is covered over the remaining groups and show the more electronegativity in the carbonyl group makes it the most reactive part of the compound. The stability of the molecule arising from hyperconjugative interaction and charge delocalization has been studied using NBO analysis. AIM confirms the presence of an intramolecular hydrogen bond between O44-H27···N14 with energy of 46.60 kcal/mol. The surface electron density core, lone pair and valance findings were confirmed by electron localization function (ELF) and localized orbital locator (LOL) studies. Intra- and intermolecular non-covalent and weak interactions (van der Waals forces) of thiazole and pyrazole were explored using the reduced density gradient (RDG) methods. The anticancerous protein 3A99 is having higher binding energy, inhibition constant and RMSD values such as -9.23 kcal/mol, 170.15 nM and 81.47 Å than 1GJ8 1XQZ. From the results, the title compound may be observed as an effective Pim-1 kinase drug.

CONFLICT OF INTEREST

The authors declare that there is no conflict of interests regarding the publication of this article.

REFERENCES

- P. Blum, A. Sagner, A. Tiehm, P. Martus, T. Wendel and P. Grathwohl, J. Contam. Hydrol., 126, 181 (2011); https://doi.org/10.1016/j.jconhyd.2011.08.004
- Y.S. Mary, C.Y. Panicker, M. Sapnakumari, B. Narayana, B.K. Sarojini, A.A. Al-Saadi, C.V Alsenoy and J.A. War, Spectrochim. Acta A Mol. Biomol. Spectrosc., 136, 483, (2015); https://doi.org/10.1016/j.saa.2014.09.061
- G. Susithra, S. Ramalingam, S. Periandy and R. Aarthi, *Egypt. J. Basic Appl. Sci.*, 4, 313 (2018); https://doi.org/10.1016/j.ejbas.2018.05.011

- S. Aayisha, T.S.R. Devi, S. Janani, S. Muthu, M. Raja, S. Sevvanthi and R. Hemamalini, *Comput. Biol. Chem*, 86, 107226 (2020); https://doi.org/10.1016/j.compbiolchem.2020.107226
- I.W. Cheney, S. Yan, T. Appleby, H. Walker, T. Vo, N. Yao, R. Hamatake, Z. Hong and J.Z. Wu, *Bioorg. Med. Chem. Lett.*, 17, 1679 (2007); https://doi.org/10.1016/j.bmcl.2006.12.086
- D. Morishita, M. Takami, S. Yoshikawa, R. Katayama, M. Kukimoto-Niino, S. Sato, T. Umehara, M. Shirouzu, K. Sekimizu, S. Yokoyama and N. Fujita, *J. Biol. Chem.*, 286, 2681 (2011); https://doi.org/10.1074/jbc.M109.092452
- V. V. Salian, B.K. Narayana, B.K. Sarojini, M.S. Kumar and A.G. Lobo, J. Mol. Struct., 1192, 91 (2019); https://doi.org/10.1016/j.molstruc.2019.04.105
- M.J. Frisch, G.W. Trucks, H.B. Schlegel, G.E. Scuseria, M.A. Robb, J.R. Cheeseman, G. Scalmani, V. Barone, B. Mennucci, G.A. Petersson, H. Nakatsuji, M. Caricato, X. Li, H.P. Hratchian, A.F. Izmaylov, J. Bloino, G. Zheng, J.L. Sonnenberg, M. Hada, M. Ehara, K. Toyota, R. Fukuda, J. Hasegawa, M. Ishida, T. Nakajima, Y. Honda, O. Kitao, H. Nakai, T. Vreven, J.A. Montgomery, Jr., J.E. Peralta, F. Ogliaro, M. Bearpark, J.J. Heyd, E. Brothers, K.N. Kudin, V.N. Staroverov, R. Kobayashi, J. Normand, K. Raghavachari, A. Rendell, J.C. Burant, S.S. Iyengar, J. Tomasi, M. Cossi, N. Rega, J.M. Millam, M. Klene, J.E. Knox, J.B. Cross, V. Bakken, C. Adamo, J. Jaramillo, R. Gomperts, R.E. Stratmann, O. Yazyev, A.J. Austin, R. Cammi, C. Pomelli, J.W. Ochterski, R.L. Martin, K. Morokuma, V.G. Zakrzewski, G.A. Voth, P. Salvador, J.J. Dannenberg, S. Dapprich, A.D. Daniels, Ö. Farkas, J.B. Foresman, J.V. Ortiz, J. Cioslowski and D.J. Fox, Gaussian 09, Gaussian, Inc., Wallingford CT (2009).
- R. Dennington, T. Kerth and J. Millam, Gauss View, Version 5.0, Semicham. Inc., Shawnee Mission KS (2009).
- 10. M.H. Jamroz, Spectrochim. Acta A Mol. Biomol. Spectrosc., 114, 220 (2013);

https://doi.org/10.1016/j.saa.2013.05.096

- T. Lu and F. Chen, J. Comput. Chem., 33, 580 (2011); https://doi.org/10.1002/jcc.22885
- E.D. Glendening and A.E. Reed, NBO Version 3.1, TCL, University of Wisconsin, Madison, USA (1998).
- 13. https://www.pymol.org
- 14. Biovia discovery studio 4.5; https://discover.3ds.com
- S. Parveen, M.A. Al-Alshaikh, C.Y. Panicker, A.A. El-Emam, B. Narayana,
 V. V. Saliyan and C. Van Alsenoy, *J. Mol. Struct.*, 1112, 136 (2016);
 https://doi.org/10.1016/j.molstruc.2016.02.018
- A.S. Devi, V.V. Aswathy, Y.S. Mary, C.Y. Panicker, S. Armakovic, S.J. Armakovic and C. Van Alsenoy, *J. Mol. Struct.*, 1148, 282 (2017); https://doi.org/10.1016/j.molstruc.2017.07.065
- K. Venil, A. Lakshmi, V. Balachandra, B. Narayana and V.V. Salian, *J. Mol. Struct.*, **1225**, 129070 (2021); https://doi.org/10.1016/j.molstruc.2019.127394
- Y.S. Mary, C.Y. Panicker, S. Armakovic, S.J. Armakovic, B. Narayana, B.K. Sarojini and C. Van Alsenoy, *J. Mol. Struct.*, 1148, 266 (2017); https://doi.org/10.1016/j.molstruc.2017.07.052

- R.A. Sheakh Mohamad, W.M. Hamad and H.J. Aziz, *Acta Cryst.*, E76, 920 (2020); https://doi.org/10.1107/S2056989020006611
- H. Behbehani and H.M. Ibrahim, *Molecules*, 17, 6362 (2012); https://doi.org/10.3390/molecules17066362
- S. Alturk, D. Avci, O. Tamer and Y. Atalay, *Comput. Theor. Chem.*, 1100, 34 (2017); https://doi.org/10.1016/j.comptc.2016.12.007
- 22. N. Colthup, Introduction to Infrared and Raman Spectroscopy, Elsevier (2012)
- B. Smith, Infrared Spectral Interpretation: A Systematic Approach, CRC Press, Washington, DC (1999).
- A. Viji, V. Balachandran, S. Babiyana, B. Narayana and V.V. Saliyan, *J. Mol. Struct.*, 1215, 128244 (2020); https://doi.org/10.1016/j.molstruc.2020.128244
- V. Arjunan, R. Anitha, S. Thirunarayanan and S. Mohan, *Chem. Data Coll.*, 11-12, 139 (2017); https://doi.org/10.1016/j.cdc.2017.09.002
- S.M. Hiremath, A. Suvitha, N.R. Patil, C.S. Hiremath, S.S. Khemalapure, S. K. Pattanayak, V.S. Negalurmath and K. Obelannavar, *J. Mol. Struct.*, 1171, 362 (2018); https://doi.org/10.1016/j.molstruc.2018.05.109
- Y.B. Shankar Rao, M.V.S. Prasad, N.U. Sri and V. Veeraiah, *J. Mol. Struct.*, **1108**, 567 (2016); https://doi.org/10.1016/j.molstruc.2015.12.008
- C. Sivakumar, V. Balachandran, B. Narayana, V.V. Salian, B. Revathi, N. Shanmugapriya and K. Vanasundari, *J. Mol. Struct.*, 1224, 129010 (2021); https://doi.org/10.1016/j.molstruc.2020.129010
- G. Socrates, *J. Chem. Educ.*, **72**, A93 (1995); https://doi.org/10.1021/ed072pA93.5
- M. Kaur, Y.S. Mary, C. Y. Panicker, H.T. Varghese, H. Yathirajan, K. Byrappa and C. Van Alsenoy, *Spectrochim. Acta A Mol. Biomol. Spectrosc.*, 120, 445 (2014); https://doi.org/10.1016/j.saa.2013.10.032
- R.M. Silverstein, F.X. Webster and D. Kiemle, Spectrometric Identification of Organic Compounds, Wiley: New York, Ed.: 7 (2005).
- 32. Y. Sert, M. Gumus, H. Gokce, I. Kani and I. Koca, *J. Mol. Struct.*, **1171**, 850 (2018);
 - https://doi.org/10.1016/j.molstruc.2018.06.069

- R.G. Parr and R.G. Pearson, J. Am. Chem. Soc., 105, 7512 (1983); https://doi.org/10.1021/ja00364a005
- E. Temel, C. Alasalvar, H. Gokce, A. Guder, C. Albayrak, Y.B. Alpaslan, G. Alpaslan and N. Dilek, *Spectrochim. Acta A Mol. Biomol. Spectrosc.*, 136, 534 (2015); https://doi.org/10.1016/j.saa.2014.09.067
- P. Kolandaivel and V. Nirmala, J. Mol. Struct., 694, 33 (2004); https://doi.org/10.1016/j.molstruc.2004.01.030
- A.E. Reed, L.A. Curtiss and F. Weinhold, *Chem. Rev.*, 88, 899 (1988); https://doi.org/10.1021/cr00088a005
- R.M. Asath, R. Premkumar, T. Mathavan and A.M.F. Benial, Spectrochim. Acta A Mol. Biomol. Spectrosc., 175, 51 (2017); https://doi.org/10.1016/j.saa.2016.11.037
- G.L. Sosa, N.M. Peruchena, R.H. Contreras and E.A. Castro, *J. Mol. Struct.*, 577, 219 (2002); https://doi.org/10.1016/S0166-1280(01)00670-4
- E.R. Johnson, S. Keinan, P. Mori-Sanchez, J. Contreras-Garcia, A.J. Cohen and W. Yang, *J. Am. Chem. Soc.*, 132, 6498 (2010); https://doi.org/10.1021/ja100936w
- A.D. Becke and K.E. Edgecombe, J. Chem. Phys., 92, 5397 (1990); https://doi.org/10.1063/1.458517
- 41. B. Silvi and A. Savin, *Nature*, **371**, 683 (1994); https://doi.org/10.1038/371683A0
- R.A. Boto, J. Contreras-García, J. Tierny and J.-P. Piquemal, *Mol. Phys.*, 114, 1406 (2015); https://doi.org/10.1080/00268976.2015.1123777
- I. Rozas, I. Alkorta and J. Elguero, J. Am. Chem. Soc., 122, 11154 (2000); https://doi.org/10.1021/ja0017864
- O. Trott and A.J. Olson, *J. Comput. Chem*, 31, 455 (2010); https://doi.org/10.1002/jcc.21334
- A. Lagunin, A. Stepanchikova, D. Filimonov and V. Poroikov, Bioinformatics, 16, 747 (2000); https://doi.org/10.1093/bioinformatics/16.8.747
- A.N. Bullock, J. Debreczeni, A.L. Amos, S. Knapp and B.E. Turk, *J. Biol. Chem.*, 280, 41675 (2005); https://doi.org/10.1074/jbc.M510711200
- 47. G.M. Morris, D.S. Goodsell, R.S. Halliday, R. Huey, W.E. Hart, R.K. Belew and A.J. Olson, *J. Comput. Chem.*, **19**, 1639 (1998); https://doi.org/10.1002/(SICI)1096-987X(19981115)19:14<1639:: AID-JCC10>3.0.CO;2-B